Yoshimura
Hangai

OCT Atlas

Springer

Nagahisa Yoshimura
Masanori Hangai

OCT Atlas

With 374 Figures

Springer

Nagahisa Yoshimura, MD, PhD
Department of Ophthalmology and Visual Sciences
Kyoto University Graduate School of Medicine,
Kyoto 6060-8507, Japan

Masanori Hangai, MD, PhD
Department of Ophthalmology
Saitama Medical University
Saitama 350-0495, Japan

ISBN-13 978-3-642-38624-4 ISBN 978-3-642-38625-1 (eBook)
DOI 10.1007/978-3-642-38625-1

Springer Medizin
© Springer-Verlag Berlin Heidelberg 2014

All Rights Reserved. No part of this book may be reproduced or transmitted in any form or by any means, electronic or mechanical, including photocopying, recording or by any information storage retrieval system, without permission from IGAKU-SHOIN LTD.

Authorized translation from the Japanese language edition, entitled: OCT Atlas; ISBN: 978-4-260-01513-4 by Nagahisa Yoshimura, Masanori Hangai; published by IGAKU-SHOIN LTD. TOKYO Copyright© 2012

Library of Congress Control Number: 2013944211

This work is subject to copyright. All rights are reserved by the Publisher, whether the whole or part of the material is concerned, specifically the rights of translation, reprinting, reuse of illustrations, recitation, broadcasting, reproduction on microfilms or in any other physical way, and transmission or information storage and retrieval, electronic adaptation, computer software, or by similar or dissimilar methodology now known or hereafter developed. Exempted from this legal reservation are brief excerpts in connection with reviews or scholarly analysis or material supplied specifically for the purpose of being entered and executed on a computer system, for exclusive use by the purchaser of the work. Duplication of this publication or parts thereof is permitted only under the provisions of the Copyright Law of the Publisher's location, in its current version, and permission for use must always be obtained from Springer. Permissions for use may be obtained through RightsLink at the Copyright Clearance Center. Violations are liable to prosecution under the respective Copyright Law.

The use of general descriptive names, registered names, trademarks, service marks, etc. in this publication does not imply, even in the absence of a specific statement, that such names are exempt from the relevant protective laws and regulations and therefore free for general use.

While the advice and information in this book are believed to be true and accurate at the date of publication, neither the authors nor the editors nor the publisher can accept any legal responsibility for any errors or omissions that may be made. The publisher makes no warranty, express or implied, with respect to the material contained herein.

Editor: Diana Kraplow, Heidelberg
Project Management: Dr. Astrid Horlacher, Heidelberg
Professional proofreading: Jesse Jung, MD, New York University School of Medicine, New York and Department of Ophthalmology, Edward S. Harkness Eye Institute, Columbia University College of Physicians and Surgeons, New York, USA; Quraish Ghadiali, MD, New York University School of Medicine, New York, USA
Cover Illustration: © Santiago Cornejo – Fotolia
Cover Design: deblik Berlin
Typesetting and Reproduction of the Figures: Fotosatz-Service Köhler GmbH – Reinhold Schöberl, Würzburg

Printed on acid-free paper

Springer Medizin is brand of Springer
Springer is part of Springer Science+Business Media (www.springer.com)

Preface

At the time of its first clinical application, optical coherence tomography (OCT) imaging was limited particularly by the clarity of images. However, OCT provided a great advantage over other diagnostic modalities, as it could noninvasively provide tomographic images of the retina of a living eye. As a result, a number of new findings in retinal diseases were made using the time-domain OCT. Later, in 2002, the second generation OCT devices (Stratus 3000 OCT©) were released and the quality of OCT images improved dramatically. Prior to the release of the first commercially available spectral-domain (SD) OCT in 2006, we had an opportunity to use this SD-OCT. I was so excited with the quality of these images, and I felt as if we were observing in vivo histopathology of retinal lesions. Furthermore, with the release of the Heidelberg Spectralis© with noise reduction technology, this further enhanced the quality of images.

OCT has now become an essential medical equipment in ophthalmic care, and I believe quality textbooks describing the functionality of OCT are very important in the education of young ophthalmologists and eye care personnel. In this book, with Professor Hangai, we chose high quality OCT images of rather common diseases as well as images of several rare diseases. We also tried to make the explanation of these OCT images as simple as possible.

Unfortunately, because the original version was published in the Japanese language and this English version is published two years after the Japanese version, there may be some obsolete descriptions and new references could be added. Even with such drawbacks, I believe this OCT Atlas will be helpful in further understanding retinal diseases.

Nagahisa Yoshimura, MD, PhD
April 2014
Kyoto with cherry blossom

Second Preface

Biological information such as color, light absorption/back-reflection, cross-sectional images, polarization, motion and function is provided by the reflection of light from the fundus. Our progress in clinically diagnosing and treating retinal diseases depends on the advancement of technology by which this biological information is extracted from the reflected light from the fundus.

Originally, the clinical basics of retinal diseases were established based on direct observation of the fundus by biomicroscopy alone. However, biomicroscopic observation was limited by the observer's inability to provide sufficient systematic, 3-dimensional information. Optical coherence tomography (OCT) now enables clinicians the ability to obtain high-resolution cross-sectional images. The reduction in speckle-noise has improved the visualization of each retinal layer and also provides imaging of pathological retinal diseases with definition similar to that of histopathology. However, in vivo OCT images are not identical to light microscopic sections, but no more than the optical images that consist of the intensity of back-reflections from each depth point within the fundus. Therefore, we need to continue to cultivate our ability to interpret the OCT B-scan images.

Interpretation of the OCT B-scan images requires both a basic knowledge of the factors affecting the acquisition of OCT B-scans and the pattern of features seen on OCT B-scans characteristic to each retinal disease. We believe that the presentation of selected cases with typical OCT images is one of the most powerful methods to efficiently learn how to interpret OCT B-scan images. Particularly, cases of common diseases we daily see would be useful to strengthen our ability to interpret and diagnose retinal diseases. We hope that this »OCT Atlas« provides a useful source of information in the interpretation of OCT images to our readers.

Masanori Hangai, MD, PhD
April 2014
Saitama with cherry blossom

Table of Contents

1 The basis of OCT interpretation . . . 1
1.1 B-scan interpretation . . . 2
1.2 Normal retina . . . 4
1.3 Normal choroidal imaging . . . 9
1.4 Displaying B-scans . . . 10
1.5 Depth resolution misinterpretations . . . 11
1.6 Artifacts . . . 13

2 Vitreoretinal interface pathology . . . 21
2.1 Idiopathic macular holes . . . 23
Case 1 Physiological PVD: Flattening of foveal depression . . . 29
Case 2 Idiopathic macular holes: Progression from stage 1 (cystoid space type) to stage 2 . . . 30
Case 3 Idiopathic macular hole: Stage 1 foveal cystoid space formation type . . . 31
Case 4 Idiopathic macular hole: Stage 1 foveal detachment type . . . 32
Case 5 Idiopathic macular hole: Stage 1 photoreceptor dehiscence type . . . 33
Case 6 Idiopathic macular hole: Stage 1 small foveal detachment type . . . 34
Case 7 Idiopathic macular hole: A case just before progression from stage 1 to stage 2 . . . 35
Case 8 Idiopathic macular hole: Typical example of stage 2 . . . 36
Case 9 Idiopathic macular hole: Postoperative course for macular hole closure under gas tamponade . . . 38
Case 9 DONFL appearance . . . 39
Case 10 Idiopathic macular hole: Postoperative course for macular hole closure . . . 40
Case 11 Idiopathic macular hole: Typical example of stage 3 . . . 41
After surgery . . . 42
Case 12 Idiopathic macular hole: Typical example of stage 4 . . . 43
Case 13 Idiopathic macular hole: Old case of stage 4 . . . 44
Stage 4 after surgery . . . 45
Case 14 Idiopathic macular holes: Progression from lamellar to full-thickness macular holes . . . 46
Case 15 Stage 1 macular hole: Spontaneous separation of perifoveal PVD . . . 47
Case 16 Stage 1 macular hole: Macular microhole formation . . . 48
Case 17 Stage 2 macular hole: Spontaneous closure . . . 49
Case 18 Stage 3 macular hole: Spontaneous closure . . . 50
Case 19 Stage 4 macular hole: Spontaneous closure . . . 51
Case 20 Traumatic macular hole: A typical example . . . 52
Case 21 Lamellar macular hole: a typical example . . . 54
Case 22 Lamellar macular hole: Differentiation from a MPH . . . 55
Macular microholes . . . 56
Case 23 Macular microhole: with macular PVD . . . 57
Case 24 Macular microhole: with complete PVD . . . 58
Case 25 Macular microhole: Case without PVD . . . 59

2.2 Idiopathic epiretinal membrane . . . 60
Case 26 Idiopathic epiretinal membrane: A typical example . . . 63
Case 27 Idiopathic epiretinal membrane: Exposure of the fibrocellular membrane . . . 64
Case 28 Idiopathic epiretinal membrane: Membrane with significant whitening . . . 65
Case 29 Idiopathic epiretinal membrane: Significant columnar structure formation . . . 66
Case 30 Idiopathic epiretinal membrane: Case ① where macular PVD has not been complete . . . 67
Case 31 Idiopathic epiretinal membrane: Case ② where macular PVD has been complete . . . 68
Case 32 Epiretinal membrane secondary to retinal hemangioma . . . 69
Case 33 Macular pseudohole: A typical example . . . 70
Case 34 Macular pseudohole: Case where macular PVD has not been complete . . . 71

2.3 Vitreomacular traction syndrome . . . 72
Case 35 Vitreomacular traction syndrome: Case showing disease development . . . 73
Case 35 Continuation . . . 74

Case 36 Vitreomacular traction syndrome: Case with macular detachment . . . 75
Case 37 Vitreomacular traction syndrome: A highly myopic eye with foveoschisis . . . 76

3 Diabetic retinopathy . . . 77
3.1 Diabetic retinopathy . . . 78

3.2 Diabetic macular edema . . . 79
Case 38 Diabetic macular edema: Early-stage case . . . 86
Case 39 Cystoid macular edema: Case with CME limited to layers anterior to the ELM . . . 87
Case 40 Cystoid macular edema: Case with CME extending to the outer retina . . . 88
Case 41 Cystoid macular edema: Exacerbation . . . 89
Case 42 Cystoid macular edema: Foveal detachment with recurrence . . . 90
Case 43 Cystoid macular edema: Subfoveal accumulation of hard exudates and the development of ischemic maculopathy . . . 91
Case 44 Cystoid macular edema: Subretinal leakage from a parafoveal cystoid space . . . 92
Continuation . . . 93
Case 45 Cystoid macular edema: Subfoveal leakage from a foveal cystoid space . . . 94
Case 46 Cystoid macular edema: Photoreceptor damage from outer plexiform layer edema . . . 95
Continuation . . . 96
Case 47 Cystoid macular edema: Microaneurysms . . . 97
Case 48 Ischemic maculopathy: Cystoid macular degeneration . . . 98
Case 49 Ischemic maculopathy: Thinned macula . . . 99
Case 50 Vitreomacular traction syndrome: A typical example . . . 100
Case 51 Proliferative diabetic retinopathy: Progressive proliferation . . . 101
Case 52 Proliferative diabetic retinopathy: Preretinal hemorrhages and vitreomacular traction syndrome . . . 102

4 Retinal vascular diseases . . . 103
4.1 Retinal vein occlusion . . . 104
Case 53 Central retinal vein occlusion: Progression from non-ischemic to ischemic ① . . . 108
Continuation . . . 109
Case 54 Central retinal vein occlusion: Progression from non-ischemic to ischemic ② . . . 110
Case 55 Central retinal vein occlusion: Ischemic type . . . 112
Case 56 Hemi-central retinal vein occlusion: Non-ischemic type . . . 113
Case 57 Branch retinal vein occlusion: Significant inner retinal layer ischemia . . . 114

4.2 Retinal artery occlusion . . . 115
Case 58 Central retinal artery occlusion: A typical example . . . 116
Case 59 Central retinal artery occlusion: Cilioretinal artery not occluded . . . 117
Case 60 Central retinal artery occlusion: Incomplete occlusion . . . 118
Case 61 Branch retinal artery occlusion: Case of good visual acuity . . . 119
Case 62 Branch retinal artery occlusion: Incomplete occlusion . . . 120

4.3 Idiopathic juxtafoveal macular telangiectasia . . . 121
Case 63 Macular telangiectasia: Yannuzzi classification Type 1 . . . 123
Case 64 Macular telangiectasia: Yannuzzi classification Type 1 . . . 124
Case 65 Macular telangiectasia: Yannuzzi classification Type 2 Stage 2 . . . 125
Case 66 Macular telangiectasia: Yannuzzi classification Type 2 Stage 3 . . . 126
Case 67 Macular telangiectasia: Yannuzzi classification Type 2 Stage 4 . . . 127
Case 68 Coats' disease: A typical example . . . 128

4.4 Retinal arterial macroaneurysm . . . 129
Case 69 Retinal arterial macroaneurysm: Subretinal hemorrhages . . . 130
Case 70 Retinal arterial macroaneurysm: Foveal detachment from an inferior arterial macroaneurysms . . . 132

5 Central serous chorioretinopathy . . . 133
5.1 Central serous chorioretinopathy . . . 134
Case 71 Acute central serous chorioretinopathy: Smoke-stack pattern . . . 139
Case 72 Acute central serous chorioretinopathy: A slowly leaking ink-blot pattern . . . 140
Case 73 Acute central serous chorioretinopathy: Intense leakage with ink-blot pattern . . . 141
Case 74 Chronic central serous chorioretinopathy: Choroidal thickening . . . 142

Case 75 Chronic central serous chorioretinopathy: A case of recurrence . . . 143
Continuation . . . 144
Case 76 Chronic central serous chorioretinopathy: Changes in the photoreceptor outer segment . . . 145
Case 77 Chronic central serous chorioretinopathy: Example of poor visual acuity . . . 146
Case 78 Acute bullous retinal detachment: A typical example . . . 147

6 Age-related macular degeneration . . . 149
6.1 Drusen . . . 153

6.2 Pigment epithelial detachment . . . 155
Case 79 Soft drusen: A typical example . . . 157
Case 80 Soft drusen: Confluent drusen . . . 158
Case 81 Cuticular drusen: Case with vitelliform detachment . . . 159
Case 82 Cuticular drusen: Fellow eye of case 81 . . . 160
Case 83 Reticular pseudodrusen: Fellow eye of RAP . . . 161
Case 84 Reticular pseudodrusen: Case with atrophic age-related macular degeneration (atrophic AMD) . . . 162
Case 85 Reticular pseudodrusen and soft drusen . . . 163
Case 86 Serous pigment epithelial detachment: Case without CNV . . . 164
Case 87 Pigment epithelial detachment: Reactive proliferation of retinal pigment epithelial cells . . . 165
Case 88 Drusenoid PED: Case where CNV is suspected . . . 166
17 months later . . . 167
Case 89 Large pigment epithelial detachment: Case where CNV is suspected . . . 168
Case 90 Pigment epithelial detachment: Case with type 1 CNV ① . . . 169
Case 91 Pigment epithelial detachment: Case with type 1 CNV ② . . . 170
Case 92 Large pigment epithelial detachment: Case where CNV is present . . . 171
Continuation . . . 172

6.3 Atrophic age-related macular degeneration . . . 173
Case 93 Atrophic age-related macular degeneration: A typical example . . . 176
Case 94 Atrophic age-related macular degeneration: Atrophic lesions of various sizes . . . 177
Case 95 Atrophic age-related macular degeneration: Fellow eye of PCV . . . 178

6.4 Choroidal neovascularization and exudative age-related macular degeneration . . . 179
Case 96 Exudative age-related macular degeneration: Type 1 CNV with a SRD . . . 181
Case 97 Exudative age-related macular degeneration: Type 1 CNV with low activity . . . 182
Case 98 Exudative age-related macular degeneration: Type 1 CNV with relatively strong exudative changes . . . 183
Six months later . . . 184
Case 99 Exudative age-related macular degeneration: Case with extensive Type 1 and 2 CNV exudative changes . . . 185
Six months after treatment with anti-VEGF treatment . . . 186
Case 100 Exudative age-related macular degeneration: Type 1 and 2 CNV with extensive serous retinal detachment . . . 187
Case 101 Exudative age-related macular degeneration: Type 1 and 2 CNV with cystic changes . . . 188
Case 102 Exudative age-related macular degeneration: Type 2 CNV localized in the fovea centralis . . . 189
Case 103 Exudative age-related macular degeneration: Type 2 CNV with strong exudative changes . . . 190

6.5 Polypoidal choroidal vasculopathy . . . 191
Case 104 Polypoidal choroidal vasculopathy: Small lesions . . . 194
Case 105 Polypoidal choroidal vasculopathy: Case confused with central serous chorioretinopathy . . . 195
After treatment with anti-VEGF treatment . . . 196
Case 106 Polypoidal choroidal vasculopathy: Fibrin deposits ① . . . 197
Case 107 Polypoidal choroidal vasculopathy: Fibrin deposits ② . . . 198
Case 108 Polypoidal choroidal vasculopathy: A large branching vascular network . . . 199
Case 109 Polypoidal choroidal vasculopathy: Large foveal cystoid space . . . 200
Enlargement of hemorrhagic pigment epithelial detachment . . . 201
Enlargement of the abnormal vascular network . . . 202
Case 110 Polypoidal choroidal vasculopathy: A large hemorrhagic pigment epithelial detachment ① . . . 203
Case 111 Polypoidal choroidal vasculopathy: A large hemorrhagic pigment epithelial detachment ② . . . 204
Spontaneous remission . . . 205

Case 112 Polypoidal choroidal vasculopathy: Optic disc type . . . 206
Continuation . . . 207
Case 113 Polypoidal choroidal vasculopathy: Polypoidal lesions and pigment epithelial detachment . . . 208
Case 114 Polypoidal choroidal vasculopathy: Tomographic notch sign . . . 209
Case 115 Polypoidal choroidal vasculopathy: Case where the branching vascular network has detached . . . 210
Case 116 Polypoidal choroidal vasculopathy: A massive lesion . . . 211

6.6 Retinal angiomatous proliferation . . . 212
Case 117 Retinal angiomatous proliferation: Stage 1 . . . 214
Case 118 Retinal angiomatous proliferation: Stage 2A . . . 215
Case 119 Retinal angiomatous proliferation: Stage 2B ① . . . 216
Case 120 Retinal angiomatous proliferation: Stage 2B ② . . . 217
Case 121 Retinal angiomatous proliferation: Stage 3 . . . 218
After treatment with anti-VEGF treatment . . . 219

6.7 Malattia leventinese . . . 220
Case 122 Malattia leventinese: A typical example . . . 221
6.8 Idiopathic choroidal neovascularization . . . 223
Case 123 Idiopathic choroidal neovascularization: A fresh case . . . 224
Case 124 Idiopathic choroidal neovascularization: Envelopment by RPE cells . . . 225
After treatment with anti-VEGF treatment . . . 226
Case 125 Idiopathic choroidal neovascularization: The scarring process . . . 227
Course without treatment . . . 228

7 Retinal degeneration . . . 229
7.1 Multiple evanescent white dot syndrome . . . 232
Case 126 Multiple evanescent white dot syndrome: A typical example . . . 233
Continuation . . . 234

7.2 Acute zonal occult outer retinopathy . . . 235
Case 127 Acute zonal occult outer retinopathy: Eye with a history of MEWDS . . . 236

7.3 Punctate inner choroidopathy . . . 238
Case 128 Punctate inner choroidopathy: Atrophic pigmented scars . . . 239
Case 129 Punctate inner choroidopathy: Case complicated by CNV (fellow eye of case 128) . . . 240
Case 130 Punctate inner choroidopathy: Yellowish-white spots and CNV . . . 241

7.4 X-linked juvenile retinoschisis . . . 242
Case 131 X-linked juvenile retinoschisis: Retinoschisis over a wide area . . . 243
Continuation . . . 244
Case 132 X-Linked juvenile retinoschisis: Retinoschisis confined to the macula . . . 245

7.5 Stargardt disease . . . 246
Case 133 Stargardt disease: A typical example . . . 247
Continuation . . . 248

7.6 Vitelliform macular dystrophy and adult-onset foveomacular vitelliform dystrophy . . . 249
Case 134 Adult-onset foveomacular vitelliform dystrophy: Vitelliform stage . . . 251
Case 135 Adult-onset foveomacular vitelliform dystrophy: Pseudohypopyon stage . . . 252
Case 136 Adult-onset foveomacular vitelliform dystrophy: The course . . . 253

7.7 Pseudoxanthoma elasticum . . . 254
Case 137 Pseudoxanthoma elasticum: A case of Type 1 CNV . . . 255
Case 138 Pseudoxanthoma elasticum: A case of Type 2 CNV . . . 256
Case 139 Pseudoxanthoma elasticum: A case of polypoidal lesions . . . 257
Case 140 Pseudoxanthoma elasticum: Outer retinal tubulation . . . 258

7.8 Cancer-associated retinopathy . . . 259
Case 141 Cancer-associated retinopathy: Damage to the outer retinal layers . . . 260
Case 142 Cancer-associated retinopathy: Retinal vasculitis . . . 261

7.9 Bietti crystalline dystrophy . . . 262
Case 143 Bietti crystalline dystrophy: A typical example . . . 263
Case 144 Bietti crystalline dystrophy: Outer retinal tubulation . . . 264

7.10 Retinitis pigmentosa . . . 265
Case 145 Retinitis pigmentosa: A typical example . . . 267
Continuation . . . 268
Case 146 Retinitis pigmentosa: Cystoid macular edema . . . 269
Case 147 Retinitis pigmentosa: Vitreomacular traction syndrome . . . 270

7.11 Fundus albipunctatus . . . 271
Case 148 Fundus albipunctatus: A typical example . . . 272

7.12 Oguchi disease . . . 274
Case 149 Oguchi disease: A typical example . . . 275
Case 150 Oguchi disease: Cystoid space formation and golden sheen fundus reflex (fellow eye of case 149) . . . 276

8 Uveitis . . . 277
8.1 Behçet disease . . . 278
Case 151 Behçet disease: Cystoid edema and foveal detachment . . . 279
Case 152 Behçet disease: Retinal atrophy . . . 280
Case 153 Behçet disease: Acute attack . . . 281

8.2 Sarcoidosis . . . 282
Case 154 Sarcoidosis: Cystoid macular edema . . . 283
Case 155 Sarcoidosis: Foveal detachment . . . 284

8.3 Vogt-Koyanagi-Harada disease . . . 285
Case 156 Vogt-Koyanagi-Harada disease: Large foveal cystoid space . . . 287
Continuation . . . 288
Case 157 Vogt-Koyanagi-Harada disease: Prominent choroidal thickening . . . 289
Continuation . . . 290
Case 158 Vogt-Koyanagi-Harada disease: Reattachment process . . . 291
Continuation . . . 292
Case 159 Vogt-Koyanagi-Harada disease: Choroidal folds . . . 293
Continuation . . . 294

8.4 Sympathetic ophthalmia . . . 295
Case 160 Sympathetic ophthalmia: After vitreous surgery . . . 296

8.5 Toxocariasis . . . 297
Case 161 Toxocariasis: Proliferative membrane . . . 298

8.6 Acute retinal necrosis (Kirisawa-type uveitis) . . . 299
Case 162 Acute retinal necrosis (Kirisawa-type uveitis): A typical example . . . 300

9 Pathologic myopia and related diseases . . . 303
9.1 Myopia . . . 304
Case 163 Intrachoroidal cavitation: A Typical example . . . 308
Case 164 Intrachoroidal cavitation: Connection with the vitreous cavity . . . 309
Case 165 Lacquer cracks: A typical example . . . 310
Case 166 Lacquer cracks: A mild case . . . 311
Case 167 ILM detachment: Case without foveoschisis . . . 312
Case 168 Myopic foveoschisis: Case without foveal detachment . . . 313
Case 169 Myopic foveoschisis: Case with foveal detachment . . . 314
One year after surgery . . . 315
Case 170 Myopic foveoschisis: Case with macular retinal detachment . . . 316
Two and a half years after surgery . . . 317
Case 171 Myopic foveoschisis: Traction from the thickened posterior vitreous cortex . . . 318
Case 172 Myopic foveoschisis: Macular hole formation . . . 319
Case 173 Myopic foveoschisis: MHRD . . . 320

Case 174 Myopic foveoschisis: Before and after surgery for MHRD . . . 321
Case 175 Myopic subretinal hemorrhages: A typical example . . . 322
Four months later . . . 323
Case 176 Myopic choroidal neovascularization: A typical example . . . 324
Case 177 Myopic choroidal neovascularization: Small CNV . . . 325
After anti-VEGF treatment . . . 326
Case 178 Myopic choroidal neovascularization: Large CNV . . . 327
Case 179 Myopic choroidal neovascularization: A young example . . . 328
One year after anti-VEGF treatment . . . 329
Case 180 Myopic choroidal neovascularization: Foveoschisis . . . 330

9.2 Dome-shaped macula and inferior staphyloma . . . 331
Case 181 Dome-shaped macula: A typical example . . . 332
Case 182 Inferior staphyloma: Serous retinal detachment . . . 333
Continuation . . . 334

10 Retinal detachment . . . 335
10.1 Rhegmatogenous retinal detachment . . . 336
Case 183 Rhegmatogenous retinal detachment: A case where retinal detachment has stopped at the fovea centralis . . . 337
Case 184 Rhegmatogenous retinal detachment: Macular detachment . . . 338
Case 185 Rhegmatogenous retinal detachment: Foveal inner segment defects . . . 339
Case 186 Optic disc pit maculopathy . . . 340

11 Lesion morphology index based on OCT . . . 341

Service Part . . . 347
Subject Index . . . 348
Case Index . . . 350

List of Abbreviations

AI	indocyanine green angiography
AMD	age-related macular degeneration
BRAO	branch retinal artery occlusion
CME	cystoid macular edema
CNS	central nervous system
CNV	choroidal neovascularization
COST	cone outer segment tip
CRAO	central retinal artery occlusion
CRV	central retinal vein
CRVO	central retinal vein occlusion (non-ischemic/ischemic) hemi-CRVO (HCRVO) from major branch RVO (BRVO)
CSC	central serous chorioretinopathy
EDI	enhanced depth imaging
EDI-OCT	enhanced depth imaging optical coherence tomography
ELM	external limiting membrane
ERM	epiretinal membrane
FA	fluorescein angiography
FAF	fundus autofluorescence
GCL	ganglion cell layer IPL = inner plexiform layer
ICC	intrachoroidal cavitation
IJRT	idiopathic juxtafoveolar retinal telangiectasia
IMT	idiopathic macular telangiectasia,
INL	inner nuclear layer
IS/OS	photoreceptor inner segment/outer segment junction
MA	microaneurysm
MHRD	macular hole retinal detachment
MP-1	microperimeter
MPPE	multifocal posterior pigment epitheliopathy
OCT	Optical Coherence Tomography
ONL	outer nuclear layer
OPL	outer plexiform layer
PCV	polypoidal choroidal vasculopat
PDT	photodynamic therapy
PED	pigment epithelial detachment
PVD	posterior vitreous detachment
RAO	retinal artery occlusion
RAP	retinal angiomatous proliferation
RNFL	retinal nerve fiber layer
RPE	retinal pigment epithelium
RRD	rhegmatogenous retinal detachment
RVO	retinal vein occlusion
SD-OCT	spectral-domain optical coherence tomography
SRD	serous retinal detachment
SRN	subretinal neovascularization
VKH	Vogt-Koyanagi-Harada disease
VMD	Vitelliform macular dystrophy

The basis of OCT interpretation

1.1 B-scan interpretation – 2
1.1.1 Factors that determine resolving power – 2
1.1.2 Removing speckle noise by multiple B-scan averaging – 3

1.2 Normal retina – 4

1.3 Normal choroidal imaging – 9

1.4 Displaying B-scans – 10

1.5 Depth resolution misinterpretations – 11

1.6 Artifacts – 13
1.6.1 The effect of involuntary eye movement – 13
1.6.2 Phenomena caused by the optical properties of tissue – 14
1.6.3 Aspects relating to measurement principles – 16
1.6.4 Sensitivity attenuation – 16

References – 19

1

1.1 B-scan interpretation

1.1.1 Factors that determine resolving power

OCT depth resolution

OCT depth resolution is determined by the wavelength band of the light source (centre wavelength and wavelength range), and is unrelated to OCT detection technologies, such as time-domain and spectral-domain (SD). Namely, OCT depth resolution (ΔZ) can be shown with the following mathematical formula:

$$\Delta Z = 0.44 \times \lambda^2/\Delta\lambda$$

(where λ is centre wavelength and Δλ is wavelength range)

According to this formula, the use of an 840 nm centre wavelength and a 40 nm wavelength range will produce depth resolution of 7.76 μm.

Most current spectral-domain OCT (SD-OCT) products use spectral ranges of 30–50 nm and centre wavelengths of 840–870 nm using superluminescent diode (SLD) light sources. This results in depth resolutions of 5–7 μm (Fig. 1-1). One exception includes the SPOCT-HR manufactured by OPTOPOL. This product uses 2 types of SLD light sources with an 85 nm spectral range in sum resulting in a high depth resolution of 3 μm (term ultrahigh resolution).

Speckle noise

In addition to depth resolution, speckle noise has an effect on the resolving power of B-scans[1]. As shown in Fig. 1-2, when B-scan images are enlarged, a low-reflective speckle pattern can be seen, known as speckle noise[2]. Speckle noise occurs when an object is scanned with coherent light, and is the most common cause of blurring to retinal layer boundaries on OCT B-scan images[1,3,4]. High speed image acquisition of SD-OCT allows effective reduction of speckle noise, which generates high resolution B-scan images.

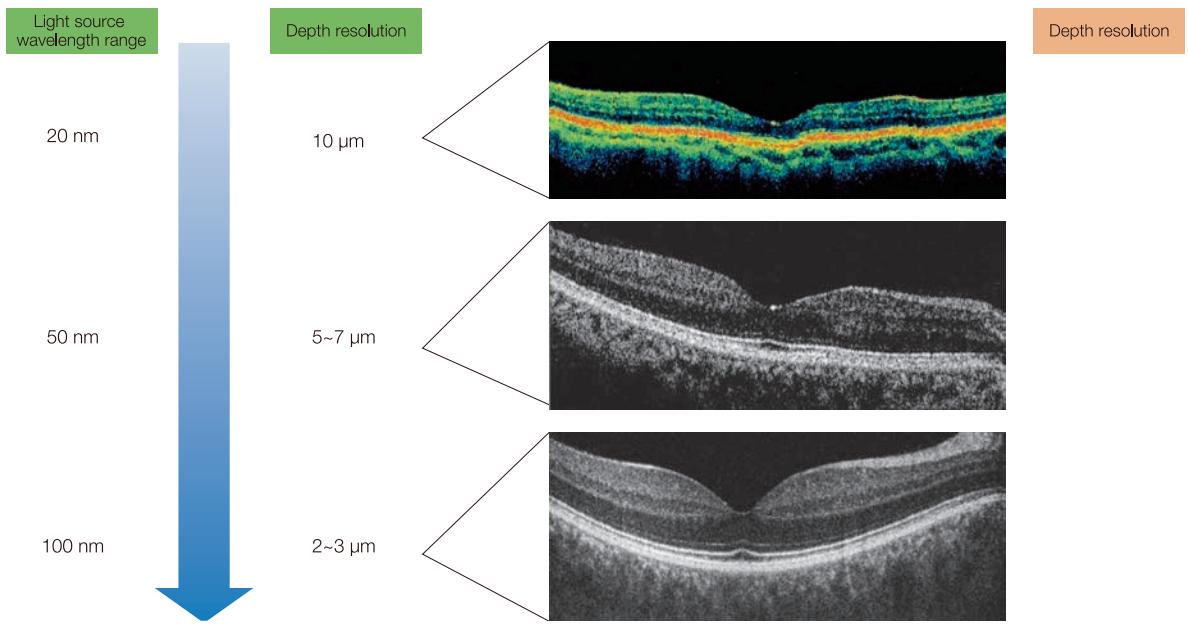

Fig. 1-1 Depth resolution and light source wavelength range
The light source wavelength range and corresponding depth resolution of commercially available OCT

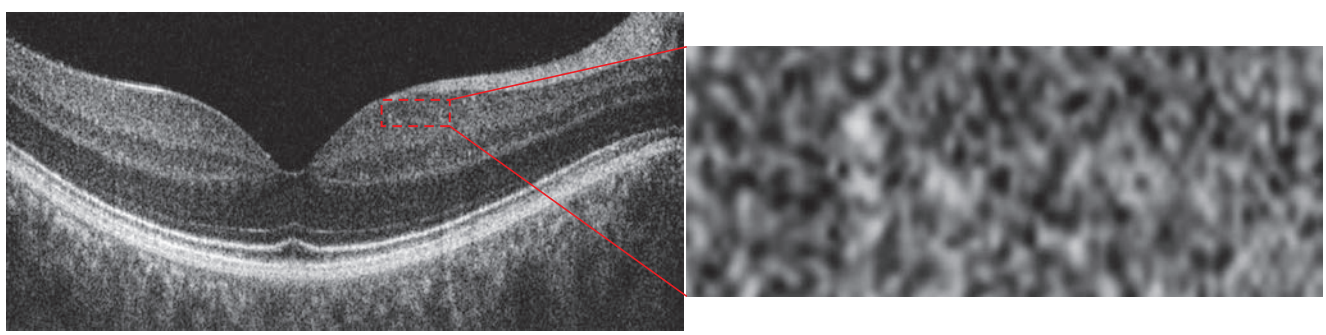

Fig. 1-2 Speckle noise
Scanning with coherent light in OCT imaging produces weakly reflective speckle pattern known as speckle noise. Speckle noise becomes apparently visible when the B-scan is enlarged.

1.1.2 Removing speckle noise by multiple B-scan averaging

Multiple B-scan averaging

Multiple B-scan averaging means performing multiple scans of the identical retinal location of interest, aligning and adding the image signals, and finally dividing by the number of scans (Fig. 1-3). Whereas the actual image is stationary, speckle noise is diluted by the reciprocal of the total number of scans since speckle noise pattern changes with every B-scan The accuracy of multiple B-scan averaging depends on the ability to take multiple scans of the exactly identical location of interest without blurring. To perform multiple B-scan averaging with high accuracy, it is important to have high-speed scanning capabilities and eye tracking. By successfully averaging an adequate number of scans, speckle noise can be sufficiently removed and retinal layer boundaries become distinct (Fig. 1-4).

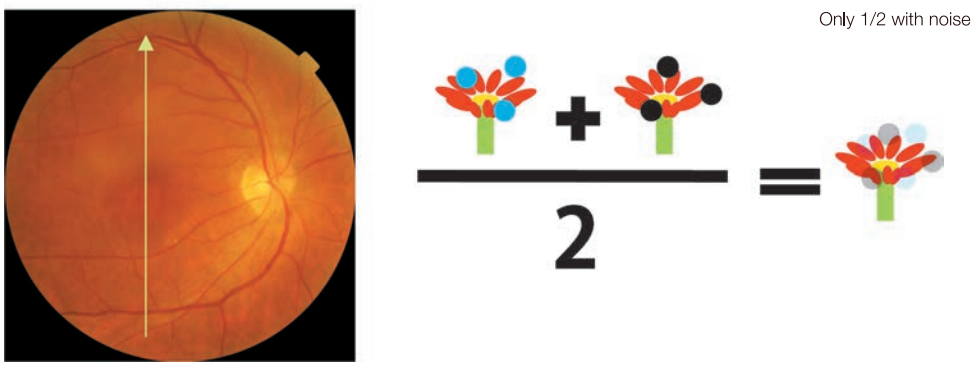

Fig. 1-3 The principle of multiple B-scan averaging

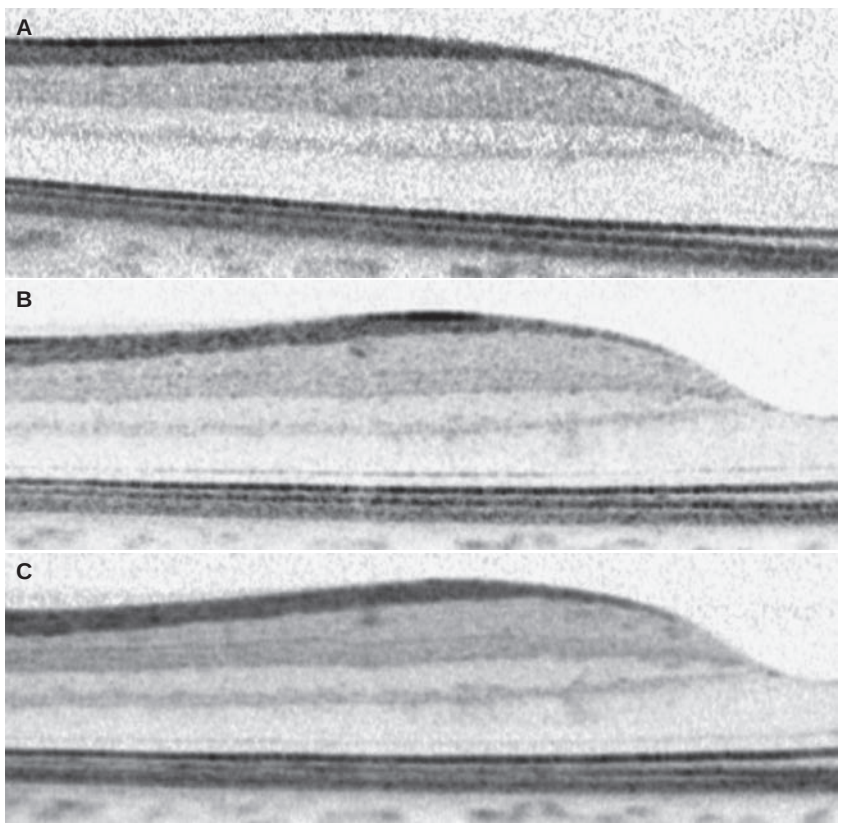

Fig. 1-4 Results of multiple B-scan averaging.
A: After 1 B-scan, **B:** after averaging 10 B-scans, **C:** after averaging 100 B-scans.
The retinal layer structures becomes more distinct with increasing number of averaged B-scans.

1

1.2 Normal retina

OCT creates an image of the intensity of light reflection and scattering in chorioretinal tissue. The »fiber layers« and »layer boundaries«, which strongly reflect light, are highly reflective, and the »cellular layers«, which weakly reflects light, are weakly reflective (Fig 1-5). In sum, there are 3 principles to retinal OCT imaging:

- Cellular layer = weakly reflective,
- Fibrous layer = highly reflective,
- Boundaries = highly reflective.

Cellular layer

The ganglion cell layer, inner nuclear layer and outer nuclear layer that are mainly comprised of neuronal cell bodies are weakly reflective. The actual outer nuclear layer is thinner than it appears, since Henle fiber layer (HFL), histologically fiber layer of the outer plexiform layer, is included in the low-reflectivity phase typically thought to be the outer nuclear layer.

Fiber layer

The nerve fibers of the retinal nerve fiber layer and the inner plexiform layer run parallel to the retinal surface. The OCT measurement beam enters almost perpendicular to this path, resulting in intense reflectivity and scattering to make it a highly reflective layer. The outer plexiform layer, however, is an exception. Since the nerve fibers of HFL tilt forward and towards the periphery of the macula[5] (Fig. 1-6), the measurement beam enters at a significant angle to the fibers' orientation. Thus, HFL becomes weakly reflective and becomes indistinguishable from the similarly weakly reflective outer nuclear layer (Fig. 1-7). However, when OCT measurement beam enters the pupil from an eccentric position, the beam obliquely reaches the retinal surface, and consequently passes the retina perpendicular to the HFL on one side (Fig. 1-6). This increases the reflectivity of HFL causing it to be a highly reflective layer.[6,7] (Fig. 1-7). This is similar to when the retinal layer tilts as a result of retinal detachment or drusen (Fig. 1-8).

The axonal endings of the synapse phase of the outer plexiform layer combine with tight junctions to form a sheet-like structure acting as the boundary surface with high reflectivity.

Boundary surface

Since photoreceptor cells orderly align themselves parallel to OCT probe light, the external limiting membrane (ELM), the photoreceptor inner segment/outer segment junction, and cone outer segment tip (COST) form the boundary surface, and can be seen as 3 highly reflective lines. Since the retinal pigment epithelium (RPE) is also an aligned unicellular layer, its apex and base each form a boundary and are visible as 2 highly reflective lines on ultrahigh resolution OCT.

Why is the RPE highly reflective even though it is made up of cells?

The reflectivity of the RPE is thought to be due to melanin pigment. However, the RPE can be seen as 2 distinct lines in 3 µm

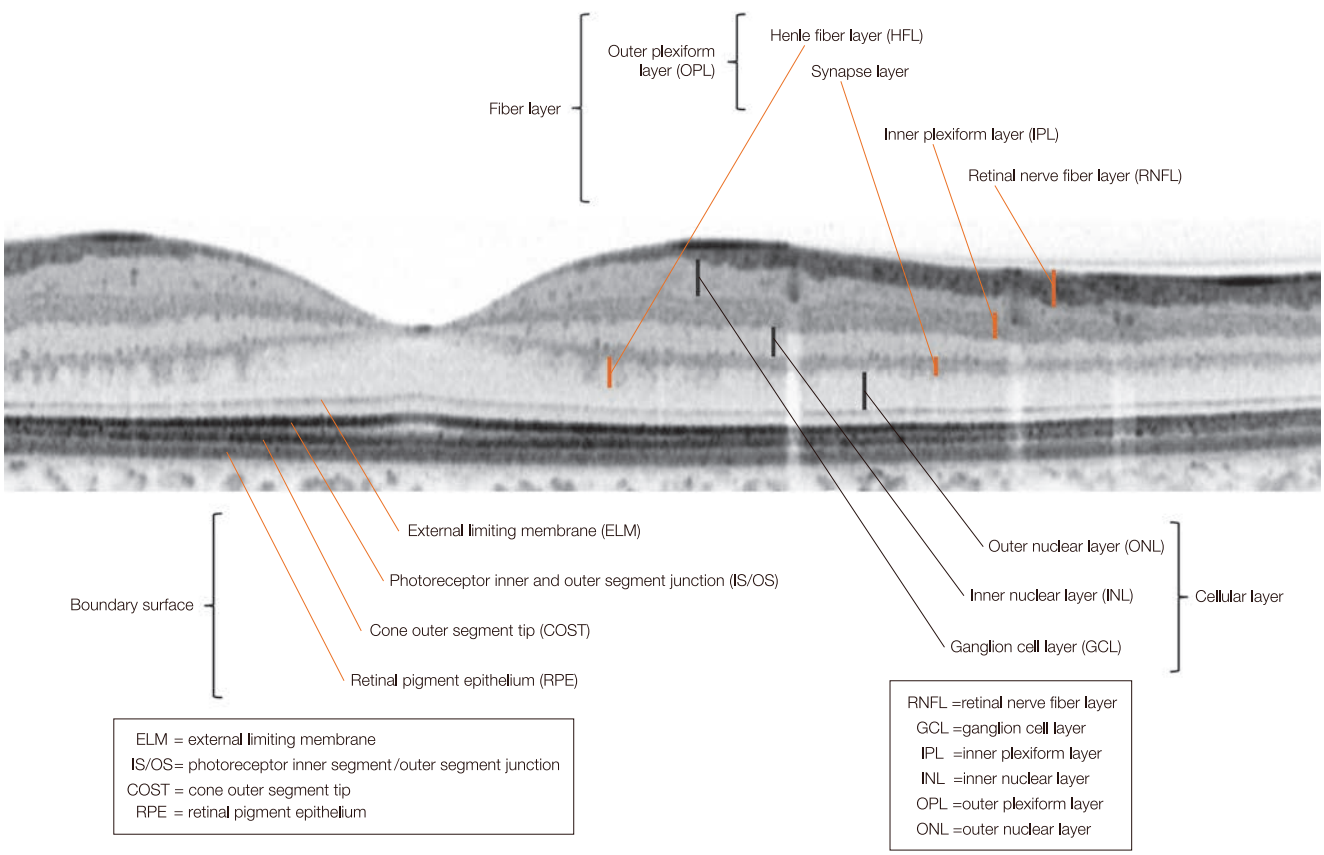

Fig. 1-5 Normal retina (speckle noise free)

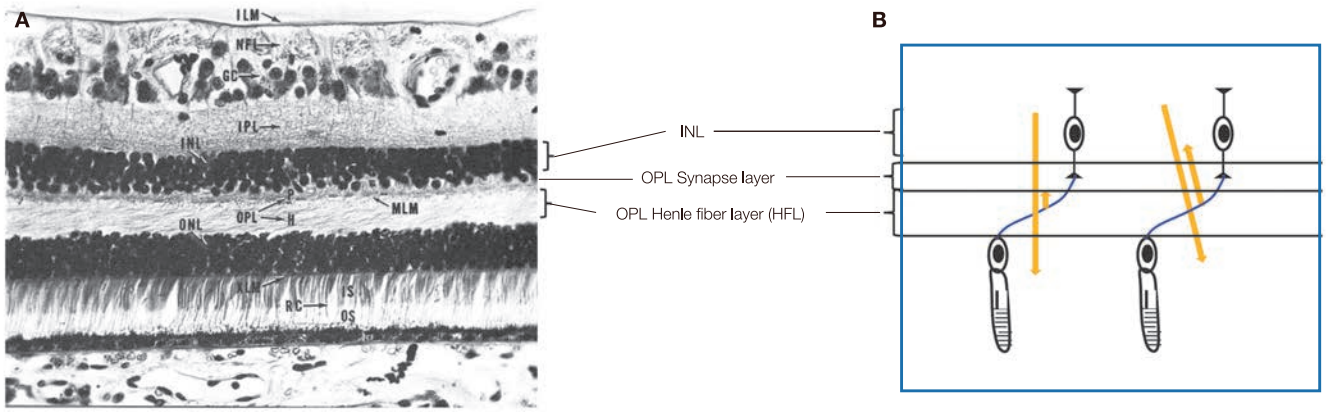

Fig. 1-6 The path of HFL
A: Light microscopic image of normal retina, **B:** diagram of the relationship between HFL and measurement beam (orange arrows). Reflectivity is enhanced when the retina is tilted and the measurement beam enters the HFL perpendicularly.
(A was modified according to Fine B, Yanoff M. Ocular Histology, 2nd ed. Harper&Row, 1979, p 57)

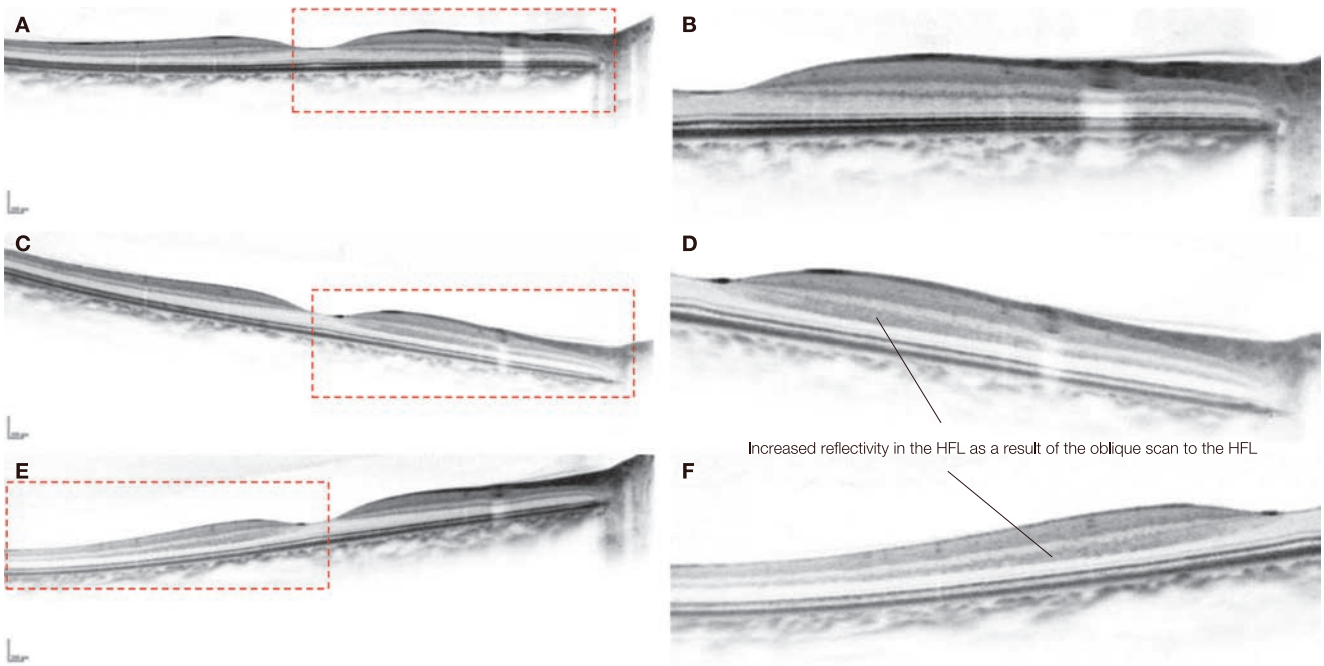

Fig. 1-7 The appearance of HFL in the normal retina
A, B: When the OCT measurement beam passes through the centre of the pupil, the HFL is obscured since there is no tilt in the retinal image. **C–F:** When the OCT measurement beam passes through the temporal side (**C, D**) and nasal side (E, F) of the pupil, the nasal retina and temporal retina each tilt backward respectively, and exhibit increased reflectivity in the HFL.

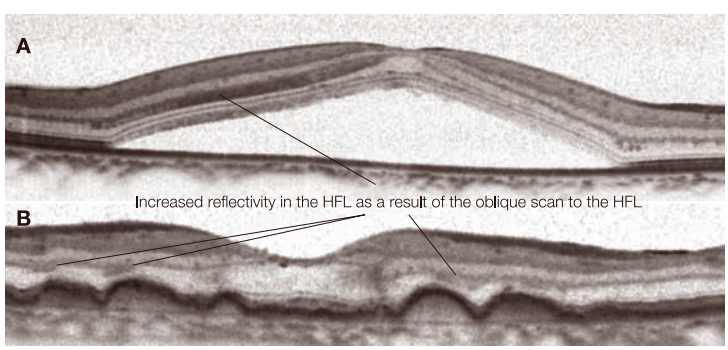

Fig. 1-8 The appearance of HFL in eyes with macular diseases
A: Serous retinal detachment (SRD) in central serous chorioretinopathy (CSCR). B: Drusen in retinal angiomatous proliferation (RAP). There are areas where HFL becomes highly reflective and thereby visible due to retinal tilt against the OCT measurement beam as a result of lesions.

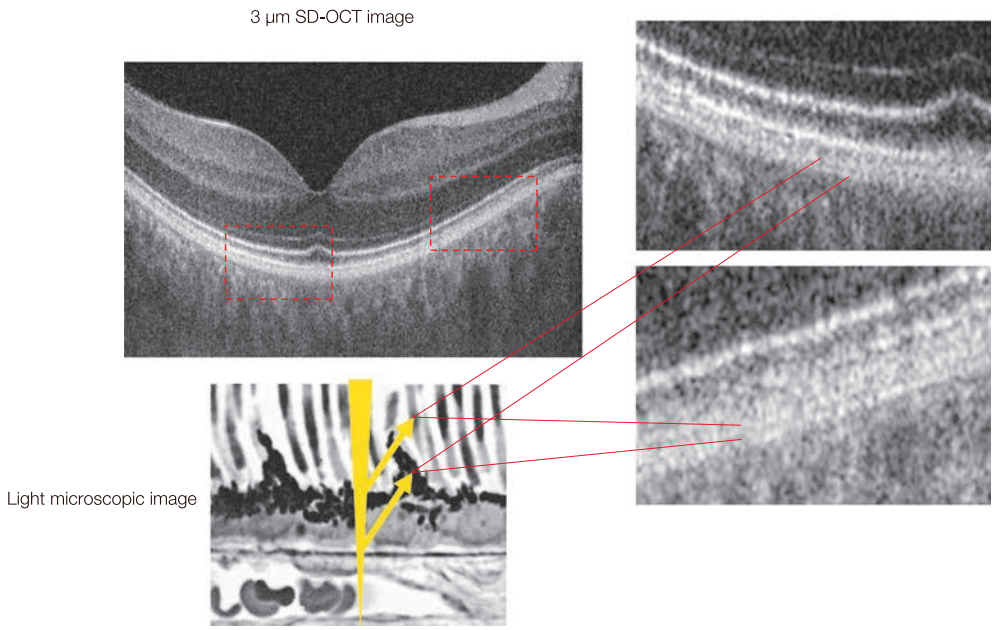

Fig. 1-9 A comparison of light microscopic and tomographic views of the retinal pigment epithelium (RPE). The RPE is seen as 2 highly reflective lines on 3 μm SD-OCT. The highly reflective RPE line is comprised of 2 highly reflective lines representing apical and basal (including Bruch's membrane) membranes and hyporeflective line between these 2 lines representing cytoplasm. These 2 lines can be distinguished in 3 μm SD-OCT, but not on standard resolution (5~7 μm) SD-OCT.
(Modified according to Fine B, Yanoff M. Ocular Histology, 2nd ed. Harper&Row, 1979, p67)

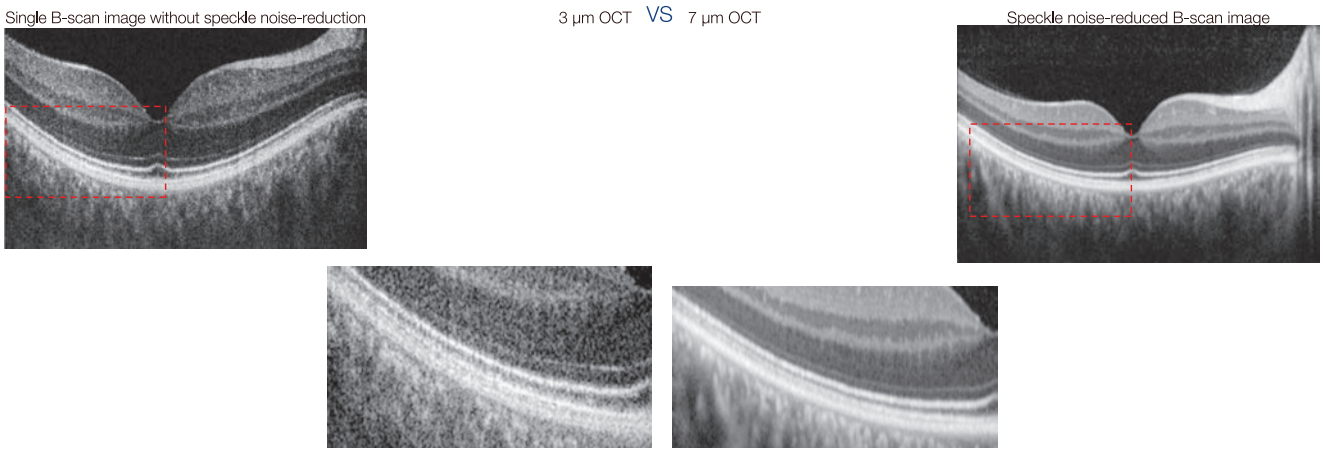

Fig. 1-10 RPE line, resolution, and speckle noise
The aggregation of RPE high reflectivity – low reflectivity – high reflectivity can be observed in 3 μm single scan SD-OCT image. However, in 7 μm OCT, only one bold highly reflective line can be seen even when speckle noise is removed.

ultrahigh resolution OCT (manufactured by Canon) (Fig. 1-9) (1). Using 5–7 μm depth resolution, only 1 aggregate line is seen even when speckle noise is removed (Fig. 1-10). The 2 highly reflective lines that can be seen in OCT with a depth resolution of 3 μm correspond to the 2 boundary surfaces that are the apex and base of the RPE, which become 2 distinct, highly reflective lines due to the low reflectivity of the cells between them. Normally, the base is consistent with the lines of Bruch's membrane. However, when an RPE detachment occurs, Bruch's membrane can be distinguished at an SD-OCT depth resolution of just 5–7 μm.

What is the natural shape of the third line?

During SD-OCT examination, one further highly reflective line can be seen between the so-called photoreceptor inner segment/outer segment junction (IS/OS) lines and the RPE. This is the third line following the ELM lines and IS/OS line, so it is referred to as the third line. It is debated as to what this line corresponds to, but when observed in ultrahigh resolution (3 μm) SD-OCT, it is thought to be the cone outer segment tip (COST) in the macular area (Fig. 1-11)[1,8]. Outside the macular area, yet another highly reflective line has been observed, thought to be the rod outer segment tip (ROST), between the IS/OS and the RPE. The COST line disappears due to milder photoreceptor cell abnormalities than the IS/OS and ELM lines.

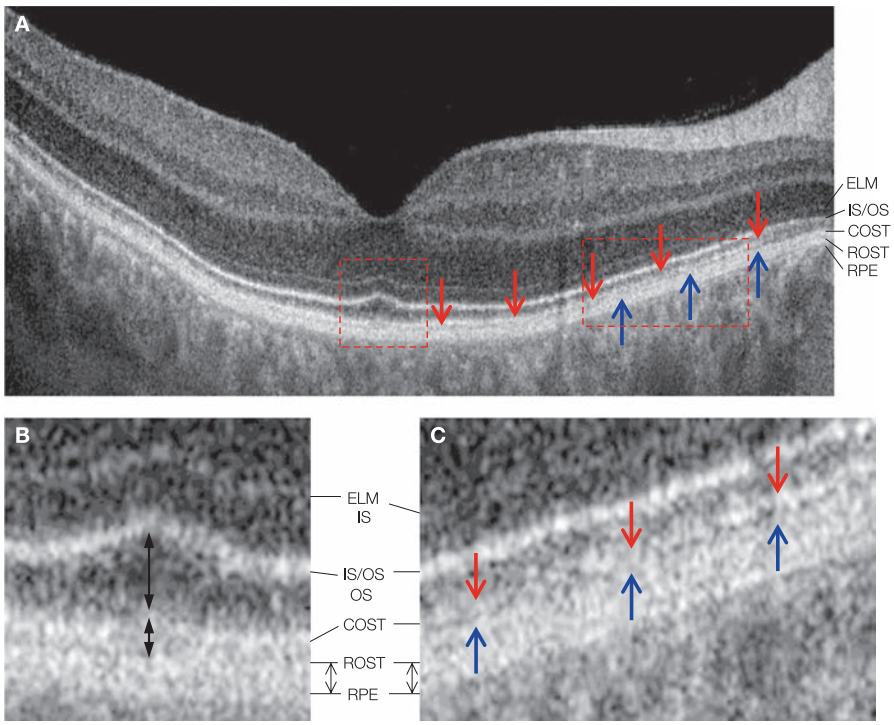

Fig. 1-11 COST and ROST in SD-OCT with a depth resolution of 3 μm
A: Horizontal B-scan. COST is observed from the fovea centralis to the outside of the macula (→), whereas ROST is observed from the periphery of the macula to the outside of the macula (→). **B**: The enlarged image of **A** representing fovea centralis. The fovea centralis OS is long and the IS/OS looks mountain-shaped, but the COST always appears to run parallel to the vicinity of the RPE, suggesting this is the cone sheath, which is enveloped by the apical processes of the retinal pigment epithelium. **C**: Periphery of the macula – outside of the macula enlarged image of A. Another line (→) was observed between the COST line (→) and the RPE apical line. This is the ROST.

The mystery of photoreceptor cell inner and outer segment junction line

The anatomical structure of the highly reflective lines that correspond to the photoreceptor inner and outer segment junction is the subject of debate.

In recent years, Drexler et al. have been able to observe individual photoreceptor cells through adaptive-optics (AO) ultra-high-resolution (UHR) SD-OCT[9] (Fig. 1-12). This AO-OCT system allows correction of chromatic and monochromatic ocular aberrations, and has enhanced lateral as well as depth resolution to micron levels (2–3 μm). Since photoreceptor cells can be distinguished in the AO UHR SD-OCT imaging, the ELM and IS/OS become dotted lines. In this imaging, ellipsoids where the mitochondria accumulates have a high reflectivity, and are thought to constitute the IS/OS line. In this OCT, we see highly reflective bands in 2 locations, immediately in front of the fovea centralis and the RPE (Fig. 1-12). Anatomically, the OS of cone photoreceptor cells terminate before reaching the RPE and are enveloped by the RPE apical processes. The outer line of these 2 high reflectivity bands is thought to be due to the COST. Independently, Spaide et al. reviewed the literature of retinal histology starting from 1990 and created a scale model of photoreceptor cells. When compared with B-scan images from Spectralis HRA + OCT the IS/OS line correspond to the ellipsoid portion of the IS and the COST line corresponds to the termination of the OS enveloped by RPE apical processes (cone sheath or contact cylinder)[10].

Symmetry of the normal retinal layer structure

Within the neural retinal layer structure, the retinal nerve fiber layer (RNFL) is symmetrical between upper and lower hemisphere. However, there is no symmetry of the RNFL nasally and temporally to the fovea centralis. In contrast, the other layers outside the RNFL (ganglion cell layer, inner plexiform layer, inner nuclear layer, outer plexiform layer, and outer nuclear layer) are symmetrical nasally and temporally to the fovea centralis in addition to having upper and lower symmetry, that is, 2-dimensionally symmetry centered at the fovea centralis.[11,12] (Fig. 1-13, 1-14).

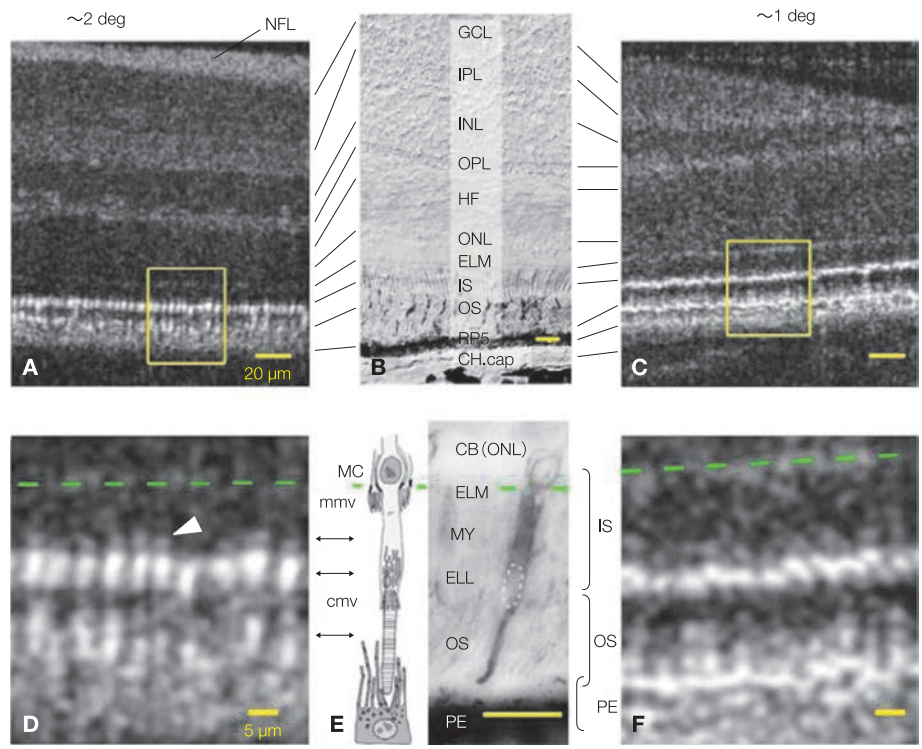

Fig. 1-12 Photoreceptor cell images on adaptive-optics ultrahigh-resolution SD-OCT
Photoreceptor cells run parallel to the optical axis and are arranged like rice plant. The highly reflective planes of the photoreceptor cells form the IS/OS lines and COST line. In AO UHR-SD-OCT, these lines appear as dotted lines, but in standard resolution SD-OCT, they appear as contiguous lines.
(Modified according to Fernández EJ, et al. Ultrahigh resolution optical coherence tomography and pancorrection for cellular imaging of the living human retina. Opt Express. 2008; 16: 11083-11094)

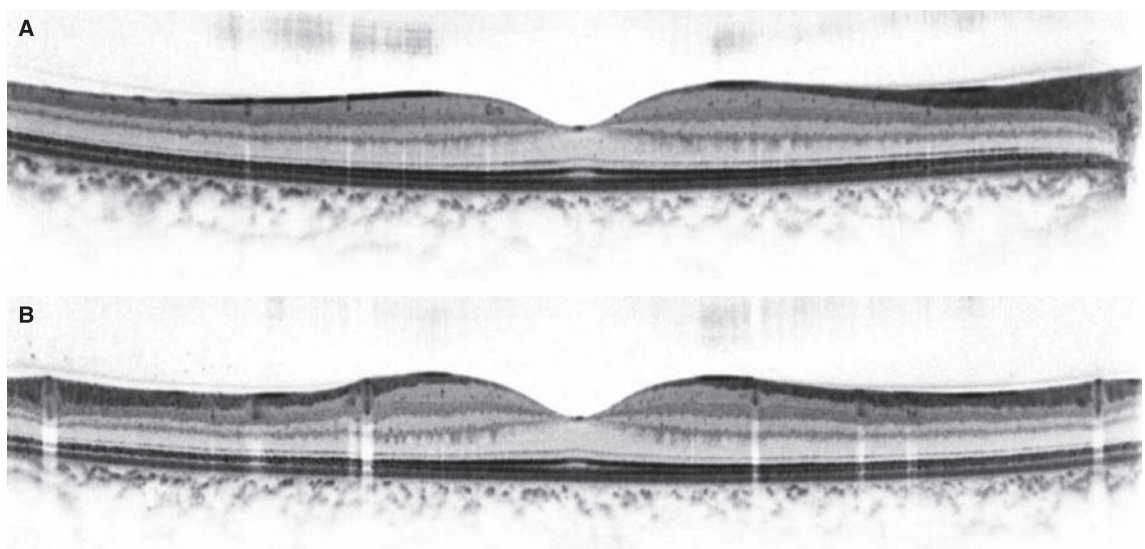

Fig. 1-13 B-scans in a normal eye
A: OCT horizontal scan. The RNFL gets thicker nasally and thinner temporally. Apart from the RNFL, all other layers are symmetrical. **B:** OCT vertical scan. All layers have vertical symmetry. The RNFL is thicker at the periphery, the outer nuclear layer is thicker at the fovea centralis, and the ganglion cell layer forms a peak outside the fovea.

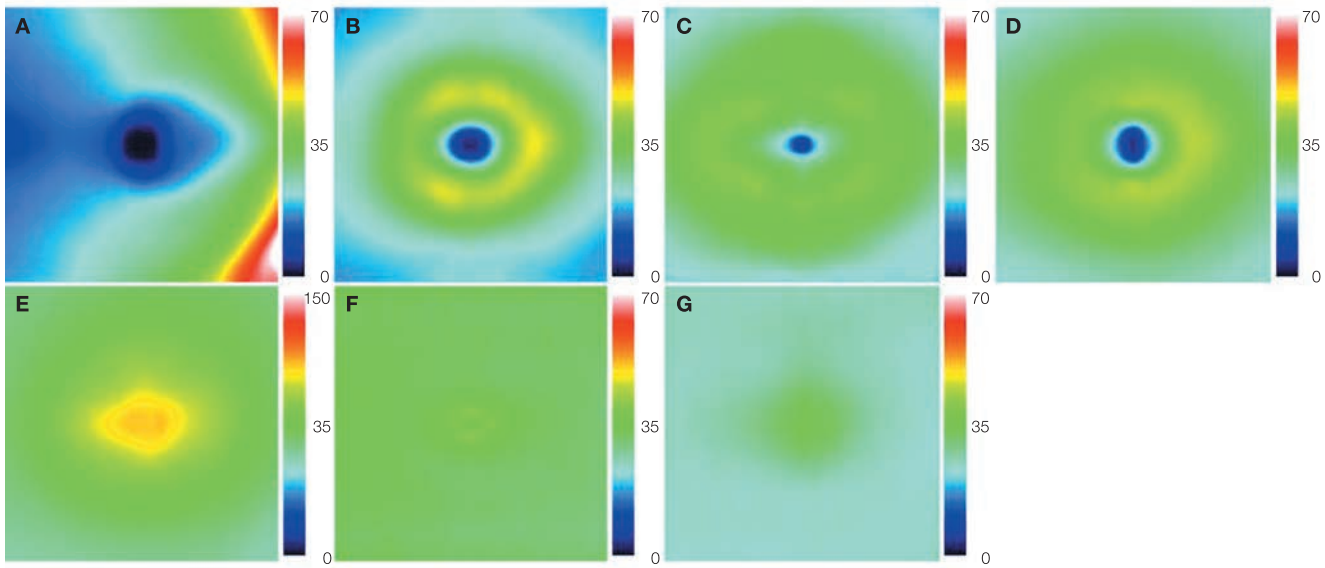

Fig. 1-14 Retinal layer thickness colour map
A: Retinal nerve fiber layer, **B:** ganglion cell layer, **C:** inner plexiform layer, **D:** inner nuclear layer, **E:** outer plexiform layer + outer nuclear layer, **F:** photoreceptor inner segment, **G:** photoreceptor outer segment. Each retinal layer has high symmetry, but the ganglion cell layer and inner nuclear layer are slightly thinner temporally.
(Modified according to Ooto S, et al. Effects of age, gender, and axial length on the three-dimensional profile of normal macular layer structures. Invest Ophthalmol Vis Sci. 2011; 52: 8769-8779)

1.3 Normal choroidal imaging

EDI-OCT

SD-OCT has a coherence gate (depth at which the interference image can be obtained) of about 2 mm. An interference signal can be obtained when the retinal tissue examined enters this coherence gate, but the signal intensity attenuates in the depth direction (see Fig. 1-35 ▶ page 18). Consequently, to obtain high-quality images in SD-OCT, it is important to bring the retinal tissue to the upper imaging range. In contrast, EDI-OCT creates an inverted mirror image as shown in Fig. 1-15. Usually, to avoid signal attenuation in the depth direction and to increase the visualization signal of the retina, the reference surface is set to the vitreous side; however, the reference surface of the inverted mirror image surface is on the choroidal side. This mirror image appears in the imaging frame when the OCT objective lens gets closer to the patient's eye during scanning. Retinal signal intensity is not high in this mirror image, but choroidal signal intensity increases. When averaging 100 scans of this mirror image, the speckle noise is removed and visualization of the choroid and

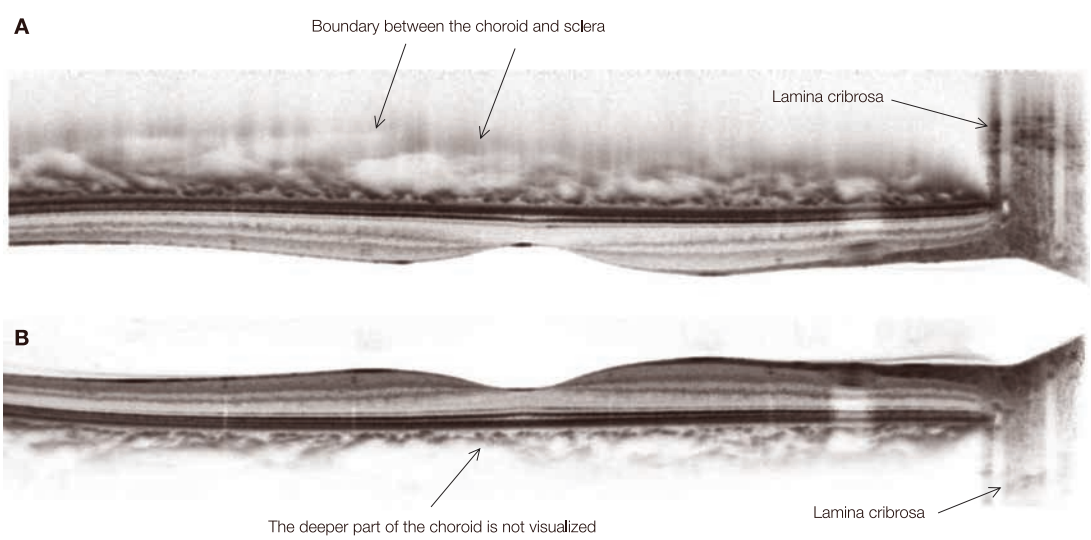

Fig. 1-15 An explanatory diagram of EDI-OCT
A: Mirror image, **B:** normal image.

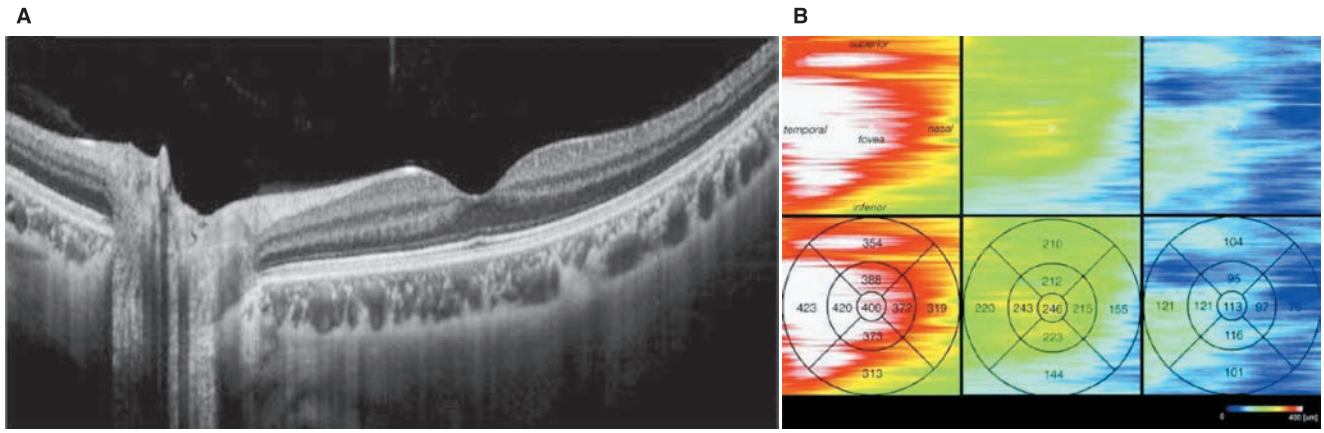

Fig. 1-16 SS-OCT B-scan image and choroidal thickness map
A: Horizontal B-scan, **B:** choroidal thickness map. From the left: hypermetropia, emmetropia, myopia.
(Modified according to Hirata M, et al. Macular choroidal thickness and volume in normal subjects measured by swept-source optical coherence tomography. Invest Ophthalmol Vis Sci. 2011; 52: 4971-4978)

lamina cribrosa is markedly improved. This imaging method is reported by Spaide et al., and is known as enhanced depth imaging (EDI)[13].

SS-OCT

Many commercially available SD-OCT use SLD light sources with centre wavelengths of 840–870 nm. Recently, 1,050 nm swept source OCT (SS-OCT) prototypes have been developed, which are known to excel in choroidal visualization (Fig. 1-16A). Since 1,050 nm light is better at permeating the RPE than 800–900 nm light it is possible to use more light in choroidal image acquisition. In addition, there is little signal intensity attenuation in the depth direction as seen in SD-OCT, resulting in clear images of not only the choroid but also of the vitreous body. With SS-OCT, averaging B-scans for choroidal thickness measurements is not required and dense raster scan can be performed to create 3-dimensional choroidal thickness maps. Currently, there are already reports on choroidal thickness of normal eyes measured using SS-OCT[14, 15] (Fig. 1-16B).

Choroidal thickness

Choroidal thickness of normal eyes decreases with older age and longer axial length[15, 16]. In addition, the choroidal thickness in the macular area is thinner nasally and thicker temporally regardless of ocular axial length[15, 17].

1.4 Displaying B-scans

Displaying reflection intensity

When the reflection intensity of light is displayed in black, the background image is white. Conversely, when it is displayed in white, the background image is black (Fig. 1-17).

Displaying false colours

False colour displays are often used to indicate the reflection distribution (Fig. 1-18). Colours are applied to the reflection intensity of light, such as warm colours for strong reflectivity and cool colours for weak reflectivity. The colours, however, do not

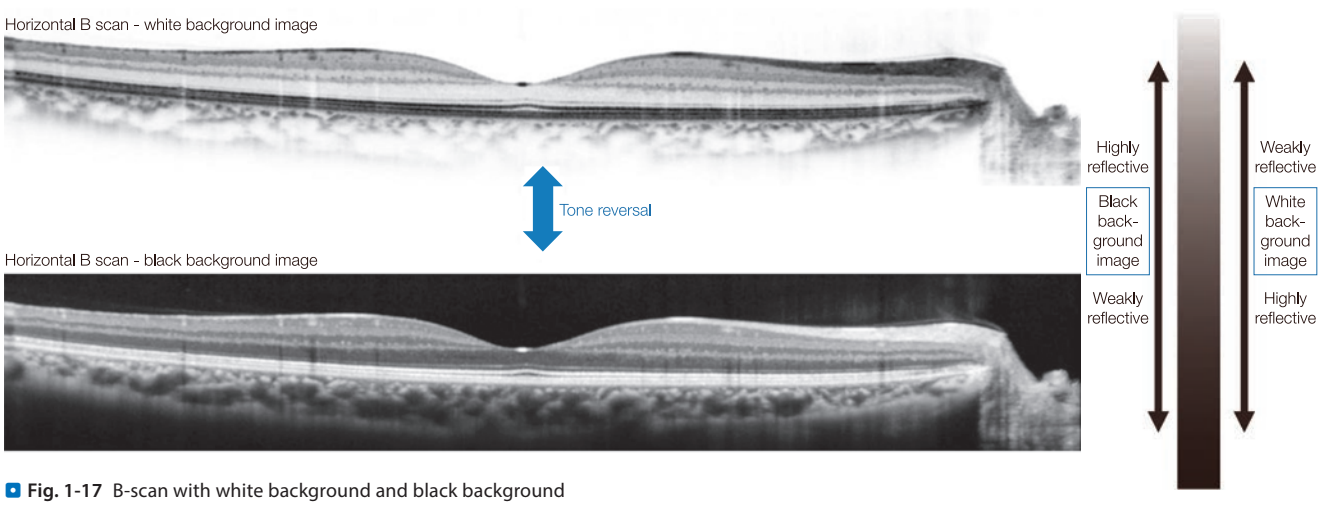

Fig. 1-17 B-scan with white background and black background

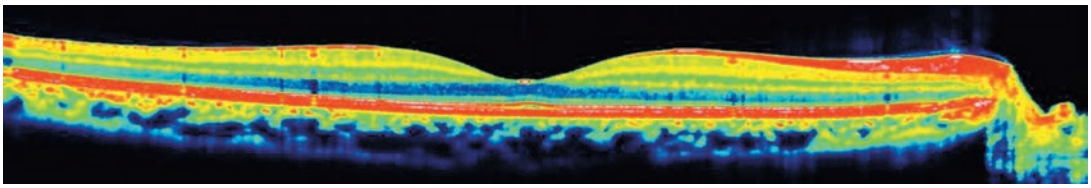

Fig. 1-18 B-scan with false colour display

have a specific meaning. In high-definition B-scans with speckle noise removed, subtle changes in reflection intensity attributed to layer boundaries or small lesions can be recognized on monochromatic displays. However, with false colour displays, subtle changes in reflective light intensity are harder to discern.

1.5 Depth resolution misinterpretations

Speckle noise removal has more impact than depth resolution on layer structure visualization

The thickness of each retinal layer in the macula exceeds 30 µm in thickness (Fig. 1-19)[11]. Thus, theoretically, if time-domain OCT with a depth resolution of 10 µm such as OCT 2000 or Stratus OCT is used, the retinal layer structure of the macula should be clearly visualized. When speckle noise is removed from Stratus OCT imaging, each retinal layer is indeed clearly visualized (Fig. 1-20)[3]. In contrast, the layer structure does not become distinct even when the depth resolution is increased to 3 µm[1].

Therefore, the removal of speckle noise is highly important in improving the resolving power of each retinal layer through OCT (Fig. 1-21, 1-22).

ELM and IS/OS boundaries can be visible with removal of speckle noise

The external limiting membrane and photoreceptor inner and outer segment junction are histologically merely boundaries, and thus have almost no thickness to them. However, if the outer nuclear layer (over 30 µm) and the IS (about 23 µm) anterior and posterior to the ELM, respectively, could be resolved, the ELM could theoretically be visualized. Similar to the previous section, analysis of these layers is indeed possible even with the OCT 2000 and Stratus OCT after speckle-noise reduction (Fig. 1-23)[3]. This indicates that the speckle noise, but not the depth resolution, is mainly responsible for the unclear visibility of the ELM and IS/OS in time-domain OCT.

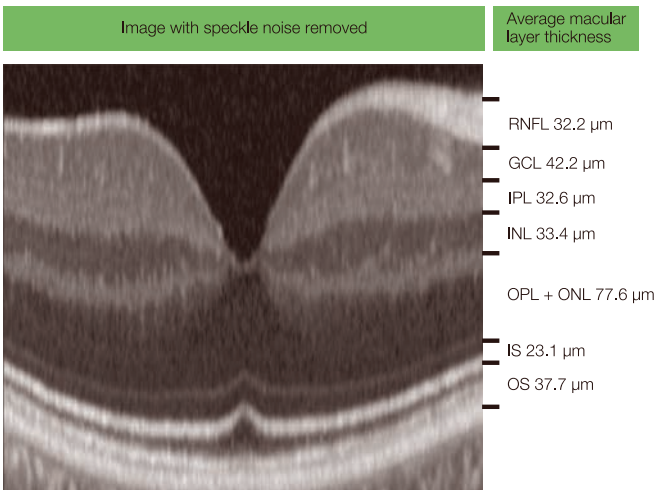

Fig. 1-19 Average macular retinal thickness
(Modified according to Ooto S, et al. Effects of age, gender, and axial length on the three-dimensional profile of normal macular layer structures. Invest Ophthalmol Vis Sci. 2011; 52: 8769-8779)

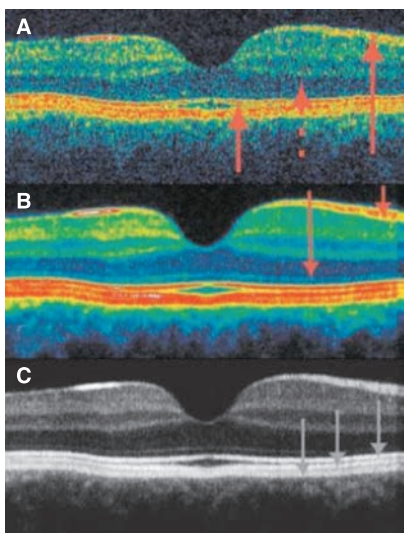

Fig. 1-20 Speckle noise removal in OCT 3000
A: B-scan. **B, C:** Image based on the averaging of 13 scans.
(Modified according to Sander B, et al. Enhanced optical coherence tomography imaging by multiple scan averaging. Br J Ophthalmol. 2005; 89: 207–212)

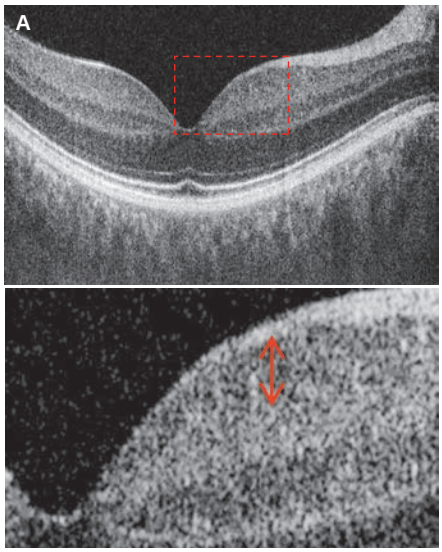

Fig. 1-21 3 µm single scan SD-OCT image without speckle noise reduction (**A**) vs. 7 µm SD-OCT image with speckle-noise removed (**B**)
Ganglion cell layer (GCL, red double arrows) boundaries are obscured even at a depth resolution of 3µm. GCL boundaries appear distinct after speckle noise removal even at a depth resolution of 7 µm.

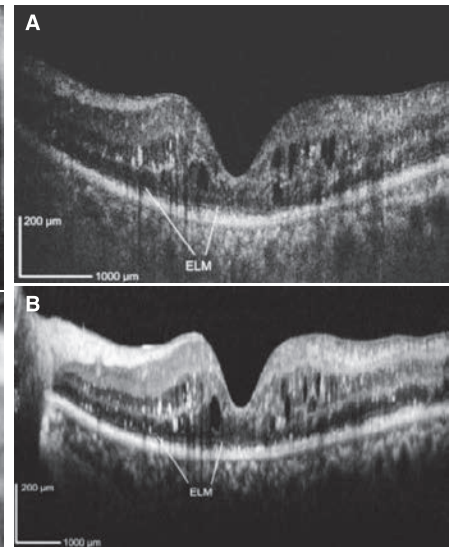

Fig. 1-22 3 µm single scan SD-OCT image without speckle noise reduction (**A**) vs. 7 µm SD-OCT image with speckle-noise removed (**B**)
Cases of cystoid macular edema. Layers where lesions exist can be clearly seen after speckle noise removal.
(Modified according to Hangai M, et al. Ultrahigh-resolution versus speckle noise-reduction in spectral-domain optical coherence tomography. Opt Express. 2009; 17: 4221-4235)

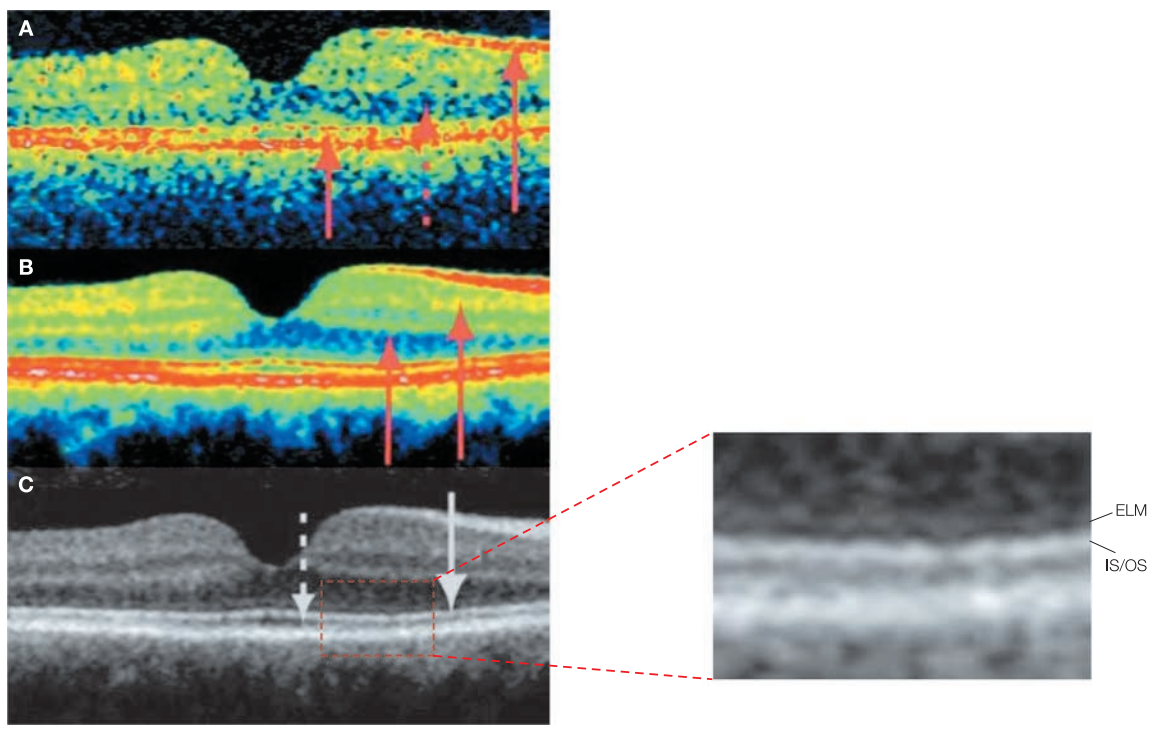

Fig. 1-23 Speckle noise removal in OCT 2000
Even with a depth resolution of 20 µm (OCT 2000), the ELM and IS/OS are visualized after an average of 9 scans is performed and speckle noise is reduced.
(According to Sander B, et al. Enhanced optical coherence tomography imaging by multiple scan averaging. Br J Ophthalmol. 2005; 89: 207-212)

1.6 Artifacts

1.6.1 The effect of involuntary eye movement

Involuntary eye movement

Involuntary eye movement is high-frequency micro-movement of the eyeball that occurs when the eyeball gazes steadily at a fixed target. These movements are composed of 3 elements: tremors, flicks, and drifts (Fig. 1-24). In time-domain OCT, distortion occurs on each B-scan image as a result of involuntary eye movement due to the slow imaging speed (Fig. 1-25). Thus, it is difficult to capture the same image and to remove speckle noise. High speed image acquisition in SD-OCT allows 3-dimensional raster scanning and precise averaging of B-scans to remove speckle noise. However, involuntary eye movement can cause jagged pattern in the 3-dimensional imaging and averaging errors in speckle-noise removal (Fig. 1-27).

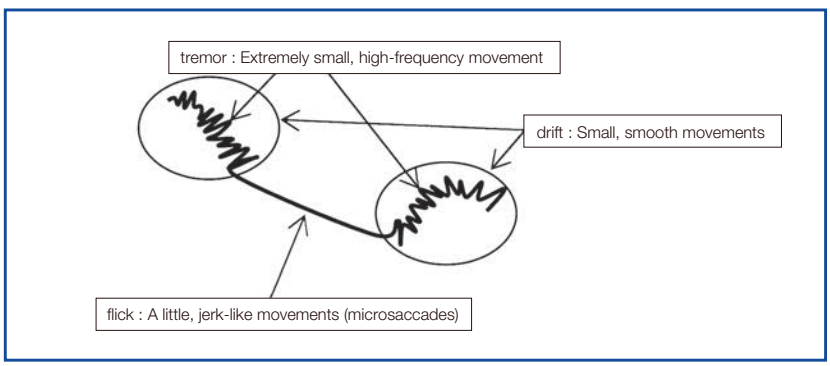

Fig. 1-24 The 3 elements of involuntary eye movement (schematic diagram)

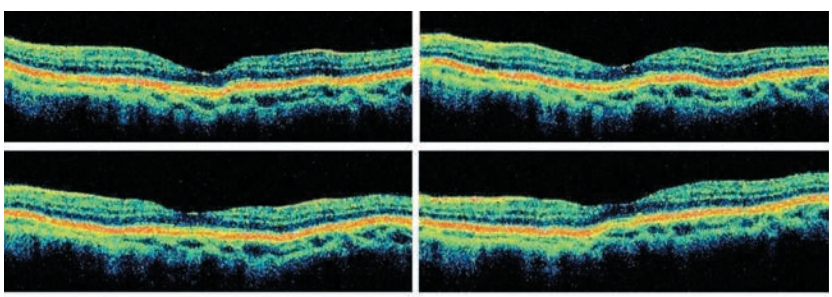

Fig. 1-25 Image distortion in time-domain OCT
The distortion is different in each scan.

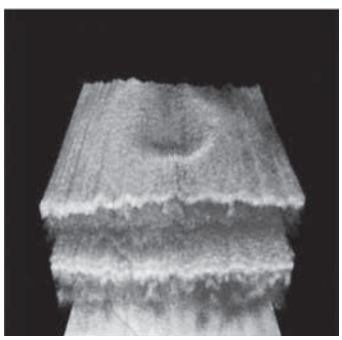

Fig. 1-26 3-dimensional image obtained with spectral-domain OCT
Involuntary eye movement can be seen as jagged patterns known as ridges.

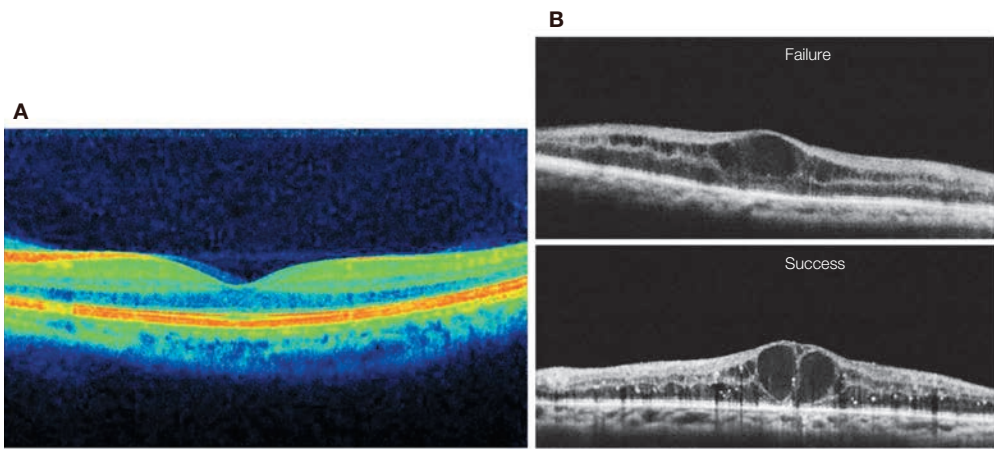

Fig. 1-27 Errors in B-scan averaging
A: An averaging error occurred due to involuntary eye movement thought to be a flick. **B:** The B-scan image appears blurred due to an averaging error thought to be the effect of a tremor.

1.6.2 Phenomena caused by the optical properties of tissue

Shadows caused by measurement beam blockage

OCT measurement beams can be blocked by 1) blood flow (Fig. 1-28) and 2) opaque lesions (Fig. 1-29), resulting in more posterior tissue not being visualized. Blood flow causes loss of the interference signal known as fringe washout. Signals lost posterior to retinal blood vessels exhibit findings known as shadows.

The effect of the blockage is stronger with more opaque lesions. Heavy hemorrhage and dense hard exudates can cause complete measurement beam blockage resulting in no visibility of posterior tissues..

High-reflectivity caused by excessive measurement beam penetration

Conversely, in lesions where retinal degeneration or atrophy is apparent, the light that is normally reflected and scattered or absorbed by intact retina and RPE reaches the posterior choroid and sclera. While usually difficult to visualize, the visualization of these tissues become enhanced (Fig. 1-30).

Low-reflectivity due to tilting

When a measurement beam is perpendicular to the nerve fibers and boundaries, the reflectivity of these structures reaches its maximum, resulting in visualization. However, when the retinal angle tilts in relation to the measurement beam due to retinal detachment or retinal pigment epithelial detachment, reflectivity of these layers becomes diminished (Fig. 1-31). Conversely, HFL, which originally runs diagonally to the outer plexiform layer, becomes highly reflective when perpendicular to the measurement beam (Fig. 1-31, Fig. 1-6 ▶ page 5).

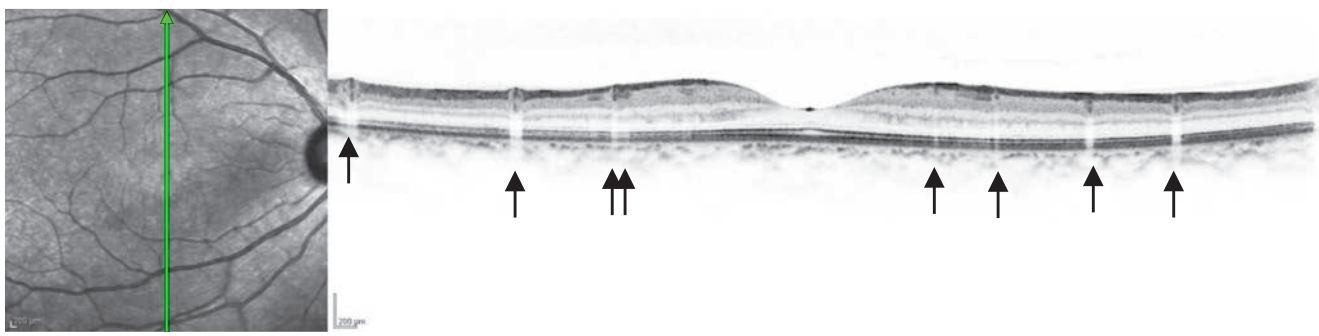

Fig. 1-28 Measurement beam blockage caused by retinal blood vessels (IR + OCT vertical scans)
Arrows (→) indicate shadows caused by retinal blood vessels

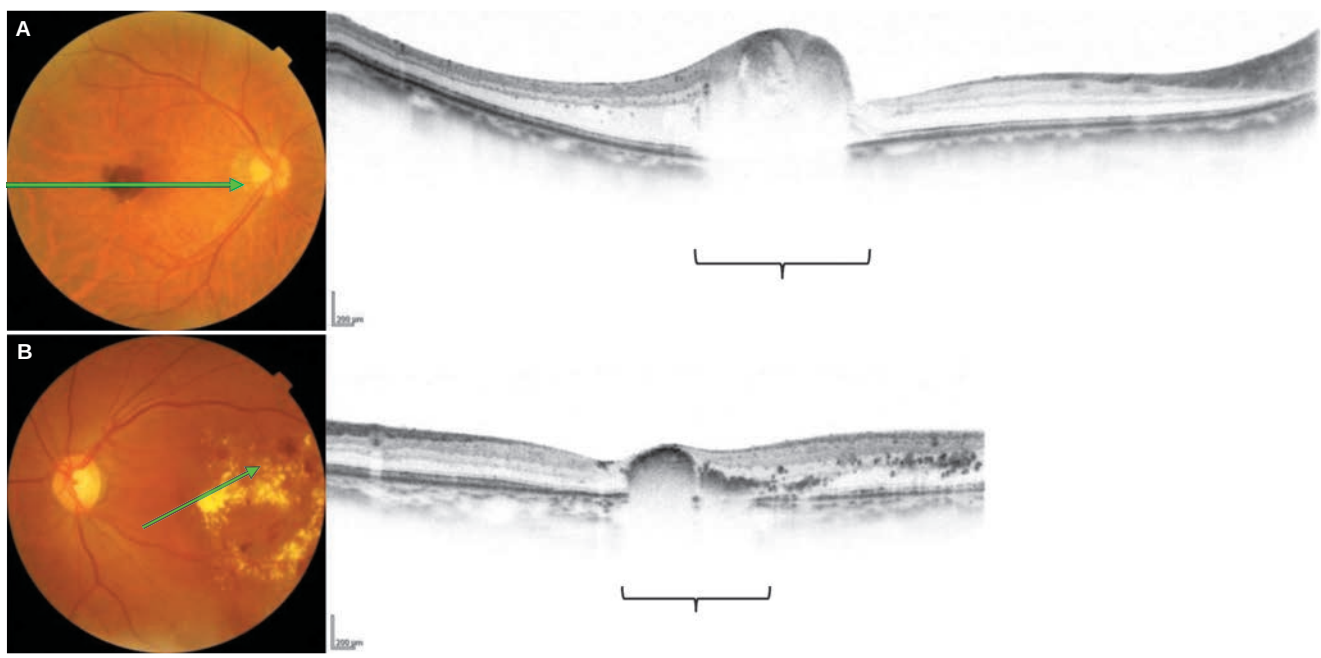

Fig. 1-29 Measurement beam blockage caused by opaque lesions (color fundus photography + OCT B-scans)
A: Due to retinal hemorrahge, **B:** due to dense hard exudates.

Fig. 1-30 Cone dystrophy (IR + OCT macula horizontal scan)
Choroidal sensitivity is remarkably high beneath the thinned and degenerated macula.

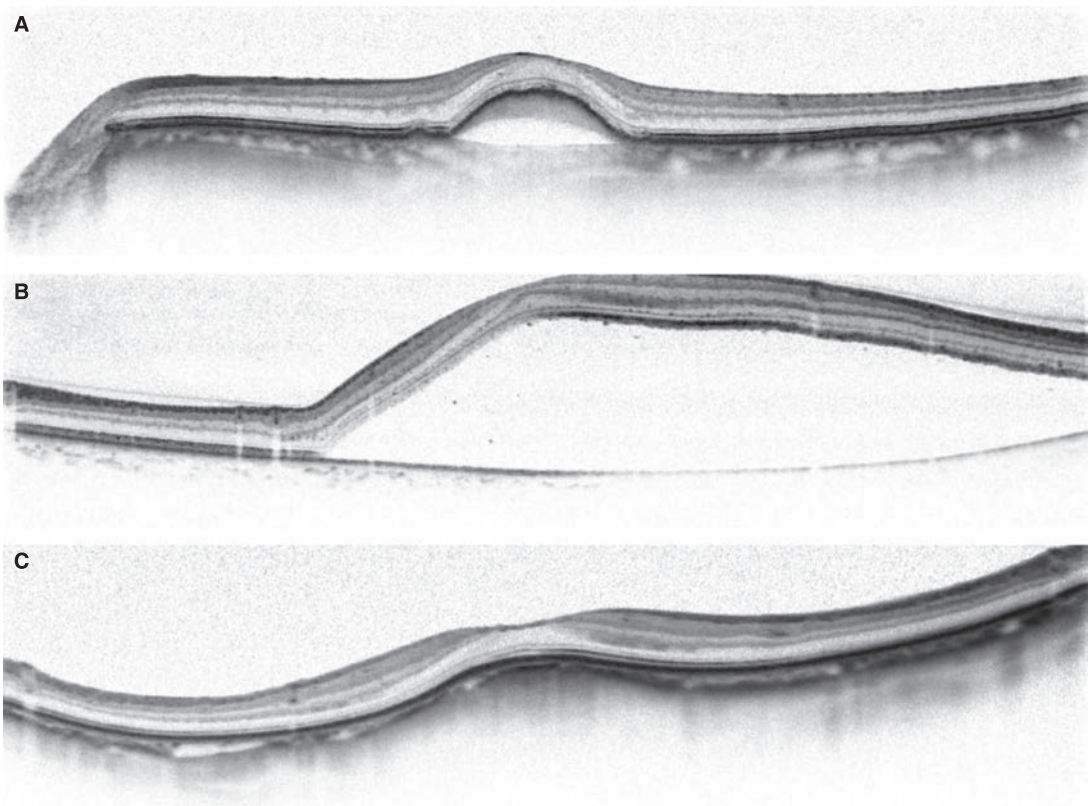

Fig. 1-31 Decrease in reflection intensity caused by retinal tilt (OCT B-scan)
A: Retinal pigment epithelial detachment. The IS/OS lines in the uninvolved retina perpendicular to the optical axis are highly reflective, whereas the reflectivity of the IS/OS lines in the retinal pigment epithelial detachment area is comparatively low. **B:** Central serous chorioretinopathy. Within the detached retina, the perpendicularly oriented portion continues to have high reflectivity while the tilted portion has comparatively low reflectivity. **C:** Dome-shaped macula. Reflectivity of each layer and IS/OS lines on the more tilted side is comparatively low.

1.6.3 Aspects relating to measurement principles

Reflection of virtual images

SD-OCT has inverted virtual images (termed mirror images) outside the imaging frame (Fig. 1-32). As a result, the virtual images of tissue and lesions sometimes enter the imaging frame. When this occurs, both real and virtual images are visualized in the imaging frame at the same time (Fig. 1-33).

Involuntary eye movements cause the vitreous body to change its position against the eye ball. Thus, opacities within the posterior vitreous cavity and posterior vitreous membrane are sometimes seen as multiple overlapping layers in B-scan images with speckle noise removed because these tissues change their position during multiple scanning for averaging (Fig. 1-33).

1.6.4 Sensitivity attenuation

Causes of sensitivity attenuation

Decreases in image sensitivity can occur from various causes.

Listed below are issues caused by imaging.

1. Being out of focus
2. The measurement beam enters the pupil eccentrically and does not intersect the retina perpendicularly
3. Image not in optimal imaging depth range
4. Insufficient eyelid opening

Listed below are issues caused by the subject.

1. Media opacity (corneal opacity, cataract, vitreous opacity)
2. Ocular surface problems (dry eye, examination immediately after contact lens wear for slit lamp examination)
3. Poor fixation

Decreases in image sensitivity reduces measurement results of retinal and retinal nerve fiber layer thickness. Since sensitivity attenuation caused by the subject are difficult to improve, effort must be made to resolve imaging-related sensitivity attenuation.

Defocusing

In OCT focusing, various mechanisms are used depending on the OCT model such as adjusting the focus in SLO imaging, and devices with automatic optimization features. Defocusing is the main cause of decreased image sensitivity (Fig. 1-34).

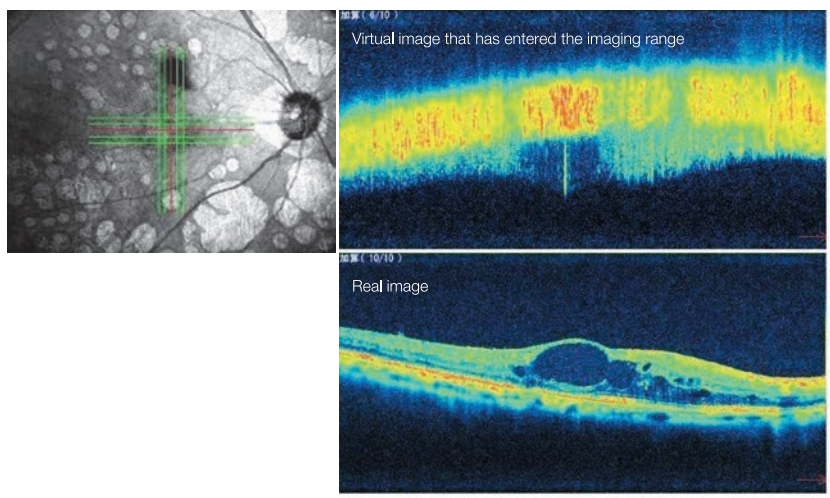

Fig. 1-32 Real images and virtual images
Usually, a virtual image is an upside down real image, and the contralateral side (lower section) is highly sensitive.

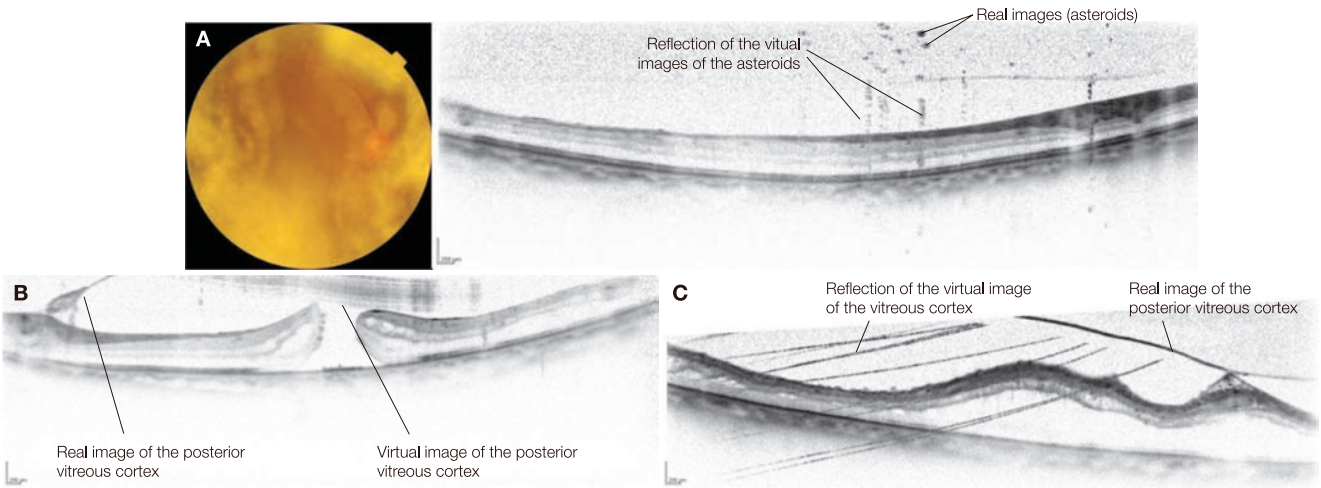

Fig. 1-33 Virtual images overlapping the real images
A: Asteroid hyalosis, **B:** Stage 3 macular hole, **C:** Vitreomacular traction syndrome.
When images are averaged, involuntary eye movement causes flickering of the posterior vitreous cortex resulting in characteristic overlap and reflection.

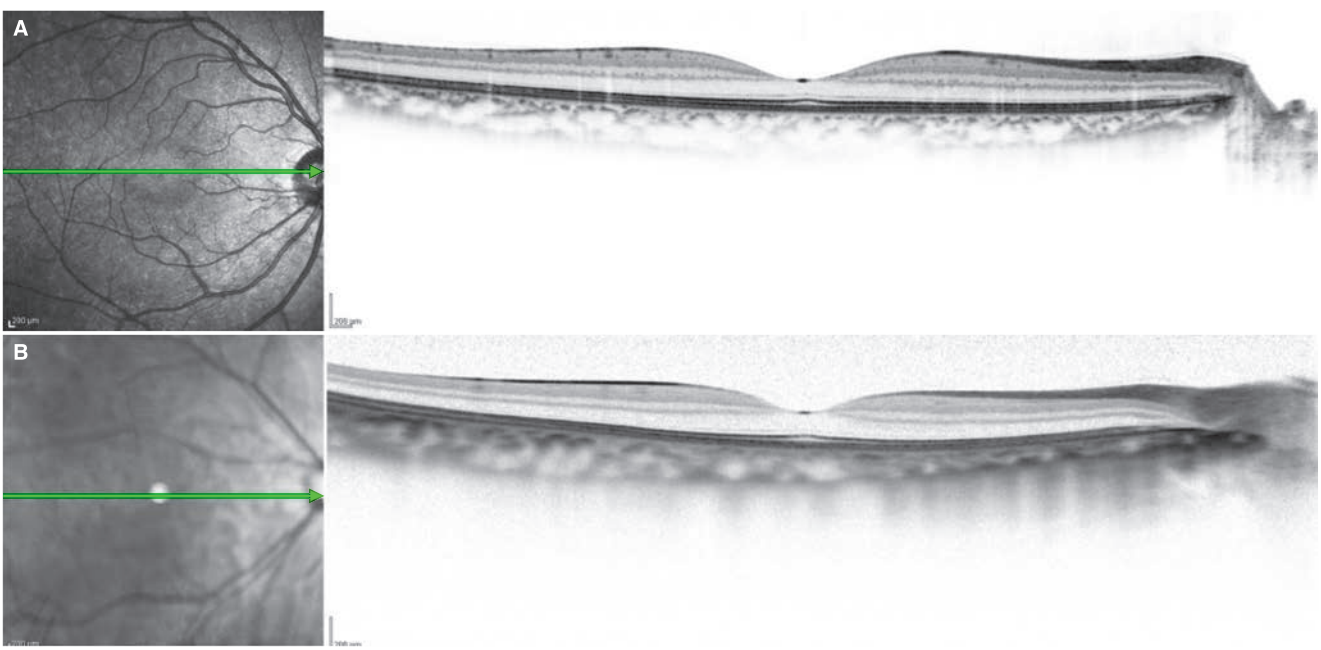

Fig. 1-34 Decreased sensitivity due to defocusing
A: Image with well-adjusted focus (Quality index 46 dB), **B:** Image with poorly adjusted focus (Quality index 29 dB).

Sensitivity attenuation along depth direction

In principle, the SD-OCT has a narrow imaging depth range for obtaining highly sensitive images. The sensitivity decreases with Imaging range (coherence gate) (Fig. 1-35, 1-36). Tissue and lesions with axially elongated structure such as severe myopia and retinal detachment are problematic (Fig. 1-37, 1-38). In the next generation swept source OCT (SS-OCT), longer imaging depth can be achieved without significant decrease in sensitivity (Fig. 1-37).

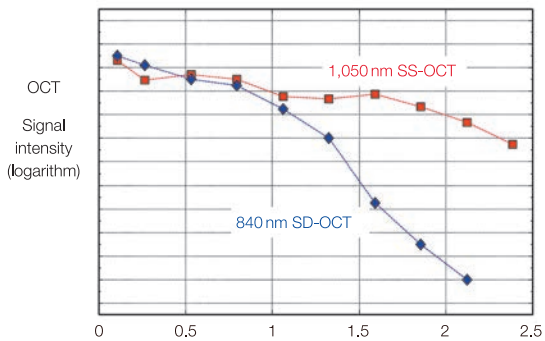

Fig. 1-35 Relationship between imaging range depth and OCT signal intensity

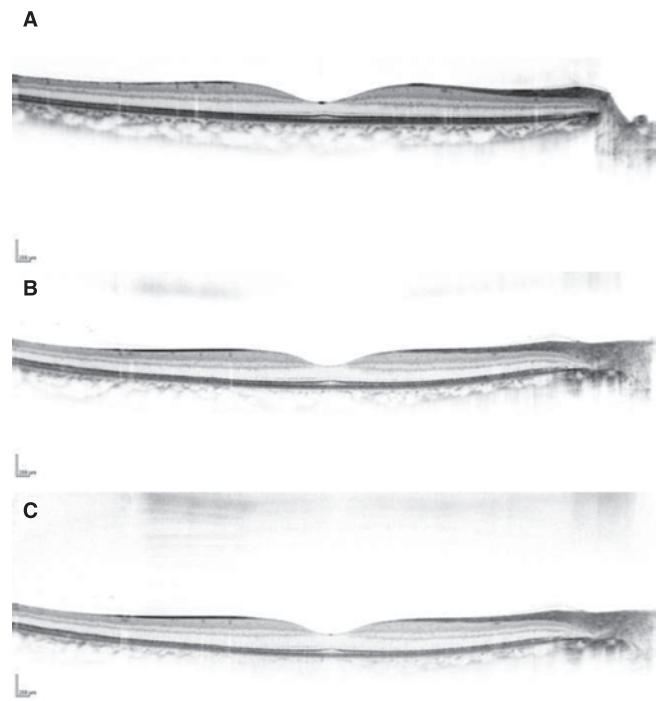

Fig. 1-36 Relationship between imaging range depth and SD-OCT signal intensity
Sensitivity attenuation increases with depth. **A**: 46 dB, **B**: 40 dB, **C**: 31 dB.

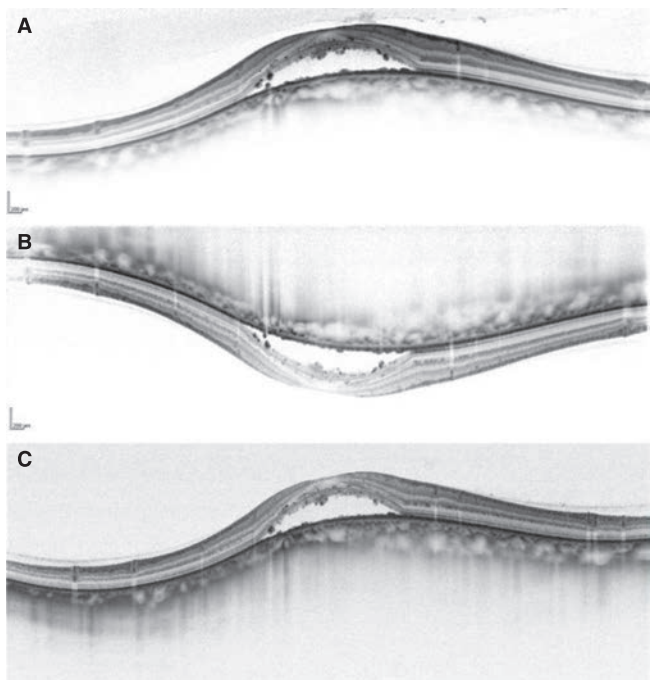

Fig. 1-37 Image of SD-OCT sensitivity attenuation compared with SS-OCT in a dome shaped macula
A: SD-OCT. Downward image sensitivity is low. **B:** EDI-OCT. Downward image sensitivity is similarly low. **C:** SS-OCT (Topcon Corporation prototype). There are no areas of apparently decreased sensitivity.

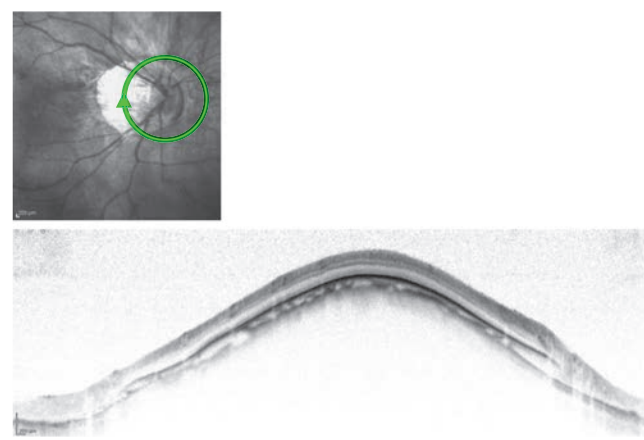

Fig. 1-38 SD-OCT sensitivity attenuation in a peripapillary circle scan
Image of retinal nerve fiber layer on a circle scan centered at the optic disc. Due to tilting of the sclera around the optic disc, severe myopia results in an image elongated along depth direction and a decreasing downward sensitivity.

References

1) Hangai M, Yamamoto M, Sakamoto A, et al. Ultrahigh-resolution versus speckle noise-reduction in spectral-domain optical coherence tomography. Opt Express. 2009; 17:4221–4235.
2) Schmitt JM, Xiang SH, Yung KM. Speckle in optical coherence tomography. J Biomed Optics. 1999; 4:95–105.
3) Sander B, Larsen M, Thrane L, et al. Enhanced optical coherence tomography imaging by multiple scan averaging. Br J Ophthalmol. 2005; 89:207–212.
4) Sakamoto A, Hangai M, Yoshimura N. Spectral-domain optical coherence tomography with multiple B-scan averaging for enhanced imaging of retinal diseases. Ophthalmology. 2008; 115:1071–1078.
5) Fine B and Yanoff M. Ocular Histology 2nd ed. Harper & Row, 1979, p57.
6) Otani T, Yamaguchi Y, Kishi S. Improved visualization of Henle fiber layer by changing the measurement beam angle on optical coherence tomography. Retina. 2011; 31:497–501.
7) Lujan BJ, Roorda A, Knighton RW, et al. Revealing Henle's fiber layer using spectral domain optical coherence tomography. Invest Ophthalmol Vis Sci. 2011; 52:1486–1492.
8) Srinivasan VJ, Monson BK, Wojtkowski M, et al. Characterization of outer retinal morphology with high-speed, ultrahigh-resolution optical coherence tomography. Invest Ophthalmol Vis Sci. 2008; 49:1571–1579.
9) Fernández EJ, Hermann B, Povazay B, et al. Ultrahigh resolution optical coherence tomography and pancorrection for cellular imaging of the living human retina. Opt Express. 2008; 16:11083–11094.
10) Spaide RF, Curcio CA. Anatomical correlates to the bands seen in the outer retina by optical coherence tomography: literature review and model. Retina. 2011; 31:1609–1619.
11) Ooto S, Hangai M, Tomidokoro A, et al. Effects of age, gender, and axial length on the three-dimensional profile of normal macular layer structures. Invest Ophthalmol Vis Sci. 2011; 52:8769–8779.
12) Curcio CA, Messinger JD, Sloan KR, et al. Human chorioretinal layer thicknesses measured in macula-wide, high-resolution histologic sections. Invest Ophthalmol Vis Sci. 2011; 52:3943–3954.
13) Spaide RF, Koizumi H, Pozzoni MC. Enhanced depth imaging spectral-domain optical coherence tomography. Am J Ophthalmol. 2008; 146:496–500.
14) Ikuno Y, Maruko I, Yasuno Y, et al. Reproducibility of retinal and choroidal thickness measurements in enhanced depth imaging and high-penetration optical coherence tomography. Invest Ophthalmol Vis Sci. 2011; 52:5536–5540
15) Hirata M, Tsujikawa A, Matsumoto A, et al. Macular choroidal thickness and volume in normal subjects measured by swept-source optical coherence tomography. Invest Ophthalmol Vis Sci. 2011; 52:4971–4978.
16) Manjunath V, Taha M, Fujimoto JG, et al. Choroidal thickness in normal eyes measured using Cirrus HD optical coherence tomography. Am J Ophthalmol. 2010; 150:325–329.
17) Ikuno Y, Tano Y. Retinal and choroidal biometry in highly myopic eyes with spectral-domain optical coherence tomography. Invest Ophthalmol Vis Sci. 2009; 50:3876–3880.

Vitreoretinal interface pathology

2.1 Idiopathic macular holes – 23
References – 28

Case 1 Physiological PVD: Flattening of foveal depressions – 29

Case 2 Idiopathic macular hole: Progression from Stage 1 (cystoid space type) to Stage 2 – 30

Case 3 Idiopathic macular hole: Stage 1 foveal cystoid space formation type – 31

Case 4 Idiopathic macular hole: Stage 1 foveal detachment type – 32

Case 5 Idiopathic macular hole: Stage 1 photoreceptor dehiscence type – 33

Case 6 Idiopathic macular hole: Stage 1 small foveal detachment type – 34

Case 7 Idiopathic macular hole: Case just before progression from stage 1 to stage 2 – 35

Case 8 Idiopathic macular holes: Typical example of stage 2 – 36

Case 9 Idiopathic macular hole: Postoperative course for macular hole closure under gas tamponade – 38

Case 9 DONFL appearance – 39

Case 10 Idiopathic macular hole: Postoperative course for macular hole closure – 40

Case 11 Idiopathic macular hole: Typical example of stage 3 – 41

Case 11 After surgery – 42

Case 12 Idiopathic macular hole: Typical example of stage 4 – 43

Case 13 Idiopathic macular hole: Old case of stage 4 – 44

Case 13 Stage 4 after surgery – 45

Case 14 Idiopathic macular hole: Progression from lamellar to full-thickness macular holes – 46

Case 15 Stage 1 macular hole: Spontaneous separation of perifoveal PVD – 47

Case 16 Stage 1 macular hole: Macular microhole formation – 48

Case 17 Stage 2 macular hole: Spontaneous closure – 49

Case 18 Stage 3 macular hole: Spontaneous closure – 50

Case 19 Stage 4 macular hole: Spontaneous closure – 51

Case 20 Traumatic macular hole: A typical example – 52

Case 21 Lamellar macular hole: A typical example – 54

Case 22 Lamellar macular hole: Differentiation from a MPH – 55

Macular microholes – 56

References – 56

Case 23 Macular microhole: with macular PVD – 57

Case 24 Macular microhole: with complete PVD – 58

Case 25 Macular microhole: Case without PVD – 59

2.2 Idiopathic epiretinal membrane – 60

References – 62

Case 26 Idiopathic epiretinal membrane: A typical example – 63

Case 27 Idiopathic epiretinal membrane: Exposure of the fibrocellular membrane – 64

Case 28 Idiopathic epiretinal membrane: Membrane with significant whitening – 65

Case 29 Idiopathic epiretinal membrane: Significant columnar structure formation – 66

Case 30 Idiopathic epiretinal membrane: Case ① where macular PVD has not been complete – 67

Case 31 Idiopathic epiretinal membrane: Case ② where macular PVD has not been complete – 68

Case 32 Epiretinal membrane secondary to retinal hemangioma – 69

Case 33 Macular pseudohole: A typical example – 70

Case 34 Macular pseudohole: Case where macular PVD has not been complete – 71

2.3 Vitreomacular traction syndrome – 72

References – 72

Case 35 Vitreomacular traction syndrome: Case showing disease development – 73

Case 35 Continuation – 74

Case 36 Vitreomacular traction syndrome: Cases with macular detachment – 75

Case 37 Vitreomacular traction syndrome: A highly myopic eye with foveoschisis – 76

2.1 Idiopathic macular holes

Background

Idiopathic macular holes occur frequently in middle-aged to elderly individuals (between 50 and 70 years of age) with emmetropia. The female to male ratio is more than 3:1[1]. Onset is seen bilaterally in over 10%. In 1988, Gass categorized the progression to hole formation into 4 stages based on biomicroscopic findings[2] and suggested that treatment by vitreous surgery was potentially effective. In 1991, Kelly and Wendel reported that full-thickness macular holes could be closed by vitreous surgery and gas tamponade[3], after which vitreous surgery became standard treatment. Currently, most macular holes can be closed in combination with internal limiting membrane peeling. Gass reflected on the findings of macular hole surgery and revised the categories himself in 1995[4]. Afterwards, the concept of foveal traction occurring during the process of posterior vitreous detachment (PVD) was proposed with the introduction of OCT in 1997, establishing the basis for understanding macular hole pathology [5–10].

Pathogenesis

The progression of physiological PVD can be elucidated by OCT[11] (Fig. 2-1, 2-2). In the course of physiological PVD, posterior vitreous cortex detachment progresses from outside of the macula, via the periphery of the macula to the fovea (Fig. 2-2A). This leads to perifoveal detachment of the posterior vitreous cortex with its persistent attachment to the fovea (termed perifoveal PVD, Fig. 2-1C, 2-2C). The remaining attachment to the fovea is resolved leading to macular PVD (Fig. 2-1D, 2-2D). Finally, a glial ring (Weiss ring) is found on the fundus image once there is separation of the posterior vitreous cortex from the optic disc, thereby completing the course of PVD (Fig. 2-1E). In idiopathic macular holes, the perifoveal PVD generates an anterior traction force towards the fovea centralis, which causes the structure of the fovea to collapse, forming full-thickness macular holes. Kishi et al. state that, PVD occurs when the thin elastic posterior wall of the premacular liquefied pocket contracts with age (Fig. 2-3)[12]. In the final stage of this process, the following 3 patterns emerge:

- full-thickness macular hole formation
- PVD is completed without progressing to full-thickness macular hole with foveal structural abnormalities remaining
- PVD is completed without evident abnormalities in foveal shape

It is not clear why the physiological PVD leads to these 3 patterns, but abnormal adhesion of the posterior vitreous cortex and fovea [13] as well as thin foveal thickness are thought to be involved.

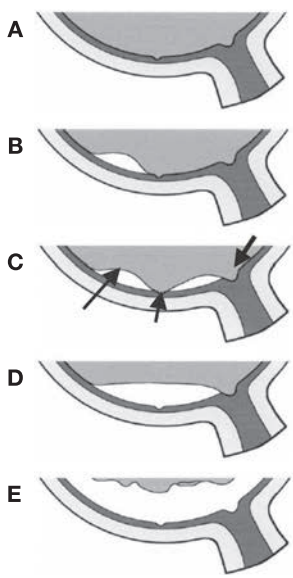

Fig. 2-1 The process of physiological PVD
(Modified according to Uchino E, et al. Initial stages of posterior vitreous detachment in healthy eyes of older persons evaluated by optical coherence tomography. Arch Ophthalmol. 2001; 119: 1475–1479)

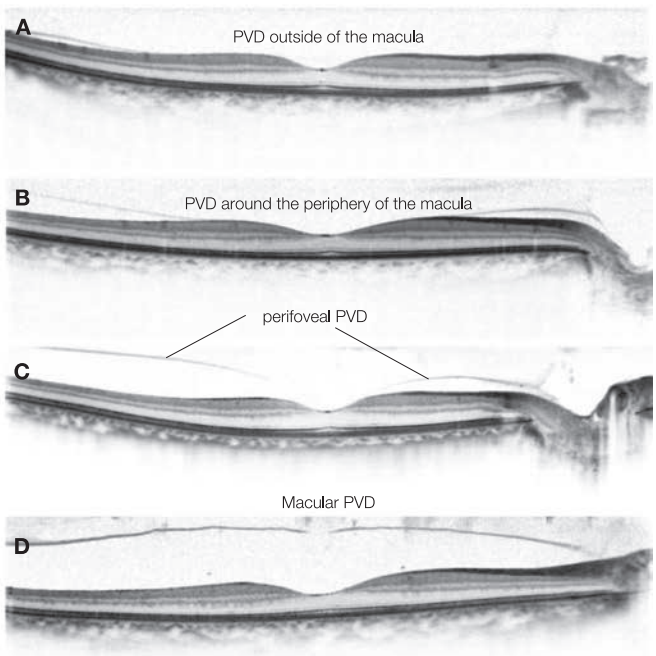

Fig. 2-2 The process of physiological PVD and OCT imaging

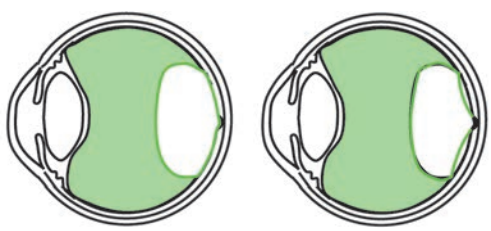

Fig. 2-3 Physiological PVD and the premacular liquefied pocket
Contraction of the posterior wall of the precortical vitreous pocket is believed to cause perifoveal PVD

Stage classification

Observations with OCT have complemented macular hole stage classifications[2, 4] based on ophthalmoscopic observations made by Gass[5–10]. However, it is difficult for Gass's Stage 1A and Stage 1B to fully support OCT findings. The essence of idiopathic macular hole onset is the disruption or removal of the Müller cell cone (illustrated below) resulting in foveal photoreceptor dehiscence at the umbo. Thus, dividing Stage 1 up based on the presence or absence of photoreceptor dehiscence is essential.

In this book, Stage 1A represents no photoreceptor dehiscence at the foveola, and Stage 1B represents dehiscence. If defined in this way, the classification is decided based on the stage of PVD and the foveal shape (■ Fig. 2-4).

Understanding macular hole stage classification better

Stage 1 is a stage where the fovea shape is variably deformed due to perifoveal PVD, but have not developed a full thickness macular hole. There are cases where foveal cystoid spaces are initially formed, cases where foveal detachment develops first, or cases where both occur (■ Fig. 2-4). Changes strongly related to visual impairment are foveal photoreceptor dehiscence, and as mentioned previously, In this book, Stage 1A is before dehiscence and Stage 1B is after dehiscence. A full-thickness macular hole forms when a cleft develops in the anterior walls of the cystoid space and foveal detachment or foveal photoreceptor dehiscence occurs. The stage where the posterior vitreous cortex and fovea are connected by a flap is Stage 2, the stage where the flap is disconnected from the fovea centralis to become an operculum and traction from the posterior vitreous cortex towards the fovea centralis is lost is Stage 3, and the stage where PVD is completed and macular hole an operculum can no longer be seen with OCT (the Weiss ring is seen on an biomicroscopy) is Stage 4. The Stage 1 roof, Stage 2 flap and Stage 3 operculum are thought to be the same tissue. When the macular holes reach full thickness, the centrifugal elevation of the edge of the macular hole progresses and visual impairment increases.

In view of the relationship with posterior vitreous detachment, in Stage 1 and Stage 2 the posterior vitreous cortex and the fovea are connected. In Stage 3 the posterior vitreous cortex is detached from the fovea, but is still connected to the optic disc. In Stage 4 posterior vitreous detachment is complete and the posterior vitreous cortex is not visualized since it is outside the OCT imaging range (■ Fig. 2-5).

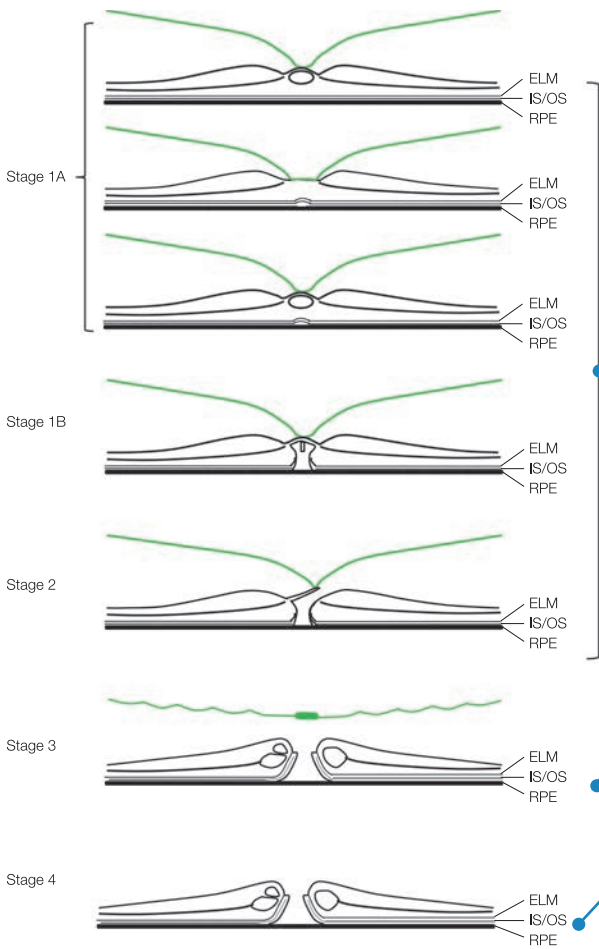

■ **Fig. 2-4** Foveal deformation and stage classifications

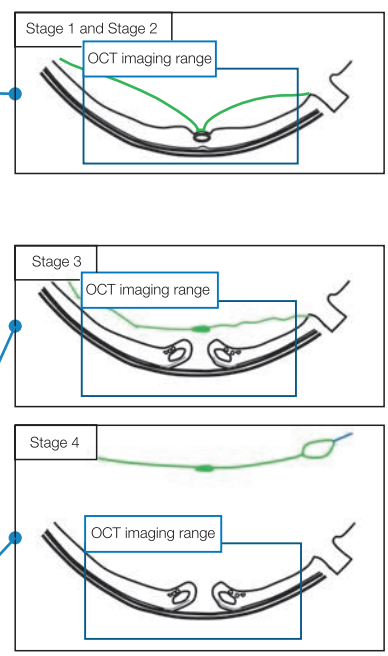

■ **Fig. 2-5** Posterior vitreous cortex and stage classifications

Spontaneous separation of perifoveal PVD and foveal deformation, in particular lamellar macular holes

In Stage 1 macular holes, defined as, the fovael deformation secondary to perifoveal PVD, the perifoveal PVD frequently separates into a completed macular PVD without progression to full thickness macular holes. This process results in various foveal deformation. When the spontaneous separation occurs in Stage 1 macular holes that have cystoid spaces with clefts in the Henle fiber layer (HFL), lamellar macular holes develop, which are characterized by the clefts remaining in the HFL and diminished fovea or parafovea (■ Fig. 2-6, 2-11)[8, 14]. On the other hand, when spontaneous separation of perifoveal PVD occurs in Stage 1 macular holes with foveal detachment or foveal photoreceptor dehiscence, the disruption of the inner and outer segments of photoreceptors in the fovea are left, which accounts for the pathogenesis of a part of macular microholes (■ Fig. 2-6, 2-7, macular microhole paragraph ► see page 58)[15]. In addition, when the perifoveal PVD is spontaneously separated, regardless of the development of a Stage 1 macular hole, abnormal contour of the foveal depression, such as flat and v-shaped foveal surface, remains (■ Fig. 2-6, 2-7). These foveal contour abnormalities are frequently seen with OCT in the fellow eye of patients with unilateral macular holes [13].

The state of fellow eyes

As mentioned above, a high rate of foveal contour abnormalities are seen in the fellow eyes of eyes with unilateral macular holes. In cases where perifoveal PVD is seen, some patients have residual foveal deformation (9%) whereas in others the normal contour is maintained (7%) (■ Fig. 2-6)[13]. When perifoveal PVD is seen in the fellow eye, macular hole incidence increases by six-fold[16]. In cases of complete PVD some patients have residual foveal deformation (17%) while others maintain a normal foveal contour (36%).

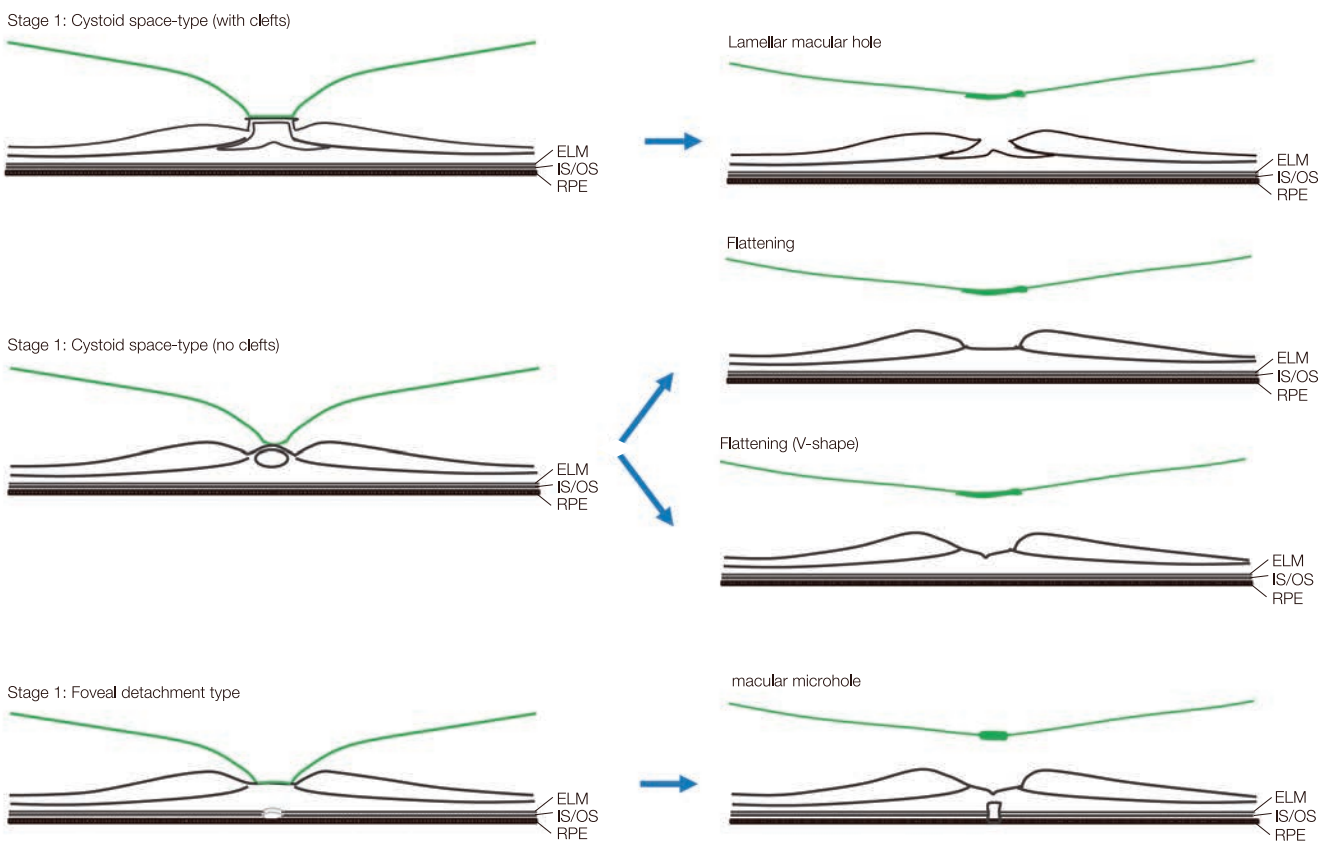

■ **Fig. 2-6** Spontaneous separation of perifoveal PVD and residual deformation of the fovea (diagram)

Spontaneous closure

While rare, spontaneous closure can occur in all stages from Stage 1 to Stage 4[17–21]. In addition, reopening can occur after spontaneous closure[22]. After spontaneous macular hole closure, the foveal depression shows abnormal contour similar to that seen after spontaneous separation of perifoveal PVD.

Postoperative visual prognosis

The macular hole closure rate has improved with internal limiting membrane peeling. In the literature, macular hole closure rates are reported to be between 76.4 and 100%. However, outcomes in postoperative visual acuity can vary greatly even when macular hole closure is achieved. Despite cases of postoperative visual acuity improving to over 1.0, there are also cases of visual acuity not changing much at all: such cases of poor visual prognosis are a remaining problem[23–28]. Although the reason why postoperative visual prognosis varies so greatly from case to case has not become apparent, the preoperative state of foveal photoreceptor cells is presumed to have an effect on prognosis. Old age, poor preoperative vision, a large macular hole diameter, a long period after onset and advanced stages are mentioned as risk factors resulting in poor visual prognosis. However, in previous reports on long-term results, only ageing, poor preoperative visual acuity and advanced stages are identified as significant risk factors[23, 28]. In addition, there are many reports that could not identify any particular significant factor. Indeed, there are cases of poor visual acuity recovery even when the period after onset has been short, the cause of which is presumed to be foveal photoreceptor cells being torn and lost during macular hole formation. This is also backed up by reports on cases where the inner segments of photoreceptor cells are included in the surgically collected macular hole opercula[29]. Moreover, when observed by OCT, there are cases where the elevated photoreceptor layer of the macular hole edges is observed without a defect of IS/OS, and other cases where a (large) part of IS/OS is defective. These findings may reflect photoreceptor inner and outer segments lost during or after macular hole formation.

Postoperative OCT findings

Even if macular hole closure is confirmed with biomicroscopy shortly after macular hole surgery (1 month after), various foveal contour abnormalities such as defects of foveal inner and outer segments, foveal detachment, loss of IS/OS and ELM reflectivity, thinning of the fovea centralis and the IS/OS and ELM lines depressed onto the retinal pigment epithelium (RPE) line can be seen with OCT. These findings are associated with visual impairment[30–35]. Among these findings, defects of foveal inner and outer segments and foveal detachment gradually decrease and disappear, and there are also cases where IS/OS and ELM reflectivity recovers[35].

Tadayoni et al. have reported the occurrence of various findings of retinal nerve fiber layer defects in the posterior pole after macular hole surgeries with internal limiting membrane peeling[36]. This feature has been thought to be dissociated retinal nerve fiber layer, because these findings are confined to the retinal nerve fiber layer when observed by vertical OCT B-scans through the fovea and retinal sensitivity abnormalities are not detected on visual field or microperimetry testing[37–39]. However, when observed by serial OCT B-scans with speckle noise removed, damage is observed from the ganglion cell layer to the inner plexiform layer particularly temporal to the macula[41, 42].

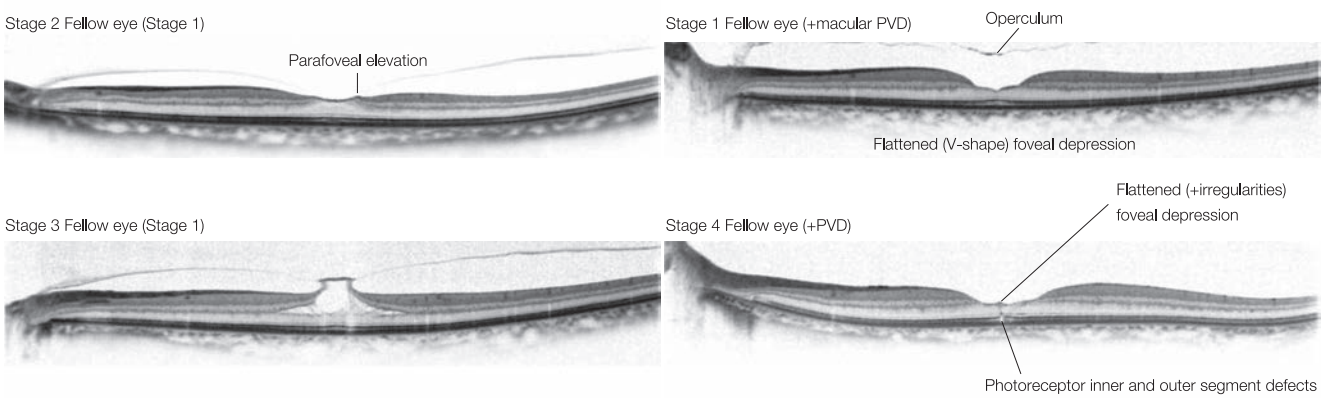

Fig. 2-7 Foveal deformation with and without spontaneous separation of perifoveal PVD in the fellow eyes of patients with a macular hole. (OCT)

Understanding perifoveal PVD and the Müller cell cone

Yamada et al. reported that the fovea centralis has a cone-shaped structure with lightfew cell nuclei that is comprised of Muller cells, referred to as the Müller cell cone (Fig. 2-8)[39]. Based on these histological findings, Gass hypothesized that the Müller cell cone function as a plug to bind together the photoreceptor cells in the foveola, and when these disconnect, there is photoreceptor dehiscence of the foveola at the umbo, leading to macular hole formation (Fig. 2-9, 2-10)[40]. Hangai et al. and Takahashi et al. observed OCT images indicating the photoreceptor layer dehiscence at the foveola associated with perifoveal PVD and isolated Muller cell cone as if perifoveal PVD pulled out the Muller cell cone, resulting in the dehiscence.[9, 10]. Thus, the function of the Müller cell cone is thought to be structural support of the fovea centralis.

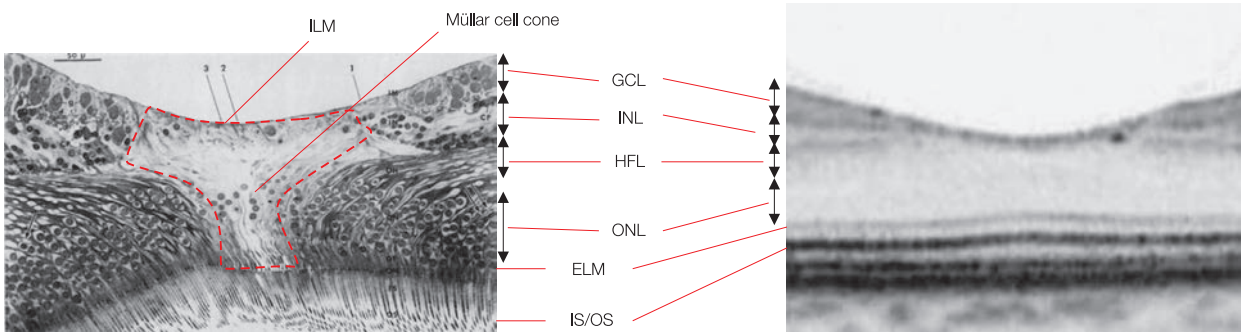

Fig. 2-8 The structure known as the fovea centralis Müller cell cone (surrounded by orange dotted line, optical light microscopic image and OCT image) (The left figure has been modified according to Yamada E. Some structural features of the fovea centralis in the human retina. Arch Ophthalmol. 1969:82; 151–159)

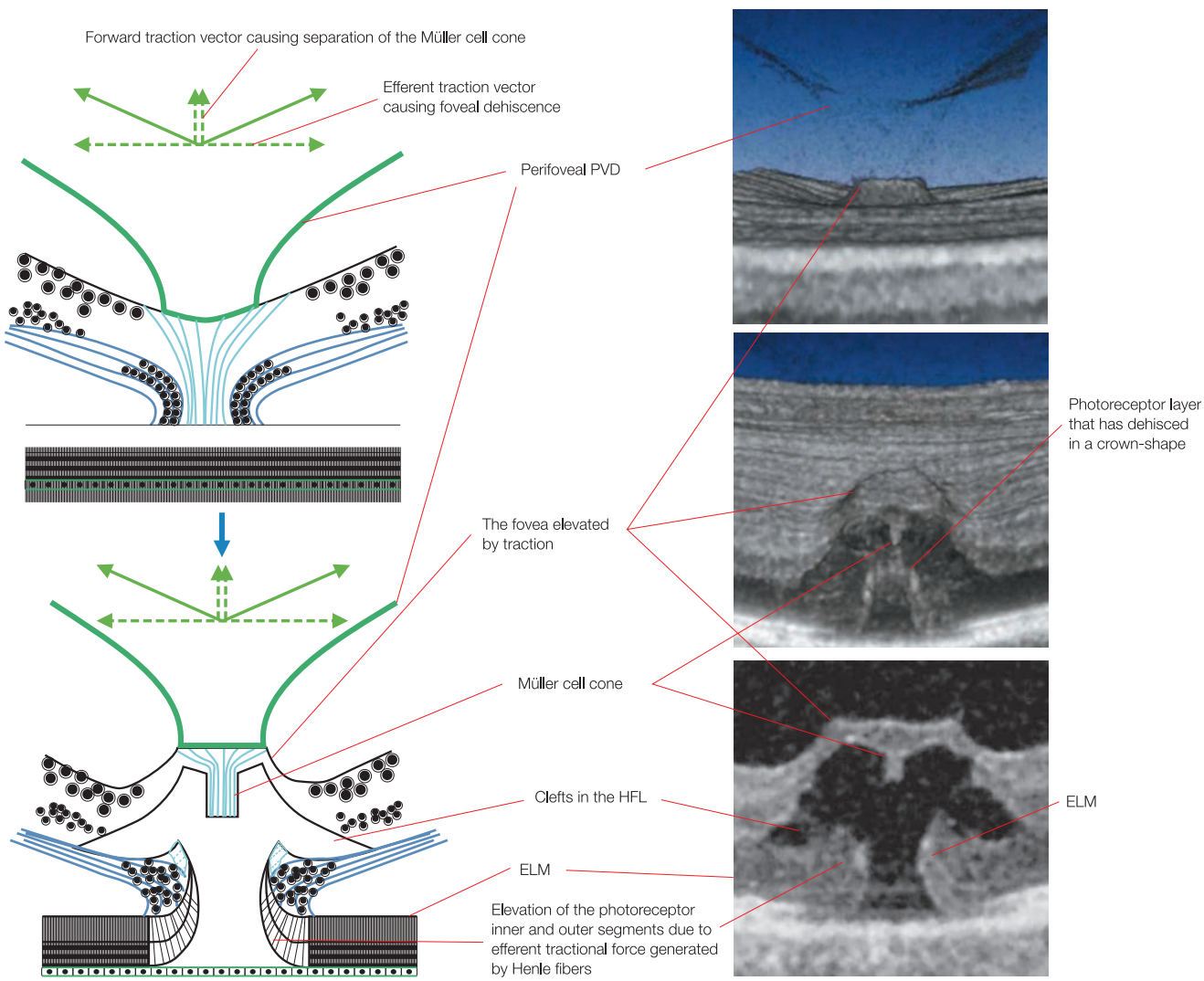

Fig. 2-9 Diagram indicating the foveal photoreceptor layer disruption
This diagram shows the involvement of the Müller cell cone in macular hole formation following the forward traction vector force generated by perifoveal PVD

Fig. 2-10 3D-OCT imaging indicating the foveal photoreceptor layer disruption
The Müller cell cone with dehiscence of the foveal photoreceptor cell layer; the surface of the fovea centralis is being pulled forward as a result of perifoveal PVD and the Muller cell cones appears over the disrupted photoreceptor layer at the umbo. (Modified according to Hangai M, et al. Three-dimensional imaging of macular holes with high-speed optical coherence tomography. Ophthalmology. 2007; 114: 763–773)

References

1) McCannel CA, Ensminger JL, Diehl NN, et al. Population-based incidence of macular holes. Ophthalmology. 2009; 116:1366–1369.
2) Gass JD. Idiopathic senile macular hole. Its early stages and pathogenesis. Arch Ophthalmol. 1988; 106:629–639.
3) Kelly NE, Wendel RT. Vitreous surgery for idiopathic macular holes. Results of a pilot study. Arch Ophthalmol. 1991; 109:654–659.
4) Gass JD. Reappraisal of biomicroscopic classification of stages of development of a macular hole. Am J Ophthalmol. 1995; 119:752–759.
5) Hee MR, Puliafito CA, Wong C, et al. Optical coherence tomography of macular holes. Ophthalmology. 1995; 102:748–756.
6) Gaudric A, Haouchine B, Massin P, et al. Macular hole formation:new data provided by optical coherence tomography. Arch Ophthalmol. 1999; 117:744–751.
7) Kishi S, Takahashi H. Three-dimensional observations of developing macular holes. Am J Ophthalmol. 2000; 130:65–75.
8) Haouchine B, Massin P, Gaudric A. Foveal pseudocyst as the first step in macular hole formation:a prospective study by optical coherence tomography. Ophthalmology. 2001; 108:15–22.
9) Hangai M, Ojima Y, Gotoh N, et al. Three-dimensional imaging of macular holes with high-speed optical coherence tomography. Ophthalmology. 2007; 114:763–773.
10) Takahashi A, Nagaoka T, Ishiko S, et al. Foveal anatomic changes in a progressing stage 1 macular hole documented by spectral-domain optical coherence tomography. Ophthalmology. 2010; 117:806–810.
11) Uchino E, Uemura A, Ohba N. Initial stages of posterior vitreous detachment in healthy eyes of older persons evaluated by optical coherence tomography. Arch Ophthalmol. 2001; 119:1475–1479.
12) Kishi S, Hagimura N, Shimizu K. The role of the premacular liquefied pocket and premacular vitreous cortex in idiopathic macular hole development. Am J Ophthalmol. 1996; 122:622–628.
13) Kumagai K, Hangai M, Larson E, et al. Vitreoretinal interface and foveal deformation in asymptomatic fellow eyes of patients with unilateral macular holes. Ophthalmology. 2011; 118:1638–1644.
14) Haouchine B, Massin P, Tadayoni R, et al. Diagnosis of macular pseudoholes and lamellar macular holes by optical coherence tomography. Am J Ophthalmol. 2004; 138:732-739.
15) Zambarakji HJ, Schlottmann P, Tanner V, et al. Macular microholes:pathogenesis and natural history. Br J Ophthalmol. 2005; 89:189–193.
16) Chan A, Duker JS, Schuman JS, et al. Stage 0 macular holes:observations by optical coherence tomography. Ophthalmology. 2004; 111:2027–2032.
17) Takahashi H, Kishi S. Optical coherence tomography images of spontaneous macular hole closure. Am J Ophthalmol. 1999; 128:519–520.
18) Tadayoni R, Massin P, Haouchine B, et al. Spontaneous resolution of small stage 3 and 4 full-thickness macular holes viewed by optical coherence tomography. Retina. 2001; 21:186–189.
19) Freund KB, Ciardella AP, Shah V, et al. Optical coherence tomography documentation of spontaneous macular hole closure without posterior vitreous detachment. Retina. 2002; 22:506–509.
20) Imai M, Ohshiro T, Gotoh T, et al. Spontaneous closure of stage 2 macular hole observed with optical coherence tomography. Am J Ophthalmol. 2003; 136:187–188.
21) Abe S, Fujiwara T, Yoshitomi T. Spontaneous closure of a stage 2 macular hole without detachment of the posterior hyaloid. Jpn J Ophthalmol. 2010; 54:633–635.
22) Kokame GT, McCauley MB. Spontaneous reopening of a spontaneously closed macular hole. Am J Ophthalmol. 2002; 133:280–282.
23) Scott IU, Moraczewski AL, Smiddy WE, et al. Long-term anatomic and visual acuity outcomes after initial anatomic success with macular hole surgery. Am J Ophthalmol. 2003; 135:633–640.
24) Da Mata AP, Burk SE, Foster RE, et al. Long-term follow-up of indocyanine green-assisted peeling of the retinal internal limiting membrane during vitrectomy surgery for idiopathic macular hole repair. Ophthalmology. 2004; 111:2246–2253.
25) Haritoglou C, Reiniger IW, Schaumberger M, et al. Five-year follow-up of macular hole surgery with peeling of the internal limiting membrane:update of a prospective study. Retina. 2006; 26:618–622.
26) Kumagai K, Furukawa M, Ogino N, et al. Long-term outcomes of internal limiting membrane peeling with and without indocyanine green in macular hole surgery. Retina. 2006; 26:613–617.
27) Passemard M, Yakoubi Y, Muselier A, et al. Long-term outcome of idiopathic macular hole surgery. Am J Ophthalmol. 2010; 149:120–126.
28) Meng Q, Zhang S, Ling Y, et al. Long-term anatomic and visual outcomes of initially closed macular holes. Am J Ophthalmol. 2011; 151:896–900.
29) Ezra E, Munro PM, Charteris DG, et al. Macular hole opercula. Ultrastructural features and clinicopathological correlation. Arch Ophthalmol. 1997; 115:1381–1387.
30) Sano M, Shimoda Y, Hashimoto H, et al. Restored photoreceptor outer segment and visual recovery after macular hole closure. Am J Ophthalmol. 2009; 147:313–318.
31) Inoue M, Watanabe Y, Arakawa A, et al. Spectral-domain optical coherence tomography images of inner/outer segment junctions and macular hole surgery outcomes. Graefes Arch Clin Exp Ophthalmol. 2009; 247:325–330.
32) Oh J, Smiddy WE, Flynn HW Jr, et al. Photoreceptor inner/outer segment defect imaging by spectral domain OCT and visual prognosis after macular hole surgery. Invest Ophthalmol Vis Sci. 2010; 51:1651–1658.
33) Wakabayashi T, Fujiwara M, Sakaguchi H, et al. Foveal microstructure and visual acuity in surgically closed macular holes:spectral-domain optical coherence tomographic analysis. Ophthalmology. 2010; 117:1815–1824.
34) Ooka E, MitamuraY, Baba T, et al. Foveal microstructure on spectral-domain optical coherence tomographic images and visual function after macular hole surgery. Am J Ophthalmol. 2011; 152:283–290.e1.
35) Bottoni F, De Angelis S, Luccarelli S, et al. The dynamic healing process of idiopathic macular holes after surgical repair:a spectral-domain optical coherence tomography study. Invest Ophthalmol Vis Sci. 2011; 52:4439–4446.
36) Tadayoni R, Paques M, Massin P, et al. Dissociated optic nerve fiber layer appearance of the fundus after idiopathic epiretinal membrane removal. Ophthalmology. 2001; 108:2279–2283.
37) Mitamura Y, Suzuki T, Kinoshita T, et al. Optical coherence tomographic findings of dissociated optic nerve fiber layer appearance. Am J Ophthalmol. 2004; 137:1155–1156.
38) Ito Y, Terasaki H, Takahashi A, et al. Dissociated optic nerve fiber layer appearance after internal limiting membrane peeling for idiopathic macular holes. Ophthalmology. 2005; 112:1415–1420.
39) Yamada E. Some structural features of the fovea centralis in the human retina. Arch Ophthalmol. 1969; 82:151–159.
40) Gass JD. Müller cell cone, an overlooked part of the anatomy of the fovea centralis:hypotheses concerning its role in the pathogenesis of macular hole and foveomacular retinoschisis. Arch Ophthalmol. 1999; 117:821–823.
41) Spaide RF. Dissociated optic nerve fiber layer appearance after internal limiting membrane removal is inner retinal dimpling. Retina. 2012; 32:1719–26.
42) Nukada K, Hangai M, Ooto S, et al. Tomographic features of macula after successful macular hole surgery. Invest Ophthalmol Vis Sci. 2013;54:2417–28.

Case 1 Physiological PVD: Flattening of foveal depression

A 68-year-old male, OS, BCVA 0.5

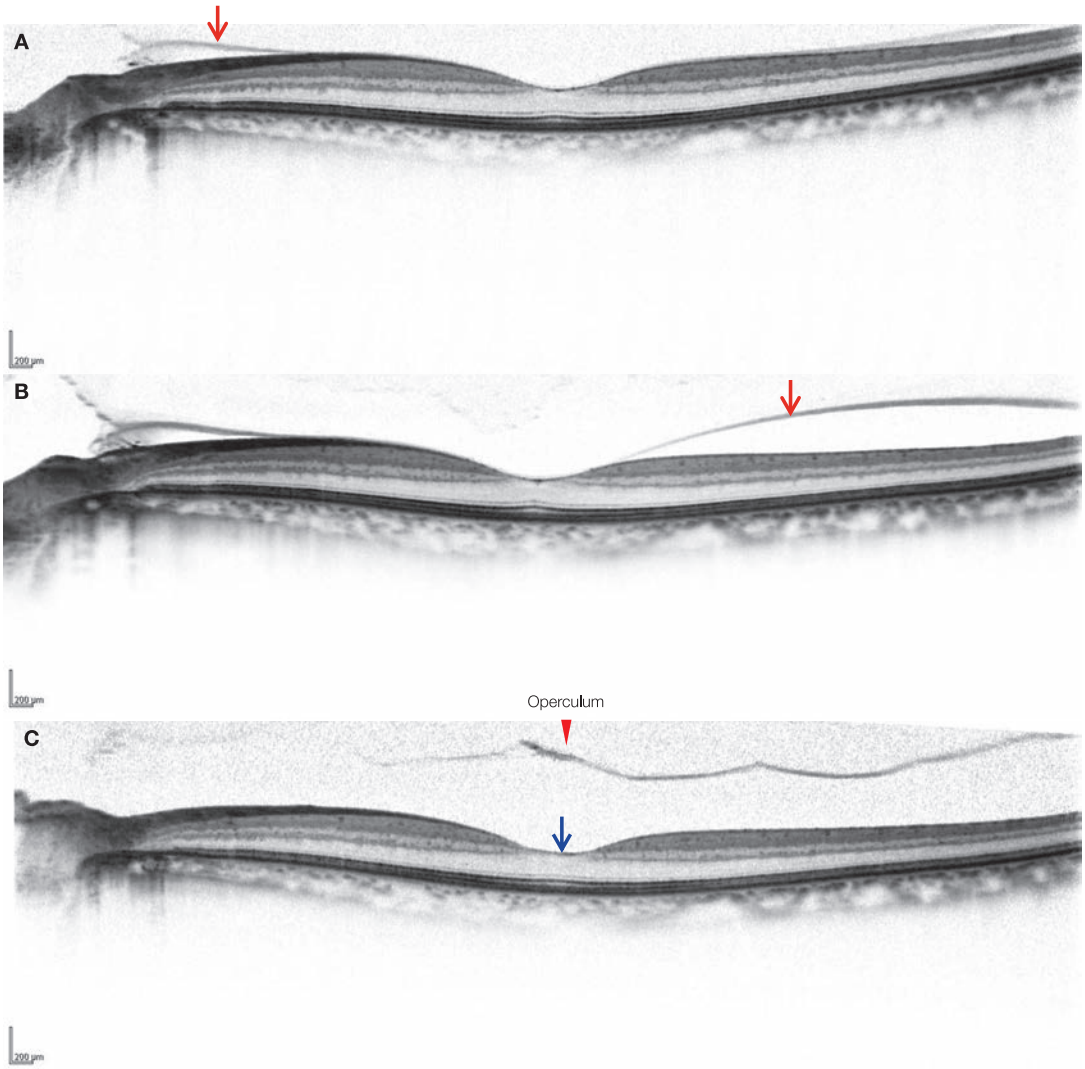

A: OCT horizontal scan of the left eye: at initial diagnosis. PVD (➔) has not yet extended to the macular area. **B:** OCT horizontal scan of the same area of the left eye: 4 months after initial diagnosis. Progression of macular PVD is evident in the temporal macula. **C:** OCT horizontal scan of the same area of the left eye: 7 months after initial diagnosis. Macular PVD is complete and an operculum appears (▶) have formed. Foveal depressions have flattened (➔)

Image interpretation points

Over the course of physiological PVD, foveal contour abnormalities may remain or appears once the posterior vitreous cortex and fovea have separated and macular PVD is complete. This case involves the fellow eye of a right eye with Stage 3 macular hole. Foveal depression have flattened. Left eye best-corrected visual acuity remains unchanged at 1.2. Abnormalities may also remain inside the fovea.

Case 2 Idiopathic macular holes: Progression from stage 1 (cystoid space type) to stage 2

A 53-year-old female, OS, BCVA 1.2 at the initial diagnosis, and 0.3 six months later

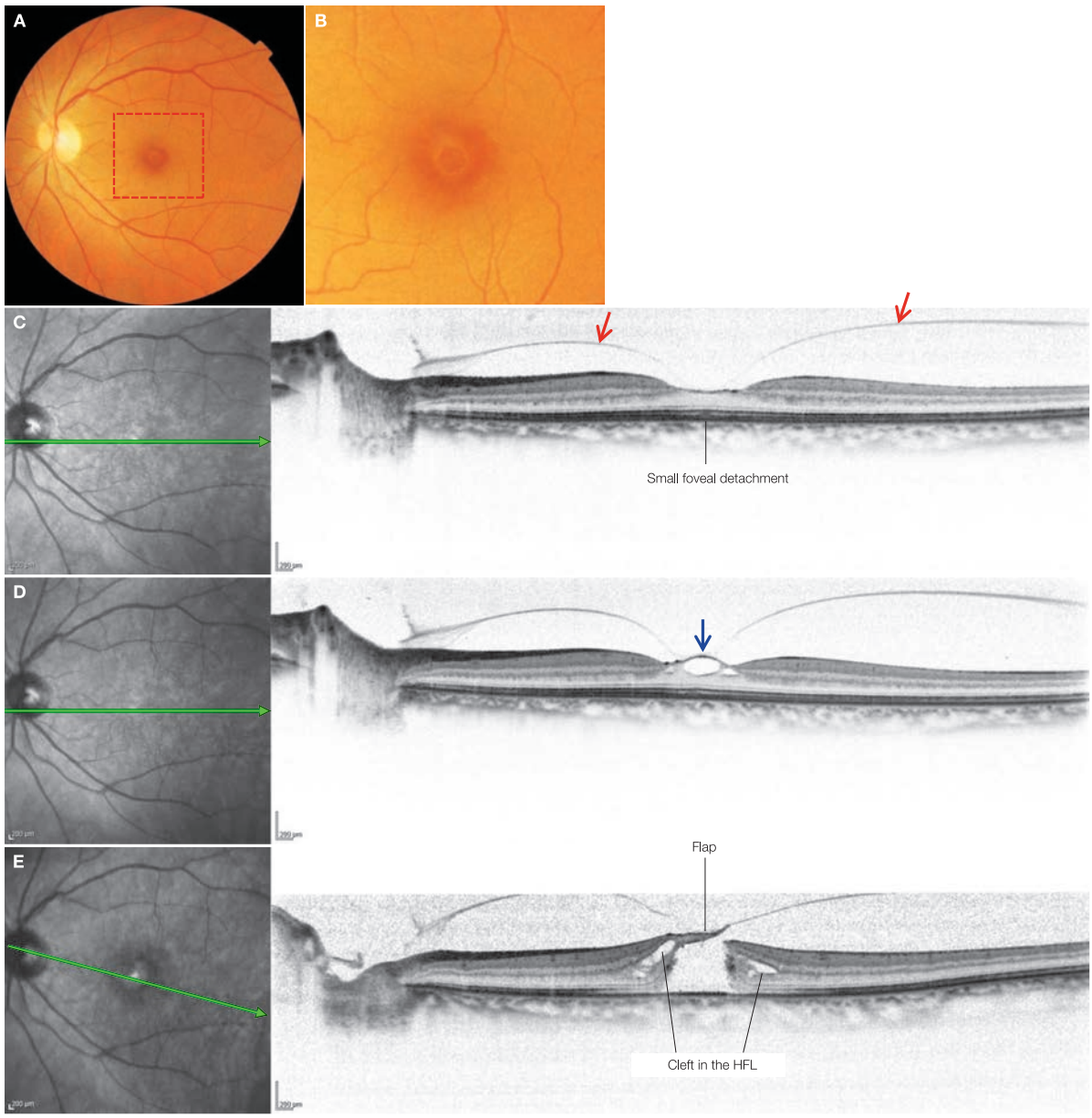

A: Color fundus photograph in the left eye, **B:** Enlarged version of A [red dashed box]: at initial diagnosis. A yellow ring can be seen in the fovea centralis. **C:** IR + OCT horizontal scan of the left eye: at initial diagnosis. Perifoveal PVD developed, the posterior vitreous cortex (➔) has pulled the fovea centralis forward and foveal depressions have been flattened. **D:** IR + OCT horizontal scan of the left eye: 4 months after initial diagnosis. Foveal cystoid space (➔) is formed. Best-corrected visual acuity is unchanged. **E:** IR + OCT horizontal scan of the left eye: 6 months after initial diagnosis. Progression to Stage 2 macular hole. Best-corrected visual acuity to 0.3

Image interpretation points

This is the fellow eye of a patient with a Stage 3 macular hole. Progression from a Stage 1 to Stage 2 macular hole was observed. At initial diagnosis, perifoveal PVD had developed, foveal depression had been flattened and small foveal detachments were observed. A cystoid space formed 4 months after initial diagnosis; 6 months after initial diagnosis the anterior wall of the cystoid space separated and the foveal photoreceptor layer dehisced into a full-thickness macular hole. Visual acuity did not decrease with the formation of cystoid space or small foveal detachment, but did decline with foveal dehiscence. The incidence of a macular hole in macular hole fellow eyes is 13–22%.

Case 3 Idiopathic macular hole: Stage 1 foveal cystoid space formation type

A 64-year-old female, OS, BCVA 1.2

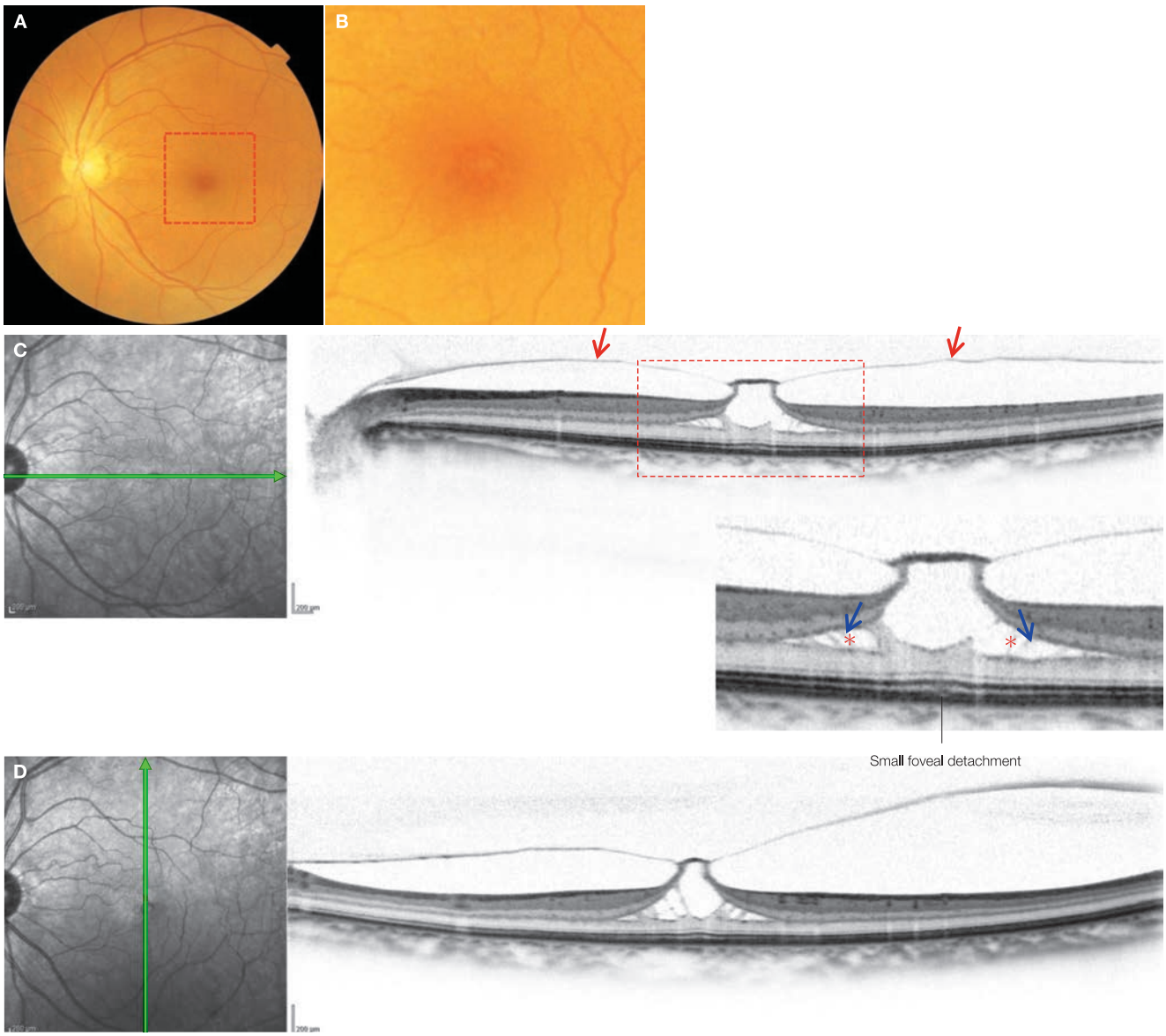

A: Color fundus photograph in the left eye, **B:** Enlarged version of A [red dashed box]: yellow ring can be seen in the fovea centralis, **C:** IR + OCT horizontal scan of the left eye + enlarged version [red dashed box]: Perifoveal PVD has been formed. The posterior vitreous cortex (→) has pulled the fovea forward, forming the cystoid space and clefts in the HFL (*). The anterior wall of the cystoid space has been lifted high up. Small foveal detachments can be seen. A columnar structure (→) thought to be Müller cells is seen in the clefts of HFL. Centrifugal forward traction towards the fovea centralis is transmitted via the columnar structure to the foveal photoreceptor layer. **D:** IR + OCT vertical scan of the left eye: same findings as in C

Image interpretation points

This is a stage 1 macular hole where a foveal cystoid space and HFL clefts are formed. Perifoveal PVD causes the elevation of the anterior wall of the cystoid space. A small foveal detachment is observed as a small protrusion of the COST line. No visual acuity decline was seen at initial diagnosis and visual acuity remained good for 6 months after initial diagnosis, if the anterior wall separation occurs together with the foveal photoreceptor dehiscence, this eye will progress to a full-thickness macular hole.

Case 4 Idiopathic macular hole: Stage 1 foveal detachment type

A 62-year-old female, OS, BCVA 0.5

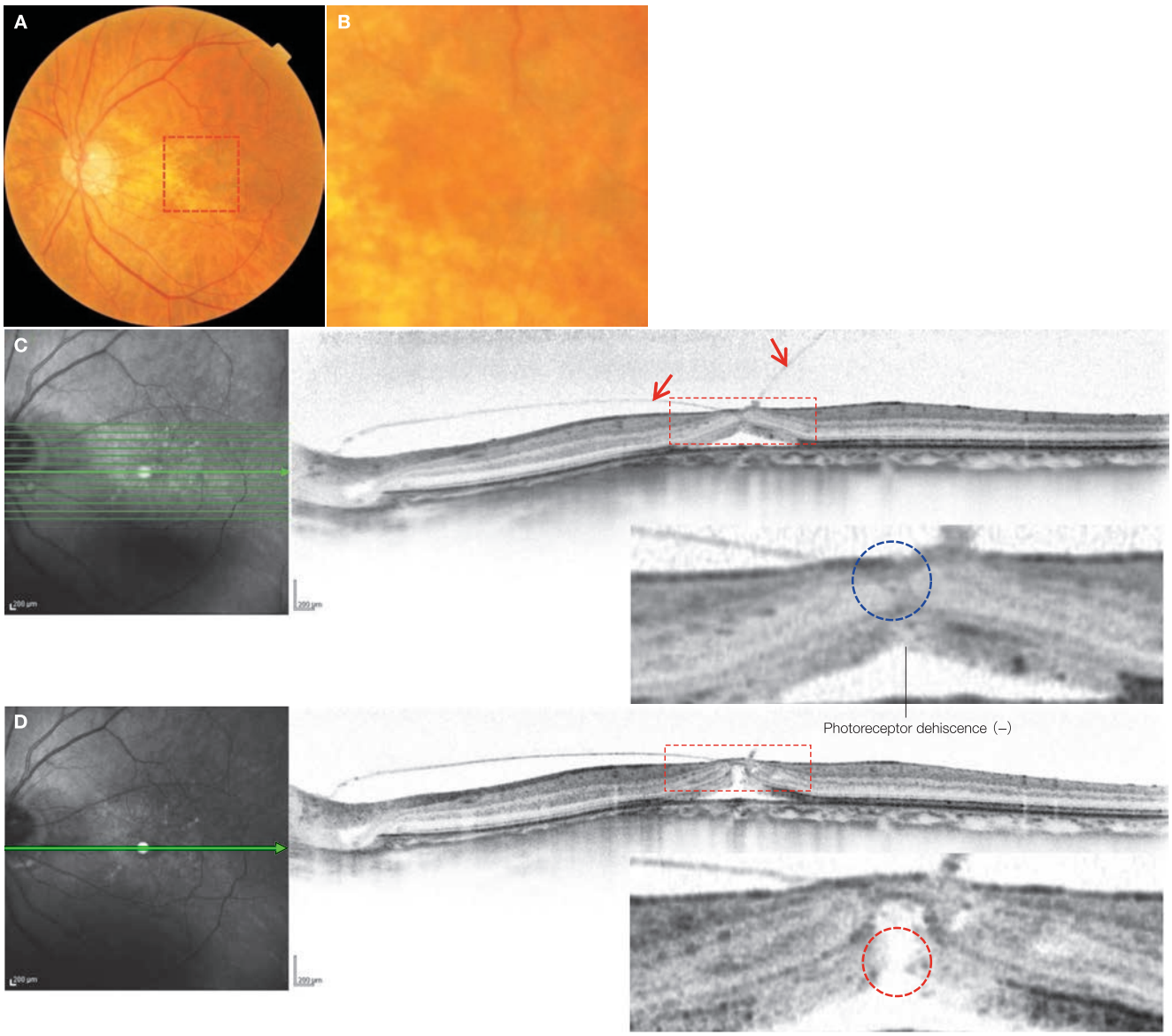

A: Color fundus photograph in the left eye: at initial diagnosis, **B:** Enlarged version of A [red dashed box]: Foveal abnormalities are obscured. **C:** IR + OCT horizontal scan of the left eye + enlarged version [red dashed box]: at initial diagnosis. Perifoveal PVD has developed, the posterior vitreous cortex (➔) has pulled the fovea forward and foveal detachment can be seen. No photoreceptor dehiscence visible, but enhanced reflectivity can be seen in the area corresponding to the Müller cell cone (blue dashed circle). **D:** IR + OCT horizontal scan of the left eye + enlarged version [red dashed box]: 1 month after initial diagnosis. Photoreceptor dehiscence has occurred (red dashed circle). Best-corrected visual acuity declined to 0.3

Image interpretation points

A stage 1 macular hole where foveal photoreceptor dehiscence was preceded by foveal detachment. There are also cases where photoreceptor layer dehiscence progresses directly from foveal detachment without foveal cystoid space formation. It is interesting that the area corresponding to the Müller cell cone becomes highly reflective before the development of photoreceptor dehiscence.

Case 5 Idiopathic macular hole: Stage 1 photoreceptor dehiscence type

A 60-year-old female, OS, BCVA 0.5

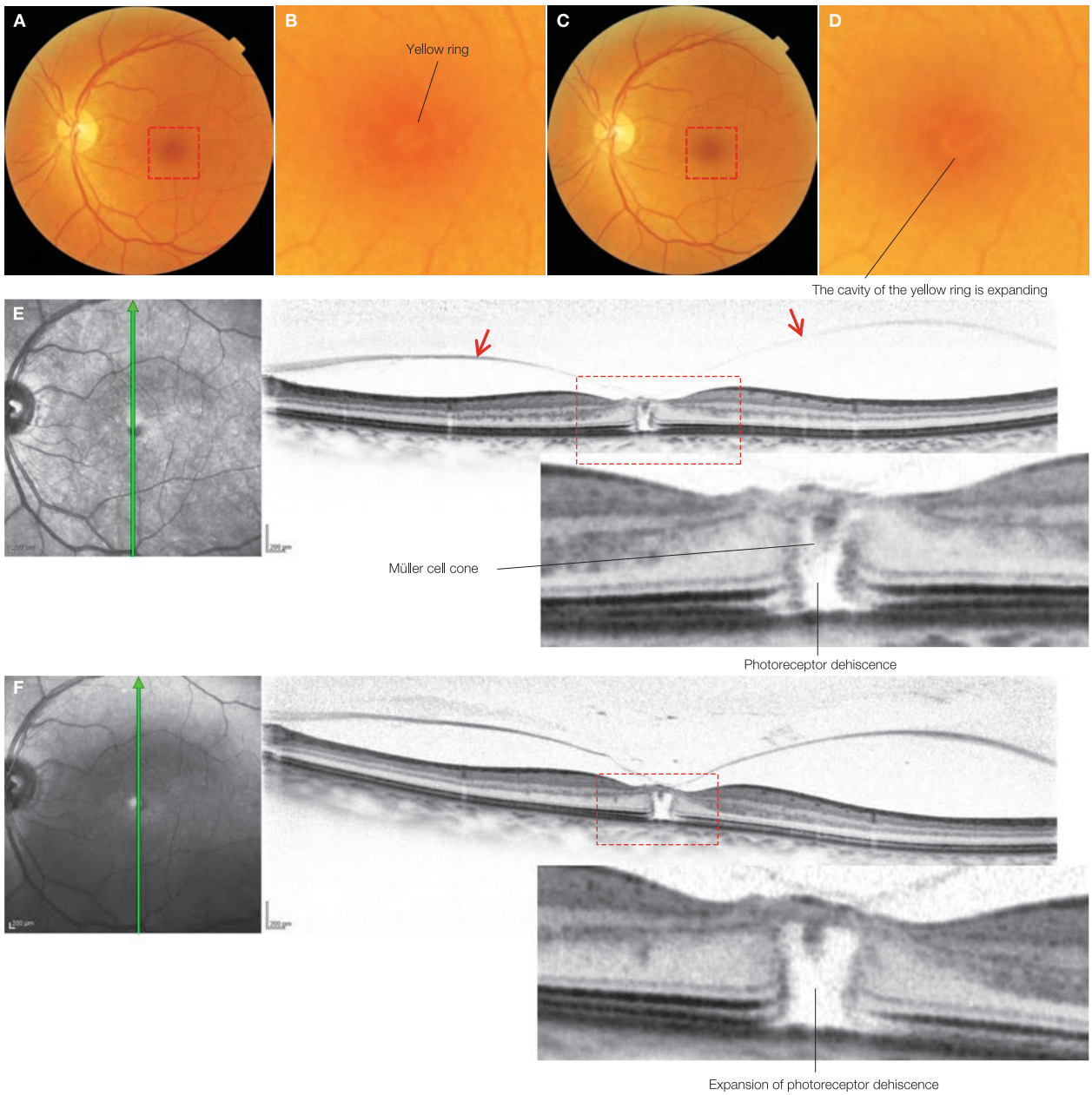

A: Color fundus photograph in the left eye, **B:** Enlarged version of A [red dashed box]: at initial diagnosis. A yellow ring is visible. **C:** Color fundus photograph in the left eye, **D:** Enlarged version of C [red dashed box]: 1 month after initial diagnosis. **E:** IR + OCT horizontal scan of the left eye + enlarged version [red dashed box]: at initial diagnosis. Photoreceptor dehiscence has occurred and the Müller cell cone can be seen. The posterior vitreous cortex (➔) in perifoveal PVD is pulling the fovea forward. **F:** IR + OCT horizontal scan of the left eye + enlarged version [red dashed box]: 1 month after initial diagnosis. The Müller cell cone is still visible; this could almost be a scan of the same area as E, but with expansion of the macular hole. Best-corrected visual acuity is unchanged

Image interpretation points

This is a case of stage 1 macular holes where photoreceptor dehiscence has occurred without forming a foveal cystoid space or foveal detachment. Contraction of the Müller cell cone is mild, which could indicate that dehiscence is just ending. This is also supported by the observation that the macular hole appears to expand scans of the same area as soon as 1 month after initial diagnosis.

Case 6 Idiopathic macular hole: Stage 1 small foveal detachment type

A 64-year-old female, OD, BCVA 0.8

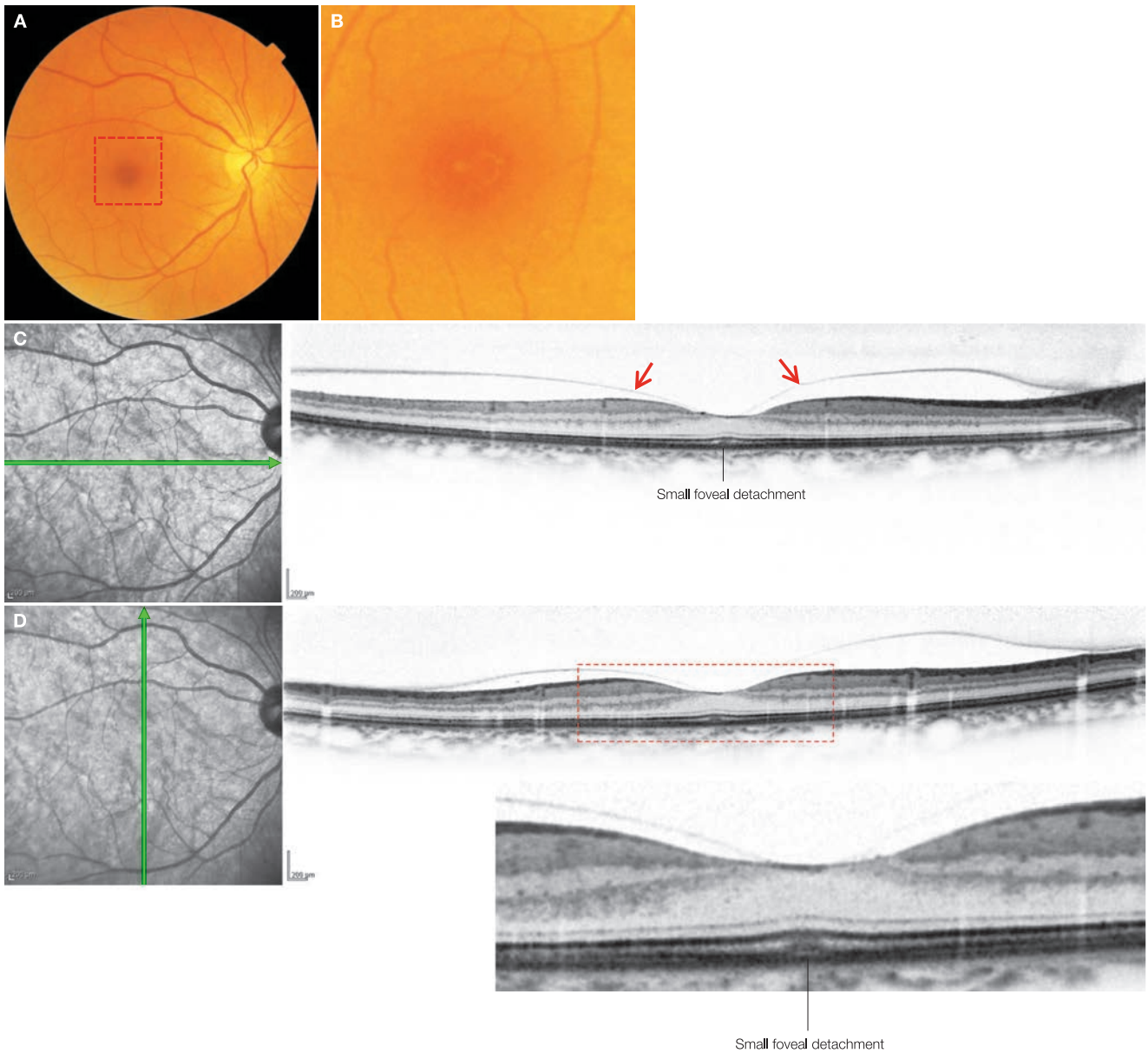

A: Color fundus photograph in the right eye, **B:** Enlarged version of A [red dashed box]: at initial diagnosis. A yellow ring can be seen in the fovea centralis. **C:** IR + OCT horizontal scan of the right eye: Perifoveal PVD has occurred, the posterior vitreous cortex (➔) has pulled the fovea centralis forward and foveal depression has flattened. Small foveal detachment, i.e., uplift of the foveal COST line and highly reflective foveal photoreceptor outer segment are seen. **D:** IR + OCT vertical scan of the right eye + enlarged version [red dashed box]: same findings as C

Image interpretation points

This is the case of a fellow eye of a patient with a stage 2 macular hole. The small protrusion in the COST line indicates the presence of small foveal detachment. Visual acuity impairment is mild. Visual acuity starts to decline once foveal dehiscence occurrs. These changes could be found because this is the fellow eye of a patient with a full-thickness macular hole.

Case 7 Idiopathic macular hole: A case just before progression from stage 1 to stage 2

A 61-year-old male, OS, BCVA 0.2

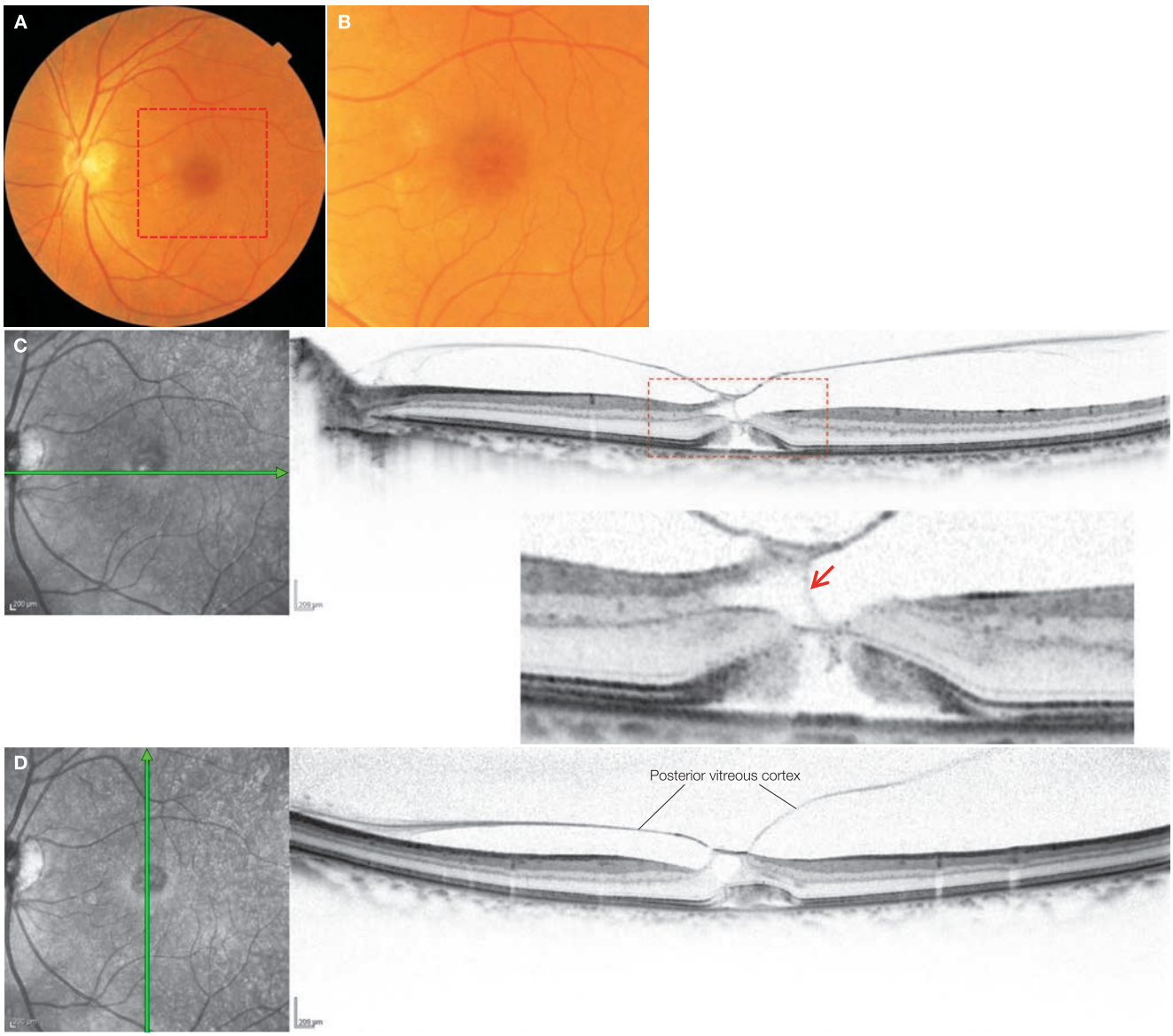

A: Color fundus photograph in the left eye, **B:** Enlarged version of A [red dashed box]: at initial diagnosis. An irregular-shaped yellow ring is visible. **C:** IR + OCT horizontal scan of the left eye + enlarged version [red dashed box]: Photoreceptor dehiscence has occurred and a flap-like elevation can be seen that is similar to the flap seen in a stage 2 macular hole, however, this macular hole is bridged by a moderately reflective thin membranous tissue connecting to the external limiting membrane. Tissue thought to be the Müller cell cone (→) can be seen in the center of the flap-like structure. Note the elongation of the photoreceptor outer segment in the elevated edge of the macular hole. **D:** IR + OCT vertical scan of the left eye: it is only evident that foveal detachment and a foveal cystoid space are present

Image interpretation points

This is a case of a stage 1 macular hole progressing to stage 2. Probably, the anterior wall of the cystoid space have separated and are changing into a flap. This has caused photoreceptor dehiscence and poor visual acuity. Usually, visual acuity impairment increases when photoreceptor dehiscence occurs.

Case 8 Idiopathic macular hole: Typical example of stage 2

A 62-year-old female, OS, BCVA 0.08

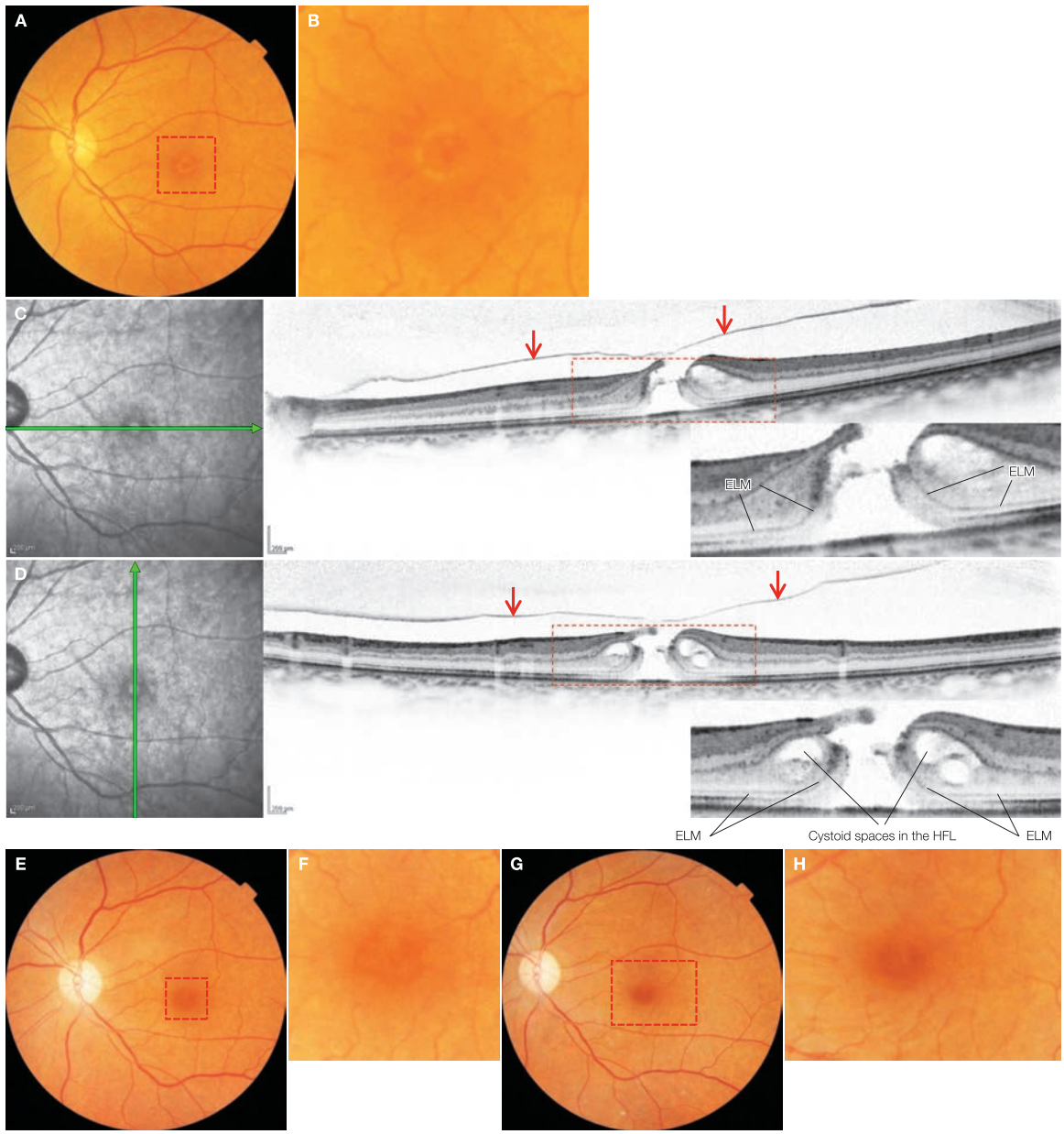

A: Color fundus photograph in the left eye, **B:** Enlarged version of A [red dashed box]: at initial diagnosis. A macular hole is with one-third the size of the optic disc diameter is seen. **C:** IR + OCT horizontal scan of the left eye + enlarged version [red dashed box], **D:** IR + OCT vertical scan + enlarged version [red dashed box]: A flaccid posterior vitreous cortex (➔) attached to the flap can be seen. The photoreceptor layer on the elevated edge of the macular hole (posterior medial to the ELM line) is preserved with few defects. **E:** Color fundus photograph in the left eye, **F: Enlarged version of** E [red dashed box]: 3 weeks after macular hole surgery. Macular hole closure can be seen. **G:** Color fundus photograph of the same eye, **H: Enlarged version of** G [red dashed box]: 6 months after surgery. Best-corrected visual acuity improved to 0.7. Dissociated optic nerve fiber layer (DONFL) appearance that was not evident 3 weeks after surgery have appeared
I: IR + OCT horizontal scan of the left eye + enlarged version [red dashed box], **J:** IR + OCT vertical scan of the left eye + enlarged version [red dashed box]: 3 weeks after surgery. Best-corrected visual acuity was 0.1. Disruption of the IS/OS at the fovea centralis and thinning of the outer nuclear layer can be seen. As the ELM approaches the RPE, indicating the significantly thin photoreceptor inner and outer segments. Defective damages to the inner retinal layers in the temporal macula are visible, although this area was not in contact with any instruments during surgery. No evident abnormalities are visible in the upper and lower retinal nerve fiber layer. **K:** IR + OCT horizontal scan of the left eye + enlarged version [red dashed box], **L:** IR + OCT vertical scan of the left eye + enlarged version [red dashed box]: 6 months after surgery. There is visible restoration of IS/OS line and COST line, and the thickness of the photoreceptor inner and outer segments has been re-instated. Nevertheless, the outer nuclear layer of the fovea centralis is still slightly thin. In addition to localized thinning of the macular upper and lower retinal nerve fiber layer consistent with DONFL appearance, there is also thinning throughout the macula compared with postoperative week 3. Particularly, temporal retinal thinning has progressed. Retinal nerve fiber layer reflectivity has disappeared and thinning is noticeable up to the ganglion cell layer.

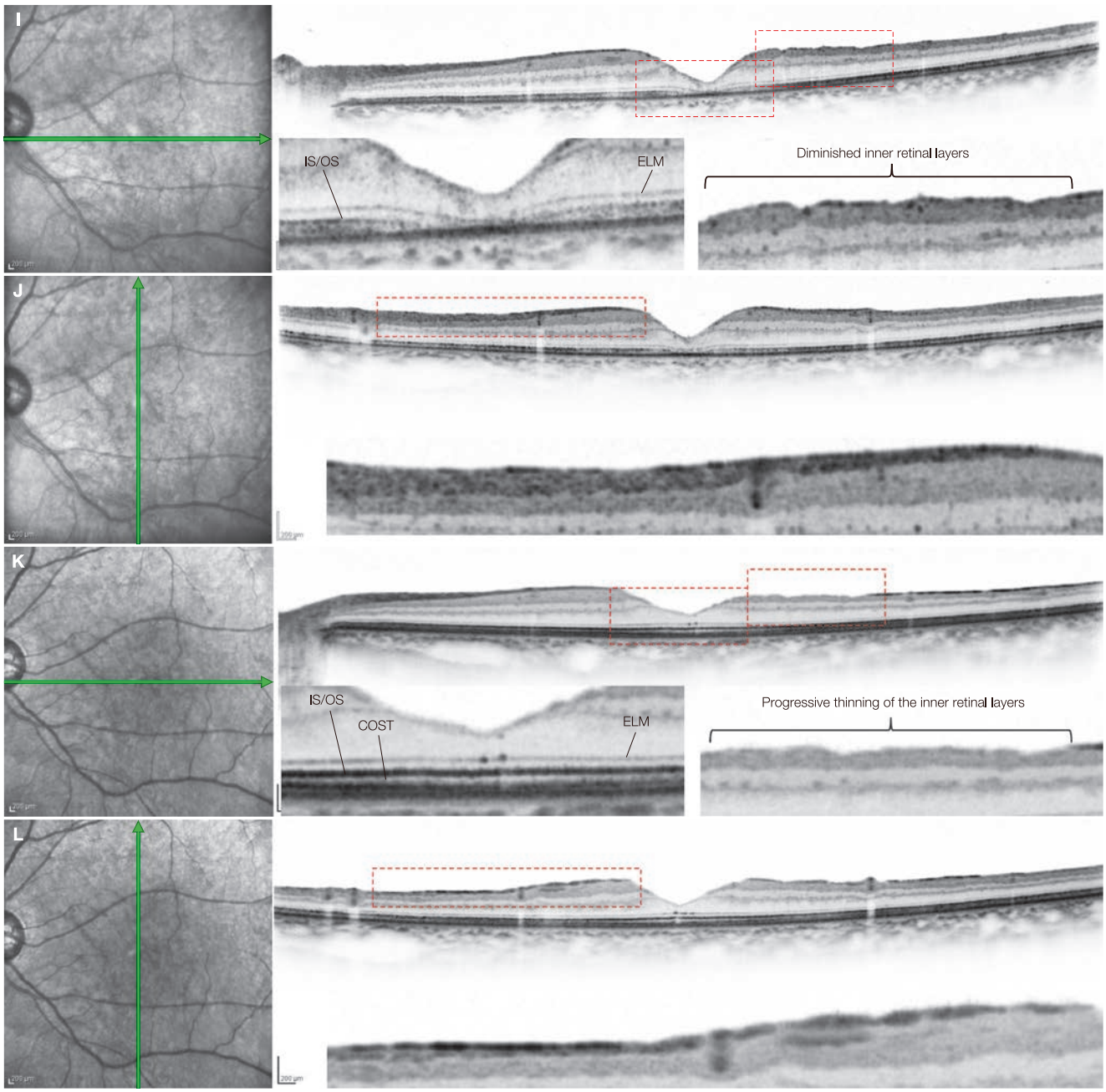

Image interpretation points

This is a typical stage 2 macular hole in which the flap is pulled forward by the posterior vitreous cortex. Cystoid spaces are formed in the HFL; the photoreceptor layer on the edge of the macular hole have been detached and elevated from the RPE. The degree of the photoreceptor damages can be estimated by the status of the photoreceptor inner and outer segments beneath the ELM line of the elevated area. In this case, there are few defects in photoreceptor inner and outer segments and the good visual acuity prognosis is expected.

Immediately after surgery, features indicating foveal photoreceptor cell damages such as disruption of the IS/OS and COST lines as well as the approach of the ELM line to the RPE can be seen. However, 6 months after surgery these abnormal findings have disappeared and each line has been restored. Nevertheless the foveal outer nuclear layer remains thinned. These 3 lines are useful in knowing the extent of the foveal photoreceptor cell damages, but it should be kept in mind that restoration may occur. DONFL appearance not seen immediately after surgery are visible in postoperative month 1–6; note the diffuse thinning in the retinal nerve fiber layer in the upper and lower parts of the macula, particularly at the DONFL sites. There is significant thinning of the temporal macula up to the ganglion cell layer. This defect is thought to be due to internal limiting membrane peeling.

Case 9 Idiopathic macular hole: Postoperative course for macular hole closure under gas tamponade

A 65-year-old female, OD, BCVA 0.2

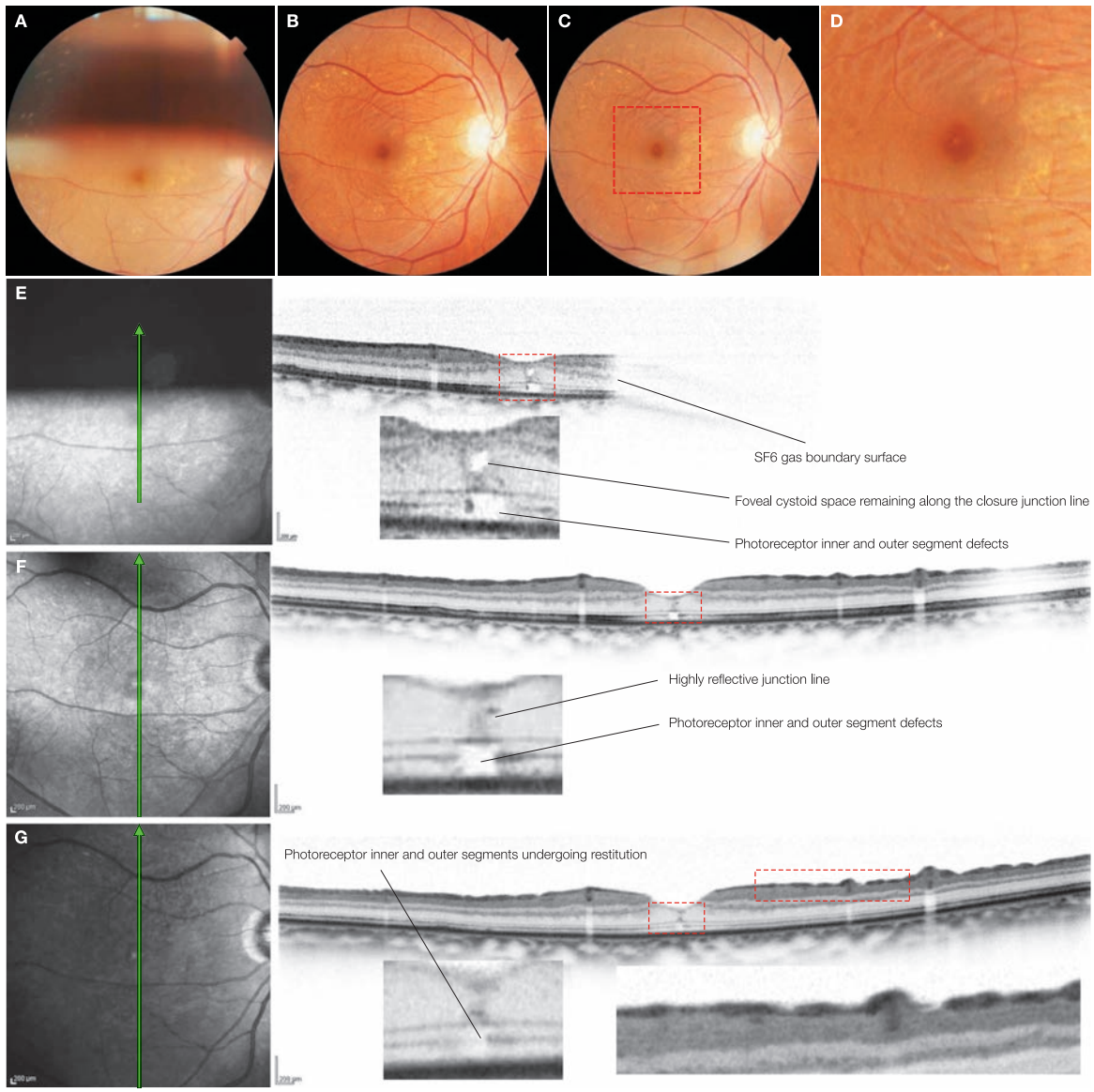

A: Color fundus photograph in the right eye: 1 week after surgery. Macular hole closure has been achieved. SF_6 gas remains. **B:** Color fundus photograph in the right eye: 1 month after surgery. Best-corrected visual acuity has improved to 0.4. Numerous arcuate striae with slightly darker color, so-called DONFL appearance, can be seen. **C:** Color fundus photograph in the right eye, **D:** Enlarged version of C [red dashed box]: 6 months after surgery. Best-corrected visual acuity is 0.4. DONFL appearance remains. **E:** IR + OCT vertical scan of the right eye + enlarged version [red dashed box]: 1 week after surgery. The macular hole have closed, but a foveal cystoid space and photoreceptor inner and outer segment defects can be seen along the closure junction line. **F:** IR + OCT vertical scan of the right eye + enlarged version [red dashed box]: The cystoid space have disappeared, and high reflectivity can be seen at the junction line in the foveal outer nuclear layer. Photoreceptor inner and outer segment defects remain. Retinal nerve fiber layer defects consistent with the arcuate striae in DONFL appearance can be seen. **G:** IR + OCT vertical scan of the right eye + enlarged version [red dashed box]: 6 months after surgery. Foveal photoreceptor inner and outer segment defects appear to have been reduced.

Image interpretation points

The macular holes are thought to have closed in 1 day after surgery. Despite closure, there are cystoid spaces, photoreceptor IS/OS defects in the junction line, and incomplete restoration of the foveal contour. This may account for the risk of macular hole reopening that increases when the gas tamponade treatment period was shortened. It takes time for photoreceptor inner and outer segment defects to disappear. Interpretation of the OCT features corresponding to DONFL appearance is addressed in the next page..

Case 9 DONFL appearance

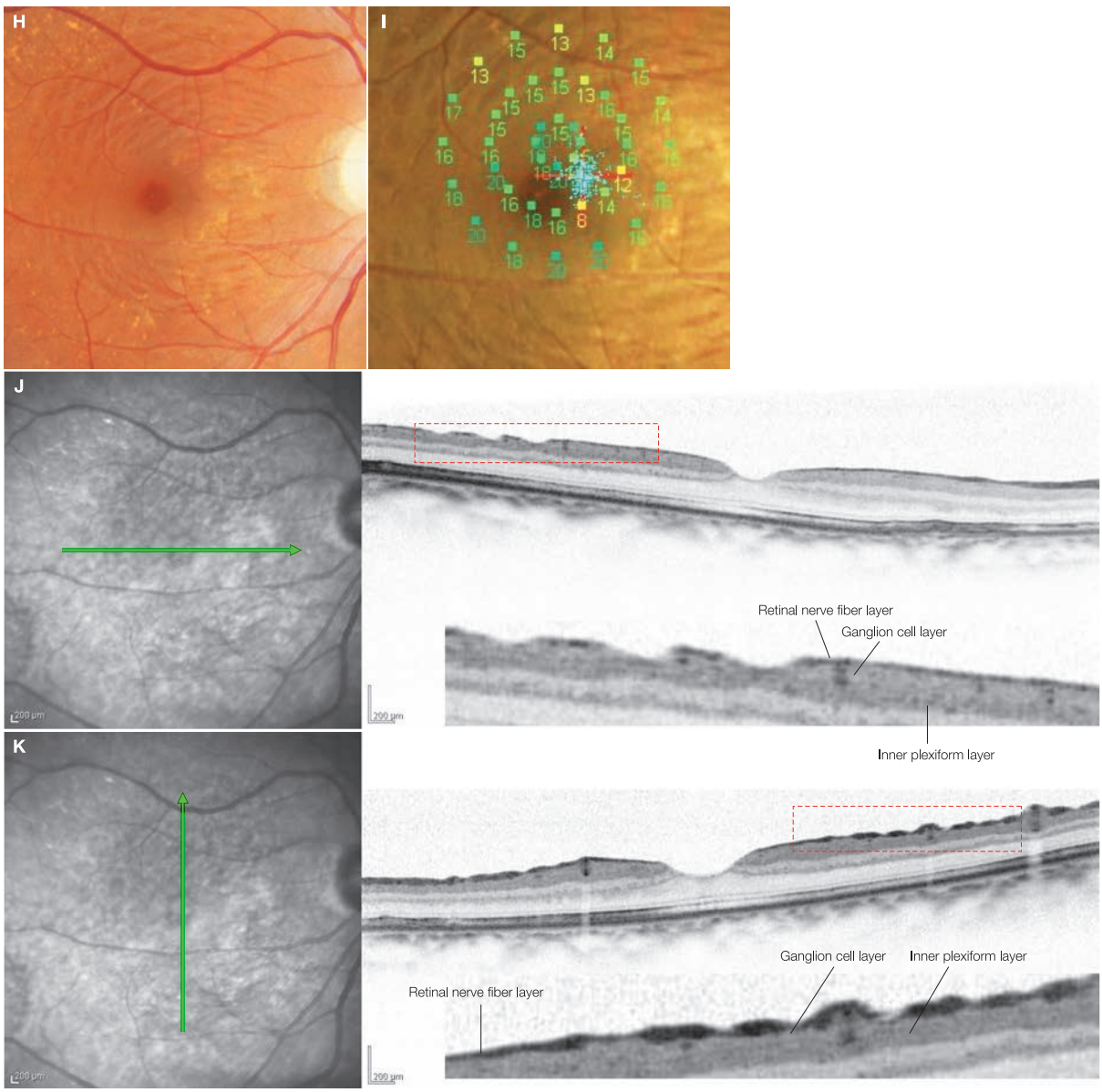

H: Color fundus photograph in the right eye: 5 months after surgery. DONFL appearance can be seen over the macular area where internal limiting membrane peeling was performed. **I:** Microperimetry-1 in the right eye: 5 months after surgery. Several points where visual sensitivity has declined to 13 dB or less are detected even outside the fovea. **J:** IR + OCT horizontal scan of right eye + enlarged version [red dashed box]: Note that the defects of the inner retinal layers in the temporal macula corresponding to the arcuate striae extend deeper than the retinal nerve fiber layer. **K:** IR + OCT vertical scan of the right eye + enlarged version [red dashed box]: Thinning of the retinal nerve fiber layer can be seen in both the superior and inferior areas of DONFL appearance.

Image interpretation points

This page shows the OCT images of DONFL appearance. While most areas of DONFL appearance show only retinal nerve fiber layer defects or thinning on a vertical scan through the fovea, the temporal areas of DONFL appearance show defects from the retinal nerve fiber layer to the ganglion cell layer and sometimes the inner plexiform layer. Since the temporal macula was not in contact with any instruments during surgery, these abnormal findings are thought to be due to inner limiting membrane peeling. In this particular case, the microperimety test points were set as dense as possible and a decline in retinal sensitivity was identified on several points. However, the sites with deep retinal defects are too small compared to the test point distribution in standard visual field and microperimetry testing to be detected by the testing.

Case 10 Idiopathic macular hole: Postoperative course for macular hole closure

Left eye of a 58-year-old female with vision corrected to 0.3

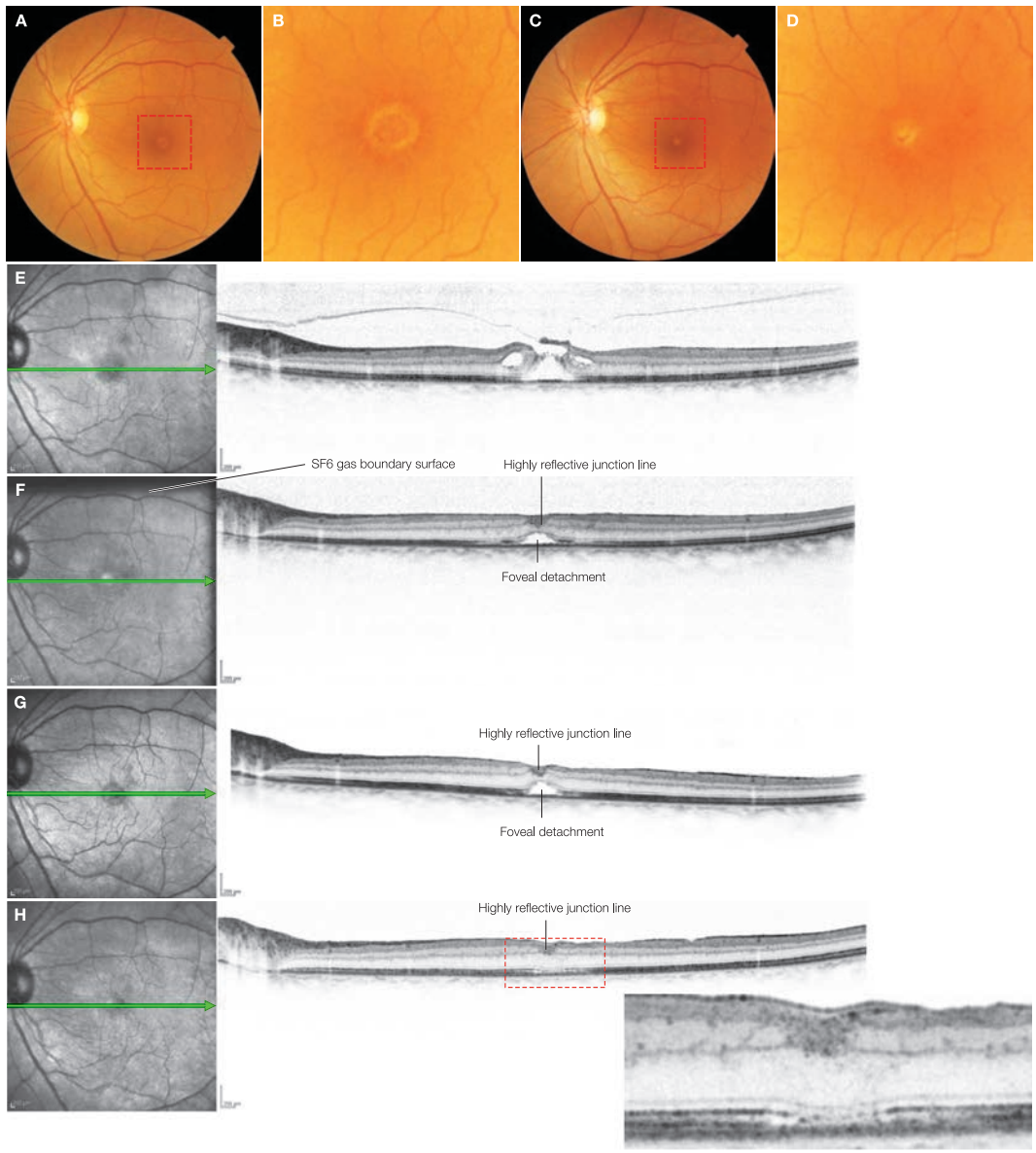

A: Color fundus photograph in the left eye, **B:** Enlarged version of A [red dashed box]: at initial diagnosis. A macular hole surrounded by a fluid cuff. **C:** Color fundus photograph in the left eye, **D:** Enlarged version of C [red dashed box]: 2 months after surgery. Best-corrected visual acuity has improved to 0.7. The macular hole has closed and a white opacity remains in the fovea centralis. **E:** IR + OCT horizontal scan of left eye: before surgery. A stage 2 macular hole. **F:** IR + OCT horizontal scan of the left eye: 9 days after surgery. The macular hole has closed, but foveal detachment remains. A part of SF_6 gas remains. High reflectivity can be seen at the junction line. **G:** IR + OCT horizontal scan of the left eye: 2 months after surgery. Foveal detachment still remains. **H:** IR + OCT horizontal scan of the left eye + enlarged version [red dashed box]: 5 months after surgery. Best-corrected visual acuity has improved to 0.7. Foveal detachment has disappeared. High reflectivity remains at the junction line. Thin membranous structure is seen on the surface of the closed macular hole. The photoreceptor outer segment is still thin.

Image interpretation points

A macular hole is thought to have closed 1 day after surgery; however, foveal detachment sometimes remains over 3 months after closure was achieved. Photoreceptor layer restitution also takes several months. Scarring formed by the migration of glial cells is thought to be involved in macular hole closure. Foveal findings 5 months after surgery revealed that thin membranous structure had formed in front of the foveal retinal nerve fiber layer. This suggests that glial cell migration results in the formation of a cellular fibrous membrane, which may be involved in macular hole closure.

Case 11 Idiopathic macular hole: Typical example of stage 3

A 65-year-old female, OS, BCVA 0.07

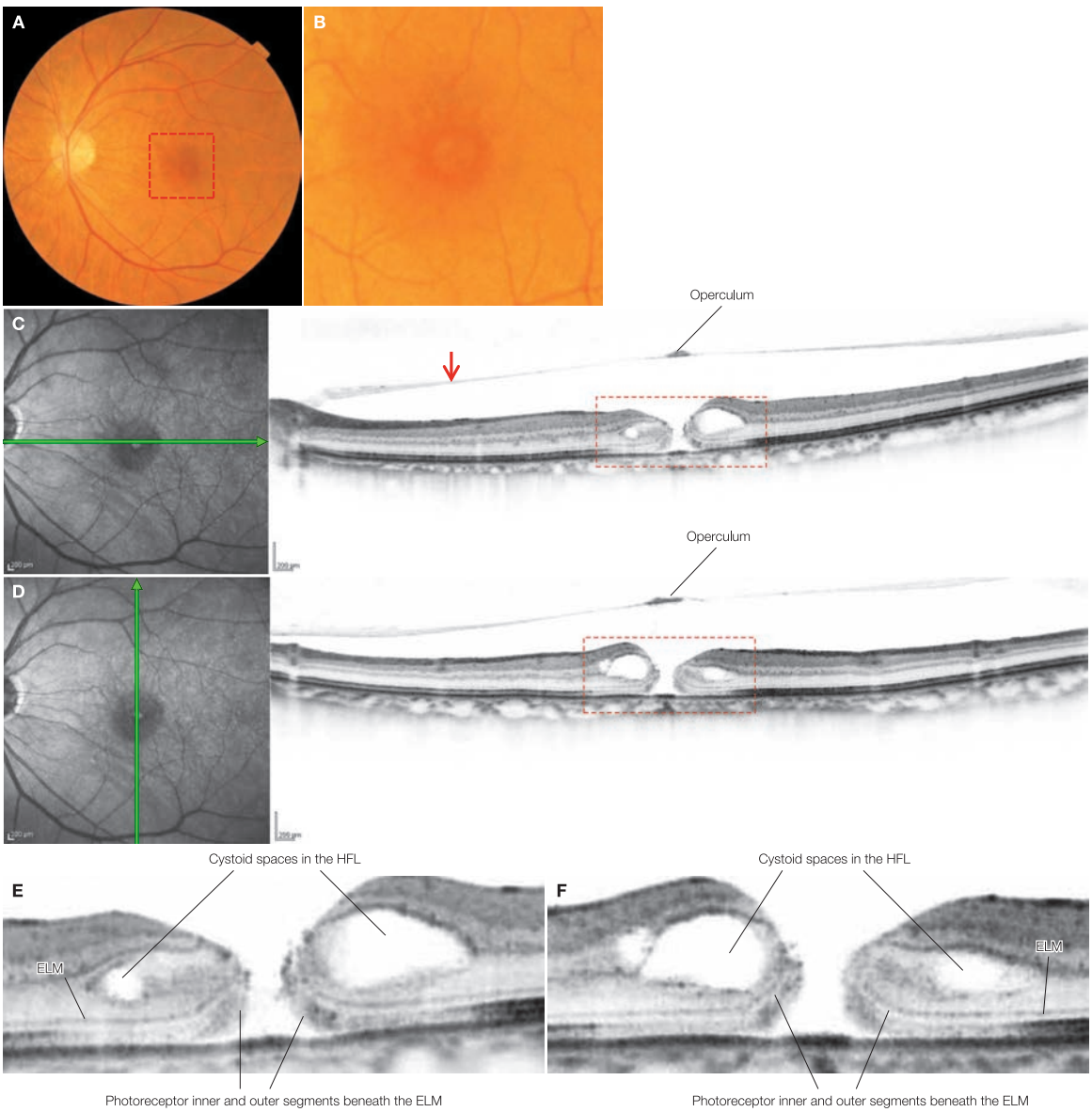

A: Color fundus photograph in the left eye, **B:** Enlarged version of A [red dashed box]: at initial diagnosis. A small macular hole with approximately one-quarter the size of the optic disc diameter is seen. **C:** IR + OCT horizontal scan of the left eye, **D:** IR + OCT vertical scan of the left eye: An operculum can be seen in the posterior vitreous cortex (➔). **E, F: Enlarged version of** C and D [red dashed box]: The photoreceptor layers beneath the ELM on the elevated edges of the macular hole are preserved with few defects.

Image interpretation points

This is a typical stage 3 macular hole, in which the posterior vitreous cortex including an operculum. No glial ring was seen with an biomicroscopic examination, the posterior vitreous cortex is attached to the optic disc, and the posterior vitreous cortex in the front of the macula is usually visible in the imaging range in OCT images. Cystoid spaces are formed in the HFL and the photoreceptor layers on the edge of the macular hole have become detached and elevated from the RPE. The degree of the photoreceptor cell disorder can be estimated by the status of the photoreceptor inner and outer segments beneath the ELM. In this example, there are few photoreceptor inner and outer segment defects and the good visual acuity prognosis can be expected.

Case 11 After surgery

A 65-year-old female, OS, BCVA 0.8

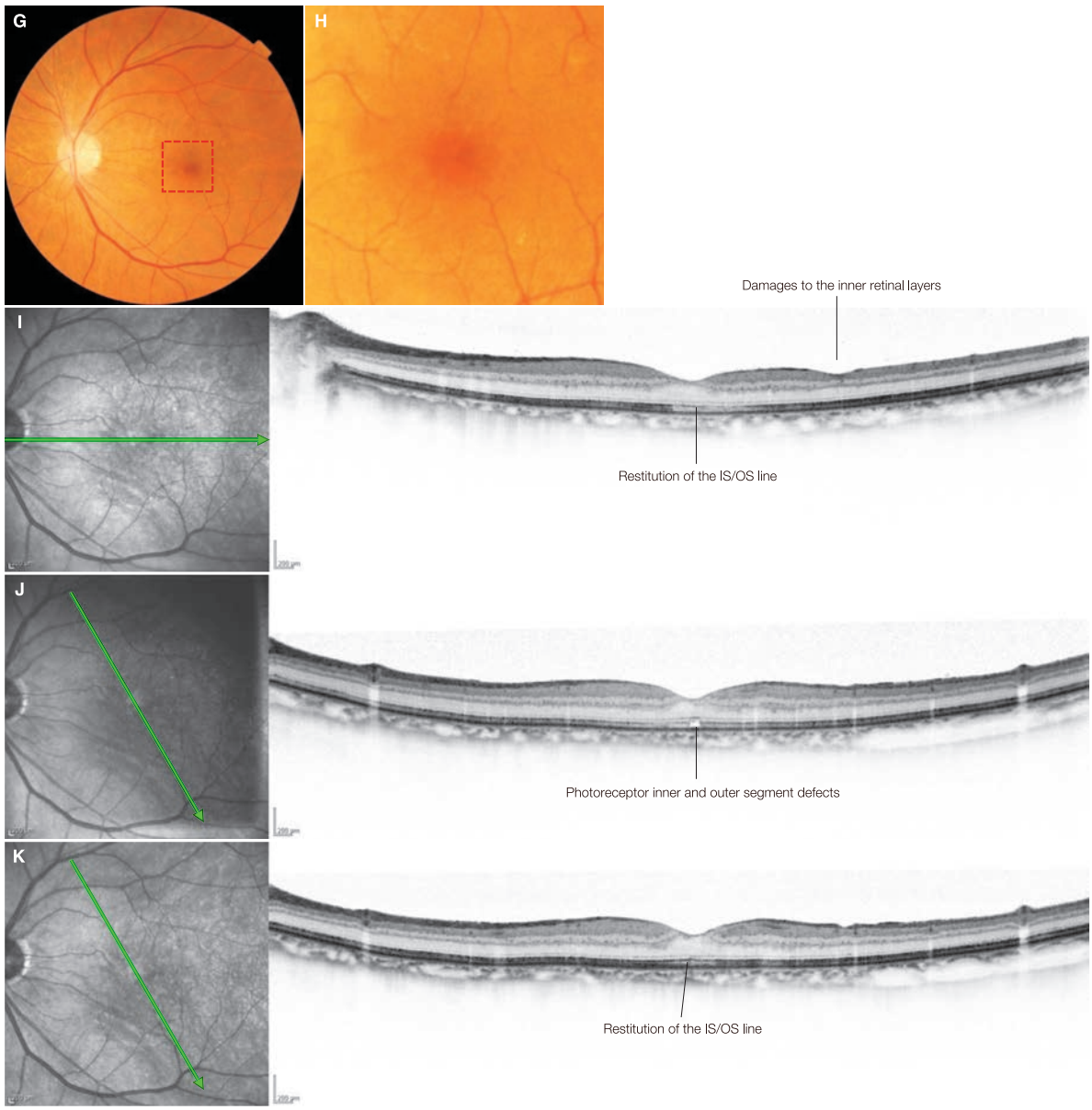

G: Color fundus photograph in the left eye, **H:** Enlarged version of A [red dashed box]: 3 weeks after macular hole surgery. Macular hole closure can be seen. **I:** IR + OCT horizontal scan of the left eye: 3 weeks after surgery. Vision corrected to 0.8. Reflectivity of foveal IS/OS line is already being restored, although it is still weak. The thickness of the photoreceptor inner and outer segments and outer nuclear layer is almost normal. Damages of the temporal inner retina can be seen. **J:** IR + OCT oblique scan of the left eye: 3 weeks after surgery. Foveal photoreceptor IS/OS defects can be seen on this scan. **K:** IR + OCT oblique scan of the left eye: 2 months after surgery. Best-corrected visual acuity has improved to 1.0. No photoreceptor IS/OS defects could be identified.

Image interpretation points

This is the fellow eye of a patient with a stage 4 macular hole. While a small inner and outer segment defect remains immediately after surgery, the IS/OS is being restored 2 months after surgery. No thinning can be seen in the outer nuclear layer or photoreceptor inner and outer segments at the fovea. The foveal contour appears to have been restored close to its normal form. The small photoreceptor inner and outer segment defect is a minor finding that cannot be identified unless dense serial scans are performed. Before surgery, there were few defects found in the inner and outer segments of the elevated edges of the macular hole, suggesting damages to foveal photoreceptor cells were not severe. The thinning of the temporal inner retinal layers is attributable to internal limiting membrane peeling.

Case 12 Idiopathic macular hole: Typical example of stage 4

A 69-year-old female, OD, BCVA 0.07

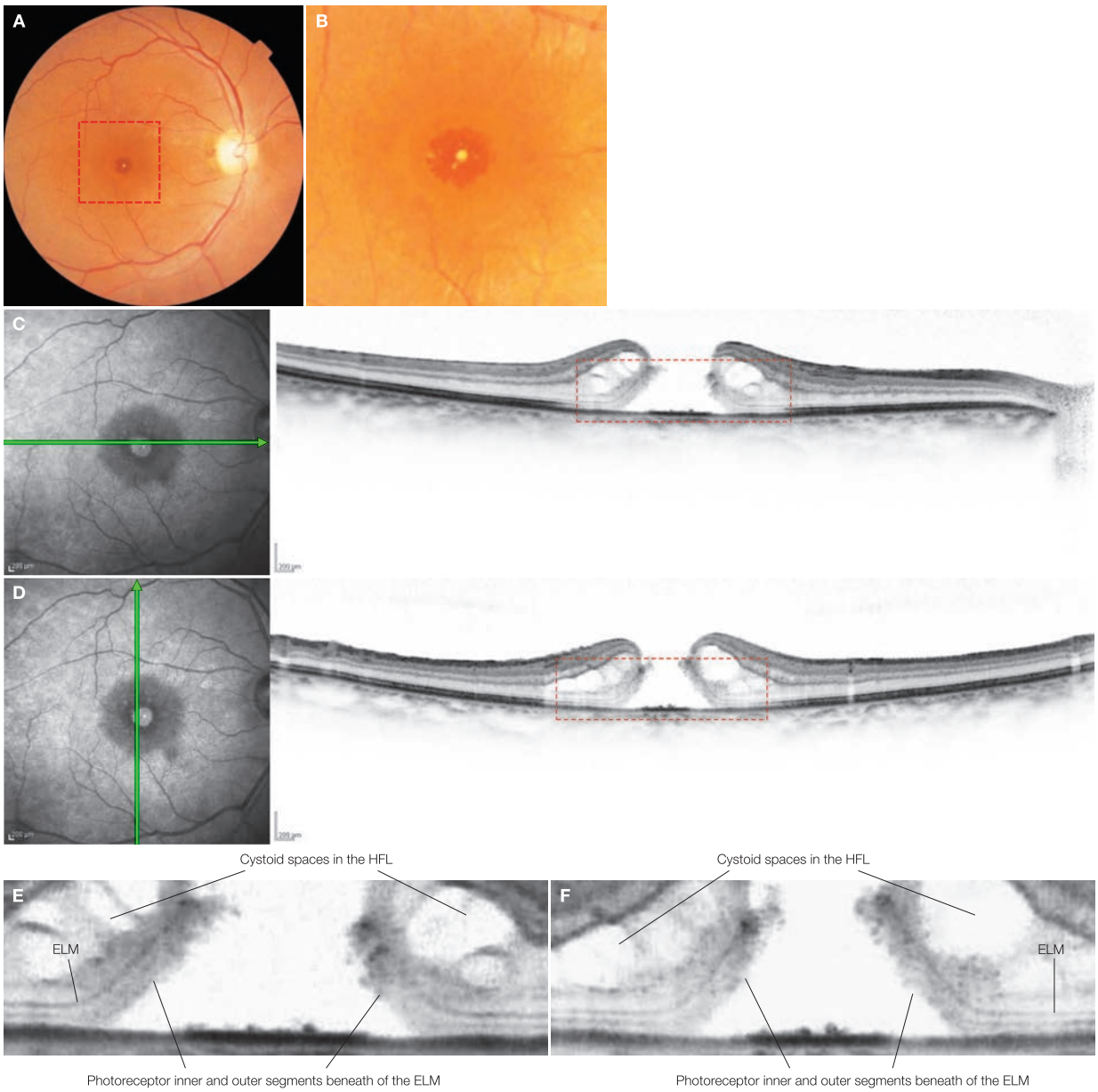

A: Color fundus photograph in the right eye, **B:** Enlarged version of A [red dashed box]: at initial consultation. A fairly large macular hole is visible measuring approximately one-half the optic disc diameter in size. **C:** IR + OCT horizontal scan of the right eye.
D: IR + OCT vertical scan of the right eye: Posterior vitreous cortex is not seen in the imaging frame. **E, F:** Enlarged version of C and D [red dashed box]: The inner and outer segments beneath the ELM on the elevated edges of the macular hole are preserved with few defects.

Image interpretation points

This is a stage 4 macular hole where a glial ring can be observed with a biomicroscopy and the posterior vitreous cortex is outside the OCT imaging frame. The status of the inner and outer segments beneath the ELM on the elevated edges of the macular hole is useful in knowing damages to foveal photoreceptor cells. In this example, there are few defects in these layers and good visual acuity prognosis is expected.

Case 13 Idiopathic macular hole: Old case of stage 4

A 73-year-old female, OD, BCVA 0.1

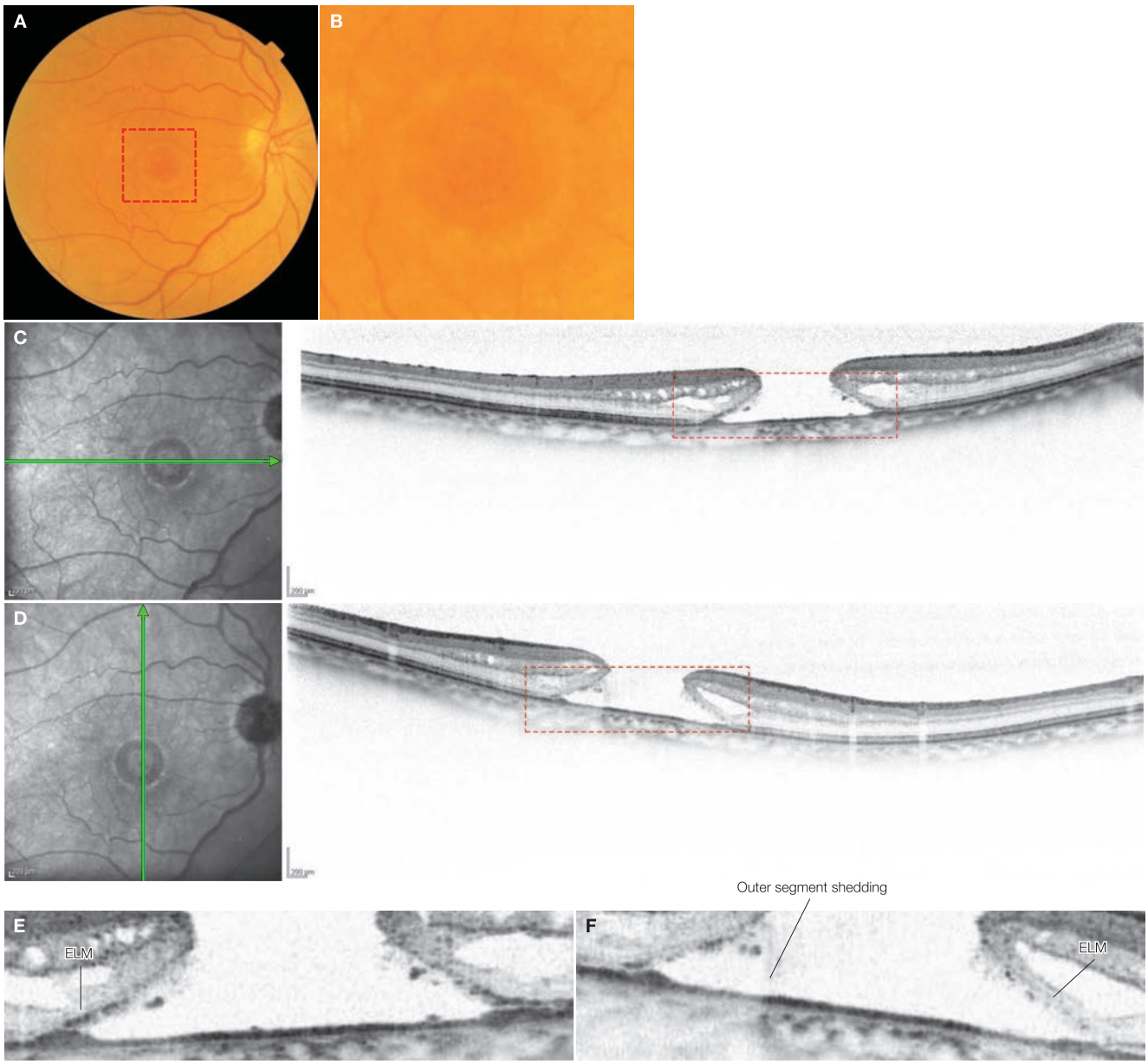

A: Color fundus photograph in the right eye, **B:** Enlarged version of A [red dashed box]: at initial diagnosis. A comparatively large macular hole approximately 1/2 the optic disc diameter can be seen. **C:** IR + OCT horizontal scan of the right eye.
D: IR + OCT vertical scan of the right eye: Cystoid spaces are significant not only in the HFL but also in the inner nuclear layer. The posterior vitreous cortex is not in the OCT imaging range.
Enlarged version of E, F, C and D [red dashed box]: Defects of the photoreceptor inner and outer segments beneath the ELM on the elevated edges of the macular hole are significant

Image interpretation points

This is the case of a stage 4 macular hole where a glial ring is seen with an biomicroscopy and the posterior vitreous cortex is outside the imaging frame. In this example, the fellow eye also has a stage 4 macular hole. Given the chronic nature of this macular hole, there is significant displacement of the fixation point as can be seen on the upper temporal portion of the macular hole. In addition to the large macular hole size, the severe defects of the inner and outer segments beneath the ELM on the elevated area illustrates serious photoreceptor damages.

Case 13 Stage 4 after surgery

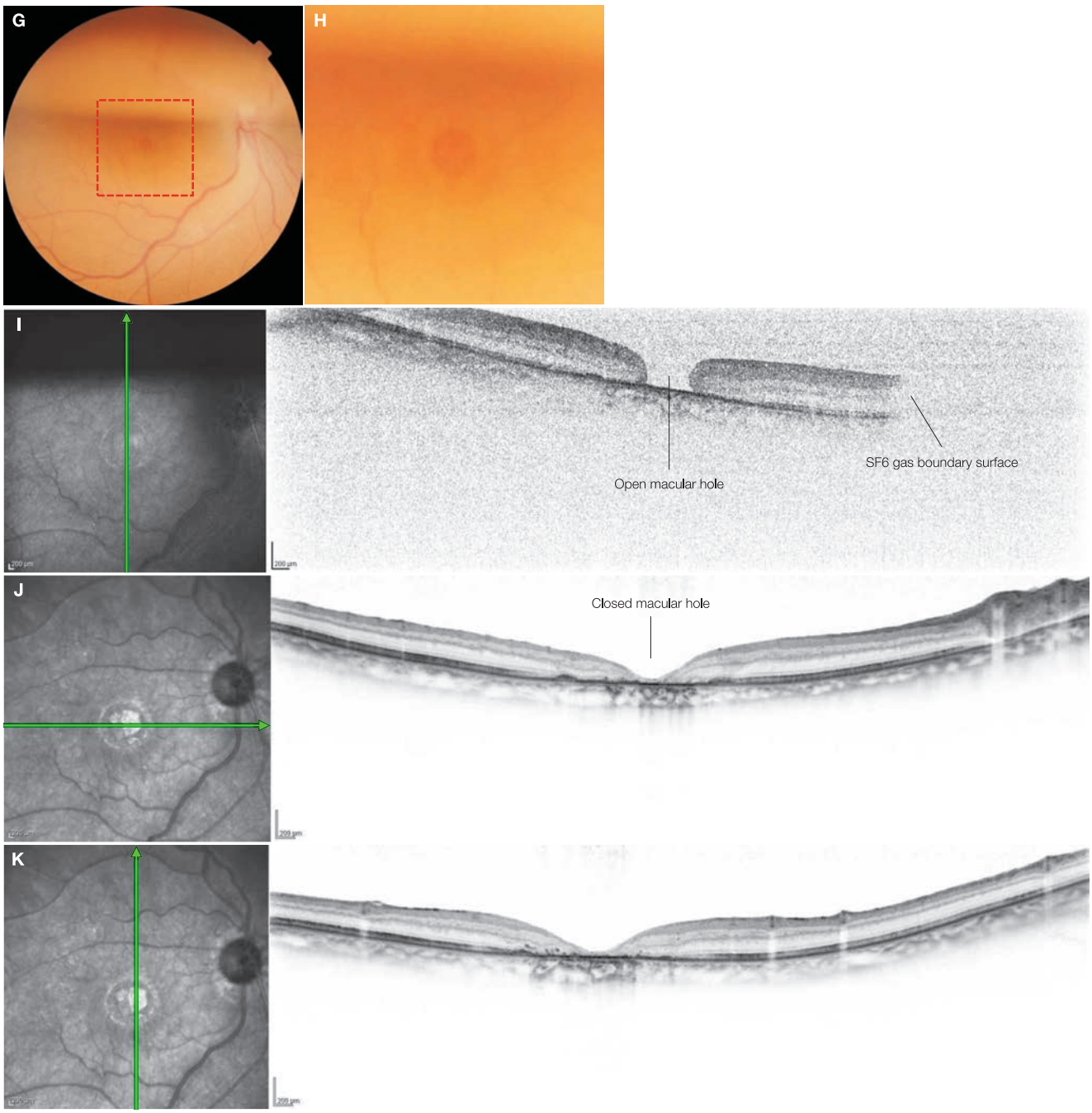

G: Color fundus photograph in the right eye, H: Enlarged version of G [red dashed box]: 1 week after first surgery. Macular hole closure has not been achieved. **I:** IR + OCT vertical scan of the right eye: 1 week after first surgery. The edge of the macular hole has become flattened, but the macular hole is not closed. SF_6 gas remains. **J:** IR + OCT horizontal scan of the right eye, **K:** IR + OCT vertical scan of the right eye: 1 month after the second surgery. Best-corrected visual acuity was 0.15. Macular hole closure has been achieved, but foveal thinning is pronounced.

Image interpretation points

This is the fellow eye of a patient with a stage 4 macular hole. In this case the macular hole was large and was only closed after a second surgery was performed. Unfortunately, there appears to be minimal nerve tissue remaining in the fovea centralis. The macular hole may have been closed by filling in with interstitial tissue such as glial tissue.

Case 14 Idiopathic macular holes: Progression from lamellar to full-thickness macular holes

A 65-year-old male, OS, BCVA 1.2

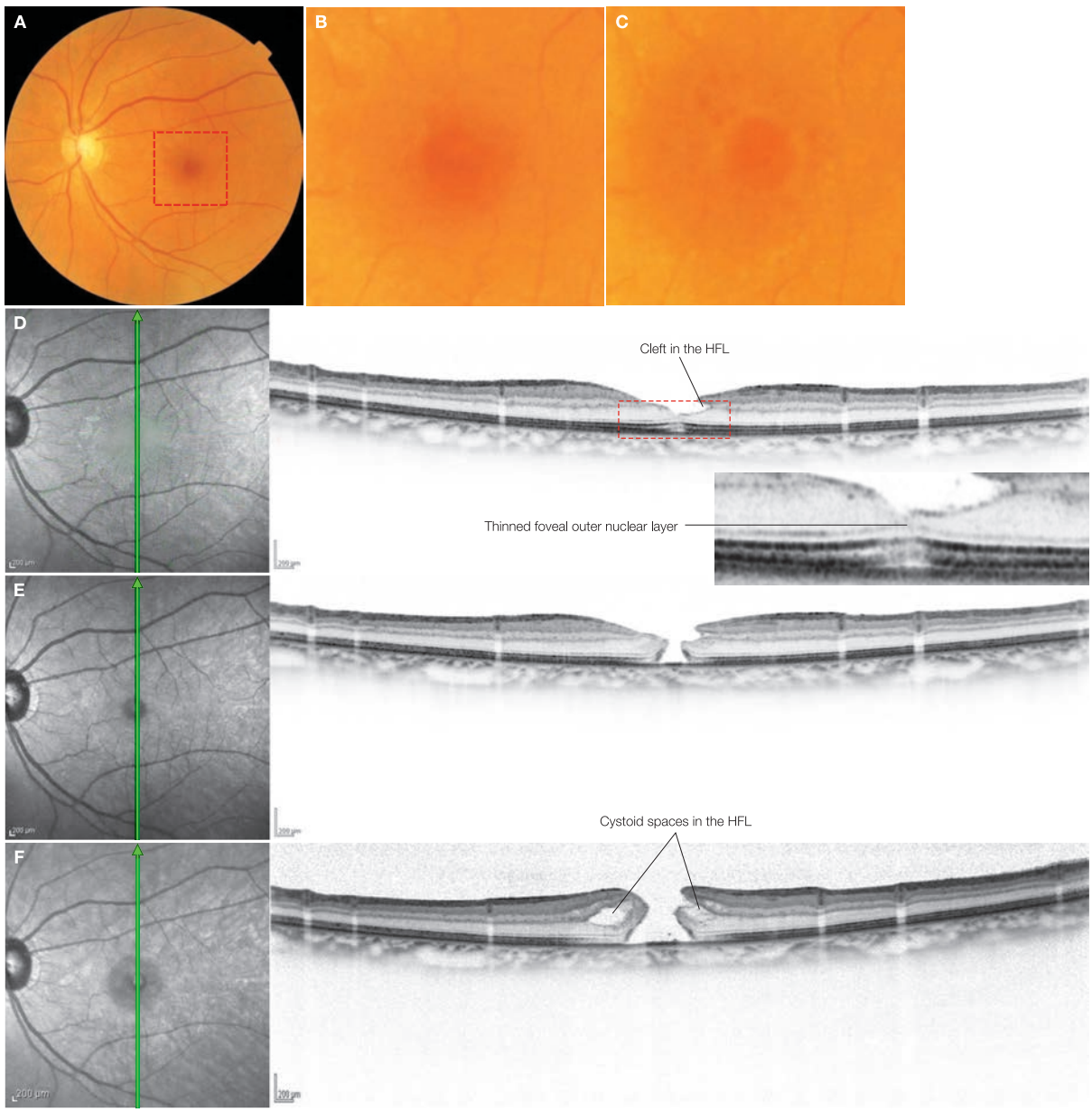

A: Color fundus photograph, **B:** Enlarged version of A [red dashed box]: at initial diagnosis. Lamellar macular hole findings are evident. **C:** Same area as **B:** 5 months after initial diagnosis. A full-thickness macular hole have developed. **D:** IR + OCT vertical scan of the left eye + enlarged version [red dashed box]: Features characteristic to lamellar macular hole, such as clefts in the HLF and diminished foveal outer nuclear layer, are evident. **E:** IR + OCT vertical scan of the left eye: 3 months after initial diagnosis. Best-corrected visual acuity has declined to 0.9. The lamellar macular hole has progressed to a full-thickness macular hole. Little elevation in the edges of the macular hole is seen. **F:** IR + OCT vertical scan of the left eye: 5 months after initial diagnosis. Best-corrected visual acuity has further declined to 0.7. Elevation in the edges of the macular hole is noted.

Image interpretation points

A lamellar macular hole develops when a perifoveal PVD spontaneously separates from the fovea in eyes with a stage 1 macular hole or when a macular hole closes spontaneously. However, this case progressed into a full-thickness macular hole after becoming lamellar. Foveal outer nuclear layer thinning is significant in a lamellar macular hole, sometimes causing foveal photoreceptor dehiscence.

Case 15 Stage 1 macular hole: Spontaneous separation of perifoveal PVD

A 46-year-old female, OD, BCVA 1.2

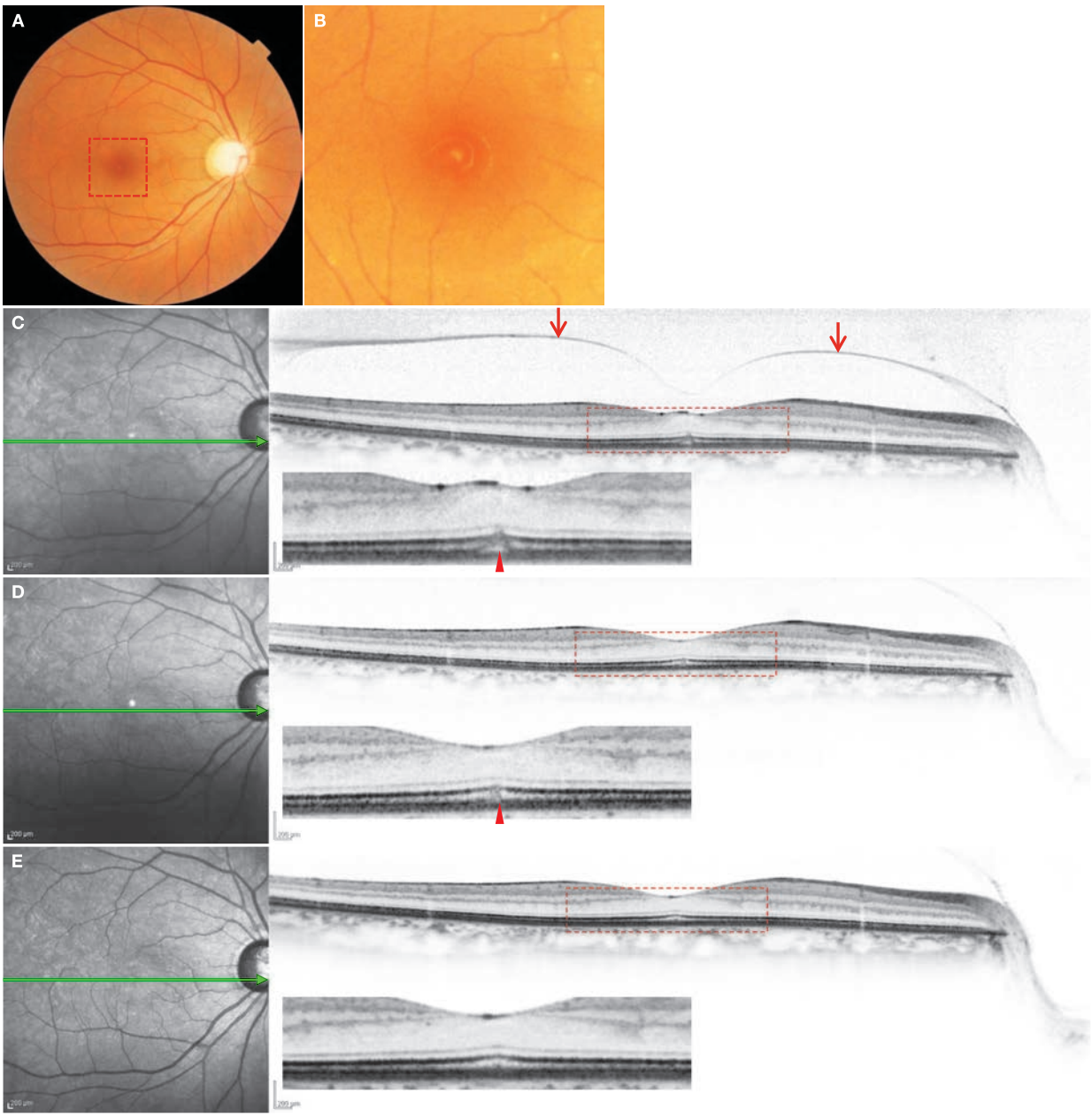

A: Color fundus photograph in the right eye, **B:** Enlarged version of A [red dashed box]: 6 months after initial diagnosis. A double yellow ring is visible. **C:** IR + OCT horizontal scan of the right eye + enlarged version [red dashed box]: 6 months after initial diagnosis. Perifoveal PVD is evident with elevation of the foveal surface and a tiny foveal detachment (►) resulting from centrifugal forward traction of the fovea centralis. → indicates the posterior vitreous cortex. **D:** IR + OCT horizontal scan of the right eye + enlarged version [red dashed box]: 9 months after initial diagnosis. Best-corrected visual acuity is 1.2. Perifoveal PVD has separated spontaneously, elevation of the foveal surface has disappeared and the foveal detachment has receded (►). **E:** IR + OCT horizontal scan of the right eye + enlarged version [red dashed box]: 12 months after initial diagnosis. Best-corrected visual acuity is 1.2. The small foveal detachment has disappeared.

Image interpretation points

A perifoveal PVD was observed at initial diagnosis, but without evidence of foveal deformation. Six months after initial diagnosis, the foveal surface was elevated and a small foveal detachment had developed; 9 months after initial diagnosis the macular PVD was complete. Elevation of the foveal surface disappeared and slight abnormal reflectivity of the photoreceptor inner and outer segments in the fovea centralis remained. 12 months after initial diagnosis, the fovea centralis was restored to normal.

Case 16 Stage 1 macular hole: Macular microhole formation

A 58-year-old female, OD, BCVA 0.8

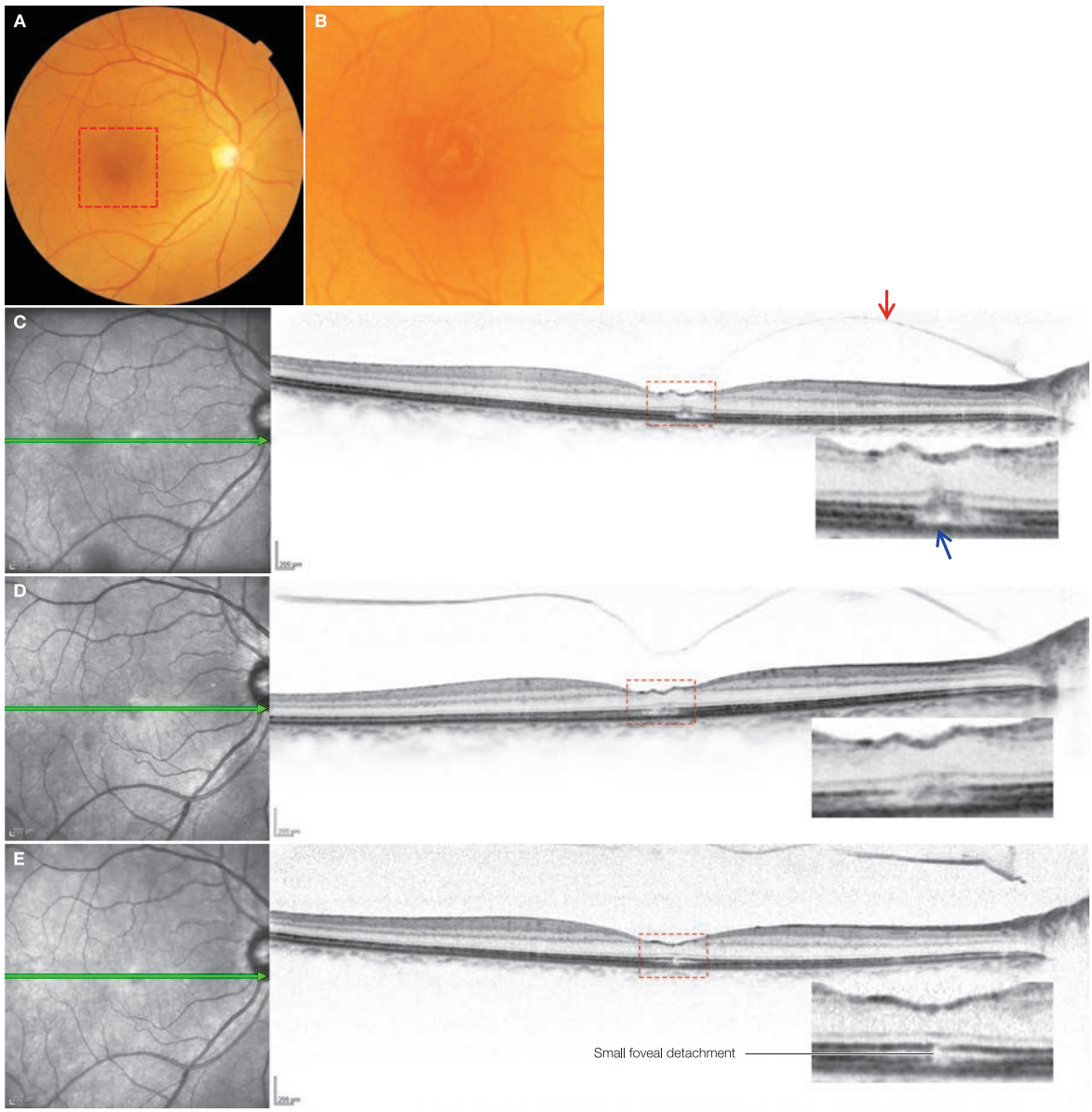

A: Color fundus photograph in the right eye, **B:** Enlarged version of A [red dashed box]: at initial diagnosis. A yellow ring is visible with a yellow dot in the center. **C:** IR + OCT horizontal scan of the right eye + enlarged version [red dashed box]: at initial diagnosis. Perifoveal PVD evident with elevation of the foveal surface and a small foveal detachment (➔) resulting from centrifugal forward traction of the fovea centralis. ➔ shows the posterior vitreous cortex. **D:** IR + OCT horizontal scan of the right eye + enlarged version [red dashed box]: 2 months after initial diagnosis. Best-corrected visual acuity is 0.9. Spontaneous separation of perifoveal PVD is in progress. **E:** IR + OCT horizontal scan of the right eye + enlarged version [red dashed box]: 3 months after initial diagnosis. Best-corrected visual acuity has improved to 1.2. Perifoveal PVD has separated and a flaccid posterior vitreous cortex can be seen. Photoreceptor inner and outer segment defects (macular microholes) remain.

Image interpretation points

Upon initial diagnosis, there was a perifoveal PVD causing elevation of the foveal surface where the posterior vitreous cortex adheres. Also seen was a small foveal detachment which was more likely a disruption of the foveal IS/OS and COST. In this case, however, foveal deformation did not worsen and the perifoveal PVD separated spontaneously. Three months after initial diagnosis, elevation of the foveal surface had receded and findings known as »a macular microhole« could be seen in the photoreceptor inner and outer segments. Best-corrected visual acuity was relatively good.

Case 17 Stage 2 macular hole: Spontaneous closure

A 72-year-old male, OD, BCVA 0.6

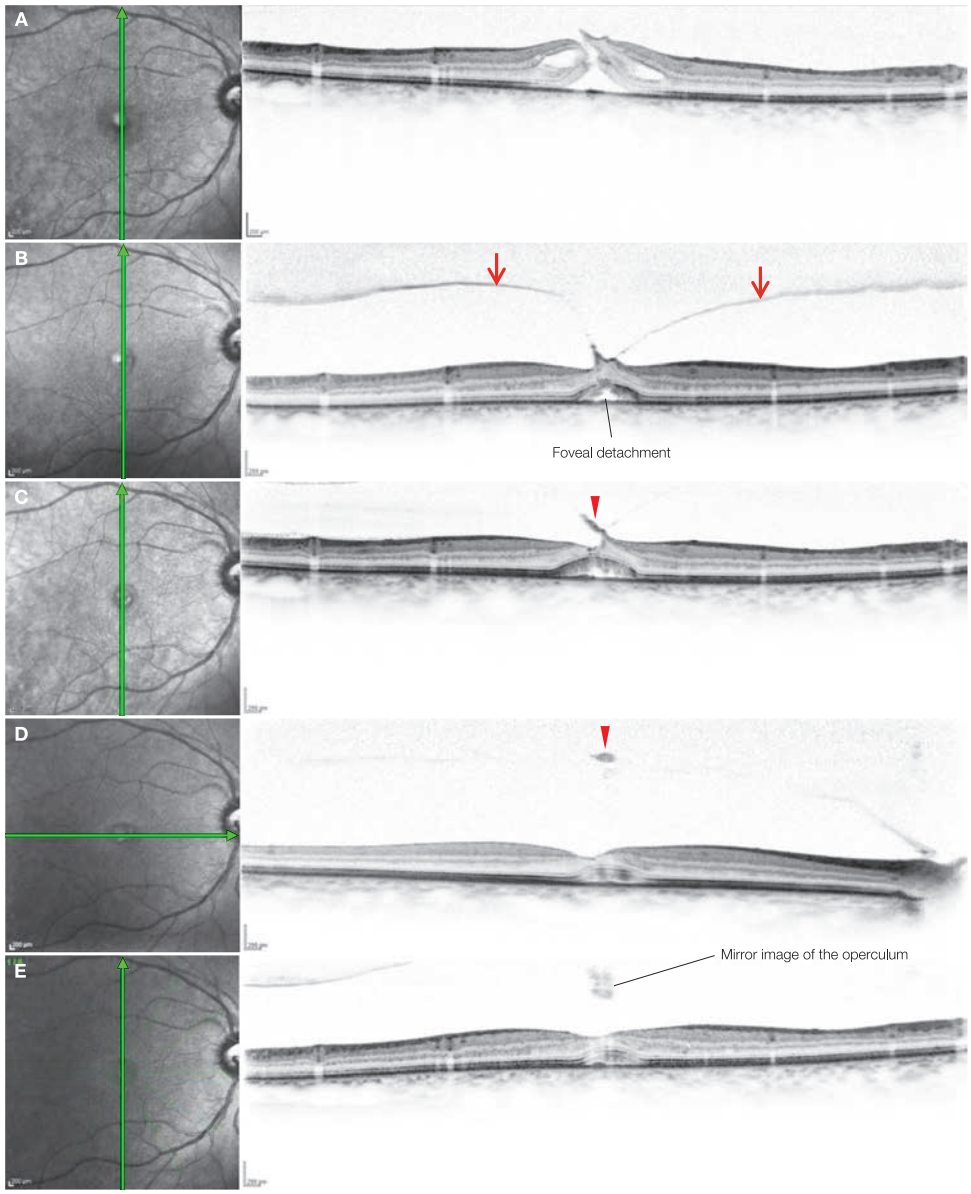

A: IR + OCT vertical scan of the right eye: at initial diagnosis. A stage 2 macular hole is seen. **B:** IR + OCT vertical scan of the right eye: 1 month after initial diagnosis. Best-corrected visual acuity has improved to 1.0. Spontaneous closure can be seen but perifoveal PVD has not separated. ➔ indicates the posterior vitreous cortex. This image appears to indicate stage 1 macular hole with foveal detachment. **C:** IR + OCT vertical scan of the right eye: 6 months after initial diagnosis. Best-corrected visual acuity is 1.2. Centrifugal forward traction resulting from perifoveal PVD continues; a flap-like foveal anterior wall is beginning to separate (►). **D:** IR + OCT horizontal scan of the right eye: 12 months after initial diagnosis. Best-corrected visual acuity is 1.2. Macular PVD is complete and an operculum (►) is attached to the posterior vitreous cortex. Foveal detachment continues to recede. **E:** IR + OCT vertical scan of the right eye: 12 months after initial diagnosis. Similar findings to D noted. A mirror image of the operculum outside the imaging range is reflected

Image interpretation points

This is an unusual case where the macular hole temporarily progressed into a stage 2 full-thickness macular hole, but spontaneously closed and returned to stage 1 regardless of the presence of perifoveal PVD. If the initial visit had been 1 month later, it would not have been evident that the hole was previously stage 2. There are instances where visual acuity is not completely improved despite spontaneous closure, however, this patient's corrected vision improved to over 1.0 with closure.

Case 18 Stage 3 macular hole: Spontaneous closure

A 68-year-old male, OD, BCVA 0.3

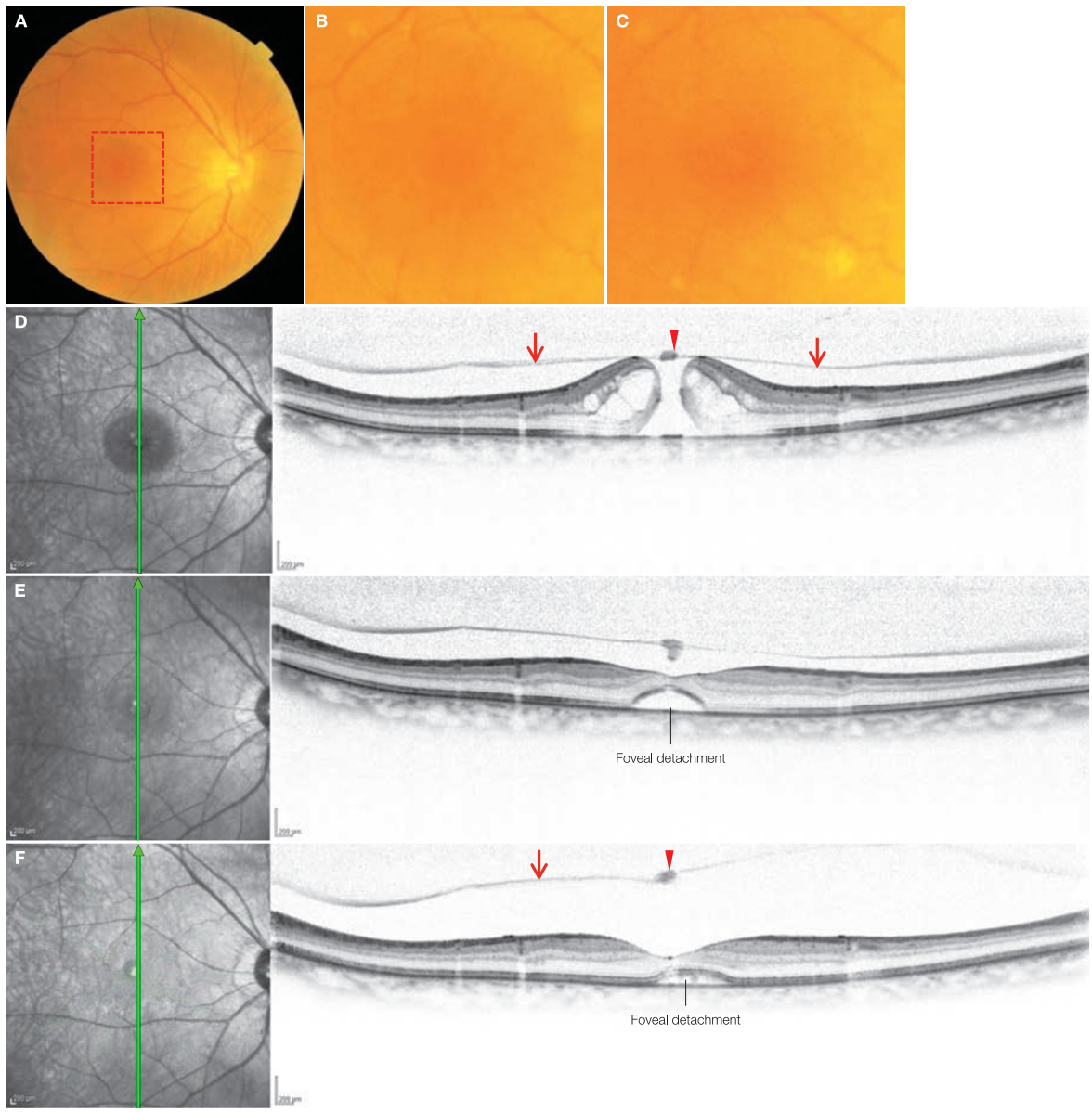

A: Color fundus photograph in the right eye, **B:** Enlarged version of A [red dashed box]: at initial diagnosis. Stage 3 macular hole is seen. **C:** Same area as **B:** 8 months after initial diagnosis. The macular hole has closed spontaneously. **D:** IR + OCT vertical scan of the right eye: at initial diagnosis. An operculum (▶) and a macular hole are seen. Cystoid spaces in the HFL and elevation of the photoreceptor layers at the edges of the macular hole are also seen. → indicates the posterior vitreous cortex. **E:** IR + OCT vertical scan of the right eye: 1 month after initial diagnosis. Visual acuity has improved to 0.5. The macular hole has closed spontaneously and the foveal detachment remains. **F:** IR + OCT vertical scan of the right eye: 8 months after initial diagnosis. Best-corrected visual acuity has improved to 0.9. Foveal detachment remains. The operculum (▶) and posterior vitreous cortex are further from the retina. The foveal depression has recovered.

Image interpretation points

This is an example of spontaneous closure of a stage 3 macular hole. The edges of the macular hole have been centrifugal elevated. Foveal detachment remained until long after spontaneous closure. Even in cases where macular holes have been closed by surgery, foveal detachment can remain for around half a year. While the spontaneous closure of macular holes is unusual, they can occur at any stage.

Case 19 Stage 4 macular hole: Spontaneous closure

A 68-year-old male, OD, BCVA 0.3

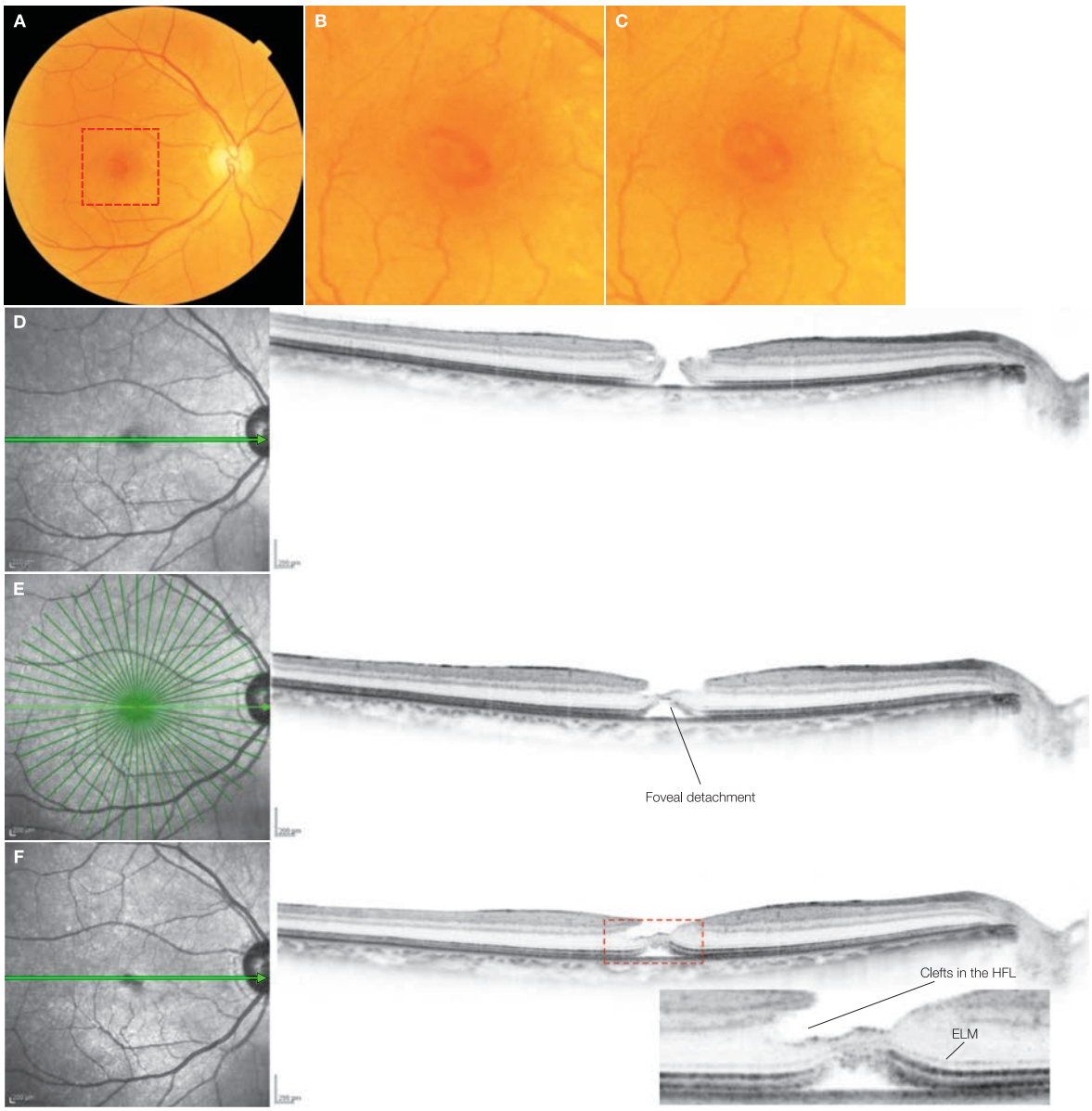

A: Color fundus photograph in the right eye, **B**: Enlarged version of A [red dashed box]: at initial diagnosis. A stage 4 macular hole is seen. **C:** Same area as **B:** 1 month after initial diagnosis. Best-corrected visual acuity has improved to 0.7. A lamellar macular hole findings is seen. **D:** IR + OCT horizontal scan of the right eye: at initial diagnosis. A full-thickness macular hole is seen. There is slight elevation in the edges of the macular hole. **E:** IR + OCT horizontal scan of the right eye 1 month after initial diagnosis. The macular hole has closed spontaneously. Features characteristic to lamellar macular holes, such as clefts in the HFL and diminished foveal outer nuclear layer, are evident. **F:** IR + OCT horizontal scan of the right eye + enlarged version [red dashed box]: 8 months after initial diagnosis. Foveal detachment and lamellar macular hole features remain. Best-corrected visual acuity has improved to 1.2. Note the remaining clefts in the HFL and thin foveal outer nuclear layer, indicating lamellar macular hole.

Image interpretation points

This is an example of spontaneous closure of a stage 4 macular hole. Features characteristic to lamellar macular holes, such as clefts in the HFL and diminished foveal outer nuclear layer, are demonstrated after spontaneous closure of the macular hole.

Although unusual, the spontaneous closure of macular holes is thought to be one of the pathogenic mechanisms of lamellar macular hole formation.

Case 20 Traumatic macular hole: A typical example

An 11-year-old male, OS, BCVA 0.3

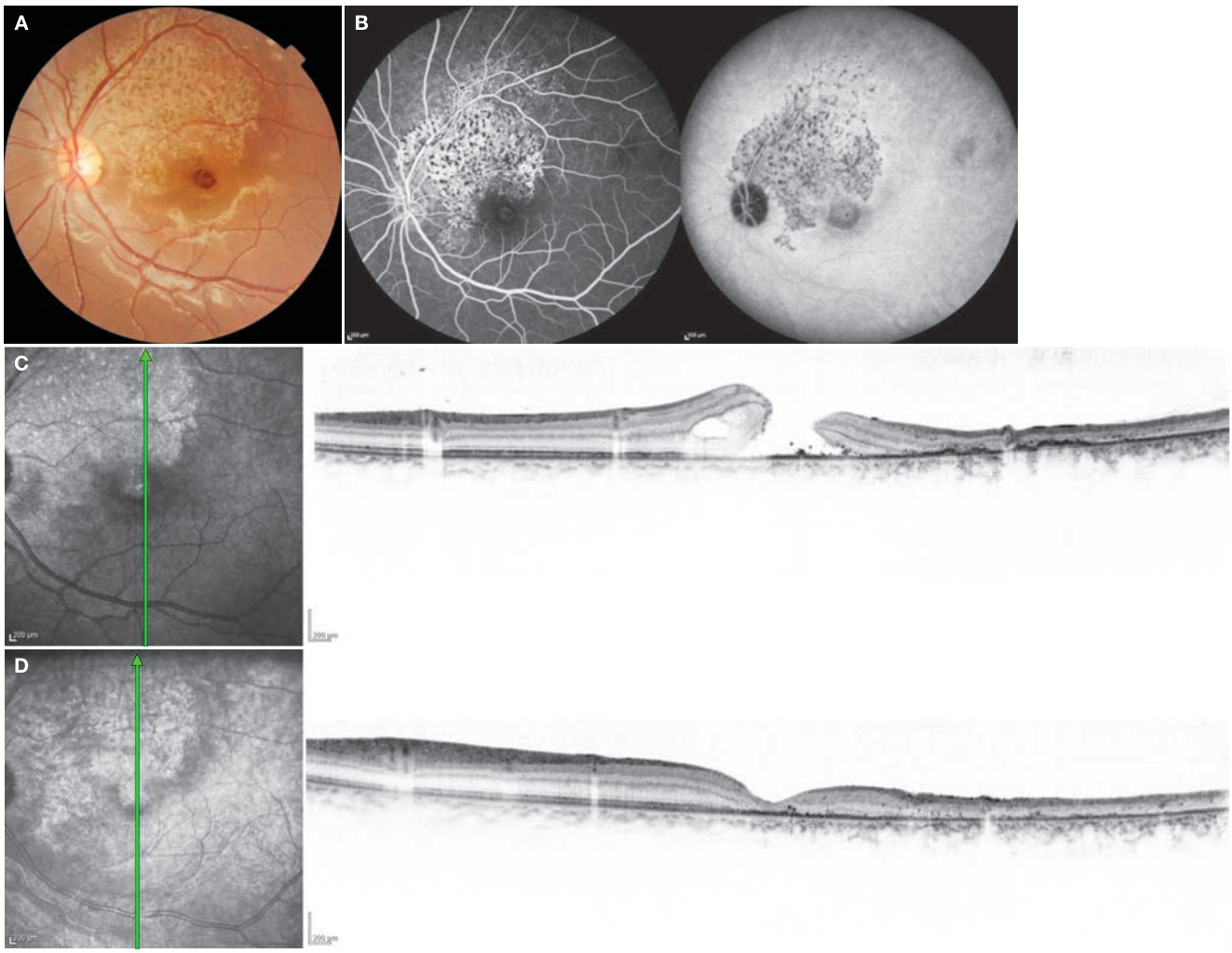

A: Color fundus photograph in the left eye: at initial diagnosis. A macular hole about half the optic disc diameter can be seen. The edges of the macular hole are irregular. The upper posterior pole of the retina appears significantly whitened as a result of commotio retinae with mottled pigmentation visible within. **B:** 10 minutes after simultaneous FA/IA angiography of the left eye: Tissue staining and mottled blockades of fluorescence is evident in the upper posterior pole of the retina. **C:** IR + OCT vertical scan of the left eye: The upper retina, particularly the outer retinal layers, are significantly atrophic. There is reactive proliferation of the RPE cells from the base of the macular hole to the area of retinal atrophy. **D:** IR + OCT vertical scan of the left eye: 3 months after surgery. Best-corrected visual acuity has improved to 0.5. The macular hole has closed, but atrophy of the fovea is significant.

Image interpretation points

This is a case of traumatic macular hole secondary to commotio retinae of the left eye caused by a football. While spontaneous closure is common, closure was achieved surgically in this case after spontaneous closure was not observed 6 months after diagnosis. Retinal atrophy of the fovea and the area of the upper macula were significant.

Understanding the difference between lamellar macular holes and macular pseudoholes

The ophthalmoscopic findings of lamellar macular holes and macular pseudoholes (MPH) are similar, whereas the pathogenesis and OCT findings differ. Lamellar macular holes can be seen when the anterior wall of stage 1 macular holes comes off or when macular holes close spontaneously. They are thought to be a pathological condition on the same spectrum as idiopathic macular holes. On the other hand, MPH are similar to epiretinal membranes (ERM) except the fovea centralis is spared from thickening due to a hole opening in the posterior vitreous cortex at the fovea centralis. These two diseases can usually be differentiated by proper interpretation of OCT images, however a definitive diagnosis is sometimes difficult without observing the process by which macular PVD occurred. The posterior vitreous cortex can remain during perifoveal PVD onset even in lamellar macular hole formation. Such cases with lamellar macular hole can be accompanied by ERM formation, leading to retinal thickening and folds. Importantly, if significant thinning is seen in the outer nuclear layer of or near the fovea centralis, it can be classified as a lamellar macular hole. This is because thinning of or near the fovea centralis occurs with centrifugal traction generated by perifoveal PVD. On the other hand, such lesions rarely occur with centripetal traction by ERM shrinkage, which is mainly associated with the pathological condition of MPH. Thinning of the outer nuclear layer in or near the fovea centralis in lamellar macular holes are sometimes progressive and can develop into full-thickness macular holes.

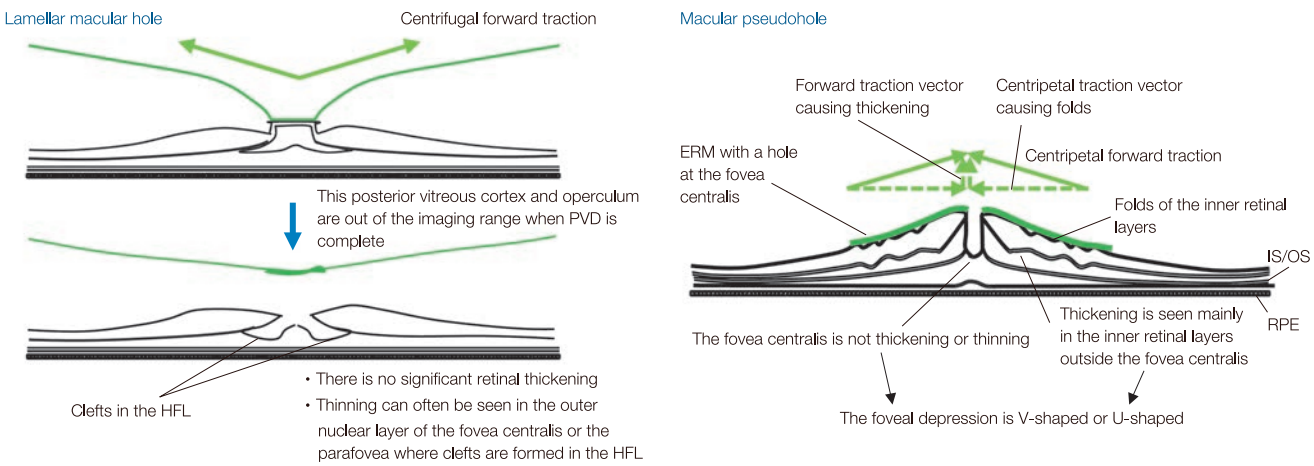

Pathology: Spontaneous separation of perifoveal PVD together with anterior wall of the cystoid space in Stage 1 macular hole, or spontaneous closure of Stage 3 and 4 macular holes
Typical OCT features [omega-shape [pumpkin-shape]
- No significant retinal thickening
- No folds can be seen in the inner retinal layers
- Clefts in the HFL are present
- Foveal or parafoveal thinning is evident

Pathology: A ERM subtype
Typical OCT features
- Retinal thickening is seen outside the fovea centralis
- The fovea centralis is neither thickening or thinning and is forming a V-shape or U-shape
- Folds are visible in the inner retinal layers

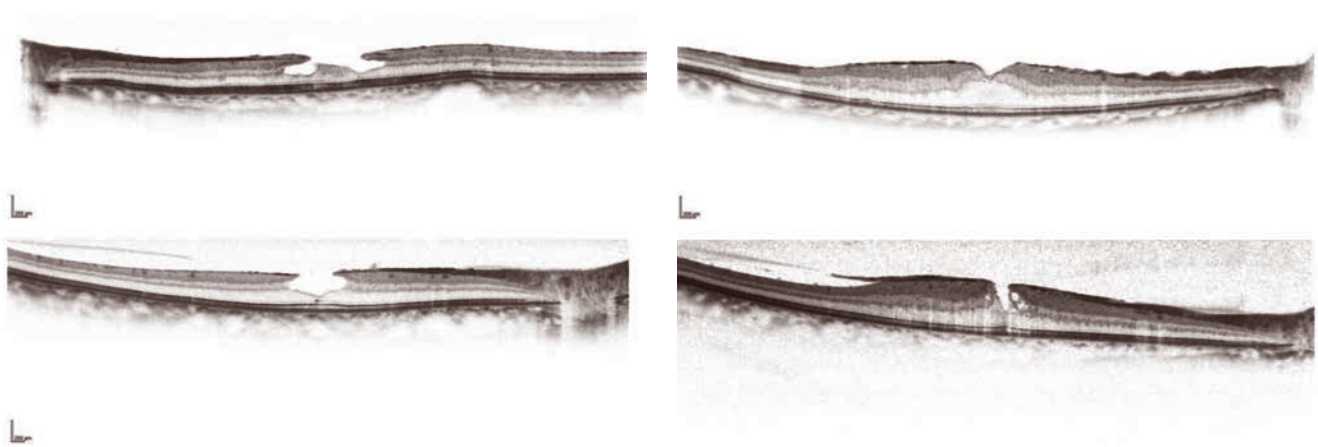

Fig. 2-11 Lamellar macular holes and MPHs

Case 21 Lamellar macular hole: a typical example

A 53-year-old female, OS, BCVA 0.3

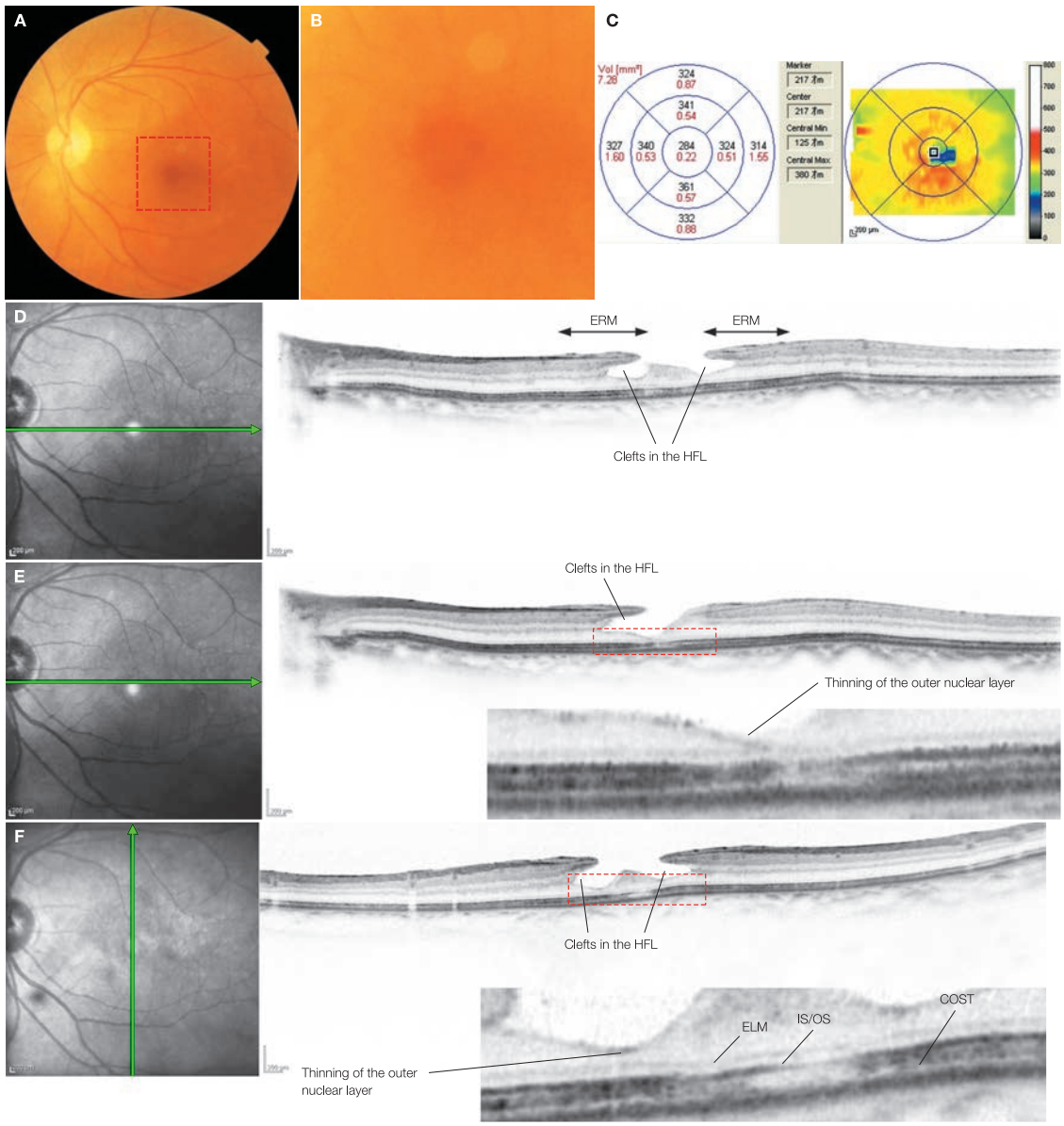

A: Color fundus photograph in the left eye, **B:** Enlarged version of A [red dashed box]: No ERM or retinal folds are visible. **C:** Retinal thickness color map of the left eye, **D:** IR + OCT horizontal scan of the left eye: ω (omega)-shaped foveal deformation is evident. Clefts in the HFL and thin ERM (↔) are evident but little macular retinal thickening or retinal folds can be seen. **E:** IR + OCT vertical scan of the left eye + enlarged version [red dashed box]: Significant thinning of the outer nuclear layer near the fovea centralis noted. Reflectivity of the IS/OS and COST is attenuated or disappearing. **F:** IR + OCT horizontal scan of the left eye + enlarged version [red dashed box]: same findings as D

Image interpretation points

This is the case of a typical lamellar macular hole showing ω-shaped foveal deformation. A lamellar macular hole is thought to be a subtype of an idiopathic macular hole where the perifoveal PVD has separated spontaneously from a stage 1 hole or when a macular hole has closed spontaneously.

In this case, clefts in the HFL and ERM are visible only on OCT, but without typical retinal thickening or folds seen with MPH. In contrast, there are areas of outer nuclear layer thinning as seen in E, which can develop into a full-thickness macular hole.

Case 22 Lamellar macular hole: Differentiation from a MPH

A 55-year-old female, OS, BCVA 0.3

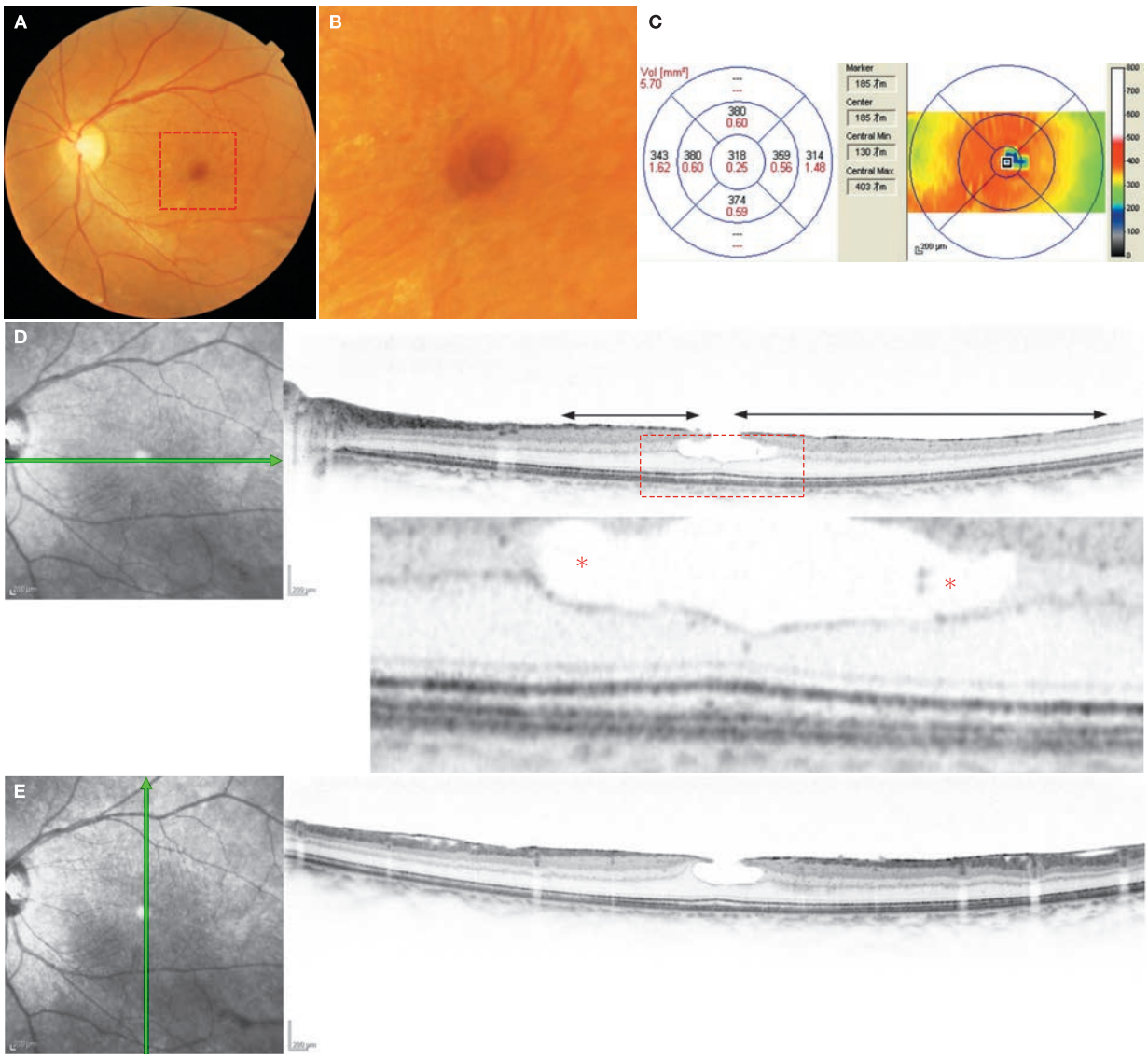

A: Color fundus photograph in the left eye, **B:** Enlarged version of A [red dashed box]: Retinal folds are visible, while membrane whitening is mild. **C:** Retinal thickness color map of the left eye. **D:** IR + OCT horizontal scan of the left eye + enlarged version [red dashed box]: ERM (↔) can be seen although retinal thickening and retinal folds are mild. The pumpkin-shaped foveal deformation is seen, which is probably formed as a result of cleft formation in the HFL (*) and inner layer protrusions due to the centripetal contraction of the ERM. The outer nuclear layer of the fovea centralis has thinned significantly. **E:** IR + OCT vertical scan of the left eye: same findings as D

Image interpretation points

This case appears to have involved both centrifugal traction by perifoveal PVD and centripetal traction by ERM as causes of foveal deformation. Here, the pumpkin-shaped foveal cavity is laterally wide. This is because this shape was formed a result of cleft formation in the HFL. In contrast, MPH foveal depressions tend to be laterally narrow.

In addition to the cleft formation, the parafoveal inner retinal layer centrally protruded as a result of centripetal shrinkage of the ERM may be responsible for the pumpkin-shaped foveal deformation. Importantly, the foveal outer nuclear layer is diminished to approximately a half of the inner and outer segment thickness. This occurs due to a centrifugal tractional force generated by perifoveal PVD in macular hole formation, but never occurs as a result of a centripetal tractional force by ERM in MPH.

In summary, the cleft in the HFL and diminished outer nuclear layer is formed by the centrifugal traction by perifoveal PVD, and the protrusion of the parafovea inner retinal layer by the centripetal traction by ERM contraction.

Macular microholes

Background

2

A macular microhole is a disease state without a well-established definition. Currently, it is loosely defined as a class of disease with a reduction in reflectivity or defect within the IS/OS line on OCT B-scan images. On funduscopic exam, 50–150 μm sharply demarcated reflections known as »red spots« are seen, while on fluorescein angiography there are no RPE changes seen. On OCT, foveal IS/OD disruption or outer retinal defects are found in or near the fovea centralis. Although there are cases without subjective complaints, symptoms are usually associated with acute onset of central scotoma, mild decrease in visual acuity and metamorphopsia. Epidemiologically, macular microholes occur in wide variety of patients ranging in age from their 20s to the elderly with no gender predilection. They are usually unilateral with 80% of cases with vision over 0.5. Typically, the vision does not worsen further and can improve as the IS/OS defects recover[4, 5].

Pathogenesis and OCT findings

It is clear that macular microholes can be caused by the PVD formation process as a result of centrifugal forward traction from the posterior vitreous cortex on the fovea centralis. In these cases, the perifoveal PVD spontaneously separates in a stage 1A macular hole. In 1/3 of the cases there is a macular PVD where the posterior vitreous cortex and operculum can be observed on OCT. When the PVD is complete, however, these are not seen in the OCT imaging range and only a Weiss' ring is seen with an biomicroscopy. While PVD formation can explain macular microholes occuring in older patients, the etiology of macular microholes is unknown in young patients without a macular PVD. Such cases need to be differentiated from trauma, solar retinopathy, or central serous chorioretinopathy. Solar retinopathy, caused by looking directly at the sun for example in observation of solar eclipse, may be diagnosed based on history, RPE abnormalities, or moderate reflectivity of all retinal layers on OCT. Central serous chorioretinopathy, on the other hand, can be differentiated based on RPE and choroidal abnormalities.

References

1) Cairns JD, McCombe MF. Microholes of the fovea centralis. Aust N Z J Ophthalmol. 1988; 16:75–79.
2) Reddy CV, Folk JC, Feist RM. Microholes of the macula. Arch Ophthalmol. 1996; 114:413–416.
3) Zambarakji HJ, Schlottmann P, Tanner V, et al. Macular microholes: pathogenesis and natural history. Br J Ophthalmol. 2005; 89:189–193.
4) Emerson GG, Spencer GR, Klein ML. Macular microholes. Retina. 2007; 27:595–600.
5) Takahashi A, Nagaoka T, Yoshida A. Stage 1-A macular hole: a prospective spectral-domain optical coherence tomography study. Retina. 2011; 31:127–147.

Case 23 Macular microhole: with macular PVD

A 72-year-old female, OS, BCVA 0.6

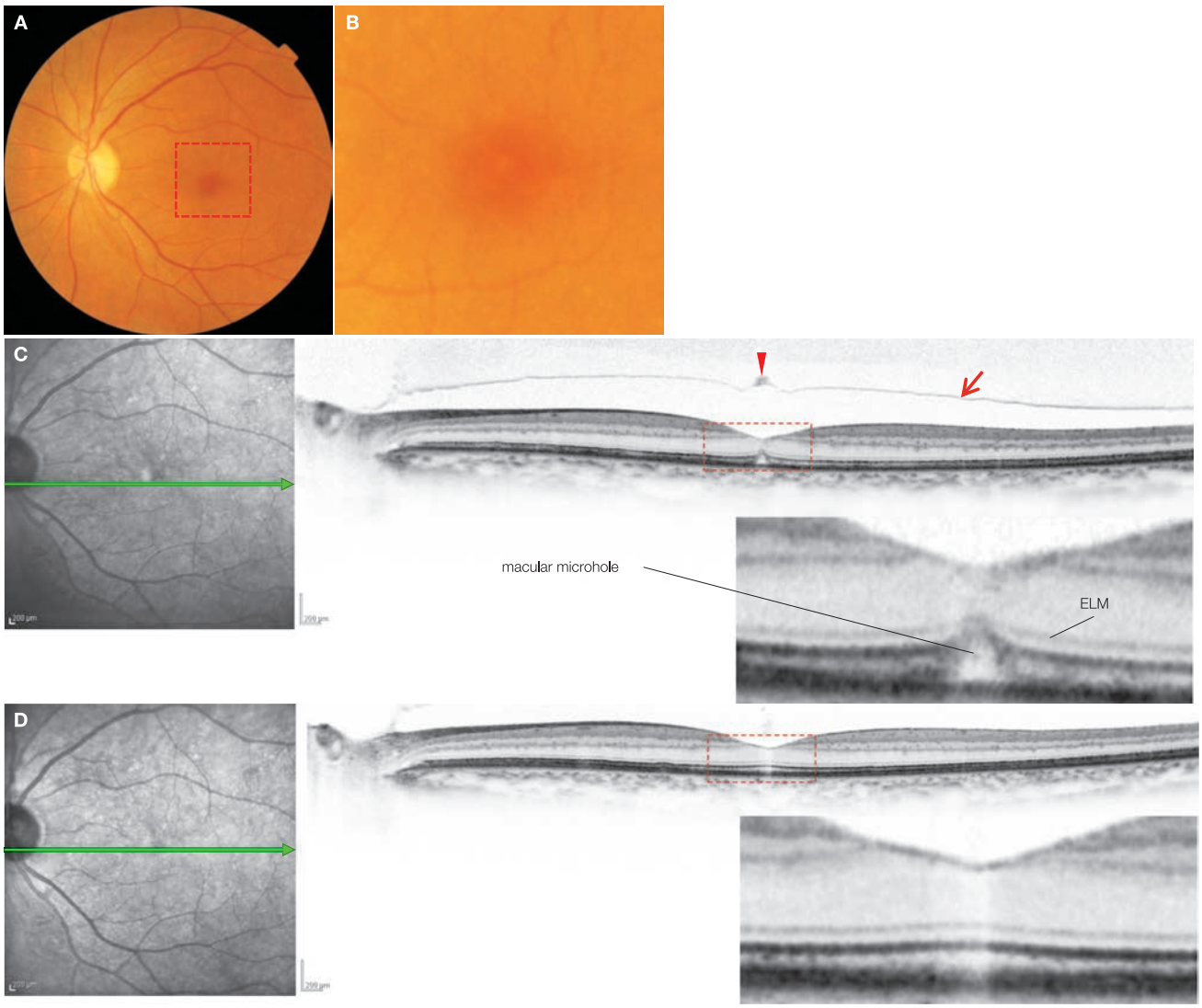

A: Color fundus photograph in the left eye, **B:** Enlarged version of A [red dashed box]: at initial diagnosis. Abnormal reflection known as a *red spot* can be seen in the fovea centralis. **C:** IR + OCT horizontal scan of the left eye + enlarged version [red dashed box]: Macular PVD has occurred, and an operculum (▶) attached to the posterior vitreous cortex (➔) is noted. Disruption of the photoreceptor IS/OS and outer segment can be observed. This is essentially the same as a small foveal detachment in a stage 1 macular hole. Abnormal high reflectivity can be seen in the foveal outer nuclear layer. This is thought to be a remnant of the foveal deformation caused by perifoveal PVD traction that was likely present prior to initial diagnosis or of spontaneous macular hole closure. The foveal depression is flattening (V-shaped). **D:** IR + OCT horizontal scan of the left eye + enlarged version [red dashed box]: 2 months after initial diagnosis. The microhole hasdisappeared and the IS/OS, ELM and COST line group has been almost restored. The V-shaped foveal depression remains.

Image interpretation points

The pathological condition known as macular microholes appears to be generated by, at least 2 different causes. A common finding of the disease group is a small foveal photoreceptor IS/OS defect or a defect of foveal inner and outer segments. A primary cause of this disease group is spontaneous separation of perifoveal PVD during the formation of a macular hole. As seen in case 16 with a stage 1A macular hole, the perifoveal PVD spontaneously separates and only a foveal photoreceptor IS/OS defect remains. In this case as seen with initial reports, the posterior vitreous cortex including an operculum is seen in front of the macula on OCT. In both this case and case 16, the posterior vitreous cortex including an operculum and foveal deformation including disruptions of the OS/OS and/or inner and outer segmentsare important diagnostic points.

Case 24 Macular microhole: with complete PVD

A 59-year-old female, OD, BCVA 0.8

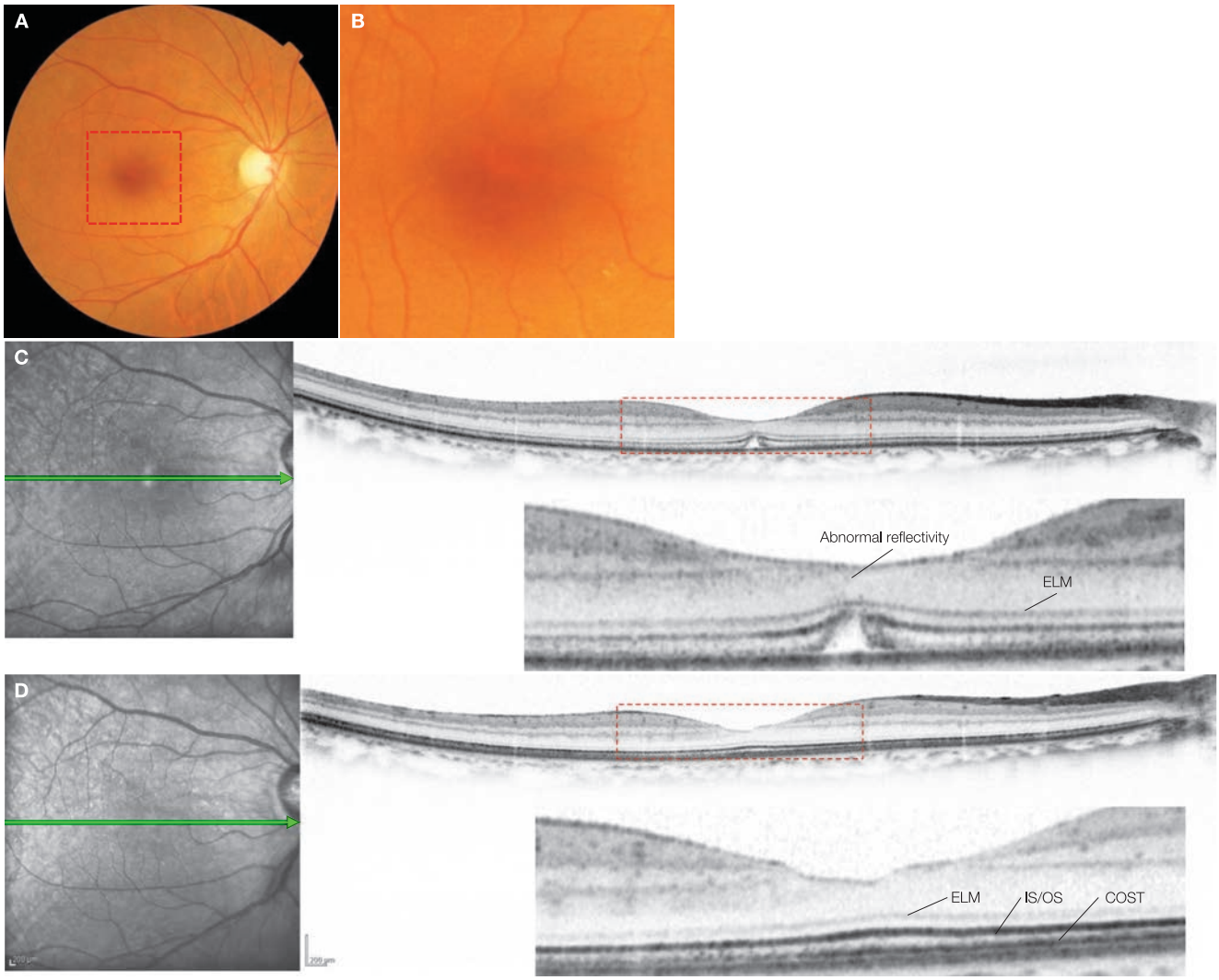

A: Color fundus photograph in the right eye, **B:** Enlarged version of A [red dashed box]: at initial diagnosis. An abnormal reflection known as »red spots« can be seen in the fovea centralis. **C:** IR + OCT horizontal scan of the right eye + enlarged version [red dashed box]: The posterior vitreous cortex cannot be seen. Note the inner and outer segment defect at the fovea centralis. This is essentially the same as a small foveal detachment in a Stage 1 macular hole. Abnormal high-reflectivity can also be seen in the foveal outer nuclear layer, which could be traces of deformation resulting from perifoveal PVD or of spontaneous macular hole closure. The foveal depression is flattening. **D:** IR + OCT horizontal scan of the right eye + enlarged version [red dashed box]: 3 months after initial diagnosis. The microhole has disappeared and the IS/OS, ELM and COST line group has been restored. The irregular foveal deformation and flattering of the foveal depression remains.

Image interpretation points

In this case, a macular microhole wes only seen in the right eye. Here, macular microhole formation is thought to be the result of spontaneous perifoveal PVD separation; however, unlike case 23, the posterior vitreous cortex cannot be seen on OCT making interpretation slightly difficult. Since a glial ring were observed by biomicroscopy, we can determine that PVD is complete. In this case, evidence for macular microholes caused by spontaneous perifoveal PVD separation is supported by the irregular deformation and flattening of the foveal depression, abnormal reflectivity of the foveal outer nuclear layer, and the spontaneous disappearance of the macular microhole.

Case 25 Macular microhole: Case without PVD

A 43-year-old female, OD, BCVA 1.0

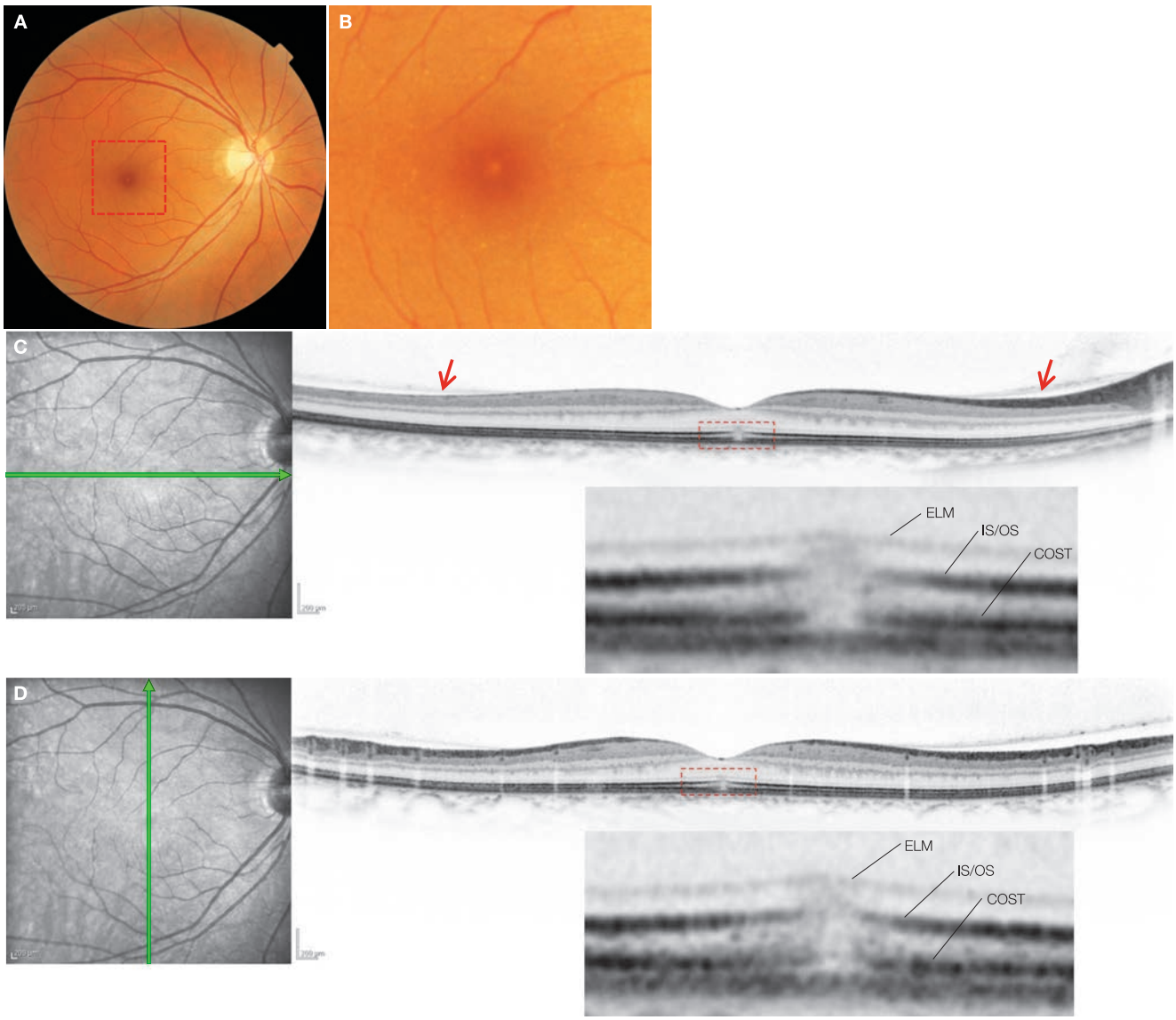

A: Color fundus photograph in the right eye, **B:** Enlarged version of A [red dashed box]: at initial diagnosis. A abnormal reflection known as »red spots« can be seen in the fovea centralis. **C:** IR + OCT horizontal scan of the right eye + enlarged version [red dashed box]: (→) shows the posterior vitreous cortex detached outside and at the periphery of the macula. **D:** IR + OCT vertical scan of the right eye + enlarged version [red dashed box]: The IS/OS and COST lines centralis are defective selectively at the fovea centralis.

Image interpretation points

This patient noticed decreased vision during a routine vision testing for contact lenses. Macular microholes were seen in both eyes. Since the PVD only occurred to the periphery of the macula, the foveal disruption does not appear to be secondary to tractional forces by the posterior vitreous cortex. After 3 years, the visual acuity and OCT findings remained unchanged. The pathogenesis of a macular microhole without macular PVD is still unknown.

2.2 Idiopathic epiretinal membrane

Background

ERM is a disease that a membrane visible with an ophthalmoscope is formed on the retinal surface of the macula, which causes retinal folds and thickening resulting in visual impairment and metamorphopsia. ERM occurs typically after PVD is complete. Cases in which there is no primary pathology known to cause ERMs are termed as idiopathic ERM. This is often seen unilaterally in the elderly and there is no gender predilection. In about 10% of idiopathic ERM cases macular PVD is not complete[1]. The membrane may appear clear, translucent, or white. The retinal folds vary from mild radial folds to severe folds accompanied by dislocation of the fovea. In severe cases, there is leakage from retinal vessels and formation of cystoid spaces. Premacular membranes resulting in eyes with retinal breaks, after retinal detachment surgeries (known as macular pucker in this case) or uveitis are known as secondary ERMs. Therefore, a detailed examination of the peripheral fundus is required.

Pathogenesis

Two hypotheses have been proposed for vitreoretinal interface membrane formation based on surgically collected tissue and histopathological findings of autopsied eyes. While different, they are not necessarily conflicting hypotheses.

Residual posterior vitreous membrane scaffolding theory (■ Fig. 2-12)

Kishi et al. demonstrated that there are elliptical defects in the posterior vitreous cortex after PVD is complete and the[2] vitreous cortex remains on the macular surface[3]. Thus, the posterior vitreous cortex can remain on the macular surface as a result of PVD. It is suggested that after the onset of PVD, cell proliferation and migration occur, with the posterior vitreous cortex remaining on the retinal surface as scaffolding. An extracellular matrix containing collagen is produced by these cells, which leads to membrane thickening. ERM is a disease that a membrane visible with an ophthalmoscope is formed on the retinal surface of the macula, which causes retinal folds and thickening resulting in visual impairment and metamorphopsia. ERM occurs typically after PVD is complete. Contraction of the fibrocellular membrane causes the retinal folds[4]. Most idiopathic ERMs are thought to occur as a result of this mechanism. The types of cells involved include glial cells differentiated into myofibroblast-like cells, vitreous cells, retinal pigment epithelium (RPE) cells, and fibrous astrocytes[5–12].

Migratory cell membrane formation theory (■ Fig. 2-13)

This theory postulates that when PVD stops around the fovea and optic disc or along the retinal blood vessels where the posterior vitreous cortex is attenuated and strongly adheres cell migration occurs through cracks in the internal limiting membrane (ILM) formed at this time due to vitreous separation as well as preexisting ILM dehiscences of the retina ans optic disc. This process forms a fibrocellular membrane through cell-cell junctions and extracellular matrix production[4]. ERM without PVD and vitreomacular traction syndrome are thought to fall into this category. Vitreomacular traction syndrome is often secondary to other retinal diseases such as diabetic maculopathy where there may be factors that strengthen vitreous traction. There are some cases in which the membrane appears to have multiple layers; this fibrocellular membrane may be the posterior vitreous cortex separated into two layers, or a complex of the ILM and posterior vitreous cortex.

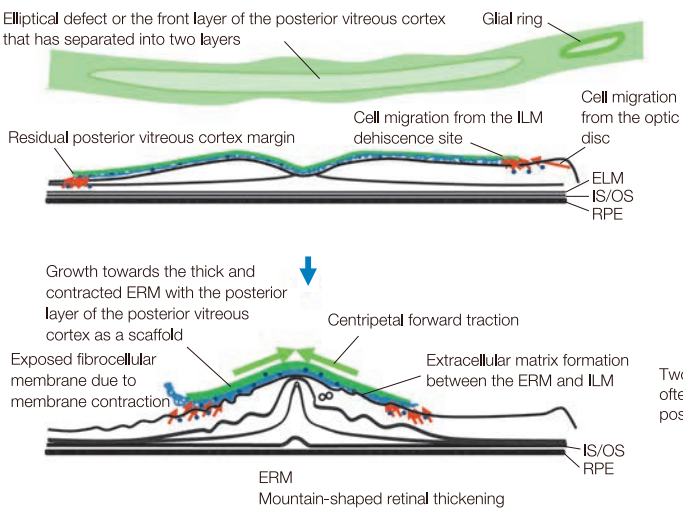

■ Fig. 2-12 Residual posterior vitreous membrane scaffolding theory

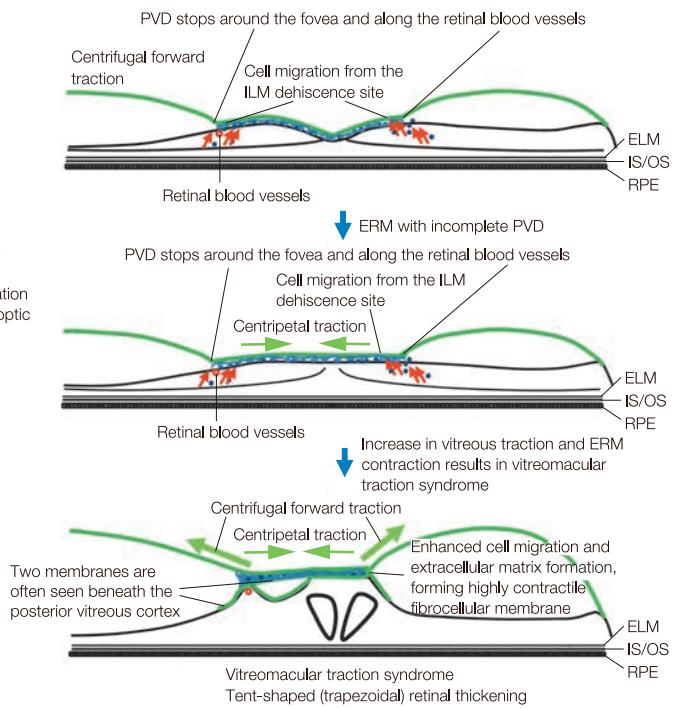

■ Fig. 2-13 Migratory cell membrane formation theory

OCT findings

On OCT, an ERM is seen as a highly reflective thick membrane. Folds are seen in the inner retinal layer beneath the membrane, but no in the membrane itself. There are cases where a gap between ERM and retinal surface is weakly reflective; there are also cases where the gap are filled with moderate reflectivity. The fibrous membrane that had been formed in a gap between ERM and macular surface, is sometimes exposed and lifted towards the vitreous cavity due to progressive contraction of the ERM. When seen on a 9 mm scan, ERM is most often present in isolation on the macular surface with no continuity from the posterior vitreous cortex (Fig. 2-12); however, in about 10% of cases, the PVD is incomplete and a thick highly reflective ERM continuing from the posterior vitreous cortex can be seen (Fig. 2-13). In addition, in cases of incomplete PVD a retinal surface ERM can sometimes be seen beneath the detached posterior vitreous cortex. In cases where the posterior vitreous cortex has been removed during surgery, a ERM remains on the macular surface in 30% of cases despite no defects in the posterior vitreous cortex.[13] To explain this phenomenon, the migratory cell membrane formation theory postulates that an ERM forms in the gaps of the posterior vitreous cortex and retina, and then the posterior vitreous cortex becomes detached from the ERM, resulting in the formation of 2 distinct membranes. Another theory postulates that the posterior vitreous cortex separates into two layers allowing the ERM to form with the posterior layer providing a scaffold after the anterior layer has detached.[14, 15].

As a result of contraction, ERMs transmit centripetal forward traction toward the fovea centralis in the macular surface causing retinal fold formation and retinal thickening. Consequently, ERM is characterized by a mountain-shaped retinal thickening, forming a peak in the fovea centralis (Figs. 2-12, 2-14)[16]. The centripetal traction vector in the retinal tangential direction causes radial folds in the inner retina that can be seen with an ophthalmoscope. In the fovea centralis, the forward traction vector mainly acts to thicken the outer nuclear layer, causing elevation of the IS/OS and a small foveal detachment. As a result, IS/OS defects occur in 24~77% of cases[17–21]. When observed with an adaptive optics scanning laser ophthalmoscope (SLO), microfolds occur on the photoreceptor cell level, which is correlated with metamorphopsia[22]. On the other hand, thickening of the parafovea occurs mainly in the inner retina, which has also been claimed to correlate with metamorphopsia.[23].

Macular pseudoholes

A macular pseudohole is a subtype of ERM, and hence forward traction by the ERM does not work toward the fovea centralis. This results in thickening of the macula with the fovea centralis remaining unthickened (Fig. 2-14). In contrast, in vitreomacular traction syndrome, centrifugal forward traction occurs resulting in a distinctive trapezoidal-shaped retinal thickening (Fig. 2-13).

Prognosis

There are cases that do not necessarily lead to loss of visual acuity even when an ERM is noted. In addition, cases where there is progressive visual acuity loss during follow-up examinations accounts for less than 10% of the total cases. ERM contraction is thought to rapidly progress and then stop.

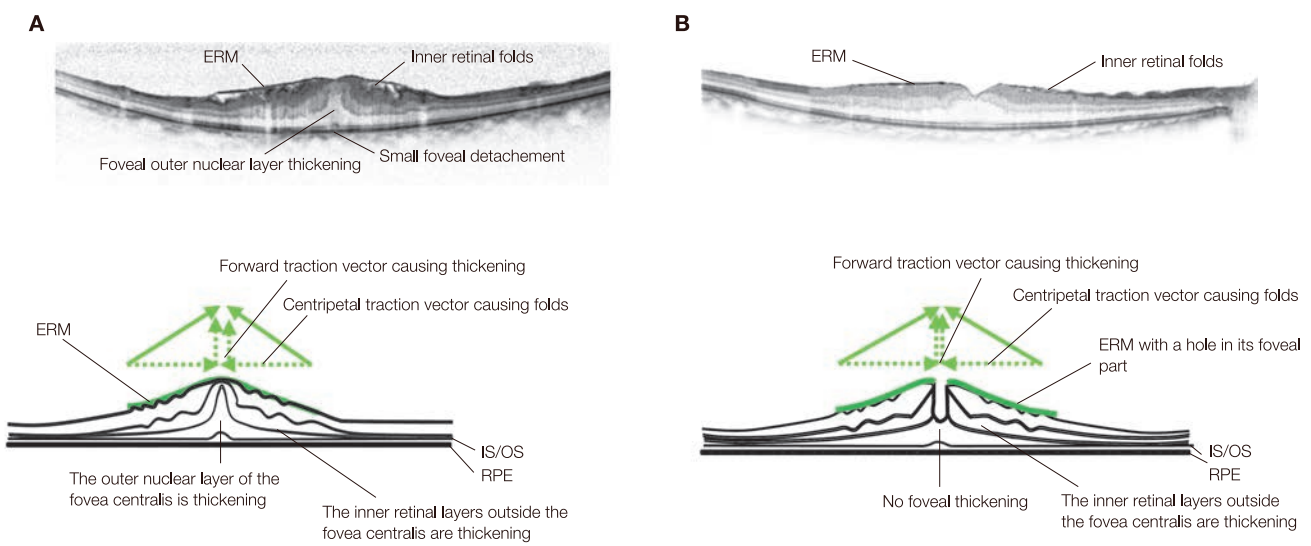

Fig. 2-14 Comparison between epiretinal membrane (**A**) and macular pseudoholes (**B**)

References

1) Sidd RJ, Fine SL, Owens SL, et al. Idiopathic preretinal gliosis. Am J Ophthalmol. 1982; 94:44–48.
2) Kishi S, Shimizu K. Oval defect in detached posterior hyaloid membrane in idiopathic preretinal macular fibrosis. Am J Ophthalmol. 1994; 118:451–456.
3) Kishi S, Demaria C, Shimizu K. Vitreous cortex remnants at the fovea after spontaneous vitreous detachment. Int Ophthalmol. 1986; 9:253–260.
4) Gass JDM. Macular dysfunction caused by epiretinal membrane contraction. Stereoscopic atlas of macular diseases. Diagnosis and treatment 4th ed., CV Mosby, St. Louis, 1997. pp176–180.
5) Clarkson JG, Green WR, Massof D. A histopathologic review of 168 cases of preretinal membrane. Am J Ophthalmol. 1977; 84:1–17.
6) Kampik A, Green WR, Michels RG, et al. Ultrastructural features of progressive idiopathic epiretinal membrane removed by vitreous surgery. Am J Ophthalmol. 1980; 90:797–809.
7) Hui YN, Goodnight R, Zhang XJ, et al. Glial epiretinal membranes and contraction. Immunohistochemical and morphological studies. Arch Ophthalmol. 1988; 106:1280–1285.
8) Smiddy WE, Maguire AM, Green WR, et al. Idiopathic epiretinal membranes. Ultrastructural characteristics and clinicopathologic correlation. Ophthalmology. 1989; 96:811–820.
9) Morino I, Hiscott P, McKechnie N, et al. Variation in epiretinal membrane components with clinical duration of the proliferative tissue. Br J Ophthalmol. 1990; 74:393–399.
10) Okada M, Ogino N, Matsumura M, et al. Histological and immunohistochemical study of idiopathic epiretinal membrane. Ophthalmic Res. 1995; 27:118–128.
11) Kampik A, Kenyon KR, Michels RG, et al. Epiretinal and vitreous membranes: comparative study of 56 cases. Retina. 2005; 25:1445–1454.
12) Bringmann A, Wiedemann P. Involvement of Müller glial cells in epiretinal membrane formation. Graefes Arch Clin Exp Ophthalmol. 2009; 247:865–883.
13) Yamashita T, UemuraA, Sakamoto T. Intraoperative characteristics of the posterior vitreous cortex in patients with epiretinal membrane. Graefes Arch Clin Exp Ophthalmol. 2008; 246:333–337.
14) Kakehashi A, Schepens CL, de Sousa-Neto A, et al. Biomicroscopic findings of posterior vitreoschisis. Ophthalmic Surg. 1993; 24:846–850.
15) Heilskov TW, Massicotte SJ, Folk JC. Epiretinal macular membranes in eyes with attached posterior cortical vitreous. Retina. 1996; 16:279–284.
16) Arichika S, Hangai M, Yoshimura N. Correlation between thickening of the inner and outer retina and visual acuity in patients with epiretinal membrane. Retina. 2010; 30:503–508.
17) Mitamura Y, Hirano K, Baba T, et al. Correlation of visual recovery with presence of photoreceptor inner/outer segment junction in optical coherence images after epiretinal membrane surgery. Br J Ophthalmol. 2009; 93:171–175.
18) Suh MH, Seo JM, Park KH, et al. Associations between macular findings by optical coherence tomography and visual outcomes after epiretinal membrane removal. Am J Ophthalmol. 2009; 147:473-480.e3.
19) Falkner-Radler CI, Glittenberg C, Hagen S, et al. Spectral-domain optical coherence tomography for monitoring epiretinal membrane surgery. Ophthalmology. 2010; 117:798–805.
20) Inoue M, Morita S, Watanabe Y, et al. Inner segment/outer segment junction assessed by spectral-domain optical coherence tomography in patients with idiopathic epiretinal membrane. Am J Ophthalmol. 2010; 150:834–839.
21) Oster SF, Mojana F, Brar M, et al. Disruption of the photoreceptor inner segment/outer segment layer on spectral domain-optical coherence tomography is a predictor of poor visual acuity in patients with epiretinal membranes. Retina. 2010; 30:713–718.
22) Ooto S, Hangai M, Takayama K, et al. High-resolution imaging of the photoreceptor layer in epiretinal membrane using adaptive optics scanning laser ophthalmoscopy. Ophthalmology. 2011; 118:873–881.
23) Watanabe A, Arimoto S, Nishi O. Correlation between metamorphopsia and epiretinal membrane optical coherence tomography findings. Ophthalmology. 2009; 116:1788–1793.

Case 26 Idiopathic epiretinal membrane: A typical example

A 76-year-old male, OD, BCVA 0.6

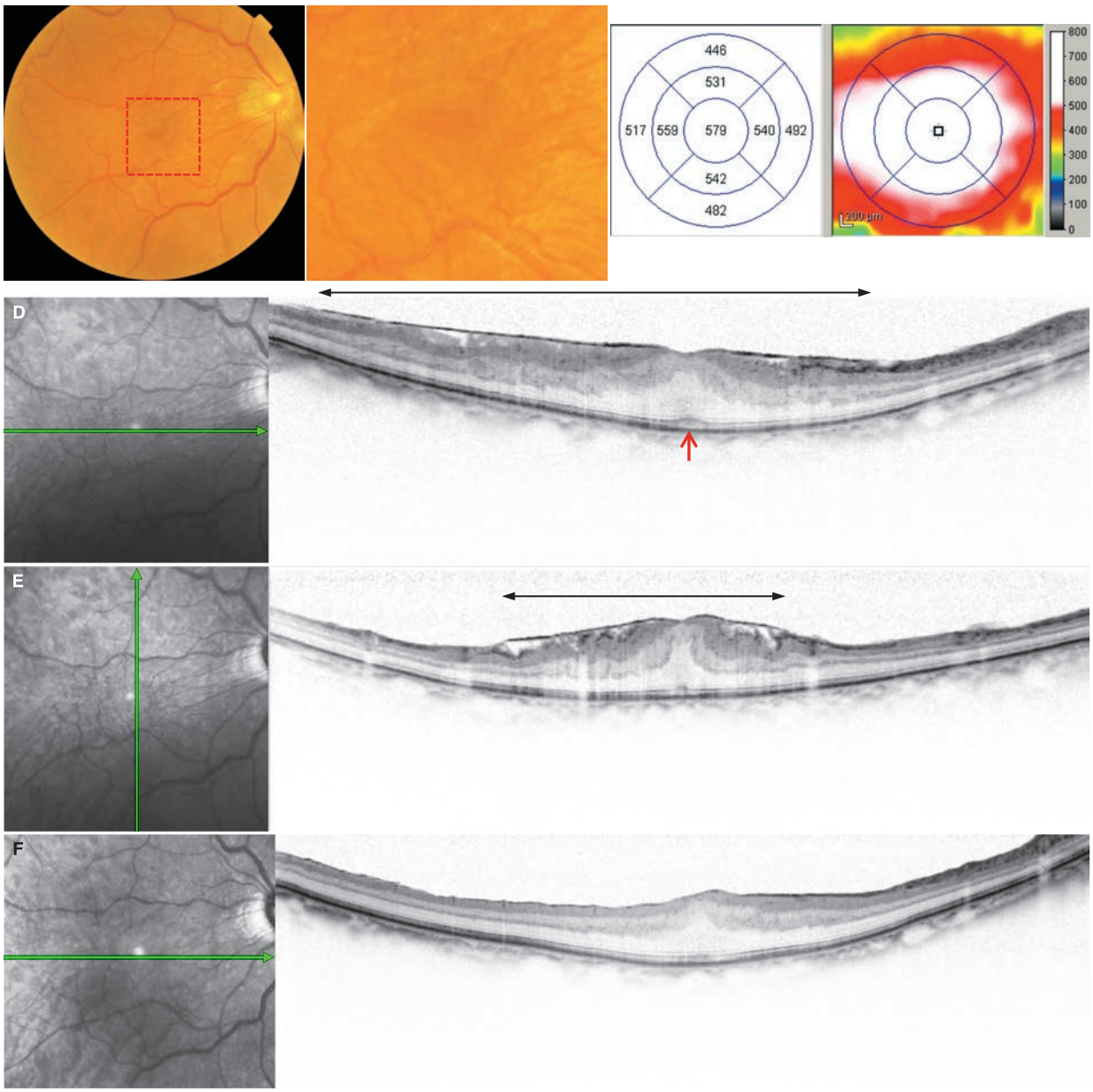

A: Color fundus photograph in the right eye: Retinal wrinkling, mild membrane whitening and tortuosity of the retinal blood vessels are noted. **B:** Enlarged version of A [red dashed box]: Same findings as A can be observed. **C:** Retinal thickness color map of the right eye, **D:** IR + OCT horizontal scan of the right eye: ERM (↔) and a small foveal detachment (➔) can be seen. **E:** IR + OCT vertical scan of the right eye: Retinal folds are noticeable in the horizontal direction. A gap between ERM (↔) and ILM appears to be vacant adherent only to the peaks of the folds. **F:** IR + OCT horizontal scan of right eye: 2 months after surgery. Retinal thickening is reduced, but the foveal depression has not been restored. Best-corrected visual acuity has improved to 0.9

Image interpretation points

ERMs are thought to occur as a result of fibrocellular membrane formation that develops when cells migrate to a gap in the residual posterior vitreous cortex and ILM in eyes with macular PVD. The area in which an ERM is formed is narrower than the 9 mm OCT scan area in most cases and ERM stumps can be seen in the images. Retinal thickening and retinal fold formation occurs as a result of concentric contraction of the residual posterior vitreous cortex. Retinal folds are noticeable on vertical scans that intersect the retinal blood vessels because ERMs strongly adhere to the blood vessels. The gap between ERM and ILM is fulfilled with moderately reflective fibrocellular membraneous tissue in some eyes while it appears to be vacant as seen in this case.

Case 27 Idiopathic epiretinal membrane: Exposure of the fibrocellular membrane

A 58-year-old female, OS, BCVA 0.8

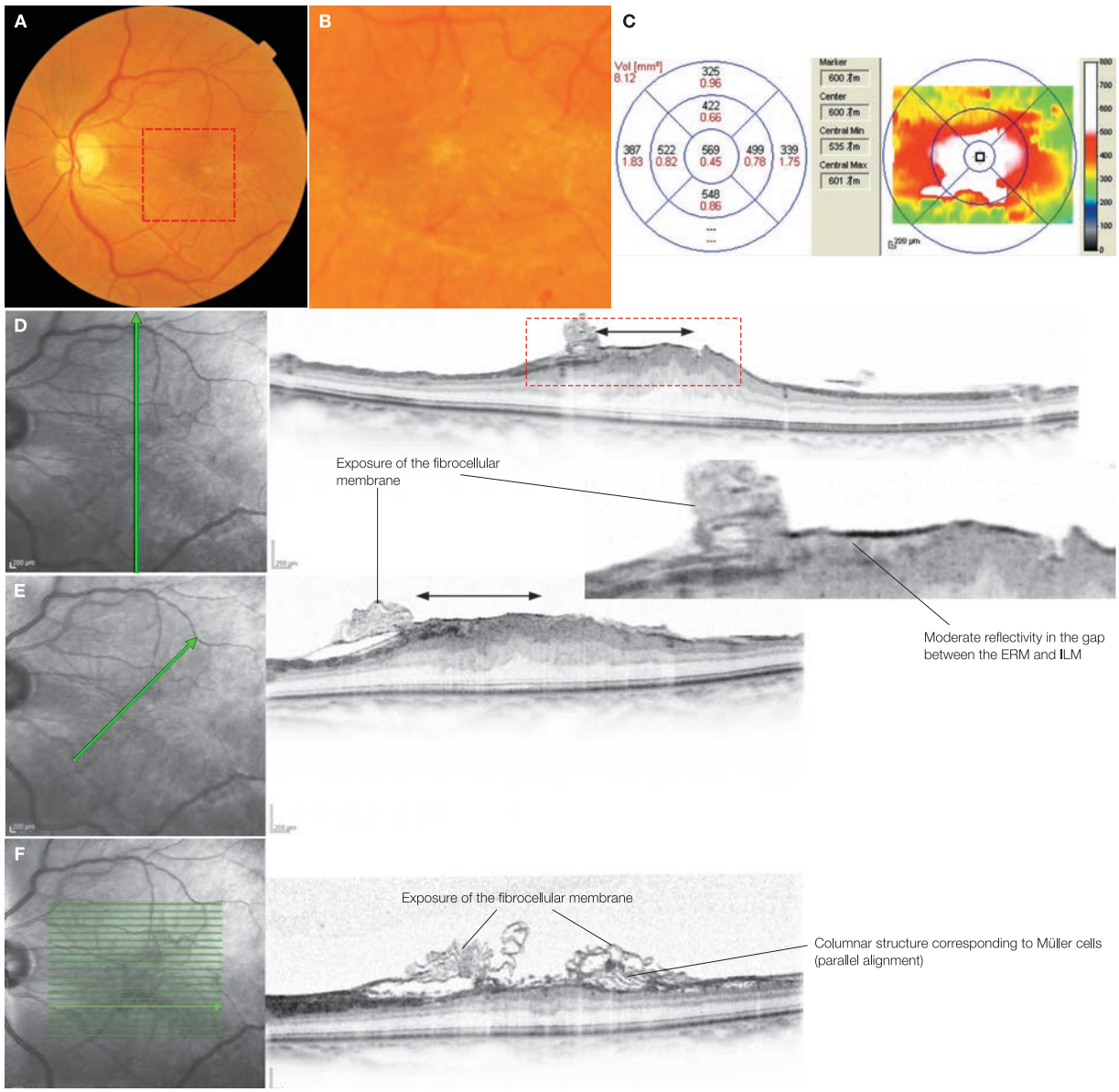

A: Left eye fundus photograph, **B:** Enlarged version of A [red dashed box]: Retinal folds, whitening and tortuosity of the retinal blood vessels can be viewed. **C:** Retinal thickness color map of the left eye. **D:** IR + OCT horizontal scan of the left eye + enlarged version [red dashed box]: Exposure of flaccid swollen fibrous tissue from ERM (↔) stumps can be seen. This extends from the moderately reflective fibrous membrane that exists between the ERM and the ILM. The IS/OS and COST lines of the fovea centralis are normal. **E:** IR + OCT oblique scan of the left eye: Same findings as D can be seen. Retinal folds are not clearly seen. This is because the gap between the ERM and ILM is fulfilled with moderately reflective fibrocellular tissue, which is also responsible for the whitening of the ERM on a color fundus photograph. ↔ shows ERM. **F:** IR + OCT horizontal scan of the left eye: Flaccid coil-shaped fibrous structures representing exposed fibrocellular membrane are clearly visible. Columnar structure running obliquely to the retina in parallel represents Muller cells in the ILM detachment. These 2 structures can be differentiated based on the characteristic pattern.

Image interpretation points

Findings of fibrous, flaccid tissue rising towards the vitreous cavity from ERM stumps is often seen. These findings are consistent with thickened white areas when viewed with an ophthalmoscope. In cases such as these, retinal folds exist but become indistinct on OCT since the gap between the ERM and ILM is fulfilled with the fibrous membrane that exhibits moderate reflectivity. These features suggest extensive fibroplasia and cell migration towards the ERM and ILM gap leading to substantial ERM contraction.

Case 28 Idiopathic epiretinal membrane: Membrane with significant whitening

A 74-year-old female, OS, BCVA 0.4

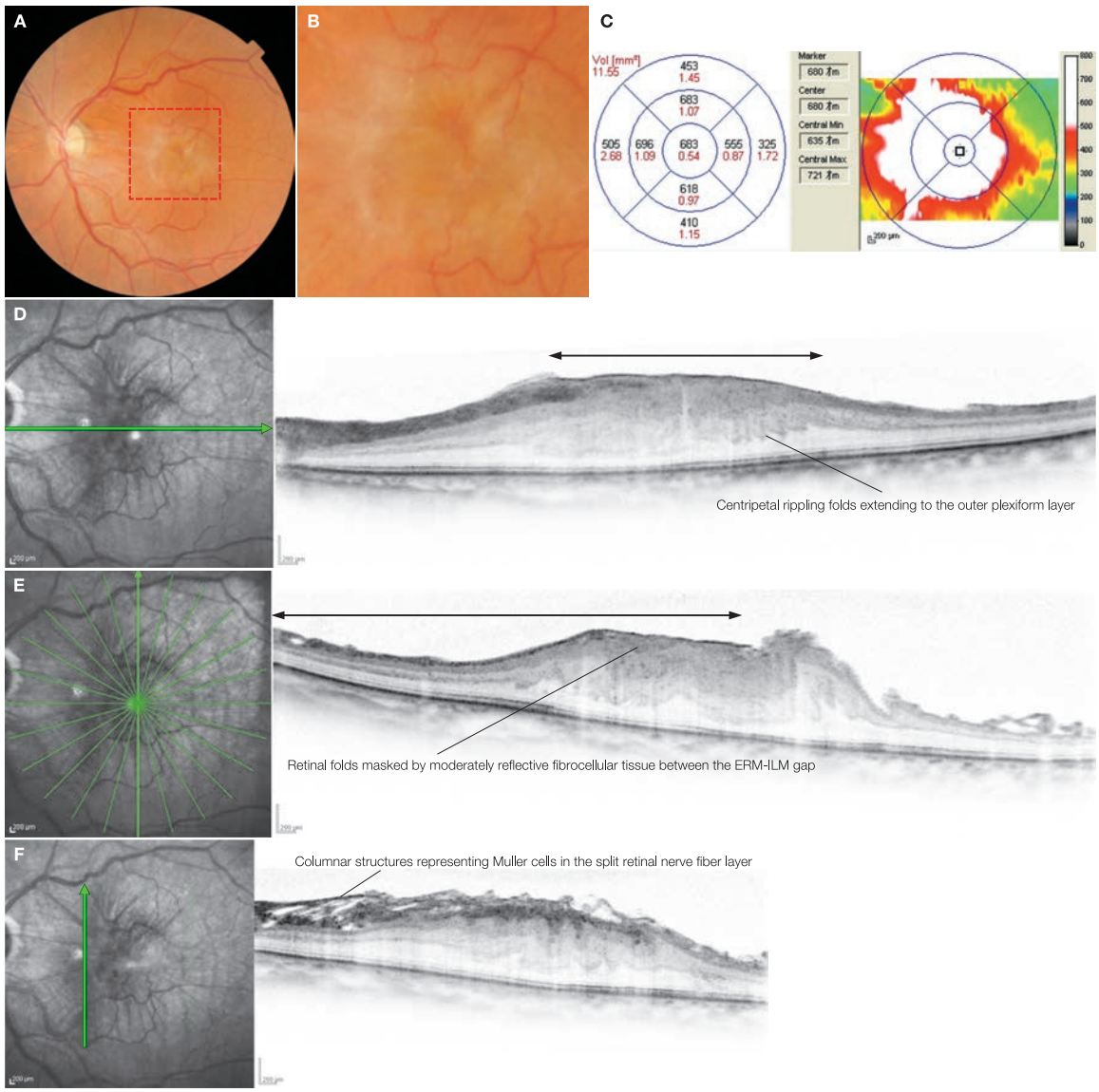

A: Color fundus photograph in the left eye, **B:** Enlarged version of A [red dashed box]: at initial diagnosis. Significant macular whitening accompanies radial retinal folds. **C:** Retinal thickness color map of the left eye: Significant thickening can be seen. **D:** IR + OCT horizontal scan of the left eye: The rippling folds extending to the outer nuclear layer indicate strong centripetal forward tractional force. The fovea centralis shows thickening of the outer nuclear layer, while the parafoveal retina shows thickening of the inner retinal layers. ↔ shows ERM. **E:** IR + OCT vertical scan of the left eye: Retinal folds that can be readily seen in the fundus photograph are indistinct. Fibrocellular membrane tissue filling the ERM and ILM gap may be responsible for the unclear visibility of retinal folds, and also for the membrane whitening. ↔ shows ERM. F: IR + OCT vertical scan of the left eye: ILM detachment or splitting of the retinal nerve fiber layer can be seen. A columnar structure thought to be Müller cells can be seen in the separation gap.

Image interpretation points

This is a case where retinal whitening and contraction are significant. The gap between the highly reflective ERM and ILM has been completely filled with moderately reflective fibrocellular membrane tissue, which is thought to be why membrane whitening is exhibited on a color fundus photograph. Significant thickening, ripples in the outer plexiform layer, and separation of the retinal nerve fiber layer demonstrate the strength of the traction. Ripples and the columnar structure corresponding to Müller cells in the retinal nerve fiber layer separation gaps show the centripetal forward traction. The end of the ERM is visible and the fibrous membrane exposed outside can sometimes be seen. This can be interpreted as findings which demonstrate that concentric contraction has progressed.

Case 29 Idiopathic epiretinal membrane: Significant columnar structure formation

A 58-year-old female, OS, BCVA 0.3

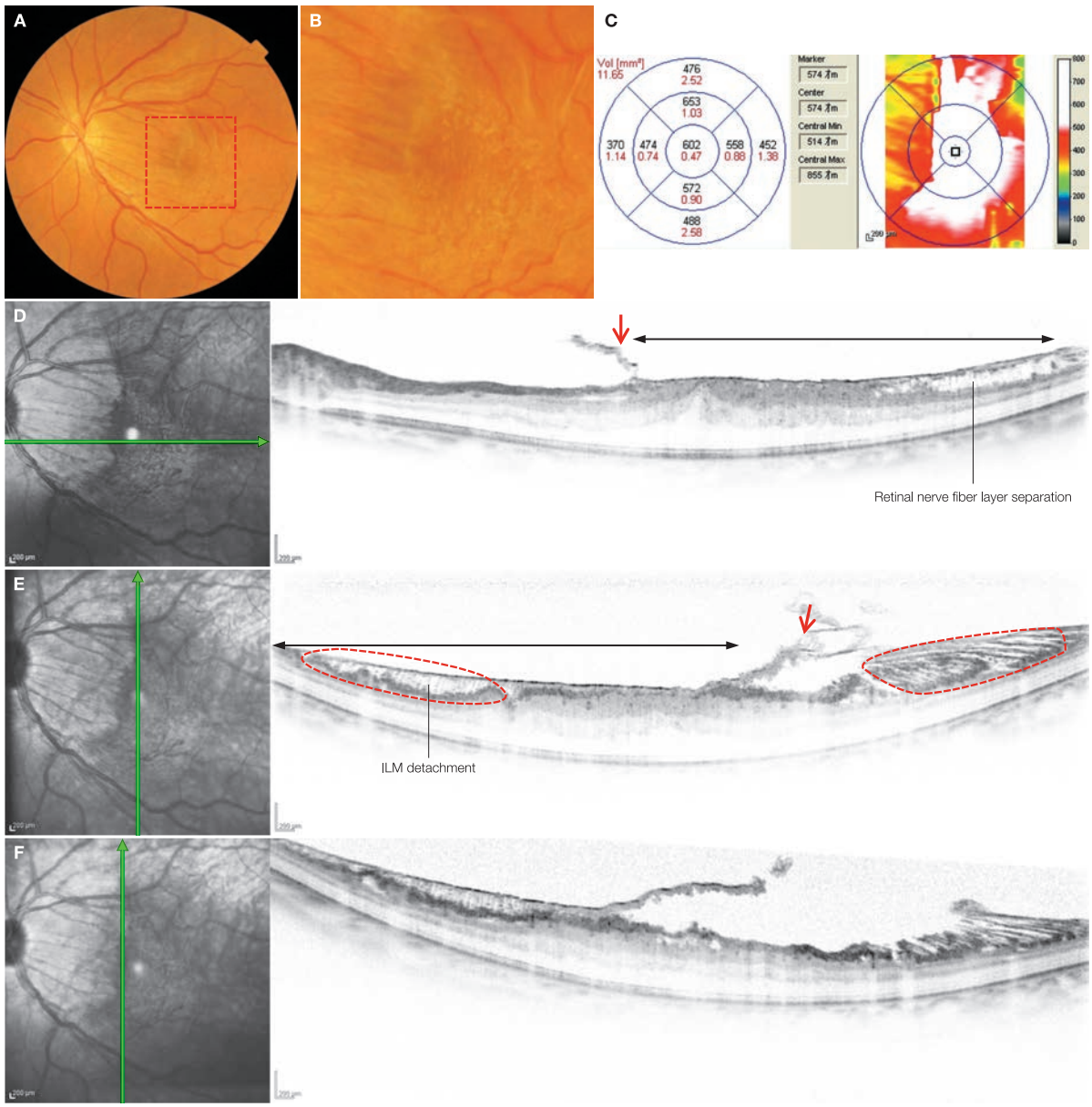

A: Color fundus photograph in the left eye, **B:** Enlarged version of A [red dashed box]: Substantial macular whitening accompanies radial retinal folds. **C:** Retinal thickness color map of the left eye. **D:** IR + OCT horizontal scan of the left eye: The ERM (↔) contracts and the fibrocellular membrane (➔) formed in the ERM and ILM gap, is exposed and becomes flaccid. The retinal nerve fiber layer is splitting and a columnar structure corresponding to Muller cells is seen in the gap. **E:** IR + OCT vertical scan of left eye: Exposure of the fibrocellular membrane (➔) can be seen. A columnar structure (red dashed circle) corresponding to Müller cells in the separation gap of the ILM detachment can be seen. The orientation of the columnar structure appears to show the direction of the traction. ↔ shows ERM. F: IR + OCT vertical scan of the left eye: A fibrocellular membrane tissue that formed between the ERM and the ILM has detached from the macular surface and has become flaccid

Image interpretation points

This is a case where whitening and contraction of ERM are substantial. Significant thickening, ripples in the inner layers, and separation of the retinal nerve fiber layer demonstrate the strength of the traction. The orientation of the columnar structure in the retinal nerve fiber layer splitting gap and beneath the detached ILM shows centripetal traction. The end of the ERM is visible and the fibrocellular membrane exposed can sometimes be seen. This can be interpreted as findings that also demonstrate that concentric contraction has progressed.

Case 30 Idiopathic epiretinal membrane: Case ① where macular PVD has not been complete

A 66-year-old female, OD, BCVA 0.7

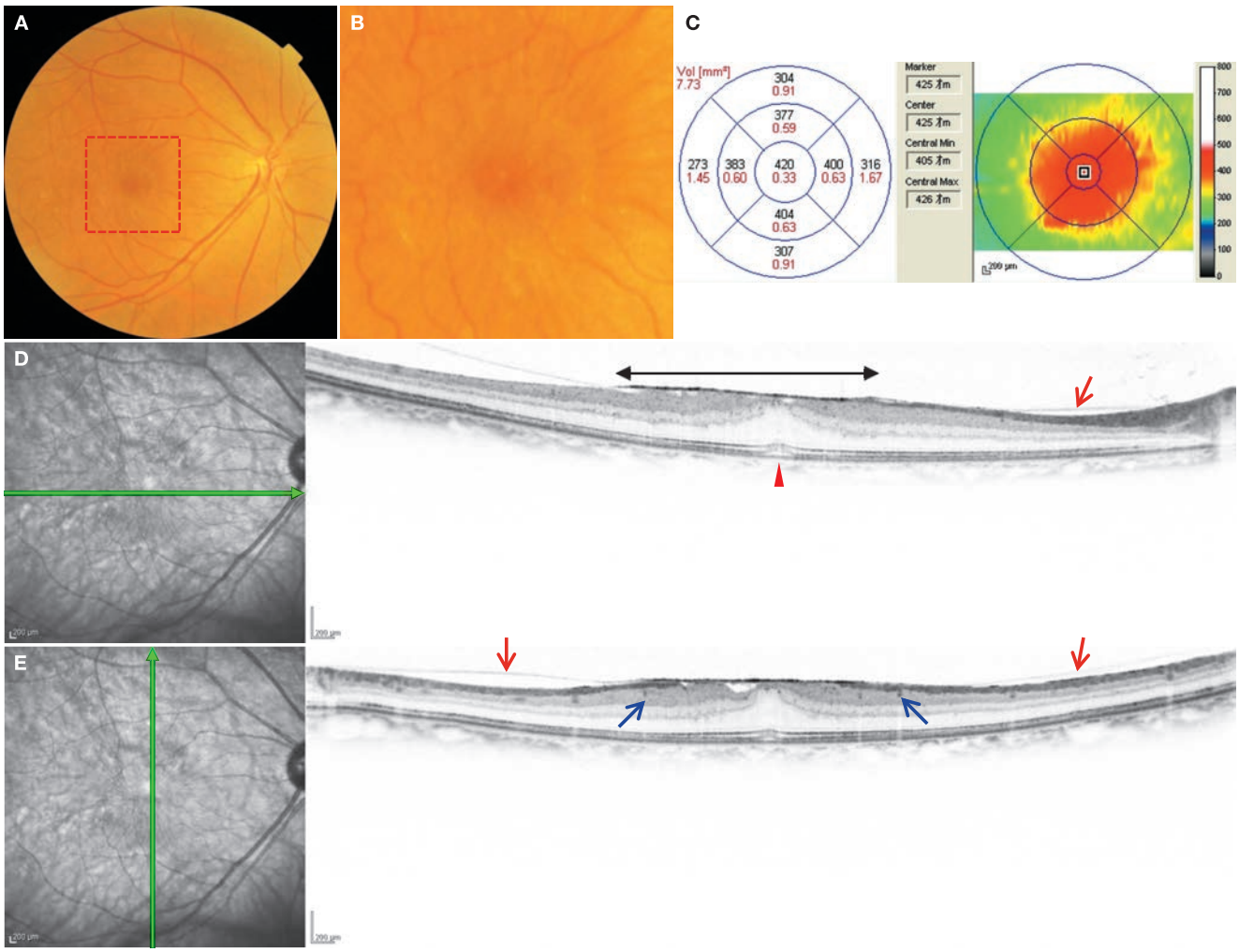

A: Color fundus photograph in the right eye, **B:** Enlarged version of A [red dashed box]: Membrane whitening and radial retinal folds can be seen. **C:** Retinal thickness color map of the right eye: Thickening is not very significant. **D:** IR + OCT horizontal scan of the right eye: The macular PVD stops at the periphery of the macula and the posterior vitreous cortex adherent to the macula has developed into the ERM ↔. Compared to the detached posterior vitreous cortex (➔), the ERM is highly reflective and linear. Contraction of ERM leads to formation of retinal folds and a small foveal detachment (▶). **E:** IR + OCT vertical scan of the right eye: PVD appears to have stopped in the retinal blood vessel area (➔). ➔ indicates the posterior vitreous cortex

Image interpretation points

This is a case where macular PVD is incomplete and has stopped at the retinal blood vessel of the macula. Cell migration occurred from cracks in the ILM along the retinal blood vessels. A fibrovascular membrane has formed in the gap between the attached posterior vitreous cortex and ILM, which is thought to develop into an ERM. Contraction occurs in the ERM development process, generating centripetal forward traction. This is similar to the pathogenic mechanism of vitreomacular traction syndrome in the disease processes include both centripetal and centrifugal traction, but the morphological changes that occur in the retina are a little different. Vitreomacular traction syndrome is trapezoidal-shaped thickening due to strong centrifugal forward traction, whereas in this case foveal thickening and retinal folds due to centripetal forward traction is primary. However, both diseases conditions may be on the same spectrum.

Case 31 Idiopathic epiretinal membrane: Case ② where macular PVD has been complete

Left eye of a 74-year-old female with vision corrected to 0.8

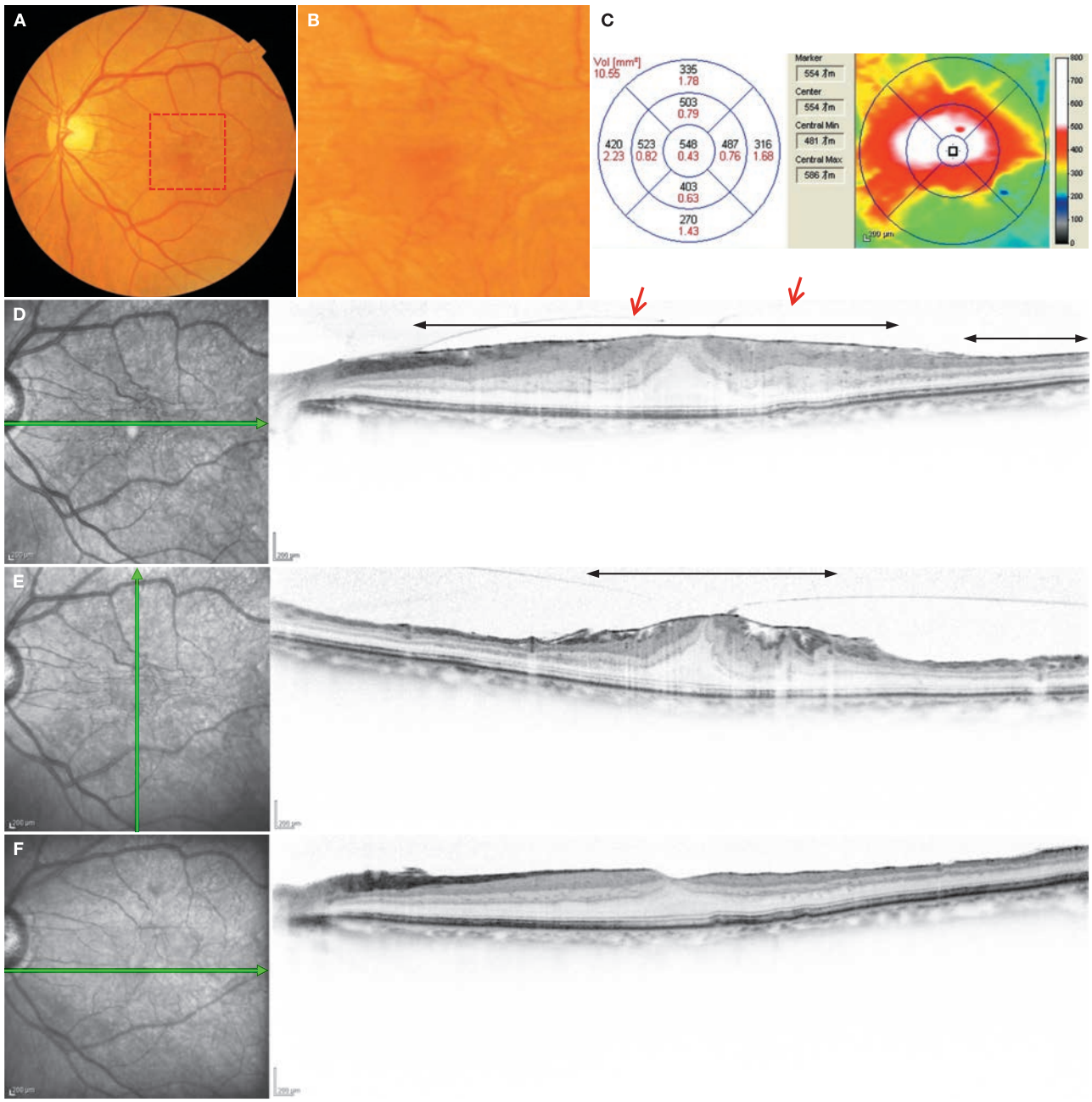

A: Color fundus photograph in the left eye, **B:** Enlarged version of A [red dashed box]: Whitening and tortuosity of the retinal blood vessels can be seen. **C:** Retinal thickness color map of the left eye. **D:** IR + OCT horizontal scan of the left eye: Macular PVD is stopping at the foveal border (➔). This state is known as perifoveal PVD. ERM (↔) is formed even in the area where PVD has progressed. **E:** IR + OCT vertical scan of the left eye: Retinal folds are noticeable in the horizontal direction. ↔ shows ERM. **F:** IR + OCT horizontal scan of left eye: 2 months after surgery. Retinal thickening has decreased. Thinning of the temporal retina that occurs when the ILM has detached cannot be seen. Thus, it is very likely that the retinal surface membrane is not the ILM, but the ERM.

Image interpretation points

In this case, the posterior vitreous cortex and ERM can be seen at the same time part way through the PVD process. An ERM is thought to be formed as a result of fibrocellular membrane formation that occurs when cells migrate to a gap in the residual posterior vitreous cortex and ILM. In this case, the posterior vitreous cortex in the macula separated into two layers and PVD only of the inner layer progressed and then stopped at the parafovea. ERM appears to be formed with the posterior layer acting as a scaffold.

Case 32 Epiretinal membrane secondary to retinal hemangioma

A 53-year-old female, OS, BCVA 0.6

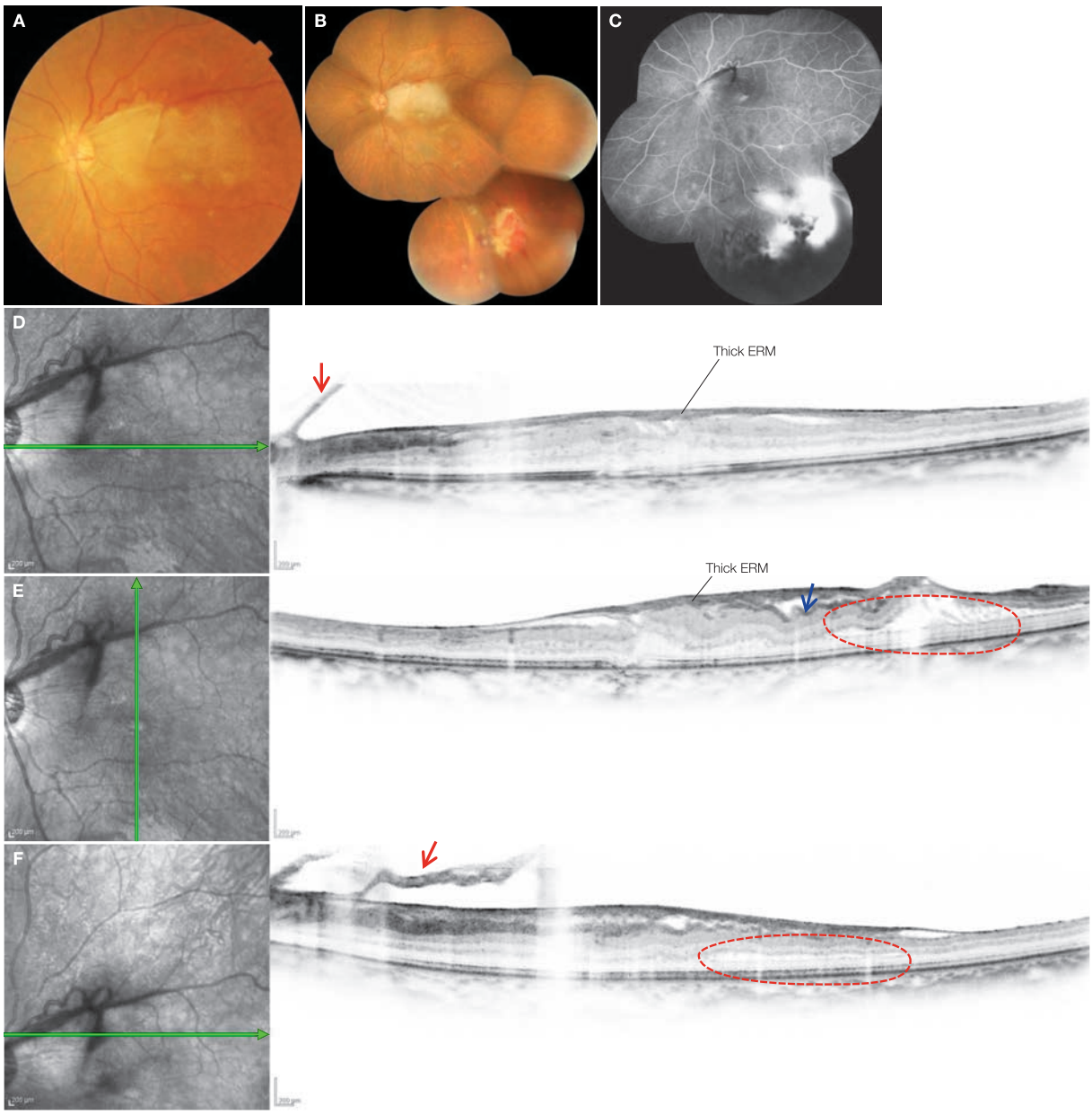

A: Color fundus photograph in the left eye: Thick, yellowish-white ERM is noticeable over a wide area of posterior pole. **B:** Left eye panoramic fundus photograph in the left eye: Hemangioma of the retina can be seen infero temporally. **C:** Panoramic fluorescein angiography (FA) in the left eye: Significant leakage from hemangioma of the retina and an avascular region in the periphery can be observed. **D:** IR + OCT horizontal scan of the left eye: Seemingly thick »rigid« ERM can be seen. Retinal thickening is mild. Retinal schisis (red dashed circle) secondary to the traction toward the retinal blood vessel can be observed superiorly. Proliferative membrane tissue rising towards the vitreous cavity is noted (➔). **E:** IR + OCT vertical scan of the left eye: Irregular retinal folds (➔) can be seen above the macula. **F:** IR + OCT horizontal scan of the left eye: Proliferative membrane tissue rising towards the vitreous cavity is noticeable (➔). Retinal schisis (red dashed circle) can be observed temporally.

Image interpretation points

This is a case of an ERM thought to be secondary to retinal hemangioma. ERM occurs frequently secondary to fundus diseases such as retinal tears, retinal vascular diseases and uveitis. In this type of ERM, there is a tendency for the area to be wider than an idiopathic ERM, the thickness of the membrane to be more significant, and increased retinal traction. Significant membrane thickening, irregularities in the retinal folds and retinoschisis formation in the outer plexiform layer are also noticeable in this case.

Case 33 Macular pseudohole: A typical example

A 73-year-old female, OD, BCVA 0.7

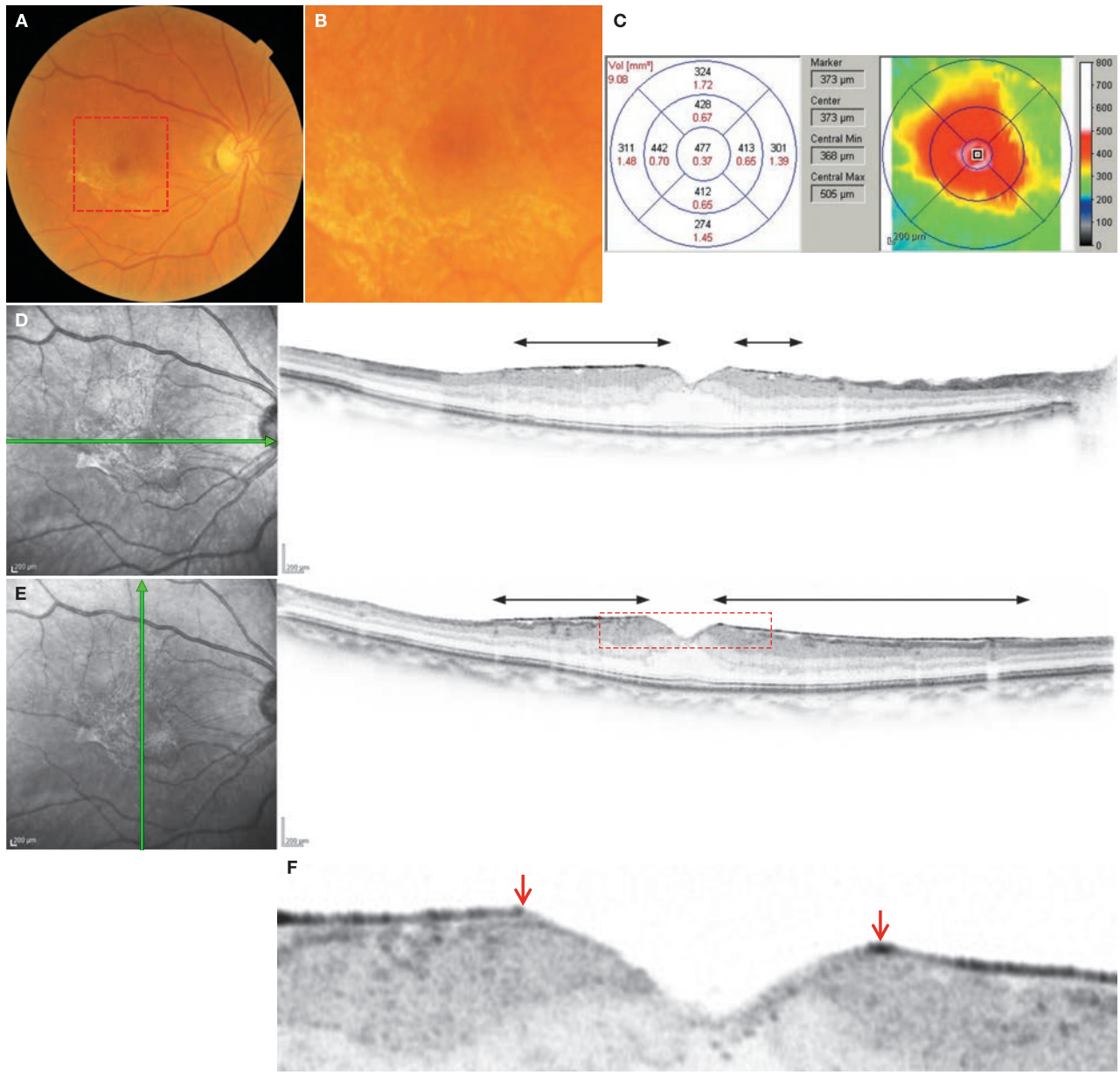

A: Color fundus photograph in the right, **B:** Enlarged version of A [red dashed box]: Significant whitening can be seen in the inferior macula. **C:** Retinal thickness color map of the right eye. **D:** IR + OCT horizontal scan of the right eye, **E:** IR + OCT vertical scan of the right eye: ERM (↔) cannot be seen in the fovea centralis, and a V-shaped foveal depression can be seen. Excluding the foveal shape, this is no different than a typical ERM OCT image. F: Enlarged version of E [red dashed box]: ERM stumps can be clearly seen (➔)

Image interpretation points

An ERM develops as a membrane characterized by concentric contraction. The posterior vitreous cortex that remains on the macular surface after PVD onset becomes scaffolding along which cell migration and fibrous membrane formation occur. Macular pseudoholes (MPH) occur as a result of the same pathogenic mechanism as ERM; however, with MPH, a hole is formed at the foveal area of the residual posterior vitreous cortex. In other words, the foveal thickening characteristic to ERM is missing. In addition, macular pseudohoes can be distinguished from lamellar macular holes by retinal findings, i.e. retinal folds, and retinal thickening outside the fovea centralis as a result of concentric contraction of ERM. Nevertheless, ERM can also form after lamellar circular hole formation sometimes making it difficult to differentiate the two entities.

Case 34 Macular pseudohole: Case where macular PVD has not been complete

A 56-year-old male, OD, BCVA 1.5

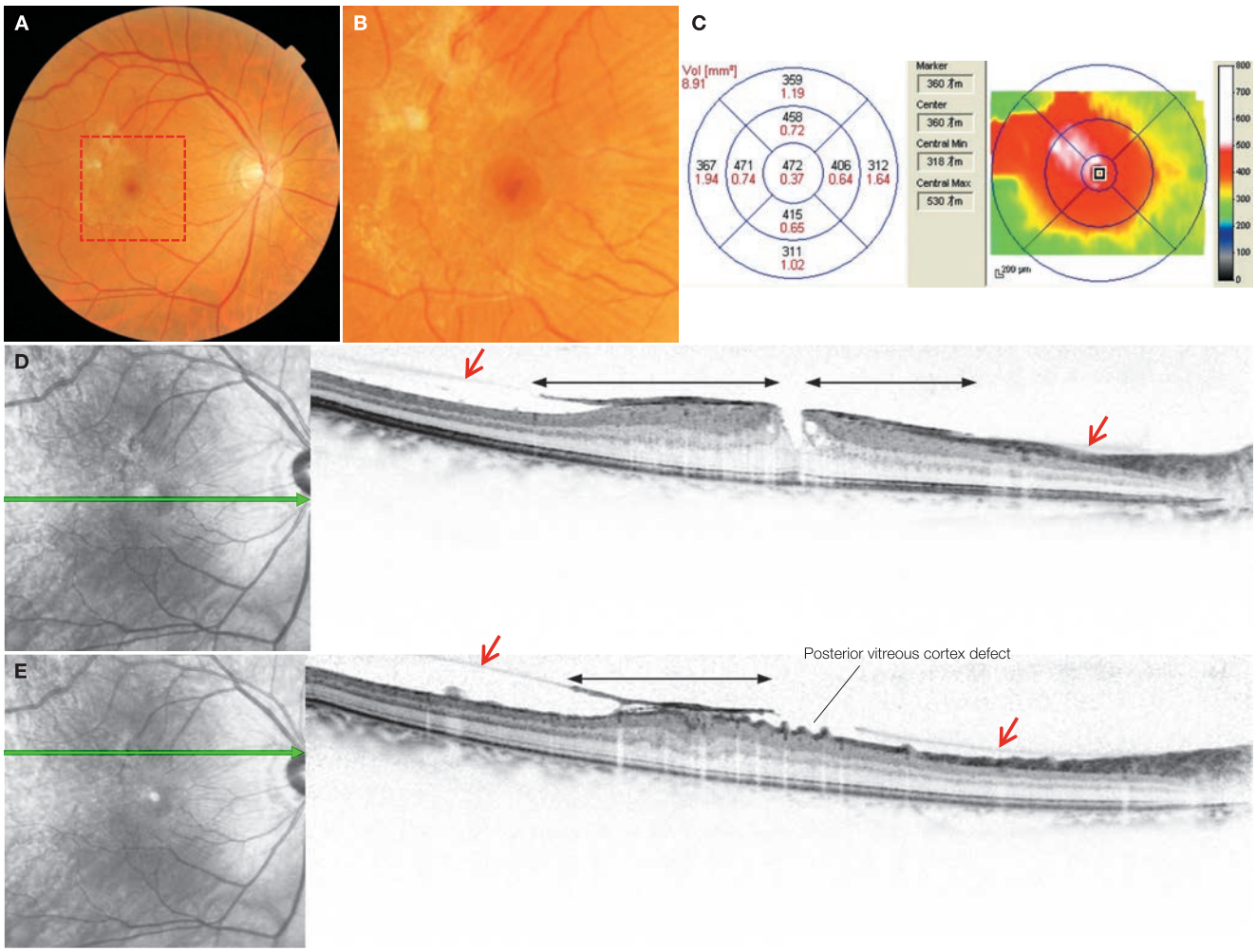

A: Color fundus photograph in the right eye, **B:** Enlarged version of A [red dashed box]: Whitening and radial retinal folds can be seen. **C:** Retinal thickness color map of the right eye. **D:** IR + OCT horizontal scan of the right eye: Thick ERM ↔ is noted. ERM cannot be seen over the fovea centralis. ERM is formed along the posterior vitreous cortex (➔). The foveal depression is V-shaped. **E:** IR + OCT horizontal scan of the right eye: ERM scan. ERM (↔), continuing from the posterior vitreous cortex (➔), can be observed. A posterior vitreous cortex defect are visible on the supero nasal ERM

Image interpretation points

This is a case of macular pseudohole where ERM is formed when the PVD has stopped in the periphery of the macula. PVD often stops along the retinal blood vessels to which the posterior vitreous cortex is firmly adherent , and thereby the dehiscence of the ILM occurs duo the traction of the detached posterior vitreous cortex toward the ILM. Cell migration often occurs through the ILM dehiscence into the gap between the posterior vitreous cortex and ILM and produces fibrocellular membrane, thus forming the ERM.

ILM dehiscence along the retinal blood vessels contraction occurs in this formation process resulting in centripetal forward traction similar to the pathogenic mechanism of vitreomacular traction syndrome. However, whereas centrifugal forward traction is primary in vitreomacular traction syndrome, causing macular trapezoidal-shaped thicknening, in this case, centripetal forward traction is primary, leading to mountain-shaped retinal thickening and fold formation in the macula. The fovea centralis exhibits a V-shaped or U-shaped depression. Despite the macular PVD being incomplete, the reason for the defect formation foveal posterior vitreous cortex defects over the fovea centralis is not known. Posterior vitreous cortex defects may occur as a result of ERM contraction, or may develop with extensive separation of the posterior vitreous cortex into two layers. In the latter hypothesis, the posterior layer is clipped out over the fovea centralis and taken away adherent to the detached anterior layer.

2.3 Vitreomacular traction syndrome

Background

Vitreomacular traction syndrome is like a stage 1 macular hole or an epiretinal membrane with incomplete macular PVD in that it occurs in conditions where the perifoveal detachment of the posterior vitreous cortex with persistent adherence of the vitreous to the fovea or retinal surface of the macula. However, the attachment to the retinal surface in this disease state is often more broad or occurs in multiple areas. Strong centrifugal forward traction is applied to the macula so that the macular area is raised into a tent shape (trapezoid) and the retina thickens. Cystoid space formation and fovea or macular detachment often accompany this disease. In 11% of cases, PVD occurs during follow-up and cystoid spaces decrease[1]. There is both a focal- and wide- adhesion type vitreomacular traction syndrome where the focal type has a vitreomacular adhesion within a central macula region with physiological strong attachment between posterior vitreous body and macular surface that was reprorted by Kishi et al. and Spaide et al. as a cause of vitreofoveal traction in the development of a macular hole[2,3] while the broad type over a wider area[4]. Vitreomacular traction syndrome often accompanies other eye diseases such as diabetic maculopathy, severe myopia, and uveitis. Abnormal vitreoretinal interface adhesion and degeneration of vitreous gel due to inflammation may be involved in the pathogenic processes of this disease. ERM cases without a PVD sometimes progress to vitreomacular traction syndrome. The pathogenesis of vitreomacular traction syndrome can be explained by the migratory cell membrane formation theory described for ERM pathogenesis earlier in this chapter. Based on this theory, the PVD stops at the strongly adhesive retinal blood vessels, fovea and optic disc with cells then migrating from cracks in the ILM and to gaps in the posterior vitreous cortex and ILM. As a result of extracellular matrix production, these migrating cells form a fibrocellular membrane which adheres to the posterior vitreous cortex and macular surface.[5] (see page 60, ◘ Fig. 2-13).

Thus, vitreomacular traction syndrome and ERM without complete macular PVD appear to have pathogenic mechanisms on the same spectrum with some different conditions. ERM may be a condition where fibrocellular membrane formation occurs primarily beneath the posterior vitreous cortex attached to the macular surface, thus leading to macular thickening and fold formation through centropetal forward traction generated by membrane contraction[4]. In contrast, vitreomacular traction syndrome may be a condition where fibrocellular membrane formation occurs beneath both attached and detached posterior vitreous cortex, thus leading to a tent-shaped elevation of the macula through centrifugal forward traction generated by the detached posterior vitreous cortex[4].

Vitreomacular traction syndrome often accompanies ERM. In these cases, the posterior vitreous cortex is presumed to separate in eyes with vitreomacular traction syndromeinto two layers where the anterior layer detaches from the retina and the posterior layer remains on the retina and becomes the origin of the ERM [4]. In histopathological observations of surgical samples and autopsied eyes, cells mainly comprising fibrous astrocytes and myofibroblasts, which were reportedly found in eyes with ERM and an extracellular matrix primarily made of collagen were found to be present in fibrocellular membrane in eyes with vitreomacular traction syndrome, supporting the speculation that these 2 diseases have common pathogenic conditions.[6–9].

References

1) Hikichi T, Yoshida A, Trempe CL. Course of vitreomacular traction syndrome. Am J Ophthalmol. 1995; 119:55–61.
2) Kishi S, Demaria C, Shimizu K. Vitreous cortex remnants at the fovea after spontaneous vitreous detachment.Int Ophthalmol. 1986; 9:253–260.
3) Spaide RF, Wong D, Fisher Y, et al. Correlation of vitreous attachment and foveal deformation in early macular hole states. Am J Ophthalmol. 2002; 133:226–229.
4) Koizumi H, Spaide RF, Fisher YL, et al. Three-dimensional evaluation of vitreomacular traction and epiretinal membrane using spectral-domain optical coherence tomography. Am J Ophthalmol. 2008; 145:509–517.
5) Gass JDM. Macular dysfunction caused by epiretinal membrane contraction. Stereoscopic atlas of macular diseases. Diagnosis and treatment 4th ed., CV Mosby, St. Louis, 1997. pp176–180.
6) Smiddy WE, Green WR, Michels RG, et al. Ultrastructural studies of vitreomacular traction syndrome. Am J Ophthalmol. 1989 15; 107:177–185.
7) Shinoda K, Hirakata A, Hida T, et al. Ultrastructural and immunohistochemical findings in five patients with vitreomacular traction syndrome. Retina. 2000; 20:289–293.
8) Gandorfer A, Rohleder M, Kampik A, et al. Epiretinal pathology of vitreomacular traction syndrome. Br J Ophthalmol. 2002; 86:902–909.
9) Chang LK, Fine HF, Spaide RF, et al. Ultrastructural correlation of spectral-domain optical coherence tomographic findings in vitreomacular traction syndrome. Am J Ophthalmol. 2008; 146:121–127.

Case 35 Vitreomacular traction syndrome: Case showing disease development

Right eye of a 74-year-old male with vision corrected to 0.8

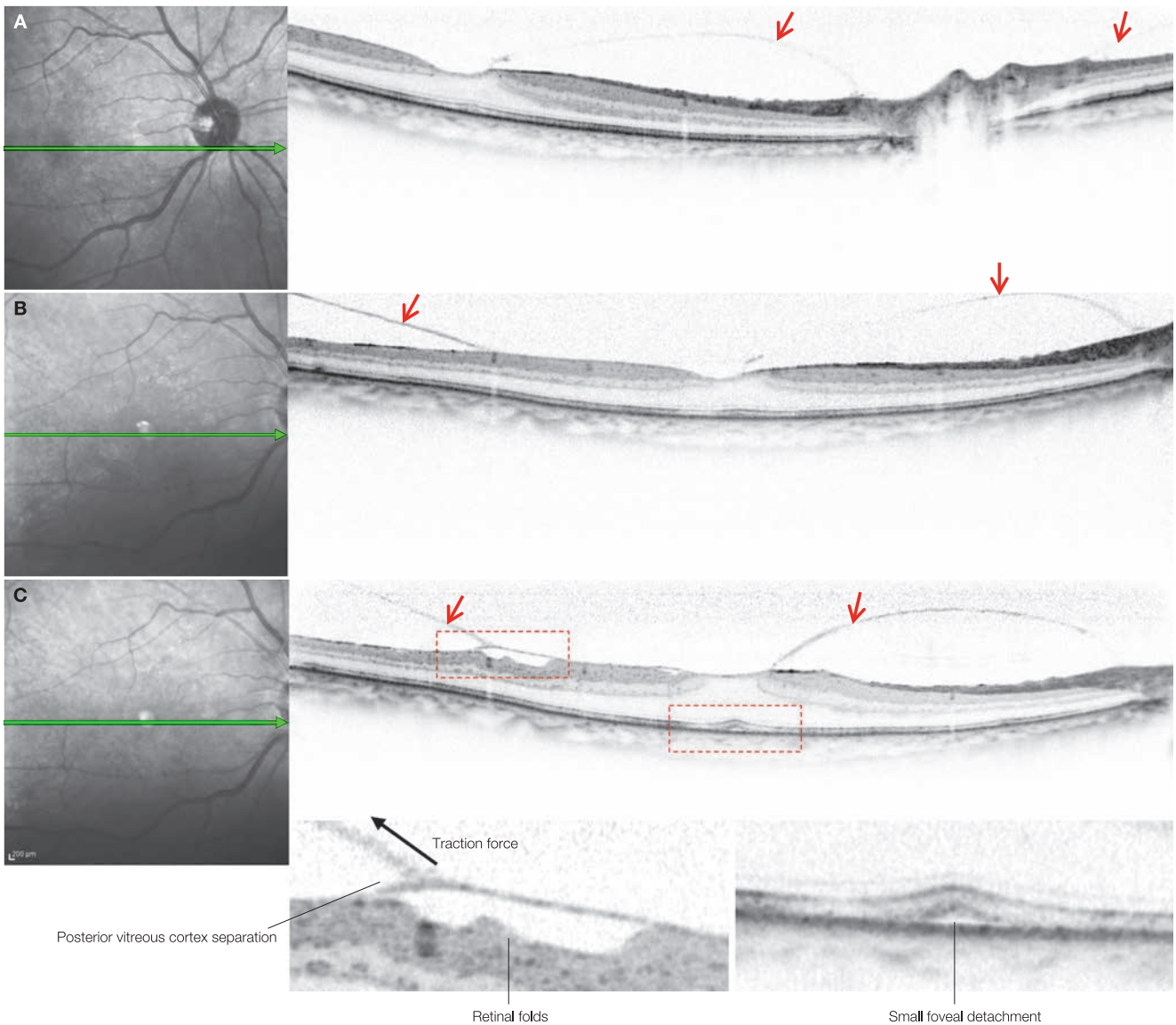

A: IR + OCT horizontal scan of the right eye, **B:** IR + OCT horizontal scan of the right eye: at initial diagnosis. Macular PVD is in progress. Adhesion of the posterior vitreous cortex (➔) remains in the optic disc, fovea centralis and the temporal macula. **C:** IR + OCT horizontal scan of the right eye + enlarged version [red dashed box]: 1 year after initial diagnosis. Best corrected visual acuity is 0.7. Macular PVD is not progressing; however, there is separation of the posterior vitreous cortex, an increase in the tension of the detached anterior layer of the posterior vitreous cortex (➔) and contraction of the posterior vitreous cortex adhered to the macular surface seen. Mild retinal thickening, retinal folds and foveal detachment are all seen. It is unknown whether the membrane of the posterior part is the ILM or the result of the separation of the posterior vitreous cortex into two layers, but the third membrane beneath these 2 membranes that appears afterwards suggests that these membranes are anterior and posterior layers separated posterior vitreous cortex. The anterior layer of the posterior vitreous cortex is causing centrifugal forward traction.

(Continues on the following page)

Case 35 Continuation

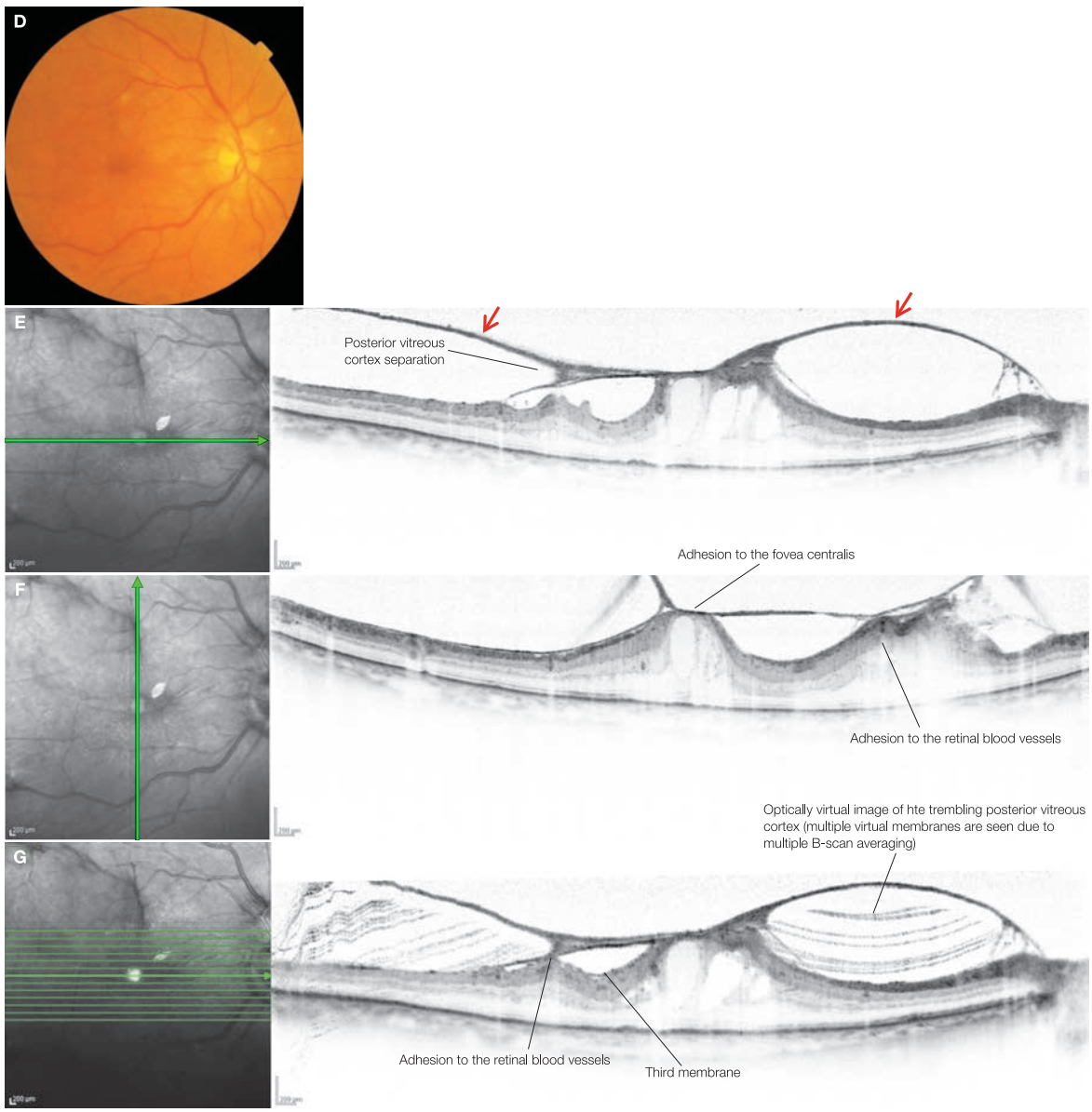

D: Color fundus photograph in the right eye: 2 years after initial diagnosis. Visual acuity reduced to 0.3. **E:** IR + OCT horizontal scan of the right eye, **F:** IR + OCT vertical scan of the right eye, **G:** IR + OCT horizontal scan of the right eye: Traction of the posterior vitreous cortex that has separated into two layers is increasing and macular area thickening is worsening. The posterior vitreous cortex (➔) is strongly adherent to the retinal blood vessels and fovea centralis and its anterior layer is applying strong centrifugal forward traction. Cystoid spaces are formed in the macula. G shows the optically virtual image of the thickened anterior layer of the posterior vitreous cortex reflected in multiple layers as an averaging artifact, which indicates that the membrane is intensely shook by eye movement. Another membrane is seen below the posterior vitreous membrane that has separated into two layers is noticeable on the retinal surface.

Image interpretation points

Cell migration and fibrocellular membrane formation resulting in strong adhesion occur on the posterior vitreous cortex and in the gap between the posterior vitreous cortex and ILM gaps while macular PVD in stopped around the fovea and along the strongly adherent retinal blood vessels. In this disease, centrifugal forward traction due to the detached posterior vitreous cortex with persistent adhesion to the fovea and blood vessels is superior to centripetal forward traction by the contraction of the ERM, thus causing the macula to thicken into a tent-shaped (trapezoid). With eye movements, the posterior vitreous cortex demonstrates significant trembling, which could enhance cell migration. In vitreomacular traction syndrome, multiple membranes are seen on OCT. In this case, it is likely that there is initially separation of the posterior vitreous membrane into two layers followed by ILM detachment as the traction worsens.

Case 36 Vitreomacular traction syndrome: Case with macular detachment

A 75-year-old female, OD, BCVA 0.3

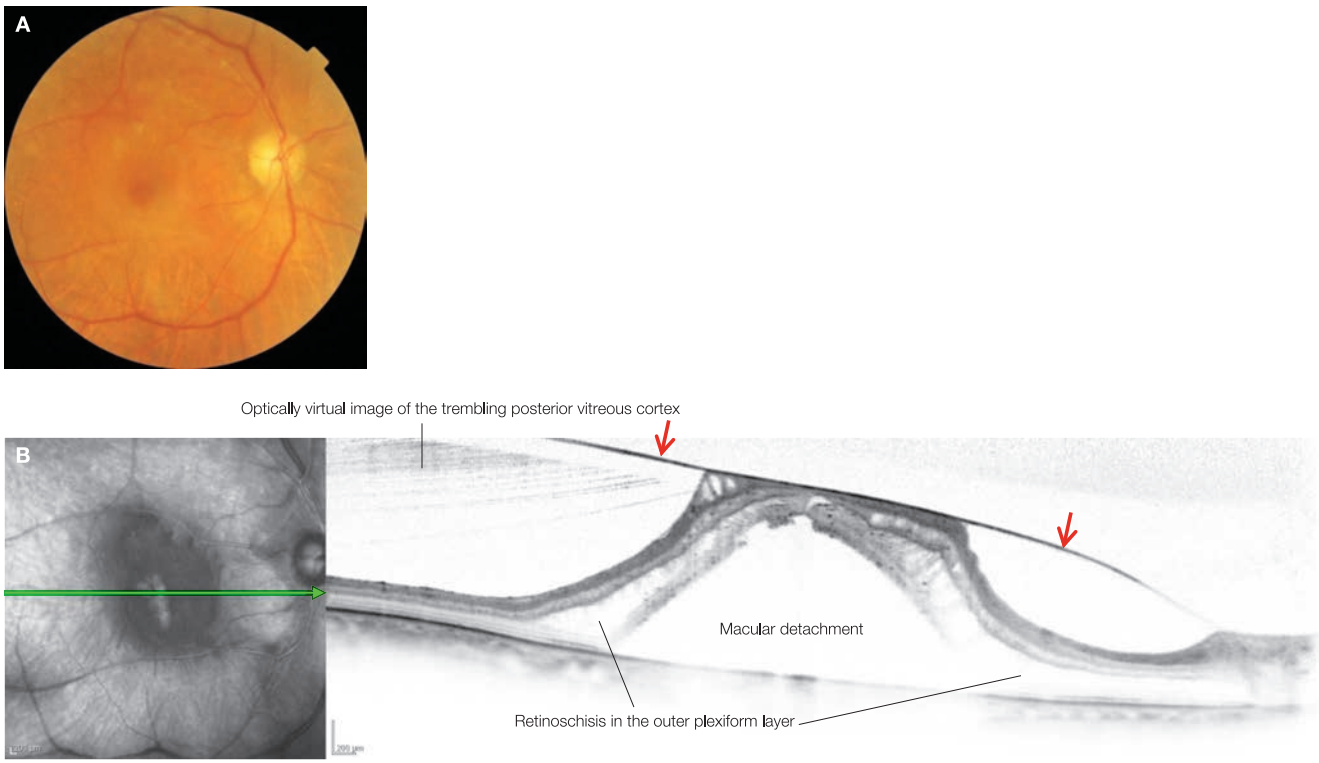

A: Color fundus photograph in the right eye: Whitening in the macula is apparent. **B:** IR + OCT horizontal scan of the right eye: The posterior vitreous cortex (➔) is thick and linear, adherent to a wide area of the macula. The retina in the macula is highly elevated to form macular detachment. The optically virtual image of the thickened posterior vitreous cortex is reflected in multiple layers as an averaging artifact and the membrane can be seen trembling significantly with eye movements. In addition, retinoschisis and a columnar structure thought to be Müller cells can be seen in the outer plexiform layer, inner nuclear layer and retinal nerve fiber layer.

Image interpretation points

This individual became aware of blurred vision one month prior to presentation. The posterior vitreous cortex has thickened and adhered to the wide area of the macula. Progression of fibrocellular membrane formation appears to have made the posterior vitreous cortex thickened and hard. The presence of macular detachment is suggestive of strong forward traction.

Case 37 Vitreomacular traction syndrome: A highly myopic eye with foveoschisis

A 71-year-old female, OS, BCVA 0.5

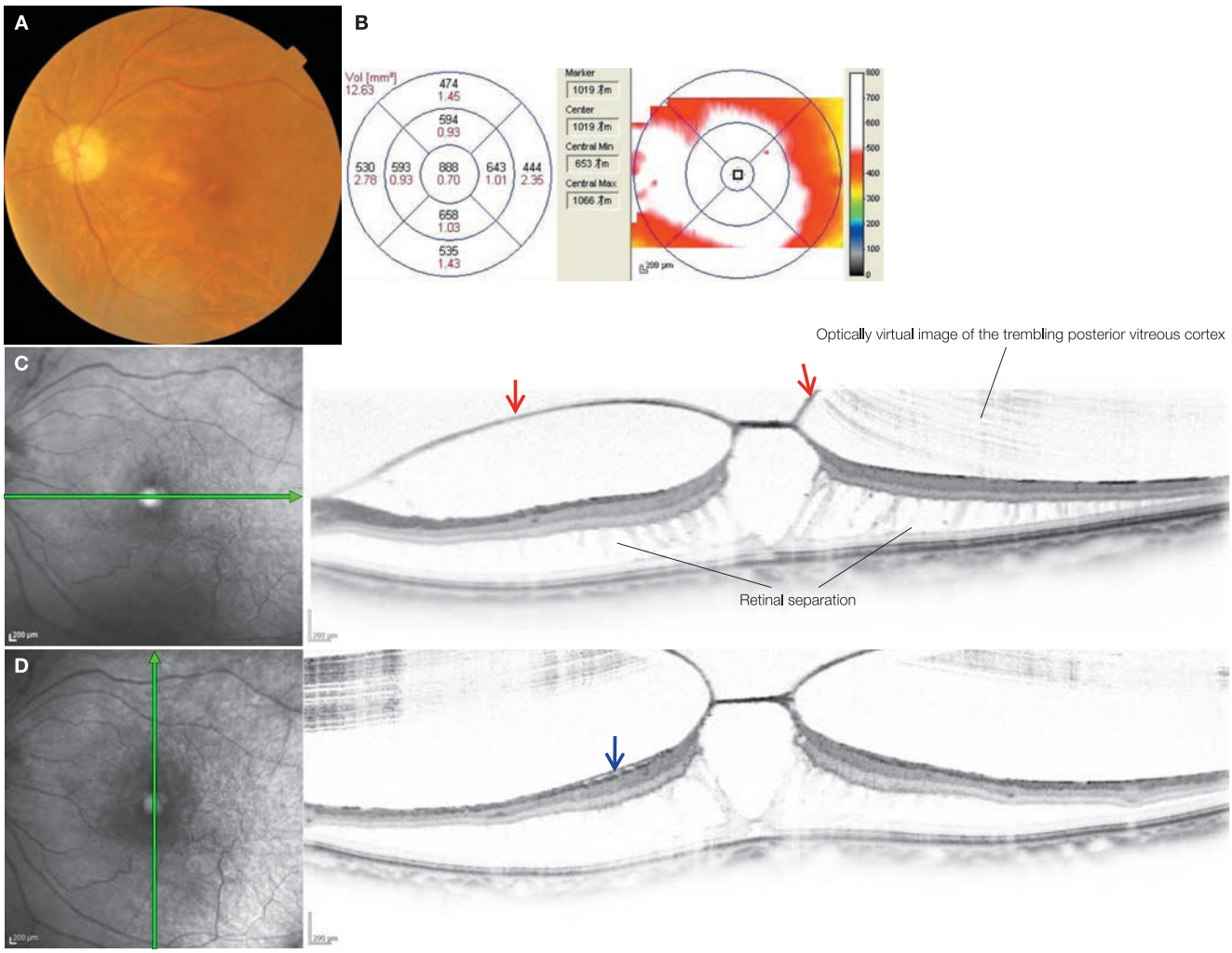

A: Color fundus photograph in the left eye: A tessellated fundus is seen. **B:** Retinal thickness color map of the left eye, **C:** IR + OCT horizontal scan of the left eye: The posterior vitreous cortex (➔) is adhered to the surface of the fovea. The fovea is highly elevated by the centrifugal forward traction, and large foveal cystoid space and retinoschisis in the outer plexiform layer are seen. The optically virtual image of the thickened posterior vitreous cortex is reflected in multiple layers as an averaging artifact, and the membrane can be seen trembling significantly with eye movements. Highly myopic eyes are susceptible to retinoschisis formation when such forward traction works on the fovea.. **D:** IR + OCT vertical scan of the left eye: A slight detachment of a thin membrane on the retinal surface in the inferior macula is visible (➔).

Image interpretation points

Vitreomacular traction syndrome tends to occur in severely myopic eyes. Adhesion of the posterior vitreous cortex to the surface of the fovea and tent-shaped thickening of the retina are characteristics of vitreomacular traction syndrome. Vitreomacular traction is one of the causes for developing myopic foveoschisis.

Diabetic retinopathy

3.1 Diabetic retinopathy – 78
3.1.1 Background – 78

3.2 Diabetic macular edema – 79
3.2.1 Background – 79
3.2.2 SD-OCT findings – 80
References – 85

Case 38 Diabetic macular edema: Early-stage case – 86

Case 39 Cystoid macular edema: Case with CME limited to layers anterior to the ELM – 87

Case 40 Cystoid macular edema: Case with CME extending to the outer retina – 88

Case 41 Cystoid macular edema: Exacerbation – 89

Case 42 Cystoid macular edema: Foveal detachment with recurrence – 90

Case 43 Cystoid macular edema: Subfoveal accumulation of hard exudates and the development of ischemic maculopathy – 91

Case 44 Cystoid macular edema: Subretinal leakage from a parafoveal cystoid spaces – 92

Case 44 Continuation – 93

Case 45 Cystoid macular edema: Subfoveal leakage from a foveal cystoid spaces – 94

Case 46 Cystoid macular edema: Photoreceptor damage from outer plexiform layer edema – 95

Case 46 Continuation – 96

Case 47 Cystoid macular edema: Microaneurysms – 97

Case 48 Ischemic maculopathy: Cystoid macular degeneration – 98

Case 49 Ischemic maculopathy: Thinned macula – 99

Case 50 Vitreomacular traction syndrome: A typical example – 100

Case 51 Proliferative diabetic retinopathy: Progressive proliferation – 101

Case 52 Proliferative diabetic retinopathy: Preretinal hemorrhages and vitreomacular traction syndrome – 102

3.1 Diabetic retinopathy

3.1.1 Background

Pathological conditions that cause visual impairment

Clinically significant pathological conditions that cause visual impairment are ① diabetic macular edema, and ② proliferative diabetic retinopathy. Although not as frequent, ③ ischemic maculopathy is also a significant cause of severe visual impairment.

Retinal capillary bed

The retinal capillary perifoveal capillary bed forms 4 layers between the retinal nerve fiber layer and inner nuclear layer. It is located at specific retinal layer boundaries, such as the external margin of the inner nuclear layer, the external margin of the ganglion cell layer, the inner margin of the inner nuclear layer, and the ganglion cell layer to the retinal nerve fiber layer (listed from the major network)[1–3]. The dilated capillaries in eyes with diabetic retinopathy can be easily seen as highly reflective spots on OCT, therefore easily recognizing the depth of the capillary bed (◘ Fig. 3-1). The perifoveal capillary bed only exists as one layer on the external margin of the ganglion cell layer[1]. There are no retinal blood vessels in the central part of the fovea, 0.5 mm wide in diameter, and it is known as the foveal avascular zone (FAZ).

Retinal capillary lesions in the early nonproliferative stage

Early changes in diabetic retinopathy occur in the retinal capillaries. Loss of capillary pericytes, microaneurysm (MA) formation and loss of endothelial cells, inversely endothelial cell aggregation, and thickening of the capillary basement membrane have been reported[4, 5]. Retinal MAs are the earliest changes that can be observed by ophthalmoscopy. More MAs indicate more severe retinopathy/maculopathy[6], and an increase in the number of MAs[7] suggest worsening of retinopathy/maculopathy[7]. Hyperpermeability occurs as a result of lesions in these capillaries, causing macular edema and hard exudate formation.

Retinal capillary lesions in the advanced nonproliferative stage

An exacerbation of hyperpermeability and capillary nonperfusion occur as retinopathy progresses. Arterioles become occluded and accumulated MAs and tortuous capillaries, which are known as intraretinal microvascular abnormalities (IRMAs) is seen in the vicinity. When capillary occlusion sites dilate, venous beading, venous tortuosity, flame-shaped hemorrhages (surface hemorrhages), and dot and blot hemorrhages (deep hemorrhages) increase. The IRMAs indicates initiation of the proliferative phase (preproliferative diabetic retinopathy).

Diabetic macular edema

Described in detail in the next page.

Soft exudate (cotton-wool spots)

Soft exudates is a common finding that can be seen not only in diabetic retinopathy but also in retinal vein occlusions, hypertensive retinopathy and HIV retinopathy; with the presence of multiple soft exudates suggesting the presence of an acute nonperfusion area formation or a wide area of nonperfusion. On OCT they can be seen as highly reflective localized thickening in the retinal nerve fiber layer (◘ Fig. 3-2). Highly reflectivity remains due to gliosis after the disappearance of the soft exudates[8].

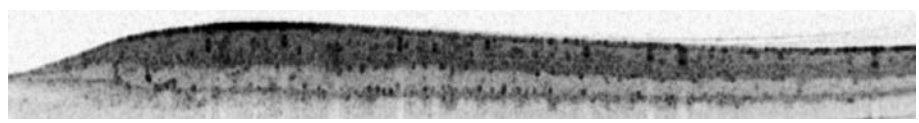

◘ **Fig. 3-1** The retinal capillary network in an OCT B-scan (case of early diabetic retinopathy)
Capillary vessels are depicted as highly reflective dots

◘ **Fig. 3-2** OCT B-scan image of soft exudates
It can be seen as highly reflective localized thickening (→) of the retinal nerve fiber layer

3.2 Diabetic macular edema

3.2.1 Background

Classification of retinal edema

Retinal edema is divided into macular edema and retinal nerve fiber layer (RNFL) edema. The former is extracellular tissue swelling due to leakage from capillaries and microaneurysms (MAs). The latter is thickening due to an increase in intracellular volume caused by a shortage in arterial blood supply, which typically occurs in soft exudate formation.

Leakage mechanism

Diabetic macular edema occurs regardless of the presence of proliferative diabetic retinopathy and is a pathological condition that destroys the foveal photoreceptors leading to permanent visual impairment. It is further divided into both focal edema and diffuse edema, based on differences in the leakage mechanism. Focal edema occurs as a result of leakage from accumulated MAs and dilated capillaries and is often surrounded by circinate exudates. Diffuse edema occurs as a result of hyperpermeability of retinal capillaries in the macula.

Macular edema patterns and retinal thickness

Otani et al. classified diabetic macular edema patterns that can be seen with OCT-2000 into sponge-like retinal swelling, cystoid macular edema, and serous retinal detachment (Fig. 3-3); and stated that visual acuity was most correlated with macular retinal thickness regardless of the type of pattern[9].

Macular exudative changes

In 15–26% of the cases that develop cystoid macular edema, repeated foveal detachment occurs due to the leakage into the subretinal space[9–11]. Lipid accumulation mainly occurs from the outer plexiform layer to subretinal space, and leads to formation of intraretinal and subretinal hard exudates[12]. Serum lipid levels are a risk factor in hard exudate formation.[13–15]

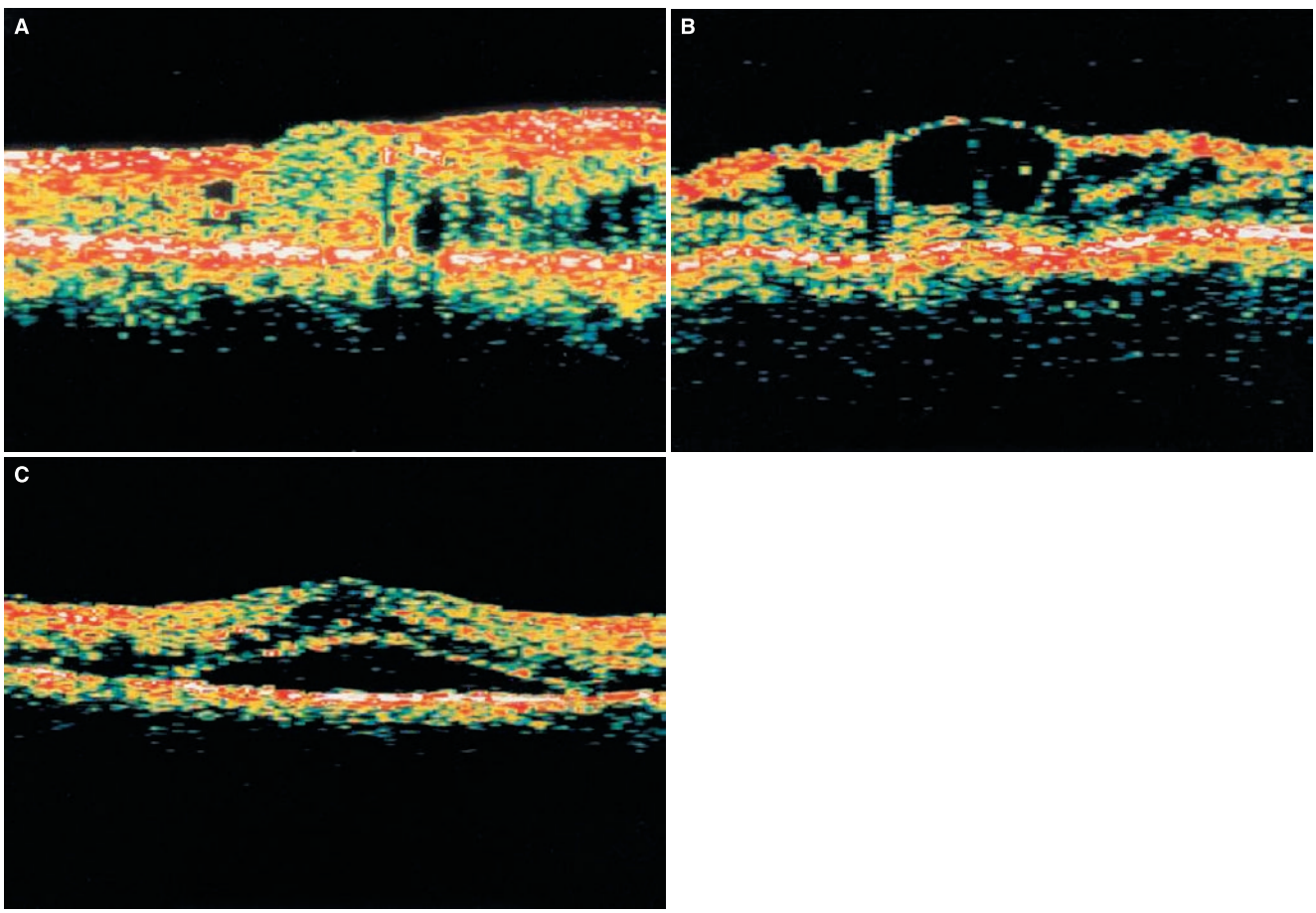

Fig. 3-3 Patterns of diabetic macular edema seen with a time-domain OCT image
A: Sponge-like retinal swelling, **B:** Cystoid macular edema, **C:** Serous retinal detachment.
(Modified according to Otani T, et al. Patterns of diabetic macular edema with optical coherence tomography. Am J Ophthalmol. 1999; 127: 688–693)

3.2.2 SD-OCT findings

Typical locations for cystoid spaces

Individual cystoid spaces can be seen with spectral-domain OCT (SD-OCT). Cystoid spaces are frequently found in the fovea centralis, parafovea, outer plexiform layer, and inner nuclear layer, and each have their own shape[16–18] (◘ Fig. 3-4). Diabetic macular edema are sometimes accompanied by foveal detachment (◘ Fig. 3-4). Among cystoid spaces, cystoid spaces in the outer plexiform layer, the fovea and parafovea, and foveal detachment are most influential in macular thickening. A variety of, sometimes complicated, lesions of diabetic macular edema are formed depending on leakage sites, leakage pressure, and properties of leaking serous fluid.

Cystoid spaces and intracavity reflectivity

SD-OCT has led to the understanding that the reflectivity intensity of cystoid spaces varies from weakly reflective to moderately reflective (◘ Fig. 3-5). This is thought to reflect the different properties of accumulating exudates in the cystoid spaces. Sometimes hemorrhages accumulate in the cystoid spaces, which then becomes highly reflective and shows niveau formation.

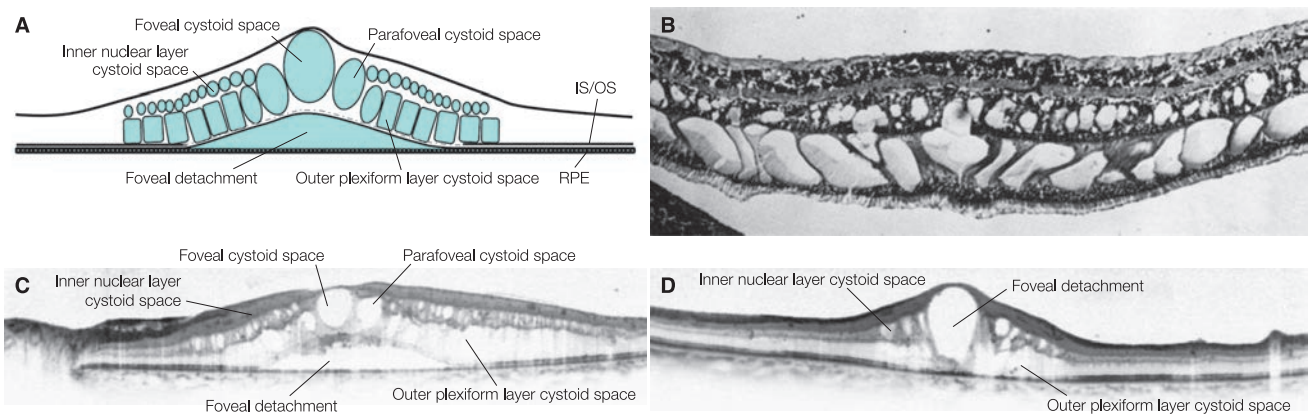

◘ **Fig. 3-4** Typical locations for cystoid spaces
A: Schema that shows the typical locations for cystoid spaces in diabetic macular edema, **B:** Light microscopic view of diabetic macular edema, **C, D:** SD-OCT images of diabetic macular edema.
(B is modified according to Gass JD, et al. Cystoid macular edema and papilledema following cataract extraction. A fluorescein fundoscopic and angiographic study. Arch Ophthalmol. 1966; 76: 646–661)

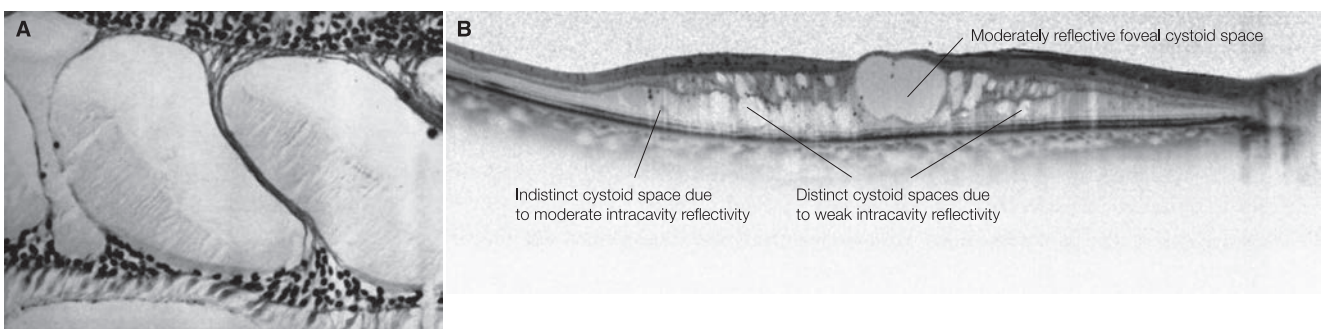

◘ **Fig. 3-5** The reflectivity intensity and accumulated fluid properties in cystoid spaces
A: »Serous exudate within thin-wall cystoid spaces« that can be seen in a tissue samples, **B:** The appearance of cystoid spaces that differs with intracavity reflectivity in OCT
(A is modified according to Tso MO. Pathological study of cystoid macular edema. Trans Ophthalmol Soc UK. 1980; 100: 408–413)

The appearance of cystoid spaces in the outer plexiform layer

When observed with SD-OCT, we can see that outer plexiform layer edema is basically comprised of cystoid spaces. When the intracavity reflections of cystoid spaces are moderate they cannot be distinguished from the septum of the cystoid spaces, making it difficult to see cystoid spaces clearly (Fig. 3-5–3-7). Thickening of the retinal nerve fiber layer can often block the OCT measurement beam, making it difficult to observe the structures including cystoid spaces below the retinal nerve fiber layer. We can figure out if it is cystoid edema through comparisons with later-phase FA.

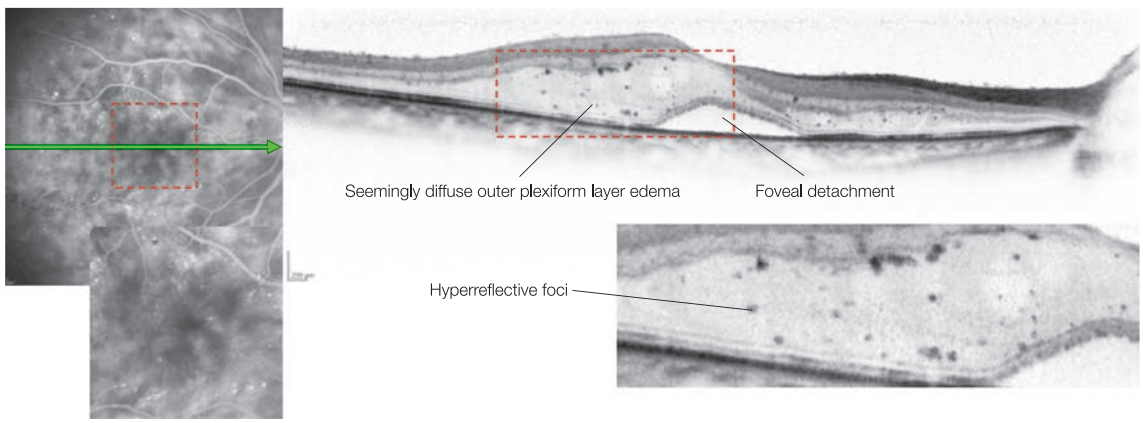

Fig. 3-6 Case of outer plexiform layer edema
The outer plexiform layer edema appears diffuse at first glance, but hyperreflective foci, accumulating in the internal walls of cystoid spaces, highlight the outline of the cystoid spaces. Cystoid macular edema is clear in FA.

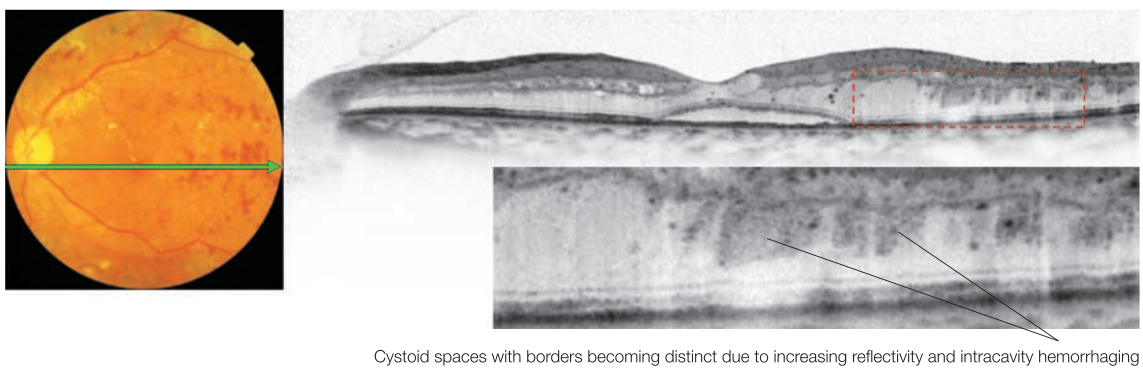

Fig. 3-7 Case of outer plexiform layer edema
The borders of the cystoid spaces are blurring when the lumen is moderately reflective, but the hemorrhages filled in some of the cystoid spaces highlight the outline of the cystoid spaces.

Hyperreflective foci

Bolz et al. reported that it is possible to see multiple highly reflective spots, which they termed as hyperreflective foci, through SD-OCT with speckle noise removed[19]. Hyperreflective foci cannot be seen with an ophthalmoscope fundus photography, or infrared imaging and are findings that cannot be clearly depicted by single-scan SD-OCT. They are smaller than the hard exudates that can be seen in fundus photography. There are distinguishing characteristics in the favorite accumulation locations and distribution patterns of hyperreflective foci, which most significantly occur in areas of outer plexiform layer edema. The foci arrange themselves in a line along cystoid space cavity walls, MA walls, the anterior border of the external limiting membrane (ELM), the posterior border of the photoreceptor inner segment in the foveal detachment area, and the anterior border of the retinal pigment epithelium (RPE) (◘ Fig. 3-8).[19] Since the retinal capillaries can also be seen as moderately reflective dots, differentiation between hyperreflective foci and retinal capillaries is necessary. It is particularly misleading if there is dilation of capillaries. However, retinal capillaries are present only in the inner nuclear layer or layers interior to it, and show weaker reflectivity than hyperreflective foci. (◘ Fig. 3-1). Hyperreflective foci are thought to be leaked lipoproteins and a precursor to hard exudates[19]. When macular edema is ameliorated by grid photocoagulation, the hyperreflective foci gather and coalesce, and become a hard exudate that can be seen with an ophthalmoscope[20]. There is no anatomical barrier to fluid movement within the retina, but the external limiting membrane (ELM) is comprised of the zonula adherens between Müller cells and photoreceptors at the base of the outer segments, and thus had very narrow gaps, which limit particularly the movement of large molecules.[21]. Hyperreflective foci cannot pass through the gaps in the ELM since they are large molecules and thereby are filtered by the ELM to align along the ELM[22]. When vascular leakage is excessive and the internal pressure of the cystoid spaces increases, the structure of the ELM likely rupture to permit hyperreflective foci to leak below the retina. The hyperreflective foci that are leaked below the retina either become trapped along the posterior margin of the inner segment or accumulate on the surface of the RPE. When foveal detachment disappears as a result of vitreous surgery, grid photocoagulation, or a natural process, it can accumulate to become thick hard exudate beneath the fovea, causing visual acuity loss[12, 22].

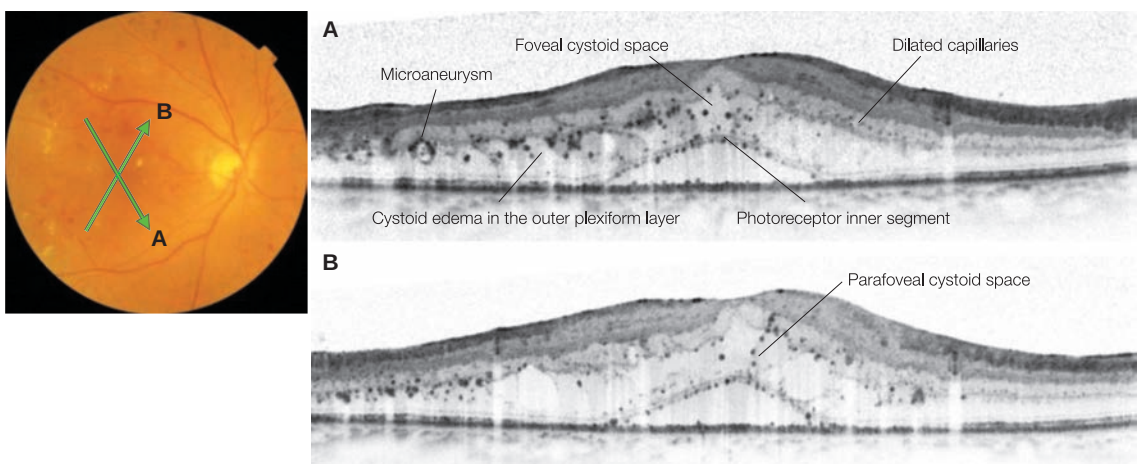

◘ Fig. 3-8 Typical localization of hyperreflective foci
Hyperreflective foci are typically found in and around outer plexiform layer edema. They are present arranged in lines along the walls of cystoid spaces, the walls of MAs, the anterior border of the ELM, the posterior margin of the photoreceptor inner segment, and the surface of the RPE

Retinal microaneurysms

Retinal microaneurysm (MA) can be seen from an early stage of diabetic retinopathy and are closely related to the disease progress[4–7]. The sizes of MAs in humans are quite variable, with 15–55 µm (vascular casting method)[23] and 14–136 µm (whole-mount immunostaining method)[24] MAs in diameter being reported. In histological observations, various types of MAs can be seen including those filled with multiple leukocytes or erythrocytes; those with various endothelium conditions, such as continuous, hypercellular, multi-layered, and defective cells; those with a thin wall or varyingly thickened and sclerotic due to hyaline degeneration, fibrosis and degenerative lipid deposits[4, 5, 25]. The majority of MAs occur from the deeper capillary bed of the inner nuclear layer[24, 25], and some can be observed extending to the outer nuclear layer[24]. MAs that extend to this depth may be involved in the edema formation in the outer plexiform layer. Utilizing SD-OCT with speckle noise removed, the depth and properties of MAs can be observed[26]. When observed with this method, MAs are circular or elliptical with a mean diameter of 118.3/111.6 µm (horizontal diameter/vertical diameter), ranging from 49.0 to 233.7 µm.[26] The spatial relationship with cystoid spaces includes isolated MAs (◘ Fig. 3-9A–E), MAs in contact with or adjacent to cystoid spaces (◘ Fig. 3-9F), and MAs that can be seen inside cystoid spaces (◘ Fig. 3-9C). The wall types of MAs include those where highly reflective rings can be seen around the entire circumference (◘ Fig. 3-9E), those where highly reflective rings can be partially seen (◘ Fig. 3-9F), and those where highly reflective rings cannot be seen (◘ Fig. 3-9G). The MAs without the ring-shaped high reflectivity were more frequently associated with cystoid spaces than those with circumferential high reflectivity[26].

Nonperfusion area and OCT findings

The nonperfusion area demonstrates significant thinning of the inner retina[26, 27]. However, when macular edema is significant, the thinning of the inner retinal layers is difficult to identify.

Visual prognosis and OCT findings

It is now possible to see and measure foveal structures indicating with the health of photoreceptor cells such as the ELM, IS/OS, and OS thickness with SD-OCT, and these indicators correlate with visual acuity in diabetic macular edema[28–31].

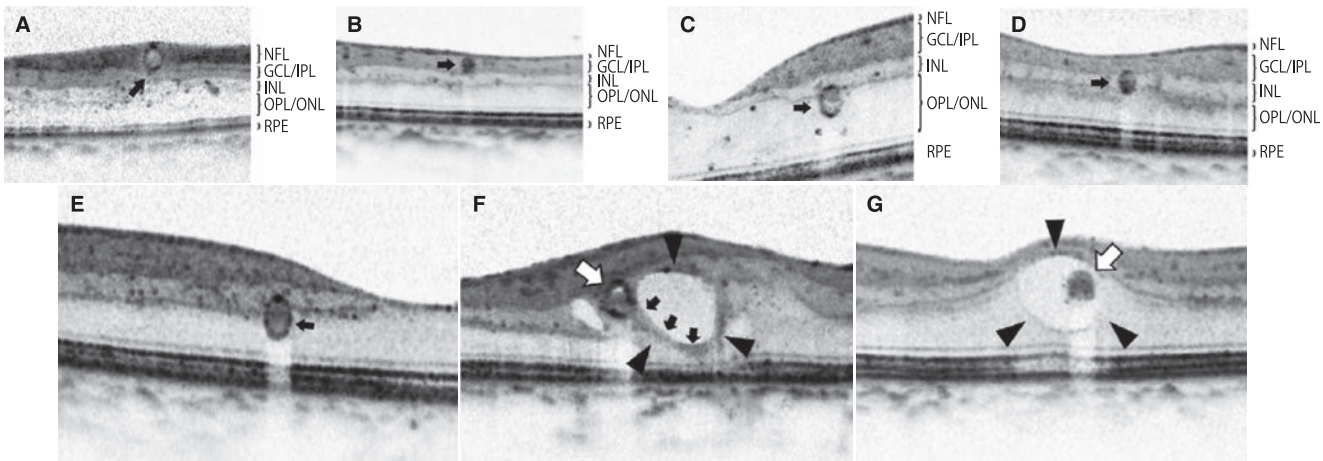

◘ **Fig. 3-9** Retinal microaneurysms seen on SD-OCT with speckle noise removed
A: Present in the retinal nerve fiber layer, **B:** Present in the ganglion cell layer and inner plexiform layer, **C:** Present in the outer plexiform layer, **D:** Present in the inner nuclear layer, **E:** Present in the outer plexiform layer, **F:** In contact with cystoid spaces, **G:** Present in the cystic cavity. Retinal MAs can be seen in various layers of the retina.
(Modified according to Horii T, et al. Optical coherence tomographic characteristics of microaneurysms in diabetic retinopathy. Am J Ophthalmol. 2010; 150: 840–848)

Mechanisms by which macular edema injure photoreceptor layer

Permanent visual impairment as a result of macular edema is caused by the destruction of the foveal photoreceptor layer. However, edema does not directly cause photoreceptor layer damage. The mechanism for photoreceptor cell destruction is complex. With SD-OCT, we are now able to observe leakages from cystoid spaces into subretinal space, and this phenomenon appears to be involved in the destruction of the foveal photoreceptor layer. When internal pressure of cystoid spaces increase, they expand to become in contact with the ELM, and thereby strong pressure is applied to the ELM. As a result, the structures of ELM as an anatomical barrier to the large molecules broken down, permitting leakage of fluid and large molecules to the photoreceptor layer and subretinal layer (◘ Fig. 3-10). This leakage repeats its stop-and-resume cycle. Photoreceptor damages appear to be due to the mechanical obstruction by the leakage and due to the accumulation of hard exudate and hemorrhages beneath the foveal photoreceptor layer. As described previously, the macular thickness is associated to visual acuity loss.One possible mechanism to account for this association is that when macular thickness become greater cystoid spaces increase in size and internal pressure, enhancing the leakage to the photoreceptor layer and subretinal space[9].

Ischemic maculopathy

Capillary nonperfusion in diabetic retinopathy typically occurs in the equator, and eventually expands to the macula as well as to the periphery. The capillary nonperfusion involving the macular, particularly the fovea, causes severe visual acuity loss. In addition, the enlargement of foveal avascular zone (FAZ) also occurs in diabetic retinopathy, leading to visual acuity loss. These disease conditions are termed ischemic maculopathy. The FAZ of 1,000 μm or less in diameter does not cause visual acuity decrease, whereas when the FAZ that expanded more than 1,000 μm causes visual acuity loss[32]. Sometimes the breakdown of the capillary bed on the temporal macula extends to the fovea leading to severe visual impairment. These disease conditions are termed ischemic maculopathy.

Ischemic maculopathy can sometimes be seen in type 1 diabetes. When observed with OCT, the fovea centralis displays cystoid macular degeneration or macular thinning. This is an important factor that impedes visual improvement even after diabetic macular edema is resolved after treatment[33].

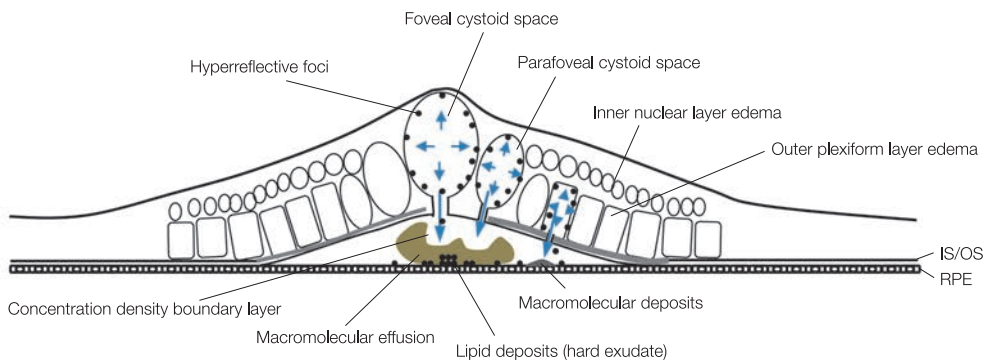

◘ Fig. 3-10 Diagram showing the leakage mechanism into the macular subretinal space
When the internal pressure of the cystoid spaces increases, contents break through the ELM and leak into the subretinal space

References

1) »Pattern and location of retinal vessels,« In The Retinal Circulation, Ed. by Wise GN, Dollery CT, Henkind P, Harper & Row. 1971, pp 20–31.
2) Iwasaki M, Inomata H. Relation between superficial capillaries and foveal structures in the human retina. Invest Ophthalmol Vis Sci. 1986; 27:1698–1705.
3) Snodderly DM, Weinhaus RS. Retinal vasculature of the fovea of the squirrel monkey, Saimiri sciureus: three-dimensional architecture, visual screening, and relationships to the neuronal layers. J Comp Neurol. 1990; 297:145–163.
4) Cogan DG, Toussaint D, Kuwabara T. Retinal vascular patterns. IV. Diabetic retinopathy. Arch Ophthalmol. 1961; 66:366–378.
5) De Venecia G, Davis M, Engerman R. Clinicopathologic correlations in diabetic retinopathy. I. Histology and fluorescein angiography of microaneurysms. Arch Ophthalmol. 1976; 94:1766–1773.
6) Klein R, Meuer SM, Moss SE, et al. The relationship of retinal microaneurysm counts to the 4-year progression of diabetic retinopathy. Arch Ophthalmol. 1989; 107:1780–1785.
7) Klein R, Meuer SM, Moss SE, et al. Retinal microaneurysm counts and 10-year progression of diabetic retinopathy. Arch Ophthalmol. 1995; 113:1386–1391.
8) Kozak I, Bartsch DU, Cheng L, et al. Hyperreflective sign in resolved cotton wool spots using high-resolution optical coherence tomography and optical coherence tomography ophthalmoscopy. Ophthalmology. 2007; 114:537–543.
9) Otani T, Kishi S, Maruyama Y. Patterns of diabetic macular edema with optical coherence tomography. Am J Ophthalmol. 1999; 127:688–693.
10) Catier A, Tadayoni R, Paques M, et al. Characterization of macular edema from various etiologies by optical coherence tomography. Am J Ophthalmol. 2005; 140:200–206.
11) Gaucher D, Sebah C, Erginay A, et al. Optical coherence tomography features during the evolution of serous retinal detachment in patients with diabetic macular edema. Am J Ophthalmol. 2008; 145:289–296.
12) Otani T, Kishi S. Tomographic findings of foveal hard exudates in diabetic macular edema. Am J Ophthalmol. 2001; 131:50–54.
13) Klein BE, Moss SE, Klein R, et al. The Wisconsin Epidemiologic Study of Diabetic Retinopathy. XIII. Relationship of serum cholesterol to retinopathy and hard exudate. Ophthalmology. 1991; 98:1261–1265.
14) Chew EY, Klein ML, Ferris FL 3rd, et al. Association of elevated serum lipid levels with retinal hard exudate in diabetic retinopathy. Early Treatment Diabetic Retinopathy Study (ETDRS) Report 22. Arch Ophthalmol. 1996; 114:1079–1084.
15) Miljanovic B, Glynn RJ, Nathan DM, et al. A prospective study of serum lipids and risk of diabetic macular edema in type 1 diabetes. Diabetes. 2004; 53:2883–2892.
16) Gass JD, Norton EW. Cystoid macular edema and papilledema following cataract extraction. A fluorescein fundoscopic and angiographic study. Arch Ophthalmol. 1966; 76:646–661.
17) Tso MO. Pathological study of cystoid macular edema. Trans Ophthalmol Soc U K. 1980; 100:408–413.
18) Wolter JR. The histopathology of cystoid macular edema. Albrecht Von Graefes Arch Klin Exp Ophthalmol. 1981; 216:85–101.
19) Bolz M, Schmidt-Erfurth U, Deak G, et al; Diabetic Retinopathy Research Group Vienna. Optical coherence tomographic hyperreflective foci:a morphologic sign of lipid extravasation in diabetic macular edema. Ophthalmology. 2009; 116:914–920.
20) Deák GG, Bolz M, Kriechbaum K, et al; Diabetic Retinopathy Research Group Vienna. Effect of retinal photocoagulation on intraretinal lipid exudates in diabetic macular edema documented by optical coherence tomography. Ophthalmology. 2010; 117:773–779.
21) Marmor MF. Mechanisms of fluid accumulation in retinal edema. Doc Ophthalmol. 1999; 97:239–249.
22) Ota M, Nishijima K, Sakamoto A, et al. Optical coherence tomographic evaluation of foveal hard exudates in patients with diabetic maculopathy accompanying macular detachment. Ophthalmology. 2010; 117:1996–2002.
23) Fryczkowski AW, Chambers RB, Craig EJ, et al. Scanning electron microscopic study of microaneurysms in the diabetic retina. Ann Ophthalmol. 1991; 23:130–136.
24) Moore J, Bagley S, Ireland G, et al. Three dimensional analysis of microaneurysms in the human diabetic retina. J Anat. 1999; 194:89–100.
25) Stitt AW, Gardiner TA, Archer DB. Histological and ultrastructural investigation of retinal microaneurysm development in diabetic patients. Br J Ophthalmol. 1995; 79:362–367.
26) Horii T, Murakami T, Nishijima K, et al. Optical coherence tomographic characteristics of microaneurysms in diabetic retinopathy. Am J Ophthalmol. 2010; 150:840–848.
27) Unoki N, Nishijima K, Sakamoto A, et al. Retinal sensitivity loss and structural disturbance in areas of capillary nonperfusion of eyes with diabetic retinopathy. Am J Ophthalmol. 2007; 144:755–760.
28) Otani T, Yamaguchi Y, Kishi S. Correlation between visual acuity and foveal microstructural changes in diabetic macular edema. Retina. 2010; 30:774–780.
29) Forooghian F, Stetson PF, Meyer SA, et al. Relationship between photoreceptor outer segment length and visual acuity in diabetic macular edema. Retina. 2010; 30:63–70.
30) Maheshwary AS, Oster SF, Yuson RM, et al. The association between percent disruption of the photoreceptor inner segment-outer segment junction and visual acuity in diabetic macular edema. Am J Ophthalmol. 2010; 150:63–67.
31) Murakami T, Nishijima K, Sakamoto A, et al. Association of pathomorphology, photoreceptor status, and retinal thickness with visual acuity in diabetic retinopathy. Am J Ophthalmol. 2011; 151:310–317.
32) Byeon SH, Chu YK, Lee H, et al. Foveal ganglion cell layer damage in ischemic diabetic maculopathy: correlation of optical coherence tomographic and anatomic changes. Ophthalmology. 2009; 116:1949–1959.
33) Jonas JB, Martus P, Degenring RF, et al. Predictive factors for visual acuity after intravitreal triamcinolone treatment for diabetic macular edema. Arch Ophthalmol. 2005; 123:1338–1343.

Case 38 Diabetic macular edema: Early-stage case

A 58-year-old male,OS, BCVA 1.2

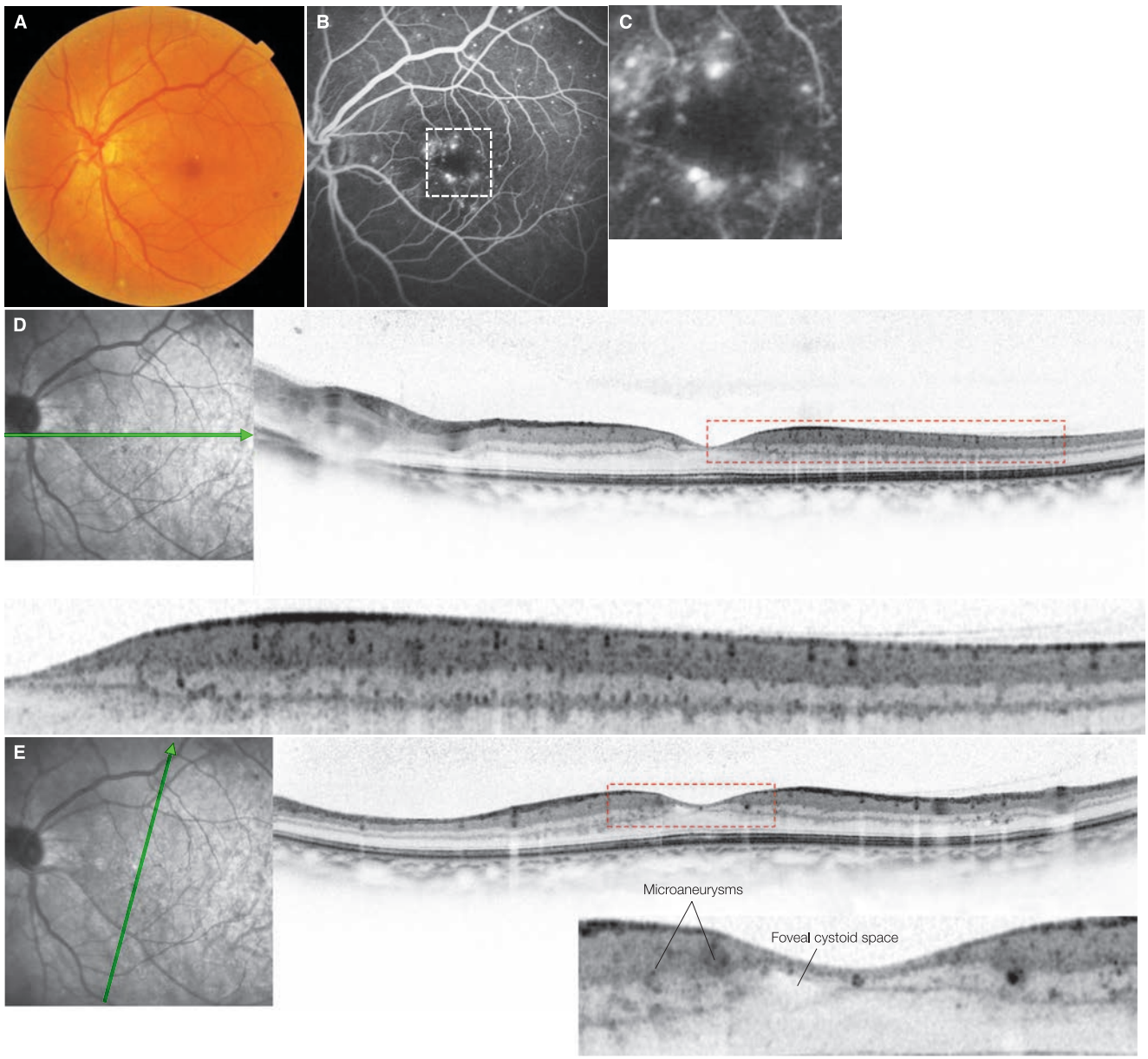

A: Left eye fundus photograph: A hard exudate and MAs can be seen in the parafovea. **B:** FA in the left eye (2 min), **C:** Enlarged version of B [white dashed box]: MAs are detected in the perifoveal capillary bed and in its vicinity. Weak fluorescent leakage can be seen. **D:** IR + OCT horizontal scan of the left eye + enlarged version [red dashed box]: The foveal depression is maintained and there is very little retinal thickening, but capillaries in the macular area are dilating and 4 rows of highly reflective spots can be observed. These rows of highly reflective spots indicate 4-layer capillary network in the external and internal margins of the inner nuclear layer, the external margin of the ganglion cell layer and the ganglion cell layer itself to the retinal nerve fiber layer. **E:** IR + OCT tilted scan of the left eye + enlarged version [red dashed box]: MAs are visible in the parafovea and a small foveal cystoid space can be noted

Image interpretation points

This is a case of early phase diabetic macular edema with minimal macular retinal thickening. MA formation and weak fluorescent leakage can be seen in the perifoveal capillary bed and very small localized cystoid spaces are visible in the parafovea and Henle‹s fibrous layer (HFL). The foveal depression is maintained and no clear retinal thickening is visible. Capillaries in the macular area are dilating, and the 4-layer capillary network can be seen more clearly than usual.

Case 39 Cystoid macular edema: Case with CME limited to layers anterior to the ELM

An 80-year-old female, OD BCVA 0.8

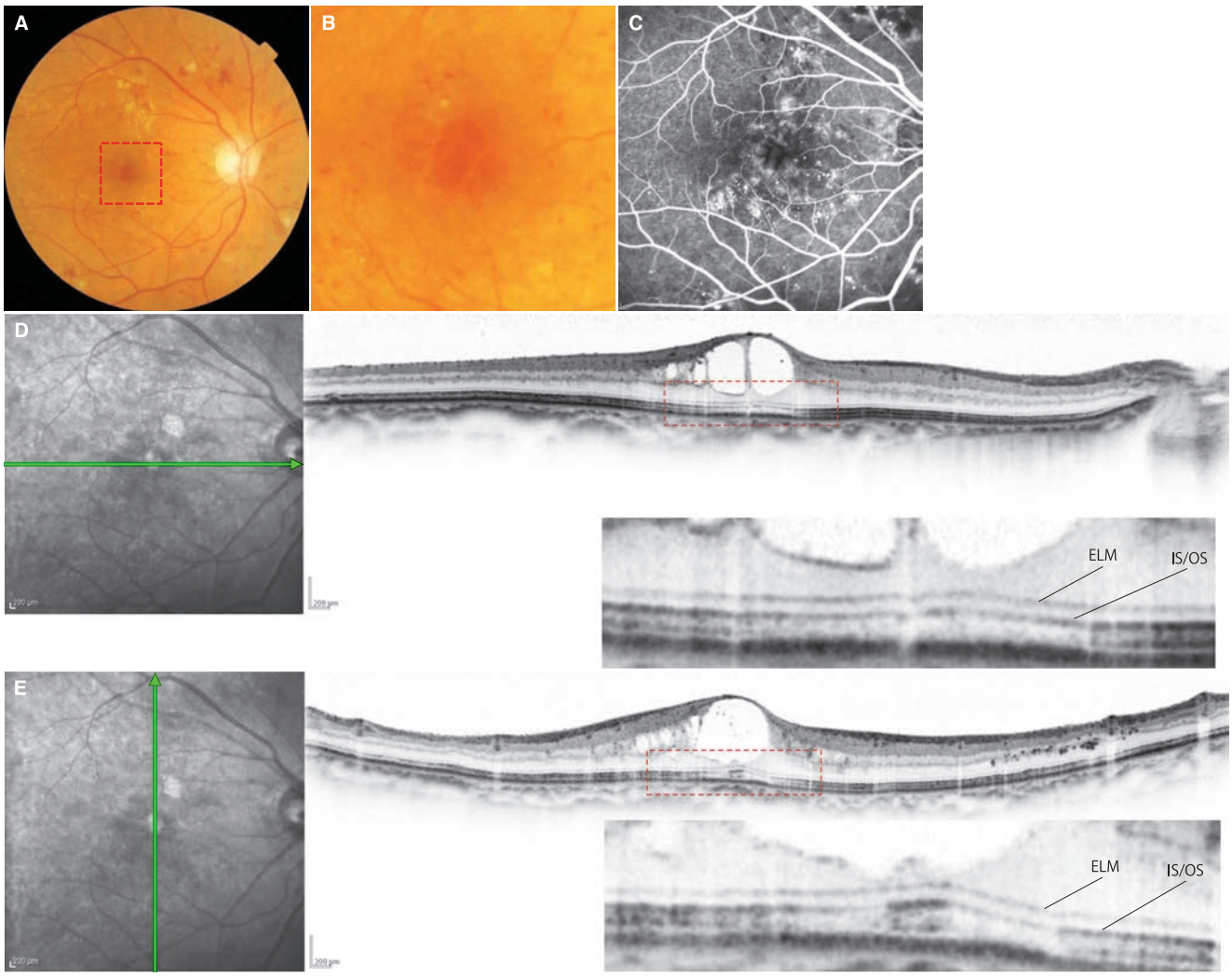

A: Color fundus photograph in the right eye, **B:** Enlarged version of A [red dashed box]: Dot and blot hemorrhages and cystoid macular edema (CME) can be seen in the macula. Hard exudates can be seen above the macula. **C:** FA in the right eye (75 sec): Multiple MAs and CME can be seen in the macula. **D**: IR + OCT horizontal scan of the right eye + enlarged version [red dashed box]: Cystoid spaces can be seen in the fovea, parafovea, and the inner nuclear layer, but no edema can be seen in the outer plexiform layer. Foveal cystoid spaces are confined anterior to the ELM line and IS/OS lines, and each line is being maintained. **E:** IR + OCT vertical scan of the right eye + enlarged version [red dashed box]: Same findings as in D can be seen

Image interpretation points

The cystoid spaces is confined to the retinal layers anterior to the ELM within the fovea, parafovea and inner nuclear layer in the vicinity of the fovea. These cystoid spaces appear to be due to the leakage from the perifoveal capillary bed. The ELM and IS/OS lines are maintained and visual acuity remains good.

Case 40 Cystoid macular edema: Case with CME extending to the outer retina

Left eye of an 80-year-old female with vision corrected to 0.2

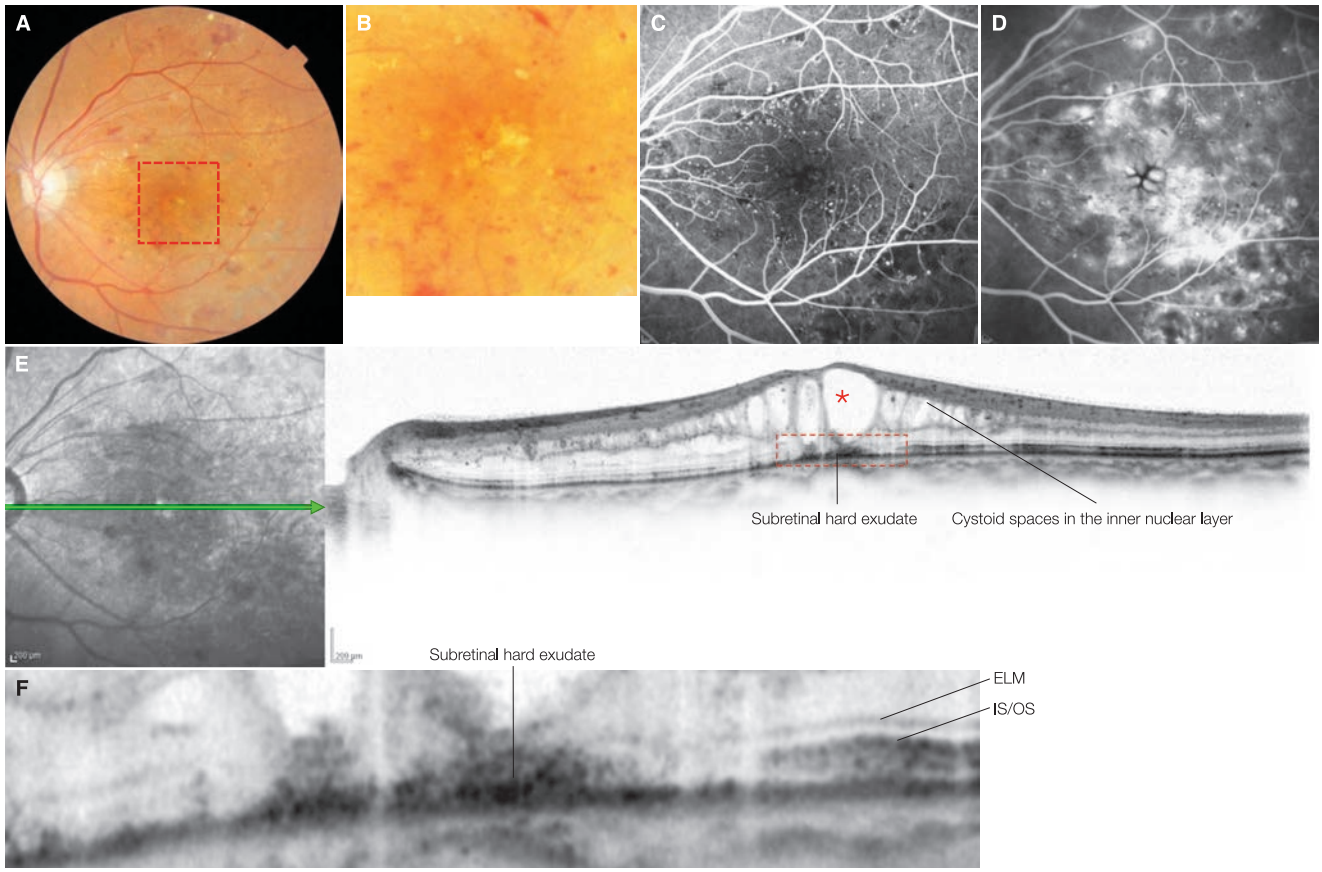

A: Color fundus photograph in the left eye, **B:** Enlarged version of A [red dashed box]: Dot and blot hemorrhages are seen over the entire macula and hard exudates can be seen in the fovea. **C:** FA in the left eye (28 sec): Multiple MAs are noted over the entire macula. **D**: FA in the left eye (5 min): CME is evident in the fovea and macular edema can be seen outside the fovea. The nonperfusion area is not visible. **E:** IR + OCT horizontal scan of the left eye: This macular edema is comprised of foveal cystoid space (*), parafoveal cystoid spaces and and inner nuclear layer cystoid spaces. A highly reflective lesion is visible beneath the fovea corresponding to accumulation of hard exudates. **F:** Enlarged version of E [red dashed box]: The ELM, IS/OS and COST lines in the fovea have disappeared

Image interpretation points

Accumulation of hard exudates beneath the fovea is one cause of severe visual impairment in diabetic macular edema. Cystoid spaces in diabetic macular edema are common in the fovea centralis, parafovea, outer plexiform layer and inner nuclear layer. As the internal pressure rises within these cystoid spaces, subretinal leakage occurs causing foveal detachment. When this accumulated fluid in the cystoid spaces passes through the ELM, a passage into the subretinal space formed. In the case of diabetic macular edema, as leakage into the subretinal space continues, hard exudates are deposited beneath the fovea leading to severe visual acuity loss.

Case 41 Cystoid macular edema: Exacerbation

A 64-year-old female, OS, BCVA 1.0

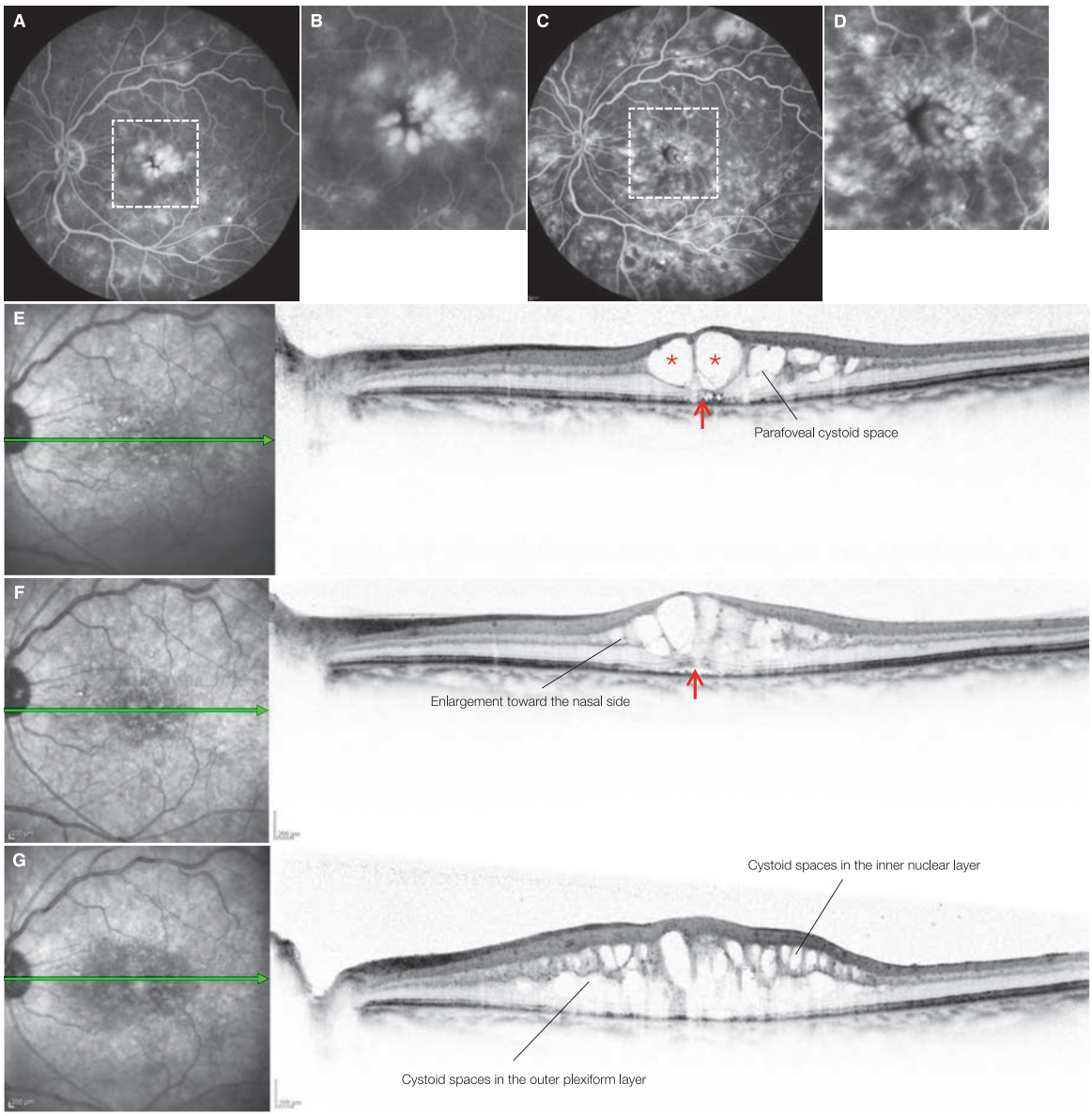

A: FA in the left eye (11 min), **B:** enlarged version of A [white dashed box]: At initial diagnosis. Typical CME in a petaloid pattern can be seen in the fovea. Leakage outside the fovea is mild. **C:** FA in the left eye (3 min), **D**: Enlarged version of C [white dashed box]: 17 months after initial diagnosis. The petaloid pattern of CME has fused and become, and a multilayered petaloid pattern can be seen outside of it. Leakage over the macula is increased. **E:** IR + OCT horizontal scan of the left eye: At initial diagnosis. Foveal and parafoveal cystoid spaces (*) in contact with the ELM line and a slight foveal detachment (➔) can be seen. **F** IR + OCT horizontal scan of the left eye: 7 months after initial diagnosis. Best-corrected visual acuity has reduced to 0.7. The edema has extended to the nasal side. Foveal detachment (➔) can be seen. **G**: IR + OCT horizontal scan of the left eye: 17 months after initial diagnosis. Best-corrected visual acuity has further decreased to 0.3. Cystoid spaces in the outer plexiform layer and inner nuclear layer over the entire macula is increased. This corresponds to the parafoveal, multilayered petaloid pattern in FA

Image interpretation points

This case show the exacerbation of diabetic macular edema. The macular edema was initially found mainly in the foveal and parafoveal regions, and then has progressed to the outer plexiform layer and inner nuclear layer of the entire macula. The lateral expansion of macular edema is observed with FA, but the extent of the edema in each retinal layer, as well as retinal thickening can be quantitatively understood with OCT. OCT also allows observation of photoreceptor damages. However, in this case, the status of ELM, IS/OS and COST lines are indistinct due to blockade of OCT measurement beams by the multiple cystoid spaces.

Case 42 Cystoid macular edema: Foveal detachment with recurrence

A 61-year-old male, OS, BCVA 0.8

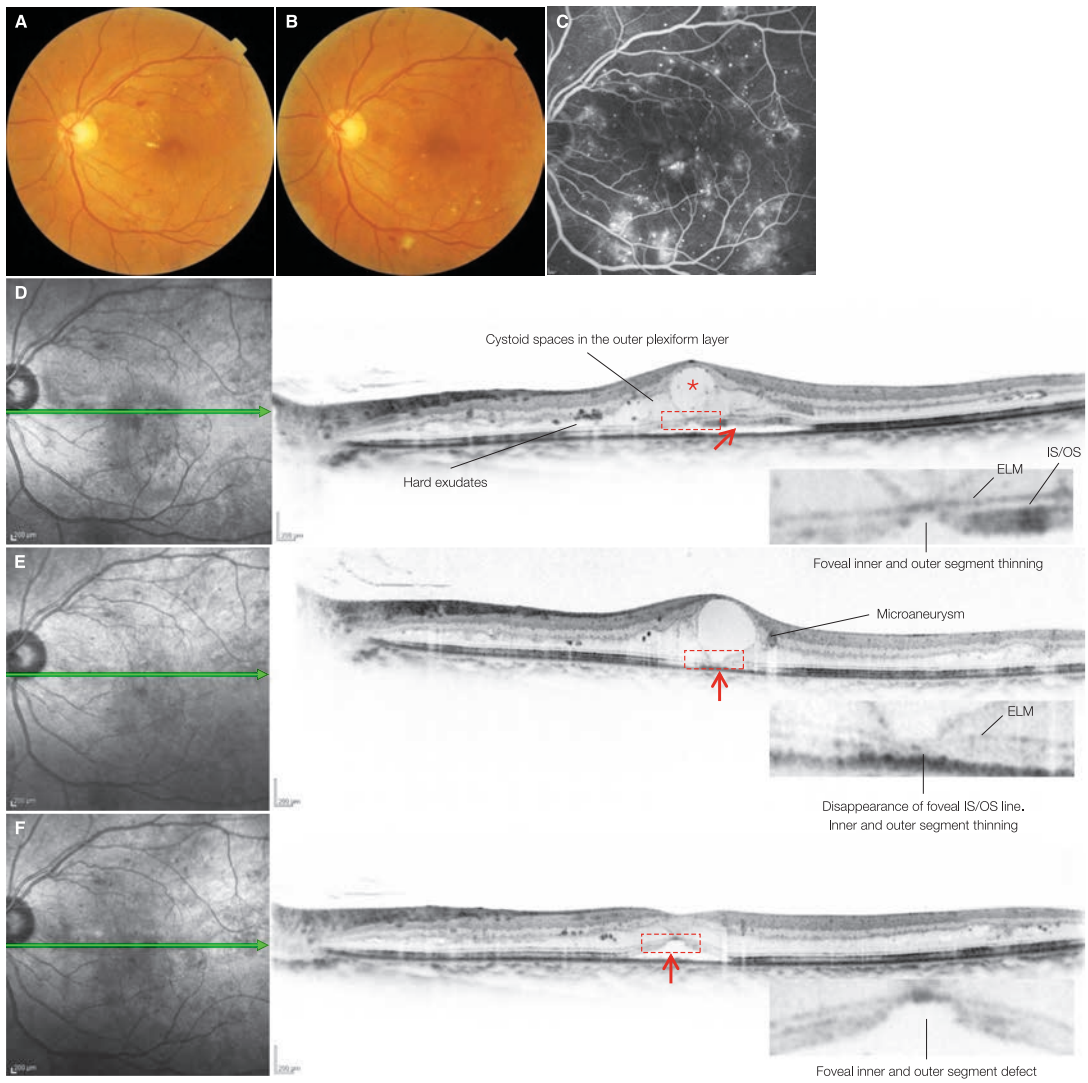

A: Color fundus photograph in the left eye: At initial diagnosis. **B:** Color fundus photograph in the left eye: 3 months after initial diagnosis. Best-corrected visual acuity has reduced to 0.4. **C:** FA in the left eye (5 min): At initial diagnosis. CME can be seen in the fovea and parafovea. **D:** IR + OCT horizontal scan of left eye + enlarged version [red dashed box]: At initial diagnosis. A foveal cystoid space (*) in contact with the ELM and foveal detachment (➔) can be seen. The inside of the cystoid spaces is moderately reflective, which is thought to be due to high viscosity fluid. The photoreceptor inner and outer segments of the fovea are diminished. **E:** IR + OCT horizontal scan of the left eye + enlarged version [red dashed box]: 3 months after initial diagnosis. The foveal detachment has subsided (➔), but foveal cystoid spaces remain. The foveal photoreceptor inner and outer segments are thinned. **F:** IR + OCT horizontal scan of the left eye + enlarged version [red dashed box]: 4 months after initial diagnosis. Best-corrected visual acuity is 0.4. Foveal detachment (➔) has reoccurred. The foveal photoreceptor inner and outer segments are lost at their entire depth.

Image interpretation points

This is a case where foveal detachment due to a foveal cystoid space repeatedly occurred,and the photoreceptor inner and outer segments in the fovea were damaged. Leakage is due to the microaneurysms of perifoveal capillary bed. The foveal cystoid space has extended to the outer retina and is connected with the subretinal space via the ELM structure. The ELM is the area where the adhesion complex between the photoreceptor inner segment and outer edges of the Müller cells is aligned, but it only exists in very narrow gaps. As the cystoid spaces expand and come into contact with the ELM, they apply strong pressure to this structure leading to its disintegration and leakage below the retina. The photoreceptor inner and outer segments become defective as this fluid pass through them, and repeated foveal detachments exacerbate the damage done to the foveal photoreceptor inner and outer segments.

Case 43 Cystoid macular edema: Subfoveal accumulation of hard exudates and the development of ischemic maculopathy

Right eye of a 59-year-old female with vision corrected to 0.7

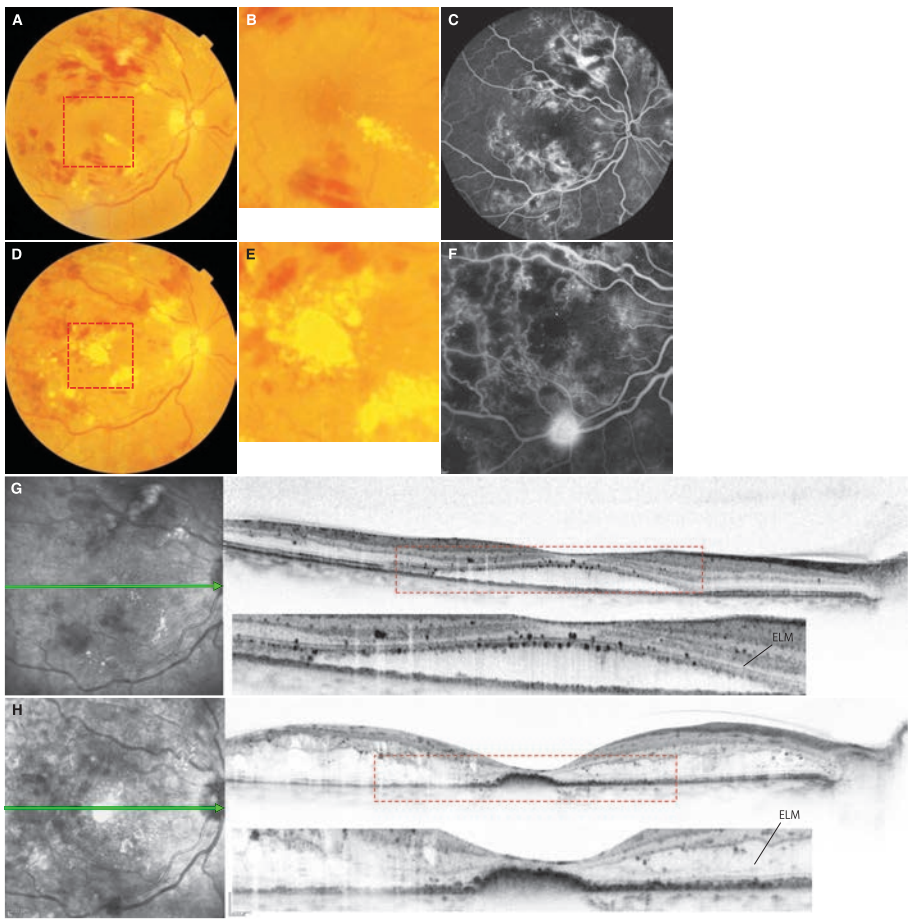

A: Color fundus photograph in the right eye, **B:** Enlarged version of A [red dashed box]: 1 month after initial diagnosis. Flame-shaped hemorrhages can be seen in the posterior pole, soft exudate is exhibited near the upper arcade vessels, and hard exudate is visible on the nasal macula. Fine yellowish-white granules are observed in the fovea. **C:** FA in the right eye (2 min): A focal nonperfusion area can be seen near the upper arcade vessels. **D:** Color fundus photograph in the right eye, **E:** Enlarged version of D [red dashed box]: 12 months after initial diagnosis. Accumulation of hard exudates beneath the foveas is noticeable. **F:** FA in the right eye (3 min): 12 months after initial diagnosis. A nonperfusion area can be seen from the fovea centralis to the upper arcade vessels. **G:** IR + OCT horizontal scan of the right eye + enlarged version [red dashed box]: 10 months after initial diagnosis. Best-corrected visual acuity is 0.7. Foveal detachment is noted and hyperreflective foci are aligned on the anterior border of the ELM and posterior margin of the photoreceptor inner segment. H: IR + OCT horizontal scan of the right eye + enlarged version [red dashed box]: Same area as G, 12 months after initial diagnosis. Best-corrected visual acuity has reduced to 0.2. Foveal detachment has disappeared, and hard exudates have accumulated on the RPE beneath the fovea centralis. The ELM and IS/OS lines have disappeared in the foveal area with hard exudate accumulation and significant thinning of the foveal photoreceptor layer can be seen. (A, D, and H were modified according to Ota M, et al. Optical coherence tomographic evaluation of foveal hard exudates in patients with diabetic maculopathy accompanying macular detachment. Ophthalmology. 2010; 117: 1196–2002)

Image interpretation points

This is a case where accumulation of hard exudates progressed beneath the fovea centralis and visual acuity loss became worse during 1 year of observation. Subfoveal accumulation of hard exudates is one of causes for visual acuity loss associated with foveal detachment. At the initial diagnosis, fine yellowish-white granules were observed in the fovea, which probably corresponds to a part of hyperreflective foci on OCT images. Foveal detachment was present, and hyperreflective foci were seen aligned in an orderly manner along the anterior border of the ELM and the posterior margin of photoreceptor inner segment. Since hyperreflective foci are large molecules, they cannot pass through gaps in the ELM and appear to be filtered through the ELM and align. The structure of the ELM eventually ruptures and the hyperreflective foci appear to become trapped in the posterior margin of the inner segment. Images showing the process of subfoveal hard exudate accumulation are not available, but it is certain that alignment of the hyperreflective foci can be observed before the subfoveal accumulation of hard exudates.

Case 44 Cystoid macular edema: Subretinal leakage from a parafoveal cystoid space

A 64-year-old male, OD, BCVA 0.4

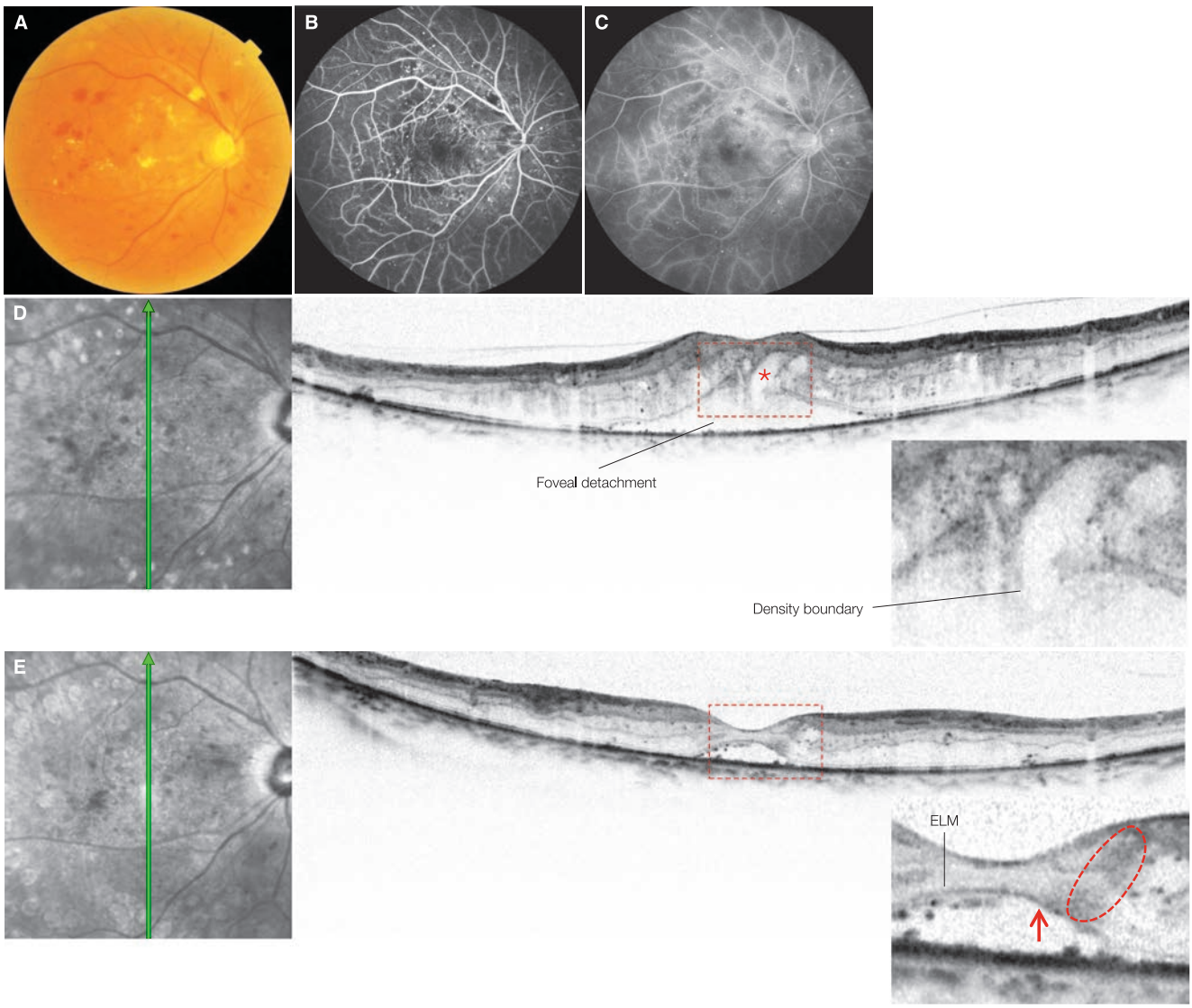

A: Color fundus photograph in the right eye: at initial diagnosis. Retinal hemorrhages and hard exudates can be seen in the macula, and soft exudates can be seen near the upper arcade vessels. **B:** FA in the right eye (1 min), **C:** FA in the right eye (13 min): At initial diagnosis. Multiple MAs are observed in the macula. Focal nonperfusion areas are seen in the peripheral macula and outside the macula. **D**: IR + OCT vertical scan of the right eye + enlarged version [red dashed box]: 6 months after initial diagnosis. Best-corrected visual acuity has reduced to 0.1. A parafoveal cystoid space (*) are opening below the retina. A density boundary is forming near the opening suggesting leakage. **E:** IR + OCT vertical scan of the right eye + enlarged version [red dashed box]: 8 months after initial diagnosis. Best-corrected visual acuity is 0.2. The parafoveal cystoid space and its opening have disappeared and an increase in reflectivity can be seen in the same area (red dashed circle). The photoreceptor inner and outer segments in the area of leakage are lost (→).
(D is modified according to and H according to Ota M, et al. Optical coherence tomographic evaluation of foveal hard exudates in patients with diabetic maculopathy accompanying macular detachment. Ophthalmology. 2010; 117: 1196–2002) (Continued on the next page)

Image interpretation points

Foveal photoreceptor layer degeneration due to foveal detachment causes visual impairment in diabetic macular edema. It is now possible to observe the process of subretinal leakage from cystoid spaces with SD-OCT. The photoreceptor inner and outer segments disappear in the area of leakage, and highly reflective lesions remain within the retina where the cystoid space with an opening was present. This, it appears that mechanical damages due to subretinal fluid efflux is one of the causes of visual acuity loss associated with repeated foveal detachment.

Case 44 Continuation

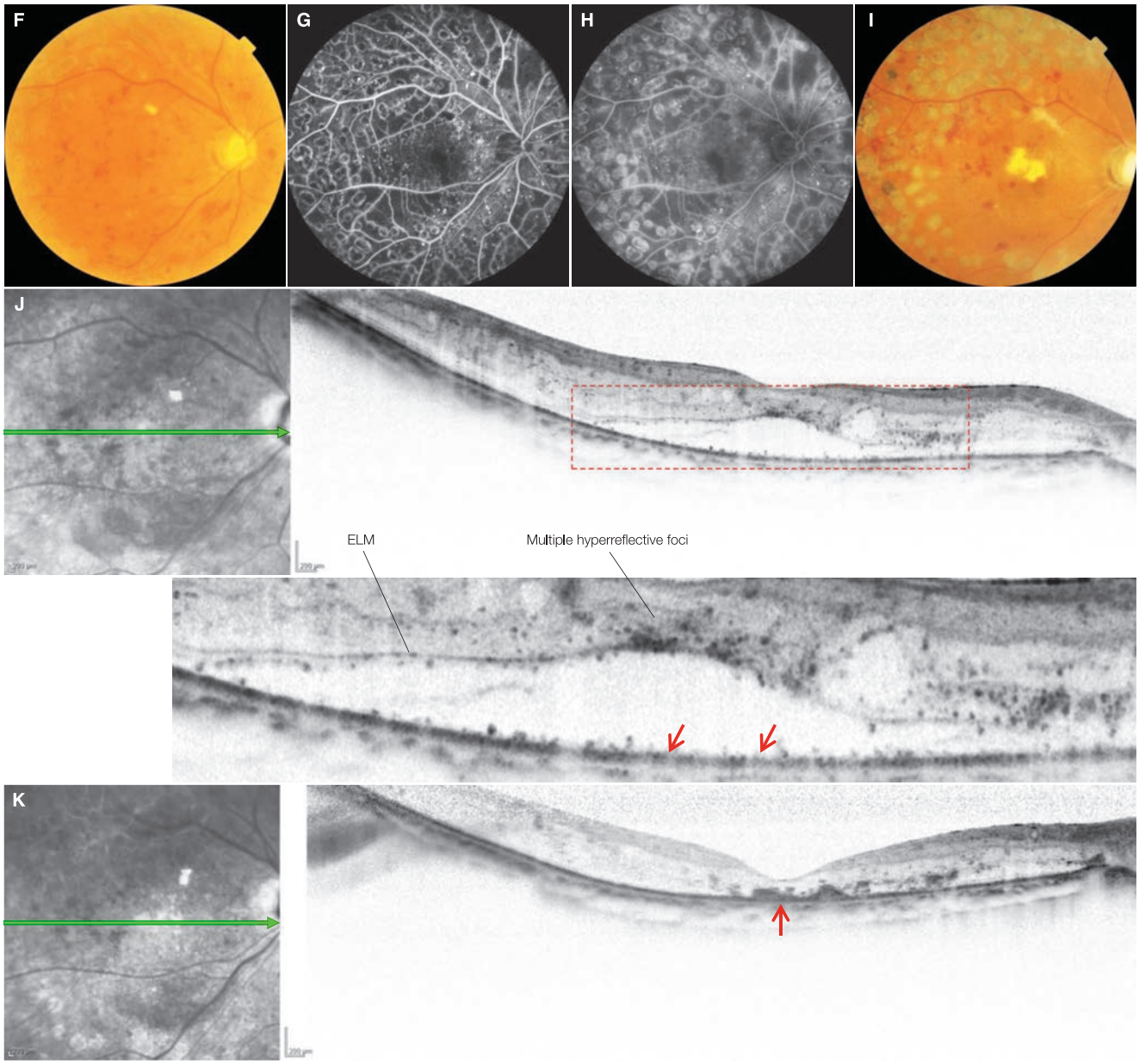

F: Color fundus photograph in the right eye: 11 months after initial diagnosis. Best-corrected visual acuity is 0.2. Hard exudates in the macula has decreased and a soft exudate has appeared above the fovea. **G:** FA in the right eye (1 min), **H:** FA in the right eye (13 min): 11 months after initial diagnosis. Multiple MAs can be seen in the macula. The nonperfusion area of the macula has expanded. **I:** Color fundus photograph in the right eye: 16 months after initial diagnosis. Visual acuity has further reduced to 0.05. Accumulation of hard exudates beneath the fovea is seen. **J:** IR + OCT horizontal scan of the right eye + enlarged version [red dashed box]: 12 months after initial diagnosis. Best-corrected visual acuity is 0.1. Hyperreflective foci can be seen in the detached outer layer of the retina, and are falling and accumulating on the RPE (→). The photoreceptor inner and outer segments have disappeared over a wide area of the macula. **K:** IR + OCT horizontal scan of the right eye: 13 months after initial diagnosis. BCVA further decreased to 0.07. One month after J, subfoveal accumulation of hard exudate is evident (→) and significant thinning in the fovea is noted.

Image interpretation points

In this case, the foveal photoreceptor layer had once undergone severe damages due to the mechanical injuries by the subretinal fluid efflux, and then subfoveal accumulation of hard exudates further enhanced the foveal damages. Multiple hyperreflective foci, which are leaked lipoproteins, accumulate along the outer retinal layers along the foveal detachment and some foci can be seen falling on the RPE. Accumulation of hard exudates beneath the fovea occurs with the disappearance of foveal detachment, and hyperreflective foci in the outer layer of the retina appears to be involved in this accumulation. Visual prognosis is poor in such cases.

Case 45 Cystoid macular edema: Subfoveal leakage from a foveal cystoid space

A 56-year-old male, OD, BCVA 0.5

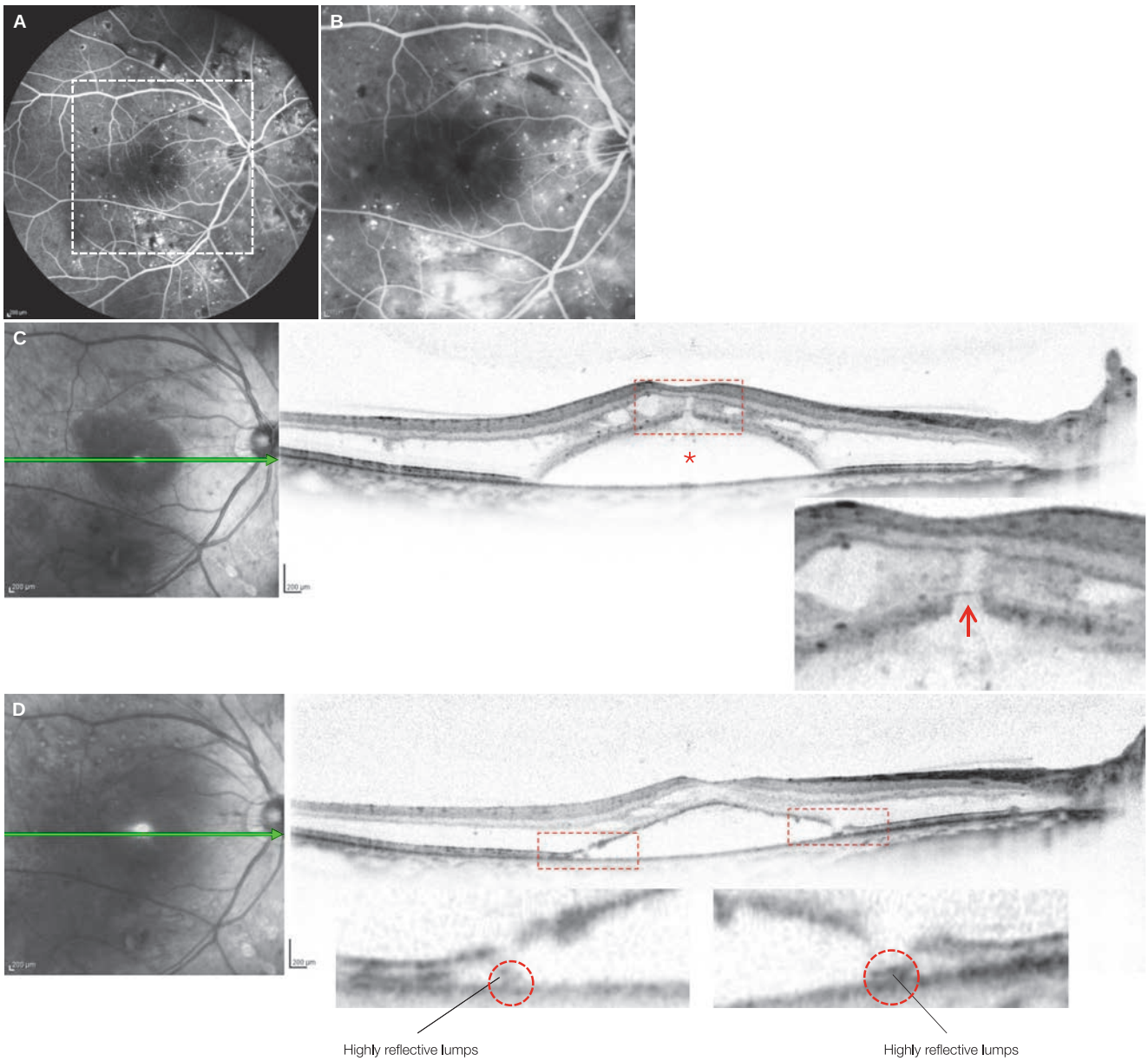

A: FA in the right eye (1 min), **B:** enlarged version of A [white dashed box]: At initial diagnosis. Scattered MAs and mild CME can be seen in the posterior pole. **C:** IR + OCT horizontal scan of the right eye + enlarged version [red dashed box]: At initial diagnosis. A leakage path (→) is formed from the shrinked foveal cystoid space to subretinal space. Diffuse moderate reflectivity is observed in the opening. * shows the foveal detachment. **D:** IR + OCT horizontal scan of the right eye + enlarged version [red dashed box]: 5 months after initial diagnosis. Multiple leakage openings from the outer plexiform layer cystoid spaces to subretinal space (red dashed square) are seen. Highly reflective lumps can be seen on the RPE beneath the openings.

Image interpretation points

Repeated foveal detachment involved in visual impairment due to diabetic macular edema appears to occur due to leakage from a foveal cystoid space, parafoveal cystoid spaces, and outer plexiform layer cystoid spaces into the subretinal space. In this case, leakage appeared to be mainly from a foveal cystoid spaces at initial diagnosis. The foveal cystoid space appears to be shrinked a result of connections between the foveal cystoid space and subretinal space. Five months after initial diagnosis, multiple leakage paths could be seen from the cystoid spaces in the outer plexiform layer. The source of leakage can sometimes change over time leading to persistence of the foveal detachment.

Case 46 Cystoid macular edema: Photoreceptor damage from outer plexiform layer edema

A 69-year-old female, OD, BCVA 0.4

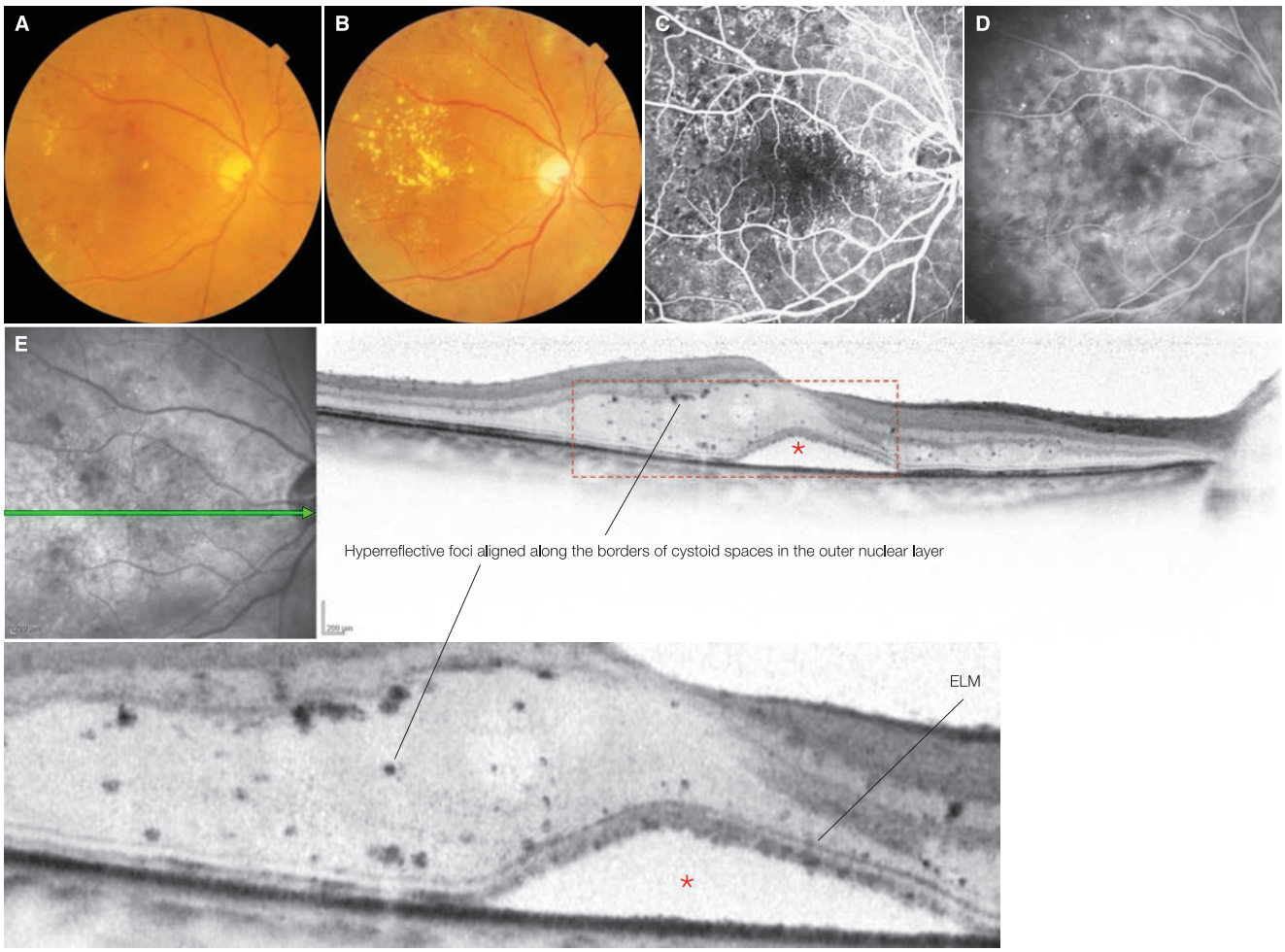

A: Color fundus photograph in the right eye: At initial diagnosis. A few of hard exudates are seen in the macula. **B:** Color fundus photograph in the right eye: 6 months after initial diagnosis. Hard exudates are increasing on the temporal macula. **C:** FA in the right eye (24 sec): 6 months after initial diagnosis. Multiple MAs are visible in the macula, but no capillary nonperfusion can be seen. **D:** FA in the right eye (8 min): Significant cystic fluorescein accumulations are noted in the entire posterior pole. **E:** IR + OCT horizontal scan of the right eye + enlarged version [red dashed box]: At initial diagnosis. Foveal detachment is visible (*). The hyperreflective foci accumulating along the internal walls of cystoid spaces highlight the outline of the cystoid spaces in the outer nuclear layer of the temporal macula.
(Continued on the next page)

Image interpretation points

This is a case representative of outer plexiform layer edema in the temporal macula, with minimal edema observed in the fovea centralis and inner nuclear layer. The changes in the outer plexiform layer appear to be diffuse at first glance, but the septum of each cystoid space is blurry due to moderate reflectivity within the cystoid space. The hyperreflective foci being aligned along the internal wall of each cystoid space help us identify the outline of the cystoid space..

Case 46 Continuation

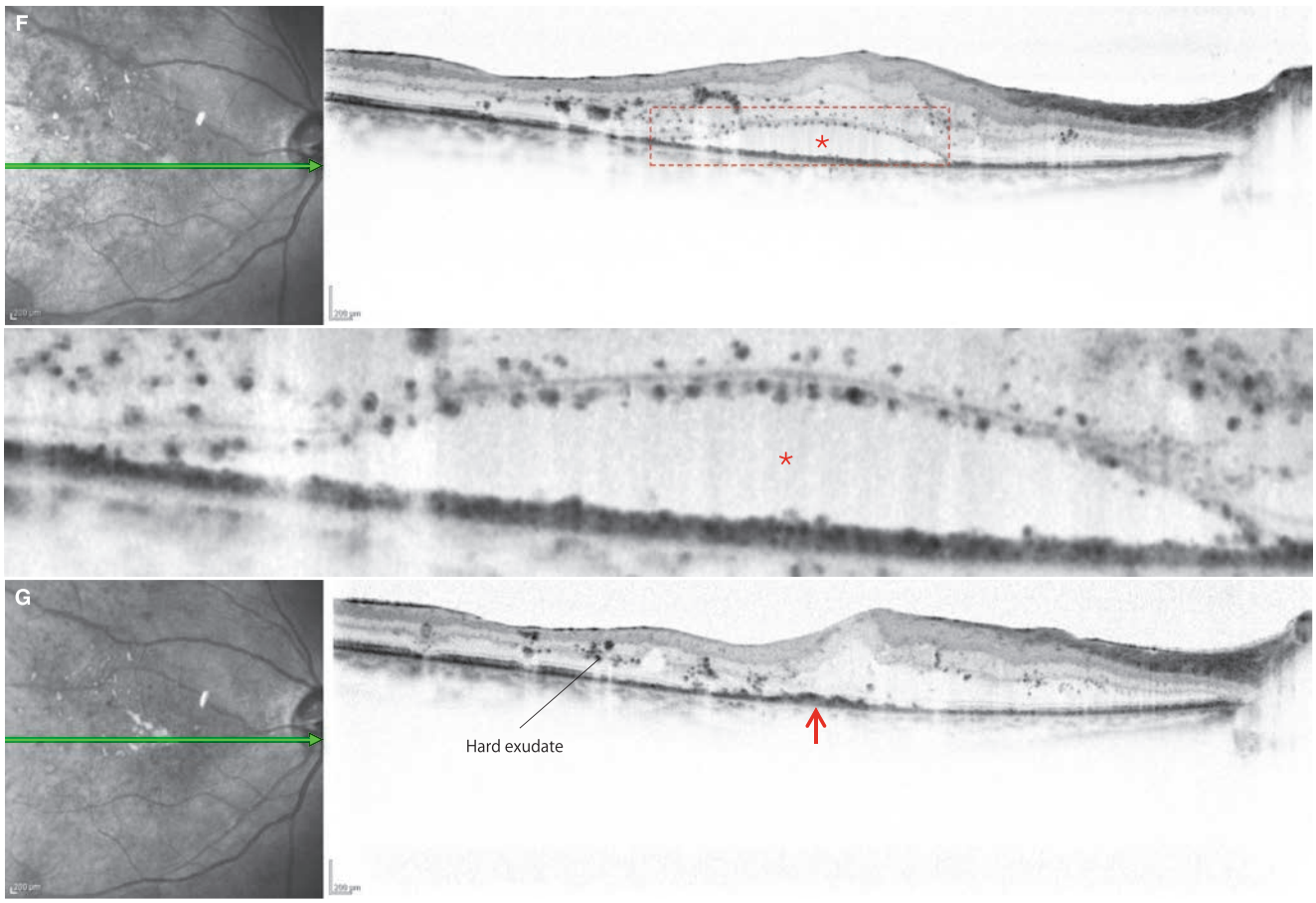

F: IR + OCT vertical scan of the right eye + enlarged version [red dashed box]: 5 months after initial diagnosis. Best-corrected visual acuity is 0.3. Grid photocoagulation was performed 1 month after diagnosis. The cystoid edema in the outer plexiform layer in the temporal macula has subsided, and hard exudate formation is evident inside the retina. Hyperreflective foci are aligned along anterior border of the ELM and posterior margin of the photoreceptor inner segment of the detached retina (*). **G:** IR + OCT horizontal scan of the right eye: 6 months after initial diagnosis. Best-corrected visual acuity is 0.3. The outer plexiform layer edema in the temporal macula that underwent grid photocoagulation has disappeared and an accumulation of hard exudate can be seen beneath the fovea centralis (→).

Image interpretation points

The cystoid edema of the outer plexiform layer in the temporal macula has disappeared after grid photocoagulation, but hard exudate is accumulating beneath the fovea centralis, causing atrophy of the foveal photoreceptor layer. Hard exudates are also formed within the retina where the cystoid spaces are disappearing. Just before hard exudates accumulate beneath the fovea centralis, hyperreflective foci were seen aligned on the anterior border of the ELM and on the posterior margin of the photoreceptor inner segment in the area of the foveal detachment. Accumulation of hard exudates cannot be seen on the RPE at this stage.

Case 47 Cystoid macular edema: Microaneurysms

A 67-year-old female, OD, BCVA 0.3

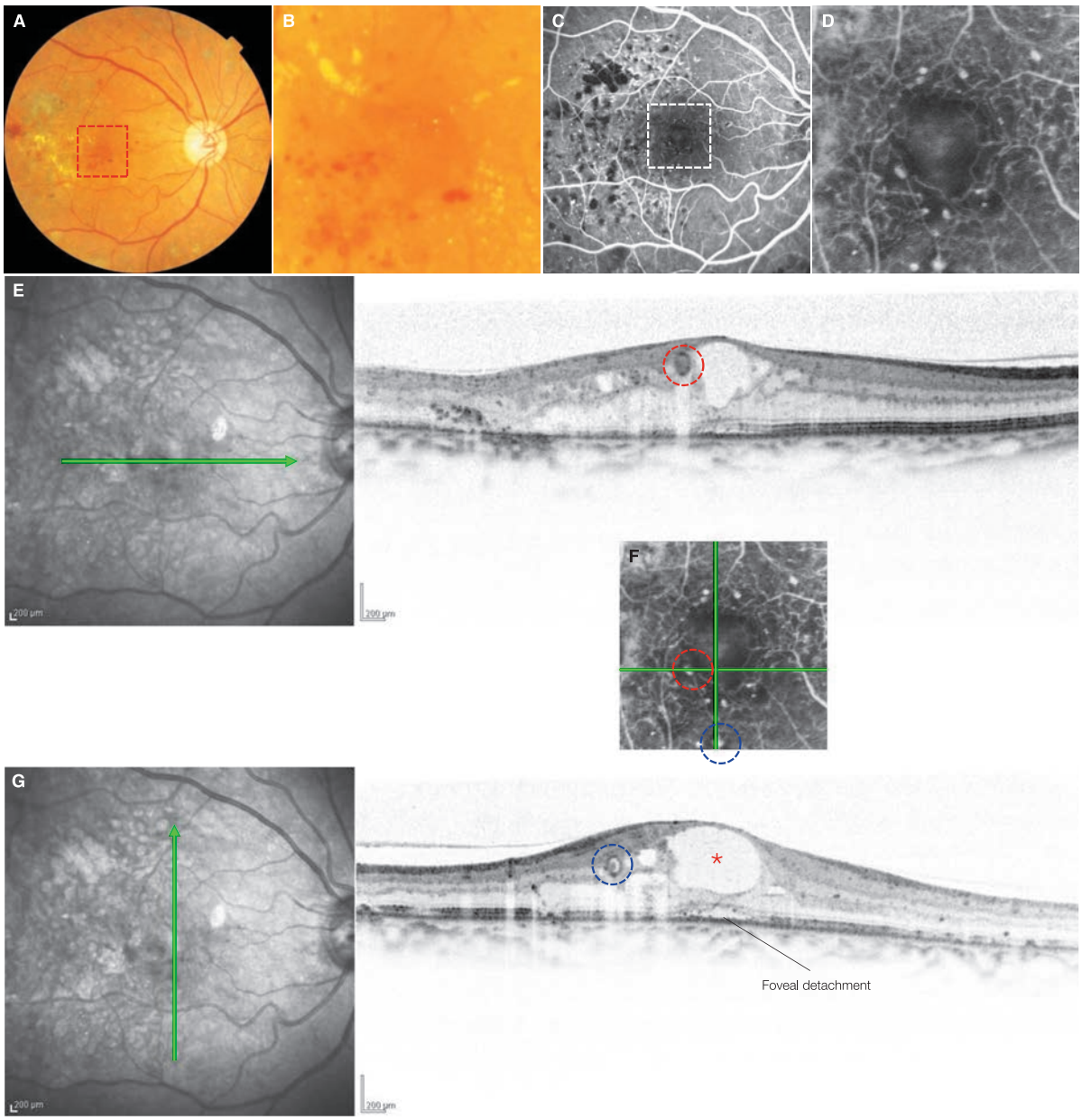

A: Color fundus photograph in the right eye, **B:** Enlarged version of A [red dashed box]: Dot and blot hemorrhages can be seen. The MAs and dot hemorrhages, which are present together in the macula, looks too similar to be distinguished on color fundus photography. **C:** FA in the right eye (1 min), **D**: Enlarged version of C [white dashed box]: Multiple MAs are visible in the perifoveal capillary bed. Destruction of the perifoveal capillary bed can also be observed. **E:** IR + OCT horizontal scan of the right eye, **F:** Same image as D: This has been redisplayed to show the alignment between the OCT B-scan images E and G and the FA image. The red and blue dashed circles showing MAs on the FA image correspond to the red and blue dashed circles in the OCT images E and G respectively. **G:** IR + OCT vertical scan of the right eye: MAs in contact with foveal cystoid spaces (*) (red dashed circle) and MAs in the vicinity of the foveal cystoid space (blue dashed circle) can be seen. Both exist at the inner nuclear layer level.

Image interpretation points

MAs are depicted on OCT B-scan images as circular/elliptical capsular structures with highly reflective walls. It is easy to discern the layer where MAs exist and their positional relationship with cystoid spaces on OCT. About 80% of MAs can be seen in the inner nuclear layer, and roughly 50% are adjacent to, in contact with or inside the cystoid spaces. MAs are enveloped by highly reflective walls of various extents, and the MAs with poor wall reflectivity are thought to be associated with cystoid space formation.

Case 48 Ischemic maculopathy: Cystoid macular degeneration

A 38-year-old female, OS, BCVA 0.01

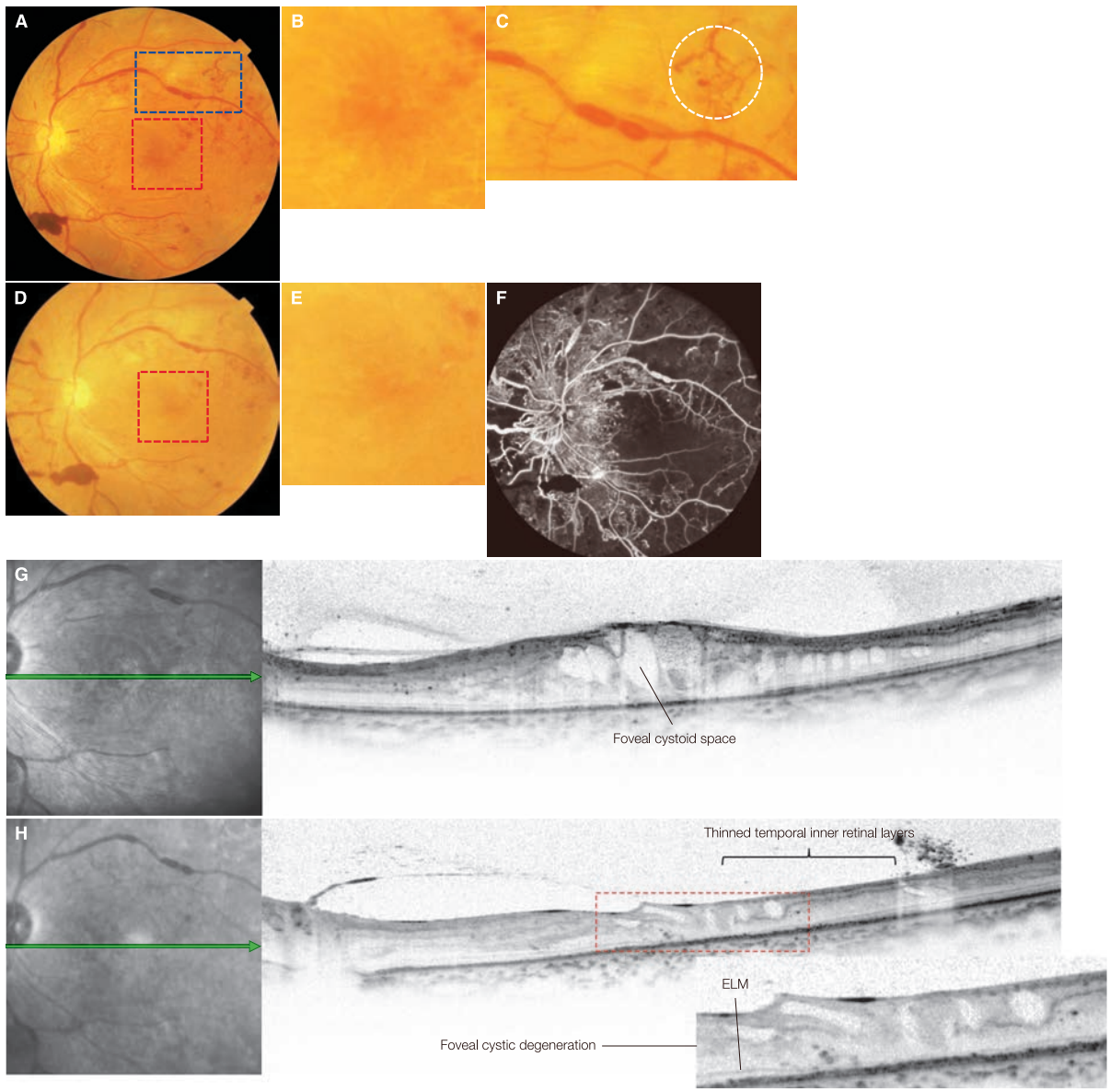

A: Color fundus photograph in the left eye, **B:** Enlarged version of A [red dashed box], C: Enlarged version of A [blue dashed box]: At initial diagnosis. Venous beading and intraretinal microvascular abnormalities (IRMAs, white dashed circle) can be seen, **D:** Color fundus photograph in the left eye, **E:** Enlarged version of D [red dashed box]: 2 months after initial diagnosis. Best-corrected visual acuity is 0.01. Preretinal hemorrhages can be seen in the lower arcade vessels. Ghost perifoveal capillary bed (no capillary blood flow) is visible. **F:** FA in the left eye (1 min): 2 months after initial diagnosis. Nonperfused area is seen in the perifoveal capillary bed and the temporal half of the macula. **G:** IR + OCT horizontal scan of the left eye: At initial diagnosis. Appearance of the cystoid edema can be seen in the macula. **H:** IR + OCT horizontal scan of the left eye + enlarged version [red dashed box]: Same area as G, 2 months after initial diagnosis. Cystoid edema has subsided, but the fovea centralis exhibits significant atrophy with cystoid spaces. There is significant thinning of the inner retinal layers on the temporal side.

Image interpretation points

This is a case that appears to be cystoid macular edema at first glance, but is actually cystoid degeneration (also termed cystic degeneration) due to macular ischemia. Remission of the macular edema is due to blood supply to the macula being cut off as a result of retinal vascular nonperfusion in the macula.

Cystic degeneration of the macula was clearly detected on OCT, and there is also significant thinning of the temporal inner layers of the retina. Currently, there are no methods of predicting the onset or established treatments for diabetic ischemic maculopathy.

Case 49 Ischemic maculopathy: Thinned macula

A 38-year-old female, OD, BCVA 0.01

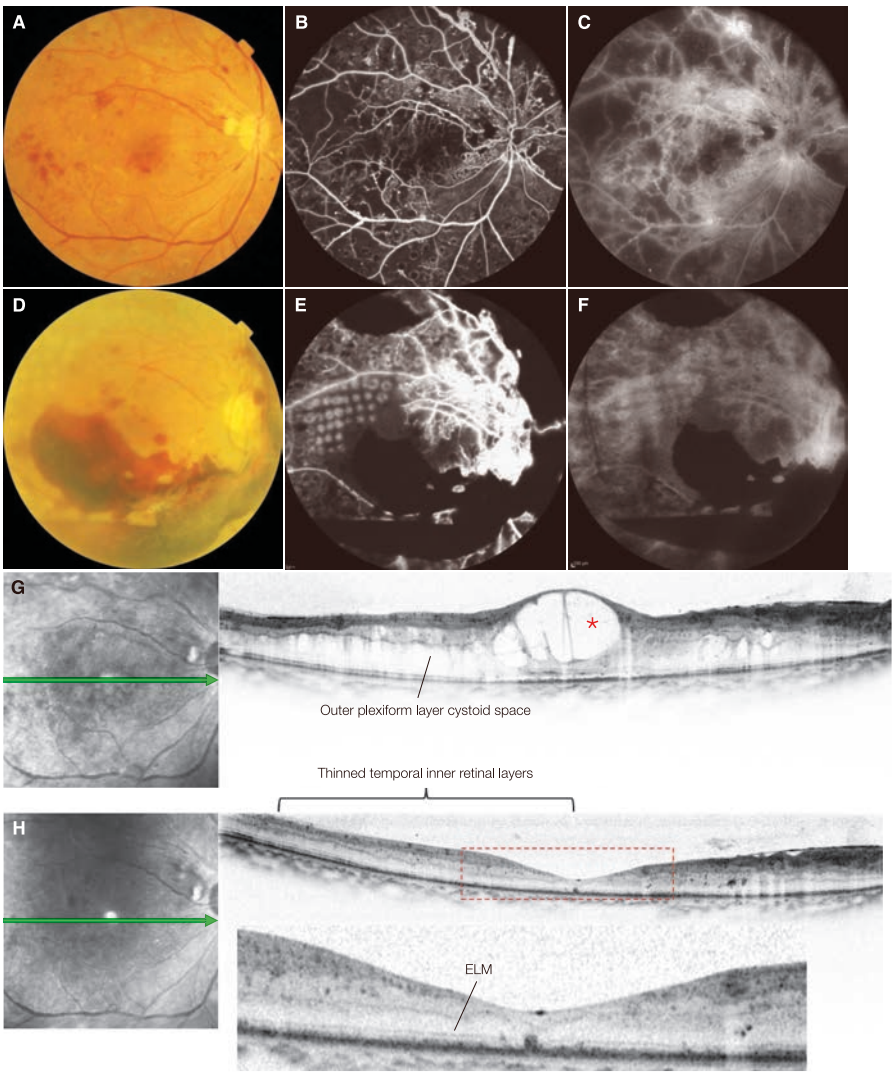

A: Color fundus photograph in the right eye: At initial diagnosis. Retinal hemorrhages, venous beading, IRMAs, and hard exudate can be seen in the posterior pole. **B:** FA in the right eye (1 min), **C:** FA in the right eye (10 min): At initial diagnosis. Nonperfusion area can be seen mainly in the equatorial area, but nonperfusion of the perifoveal capillary bed and temporal macula is also observed. Leakage from superior retinal neovascular vessels can be seen. **D:** Color fundus photograph in the right eye: 5 months after initial diagnosis. Best-corrected visual acuity is 0.01. Preretinal hemorrhages have occurred. Niveau formation of subhyaloid hemorrhages can be seen. Photocoagulation scars produced by PASCAL (PAttern SCAnning Laser) Photocoagulator (OptiMedica Corporation, Santa Clara, CA) can be seen. **E:** FA in the right eye (90 sec), **F:** FA in the right eye (13 min): 5 months after initial diagnosis. Blocking of fluorescence due to preretinal hemorrhages, but nonperfusion is evident over a wide macular area. **G:** IR + OCT horizontal scan of the right eye: At initial diagnosis. Foveal and parafoveal cystoid spaces (*) are noted. **H:** IR + OCT horizontal scan of the right eye + enlarged version [red dashed box]: Same area as G, 2 months after initial diagnosis, 3 months before the preretinal hemorrhages. Best-corrected visual acuity is 0.02. The CME has completely subsided, but the fovea centralis exhibits significant thinning. The ELM line is visible, but the IS/OS lines are not. Thinning of the inner retinal layer of the macula is significant, and the foveal depression appears flattened and enlarged.

Image interpretation points

In this case, before the vitreous hemorrhages occurred, capillary nonperfusion in the macula progressed rapidly resulting in foveal atrophy and leading to severe visual impairment. Such acute development of perifoveal capillary bed nonperfusion is common in type 1 diabetes. Remission of the macular edema is due to blood supply to the macula being cut off as a result of retinal vascular nonperfusion in the macula. Thinning of the fovea centralis and inner retinal layers of the macula can be seen with OCT. Panretinal photocoagulation was performed but could not prevent the progression of diabetic ischemic maculopathy. Currently, there are no established treatments for diabetic ischemic maculopathy.

Case 50 Vitreomacular traction syndrome: A typical example

A 71-year-old female, OD, BCVA 0.07

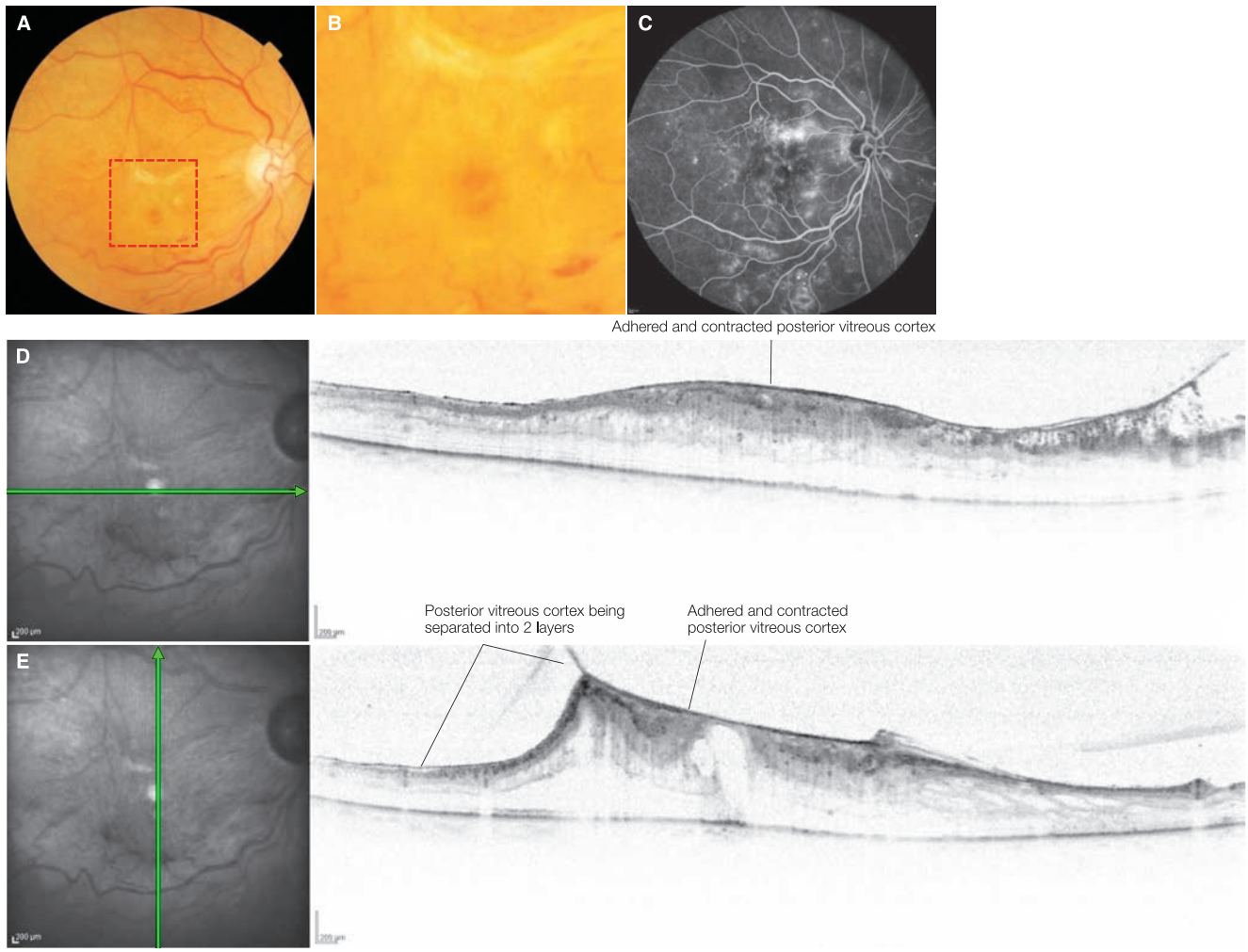

A: Color fundus photograph in the right eye, **B:** Enlarged version of A [red dashed box]: Significant macular whitening and capillary tortuosity due to the ERM is seen. **C:** FA in the right eye (3 min): FA from 6 months before initial diagnosis. Leakage in the macular area can be seen. **D:** IR + OCT horizontal scan of the right eye: Adhesion of the posterior vitreous cortex to the entire macula is exhibited in the horizontal scan passing through the fixation point. **E:** IR + OCT vertical scan of the right eye: Adhesion of the posterior vitreous cortex to the macula can be observed over a wide area, and the macula is being elevated into a tent-shape. The posterior vitreous cortex was separated into 2 layers.

Image interpretation points

Vitreomacular traction syndrome is common with diabetic macular edema, but the adhesion of the posterior vitreous cortex is often wider than vitreomacular traction syndrome associated with other retinal diseases. This appears be due to abnormal adhesion occurring over a wider area of the vitreoretinal interface in diabetic macular edema. There are many cases where the entire macula is lifted into a tent-shape.

Case 51 Proliferative diabetic retinopathy: Progressive proliferation

A 29-year-old male, OS, BCVA 0.4

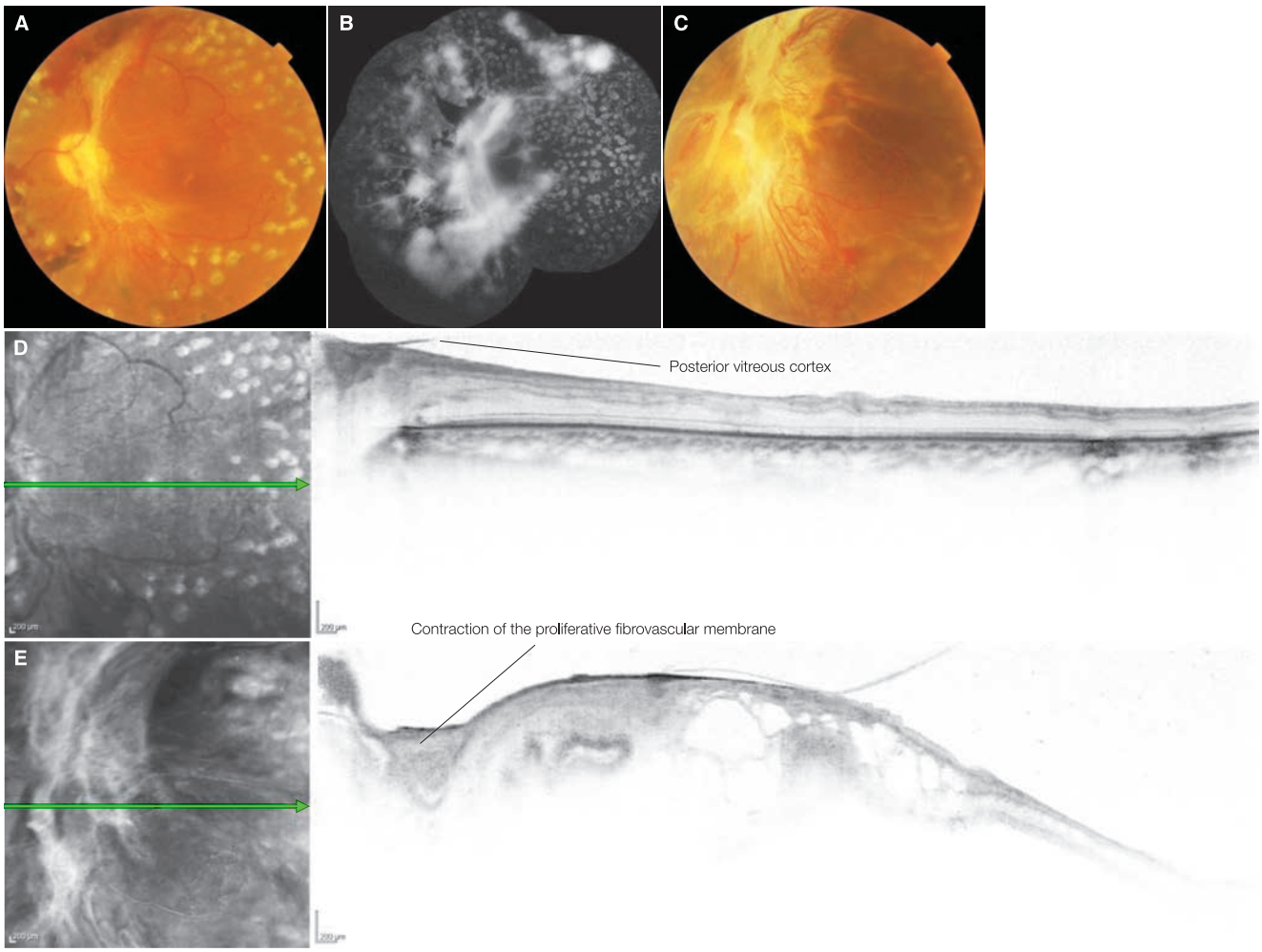

A: Color fundus photograph in the left eye: At initial diagnosis. Mild fibrovascular membrane is seen from the optic disc along the upper and lower arcades, and focal preretinal hemorrhages above the optic disc. **B:** FA montage of the left eye (10 min): Significant fluorescein leakage can be seen from neovascularization of the disc (NVD) and elsewhere on the retina (NVE) . Panretinal photocoagulation is performed to a certain extent. **C:** Color fundus photograph in the left eye: 3 months after initial diagnosis. Best-corrected visual acuity in this left eye is now finger counting directly in front of the eye. Tractional retinal detachment has occurred due to rapid proliferation of the fibrovascular membrane. **D:** IR + OCT horizontal scan of the left eye: At initial diagnosis. No retinal detachment is visible. **E:** IR + OCT horizontal scan of the left eye: 3 months after initial diagnosis. Best-corrected vision is finger counting directly in front of the left eye. The macula is detached as if being pulled by the optic disc due to contraction of the proliferative fibrovascular membrane. The RPE is poorly depicted on OCT due to the elongation of the eye in the longitudinal direction.

Image interpretation points

This case represents the exacerbation process of proliferative diabetic retinopathy. At initial diagnosis, neovasculaization of the disc (NVD) and elsewhere on the retina (NVE) are present, but visual acuity remained good since there was minimal damage to the macula. During follow-up after the addition of retinal photocoagulation, there was rapid progress of proliferative changes resulting in a macular tractional retinal detachment. Earlier surgical intervention would have been preferable.

Case 52 Proliferative diabetic retinopathy: Preretinal hemorrhages and vitreomacular traction syndrome

A 37-year-old female, OS, BCVA 0.3

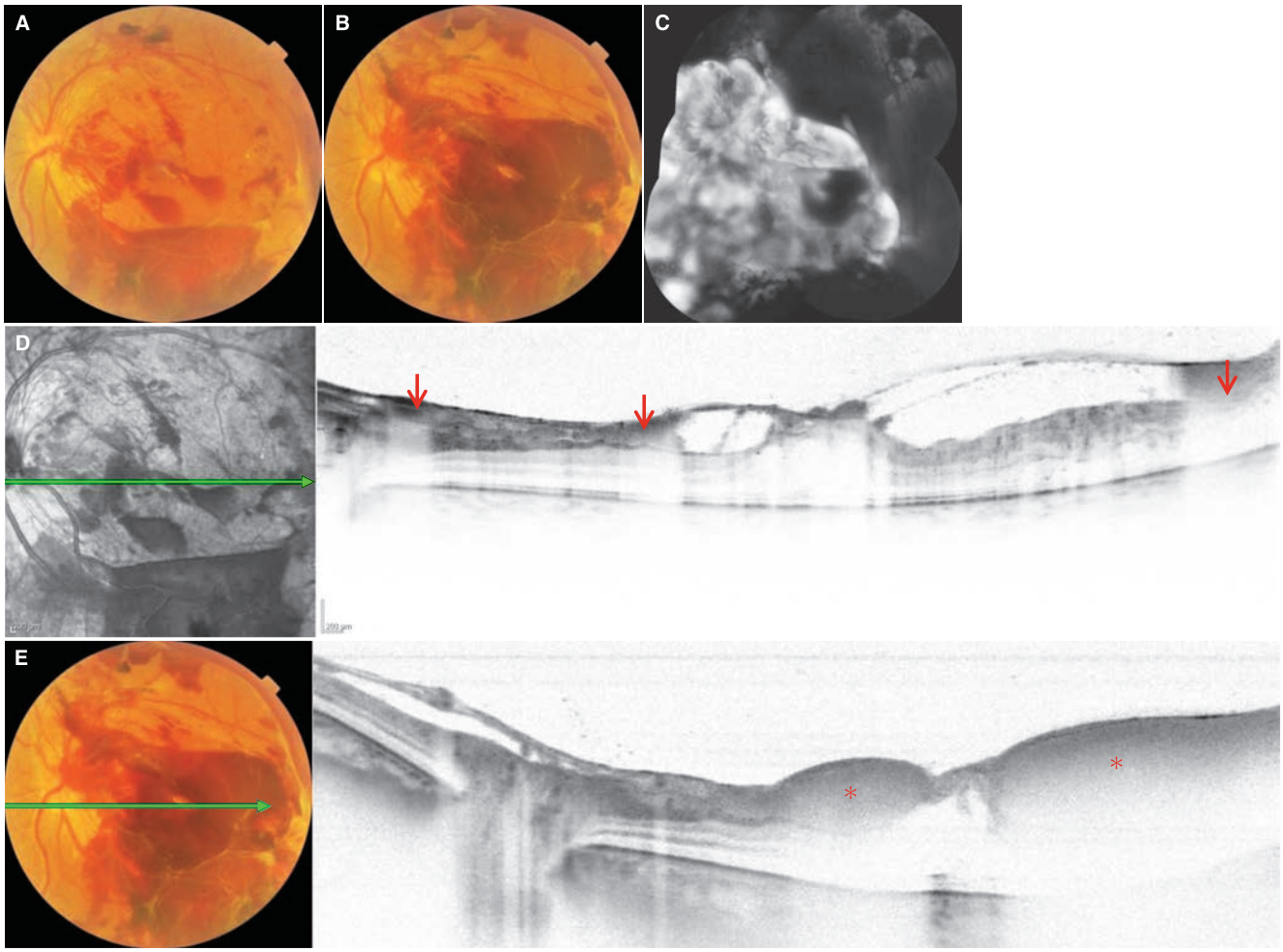

A: Left eye fundus photograph: At initial diagnosis. Neovascularization of the disc (NVE) and fibrovascular membrane from the optic disc along the arcade vessels can be seen, and preretinal hemorrhages are seen in the posterior pole with niveau along the inferior arcade. **B:** Color fundus photograph: 2 weeks after initial diagnosis. Preretinal hemorrhages have remarkably increased. There is only few hemorrhages in the fovea. **C:** FA in the left eye (10 min), panorama: Fibrovascular membrane is formed over the posterior pole including the optic disc, and significant fluorescein leakage is seen. **D**: IR + OCT horizontal scan of the left eye: At initial diagnosis. Vitreomacular traction syndrome can be observed. Hemorrhages can be seen between the posterior vitreous cortex and the retina l surface (➔). **E:** Color fundus photograph + SS-OCT horizontal scan of the left eye: 2 weeks after initial diagnosis. Gaps between the posterior vitreous cortex and the retina l surface are filled with hemorrhages (*). It is obvious that vitreomacular traction is present.

Image interpretation points

Preretinal hemorrhages can accumulate between the posterior vitreous cortex and retina l surface in cases where PVD has not occurred. In this case vitreomacular traction syndrome preceded massive preretinal hemorrhages. Large amounts of preretinal hemorrhages are accumulating and filling the gaps between the posterior vitreous cortex and the retina l surface. Even though retinal lesions cannot be visualized by SD-OCT, SS-OCT can provide images that allow interpretation of retinal pathology hiding beneath the massive preretinal hemorrhages.

Retinal vascular diseases

4.1 Retinal vein occlusion – 104
References – 106

Case 53 Central retinal vein occlusion: Progression from non-ischemic to ischemic ① – 108

Case 53 Continuation – 109

Case 54 Central retinal vein occlusion: Progression from non-ischemic to ischemic ② – 110

Case 55 Central retinal vein occlusion: Ischemic type – 112

Case 56 Branch retinal vein occlusion: Non-ischemic type – 113

Case 57 Branch retinal vein occlusion: Significant inner layer ischemia – 114

4.2 Retinal artery occlusion – 115
References – 115

Case 58 Central retinal artery occlusion: A typical example – 116

Case 59 Central retinal artery occlusion: Cilioretinal artery not occluded – 117

Case 60 Central retinal artery occlusion: Incomplete occlusion – 118

Case 61 Hemi central retinal artery occlusion: Case of good visual acuity – 119

Case 62 Branch retinal artery occlusion: Incomplete occlusion – 120

4.3 Idiopathic juxtafoveal macular telangiectasia – 121
References – 122

Case 63 Macular telangiectasia: Yannuzzi classification Type 1 – 123

Case 64 Macular telangiectasia: Yannuzzi classification Type 1 – 124

Case 65 Macular telangiectasia: Yannuzzi classification Type 2 Stage 2 – 125

Case 66 Macular telangiectasia: Yannuzzi classification Type 2 Stage 3 – 126

Case 67 Macular telangiectasia: Yannuzzi classification Type 2 Stage 4 – 127

Case 68 Coats' disease: A typical example – 128

4.4 Retinal arterial macroaneurysm – 129
References – 129

Case 69 Retinal arterial macroaneurysm: Subretinal hemorrhages – 130

Case 70 Retinal arterial macroaneurysm: Foveal detachment from an inferior arterial macroaneurysms – 132

4.1 Retinal vein occlusion

Background

When the central retinal vein or its branches are occluded, the upstream vein dilates and becomes tortuous; flame-shaped or spotted retinal hemorrhages can occur depending on the depth of bleeding. The main cause of visual impairment is macular edema. When significant retinal ischemia causes retinal neovascularization and iris rubeosis, this can lead to visual impairment due to vitreous hemorrhages and neovascular glaucoma.

Central retinal vein occlusion

Central retinal vein occlusion (CRVO) occurs due to a central retinal venous obstruction mainly caused by thrombosis forming at the lamina cribrosa level in the optic disc.[1] The central retinal vein sometimes divides into two branches when it exits the optic nerve; if one side is occluded, this results in a hemi-CRVO. The incidence of CRVO is 0.1–0.5%.[1–3] In the elderly, CRVO often accompanies systemic disorders such as hypertension, diabetes, ischemic (arteriosclerotic) heart disease[4–10], and glaucoma.[4–7, 10] Aspirin and/or warfarin have also been reported as risk factors.[9] In contrast, vasculitis is typically associated with the onset of CRVO in young patients. However, the cause of CRVO in young patients is often unclear, and in such cases congenital abnormalities of the central retinal vein at the level of the lamina cribosa is suspected.[11] Bilateral involvement is seen in about 10–15% of elderly patients, but in the majority of younger patients, the onset is in just one eye.[11, 12] CRVO is classified into non-ischemic and ischemic based on the extent of the capillary bed nonperfusion, which corresponds to Hayreh's classifications of venous stasis retinopathy and hemorrhagic retinopathy.[13] The incidence of non-ischemic CRVO is approximately twice that of ischemic, but when followed long-term for one and a half years, 18.6–34% of non-ischemic CRVO progress to ischemic CRVOs.[14, 15] Non-ischemic CRVO includes cases with a relatively good prognosis where visual acuity and the ocular fundus almost normalize naturally, although the prognosis is poor when macular edema is more advanced.

In addition to advanced macular edema, the development of macular ischemia and subsequent neovascular glaucoma are further causes of poor prognosis in ischemic CRVO. Neovascular glaucoma typically occurs within 3–4 months after CRVO onset. Visual prognosis is good in cases where visual acuity at the time of diagnosis is 0.5 or above, whereas visual improvement is not achieved in the majority of cases under 0.1.[15] Ischemic maculopathy as a result of capillary nonperfusion including perifoveal capillary bed also appears to underlie such severe visual impairment. The extent of retinal capillary nonperfusion is responsible for both the visual prognosis and the risks of developing neovascular glaucoma. It is common to define an ischemic CRVO as having a nonperfusion area with a diameter of 10-fold disc diameter or more,[16] but when dense retinal hemorrhages are present immediately after onset, it is not easy to determine the nonperfusion area fluorescein angiography because of blocking of fluorescence light by the hemorrhages. In such cases, poor visual acuity and visual field results, relative afferent pupillary defect , poor visual function tests such as an electroretinogram, multiple soft exudates, extension of the intraretinal circulation time,[17] and significant fluorescein leakage on FA suggest ischemic CRVO.

OCT findings

It has now become possible to quantitatively assess the extent of macular edema in CRVO with OCT. OCT is becoming an essential test for evaluating the effects of medical therapies that use anti-vascular endothelial growth factor drugs and/or steroid drugs, evaluating recurrence, and determining the effects of grid photocoagulation and vitreous surgery. In addition, OCT can detect structures of macular edema such as cystoid spaces and serous retinal detachment (SRD, also termed foveal detachment) that other tests, including FA, cannot.[18–21] It was previously believed that SRD accompanied severe CRVO, but we have now observed that SRD accompanies a higher percentage (about 80%) than previously thought thanks to OCT.[18, 21] Most SRDs (about 70%) can be seen as cone-shaped, small foveal detachments, and are thought to progress to dome-shaped SRDs based on the mechanism shown in Fig. 4-1.[21] The highest percentage of cystoid spaces can be seen in the fovea centralis, inner nuclear layer, and outer plexiform layer (all >80%). It was shown that a foveal cystoid space reaching the external limiting membrane (ELM) result in poor visual acuity.[19] Macular edema in CRVO exhibits maximum thickness in the fovea centralis, but the correlation between the thickness and visual acuity is not high.[22] This appears to be because, although macular ischemia is most strongly associated with visual impairment, the macular thickening due to macular edema does not necessarily reflect the severity of macular ischemia. In practice, the state of the IS/OS line, which is the index for the photoreceptor integrity, correlates with visual acuity more than foveal retinal thickness.[23] Such observations of a foveal cystoid space and the IS/OS line are useful, but when retinal hemorrhages and cystoid edema are extensive, the photoreceptor IS/OS line cannot be clearly seen due to blocking of OCT measurement beams.

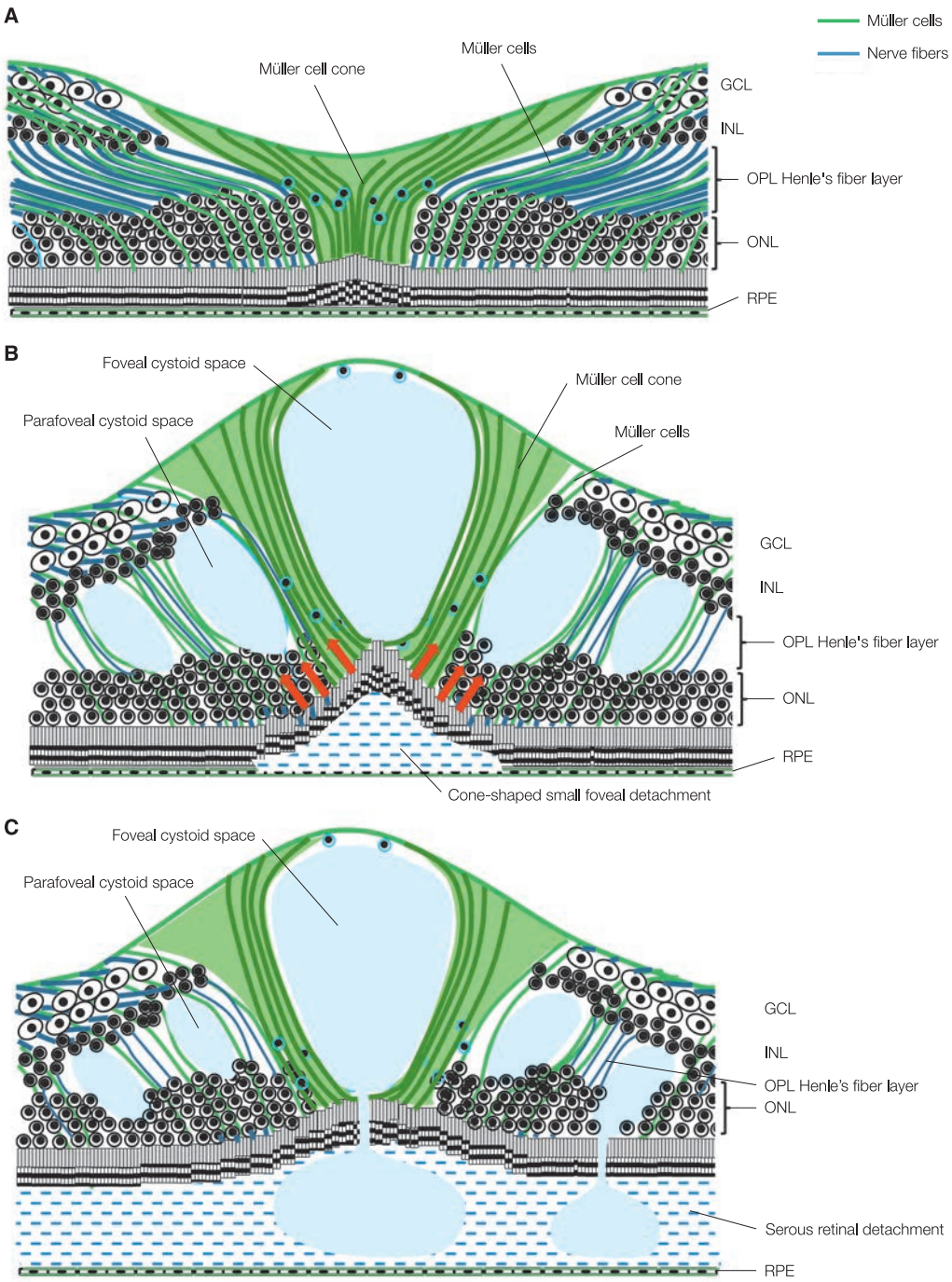

Fig. 4-1 Schematic diagram of serous retinal detachment development in retinal vein occlusion
A: The structure of the fovea centralis is drawn. The Müller cell cone in the foveola is highlighted in light green, and the Müller cells in the Muller cell cone and parafovea are highlighted in deep green lines and the nerve fibers are highlighted in blue lines. **B:** When cystoid spaces form in the fovea centralis and parafovea, the Müller cells are stretched as a result of the spatial expansion, consequently pulling the photoreceptor layer and leading to a cone-shaped small foveal detachment (➔). **C:** Holes develop in the ELM and photoreceptor inner and outer segments, and fluids and sometimes hemorrhages leak from within the cystoid spaces into the subretinal space causing serous retinal detachment. GCL=ganglion cell layer, INL=inner nuclear layer, OPL=outer plexiform layer, RPE=retinal pigment epithelium, ONL=outer nuclear layer. (Modified according to Tsujikawa A, et al. Serous retinal detachment associated with retinal vein occlusion. *Am J Ophthalmol.* 2010; 149: 291–301)

Branch retinal vein occlusion

Branch retinal vein occlusion (BRVO) occurs due to thrombus forming at an arteriovenous crossing.[24] The retinal artery and vein at the crossing share common wall, and the vein is susceptible to pressure from the artery. BRVO is associated with hypertension in about 3/4 of cases.[4, 7, 8] Venous occlusion areas are most common in the superotemporal arteriovenous crossing of the retina. BRVO develops in both eyes in 5–6% of cases upon initial diagnosis and develops in the fellow during follow-up in another 10% of cases. The causes of reduced visual acuity are macular edema and retinal hemorrhages (particularly hemorrhages extending to the foveal and parafoveal cystoid spaces), in the early stage and prolonged macular edema, pigmentation of the fovea centralis, epiretinal membrane, vitreous hemorrhages, and rhegmatogenous retinal detachment in the late to end stages. Visual acuity is good when there is no macular edema, but vision declines below 0.5 when macular edema occurs. A baseline mean visual acuity is reportedly 0.15-0.2, which is worse than thought. With a natural course, vision rarely improves so much after 6 months, but will improve significantly within 2 years (by an average of 28 letters in ETDRS). Macular edema reportedly regressed in 18% of cases 4.5 months after the patients had become aware of reduced visual acuity, while patients developed macular edema in 41% of the cases within 7.5 months.[25] Collateral circulation spanning the nonperfusion area and temporal horizontal raphe often form when retinal hemorrhages are absorbed.

OCT findings

Macular retinal thickness measurements using OCT have become indispensable in the follow-up of BRVO macular edema and assessing therapeutic effects. OCT has a higher detection rate for CME than FA, and is able to detect the SRD that FA cannot find. We have come to understand that SRD accompanying BRVO is not unusual when observed using OCT.[26] Macular edema in BRVO differs from that in CRVO in that significant macular thickening occurs only on the nonperfused side and in the fovea, and therefore observation with vertical B scans is useful. Foveal cystoid spaces, parafoveal cysts, and SRD even extend to the perfused side. The nonperfusion in the distal area that does not involve the macula can cause a macular SRD.[27] BRVO does share several characteristics in macular edema with that of CRVO. Specifically, these include: ① the SRD appears as a cone-shaped small foveal detachment, and progresses to a dome-shaped SRD,[21] ② the cystoid spaces are most frequently seen in the fovea centralis, inner nuclear layer, and outer plexiform layer, eventually resulting in poor vision when the foveal cystoid space reach the ELM,[19] and ③ the IS/OS line, which is an index for the photoreceptor integrity, are correlated with visual acuity.[28–30] In the acute phase, the occluded side of the fovea centralis cannot be clearly seen when there is significant retinal hemorrhages and cystoid macular edema. Cases where visual acuity remains poor despite resolved macular edema often are due to accompanying macular area pigmentation and thinning of the macular area photoreceptor inner and outer segments and outer nuclear layer. Several etiologies including SRD and subretinal efflux of retinal hemorrhages may explain the damage to the outer layer of the retina.

References

1) Green WR, Chan CC, Hutchins GM, et al. Central retinal vein occlusion: a prospective histopathologic study of 29 eyes in 28 cases. Trans Am Ophthalmol Soc. 1981; 79:371–422.
2) Klein R, Klein BE, Moss SE, et al. The epidemiology of retinal vein occlusion: the Beaver Dam Eye Study. Trans Am Ophthalmol Soc. 2000; 98: 133–141.
3) Mitchell P, Smith W, Chang A. Prevalence and associations of retinal vein occlusion in Australia. The Blue Mountains Eye Study. Arch Ophthalmol. 1996; 114: 1243–1247.
4) Appiah AP, Greenidge KC. Factors associated with retinal-vein occlusion in Hispanics. Ann Ophthalmol. 1987; 19:307–309, 312.
5) Rath EZ, Frank RN, Shin DH, et al. Risk factors for retinal vein occlusions. A case-control study. Ophthalmology. 1992; 99:509-514.
6) The Eye Disease Case-Control Study Group. Risk factors for central retinal vein occlusion. Arch Ophthalmol. 1996; 114:545–554.
7) Sperduto RD, Hiller R, Chew E, et al. Risk factors for hemiretinal vein occlusion: comparison with risk factors for central and branch retinal vein occlusion: the eye disease case-control study. Ophthalmology. 1998; 105: 765–771.
8) Hayreh SS, Zimmerman B, McCarthy MJ, et al. Systemic diseases associated with various types of retinal vein occlusion. Am J Ophthalmol. 2001; 131:61–77.
9) Koizumi H, Ferrara DC, Bruè C, et al. Central retinal vein occlusion case-control study. Am J Ophthalmol. 2007; 144:858–863.
10) Klein R, Moss SE, Meuer SM, et al. The 15-year cumulative incidence of retinal vein occlusion: the Beaver Dam Eye Study. Arch Ophthalmol. 2008; 126:513–518.
11) Walters RF, Spalton DJ. Central retinal vein occlusion in people aged 40 years or less: a review of 17 patients. Br J Ophthalmol. 1990; 74: 30–35.
12) Pollack A, Dottan S, Oliver M. The fellow eye in retinal vein occlusive disease. Ophthalmology. 1989; 96:842–845.
13) Hayreh SS. Classification of central retinal vein occlusion. Ophthalmology. 1983; 90:458-474.
14) Hayreh SS, Zimmerman MB, Podhajsky P. Incidence of various types of retinal vein occlusion and their recurrence and demographic characteristics. Am J Ophthalmol. 1994; 117:429–441.
15) The Central Vein Occlusion Study Group. Natural history and clinical management of central retinal vein occlusion. Arch Ophthalmol. 1997; 115:486–491
16) The Central Vein Occlusion Study Group. Baseline and early natural history report. Arch Ophthalmol. 1993; 111:1087–1095.
17) Sinclair SH, Gragoudas ES. Prognosis for rubeosis iridis following central retinal vein occlusion. Br J Ophthalmol. 1979; 63:735–743
18) Ozdemir H, Karacorlu M, Karacorlu S. Serous macular detachment in central retinal vein occlusion. Retina. 2005; 25:561–563.
19) Yamaike N, Tsujikawa A, Ota M, et al. Three-dimensional imaging of cystoid macular edema in retinal vein occlusion. Ophthalmology. 2008; 115:355–362.
20) Jittpoonkuson T, Garcia PM, Rosen RB. Correlation between fluorescein angiography and spectral-domain optical coherence tomography in the diagnosis of cystoid macular edema. Br J Ophthalmol. 2010; 94:1197–1200.
21) Tsujikawa A, Sakamoto A, Ota M, et al. Serous retinal detachment associated with retinal vein occlusion. Am J Ophthalmol. 2010; 149: 291–301.
22) Scott IU, Van Veldhuisen PC, Oden NL, et al; SCORE Study Investigator Group. SCORE Study report 1: baseline associations between central retinal thickness and visual acuity in patients with retinal vein occlusion. Ophthalmology. 2009; 116:504–512.

23) Ota M, Tsujikawa A, Kita M, et al. Integrity of foveal photoreceptor layer in central retinal vein occlusion. Retina. 2008; 28:1502–1508.
24) Frangieh GT, Green WR, Barraquer-Somers E, et al. Histopathologic study of nine branch retinal vein occlusions. Arch Ophthalmol. 1982; 100: 1132–1140.
25) Rogers SL, McIntosh RL, Lim L, et al. Natural history of branch retinal vein occlusion: an evidence-based systematic review. Ophthalmology. 2010; 117:1094–1101.
26) Spaide RF, Lee JK, Klancnik JK Jr, et al. Optical coherence tomography of branch retinal vein occlusion. Retina. 2003; 23:343–347.
27) Otani T, Yamaguchi Y, Kishi S. Serous macular detachment secondary to distant retinal vascular disorders. Retina. 2004; 24:758–762.
28) Murakami T, Tsujikawa A, Ohta M, et al. Photoreceptor status after resolved macular edema in branch retinal vein occlusion treated with tissue plasminogen activator. Am J Ophthalmol. 2007; 143:171–173.
29) Ota M, Tsujikawa A, Murakami T, et al. Association between integrity of foveal photoreceptor layer and visual acuity in branch retinal vein occlusion. Br J Ophthalmol. 2007; 91:1644–1649.
30) Ota M, Tsujikawa A, Murakami T, et al. Foveal photoreceptor layer in eyes with persistent cystoid macular edema associated with branch retinal vein occlusion. Am J Ophthalmol. 2008; 145:273–280.

Case 53 Central retinal vein occlusion: Progression from non-ischemic to ischemic ①

A 54-year-old male, OD, BCVA 0.3

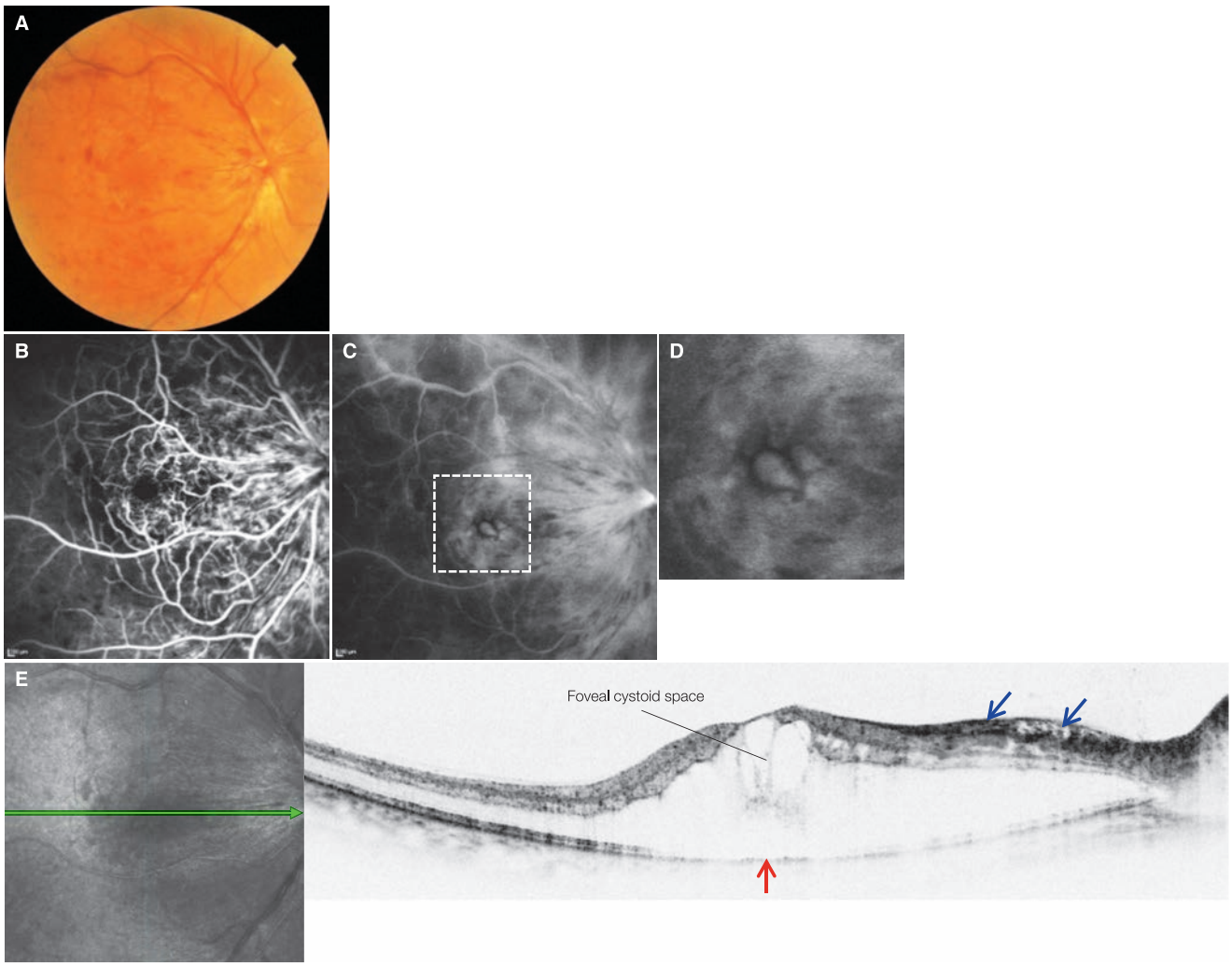

A: Color fundus photograph in the right eye: At initial diagnosis. Flame-shaped and blot retinal hemorrhages, dilation and mild tortuosity of retinal veins, optic disc edema as well as retinal whitening surrounded by soft exudates can be seen. **B:** FA in the right eye (36 sec), **C:** FA in the right eye (10 min), **D:** enlarged version of C [white dashed box]: At initial diagnosis. This is a non-ischemic CRVO where capillary nonperfusion is hardly visible. CME is present. **E:** IR + OCT horizontal scan of the right eye: At initial diagnosis. Significant CME and cone-shaped small foveal detachments (→) are noted. Significant edema (→) in the retinal nerve fiber layer corresponding to a soft exudate is seen.

Case 53 Continuation

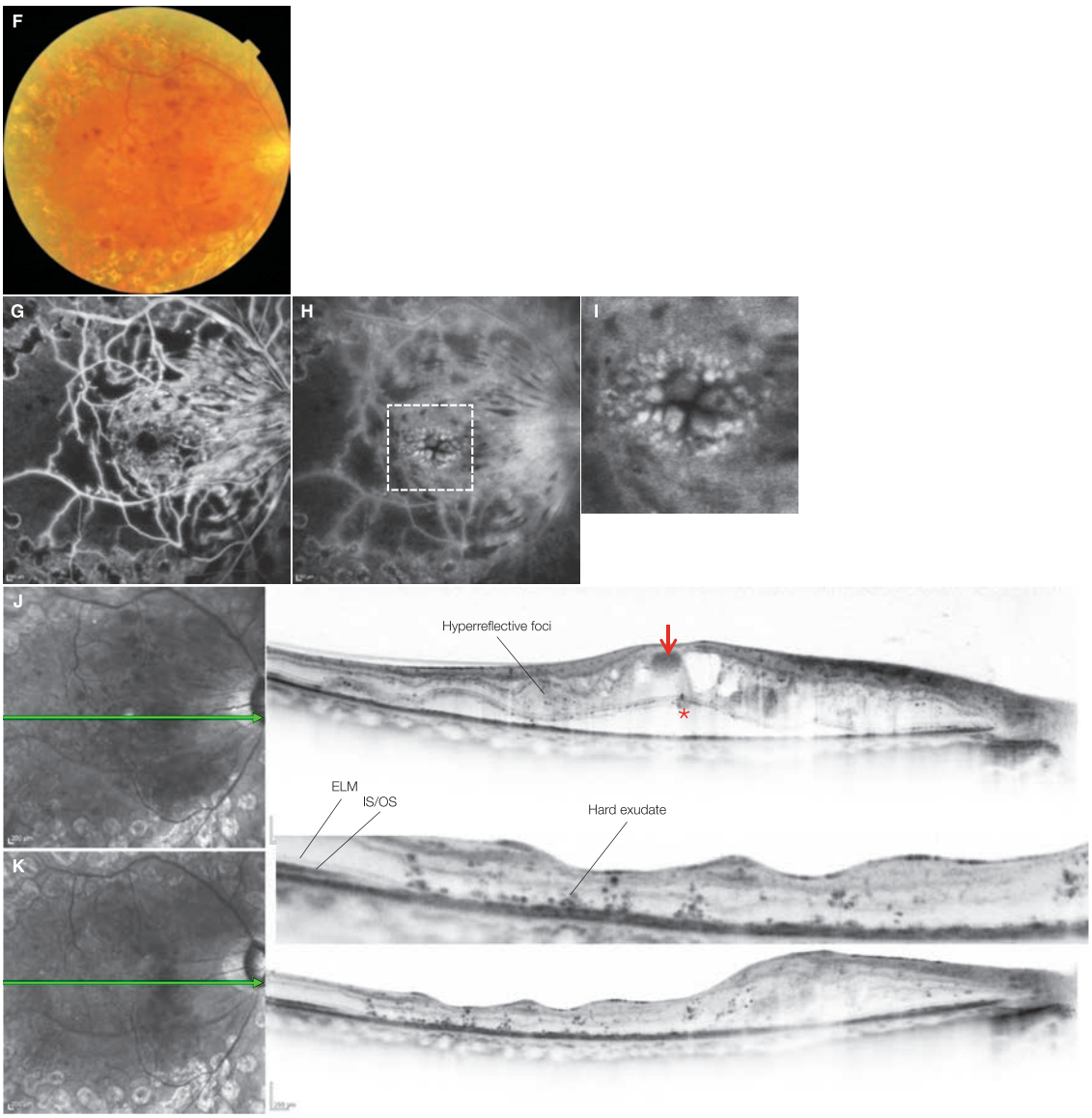

F: Color fundus photograph in the right eye: 2 months after initial diagnosis and after panretinal photocoagulation. Best-corrected visual acuity remains to be 0.3. **G:** FA in the right eye (1 min), **H:** FA in the right eye (10 min), **I:** enlarged version of H [white dashed box]: 2 months after initial diagnosis. A wide, nonperfusion area excluding the area from the macula to the optic disc is formed and thus has progressed to ischemic CRVO. The area of CME has slightly expanded. **J:** IR + OCT horizontal scan of the right eye: Same scan as E 2 months after initial diagnosis. Hemorrhages are noticeable in foveal and outer plexiform layer cystoid spaces. Hemorrhages in the foveal cystoid space are thick and cause measurement beam blocking (➔). SRD is expanding in a dome-shape fashion (*). Hyperreflective foci as described in the section on diabetic retinopathy can be seen. **K:** IR + OCT horizontal scan of the right eye: Same scan as E 6 months after initial diagnosis. Best-corrected visual acuity is 0.2. The CME and SRD have disappeared 3 months after vitreous surgery combined with ILM peeling, but there is significant thinning of the retinal inner layers and the photoreceptor layer from the fovea centralis to the temporal macula. Loss of the outer nuclear layer and IS/OS reflectivity is present throughout the macula. Note the hard exudates on the temporal macula.

Image interpretation points

This is a case of CRVO combined with diabetic retinopathy which progressed from non-ischemic to ischemic 2 months after initial diagnosis. Meanwhile, the CME remained and the SRD has changed from a cone-shaped small foveal detachment to dome-shaped SRD. Hemorrhages are accumulating in foveal cystoid space. The macular edema and SRD disappeared 6 months later and significant retinal thinning is present in the temporal macula. Thinning of the inner layers is due to the formation of a nonperfusion area, and although the cause of outer layer thinning and the loss of IS/OS reflectivity remains unclear, CME and SRD are suspected to be involved.

Case 54 Central retinal vein occlusion: Progression from non-ischemic to ischemic ②

A 65-year-old male, OS, BCVA 0.2

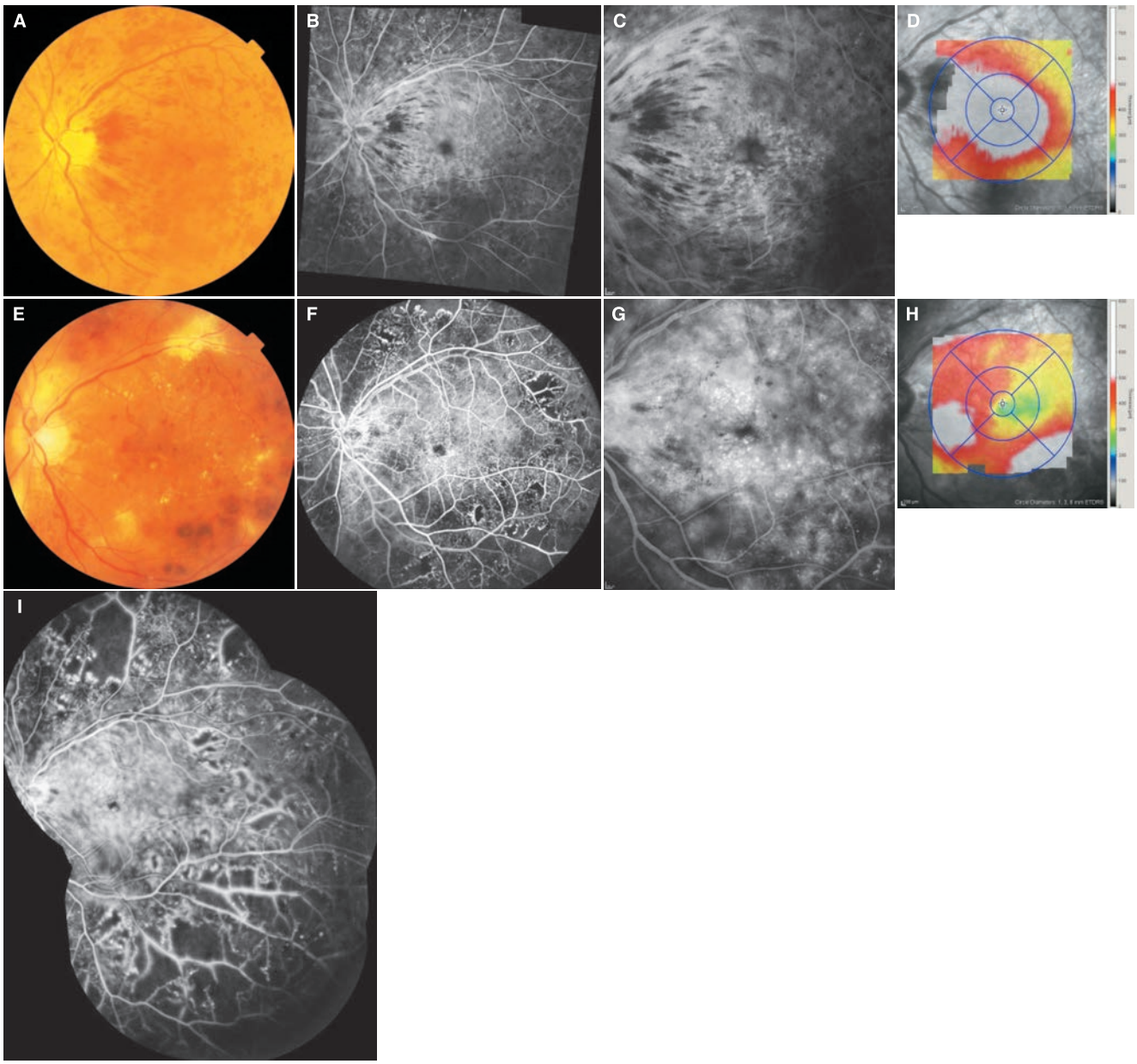

A: Color fundus photograph in the left eye: At initial diagnosis. Flame-shaped and blot retinal hemorrhages are visible. **B:** 1-minute left eye FA, **C:** FA in the left eye (5 min): At initial diagnosis. CME is exhibited. Nonperfusion is not found. **D:** Macular thickness map of the left eye: Significant thickening is observed over the entire macula. **E:** Color fundus photograph in the left eye: 20 months after initial diagnosis. Best-corrected visual acuity is 0.1. The flame-shaped retinal hemorrhages have disappeared and spotted retinal hemorrhages can be seen in the fovea centralis and outside the macula. Exudative changes are significant. **F:** FA in the left eye (1 min), **G:** FA in the left eye (10 min): 20 months after initial diagnosis. CME remains. A area of nonperfusion is observed outside the macula. **H:** Macula thickness map of the left eye: 20 months after initial diagnosis. Thickening in the centre of the macula has subsided, whereas thickening remains on the nasal side and inferotemporal side. **I:** FA montage of the left eye (75 sec): 20 months after initial diagnosis. A wide area of nonperfusion has formed outside the arcade vessels

J: Color fundus photograph in the left eye + enlarged version + OCT horizontal scan: At initial diagnosis. Typical acute phase CME images can be seen. Foveal cystoid spaces (*), inner nuclear layer small cystoid spaces, outer plexiform layer cystoid spaces, and cone-shaped foveal detachments are present. **K:** Color fundus photograph in the left eye + enlarged version + OCT horizontal scan: Same scan 7 months after initial diagnosis, and 3 months after vitreous surgery combined with ILM peeling. Best-corrected visual acuity further decreased to 0.05. Macular CME has subsided on the temporal side, but remains on the nasal side. Macular retinal hemorrhages are visible in the outer plexiform layer and beneath the fovea centralis. The IS/OS on the temporal side are disrupted. **L:** Color fundus photograph in the left eye + enlarged version + OCT horizontal scan: Same scan 20 months after initial diagnosis. The CME in the nasal macula has become less severe. Retinal hemorrhages remain beneath the fovea centralis, and foveal IS/OS reflectivity has been lost.

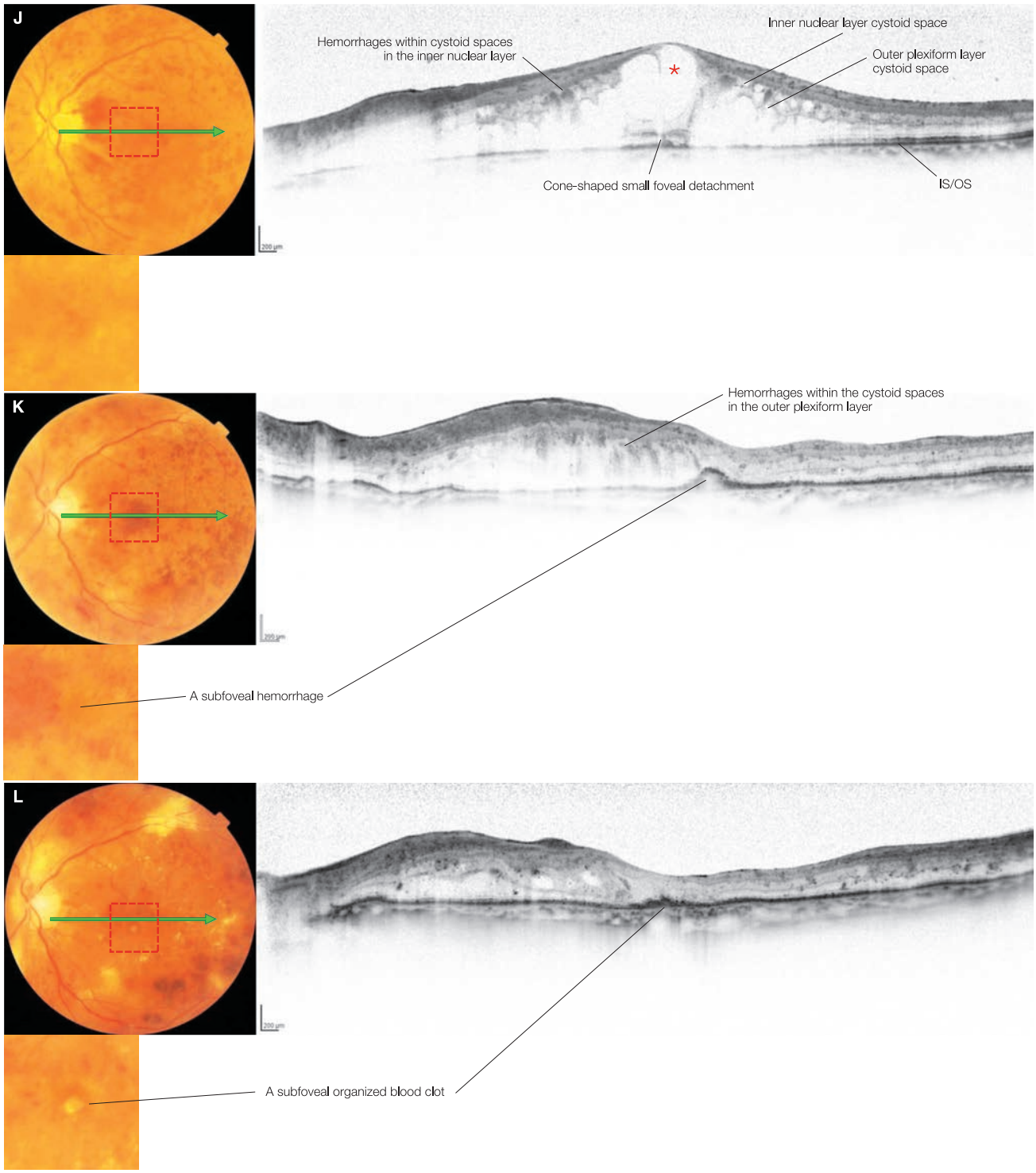

Image interpretation points

This is a case where reduced visual acuity is noted as a result of non-ischemic CME/Vitreous surgery combined with ILM peeling was performed. Flame-shaped retinal hemorrhages, which is hemorrhages in the retinal nerve fiber layer, have disappeared over time, while the deeper blot hemorrhages have worsened. Afterwards, exudative changes have progressed, and a nonperfusion area has been formed mainly outside the arcade vessels, subsequently requiring panretinal photocoagulation. Persistent retinal hemorrhages can be seen beneath the fovea centralis. Finally, visual prognosis was poor due to the breakdown of the foveal structure such as the disappearance of foveal IS/OS reflectivity, which is thought to be caused by the retinal hemorrhages beneath the fovea centralis.

Case 55 Central retinal vein occlusion: Ischemic type

A 72-year-old male, OS, BCVA 0.08

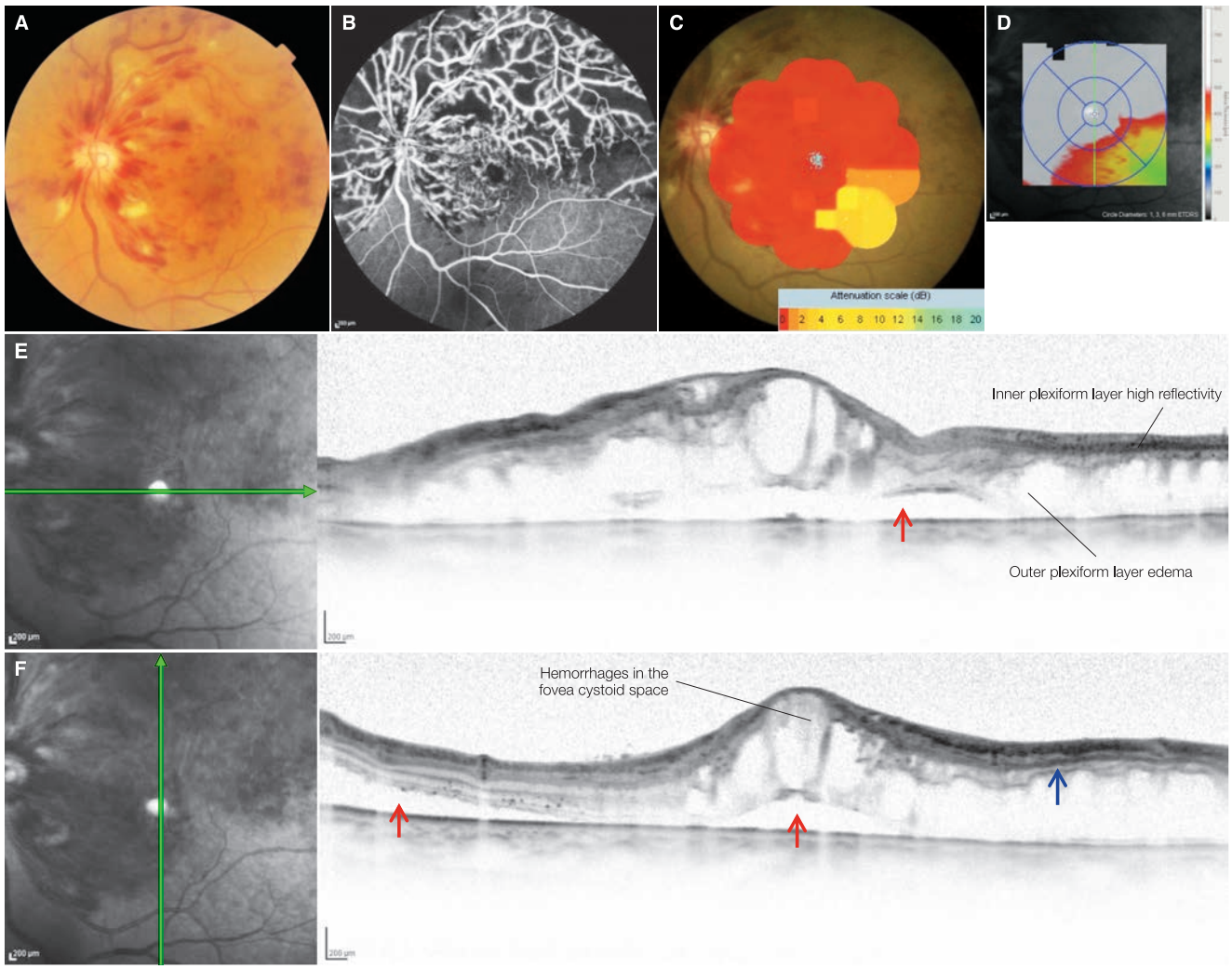

A: Color fundus photograph in the left eye: Excluding the lower area, flame-shaped and blot retinal hemorrhages and multiple soft exudates are exhibited. **B:** FA in the left eye (1 min): Including the macula, a nonperfusion area is formed circumferentially in roughly the upper 240-degree retinal area around the optic disc. **C:** Microperimetry-1 of the left eye: Excluding the lower temporal side, no retinal sensitivity can be detected in the macula. **D:** Macular thickness map of the left eye: Excluding the temporal side, the retina is thickened in the macular area. **E:** IR + OCT horizontal scan of the left eye, **F:** IR + OCT vertical scan of the left eye: There are CME and SRD (→) is extending to the lower arcade. Increased reflectivity (→) of the synapse phase of the outer plexiform layer can be seen.

Image interpretation points

At initial diagnosis, a wide area of nonperfusion spanning roughly the upper 240 degrees of the retina including the macula was seen on FA and diagnosed as ischemic CRVO. Visual acuity is poor. High reflectivity of the synapse phase of the outer plexiform layer suggests deepest capillary occlusion. Both the upper and lower first branch of the central retinal vein are dilated, and on FA, laminar flow started at approximately 23 seconds in the lower vein in FA, whereas the start of laminar flow was delayed by 7 seconds (at 30 seconds) in the upper vein. In general, hemi-CRVO is caused by occlusion of just one branch of the central retinal vein in cases where the central retinal vein divides into two branches as it exits the optic nerve. This case is an example of both branches being occluded near the branching therefore exhibiting the same findings as a CRVO, but the extent of occlusion differs and the perfusion in the lower portion of the retina is relatively preserved.

Case 56 Hemi-central retinal vein occlusion: Non-ischemic type

Right eye of a 68-year-old male with vision corrected to 0.7

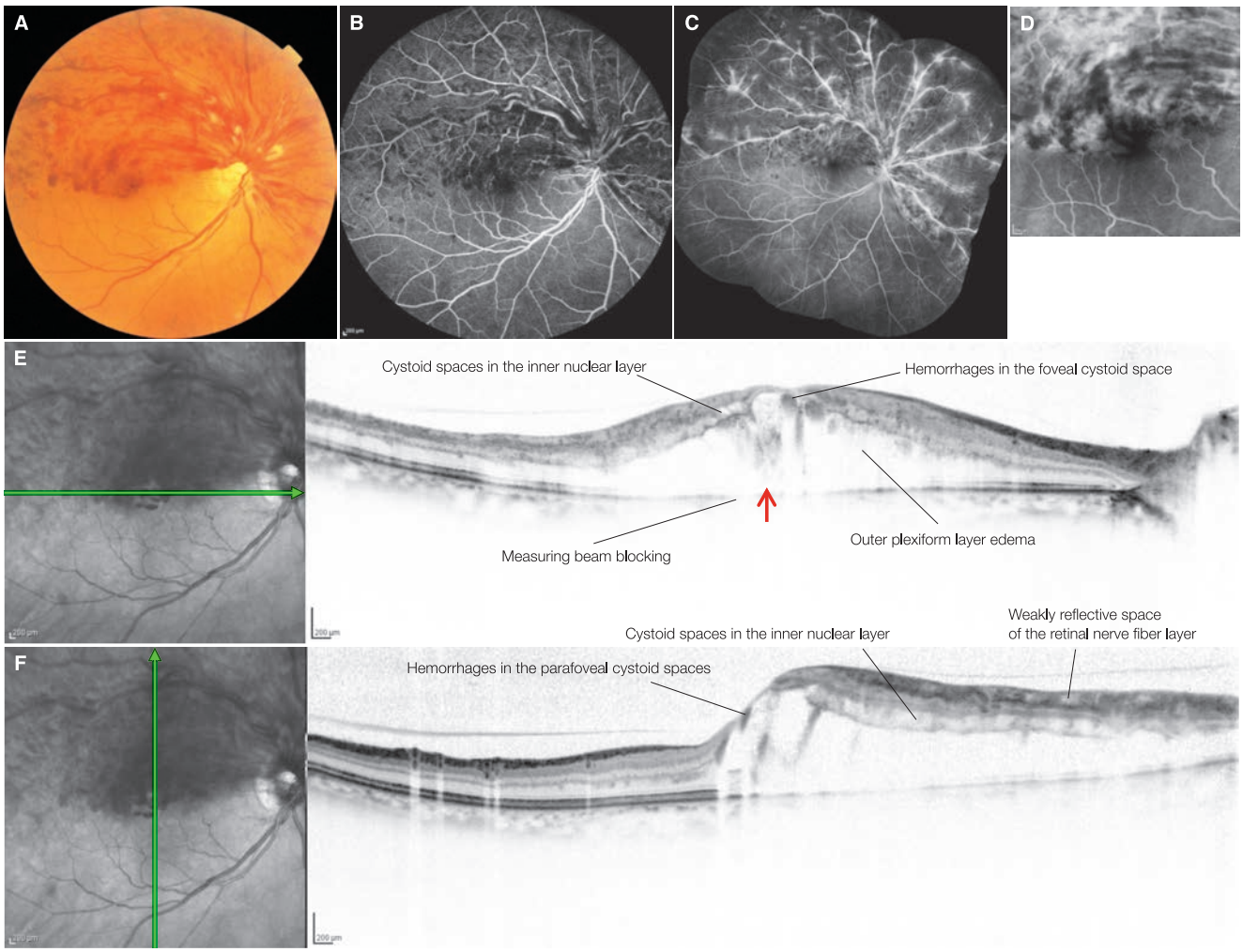

A: Color fundus photograph in the right eye: Flame-shaped and blot retinal hemorrhages and multiple soft exudates are visible in the upper half of the retina. Retinal hemorrhages can also be seen in the fovea centralis. **B:** FA in the right eye (30 sec), **C:** FA montage of the right eye (2 min), **D:** 8-minute right eye macular area FA: Dilation, tortuosity, and leakage of the retinal veins are observed. There is no areas of retinal nonperfusion. CME can be seen in the upper half of the fovea centralis. **E:** IR + OCT horizontal scan of the right eye: CME and small cone-shaped foveal detachments (→) are noted. **F:** IR + OCT vertical scan of the right eye: CME is noted. A small number of hemorrhages are noticeable in the foveal cystoid spaces. Weakly reflective spaces are visible in the retinal nerve fiber layer.

Image interpretation points

Soft exudates can be seen, suggesting that ischemia of the retinal surface layer is significant. However, an area of nonperfusion cannot be seen with FA, therefore this is a non-ischemic CRVO. OCT vertical scans are useful in the diagnosis of hemi-CRVO and understanding its pathology.

Case 57 Branch retinal vein occlusion: Significant inner retinal layer ischemia

Right eye of a 56-year-old female with vision corrected to 0.06

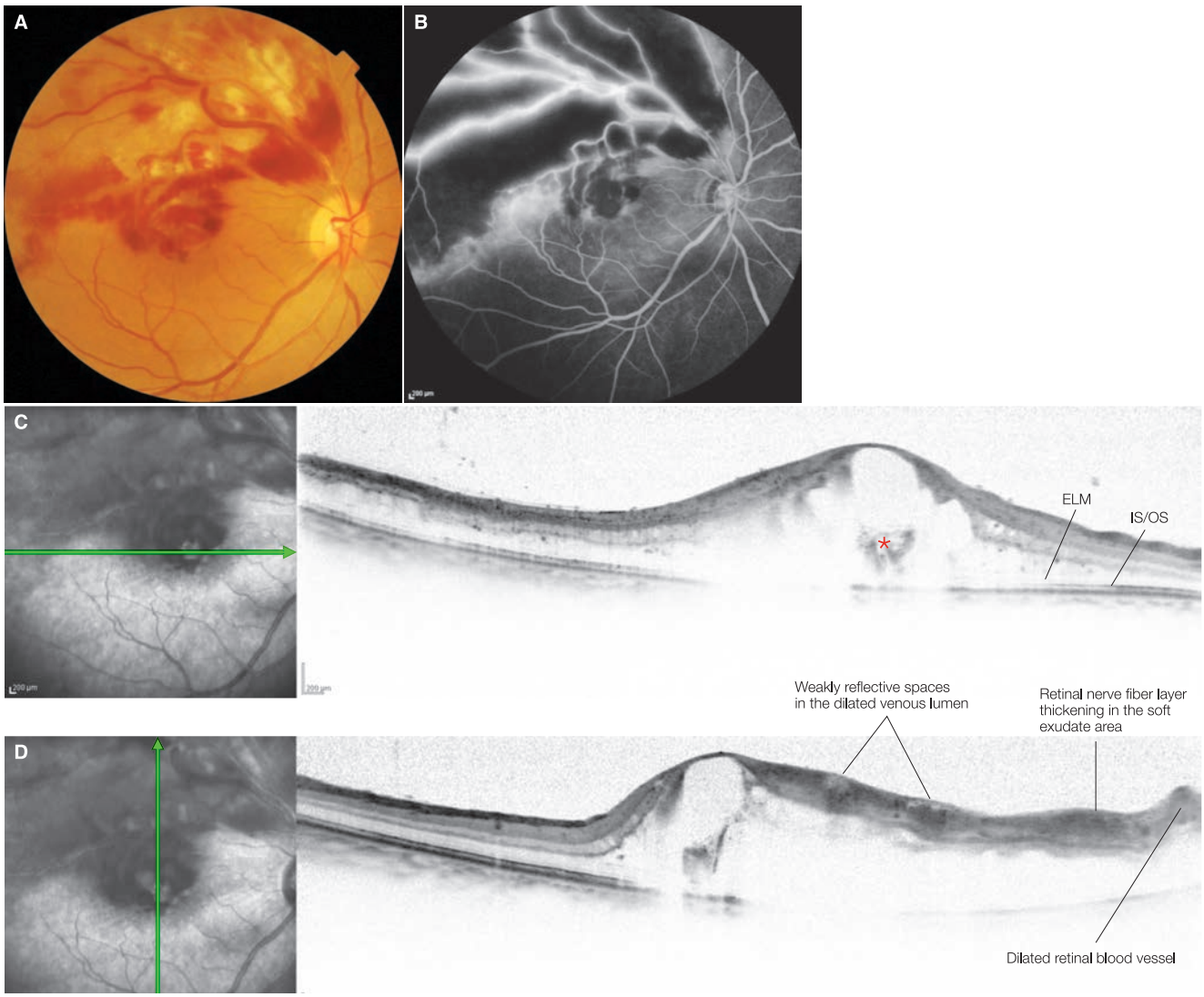

A: Color fundus photograph in the right eye: Dilation of the upper first branch of the central retinal vein and significant flame-shaped retinal hemorrhages in the circumference of the perfusion area of this branch including the fovea centralis can be seen. Retinal hemorrhages are relatively scarce and multiple soft exudates are observed in the central part of the perfusion area of the branch. **B:** FA in the right eye (1 min): Almost all arterioles, venules and capillaries are not perfused. **C:** IR + OCT horizontal scan of the right eye: Hemorrhages are visible in the foveal cystoid space (*). **D:** IR + OCT vertical scan of the right eye: The dilated venous lumen is weakly reflective and no blocking of the imaging beam resulting from blood flow are noted, suggesting a significant decrease in perfusion. The retinal nerve fiber layer edema consistent with soft exudates is is thickened in a non-cystic manner. The posterior portion of the inner layer of the retina is not only poorly defined due to the effect of blocked imaging beams resulting from the retinal hemorrhages and the increased reflectivity of the inner retinal layer.

Image interpretation points

This is a case where retinal arterioles and venules as well as retinal capillaries were acutely occluded, leading to the significant retinal ischemia. As ischemia acutely progresses, the axonal flow of ganglion cells is impaired and soft exudates form. This appears as non-cystic, localized thickening of the retinal nerve fiber layer on OCT. Weak reflectivity of the dilated and occluded vein lumen can be seen in this case, suggesting that the perfusion of the veins are significantly decreased. The significant edema would be present in the inner nuclear layer and outer plexiform layer, but are not depicted due to blocking of the imaging beams by the increased reflectivity of the inner retina.

4.2 Retinal artery occlusion

Background

Retinal artery occlusion (RAO) is a disease in which the central retinal artery or one of its major branches is occluded. Causes of this are considered to be embolus, thrombus, narrowing of blood vessels, vasospasm or decreased arterial blood flow, of which embolus is the most common cause. Many cases are due to thrombus from arteriosclerotic plaques in the carotid artery or cardiac valves. Bacteria (bacterial endocarditis), lipids, tumor (cardiac mucosal tumor) and air bubbles may also cause this disease. In young people, RAO can be associated with antiphospholipid syndrome. Patients become aware of sudden impairment to their vision and visual field. Sometimes, a sudden loss of vision (amaurosis fugax) lasting 1–2 minutes precedes RAO. This occurs frequently in those around 60 years of age, especially in men, and 3/4 of the patients over 40 years of age have abnormalities in carotid artery.

In Central retinal artery occlusion (CRAO) exhibits widespread whitening of the fundus except in the foveola, which are not supplied by retinal blood vessels. This fundus appearance is known as a cherry-red spot. Uniform retinal whitening is evident when occlusion is complete, and in cases of incomplete occlusion, mottled whitening is found to various extents. When the cilioretinal artery is spared, the retina escapes whitening in a limited area between the optic disc and fovea therefore preserving vision to a certain extent.

If occlusion is formed more distal to the branching of the central retinal artery or in the arteriolar level, acute ischemic retinopathy is localized. This presents as BRVO and vision is relatively preserved. In BRAO either the upper or lower temporal retina demonstrates retinal whitening.

OCT findings

Increased reflectivity of the inner retinal layers and mild to moderate retinal thickening consistent with retinal whitening can be seen in the acute stage.[1–4] This is due to intracellular swelling and cytolysis.[5] The retina may recover if the ischemia due to arterial occlusion resolves within 100 minutes, but if time exceeds this limit, cells undergo necrosis and lead to irreversible damage.[6]

When an acute RAO is observed with OCT, the increased reflectivity resulting from retinal arterial occlusion can be seen from the retinal nerve fiber layer to the outer plexiform layer. Reflectivity from the outer nuclear layer to the photoreceptor inner and outer segments declines due to blocking of measurement beams by the highly reflective inner layers. However, little damages to these outer layers occur in RVO. If retinal artery obstruction is incomplete, an increase in reflectivity occurs in the limited retinal layers, such as retinal nerve fiber layer-ganglion cell layer and inner nuclear layer-outer plexiform layer, or is limited to columnar regions of the ganglion cell layer or inner nuclear layer. In BRAO and CRAO with the cilioretinal artery spared, no high reflectivity is found outside the area of nonperfusion. In 3–4 weeks, selective thinning of the inner retinal layers occurs diffusely and progresses further over the course of several months. Retinal thickness becomes roughly 60% of that prior to onset, but foveal thickness remains unchanged leading to loss of the foveal depression.[3, 4, 7, 8] The structure of the inner layers is preserved in the area where perfusion remained intact.

References

1) Ozdemir H, Karacorlu S, Karacorlu M. Optical coherence tomography findings in central retinal artery occlusion. Retina. 2006; 26:110–112
2) Karacorlu M, Ozdemir H, Arf Karacorlu S. Optical coherence tomography findings in branch retinal artery occlusion. Eur J Ophthalmol. 2006; 16: 352–353.
3) Ikeda F, Kishi S. Inner neural retina loss in central retinal artery occlusion. Jpn J Ophthalmol. 2010; 54:423–429.
4) Ritter M, Sacu S, Deák GG, et al. In vivo identification of alteration of inner neurosensory layers in branch retinal artery occlusion. Br J Ophthalmol. 2012 ; 96 : 201–207.
5) Kroll AJ. Experimental central retinal artery occlusion. Arch Ophthalmol. 1968; 79:453–469
6) Hayreh SS, Kolder HE, Weingeist TA. Central retinal artery occlusion and retinal tolerance time. Ophthalmology. 1980; 87:75–78.
7) Leung CK, Tham CC, Mohammed S, et al. In vivo measurements of macular and nerve fibre layer thickness in retinal arterial occlusion. Eye (Lond). 2007; 21:1464–1468.
8) Takahashi H, Iijima H. Sectoral thinning of the retina after branch retinal artery occlusion. Jpn J Ophthalmol. 2009; 53:494–500.

Case 58 Central retinal artery occlusion: A typical example

A 69-year-old male, OS, BCVA hand motion

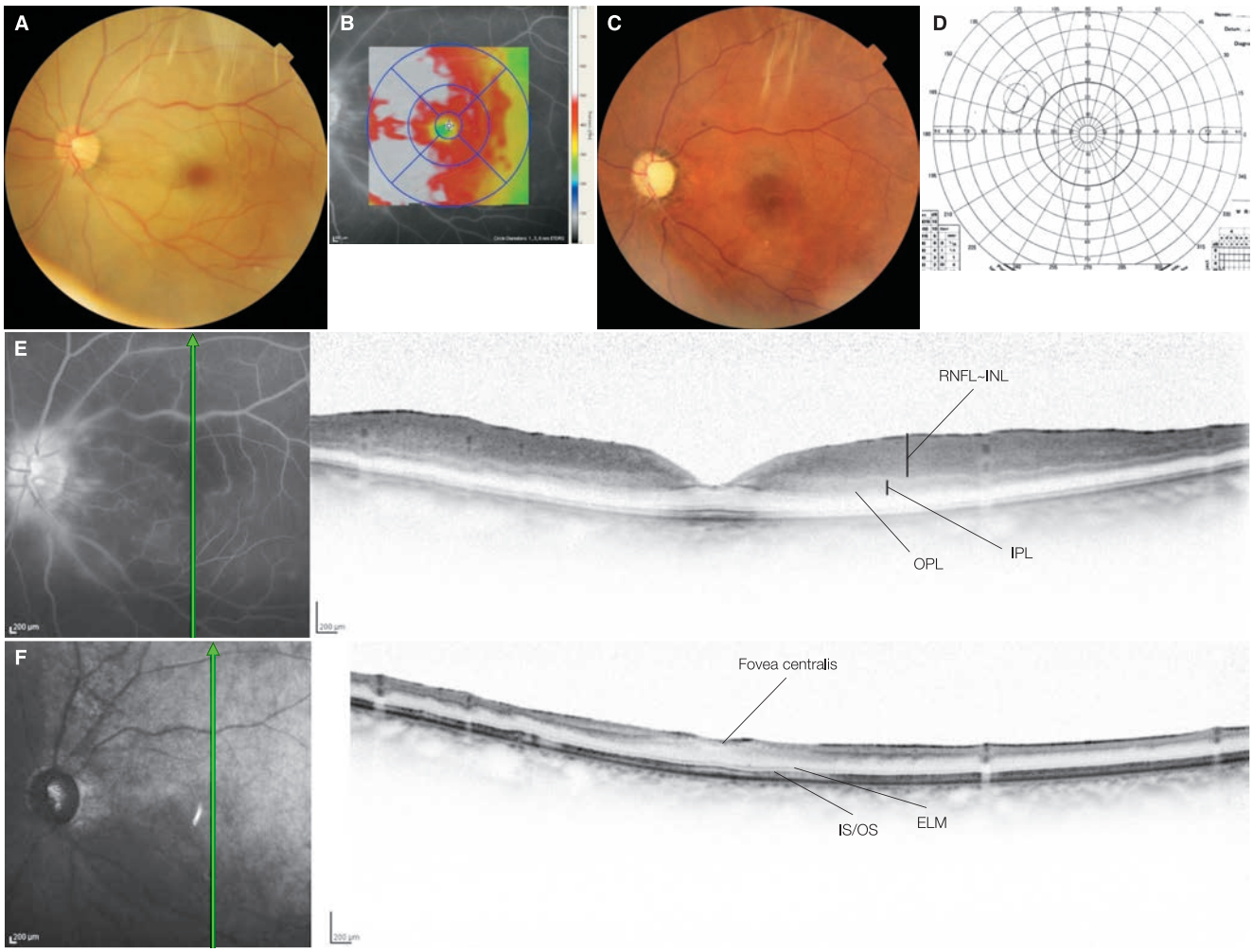

A: Color fundus photograph in the left eye: At initial diagnosis. Retinal whitening of the entire posterior pole with a cherry-red spot is seen. **B:** Macular thickness map of the left eye: Significant thickening exceeding 500 µm can be seen particularly on the nasal macula. **C:** Color fundus photograph in the left eye: 2 months after initial diagnosis. Best-corrected visual acuity is hand motion. Retinal whitening has disappeared and sheathing of the retinal arteries is observed. The optic disc is atrophic and pale.
D: Goldmann visual field of the left eye: 2 months after initial diagnosis. A small island of visual field remains in the temporal periphery. **E:** IR + OCT vertical scan of the left eye: At initial diagnosis. There is markedly increased reflectivity and thickening seen from the retinal nerve fiber layer to the inner plexiform layer of the entire posterior pole, and layer boundaries are blurring. There is decreased reflectivity of the photoreceptor IS/OS and RPE except in the fovea centralisdue to blocking of OCT measurement beam. **F:** IR + OCT vertical scan of the left eye: 2 months after initial diagnosis. The inner retinal layers of the posterior pole are diffusely diminished, and the foveal depression has mostly disappeared. In comparison, the thickness of the outer nuclear layer and photoreceptor inner and outer segments remain unchanged, and the IS/OS and ELM lines are preserved.

Image interpretation points

This is a typical example of CRAO where retinal whitening with a cherry-red spot can be seen. There is significant increase in reflectivity from the retinal nerve fiber layer to the inner plexiform layer, and the inner nuclear layer remains relatively hyporeflective. Two months after initial diagnosis, there is significant thinning of the inner retinal layer. Even 4 months after initial diagnosis, visual acuity is not improved with hand motion and the visual field is lost except for a small island of remaining in the temporal periphery.

Case 59 Central retinal artery occlusion: Cilioretinal artery not occluded

A 73-year-old femaleOD, BCVA 0.6

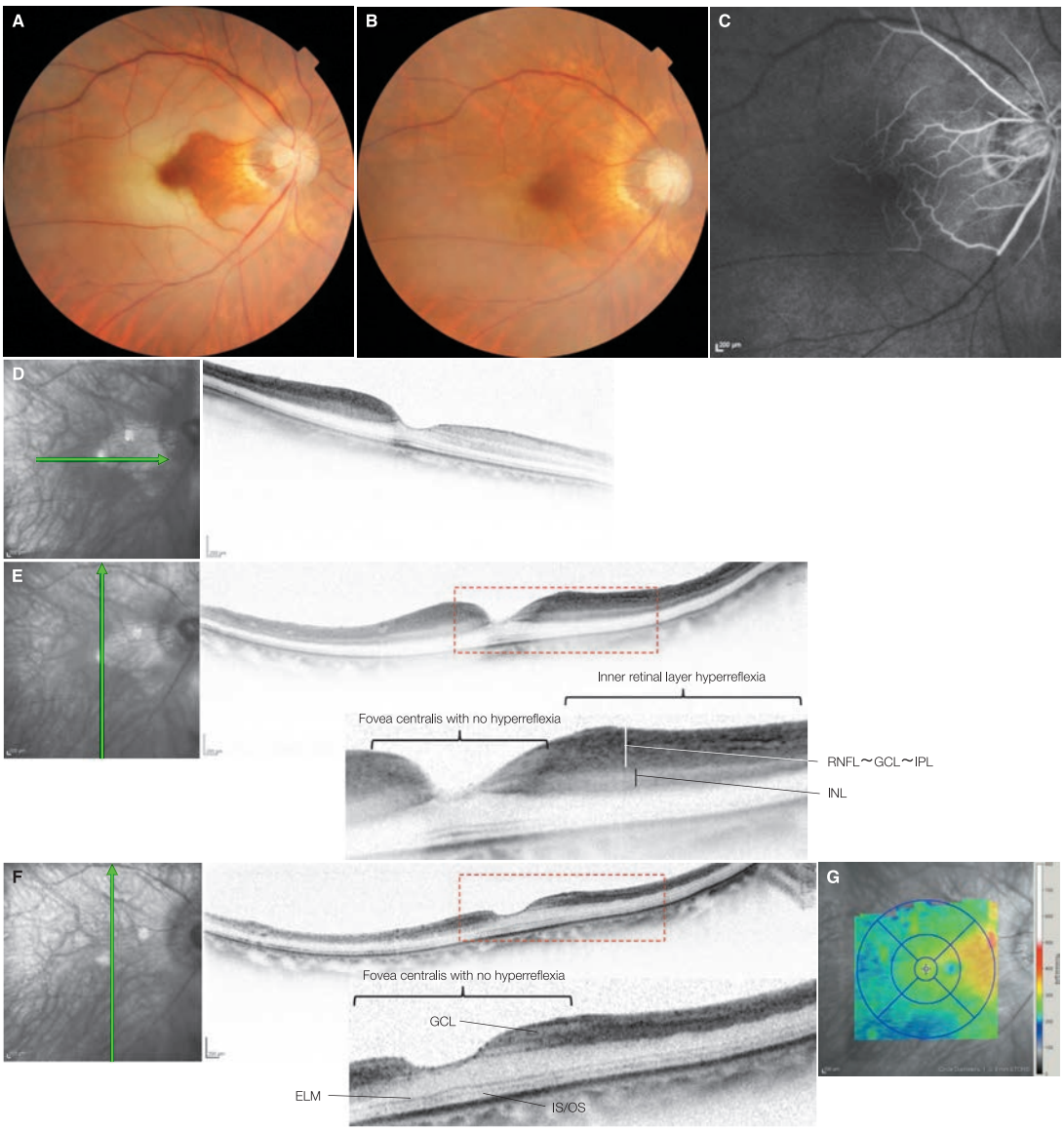

A: Color fundus photograph in the left eye: During initial diagnosis. Retinal whitening can be seen except in the area perfused by the cilioretinal artery. **B:** Color fundus photograph in the right eye: 3 weeks after initial diagnosis. Best-corrected visual acuity has decreased to 0.2. Retinal whitening has subsided. **C:** FA in the right eye (26 sec): The filling of the fluorescein dye is only visible in the area perfused by the cilioretinal artery with retrograde filling of proximal veins and arteries via the optic disc collateral circulation. **D:** IR + OCT horizontal scan of the right eye, **E:** IR + OCT vertical scan of the right eye [red dashed box]: At initial diagnosis. Hyperreflectivity and thickening of the inner retinal layers are observed except in the nasal macula, and layer boundaries are blurring. Only the layers in the fovea centralis where there is less increase in reflectivity can be clearly distinguished. **F:** IR + OCT vertical scan of the right eye + enlarged version [red dashed box]: 3 weeks after initial diagnosis. Best-corrected visual acuity has reduced to 0.2. The inner layers of the retina are diminished, but remains highly reflective. The inner layers of the fovea centralis is also thinned, but can be clearly distinguished because there is little increase in reflectivity. **G:** Retinal thickness map of the right eye: Significant decrease in the macular thickness is noted.

Image interpretation points

When the cilioretinal artery remains perfused, the retina avoids whitening in a very limited area sandwiched between the optic disc and macula. On OCT, excluding the nasal side and fovea centralis, retinal inner layer hyperreflectivity and thickening is observed in the macula. The retinal inner layers have rapidly atrophied in 3 weeks, but the hyperreflectivity persists. The structure of the retinal layers is clearly visible in the fovea centralis. Whitening with sparing of the fovea centralis can be seen in approximately 2/3 of cases and as in this case, final visual acuity recovered to 0.2.

Case 60 Central retinal artery occlusion: Incomplete occlusion

A 63-year-old male, OS, BAVA finger count

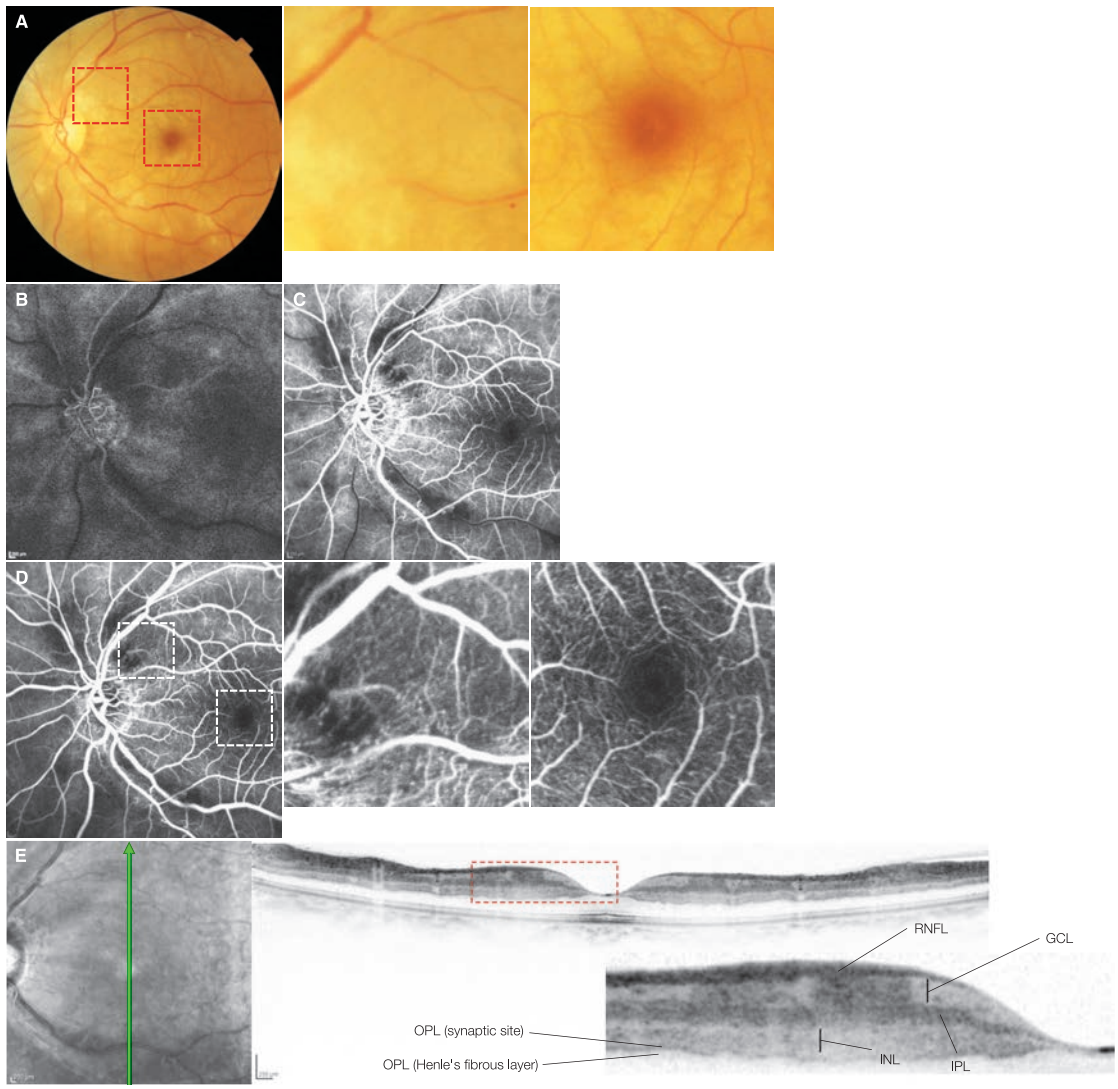

A: Color fundus photograph in the left eye + enlarged version [red dashed box]: Retinal whitening and a cherry-red spot are visible over the entire posterior pole. Soft exudates-like lesions are formed along the arcade vessels, and the whitening in the macular area is irregular with less whitening around the arterioles. **B:** FA in the left eye (21 sec): Retinal arterial filling is delayed by several seconds. The filling of choroidal circulation is already beginning. **C:** FA in the left eye (29 sec): Venous laminar flow extends close to the optic disc. **D:** FA in the left eye (66 sec) + enlarged version [white dashed box]: Note the retinal capillary filling in the macular area. Nonperfusion and narrowing of the arterioles around the arcade vessels can be seen. **E:** IR + OCT vertical scan of the left eye + enlarged version [red dashed box]: Significant increase in reflectivity of the ganglion cell layer, inner nuclear layer and inner and outer plexiform layer is observed. In particular, hyperreflectivity can be seen in a columnar pattern within the ganglion cell layer. The outer plexiform layer demonstrates undulations.

Image interpretation points

In normal eyes, central retinal artery begins to fluoresce approximately in 10 to 15 second after dye injection (1 to 3 seconds after choroidal flush). This case was delayed to 21 seconds in retinal artery filling. Eight seconds later, the laminar flow reached the vein near the optic disc, and thus the retinal circulation time (normally ranging 6.3–13 seconds) was normal. Based on these findings, this case likely demonstrates incomplete occlusion of the central retinal artery. Retinal whitening and a cherry-red spots can be seen over the entire posterior pole, but the macula remains perfused and has avoided retinal whitening in the area around the arterioles. Soft exudate-like lesions are present along the arcade vessels, and nonperfusion and narrowing of the arterioles are noted. On OCT images, increased reflectivity in a columnar pattern is evident in the ganglion cell layer. Irregularities of the hyperreflectivity indicating inner retinal ischemia suggest regional differences in the amount of ischemia corresponding to irregularities in retinal whitening. In this case, best-corrected visual acuity has improved to 0.04 6 months after initial diagnosis.

Case 61 Branch retinal artery occlusion: Case of good visual acuity

A 58-year-old female, OD, BCVA 1.5

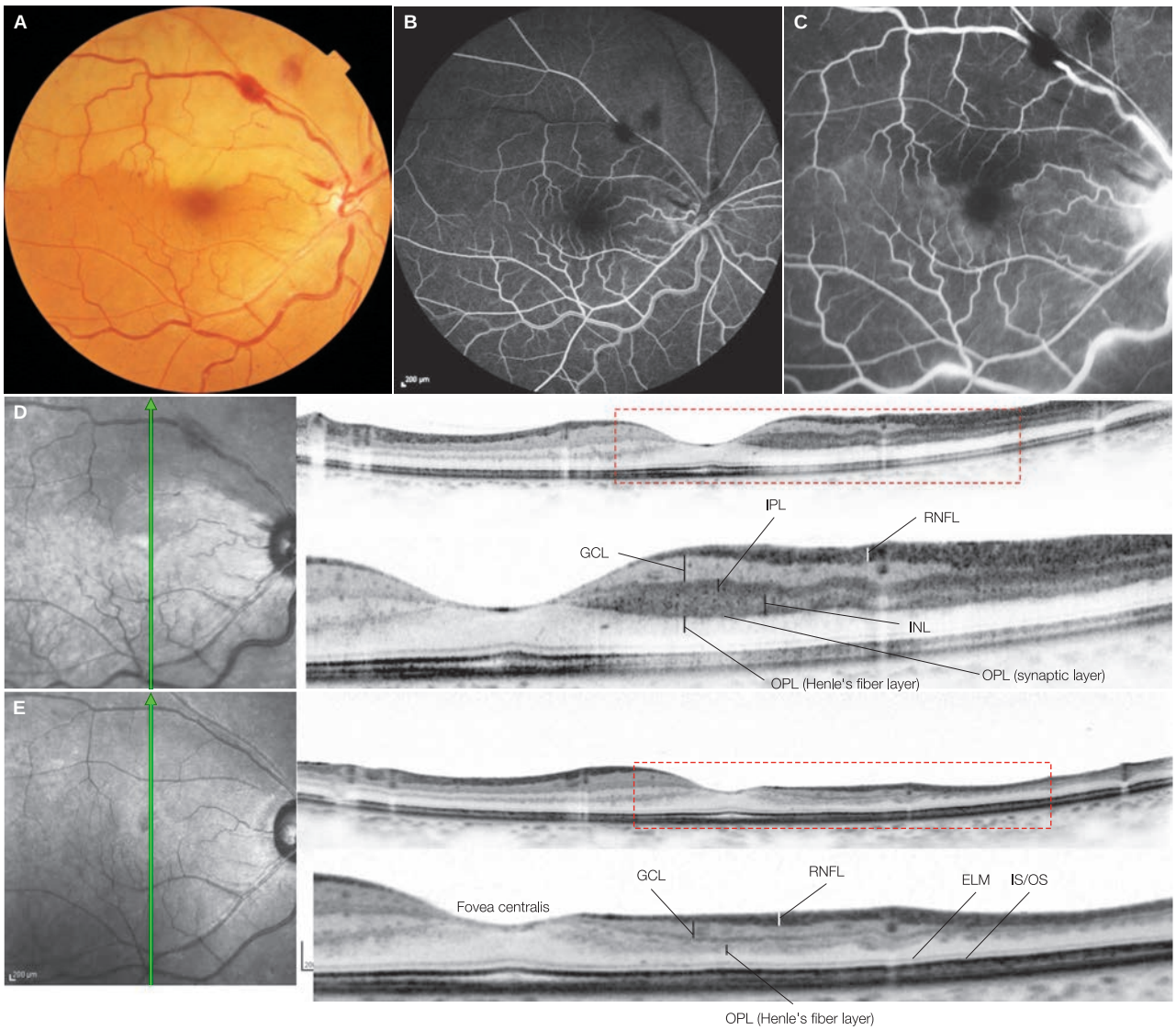

A: Color fundus photograph in the right eye: At initial diagnosis. Whitening can be seen in the upper half of the retina. Dilation and tortuosity of the upper and lower veins are seen along with accompanying retinal hemorrhages in the upper retina. **B:** FA in the right eye (28 sec): There was no difference in the arterial filling time between the upper and lower retina, but filling of the upper vein is delayed; there is no filling in the upper veins whereas the laminar flow is seen in the lower veins. **C:** FA in the right eye (5 min): The artery in the upper retina is narrowed. **D:** IR + OCT vertical scan of the right eye + enlarged version [red dashed box]: As is clear when comparing the upper and lower retina, significantly increased reflectivity can be observed in the inner plexiform layer, inner nuclear layer and outer plexiform layer, but not in the ganglion cell layer. There is little retinal thickening. **E:** IR + OCT vertical scan of the right eye + enlarged version [red dashed box]: 2 years after initial diagnosis. Best-corrected visual acuity remains to be 1.5. The inner layers of the area of occlusion are severely diminished, but the considerable amount of the retinal nerve fiber layer and ganglion cell layer remains. The foveal structure and outer layers in the area of occlusion appear almost preserved.

Image interpretation points

This is a BRVO case where one major branch of the central retinal artery was occluded immediately distal to the branching. Along with the whitening of the retina, this case demonstrates dilation and tortuosity of the upper and lower retinal veins as well as retinal hemorrhages. Thus, impending CRVO appears to have concurred with BRAO. On OCT, the reflectivity of the inner plexiform layer, inner nuclear layer and outer plexiform layer is significantly enhanced. This hyperreflectivity on OCT and retinal whitening reflect the same pathological condition. Visual prognosis is much better central retinal artery occlusion. This is because the fovea and lower retina are almost intact.

Case 62 Branch retinal artery occlusion: Incomplete occlusion

A 59-year-old male, OD, BCVA 1.5

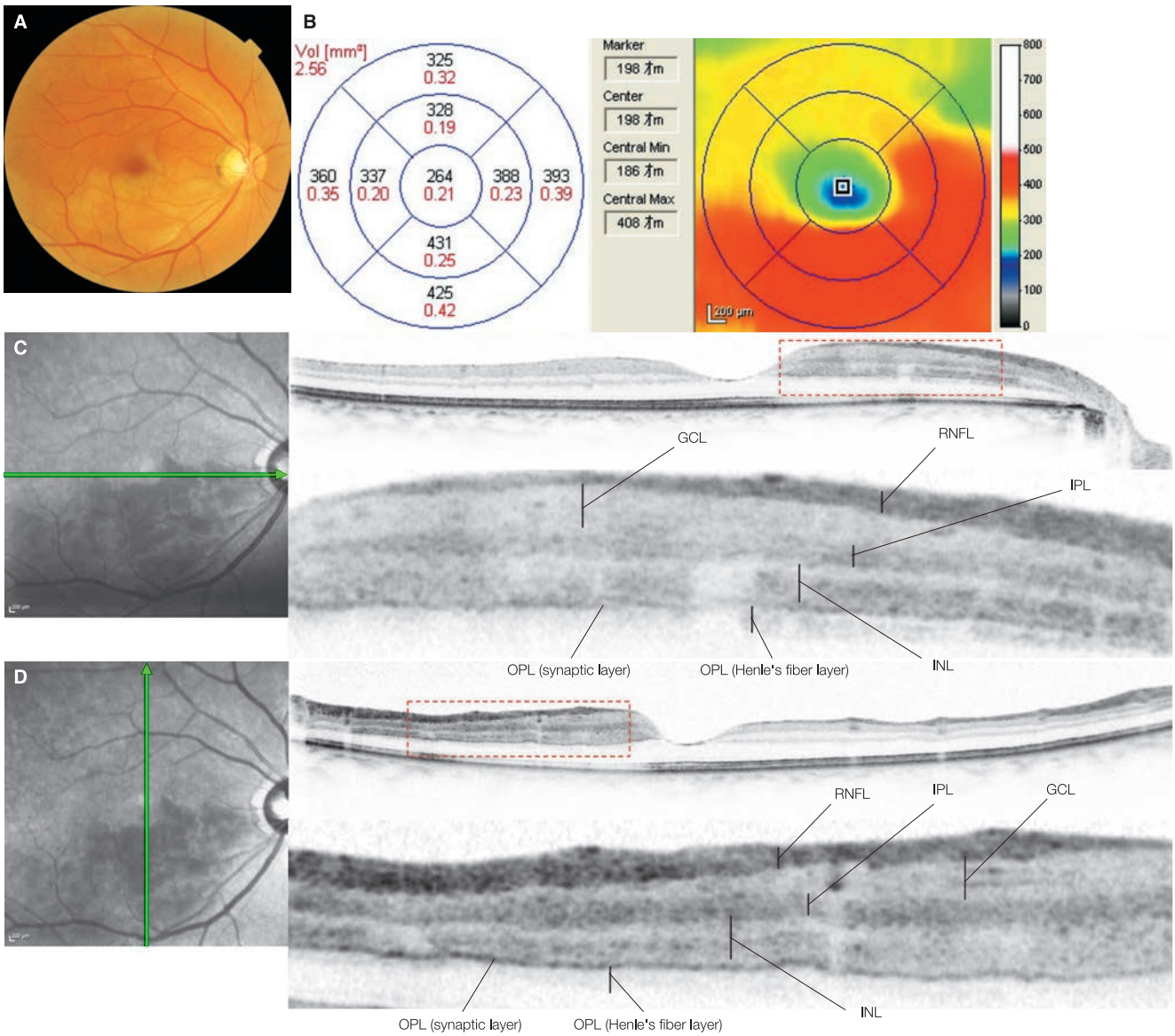

A: Color fundus photograph in the right eye: At initial diagnosis. Retinal whitening can be seen in the lower posterior pole. **B:** Macular thickness map of the right eye: Moderate thickening is noted in the inferior macula. **C:** IR + OCT horizontal scan of the right eye + enlarged version [red dashed box], **D:** IR + OCT vertical scan of the right eye + enlarged version [red dashed box]: Enhanced reflectivity is mainly seen from the inner plexiform layer to the outer plexiform layer in a columnar pattern. Outer half part of the inner nuclear layer is exhibiting high reflectivity. In addition, the reflectivity in each layer is increased in a columnar pattern. The IS/OS and RPE reflectivity in the posterior portion of the highly reflective area is decreased due to blocking of OCT measurement beam.

Image interpretation points

This is a lower BRAO. The increase in reflectivity was limited to partial both along the depth and lateral direction, indicating incomplete occlusion along the depth and lateral direction. The increase in the reflectivity of the inner nuclear layer was limited its deeper half portion, suggesting that the occlusion took place primarily in the retinal capillary bed along the external margin of the inner nuclear layer. Based on these findings, it is possible that ischemia as a result of the disruption of blood flow in the capillary network of the inner nuclear layer in the outer margin is significant, whereas ischemia in the capillary network region of the inner nuclear layer is not as significant. Highly reflective cylindrical areas can be seen in each layer, and significant »speckled« areas of ischemia may exist.

4.3 Idiopathic juxtafoveal macular telangiectasia

Classification

Idiopathic juxtafoveal macular telangiectasia (MacTel), which was originally described by Gass as idiopathic juxtafoveolar retinal telangiectasia (IJRT), is a syndrome characterized by the non-diabetic dilation of parafoveal capillaries and subsequent development of macular lesions that cause a slow decline in visual acuity.[1] According to Gass and Blodi,[2] IJRT can be divided into 3 groups based on fundus photograph and FA findings (Group 1–3), and each group can be further subdivided. Their initial classification encompassed specific disease types, but Yannuzzi et al.[3] excluded these specific disease types and created a more practical system by simplifying the classification. In the Yannuzzi classification, after the extremely rare Group 3 (occlusive telangiectasia) is excluded, the disease is classified into Type 1 (aneurysmal telangiectasia) and Type 2 (perifoveolar telangiectasia) as shown in ◘ Table 4-1. Type 2, which was previously divided into 5 stages, is subclassified into just nonproliferative and proliferative. Currently, the Yannuzzi classification is commonly used, and Gass and Blodi's stage classification is used for the subclassification of Type 2.

Pathology

Yannuzzi classification Type 1 and Type 2 can be considered different diseases. Type 1 is common in men and is unilateral. Exudative lesions due to telangiectasis of the temporal side of the parafovea are a characteristic. Telangiectasis, capillary aneurysms, cystoid macular edema (CME) and circinate hard exudate are found, and on FA fluorescent leakage can be seen mainly on the temporal macula. When observed with OCT in the majority of cases, the macula is thickened due to CME, which is sometimes accompanied by foveal detachment. These findings are similar to diabetic macular edema, so differentiation is necessary. Type 1 develops in adults and is thought to be a congenital capillary abnormality confined to the parafoveal area, and in a sense, it is considered a subtype of Coats' disease.

Yannuzzi classification Type 2 has no gender difference and is bilateral. MacTel Type 2 has few exudative lesions, and telangiectasis and fluorescent leakage without retinal thickening. No exudative lesions such as MAs, CME, or hard exudates are visible. In Type 2, singular findings are observed on the temporal side of the parafovea from an early stage. A decrease in retinal transparency, telangiectasis and fluorescein leakage on FA, enhancement of macular autofluorescence, enhanced confocal blue reflectance on red-free imaging, and a decrease in macular pigment can also be seen. The area of enhanced confocal blue reflectance and decreased macular pigment are almost identical in area; and wider than the area of fluorescein leakage and enhanced autofluorescence.[4] Green et al. showed small, extracellular fluid pooling localized in the inner layer of the retina on light microscopic images of one eye diagnosed as Type 2.[5] Yannuzzi et al. also observed thickening of the macular retina on OCT.[3] However in practice, retinal thickening is not evident in the majority of Type 2 cases on OCT.[6–10] Instead, a foveal defect covered by the ILM on the anterior border described by Yannuzzi et al. as an inner lamella cyst is a characteristic feature.[3] Type 2 differs from Type 1 in that the main form of the disease is degeneration and atrophy of the fovea centralis. Gass thought the telangiectasis and resulting decline of metabolic function in Group 2A make the cells in the inner retinal layers, in particular Müller cells, be exposed to chronic nutritional deprivation leading to the degeneration of these cells and the connecting photoreceptor cells.[11] It was recently demonstrated that 3 types of Müller cell markers were negative in the foveal site where macular pigment was not detected in immunohistochemistry of a Type 2 autopsied eye, which supports Gass' hypothesis.[12]

◘ **Table 4-1** The Gass classification and the Yannuzzi classification

IJRT (Gass-Blodi)	IMT (Yannuzzi)
Group 1A: visible and exudative IJRT	Type 1 (aneurysmal telangiectasia)
Group 1B: visible, exudative and focal IJRT	
Group 2A	Type 2 (perifoveal telangiectasia)
Stage 1: occult telangiectatic vessels	
Stage 2: loss of transparency without clinically evident telangiectatic vessels	
Stage 3: prominent dilated right-angle retinal venules	
Stage 4: retinal pigment hyperplasia into the retina	
Stage 5: SRN from proliferation of intraretinal capillaries	
Group 2B: juvenile occult familial IJRT	
Group 3A: occlusive IJRT	
Group 3B: occlusive IJRT with CNS vasculopathy	

CNS = central nervous system, IJRT = idiopathic juxtafoveolar retinal telangiectasia, IMT = idiopathic macular telangiectasia, SRN = subretinal neovascularization
(Created with reference to Yannuzzi LA, et al. Idiopathic macular telangiectasia. Arch Ophthalmol. 2006; 124: 450–460)

OCT findings

The characteristic OCT findings in Type 1 is CME mainly around the temporal side of the parafovea. Cystoid spaces can be typically seen in the fovea centralis, parafovea, inner nuclear layer, and outer plexiform layer, and the retina is significantly thickened. Sometimes a foveal detachment may occur. Foveal cystoid spaces fuse with surrounding cystoid spaces to become larger as the disease progresses. In addition, dilated capillaries are seen as highly reflective dots located in lines between the retinal nerve fiber layer and external margin of the inner nuclear layer. Capillary microaneurysms are also visible.

Characteristic Type 2 OCT findings include a lack of significant retinal thickening, and defective changes like cystoid cystic degeneration, known as an inner lamellar cyst, seen in the fovea centralis or the temporal side of the parafovea.[3] The defective changes appears to start in the inner retina because an early inner lamellar cyst is bordered anteriorly by the internal limiting membrane.[3] Cystoid spaces extend to the outer layers of the retina and cause photoreceptor layer defects as the disease progresses. However, IS/OS line irregularities can be observed from an early stage. Dilated capillaries are not so evident as in Type 2.

Cystoid spaces are formed in both Type 1 and Type 2, but their pathologies are completely different. The cystoid space formation in Type 1 is basically identical with the CME in diebetic macular edema and RVO, which is caused by retinal vascular leakage and results in evident macular thickening. In Type 2, the cystoid spaces are associated with minimal exudative changes, such as weak fluorescein leakage and slight retinal thickening if any, which can be interpreted as cystoid degeneration as a result of the loss of the retinal cells.[6–10]

References

1) Gass JD. A fluorescein angiographic study of macular dysfunction secondary to retinal vascular disease. V. Retinal telangiectasis. Arch Ophthalmol. 1968; 80:592–605
2) Gass JD, Blodi BA. Idiopathic juxtafoveolar retinal telangiectasis. Update of classification and follow-up study. Ophthalmology. 1993; 100:1536–1546.
3) Yannuzzi LA, Bardal AM, Freund KB, et al. Idiopathic macular telangiectasia. Arch Ophthalmol. 2006; 124:450–460.
4) Charbel Issa P, Berendschot TT, Staurenghi G, et al. Confocal blue reflectance imaging in type 2 idiopathic macular telangiectasia. Invest Ophthalmol Vis Sci. 2008; 49:1172–1177.
5) Green WR, Quigley HA, De la Cruz Z, et al. Parafoveal retinal telangiectasis. Light and electron microscopy studies. Trans Ophthalmol Soc U K. 1980; 100:162–170.
6) Gaudric A, Ducos de Lahitte G, Cohen SY, et al. Optical coherence tomography in group 2A idiopathic juxtafoveolar retinal telangiectasis. Arch Ophthalmol. 2006; 124:1410–1419.
7) Albini TA, Benz MS, Coffee RE, et al. Optical coherence tomography of idiopathic juxtafoveolar telangiectasia. Ophthalmic Surg Lasers Imaging. 2006; 37:120–128.
8) Surguch V, Gamulescu MA, Gabel VP. Optical coherence tomography findings in idiopathic juxtafoveal retinal telangiectasis. Graefes Arch Clin Exp Ophthalmol. 2007; 245:783–788
9) Paunescu LA, Ko TH, Duker JS, et al. Idiopathic juxtafoveal retinal telangiectasis: new findings by ultrahigh-resolution optical coherence tomography. Ophthalmology. 2006 ; 113:48–57.
10) Cohen SM, Cohen ML, El-Jabali F, et al. Optical coherence tomography findings in nonproliferative group 2a idiopathic juxtafoveal retinal telangiectasis. Retina. 2007; 27:59–66.
11) Gass JDM. Retinal capillary diseases. In: Stereoscopic Atlas of Macular Diseases: Diagnosis and Treatment. 4th ed. Vol 1 CV. Mosby, St. Louis, 1997. pp 506–511.
12) Powner MB, Gillies MC, Tretiach M, et al. Perifoveal Müller cell depletion in a case of macular telangiectasia type 2. Ophthalmology. 2010; 117:2407–2416.

Case 63 Macular telangiectasia: Yannuzzi classification Type 1

A 54-year-old male, OS, BCVA 0.9

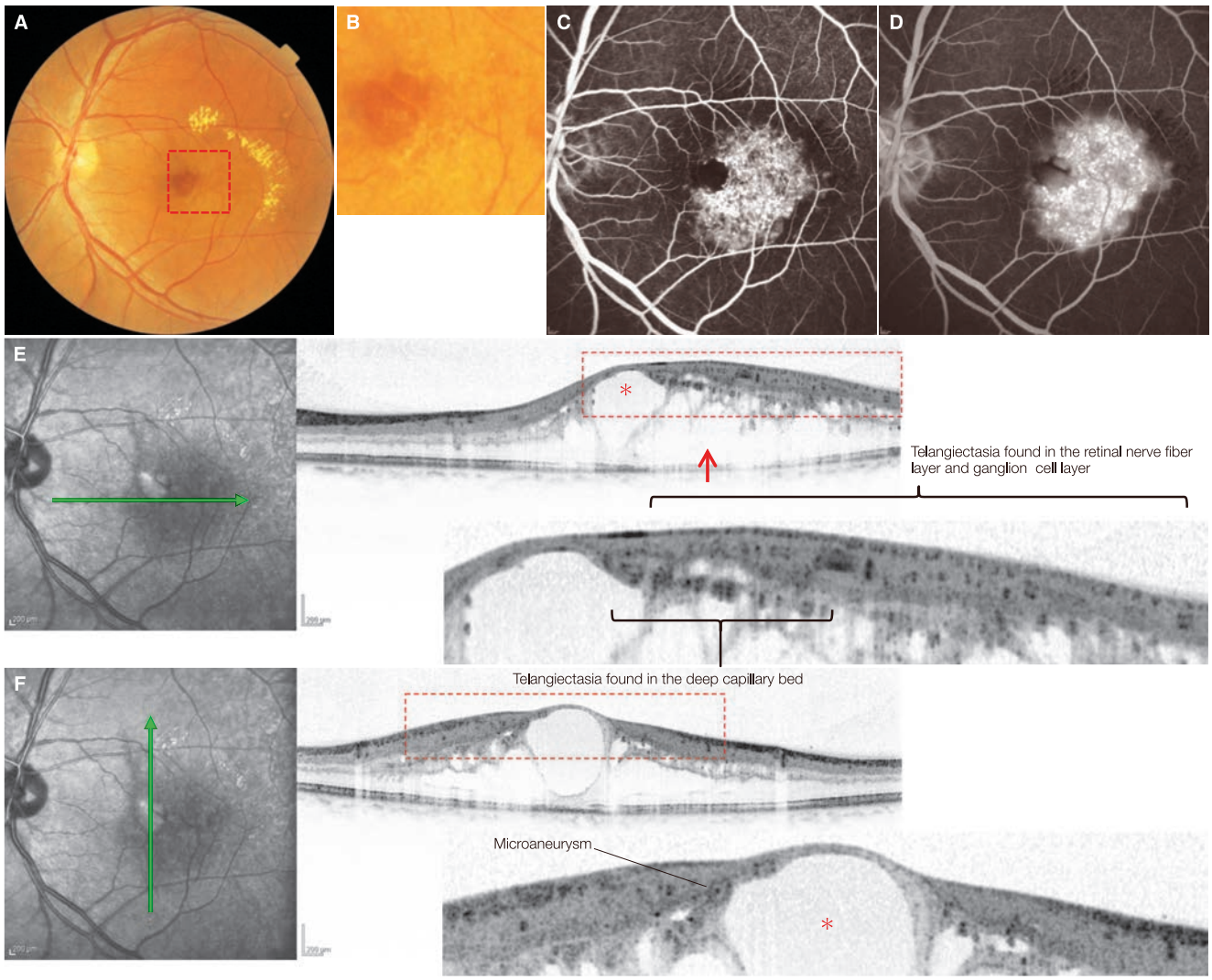

A: Color fundus photograph in the left eye, **B:** Enlarged version of A [red dashed box]: Circinate retinopathy can be seen centered at the temporal side of the parafovea. CME is present in the fovea centralis. **C:** FA in the left eye (54 sec): Telangiectasis and capillary MAs are visible in the area surrounded by the circinate retinopathy. **D:** FA in the left eye (5 min): Fluorescein leakage and fluorescein pooling into the cystoid spaces are exhibited. **E:** IR + OCT horizontal scan of the left eye + enlarged version [red dashed box]: A foveal cystoid space (*), outer plexiform layer cystoid spaces (→), and inner nuclear layer cystoid spaces are noted. Dilated capillaries are seen as 3 lines of highly reflective dots located along the boundary between the retinal nerve fiber layer and ganglion cell layer, external margin of the ganglion cell layer, and the inner nuclear layer. **F:** IR + OCT vertical scan of the left eye + enlarged version [red dashed box]: Note the capillary aneurysms in the margins of the foveal cystoid spaces (*).

Image interpretation points

Yannuzzi classification Type 1 is common in men, unilateral, and characterized by telangiectasis and retinal thickening on the temporal side of the parafovea accompanied by exudative lesions. In this case, telangiectasia, capillary aneurysms, CME and hard exudate were observed with an ophthalmoscope, and fluorescein leakage was seen on the temporal side of the fovea centralis by FA. Impressively, 3 layers of telangiectasia in the retinal capillary network can be observed by OCT. It is worth noting the capillary aneurysms in the margins of the cystoid spaces.

Case 64 Macular telangiectasia: Yannuzzi classification Type 1

A 57-year-old male, OD, BCVA 1.0

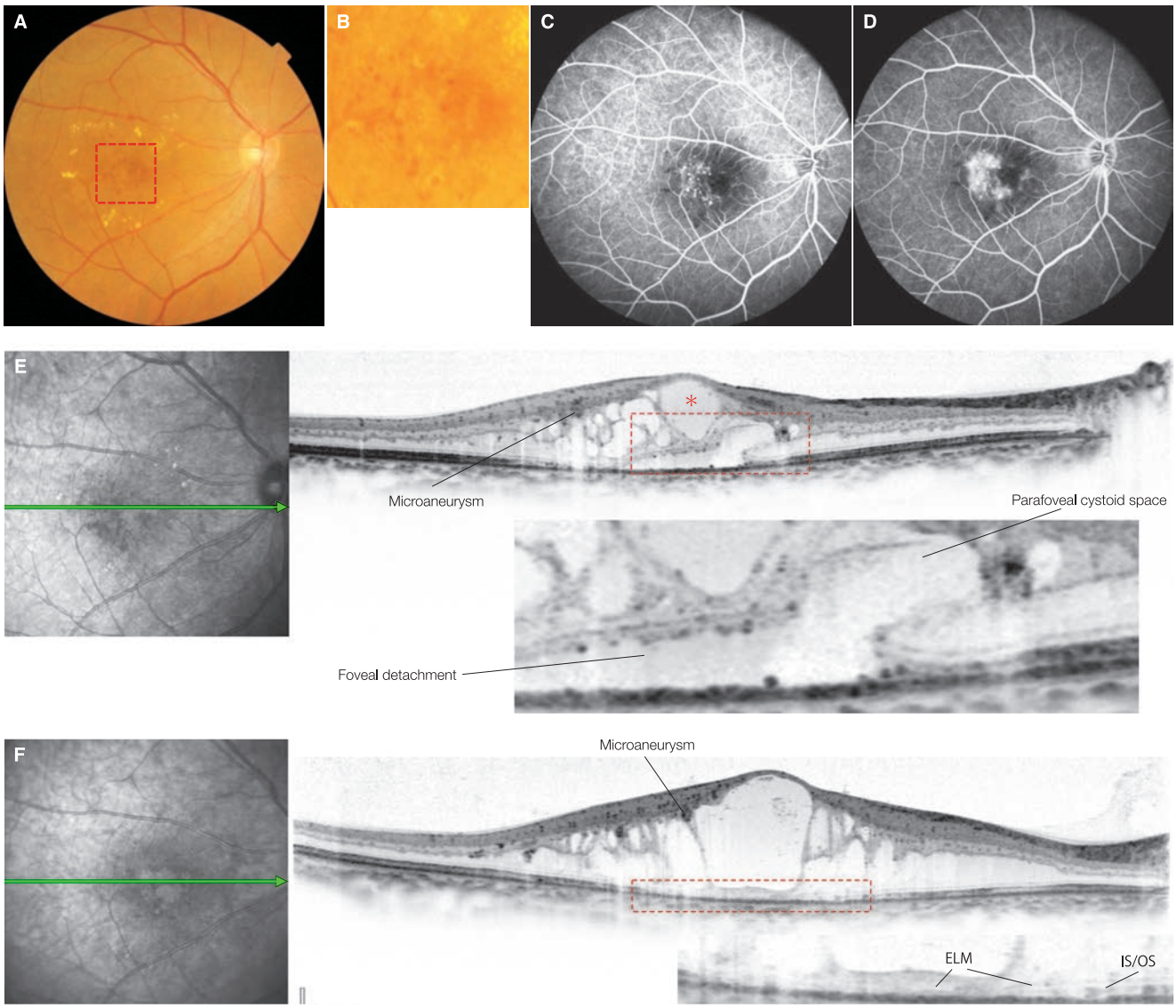

A: Color fundus photograph in the right eye, **B:** Enlarged version of A [red dashed box]: Circinate retinopathy can be seen centered on the temporal side of the parafovea. CME is visible in the fovea centralis. **C:** FA in the right eye (1 minute): Telangiectasia and capillary aneurysms are observed on the temporal side of the parafovea. **D:** 4-minute right eye FA: Fluorescein leakage from the capillary aneurysms is noted. **E:** IR + OCT horizontal scan of the right eye + enlarged version [red dashed box]: Foveal cystoid space (*), and cystoid spaces in the outer plexiform layer and inner nuclear layer can be observed. Adjacent parafoveal cystoid space are connected to a foveal detachment. **F:** IR + OCT horizontal scan of the right eye + enlarged version [red dashed box]: 18 months after initial diagnosis. Best corrected visual acuity declined to 0.5. The foveal detachment has disappeared, while the foveal cystoid spaces and parafoveal cystoid spaces have fused and expanded. The photoreceptor IS/OS beneath the cystoid space demonstrates significant atrophy. Note the dilated capillary aneurysm in the inner nuclear layer near the border of the parafoveal cystoid space.

Image interpretation points

In this case, fluid is leaking from the parafoveal cystoid spaces to below the retina, causing a foveal detachment. Eighteen months after initial diagnosis, the foveal detachment has disappeared, but the photoreceptor IS/OS beneath the expanded cystoid space created from the fusion and expansion of foveal and parafoveal cystoid spaces is atrophic, consistent with a decline in visual acuity. The exudative lesions of Yannuzzi classification Type 1 can exacerbate slowly, but when fluid accumulation into the subretinal space occurs, the progression of the decline in visual acuity is relatively quick.

Case 65 Macular telangiectasia: Yannuzzi classification Type 2 Stage 2

A 75-year-old female, OS, BCVA 1.0

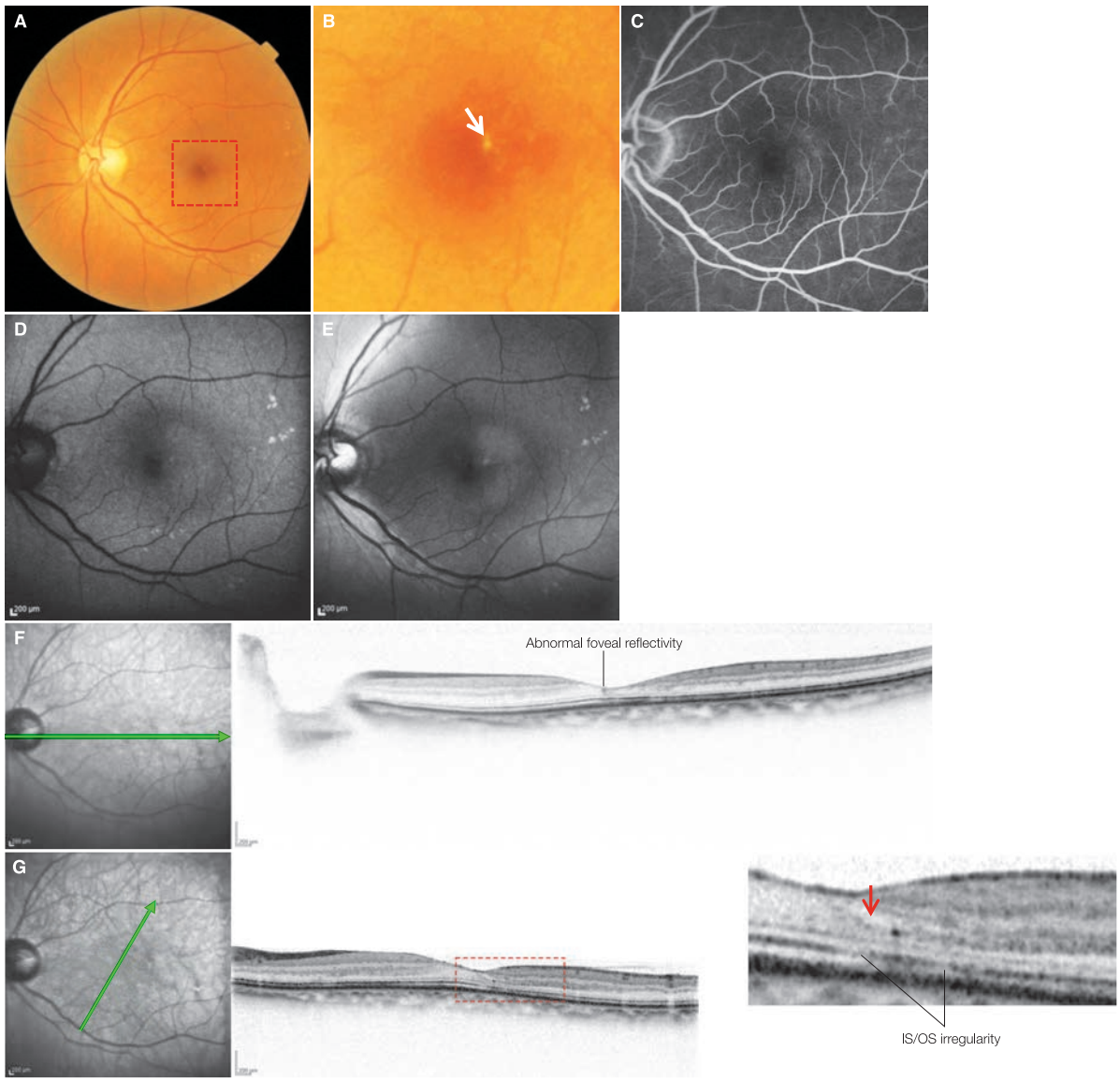

A: Color fundus photograph in the left eye, **B:** Enlarged version of A [red dashed box]: A slight decline in retinal transparency and crystalline deposits (⇒) are visible on the temporal side of the parafovea. **C:** FA in the left eye (5 minutes): Although subtle and diffuse hyperfluorescence can be seen on the temporal side of the parafovea, neither telangiectasia nor microaneurysms are observed. **D:** Fundus autofluorescence (FAF) in the left eye, **E:** Red-free imaging in the left eye: Enhancement of FAF and blue light enhancement reflectivity is observed in a semi-circular area on the temporal side of the parafovea. It is slightly wider than the area of hyperfluorescence on FA. **F:** IR + OCT horizontal scan of the left eye: The foveal depression has flattened due to atrophy of the temporal side of the parafovea and IS/OS line irregularities are noted. **G:** IR + OCT oblique scan of the left eye + enlarged version [red dashed box]: There is lamellar cystic degeneration (➔) on the temporal side of the parafovea and no retinal thickening.

Image interpretation points

Yannuzzi classification Type 2 has no gender difference, bilateral, and characterized by telangiectasia and hyperfluorescence without retinal thickening on the temporal side of the parafovea. This case corresponds to Gass-Blodi classification Stage 2: on the temporal side of the parafovea, a slight decrease in retinal transparency, crystalline deposits, weak and diffuse hyperfluorescence on FA, enhanced autofluorescence, and blue light hyperreflectivity in red-free imaging can be observed. Instead of CME or retinal thickening, OCT imaging typically demonstrates retinal thinning. Cystic degeneration, known as an inner lamellar cyst, also occurs in the temporal parafoveal area of the macula. IS/OS line irregularities can be seen, suggesting that damage to the photoreceptor cells is also present.

Case 66 Macular telangiectasia: Yannuzzi classification Type 2 Stage 3

A 75-year-old female, OD, BCVA 0.8

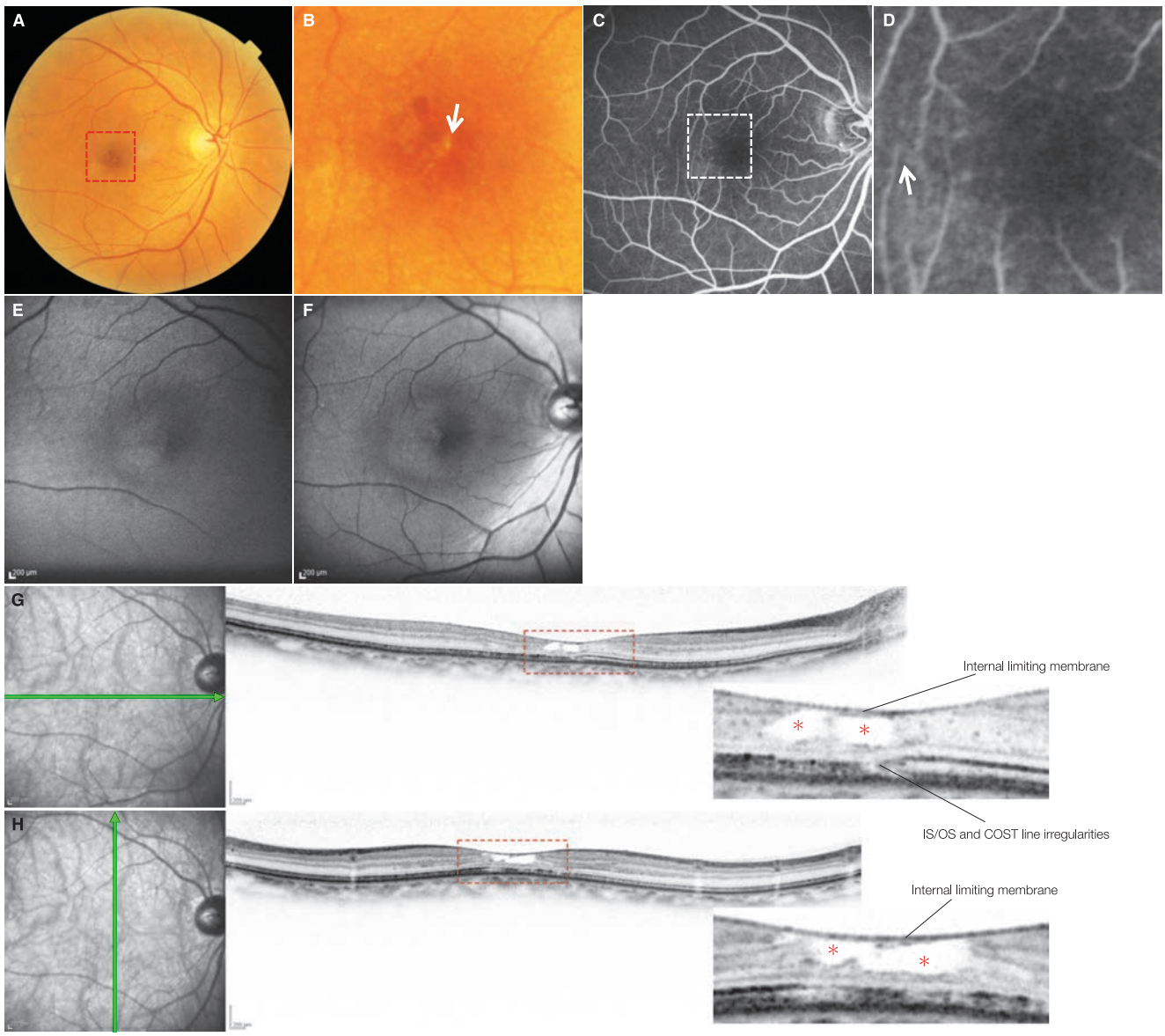

A: Color fundus photograph in the right eye, **B:** Enlarged version of A [red dashed box]: A slight decline in retinal transparency and crystalline deposits (⇒) are noted on the temporal side of the parafovea. **C:** FA in the right eye (50 seconds): **D:** Enlarged version of C [white dashed box]: Dilated and right-angled retinal venule (⇒) are observed on the temporal side of the parafovea. **E:** FAF in the right eye, **F:** Red-free imaging in the right eye: Enhanced autofluorescence and blue light hyperreflectivity are visible in a semi-circular area on the temporal side of the parafovea and is larger than the hyperfluorescence area on FA. **G:** IR + OCT horizontal scan of the right eye + enlarged version [red dashed box], H: IR + OCT vertical scan of the right eye + enlarged version [red dashed box]: Lamellar cystic degeneration (*) can be seen in the fovea centralis. The margins of the cystoid spaces are irregular. No retinal thickening is visible. Note the irregularities in the IS/OS and COST lines.

Image interpretation points

This case shows the right-angle retinal venule, consistent with Gass-Blodi classification Stage 3. On the temporal side of the parafovea, slight decrease in retinal transparency, crystalline deposits, weak and diffuse hyperfluorescence on FA, enhanced autofluorescence, and blue light hyperreflectivity in red-free imaging are observed. By OCT, no CME or retinal thickening is noticeable, but cystic degeneration, known as an inner lamellar cyst is present in the temporal parafoveal area of the macula. The term, »inner«, is derived from the fact that the anterior border of the cystoid space is the ILM. Irregularities in the IS/OS and COST lines are clearly visible, and there is thinning of the OS in the temporal portion of the parafovea.

Case 67 Macular telangiectasia: Yannuzzi classification Type 2 Stage 4

A 58-year-old male, OS, BCVA 0.7

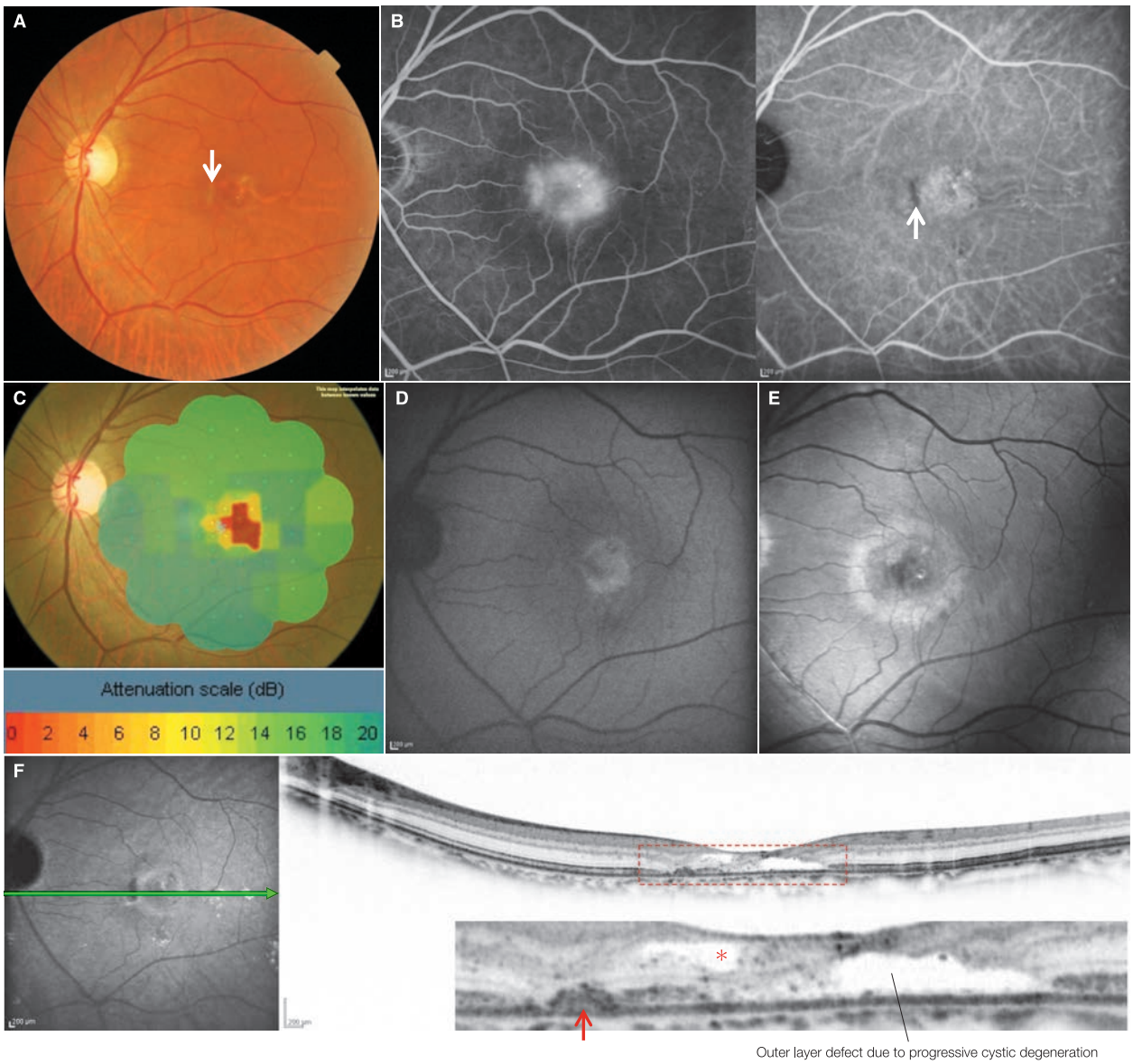

A: Color fundus photograph in the left eye: RPE hyperplasia can be seen on the nasal side of the parafovea (⇒). **B:** FA + IA in the left eye (5 minutes): Fluorescein hyperfluorescence is exhibited in the fovea and parafovea. Hypofluorescence due to light blocking by RPE are also observed on FA (⇒). **C:** Microperimetry -1 of the left eye: A scotoma is visible on the temporal side of the parafovea. **D:** FAF in the left eye: There is increased autofluorescence in the fovea centralis. **E:** Red-free imaging of the left eye: Annular blue light hyperreflectivitiy can be observed. It is wider than the area of hyperfluorescence on FA. **F:** IR + OCT horizontal scan of the left eye + enlarged version [red dashed box]: Defects are found in the outer layers of the retina on the temporal side of the parafovea. Lamellar cystic degeneration (*) of the inner layers can be seen. The margins of the cystoid spaces are irregular. No retinal thickening is visible. Areas of RPE hyperplasia (➔) are also present.

Image interpretation points

This case corresponds to Gass-Blodi classification Stage 4, as RPE hyperplasia can be seen. Cystic degeneration, known as an inner lamellar cyst, has developed into photoreceptor layer defects in the corresponding area of strong fluorescein hyperfluorescence seen on FA. The outer layer defect area causes the scotoma on microperimetry -1. Best corrected visual acuity maintained at 0.7 due to the preservation of the outer layers on the nasal side of the fovea centralis. Outside of the foveal centralis where the damage is more significant, the annular region of blue light hyperreflectivity on red-free imaging is seen. Blue light hyperreflectivity is thought to correspond to the loss of macular pigment (lutein and zeaxanthine).

Case 68 Coats' disease: A typical example

A 4-year-old girl, OD, BCVA 0.06

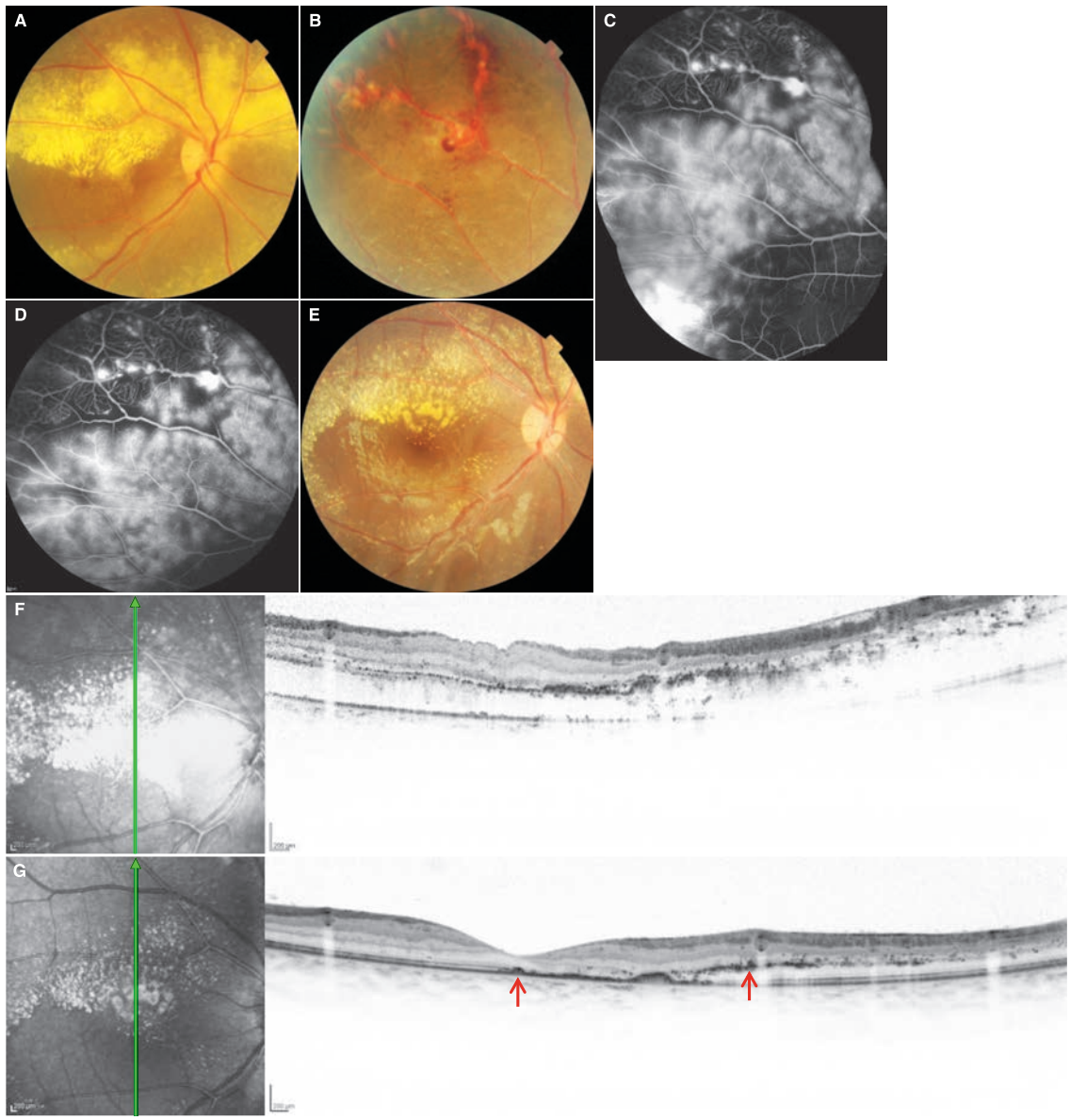

A: Color fundus photograph in the right eye: At initial diagnosis. A large amount of hard exudates and a wide area of SRD can be seen from the posterior pole to the upper retina. **B:** Color fundus photograph of the periphery in the right eye: At initial diagnosis. Irregular dilation and aneurysms are visible in the retinal blood vessels and capillaries in the upper temporal periphery. **C:** FA in the right eye (3 minutes, 30 seconds), **D:** FA in the left eye (4 minutes, 30 seconds): At initial diagnosis. Fluorescein leakage is observed from aneurysms in the peripheral retina and capillaries in the wide area inferior to the aneurysms. **E:** Color fundus photograph in the right eye: Five months after cryopexy. Visual acuity has improved to 0.6. SRD above the posterior pole has disappeared and a decrease in hard exudate is noted. **F:** IR + OCT vertical scan of the right eye: At initial diagnosis. SRD is exhibited over the entire posterior pole. **G:** IR + OCT vertical scan of the right eye: 5 months after cryopexy. Retinal detachment is subsiding, and hard exudates (→) remains below the retina and in the outer plexiform layer.

Image interpretation points

Coats' disease is non-familial, usually with unilateral onset, and common in men. It develops during infancy and childhood. When Coats' disease develops in adults and is confined to the parafovea, it is considered a disease similar to Yannuzzi Type 1. It starts with abnormalities in the peripheral capillaries, forming irregular dilation and aneurysms in the retinal blood vessels, and causing a large amount of hard exudates and SRD over a wide area. Sometimes, neovascular glaucoma may subsequently develop. Laser photocoagulation or cryopexy of the abnormal blood vessels is effective.

4.4 Retinal arterial macroaneurysm

Retinal arterial macroaneurysm is a disease that is common in women aged 60–70 years.[1, 2] It occurs readily in elderly persons with hypertension and arteriosclerosis. Unilateral onset is most common, but bilateral onset is seen in 10%. It is usually sporadic in the first to 3rd of the 4 arterial branches, but can occur in multiple sites. Although rare, it can occur in the cilioretinal artery and optic disc. It sometimes coincides with retinal vein occlusion. The macroaneurysms sometimes show pulsation, but it is unknown whether or not this finding is a risk factor for hemorrhages. The main causes of reduced visual acuity are hemorrhages below the retina and the ILM as a result of a rupture of retinal arterial macroaneurysm, and macular edema and foveal detachment as a result of leakage from it.[3] It can also be the cause of vitreous hemorrhage. The visual prognosis is relatively good in most cases with macular edema or vitreous hemorrhage alone, but a large number of hemorrhages below the fovea centralis can lead to poor visual prognosis.[4] Visual prognosis is also poor when macular edema is prolonged and circinate retinopathy is formed.[5, 6] Retinal arterial macroaneurysm can usually be seen with an ophthalmoscope, but where there is significant sub-ILM or vitreous hemorrhages obscuring the retinal arterial macroaneurysm, it is necessary to detect it by FA or IA for diagnosis.

One finding that is interesting is that despite the retinal arterial macroaneurysm being present in the arcade arteries, fluid can leak through the outer plexiform layer causing a foveal detachment and lead to visual impairment.[5, 7] Retinal arterial macroaneurysm is thought to form a linear cleft in the arterial wall, in which smooth muscle cell abnormalities and fibrosis of the retinal arterial wall has progressed. The macroaneurysm is covered by a laminated membrane formed by fibrin and platelets,[2] and thus the cleft may close spontaneously.

References

1) Rabb MF, Gagliano DA, Teske MP. Retinal arterial macroaneurysms. Surv Ophthalmol. 1988; 33:73–96.
2) Gass JDM. Macular dysfunction caused by retinal vascular diseases. In: Stereoscopic atlas of macular diseases 4th ed, Vol 1. CV Mosby, St. Louis, 1997. pp 437–599.
3) Lavin MJ, Marsh RJ, Peart S, et al. Retinal arterial macroaneurysms: a retrospective study of 40 patients. Br J Ophthalmol. 1987; 71:817–825.
4) Tonotsuka T, Imai M, Saito K, et al. Visual prognosis for symptomatic retinal arterial macroaneurysm. Jpn J Ophthalmol. 2003; 47:498–502.
5) Tsujiawa A, Sakamoto A, Ota M, et al. Retinal structural changes associated with retinal arterial macroaneurysm examined with optical coherence tomography. Retina. 2009; 29:782–792.
6) Tezel TH, Günalp I, Tezel G. Morphometric analysis of exudative retinal arterial macroaneurysms: a geometrical approach to exudate curves. Ophthalmic Res. 1994; 26:332–339.
7) Takahashi K, Kishi S. Serous macular detachment associated with retinal arterial macroaneurysm. Jpn J Ophthalmol. 2006; 50:460–464.

Case 69 Retinal arterial macroaneurysm: Subretinal hemorrhages

An 82-year-old female, OD, BCVA 0.05

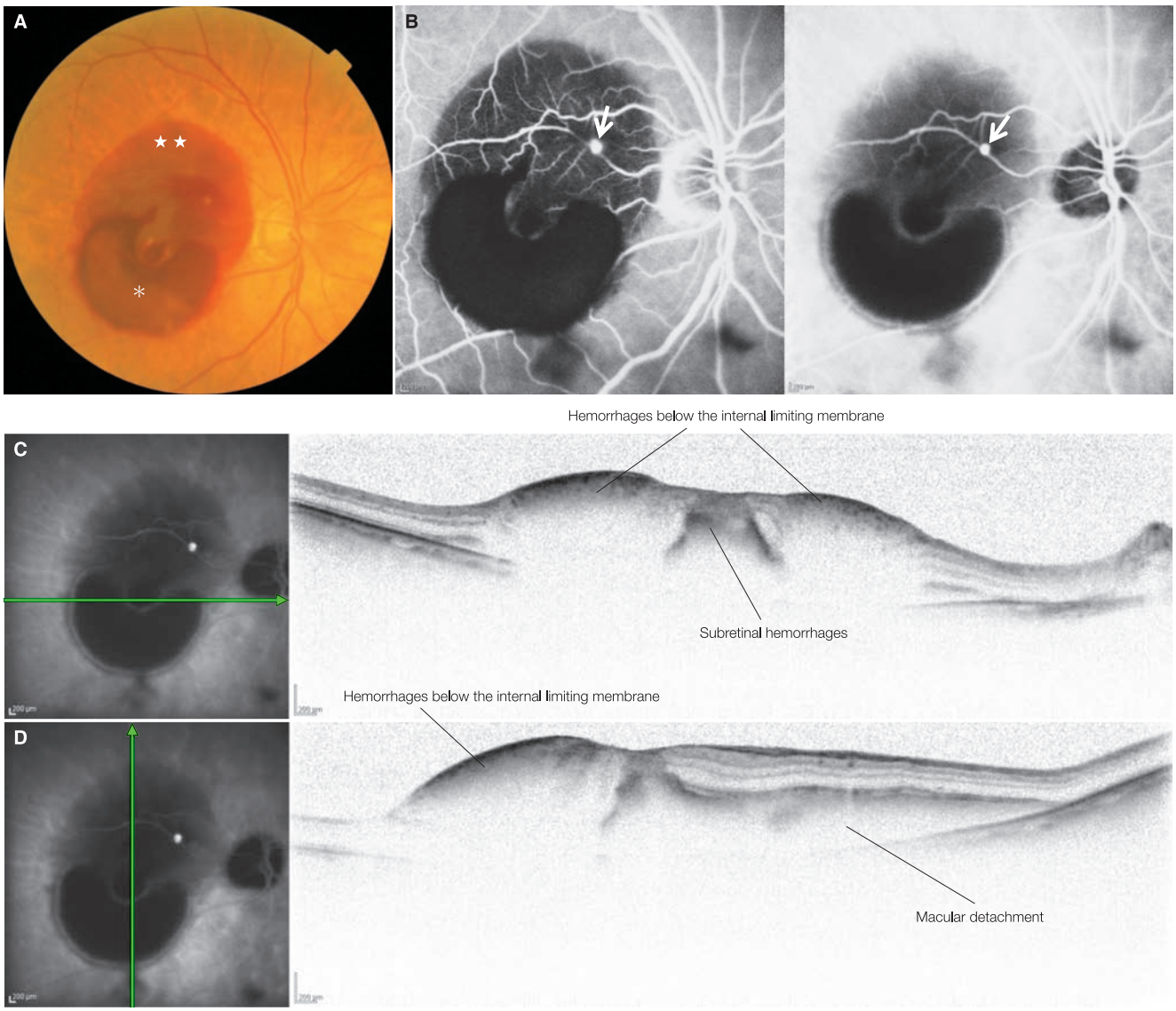

A: Color fundus photograph in the right eye: Hemorrhages below the ILM (❄) are evident in the inferior macula, and subretinal hemorrhages (☆☆) cover the entire macula. The choroid of the fovea centralis cannot be visualized. **B:** FA + IA in the right eye (1 minute): A retinal arterial macroaneurysm is visible (⇒). **C:** IR + OCT horizontal scan of the right eye: Hemorrhages below the ILM and hemorrhagic macular detachment are noted. **D:** IR + OCT vertical scan of the right eye: Same findings as C

Image interpretation points

Rupture of a retinal arterial macroaneurysm is often the cause of bleeding into below the ILM and retina, resulting in visual impairment. Hemorrhages block measurement beams so the posterior tissue is not visualized. Hemorrhages below the ILM can be removed with vitreous surgery and are infrequently the cause of poor visual prognosis. However, as in this case where a large amount of subretinal hemorrhages below the fovea centralis prevent the choroid from being visualized, the visual prognosis is poor. Gas tamponade was performed for this case, but visual improvement was limited to 0.15.

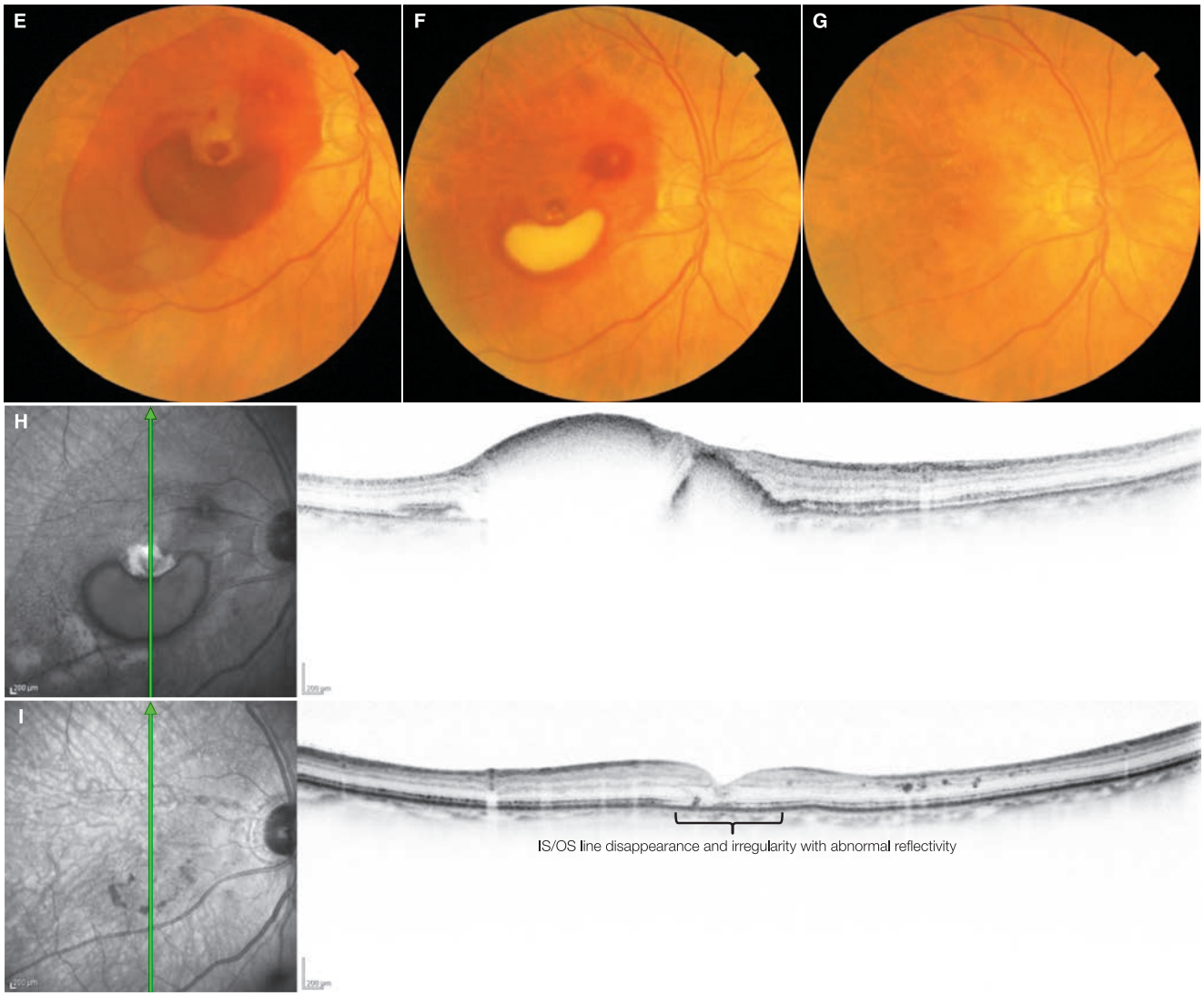

E: Color fundus photograph in the right eye: One week after gas tamponade. The subretinal hemorrhages have moved to outside the macula and choroidal visibility near the fovea centralis has improved. **F:** Color fundus photograph in the right eye: Two months after gas tamponade. Best corrected visual acuity is 0.08. Hemorrhages below the ILM are organized. Subretinal hemorrhages have been considerably absorbed. **G:** Color fundus photograph in the right eye: Nine months after surgery. Best corrected visual acuity has improved to 0.15. Hemorrhages below the ILM and subretinal hemorrhages have mostly disappeared. **H:** IR + OCT vertical scan of the right eye: One week after gas tamponade. Hemorrhages remain in the fovea centralis, but it is noticeable that the ones in the superior macula have been largely absorbed. The subretinal hemorrhage in the inferior macula is unclear due to the blocking effect as a result of hemorrhages below the ILM. I: IR + OCT vertical scan of the right eye: Subfoveal hemorrhages have disappeared. Note the disappearance, and irregularities of the IS/OS line and abnormal reflectivity of the foveal photoreceptor layer.

Case 70 Retinal arterial macroaneurysm: Foveal detachment from an inferior arterial macroaneurysms

A 73-year-old male, OS, BCVA 0.2

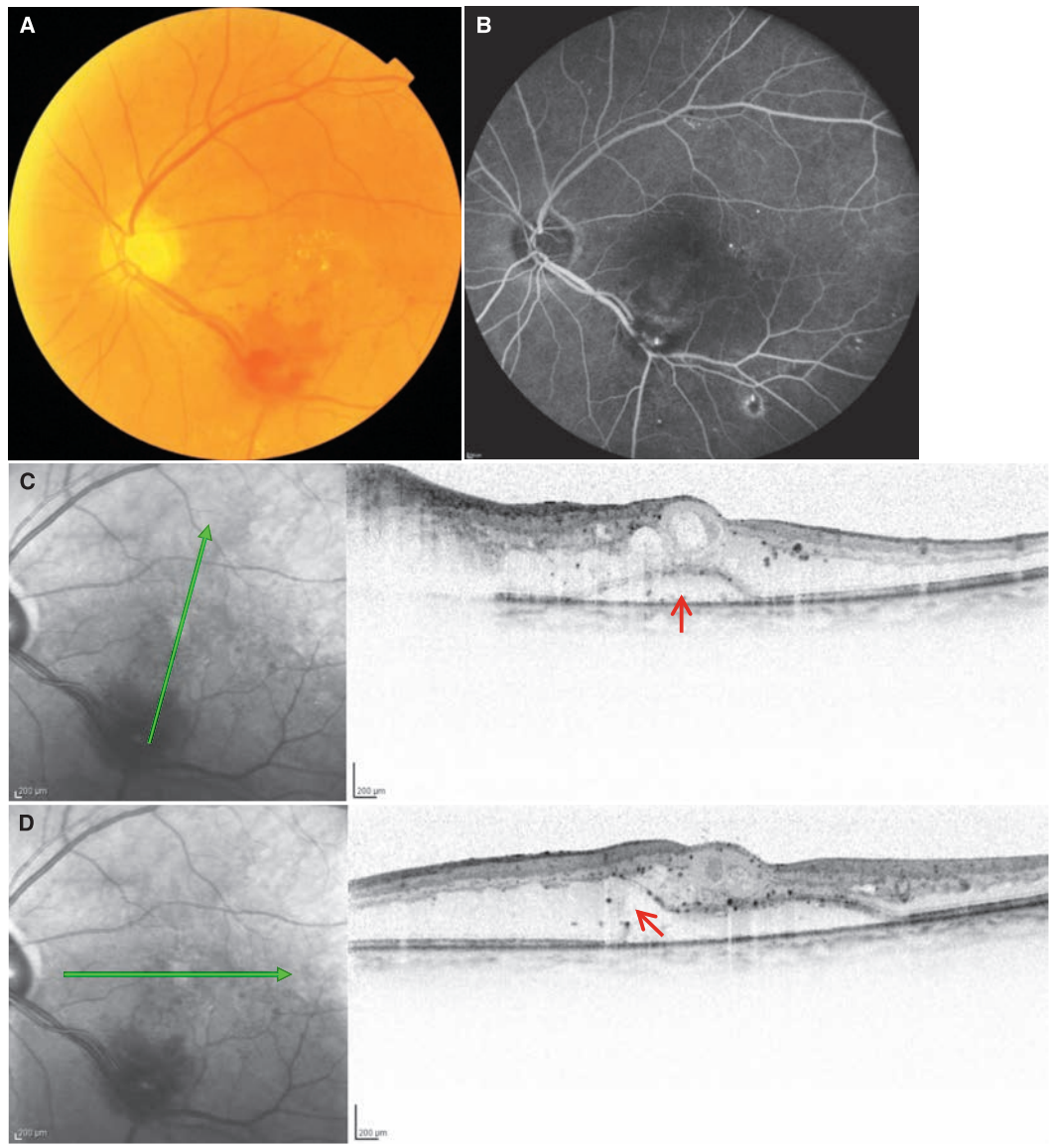

A: Color fundus photograph in the left eye: An arterial macroaneurysm and retinal hemorrhages are visible along the inferior retinal arcade. Hard exudates can be seen in the fovea centralis. **B:** FA in the left eye (2 minutes): The arterial macroaneurysm is seen in the inferior retinal arcade. **C:** IR + OCT oblique scan of the left eye: Outer plexiform layer edema is noted over a wide area from the arterial macroaneurysm to the inferonasal side of the macula. Foveal cystoid spaces and foveal detachment (➔) can also be observed. **D:** IR + OCT horizontal scan of the left eye: The parafoveal cystoid space in the outer plexiform layer is opening into the subretinal space (➔).
(A, B are modified according to Tsujikawa A, et al. Retinal structural changes associated with retinal arterial macroaneurysm examined with optical coherence tomography. Retina. 2009; 29: 782–792)

Image interpretation points

A leakage from retinal arterial macroaneurysm in the inferior arcade often spreads out into the fovea centralis leading to foveal cystoid edema and detachment, resulting in visual impairment. As in this case, outer plexiform layer edema is contiguous with the retinal arterial macroaneurysm. However, in cases where SRD is confined to the vicinity of the fovea centralis, it is thought that fluid leaking from the retinal arterial macroaneurysm flows through the outer plexiform layer like an underground stream and pools in the fovea centralis. Outer plexiform layer cystoid spaces near the fovea centralis are thought to coalesce with the subretinal space and cause foveal detachment.

Central serous chorioretinopathy

5.1 Central serous chorioretinopathy – 134
References – 138

Case 71 Acute central serous chorioretinopathy: Smoke-stack pattern – 139

Case 72 Acute central serous chorioretinopathy: A slowly leaking ink-blot pattern – 140

Case 73 Acute central serous chorioretinopathy: Intense leakage with ink-blot pattern – 141

Case 74 Chronic central serous chorioretinopathy: Choroidal thickening – 142

Case 75 Chronic central serous chorioretinopathy: A case of recurrence – 143

Case 75 Continuation – 144

Case 76 Chronic central serous chorioretinopathy: Changes in the photoreceptor outer segment – 145

Case 77 Chronic central serous chorioretinopathy: Example of poor visual prognosis – 146

Case 78 Acute bullous retinal detachment: A typical example – 147

5.1 Central serous chorioretinopathy

Background

Central serous chorioretinopathy (CSC) is a disease that causes a flat serous retinal detachment (SRD) in the macular area without any known other causes. Patients become aware of metamorphopsia, scotoma, and micropsia. In its acute form, the decrease in visual acuity is mild, and the visual prognosis is typically good if the condition does not become chronic. CSC is common in middle-aged men (male: female=10:1), stress can be a catalyst for onset, and a connection with type A personalities has been observed. The use of steroids is also involved in the onset and exacerbation of this disease.

Pathology

Breakdown of the outer blood-retinal barrier formed by the retinal pigment epithelium (RPE) was thought to be linked to the onset of CSC. In recent years, choroidal hyperpermeability has been suggested based on observation of abnormal choroidal tissue stains by indocyanine green angiography (IA).[1] Furthermore, increased choroidal thickness has also been observed using EDI-OCT. The results of such studies allowed us to consider the pathogenic mechanism involved in SRD formation: »increased choroidal permeability → choroidal stromal hypertension → breakdown of the outer blood-retinal barrier at the RPE.

Disease type and fluorescein fundus angiography

Typical (acute) CSC

- **FA**

The early stage starts with punctate hyperfluorescence; and during the late stages, severe leakage patterns known as ink-blots and smoke-stacks may appear.

The ink-blot pattern quickly leaks within the dome-shaped pigment epithelial detachment (PED) and produces a stained appearance of the exudate beneath the RPE. There is a type that diffusely leaks from within the PED to below the retina (Fig. 5-1), and a type that quickly leaks below the retina (Fig. 5-2). The latter is very similar to the smoke-stack pattern and leaks heavily from a pinhole break of the RPE, but since rapid diffusion below the retina is prevented by fibrin clots

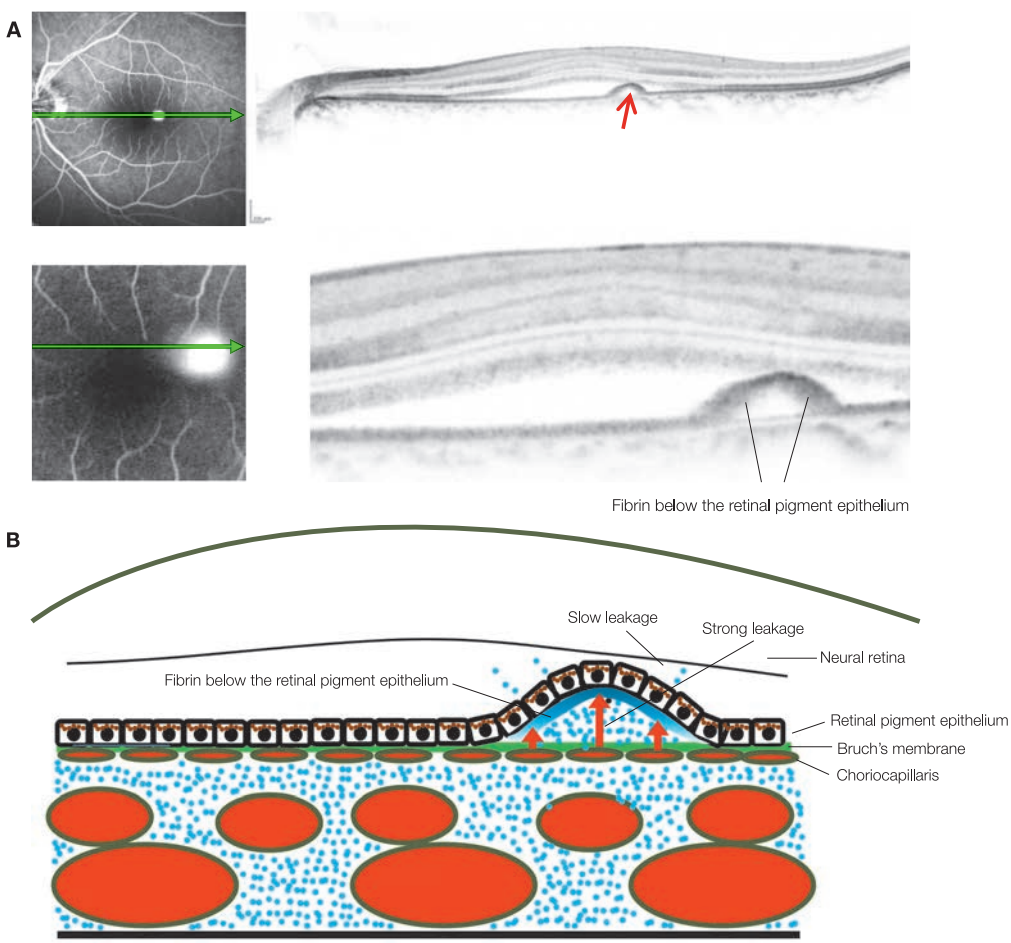

Fig. 5-1 Ink-blot pattern: Type that diffusely leaks below the retina
A: FA + OCT horizontal scan + enlarged version. The pooling of the dye (ink-blot pattern) can be seen on FA. PED (→) is visualized at this site by OCT. In the enlarged image, fibrin is not detected below the retina; instead it is located within the PED.
B: Diagram. Significant leakage from the choroid is being blocked by fibrin within the PED and causes slow spreading of dye into the retina. The characteristic of PED in this type is a dome-shaped swelling

surrounding the leakage, an ink-blot pattern with irregular configuration appears.

The smoke-stack pattern represents heavy leakage from the pinhole RPE break at the border or in the center of the PED that streams superiorly. The PED flattens as if it has collapsed and leakage fluid does not accumulate within the PED; so it does not accompany an ink-blot pattern that reflects the form of the PED (Fig. 5-3).

IA

Choroidal filling delay, dilation of the choroidal veins, and mid- to late-stage abnormal choroidal tissue staining indicating choroidal vessel hyperpermeability can be seen. These abnormal features are frequently noticeable even where there are any particular findings on FA and often remains even after SRD has resolved.

Chronic CSC

Extensive RPE dysfunction can be seen, and is characterized by the prolongation and recurrence of SRD. When the SRD is confined to around the disc, the periphery of the macula, and outside the macula during initial onset, there are no subjective symptoms; so examinations will sometimes expose cases that are already recurring or protracted at the initial visit. SRD is similar with acute CSC but shows a relatively smaller detachment. In addition, subretinal deposits, yellowish-white deposits, RPE atrophy, and pigmentation are often observed. Concentrated subretinal fluid spreads downward with gravity; and when this is prolonged, extensive RPE atrophy occurs in the inferior retina resulting in RPE atrophic tracts expressed by tear drops and flasks.

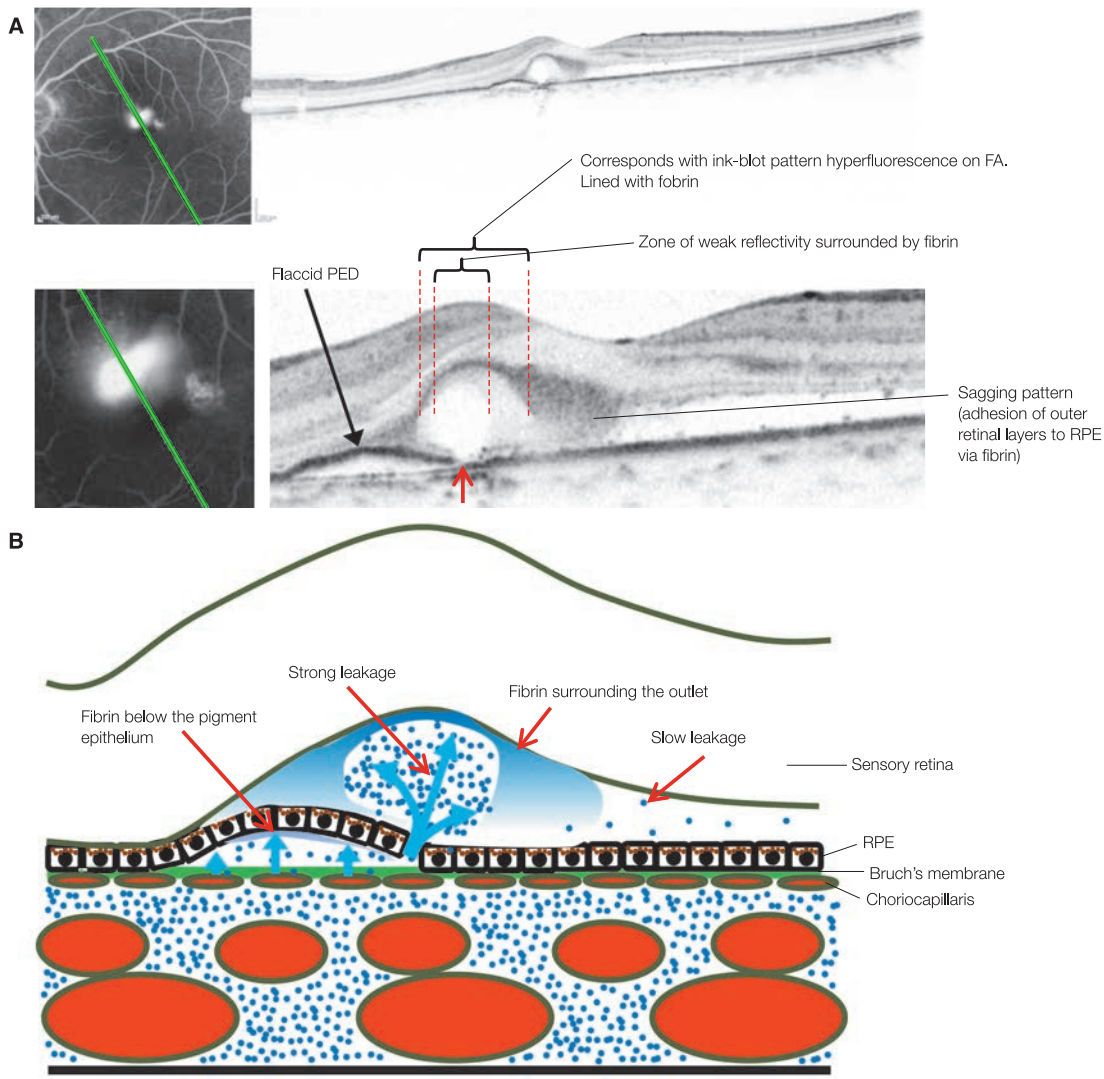

Fig. 5-2 Ink-blot pattern: Type that quickly leaks underneath the retina
In some cases with the ink-blot pattern, fibrin accumulates surrounding the leaking point of the RPE, and a circular space is formed where leakage fluid pools. The leakage fluid slowly spreads through the fibrin capsule into the subretinal space. The PED stops swelling and relaxes. In such cases, the IS/OS line is sometimes visible around the defect area, suggesting another possibility that the leakage generates a cystoid space in the outer retinal layers similar to Harada's disease. **A:** FA + OCT oblique scan + enlarged version. Rapid leakage can be seen on FA. Small defects (→) are observed in the RPE by OCT, and the PED is becoming flaccid. Fibrin is accumulating to envelop the RPE defect area, and the inside is weakly reflective. **B:** Diagram. Leakage fluid is rapidly flowing through the small defect in the RPE to underneath the retina. Fibrin is surrounding the leaking point of the RPE.

- **FA**

Diffuse, weak leakage is more frequent than clear pin-point leakage. There are many cases without distinct leakage points. RPE dysfunction can be seen as window defects.

- **IA**

Choroidal abnormal findings are observed over a wide area as in the typical example.

Acute bullous retinal detachment

Numerous SRDs and PEDs in the posterior pole and equatorial area occasionally occurs secondary to CSC. The SRDs sometimes become confluent and lead to bullous retinal detachments that extend into the inferior fundus. This is thought to be the fulminant form of CSC. In practice, many patients have a present or past history of CSC. Cases without systemic diseases are common in middle-aged men. Renal transplant patients and patients with systemic diseases receiving systemic steroids as treatment are also affected. Gender is not relevant in such cases. Yellowish-white fibrin deposits beneath the retina can be seen with a relatively large PED.

- **FA**

In the early phase, there are multiple punctiform leakage spots, which exhibits significant fluorescein leakage in later phases.

Prognosis

There are many cases of spontaneous remission, and in a large portion, visual acuity improves substantially without treatment. However, even if visual acuity is restored to 1.0 and above, numerous disorders such as a decrease in color sensitivity, a decrease in contrast sensitivity, relative scotoma, micropsia, and metamorphopsia may persist. Visual acuity remains below 0.7 in roughly 5% of cases. Patients with prolonged or recurrent SRD sometimes show visual impairments of below 0.1. The visual prognosis of cases where the SRD is large is worse compared to those where it is small. When the SRD is in remission, there are cases where the ocular fundus is almost restored to normal, but the majority exhibit irregular depigmentation of the RPE or extensive RPE atrophy. 20–30% of cases undergo at least one recurrence. RPE abnormalities are also seen in the fellow eye in 1/3 of cases, but less than 20% result in SRD.

OCT findings

In acute CSC, the following findings have been reported thanks to time-domain OCT: SRD, thickening, high reflectivity and irregularities (granulation) of the detached foveal retina, RPE abnormalities, sub- and intraretinal deposits, fibrin,[1–10] thinning of the fovea as in cases of poor visual recovery after reattachment, as well as attenuation or disappearance of the foveal ELM and IS/OS reflectivity, and cystic degeneration.[4, 11, 12] The usefulness of OCT in the diagnosis and pathological understanding of CSC has been well known. In practice, even shallow SRDs which cannot be clearly determined with an biomicroscopy or fluorescein fundus angiography can be detected by OCT.[13] An even more accurate pathological understanding is possible with SD-OCT.

Acute CSC

- **Detached sensory retina**

Roughly 1–2 months after onset, the photoreceptor outer segments (OS) maintain homogeneous reflectivity and thickness, but after 2 months, OS irregularities form including OS thickness heterogeneity, elongation of the foveal OS, and OS high reflectivity.[14, 15] As the period after initial onset becomes more prolonged, highly reflective spots corresponding to ophthalmoscopically-identified subretinal deposits become more significant, foveal OS elongation becomes more noticeable, part of the elongated OS starts shedding, and these shed OS can be seen above the RPE. The shed OS appears highly reflective on infrared imaging.

- **Subretinal findings and the RPE**

RPE defects thought to be leakage points can be seen in or at the edge of the PED. There may be a fibrin clot that covers the RPE defect and weakly reflective zone within the fibrin clot believed to form due to fresh leakage fluid.[16, 17] There are cases where tense, dome-shaped PED can be seen and those with relaxed, concave PED. Location of fibrin clot formation and PED shapes are closely related to leakage patterns (Fig. 5-1–5-3).

Chronic CSC

- **Detached sensory retina**

The SRD is flat and can sometimes only be seen with OCT.[12] The above-mentioned photoreceptor OS irregularities (OS thickness heterogeneity, OS thickening, OS high reflectivity, and OS shedding) and sub- and intra- retinal deposits are significant due to chronicity. If CSC is further prolonged or recurrence occurs, this can cause significant foveal thinning.

- **Subretinal findings and the RPE**

The PED often can be relaxed, flat, and exist over a wide area. These PEDs cannot be determined on an biomicroscopy. The presence of PED can be easily determined on OCT because the linear Bruch's membrane is visible beneath PED.

Reattached sensory

In patients with good visual acuity, there are often no abnormalities in the foveal ELM, IS/OS and COST lines, and foveal thickness tends to be normal.

As the decrease in visual acuity progresses, foveal retinal thickness thins and the ELM, IS/OS, and COST lines become irregular or disappear over a wide area.[12, 14, 18] Lack of reflectivity of the IS/OS and COST lines and thinning of the foveal portion of the retina are findings correlated with the number of foveal cone photoreceptor cells.[19] The reflectivity lines most easily affected from the early stage are ① COST, ② IS/OS, and ③ ELM, in that order. Even in eyes with good visual acuity, IS/OS and COST line irregularities confined to outside the fovea centralis are commonly encountered. A decrease in retinal sensitivity consistent with these sites can also be observed.[20]

The choroid

It was previously known that choroidal vessel hyperpermeability existed in CSC.[1] Improved visualization of the choroid using EDI-OCT has demonstrated that the choroid indeed thickens in CSC.[21] Choroidal thickening accompanying choroidal vessel hyperpermeability is sometimes even detected in the fellow eye where CSC has not developed.[22] Photodynamic therapy (PDT) and laser photocoagulation are both effective in treating SRD in CSC; however PDT improves choroidal thickening, whereas it persists even after laser photocoagulation was successfully done.[23]

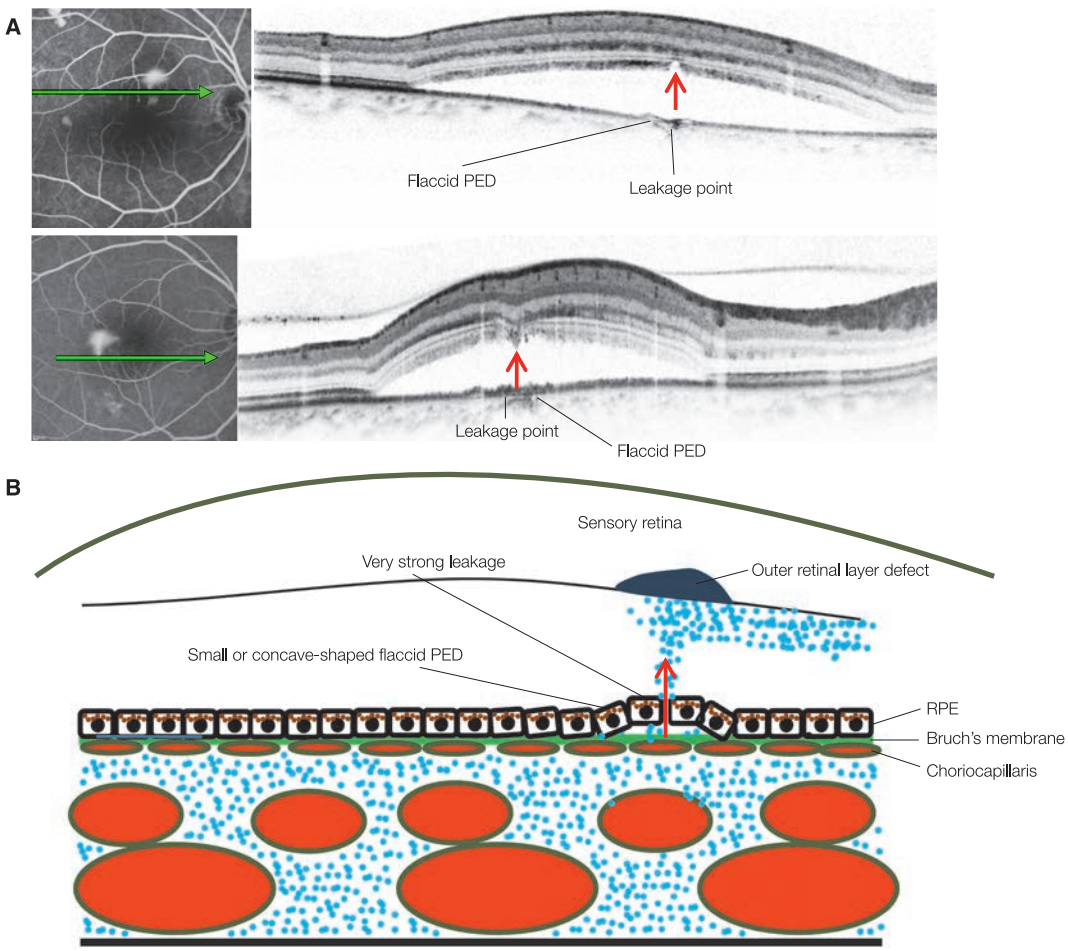

Fig. 5-3 Smoke-stack pattern
A: FA + OCT horizontal scan. A smoke-stack pattern of fluorescein leakage is visible on FA. Concave-shaped flat PED can be seen on OCT and the leakage point is also visualized. Outer retinal defect (➔) due to jet stream can be seen. **B:** Diagram. Leakage fluid is not accumulating beneath the pigment epithelium, but instead, is strongly flowing into the subretinal space. Fibrin is not accumulating beneath the RPE or the retina. Leakage spots are consistent with small or concave-shaped PED.

References

1) Iida T, Kishi S, Hagimura N, et al. Persistent and bilateral choroidal vascular abnormalities in central serous chorioretinopathy. Retina. 1999; 19:508–512.
2) Hee MR, Puliafito CA, Wong C, et al. Optical coherence tomography of central serous chorioretinopathy. Am J Ophthalmol. 1995; 120:65–74.
3) Iida T, Hagimura N, Sato T, et al. Evaluation of central serous chorioretinopathy with optical coherence tomography. Am J Ophthalmol. 2000; 129:16–20.
4) Wang MS, Sander B, Larsen M. Retinal atrophy in idiopathic central serous chorioretinopathy. Am J Ophthalmol. 2002; 133:787–793.
5) Piccolino FC, de la Longrais RR, Ravera G, et al. The foveal photoreceptor layer and visual acuity loss in central serous chorioretinopathy. Am J Ophthalmol. 2005; 139:87–99.
6) Montero JA, Ruiz-Moreno JM. Optical coherence tomography characterisation of idiopathic central serous chorioretinopathy. Br J Ophthalmol. 2005; 89:562–564.
7) Saito M, Iida T, Kishi S. Ring-shaped subretinal fibrinous exudate in central serous chorioretinopathy. Jpn J Ophthalmol. 2005; 49:516–519.
8) Hussain N, Baskar A, Ram LM, et al. Optical coherence tomographic pattern of fluorescein angiographic leakage site in acute central serous chorioretinopathy. Clin Experiment Ophthalmol. 2006; 34:137–140.
9) Mitarai K, Gomi F, Tano Y. Three-dimensional optical coherence tomographic findings in central serous chorioretinopathy. Graefes Arch Clin Exp Ophthalmol. 2006; 244:1415–1420.
10) Kon Y, Iida T, Maruko I, Saito M. The optical coherence tomography-ophthalmoscope for examination of central serous chorioretinopathy with precipitates. Retina. 2008; 28:864–869.
11) Iida T, Yannuzzi LA, Spaide RF, et al. Cystoid macular degeneration in chronic central serous chorioretinopathy. Retina. 2003; 23:1–7.
12) Eandi CM, Chung JE, Cardillo-Piccolino F, et al. Optical coherence tomography in unilateral resolved central serous chorioretinopathy. Retina. 2005; 25:417–421.
13) Wang M, Sander B, Lund-Andersen H, et al. Detection of shallow detachments in central serous chorioretinopathy. Acta Ophthalmol Scand. 1999; 77:402–405.
14) Ojima Y, Hangai M, Sasahara M, et al. Three-dimensional imaging of the foveal photoreceptor layer in central serous chorioretinopathy using high-speed optical coherence tomography. Ophthalmology. 2007; 114: 2197–2207.
15) Matsumoto H, Kishi S, Otani T, et al. Elongation of photoreceptor outer segment in central serous chorioretinopathy. Am J Ophthalmol. 2008; 145:162–168.
16) Fujimoto H, Gomi F, Wakabayashi T, et al. Morphologic changes in acute central serous chorioretinopathy evaluated by Fourier-domain optical coherence tomography. Ophthalmology. 2008; 115:1494–1500.
17) Shinojima A, Hirose T, Mori R, et al. Morphologic findings in acute central serous chorioretinopathy using spectral domain-optical coherence tomography with simultaneous angiography. Retina. 2010; 30:193–202.
18) Matsumoto H, Sato T, Kishi S. Outer nuclear layer thickness at the fovea determines visual outcomes in resolved central serous chorioretinopathy. Am J Ophthalmol. 2009; 148:105–110.
19) Ooto S, Hangai M, Sakamoto A, et al. High-resolution imaging of resolved central serous chorioretinopathy using adaptive optics scanning laser ophthalmoscopy. Ophthalmology. 2010; 117:1800–1809.
20) Ojima Y, Tsujikawa A, Hangai M, et al. Retinal sensitivity measured with the micro perimeter 1 after resolution of central serous chorioretinopathy. Am J Ophthalmol. 2008; 146:77–84.
21) Imamura Y, Fujiwara T, Margolis R, et al. Enhanced depth imaging optical coherence tomography of the choroid in central serous chorioretinopathy. Retina. 2009; 29:1469–1473.
22) Maruko I, Iida T, Sugano Y, et al. Subfoveal choroidal thickness in fellow eyes of patients with central serous chorioretinopathy. Retina. 2011; 1603–1608.
23) Maruko I, Iida T, Sugano Y, et al. Subfoveal choroidal thickness after treatment of central serous chorioretinopathy. Ophthalmology. 2010; 117: 1792–1799.

Case 71 Acute central serous chorioretinopathy: Smoke-stack pattern

A 48-year-old male, OD, BCVA 1.0

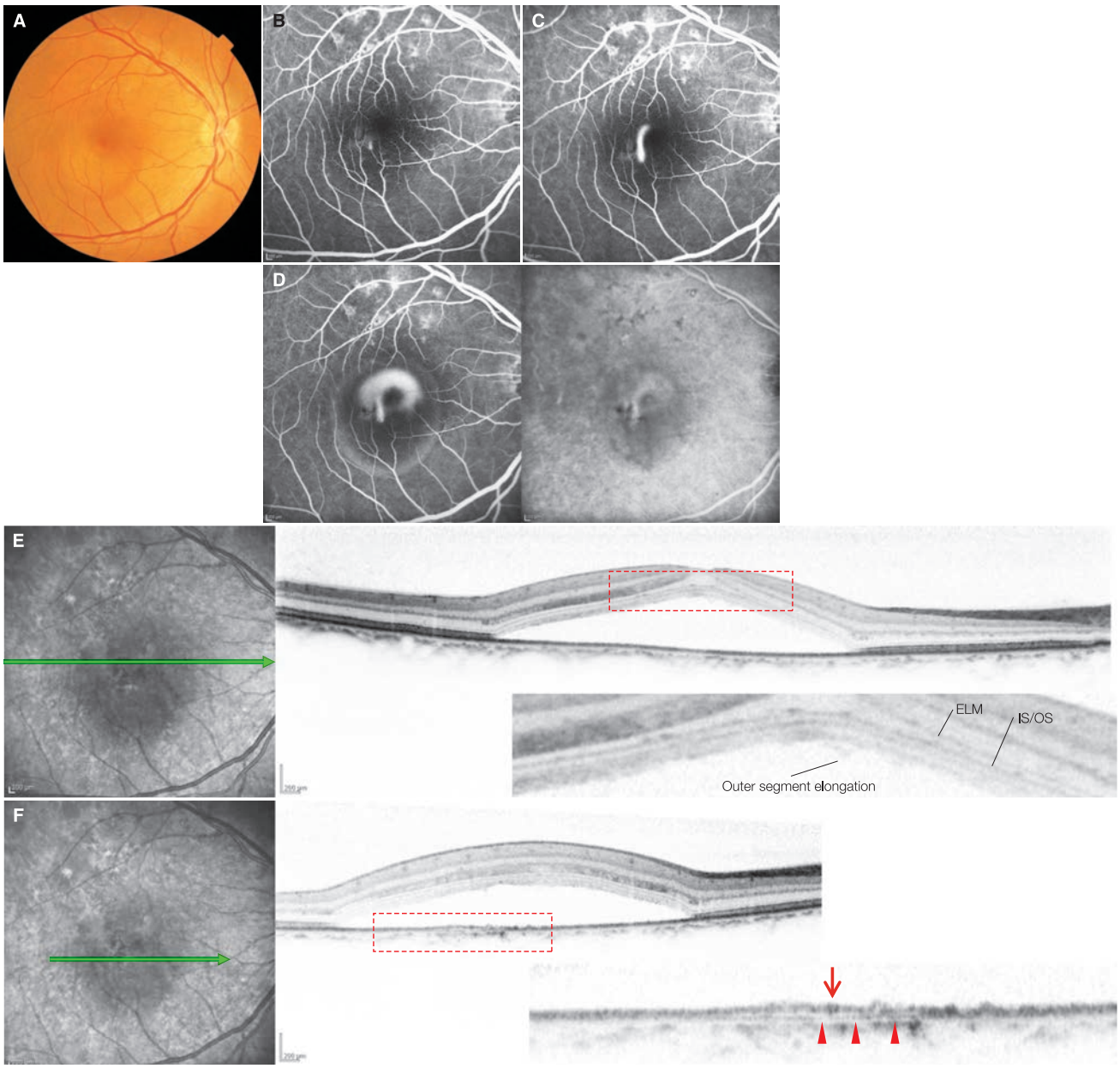

A: Color fundus photograph in the right eye: At initial visit. One week after onset. SRD two times the diameter of the optic disc is noted in the macula. **B:** FA in the right eye (45 seconds): A leakage point can be seen on the inferior temporal side of the parafovea. **C:** FA in the right eye (2 minute): Extensive leakage in a smoke-stack pattern is visible. **D:** FA + IA in the right eye (12 minutes): Filling of the dye in the subretinal space shows fungiform pattern. On IA stains abnormally in the superior macula due to choroidal hyperpermeability. **E:** IR + OCT horizontal scan of the right eye + enlarged version [red dashed box]: During initial diagnosis. The photoreceptor outer segments exhibit relatively homogeneous reflectivity, and the thickness is also uniform. Elongation is noted only in a small part of the OS. **F:** IR + OCT horizontal scan of the right eye + enlarged version [red dashed box]: A flat PED (➔) is seen over the flaccid PED including the leakage point. (►) indicates Bruch's membrane

Image interpretation points

It is common to see relatively homogeneous reflectivity and thickness of the OS in CSC within 1–2 months of acute onset. In this case, the patient became aware of metamorphopsia and visual impairment one week before being referred to the outpatient clinic. The patient had a history of CSC that had spontaneously resolved roughly 6 years earlier. This is a recurrence, but the abnormal OS findings were mild. A flaccid, flat PED could be seen in the area of the smoke-stack pattern leakage point.

Case 72 Acute central serous chorioretinopathy: A slowly leaking ink-blot pattern

A 43-year-old male, OS, BCVA 1.5

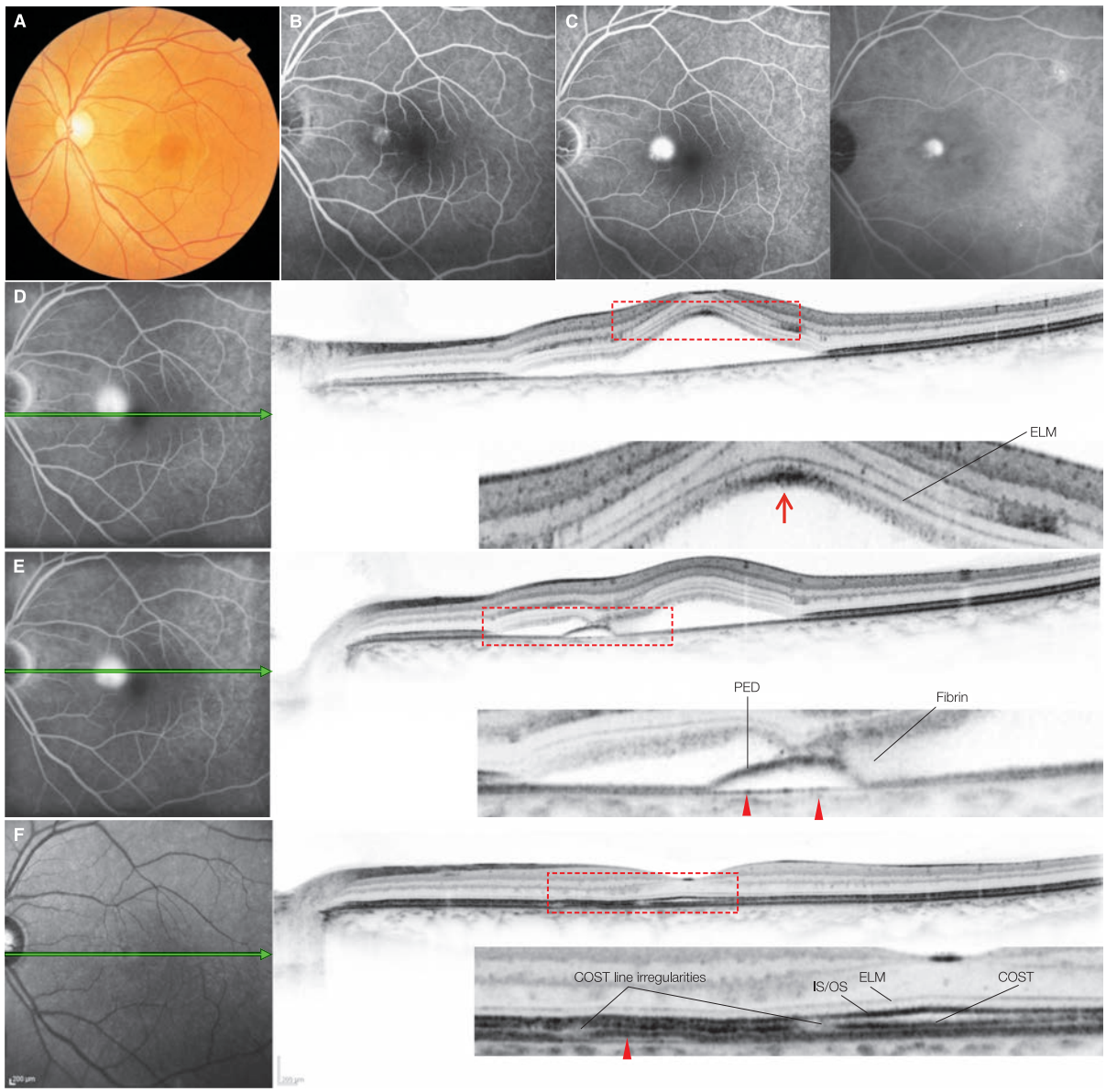

A: Color fundus photograph in the left eye: During initial diagnosis. Eight days after onset. SRD two times the diameter of the optic disc is noted in the macula. **B:** FA in the left eye (80 seconds): During initial diagnosis. A leakage point can be seen on the nasal side of the macula. **C:** FA + IA in the left eye (10 minutes): Fluorescein filling with typical ink-blot pattern is exhibited. ICG stains abnormally due to choroidal hyperpermeability, which is evident on the temporal side of the macula. **D:** IR + OCT horizontal scan of left eye + enlarged version [red dashed box]: During initial diagnosis. The photoreceptor OS is uniform in thickness but highly reflective (➔). **E:** IR + OCT horizontal scan of the left eye + enlarged version [red dashed box]: During initial diagnosis. A dome-shaped PED consistent with a round pooling of fluorescein can be seen. A part of the outer retinal layer is pulled down to attach on the RPE by the adhesive force of fibrin and exhibits a dripping pattern. (►) indicates Bruch's membrane. **F:** IR + OCT horizontal scan of left eye + enlarged version [red dashed box]: Spontaneous remission of SRD 8 months after initial diagnosis. Corrected visual acuity has improved to 1.2. No foveal abnormalities are visible, but COST line irregularities can be seen on the nasal side of the parafovea. IS/OS and ELM irregularities are indistinct. (►) indicates Bruch's membrane.

Image interpretation points

This is a case of spontaneous resolution of acute CSC 8 months after onset. In this case, fluid from the choroid leaked heavily within the PED resulting in the dome-shaped appearance and is also slowly leaking to underneath the retina causing a SRD.

The sub-RPE fluorescein pooling exhibits an ink-blot pattern. There is likely less heavy leakage below the retina due to the fibrin restricting the flow of fluid. The photoreceptor OS generally becomes highly reflective as time progresses.

Case 73 Acute central serous chorioretinopathy: Intense leakage with ink-blot pattern

A 38-year-old male, OS, BCVA 0.7

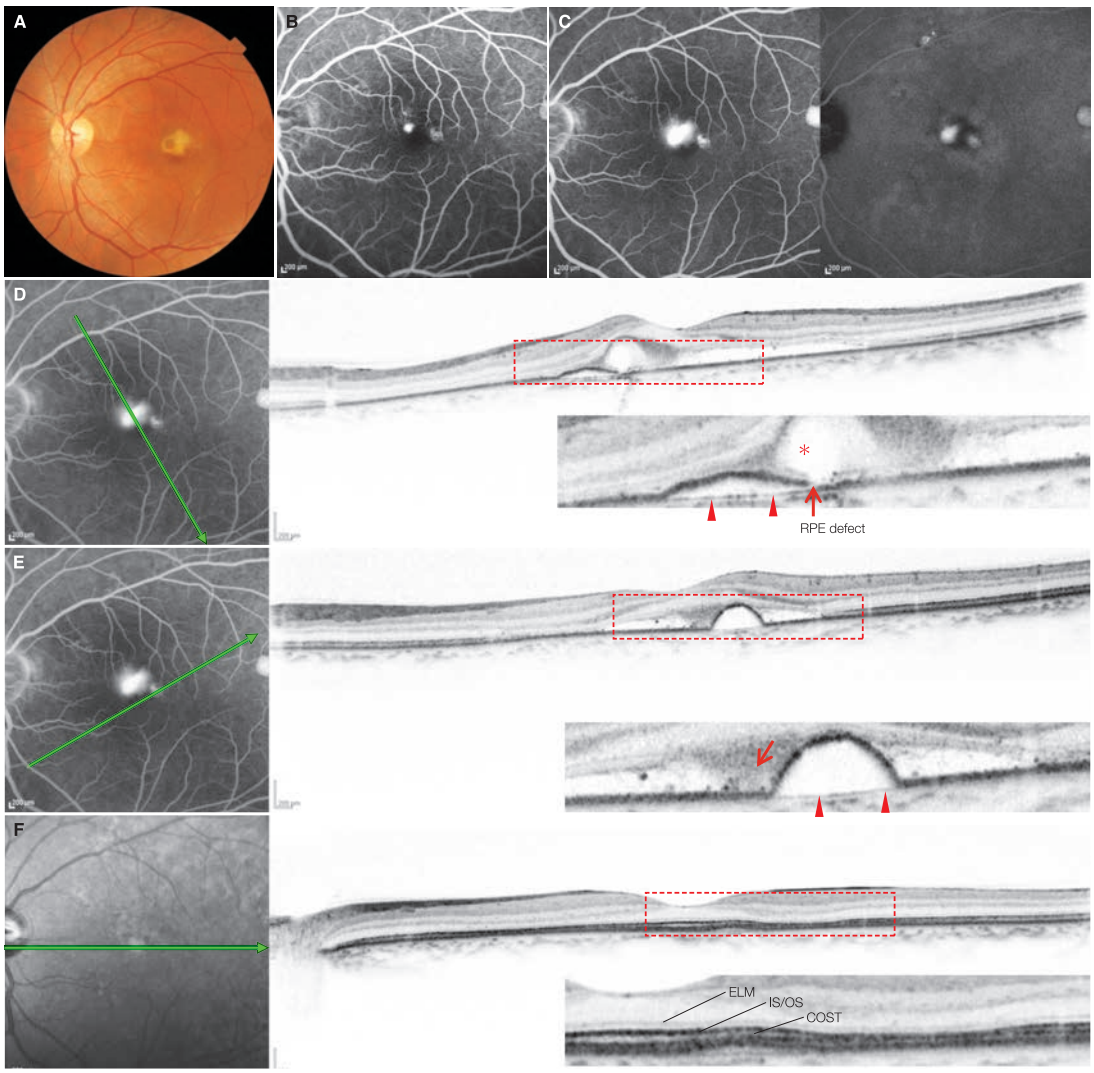

A: Color fundus photograph in the left eye: During initial diagnosis. Four months after onset. Round (with a clear zone in the center) fibrin is noted in the fovea. **B:** FA in the left eye (1 minute): During initial diagnosis. A leakage point can be seen on the superior nasal side of the fovea. A resolved leakage spot is observed on the superior temporal side of the parafovea. **C:** FA + IA in the left eye (10 minutes): Fluorescein filling with an ink-blot pattern is visible. ICG stains abnormally due to choroidal hyperpermeability, which can be observed in the macula. **D:** IR + OCT oblique scan of the left eye + enlarged version [red dashed box]: During initial diagnosis. Scan passes through the enlarged, round area of dye filling. RPE defect (➔) can be seen at the border of the PED, and a weakly reflective round area (*), consistent with the clear on fundus photographs, is seen on the RPE defect surrounded by the moderately reflective fibrin, indicating significant leakage from the defect. The PED has lost its tension. (►) indicates Bruch's membrane. **E:** IR + OCT horizontal scan of the left eye + enlarged version [red dashed box]: During initial diagnosis. Scan passes through the resolved leakage spots. Dome-shaped PED and fibrin clots (➔) in contact with the PED on the nasal side are noticeable. (►) indicates Bruch's membrane. **F:** IR + OCT horizontal scan of the left eye + enlarged version [red dashed box]: Two years after initial diagnosis. The SRD has disappeared and best-corrected visual acuity has improved to 1.5. No foveal abnormalities are visible, but disappearance of the COST line on the temporal macula can be seen. No IS/OS or ELM irregularities are noted.

Image interpretation points

This is a case of a patient referred 4 months after onset of symptoms. Laser photocoagulation was performed 1.5 months after the initial diagnosis and the SRD regressed the next day. Highly active leakage spots, as in this case, have significant leakage to below the retina via the defect point at the border of the PED. Since the leakage fluid flows through the PED without pooling, the PED becomes flaccid. Fibrin clots have formed below the retina, and the leakage fluid forms weakly reflective cavities within the fibrin clots, which correspond to an ink-blot pattern on FA. Dome-shaped PED is seen in the resolved leakage spot, and subretinal leakage decreases due to fibrin plugs (just before cessation).

Case 74 Chronic central serous chorioretinopathy: Choroidal thickening

A 42-year old male, OS, BCVA 0.4

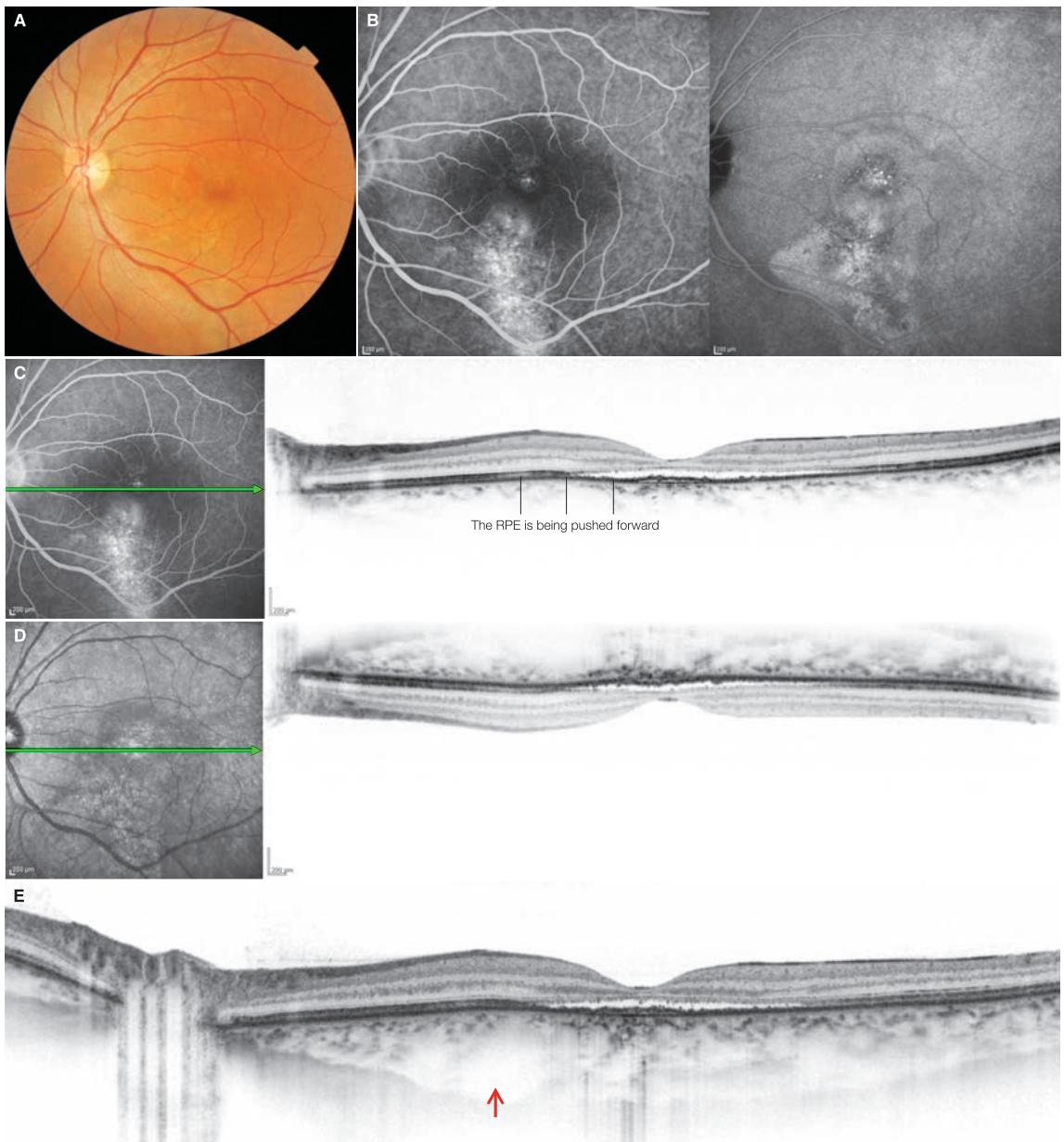

A: Color fundus photograph in the left eye: Six months after onset. A shallow SRD and subretinal deposits can be seen in the macula. **B:** FA + IA in the left eye (15 minutes): Diffuse hyperfluorescence (FA) and choroidal hyperpermeability (IA) are noted in and inferior to the fovea centralis. An atrophic tract is observed in the inferior posterior pole. **C:** FA + OCT horizontal scan of the left eye, **D:** IR + EDI-OCT horizontal scan of the left eye: Thinning of the fovea and a flat large PED are visible. There is choroidal thickening throughout the entire posterior pole. In the sites where choroidal thickening is most significant, the anterior scleral border cannot be seen. **E:** 1 µm SS-OCT of the left eye: Choroidal thickening and a weakly reflective cavity (→) between the sclera and choroid are clearly visible over the entire macular area.

Image interpretation points

This is a case of chronic CSC with recurrence in both eyes for 5 years. In this current presentation, the initial diagnosis was 6 months after onset of symptoms. The extent of the choroidal thickening could be clearly visualized using 1 µm SS-OCT (swept source OCT).

A weakly reflective cavity exists between the anterior scleral border and posterior choroid, and choroidal thickening in that area is significant. The RPE appears to be pushed forward by the choroidal thickening. Three months after initial diagnosis, the SRD has spontaneously regressed but the choroidal thickening remains.

Case 75 Chronic central serous chorioretinopathy: A case of recurrence

A 52-year-old female, OD, BCVA 0.9

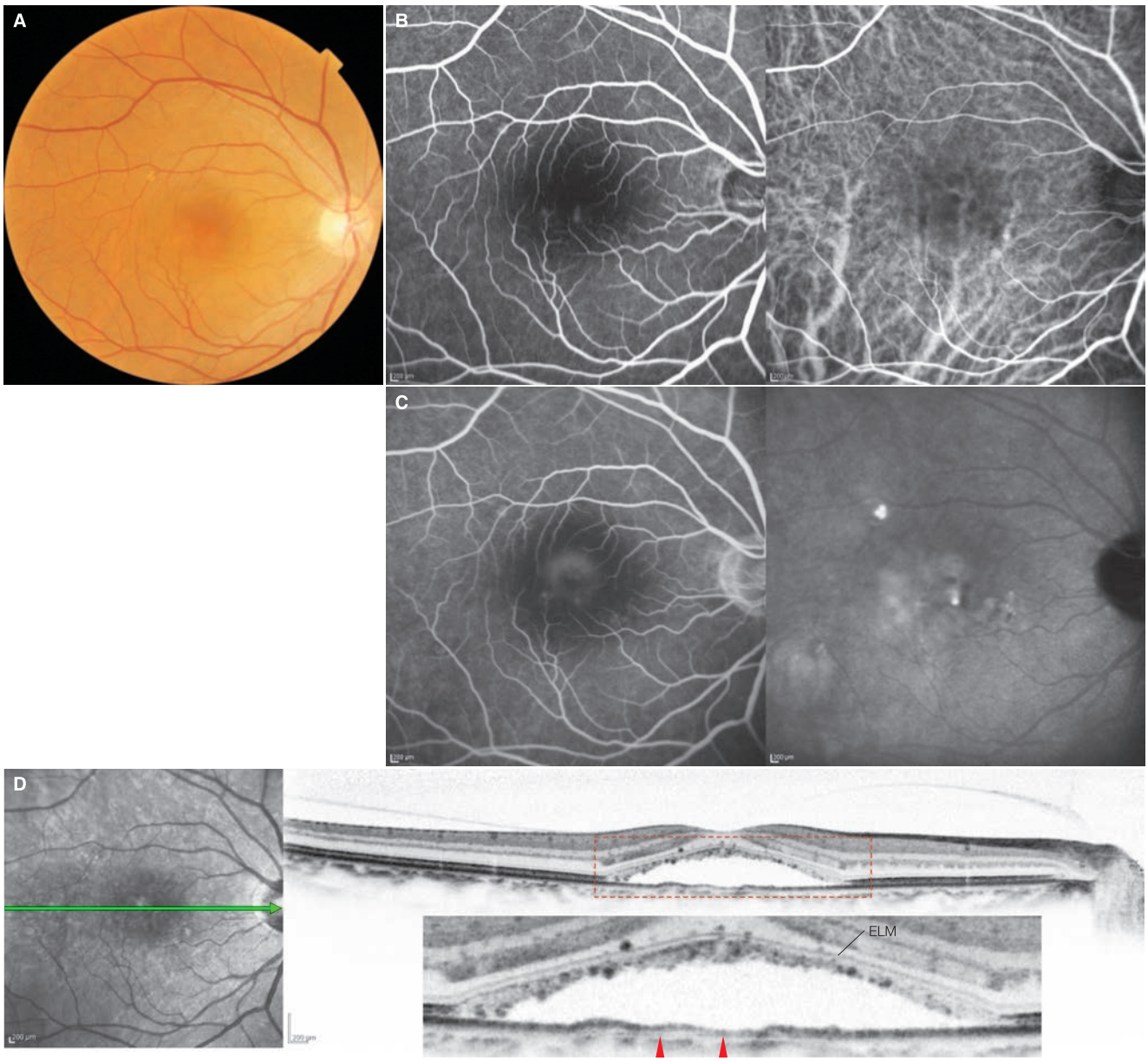

A: Color fundus photograph in the right eye: During initial diagnosis. One week after onset. SRD 1.5 times the diameter of the optic disc can be seen. **B:** FA + IA in the right eye (1 minute): During initial diagnosis. A leakage point visible on the inferior nasal side of the fovea centralis. **C:** FA + IA in the right eye (11 minutes): Mild smoke-stack pattern leakage can be seen. **D:** IR + OCT horizontal scan of the right eye + enlarged version [red dashed box]: During initial diagnosis. Uneven thickness and irregular posterior surface of the photoreceptor OS are already noticeable in the detached retina, and punctate highly reflective dots exist in the internal margin of the ELM and in the photoreceptor OS. A flat PED can be seen over the entire fovea centralis. (▶) indicates Bruch's membrane

(Continued on the next page)

Case 75 Continuation

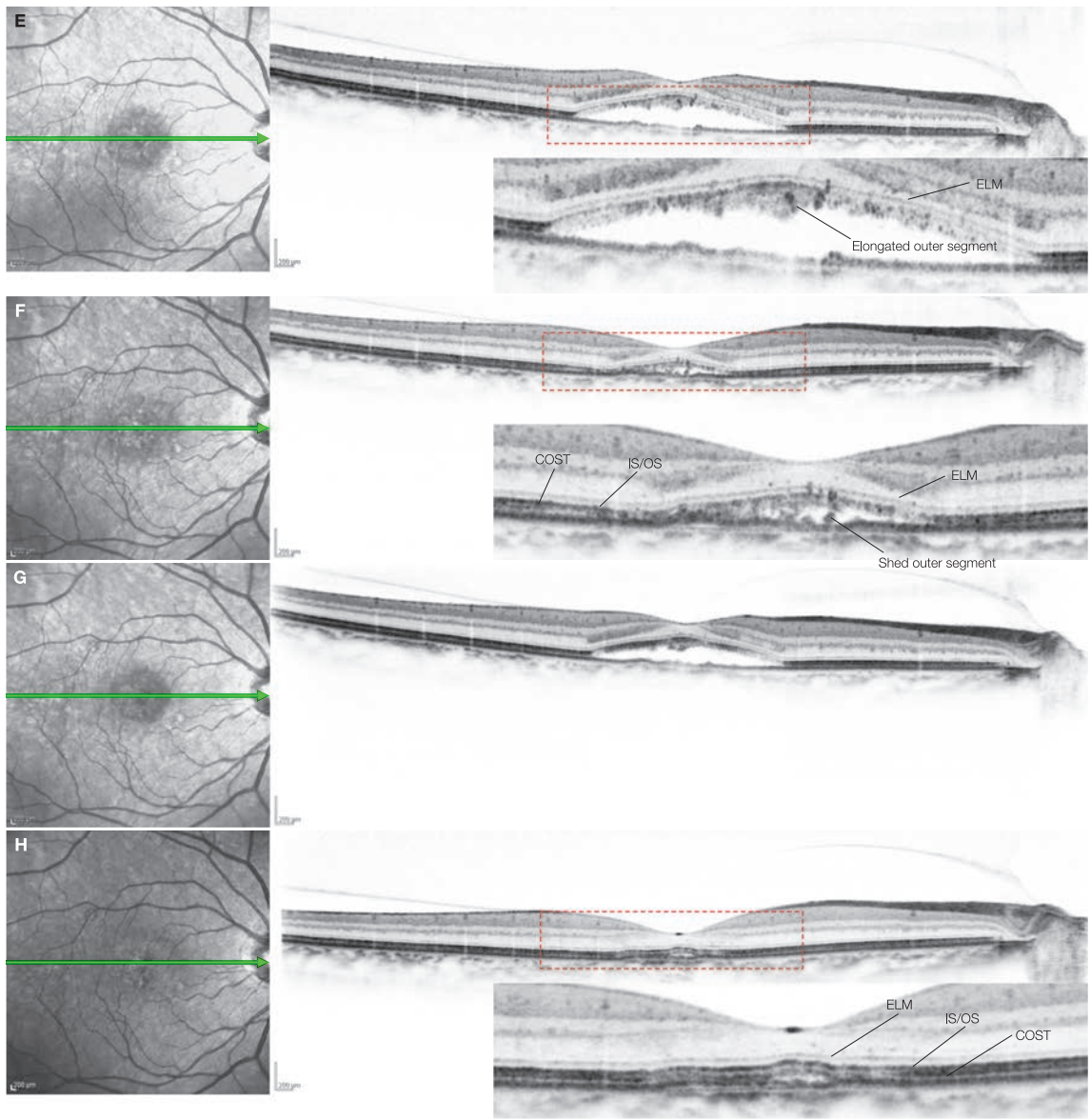

E: IR + OCT horizontal scan of the right eye + enlarged version [red dashed box]: Three months after initial diagnosis. Best-corrected visual acuity is 1.0. There is no remission of the SRD, and elongation of the foveal OS is significant. **F:** IR + OCT horizontal scan of the right eye + enlarged version [red dashed box]: Ten months after initial diagnosis. Best-corrected visual acuity is 1.5. The SRD that initially showed no remission for 7 months after initial diagnosis has started to recede. The elongated foveal photoreceptor OS has shed and deposited on the RPE. The reattached IS/OS is distinct, but the COST line remains lost. **G:** IR + OCT horizontal scan of the right eye: 12 months after initial diagnosis. Best-corrected visual acuity is 1.2. Recurrent exacerbation of the SRD. Hyperreflectivity of the photoreceptor outer segment is noted. **H:** IR + OCT horizontal scan of the right eye + enlarged version [red dashed box]: 14 months after initial diagnosis. Best-corrected visual acuity is 1.2. The SRD has almost disappeared, and the foveal IS/OS and COST lines have been restored, but they are still irregular.

Image interpretation points

This was a case of prolonged SRD over approximately 14 months, where there was repeated episodes of remission and exacerbation. The patient became aware of metamorphopsia one week prior to being referred, but the irregular form of the photoreceptor OS suggested the SRD was not a recent event. Elongation of the foveal photoreceptor OS, and OS tip shedding and deposition on the RPE were also observed.

Long-term abnormalities were seen in the foveal photoreceptor OS, but the IS/OS and COST lines were quickly restored after reattachment 14 months after initial diagnosis, therefore maintaining good visual acuity. There are cases where visual acuity is good despite a long detachment period as in this case. It appears that simply the length of the detachment period is not the only cause of poor visual prognosis.

Case 76 Chronic central serous chorioretinopathy: Changes in the photoreceptor outer segment

Right eye of a 41-year-old male with vision corrected to 0.8

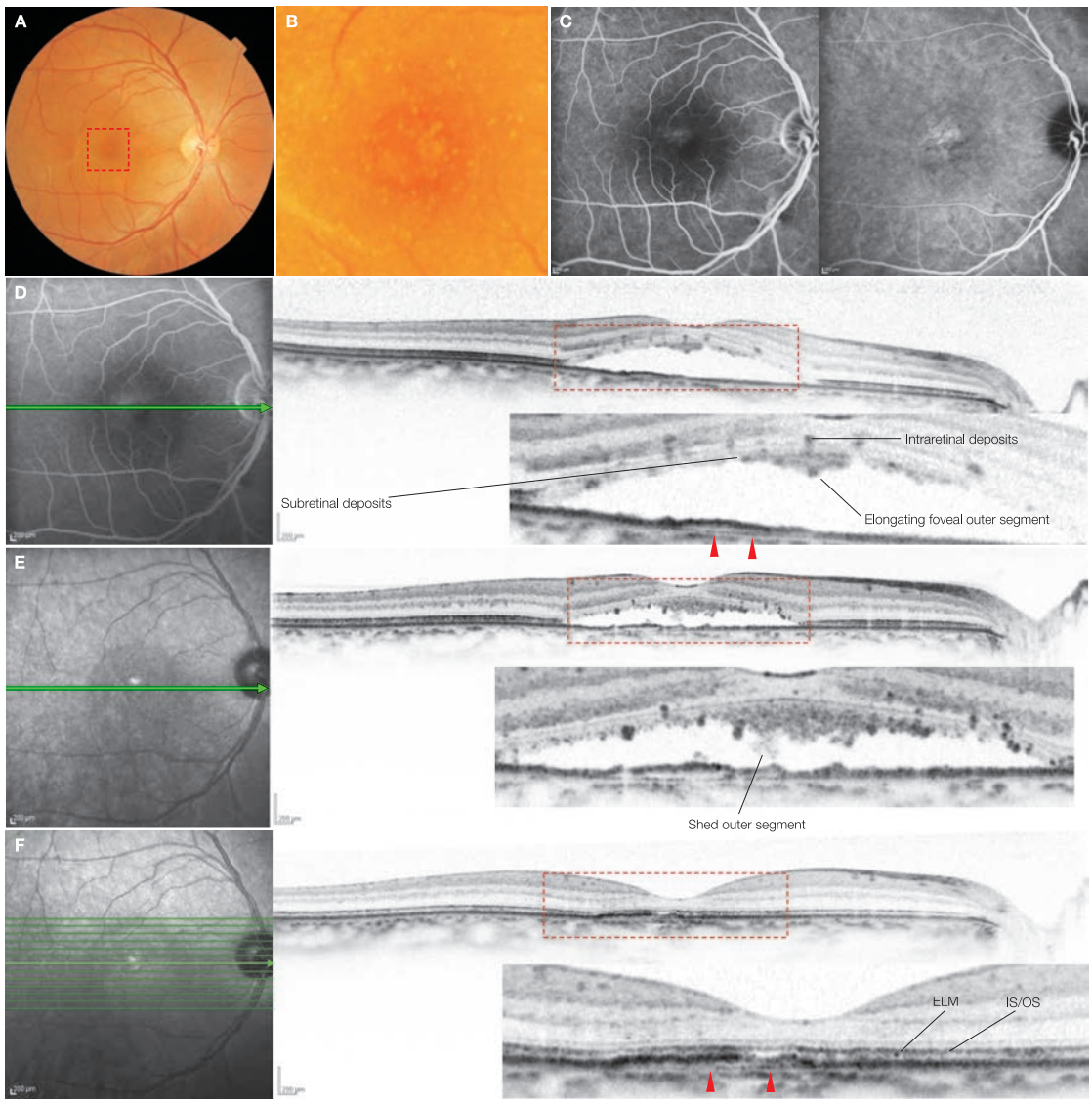

A: Color fundus photograph in the right eye: During initial diagnosis. Four months after onset. A SRD two times the diameter of the optic disc is noted. **B:** Enlarged version of A [red dashed box]: Subretinal deposits are visible in the fovea centralis. **C:** FA + IA in the right eye (11 minutes): During initial diagnosis. Weak leakage can be observed in the superior fovea centralis. ICG stains abnormally due to choroidal hyperpermeability in the fovea centralis. **D:** IR + OCT horizontal scan of the right eye + enlarged version [red dashed box]: During initial diagnosis. SRD is seen. Highly reflective OS and dots corresponding to foveal OS elongation and subretinal deposits on fundus photographs, respectively, are seen. A flat PED can be seen. (►) indicates Bruch's membrane. **E:** IR + OCT horizontal scan of the right eye + enlarged version [red dashed box]: Seven months after initial diagnosis. Best-corrected visual acuity is 0.9. There is exacerbation of the amount of foveal OS elongation and sub- and intraretinal deposits. Shedding of the OS has started. **F:** IR + OCT horizontal scan of the right eye + enlarged version [red dashed box]: Two years and 6 months after initial diagnosis. The IS/OS line has been restored, but thinning is evident in the fovea centralis, and the COST line has not recovered over a wide macular area. (►) indicates Bruch's membrane. Best-corrected visual acuity is 1.0.

Image interpretation points

This was a case of chronic CSC where 4 months had passed since initial diagnosis, and significant changes could be seen in the foveal photoreceptor OS, although relatively good visual acuity was maintained. The area of leakage was within the fovea centralis, and upon follow-up 8 months after initial diagnosis, the SRD disappeared. Eleven months after initial diagnosis, the SRD recurred, but disappeared again at 13 months, with no subsequent recurrences. Foveal thinning was observed and although the COST had not been restored, the IS/OS line had clearly been restored despite being irregular. Resolution of good visual acuity occurred as well.

Case 77 Chronic central serous chorioretinopathy: Example of poor visual acuity

A 70-year-old male, OS, BCVA 0.1

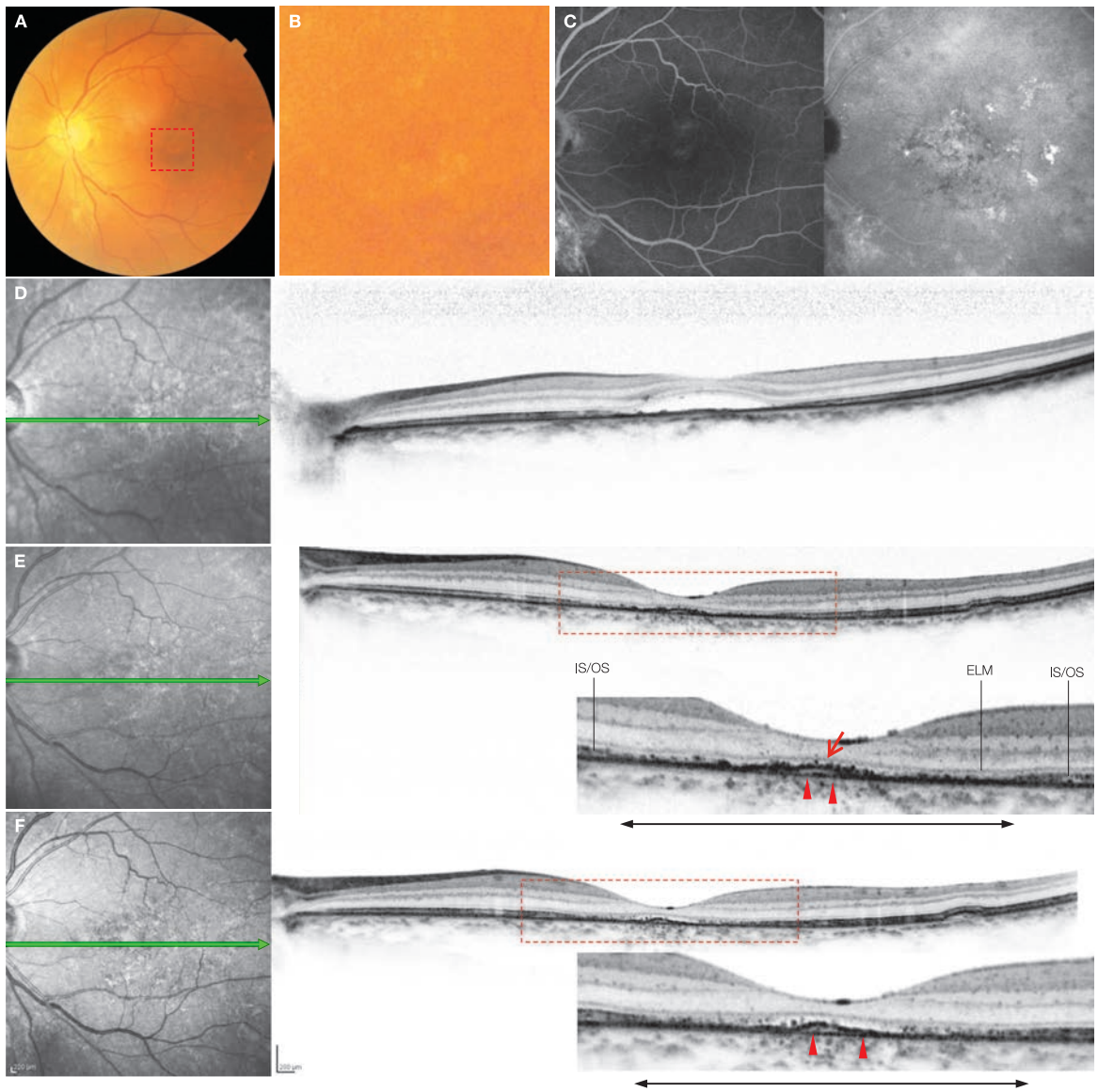

A: Color fundus photograph in the left eye: During initial diagnosis. Four years after onset. SRD with the diameter of one optic disc and foveal subretinal deposits are visible. **B:** Enlarged version of A [red dashed box]: A decrease in RPE pigment of the fovea centralis is observed. **C:** FA + IA in the left eye (14 minutes): During initial diagnosis. Diffuse, weak fluorescein leakage is seen in the fovea centralis. ICG stains abnormally due to choroidal hyperpermeability over a wide area of the posterior pole. **D:** IR + OCT horizontal scan of the left eye + enlarged version [red dashed box]: During initial diagnosis. A flat SRD can be seen. **E:** IR + OCT horizontal scan of the left eye + enlarged version [red dashed box]: Two months after initial diagnosis. The SRD has disappeared. Best-corrected visual acuity has improved to 0.6. The fovea centralis is thin and the IS/OS and COST lines within the (↔) area of the macula have been lost. Reactive hyperplasia (➔) of the RPE can be seen. (►) indicates Bruch's membrane. **F:** IR + OCT horizontal scan of the left eye + enlarged version [red dashed box]: Six months after initial diagnosis. Thinning of the fovea centralis has progressed further; IS defects are noted, and best-corrected visual acuity has once again decreased to 0.1. Almost no restoration of the IS/OS and COST lines can be seen within the (↔) area. (►) indicates Bruch's membrane

Image interpretation points

This is a case of chronic CSC that has caused severe foveal destruction. The patient became aware of metamorphopsia and visual impairment approximately 4 years prior to diagnosis. During initial diagnosis, choroidal hyperpermeability was seen over a wide area, and significant abnormalities were visible in the RPE. One month after initial diagnosis, reattachment was achieved after performing PDT. With time, extensive foveal thinning as well as IS/OS and COST line disappearance became apparent. It is notable that foveal thinning and visual acuity loss progressed even after reattachment.

Case 78 Acute bullous retinal detachment: A typical example

A 56-year-old male, OU, BCVA 1.5 OD and 0.9 OS

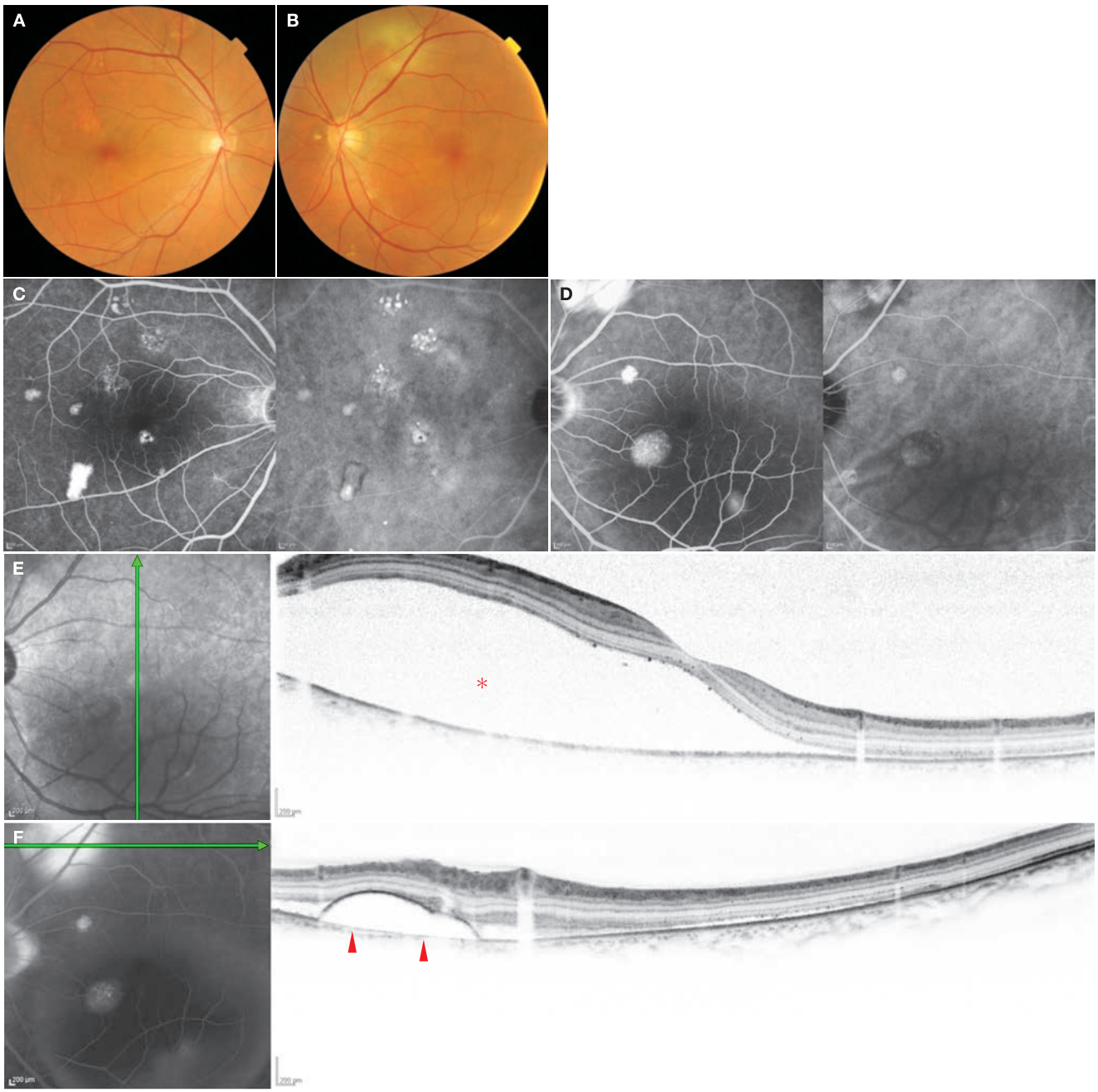

A: Color fundus photograph in the left eye, **B:** Color fundus photograph in the left eye: Multiple PEDs are seen in both eyes. Yellowish-white fibrin deposits are visible on the superior arcade of the left eye. **C:** FA + IA in the right eye (8 minutes), **D:** FA + IA in the left eye (15 minutes): Multiple PEDs are evident in both eyes. Significant fluorescein leakage from the PED is noted above the optic disc of the left eye. **E:** IR + OCT vertical scan of the left eye: A large SRD (*) can be seen within the macula extending inferiorly. **F:** FA + OCT horizontal scan of the left eye: Note a large dome-shaped PED in the site of significant fluorescein accumulation. (▶) indicates Bruch's membrane

Image interpretation points

Bullous retinal detachment differs from CSC in that there are many (frequently more than 3) PEDs. The patient became aware of reduced visual acuity in the left eye 17 days before initial diagnosis. Twenty days after initial diagnosis, PDT was performed on the left eye and the SRD disappeared and visual acuity improved to 1.5. There was no recurrence after 2 years.

Age-related macular degeneration

6.1 Drusen – 153

6.2 Pigment epithelial detachment – 155
6.2.1 References – 156

Case 79 Soft drusen: A typical example – 157

Case 80 Soft drusen: Fused drusen – 158

Case 81 Cuticular drusen combination vitelliform detachment – 159

Case 82 Cuticular drusen: Fellow eye of case 81 – 160

Case 83 Reticular pseudodrusen: Fellow eye of RAP – 161

Case 84 Reticular pseudodrusen: Case with atrophic age-related macular degeneration (atrophic AMD) – 162

Case 85 Reticular pseudodrusen and soft drusen – 163

Case 86 Serous pigment epithelial detachment: Case without CNV – 164

Case 87 Pigment epithelial detachment: Reactive proliferation of retinal pigment epithelial cells – 165

Case 88 Drusenoid PED: Case where CNV is suspected – 166

Case 88 17 months later – 167

Case 89 Large pigment epithelial detachment: Case where CNV is suspected – 168

Case 90 Pigment epithelial detachment: Case with type 1 CNV ① – 169

Case 91 Pigment epithelial detachment: Case with type 1 CNV ② – 170

Case 92 Large pigment epithelial detachment: Case where CNV is present – 171

Case 92 Continuation – 172

6.3 Atrophic age-related macular degeneration – 173
6.3.1 References – 175

Case 93 Atrophic age-related macular degeneration: A typical example – 176

Case 94 Atrophic age-related macular degeneration: Atrophic lesions of various sizes – 177

Case 95 Atrophic age-related macular degeneration: Fellow eye of PCV – 178

6.4 Choroidal neovascularization and exudative age-related macular degeneration – 179

6.4.1 References – 180

Case 96 Exudative age-related macular degeneration: Type 1 CNV with a SRD – 181

Case 97 Exudative age-related macular degeneration: Type 1 CNV with low activity – 182

Case 98 Exudative age-related macular degeneration: Type 1 CNV with relatively strong exudative changes – 183

Case 98 Six months later – 184

Case 99 Exudative age-related macular degeneration: Case with extensive Type 1 and 2 CNV exudative changes – 185

Case 99 Six months after treatment with anti-VEGF treatment – 186

Case 100 Exudative age-related macular degeneration: Type 1 and 2 CNV with extensive serous retinal detachment – 187

Case 101 Exudative age-related macular degeneration: Type 1 and 2 CNV with cystic changes – 188

Case 102 Exudative age-related macular degeneration: Type 2 CNV localized in the fovea centralis – 189

Case 103 Exudative age-related macular degeneration: Type 2 CNV with strong exudative changes – 190

6.5 Polypoidal choroidal vasculopathy – 191

6.5.1 References – 193

Case 104 Polypoidal choroidal vasculopathy: Small lesions – 194

Case 105 Polypoidal choroidal vasculopathy: Case confused with central serous chorioretinopathy – 195

Case 105 After treatment with anti-VEGF formulation – 196

Case 106 Polypoidal choroidal vasculopathy: Fibrin deposits ① – 197

Case 107 Polypoidal choroidal vasculopathy: Fibrin deposits ② – 198

Case 108 Polypoidal choroidal vasculopathy: A large branching vascular network – 199

Case 109 Polypoidal choroidal vasculopathy: Large foveal cystoid space – 200

Case 109 Enlargement of hemorrhagic pigment epithelial detachment – 201

Case 109 Enlargement of the branching vascular network – 202

Case 110 Polypoidal choroidal vasculopathy: A large hemorrhagic pigment epithelial detachment ① – 203

Case 111 Polypoidal choroidal vasculopathy: A large hemorrhagic pigment epithelial detachment ② – 204

Case 111 Spontaneous remission – 205

Case 112 Polypoidal choroidal vasculopathy: Optic disc type – 206

Case 112 Continuation – 207

Case 113 Polypoidal choroidal vasculopathy: Polypoidal lesions and pigment epithelial detachment – 208

Case 114 Polypoidal choroidal vasculopathy: Tomographic notch sign – 209

Case 115 Polypoidal choroidal vasculopathy: Case where the branching vascular network has detached – 210

Case 116 Polypoidal choroidal vasculopathy: A massive lesion – 211

6.6 Retinal angiomatous proliferation – 212

6.6.1 References – 213

Case 117 Retinal angiomatous proliferation: Stage 1 – 214

Case 118 Retinal angiomatous proliferation: Stage 2A – 215

Case 119 Retinal angiomatous proliferation: Stage 2B ① – 216

Case 120 Retinal angiomatous proliferation: Stage 2B ② – 217

Case 121 Retinal angiomatous proliferation: Stage 3 – 218

Case 121 After treatment with anti-VEGF treatment – 219

6.7 Malattia leventinese – 220

6.7.1 References – 220

Case 122 Malattia leventinese: A typical example – 221

6.8 Idiopathic choroidal neovascularization – 223

6.8.1 References – 223

Case 123 Idiopathic choroidal neovascularization: A fresh case – 224

Case 124 Idiopathic choroidal neovascularization: Envelopment by RPE cells – 225

Case 124 After treatment with anti-VEGF formulation – 226

Case 125 Idiopathic choroidal neovascularization: The scarring process – 227

Case 125 Course without treatment – 228

6.1 Drusen

Background

Drusen are the general term for small, round, yellowish-white slightly elevated lesions that can be seen in the ocular fundus as a result of age-related changes. Drusen are generally classified into soft drusen and hard drusen where soft drusen are a significant risk factor of age-related macular degeneration (AMD) along with hyperpigmentation of the retinal pigment epithelium (RPE)[1–3]. There are peculiar forms of drusen, such as cuticular drusen (formerly known as basal laminar drusen) and reticular pseudodrusen.

Soft drusen and hard drusen

Various classifications are used for drusen, among which the classification based on drusen size (soft drusen v.s. hard drusen) has been most commonly used. If the diameter of the drusen is 63 μm or above (with the diameter of the vein entering the optic disc margin at 125 μm as a reference), they are soft drusen. Below this size they are classified as hard drusen[4]. As they are differentiated by size alone, there is no actual difference between soft and hard drusen.

OCT findings

As shown in ◘ Fig. 6-1, soft drusen appear as protrusions of the RPE into the retina and as a straight thin line posterior to the elevated RPE (►) on OCT. This thin line is thought to be Bruch's membrane[5]. In general, when the RPE is elevated from Bruch's membrane [pigment epithelial detachment (PED) or drusen], the straight line of Bruch's membrane becomes clearly visible. In contrast, when there is no RPE elevation (the normal state), the line of Bruch's membrane is not delineated. Detecting Bruch's membrane line in this way can be considered an abnormal finding.

The space between the elevated RPE and Bruch's membrane corresponds to the contents of the drusen. As shown in ◘ Fig. 6-1, the contents are sometimes moderately reflective and sometimes barely reflective at all.

Drusenoid PED

Large soft drusen cannot be distinguished from PED on biomicroscopic or OCT observation. Confluent large soft drusen are known as drusenoid PED. Drusenoid PED is frequently accompanied by choroidal neovascularization (CNV). It should be noted that, in cases of drusenoid PED, serous retinal detachment (SRD) can be seen below the sensory retina between large drusen. These findings do not indicate the presence of CNV, but are instead due to the retina being lifted up by the drusen[6]. According to the International Classification of AMD, eyes with multiple soft drusen are diagnosed as having early ARM (early age-related maculopathy) and can easily develop exudative or atrophic AMD.

Cuticular drusen

Cuticular drusen (also basal laminar drusen) are another specific kind of drusen. These drusen are relatively rare in Japan but can be seen in cases of familial drusen (malattia leventinese). Countless hyperfluorescent dots are distinctive findings that can be seen on FA imaging (milky-way or stars-in-the-sky). The location of these drusen is beneath the RPE, which is the same as typical drusen. The cause of these small hyperfluorescent dots on FA is likely damages to the RPE cells as a result of steep protrusion of drusen into the RPE. These damaged sites exhibit hyperfluorescence due to window defects. Since Japanese people sometimes have a high melanin content in their RPE cells, stars-in-the-sky findings are not seen so often.

In typical cases, small, steep protrusions in the RPE known as »sawtooth figure« are visible on OCT. The case shown in ◘ Fig. 6-2 is of familial drusen where countless small, hyperfluorescent dots are scattered around the foveal lesions. When observed with OCT, these protruding lesions can be seen spreading not only to the outer nuclear and outer plexiform layer but also to the inner nuclear layer.[7, 8]. Cuticular drusen can cause vitelliform detachment (yolk-like retinal detachment)[9, 10].

Reticular pseudodrusen

In recent years, reticular pseudodrusen (or reticular drusen) have become a topic of interest. According to a report on a Beaver Dam study, the prevalence at baseline of these drusen was 0.7% of the total population, more common in women than in men, and the cumulative incidence over 15 years was 3%[11]. The presence or absence of reticular drusen was determined with only fundus photographs in this study, however, the frequency of identification may have been even higher if fundus autofluorescence or OCT had been used. The importance of this type of drusen has been growing with the increase in elderly individuals.

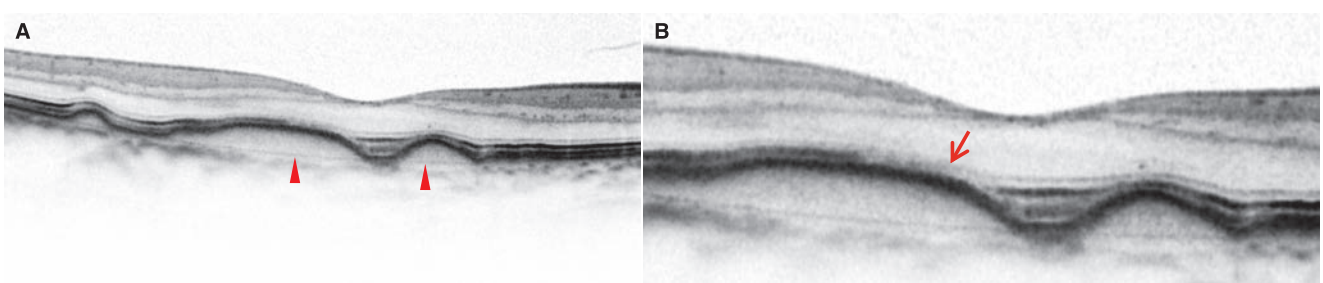

◘ **Fig. 6-1** OCT image of typical drusen
A: Drusen is seen as protrusions of the RPE. (►) indicates Bruch's membrane. **B:** Enlarged version of A. Part of the photoreceptor inner and outer segment junction on the drusen is becoming indistinct (➔) and the outer retinal layers on the drusen are atrophic.

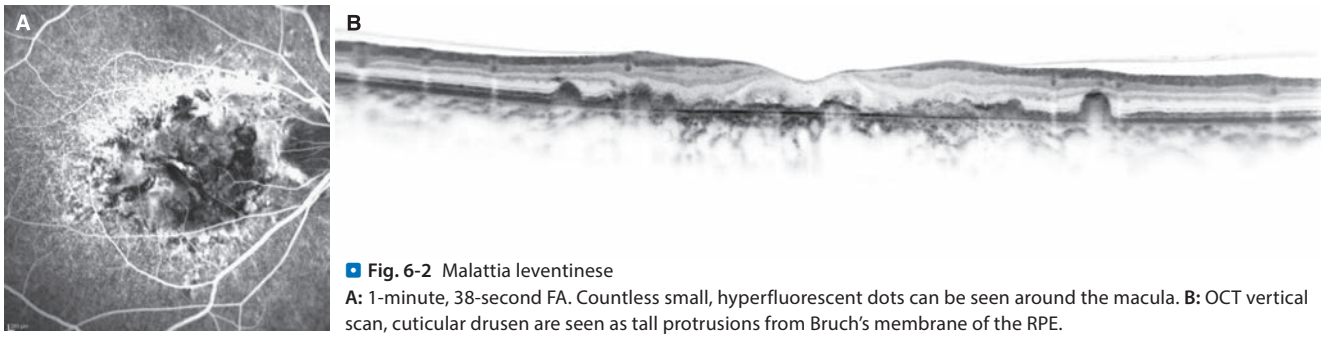

Fig. 6-2 Malattia leventinese
A: 1-minute, 38-second FA. Countless small, hyperfluorescent dots can be seen around the macula. **B:** OCT vertical scan, cuticular drusen are seen as tall protrusions from Bruch's membrane of the RPE.

Reticular pseudodrusen have been documented for a long time, but their properties have become clearer with characterization based on OCT findings[8]. In OCT images, deposits on the apical side of RPE can be seen as triangular shapes, which differ from typical drusen (Fig. 6-3). Zweifel et al. have divided reticular pseudodrusen into three stages based on these OCT findings (Fig. 6-4)[12]. Reticular pseudodrusen are considered closely associated with the onset of exudative and atrophic AMD.

Reticular drusen can occur in combination with normal pseudodrusen.

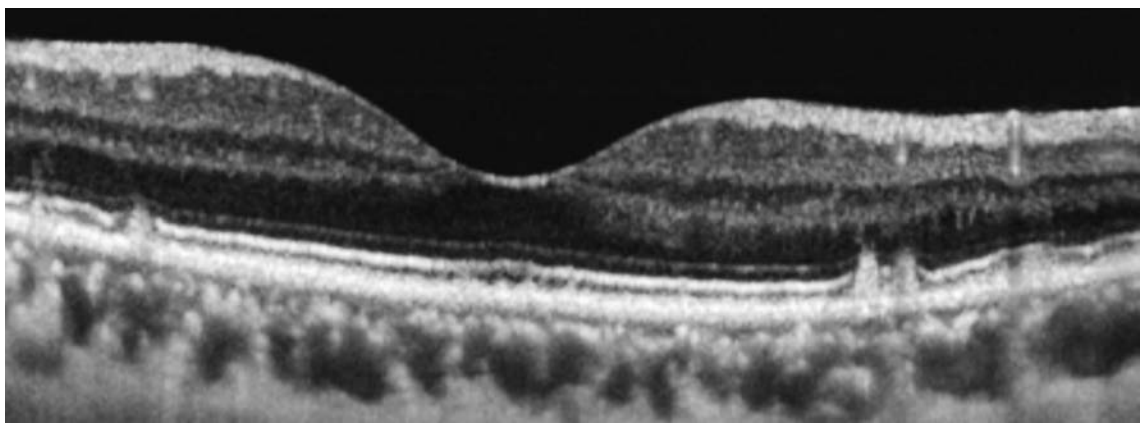

Fig. 6-3 Reticular pseudodrusen
Highly reflective deposits are seen between the RPE and sensory retina. Stage 1 reticular pseudodrusen can be seen in the fovea centralis and two Stage 3 reticular pseudodrusen can be seen to the right of the fovea. This image was acquired with a 1,050 nm wavelength prototype swept-source OCT.

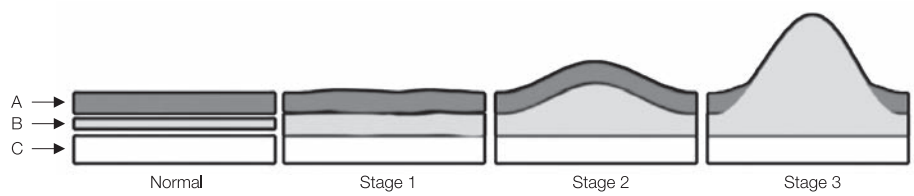

Fig. 6-4 Stage classification of reticular pseudodrusen
A is the photoreceptor inner and outer segment junction (IS/OS) line, B is the COST line, and C indicates the RPE. In Stage 1, deposits do not push up the line of the IS/OS line. In Stage 2 the IS/OS line is pushed up into the retina. In Stage 3 the deposits pass through this line.
(Modified according to Zweifel SA, et al. Reticular pseudodrusen are subretinal drusenoid deposits. Ophthalmology. 2010; 117: 303-312)

6.2 Pigment epithelial detachment

Pigment epithelial detachment (PED) is the state in which the RPE detach from Bruch's membrane between the RPE basal lamina and inner collagen fiber layer of Bruch's membrane. The origin of the fluid accumulated between the detached RPE and Bruch's membrane is thought to be the choroid according to Gass's theory[2], and the sensory retina according to Bird and Marshall's theory[13]. When CNV is present, CNV itself and exudations derived from CNV are depicted in OCT images as an origin of the fluid.

The report by Hartnett et al. is well known as a traditional classification for PED[14]. In this classification, PED is divided into pseudo-vitelliform PED, confluent drusen, serous PED, vascular PED, hemorrhagic PED and retinal vascular abnormality; here vascular PED and hemorrhagic PED can be considered the same. PED accompanied by retinal vascular abnormality is currently described as PED accompanied by retinal angiomatous proliferation (RAP). According to this report, visual prognosis varies greatly based on the type of PED. All cases of PED accompanied by vascular PED, hemorrhagic PED, and RAP eventually become scar lesions. On the other hand, the prognosis for pseudo-vitelliform PED and confluent drusen is relatively good, whereas serous PED falls into an intermediate category of prognosis (Table 6-1).

PED accompanied by polypoidal choroidal vasculopathy (PCV) is also significant in Japan. About half the cases of PCV are known to have PED during initial diagnosis[15]. Fig. 6-5 is PED seen in PCV. Two successive PEDs can be seen, but the reflectivity inside the two PEDs differs greatly. The PED on the left is weakly reflective and the adjacent one on the right is moderately reflective. In general, the content of a PED exhibiting low reflectivity on OCT is not fibrovascular, whereas the content of a PED exhibiting moderate or high reflectivity is considered fibrovascular. Given its high reflectivity, the PED on the right side of this image is thought to have CNV (Fig. 6-5).

Table 6-1 Classification and natural course of pigment epithelial detachment

Type of PED	Outcome			Follow-up period
	Unchanged	Atrophic lesions	Scar lesions	
Pseudo-vitelliform PED	40%	60%	0%	21 months
Confluent drusen	22%	65%	9%	41 months
Serous PED	28%	38%	34%	30 months
Vascular PED	0%	0%	100%	36 months
Hemorrhagic PED	0%	0%	100%	14 months
Retinal vascular abnormality	0%	0%	100%	Immediate laser treatment

(Modified according to Hartnett ME, et al. Classification of retinal pigment epithelial detachments associated with drusen. Graefes Arch Clin Exp Ophthalmol. 1992; 230: 11-19)

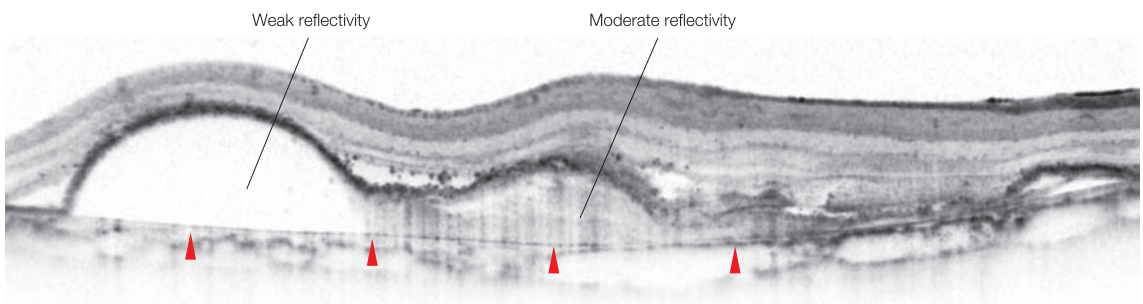

Fig. 6-5 PED and the reflectivity intensity of its contents
The contents of PEDs have various reflectivity intensities. In general, if it is weakly reflective, then no CNV is thought to exist, whereas in cases where moderate or high reflectivity is exhibited, CNV is thought to be present. In this figure, the right fibrovascular PED includes CNV. (►) indicates Bruch's membrane.

6.2.1 References

1) Gass JDM. Pathogenesis of disciform detachment of the neuroepithelium. III. Senile disciform macular degeneration. *Am J Ophthalmol*. 1967; 63:617–644.
2) Gass JD. Drusen and disciform macular detachment and degeneration. *Arch Ophthalmol*. 1973; 90:206–217.
3) The International ARM Epidemiology Study Group. An international classification and grading system for age-related maculopathy and age-related macular degeneration. *Surv Ophthalmol*. 1995; 39:367–374.
4) Klein R, Davis MD, Magli YL, et al. The Wisconsin age-related maculopathy grading system. *Ophthalmology*. 1991; 98:1128–1134.
5) Pircher M, Goetzinger E, Findl O, et al. Human macula investigated in vivo with polarization-sensitive optical coherence tomography. *Invest Ophthalmol Vis Sci*. 2006; 47:5487–5494.
6) Sikorski BL, Bukowska D, Kaluzny JJ, et al. Drusen with accompanying fluid underneath the sensory retina. *Ophthalmology*. 2011; 118:82–92.
7) Spaide RF, Curcio C. Drusen characterization with multimodal imaging. *Retina*. 2010; 30:1441–1454.
8) Souied EH, Leveziel N, Letien V, et al. Optical coherent tomography features of malattia leventinese. *Am J Ophthalmol*. 2006; 141:404–407.
9) Gass JD, Jallow S, Davis B. Adult vitelliform macular detachment occurring in patients with basal laminar drusen. *Am J Ophthalmol*. 1985; 99:445–459.
10) Freund KB, Laud K, Lima LH, et al. Acquired vitelliform lesions. correlation of clinical findings and multiple modality analyses. *Retina*. 2011; 31:13–25.
11) Klein R, Meuer SM, Knudtson MD, The epidemiology of retinal reticular drusen. *Am J Ophthalmol*. 2008; 145:317–326
12) Zweifel SA, Spaide RF, Curcio CA, et al. Reticular pseudodrusen are subretinal drusenoid deposits. *Ophthalmology*. 2010; 117:303–312.
13) Bird AC, Marshall J. Retinal pigment epithelial detachments in the elderly. *Trans Ophthalmol Sco U K*. 1986; 105:674–682.
14) Hartnett ME, Weiter JJ, Garsd A, et al. Classification of retinal pigment epithelial detachments associated with drusen. *Graefes Arch Clin Exp Ophthalmol*. 1992; 230:11–19.
15) Tsujikawa A, Sasahara M, Otani A, et al. Pigment epithelial detachment in polypoidal choroidal vasculopathy. *Am J Ophthalmol*. 2007; 143:102–111.

Case 79 Soft drusen: A typical example

A 63-year-old female, OD, BCVA 0.8

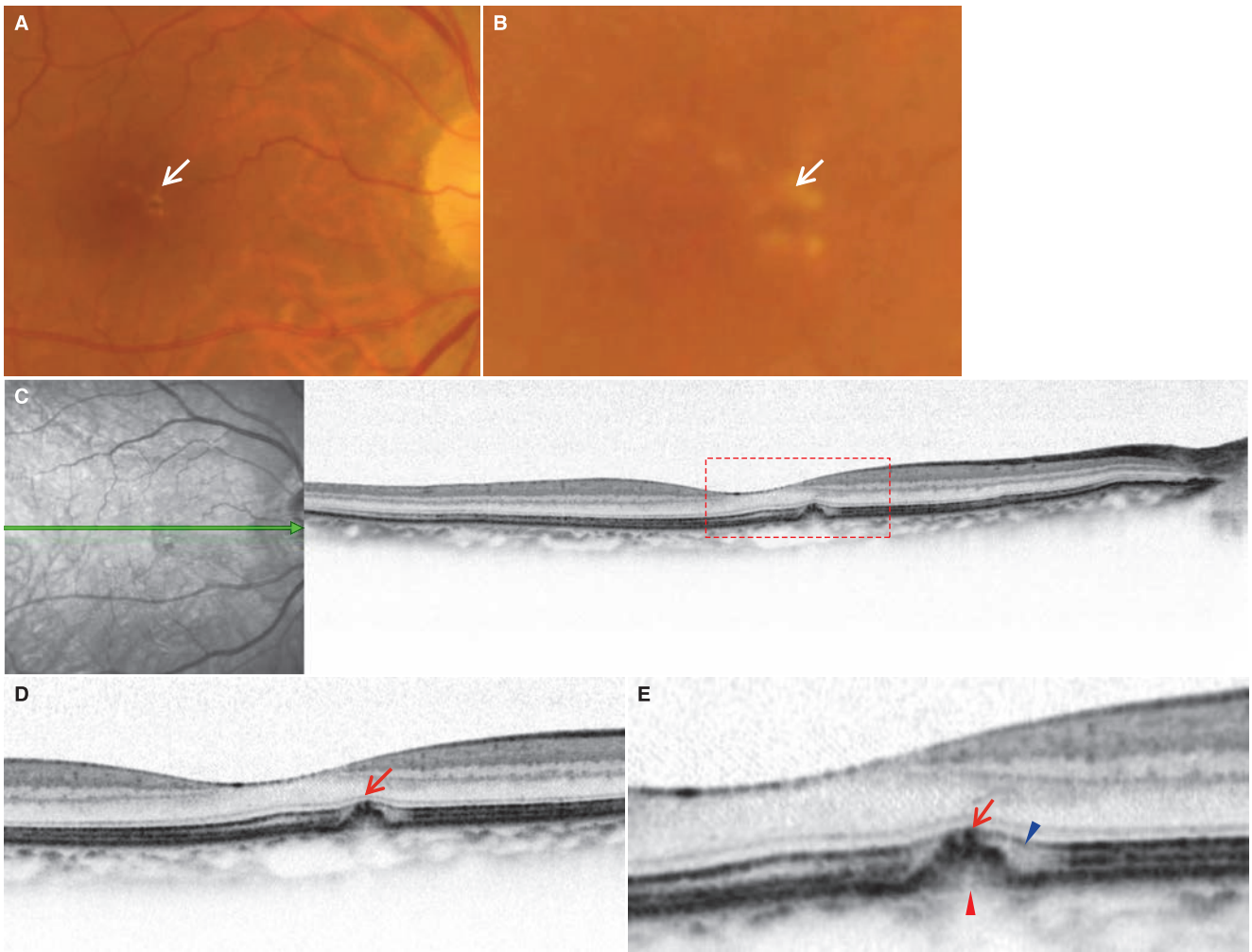

A: Color fundus photograph in the right eye, **B:** Enlarged version of A: Small drusen (⇛) can be seen. The diameter is larger than the diameter of the retinal vein that enters the optic disc, so they are soft drusen. **C:** IR + OCT horizontal scan of the right eye: The drusen can be seen as protrusions of the RPE. **D:** Enlarged version of C [red dashed box]: The RPE protrusions are clearly visible (➔). **E:** Even larger version of D: RPE proliferation (➔) in the apex of the drusen is visible. The RPE proliferation is in contact with the photoreceptor inner and outer segment junction (IS/OS). A part of the COST line is disrupting immediately nasal to the junction (►). The ELM is normal despite an anterior projection being visible. A reflectivity thought to be Bruch's membrane is only slightly visible at the base of the drusen (immediately above (►)).

Image interpretation points

This is a case of typical, small soft drusen. Drusen are frequent findings in aged patients. In this case a detailed observation with OCT allowed visualization of the disruption of COST line.

In addition, near the apex of the drusen, the gap between the IS/OS line and RPE is shortened. In this case, the inside of the drusen appear moderately reflective.

Case 80 Soft drusen: Confluent drusen

A 75-year-old male, OD, BCVA 0.8

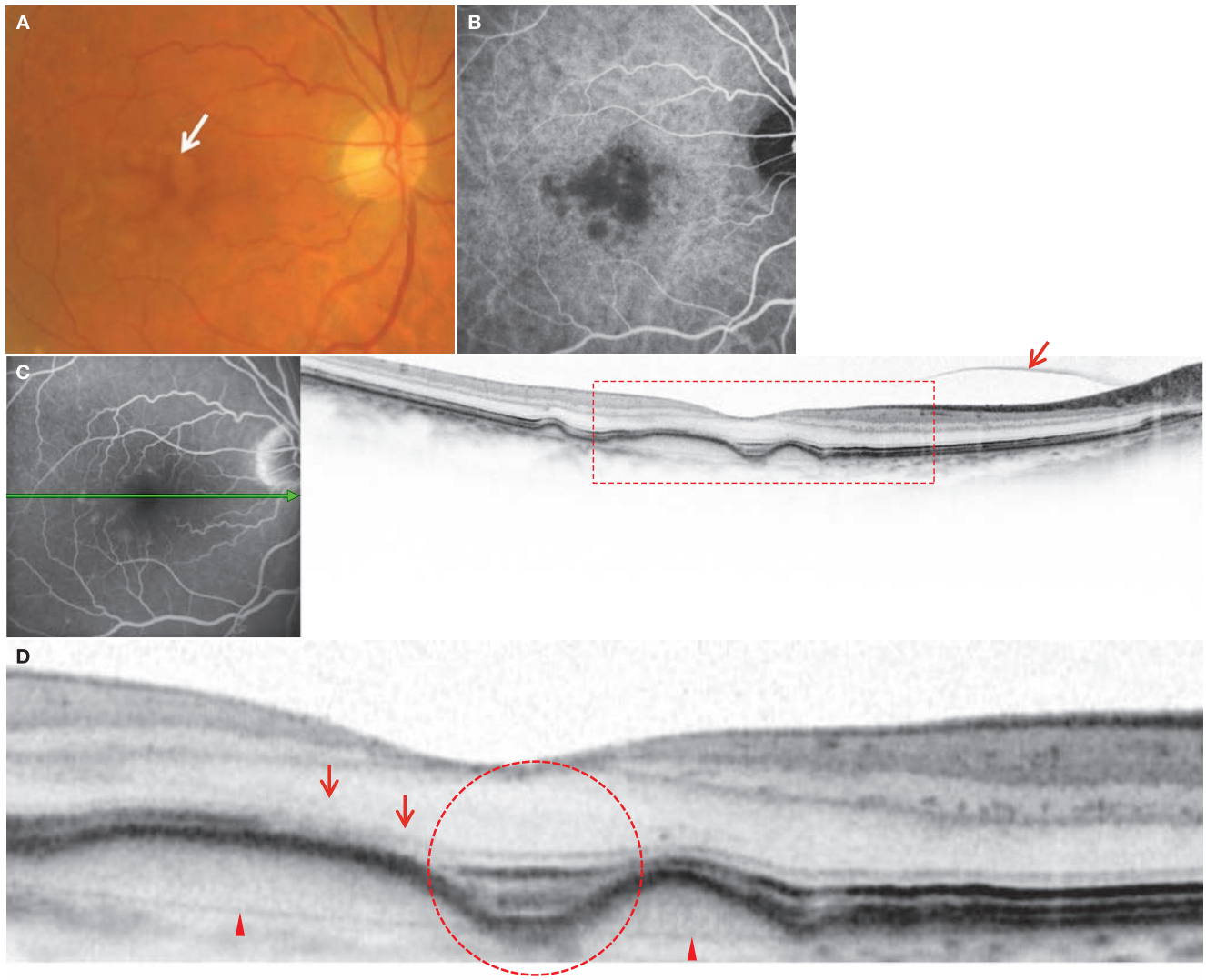

A: Color fundus photograph in the right eye: Large drusen are numerous (⇛). **B:** IA in the right eye (5 minutes): The drusen appear hypofluorescent on IA. CNV is not detected. **C:** FA + OCT horizontal scan of the right eye: The content of the drusen appears moderately reflective. The posterior vitreous cortex is visible (➔) **D:** Enlarged version of C [red dashed box]: A straight line representing Bruch's membrane is seen at the base of the drusen (►). Parts of the ELM, IS/OS and COST lines are disrupting in the apex of the drusen or the PED (➔). The outer retinal layer structure of the fovea centralis is being preserved as normal (red dashed circle).

Image interpretation points

Large drusen are pathologically the same as PED. In this case, damage to the outer retinal layers in contact with the apex of the temporal largest druse is noticeable even though visual acuity is somewhat preserved at 0.8. As shown in the red dashed circle in D, the may be due to the fact that the outer retinal layer structure in the fovea centralis is relatively healthy. While the content of the drusen is exhibiting fairly homogeneous moderate reflectivity, the presence of CNV is unlikely. This is consistent with CNV not being seen on IA.

Case 81 Cuticular drusen: Case with vitelliform detachment

A left eye of a 79-year-old female, OS, BCVA 1.2

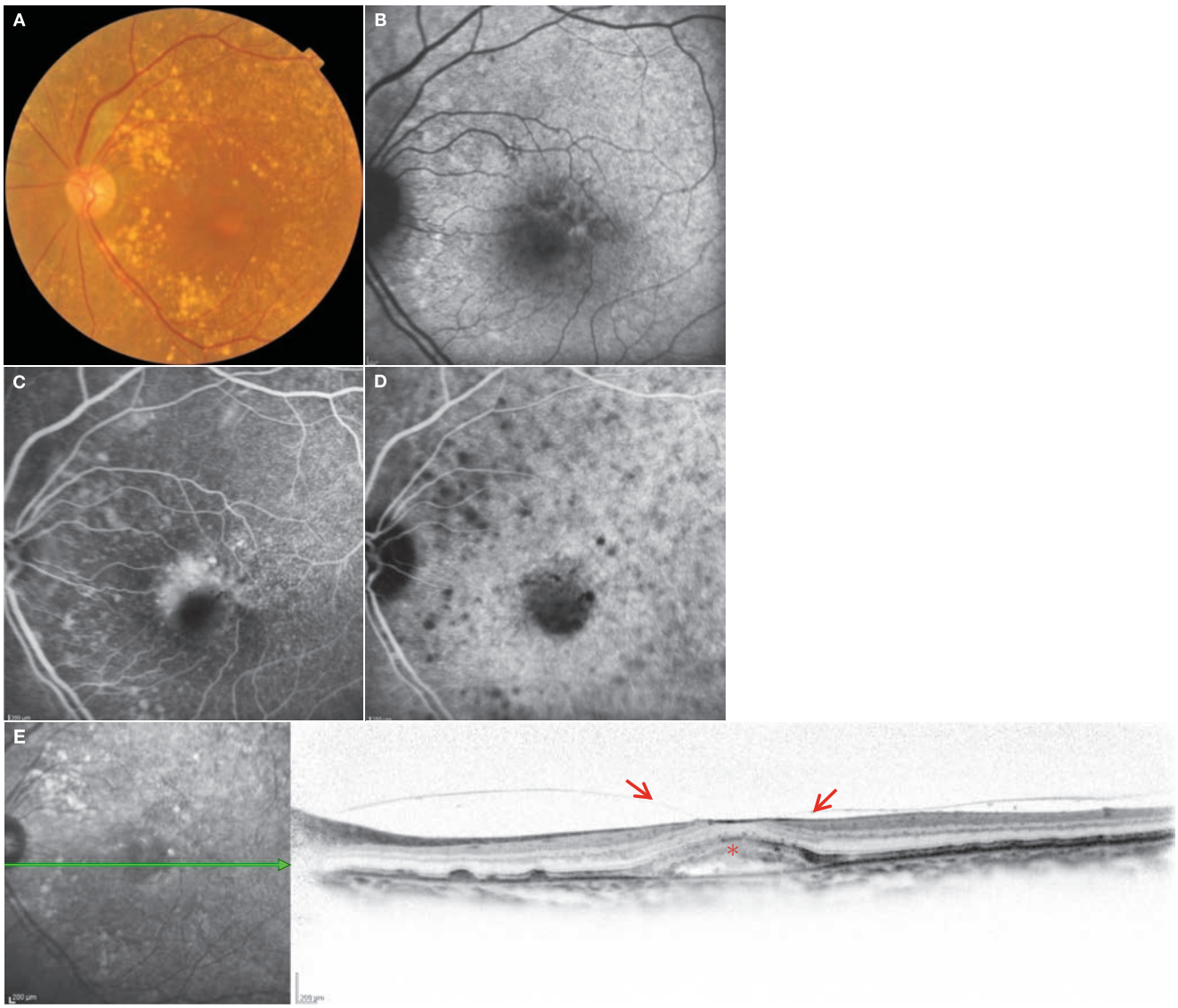

A: Color fundus photograph in the left eye: A accumulation of large soft drusen can be seen temporal to the optic disc. Yellow spots about 1/2 the diameter of the optic disc are present in the fovea centralis. Small soft drusen are scattered temporal to the fovea centralis. **B:** FAF in the left eye: Relatively strong hyperfluorescence is visible temporal to the fovea centralis. The fovea centralis is exhibiting round hypofluorescence, and small hypofluorescent foci are scattered around it. **C:** FA in the left eye (10 minutes, 18 seconds): Relatively strong hyperfluorescence can be seen nasal to the fovea centralis. Countless small hyperfluorescent dots are visible in the temporal macula, exhibiting a »stars-in-the-sky« image. **D:** IA in the left eye (10 minutes, 18 seconds): Hypofluorescence is observed in the inferior fovea, which looks like a niveau. Relatively large hypofluorescent foci and small hyperfluorescent foci are mixed together and scattered around the fovea centralis. **E:** IR + OCT horizontal scan of the left eye: Anterior centrifugal traction towards the fovea centralis as a result of the posterior vitreous cortex (➔) is appreciated (perifoveal PVD is occurring). The foveal retina has detached (vitelliform detachment) and a deposit, the result of shedding of the photoreceptor outer segment, can be seen (✻). Typical cuticular drusen images could not be appreciated with this scan.

Image interpretation points

Cuticular drusen were also referred to as basal laminar drusen. At one time, cuticular drusen were thought to occur due to nodular thickening of the RPE basal lamina, and their location was thought to differ from typical soft drusen. Later, it was revealed that both existed between the RPE basal lamina and Bruch's membrane, and that there were no differences in composition. Therefore, it is now common to use the term cuticular drusen. On fluorescein angiography (FA), cuticular drusen exhibit a distinctive pattern known as »stars-in-the-sky«. In addition, they can be combined with acquired vitelliform lesions, as seen in this case.

Case 82 Cuticular drusen: Fellow eye of case 81

A 79-year-old female, OD, BCVA 1.2

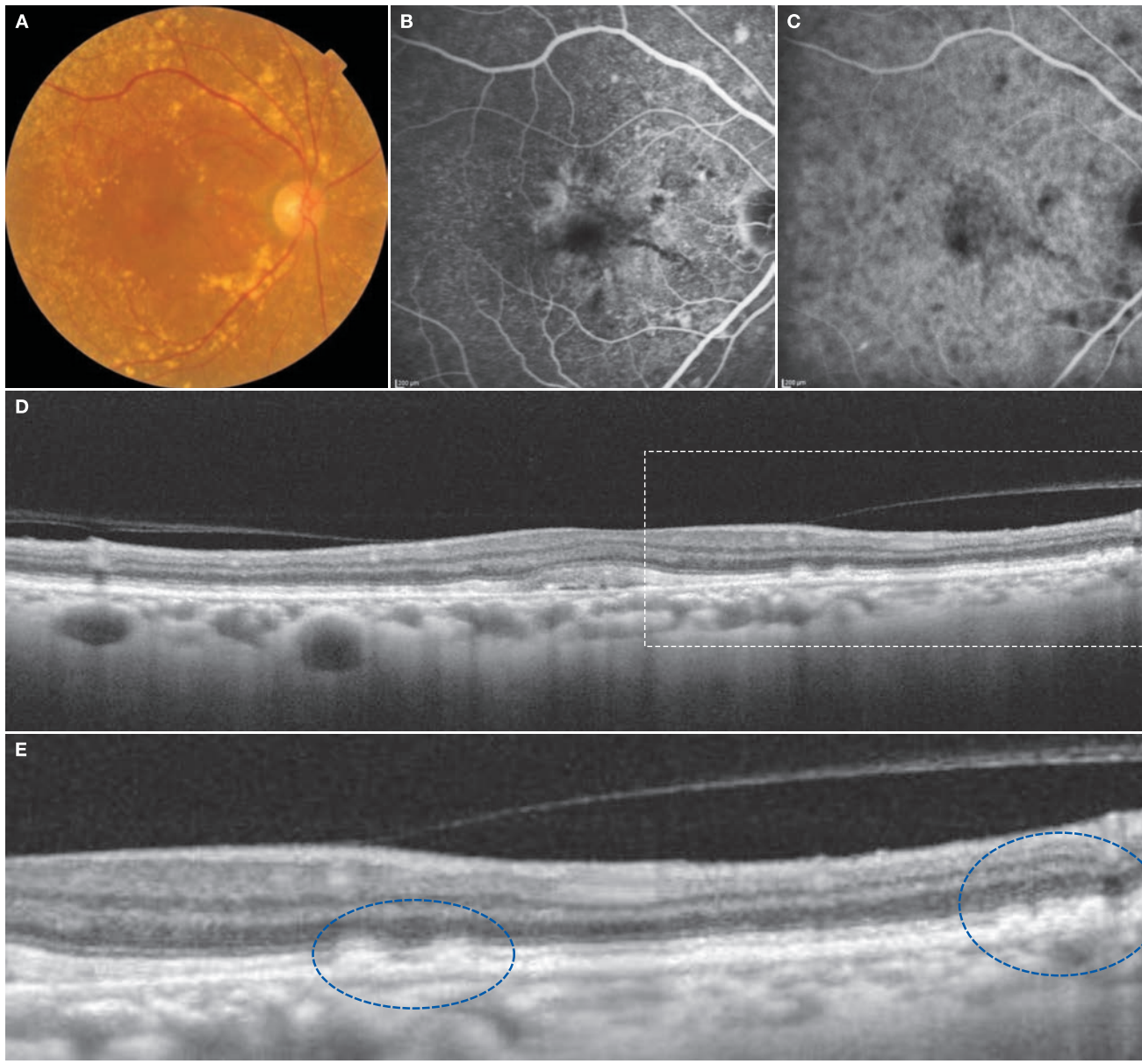

A: Color fundus photograph in the right eye: Right eye of case 81. Large soft drusen and cuticular drusen can be seen similar to the left eye. **B:** FA in the right eye (6 minutes, 8 seconds): The cuticular drusen are exhibiting a »stars-in-the-sky« pattern. Hyperfluorescence and hypofluorescence are mixed in the fovea centralis due to acquired vitelliform lesions. **C:** IA in the right eye (6 minutes, 8 seconds): The fovea centralis is exhibiting hypofluorescence. Small hypofluorescent foci are scattered over the posterior pole. **D:** OCT horizontal scan of the right eye: Perifoveal PVD is observed, similar to the left eye. There is a vitelliform detachment in the fovea centralis. **E:** Enlarged version of D [white dashed box]: A »saw-tooth pattern« is seen in the blue dashed circle area.

Image interpretation points

Cuticular drusen have been known to be combined with acquired vitelliform lesions, as seen in case 81. In this case, anterior centrifugal traction towards the fovea centralis as a result of the posterior vitreous detachment can be seen in both eyes. Hence, the possibility that this traction is causing the acquired vitelliform lesions cannot be denied.

Case 83 Reticular pseudodrusen: Fellow eye of RAP

A 78-year-old female, OS, BCVA 1.2

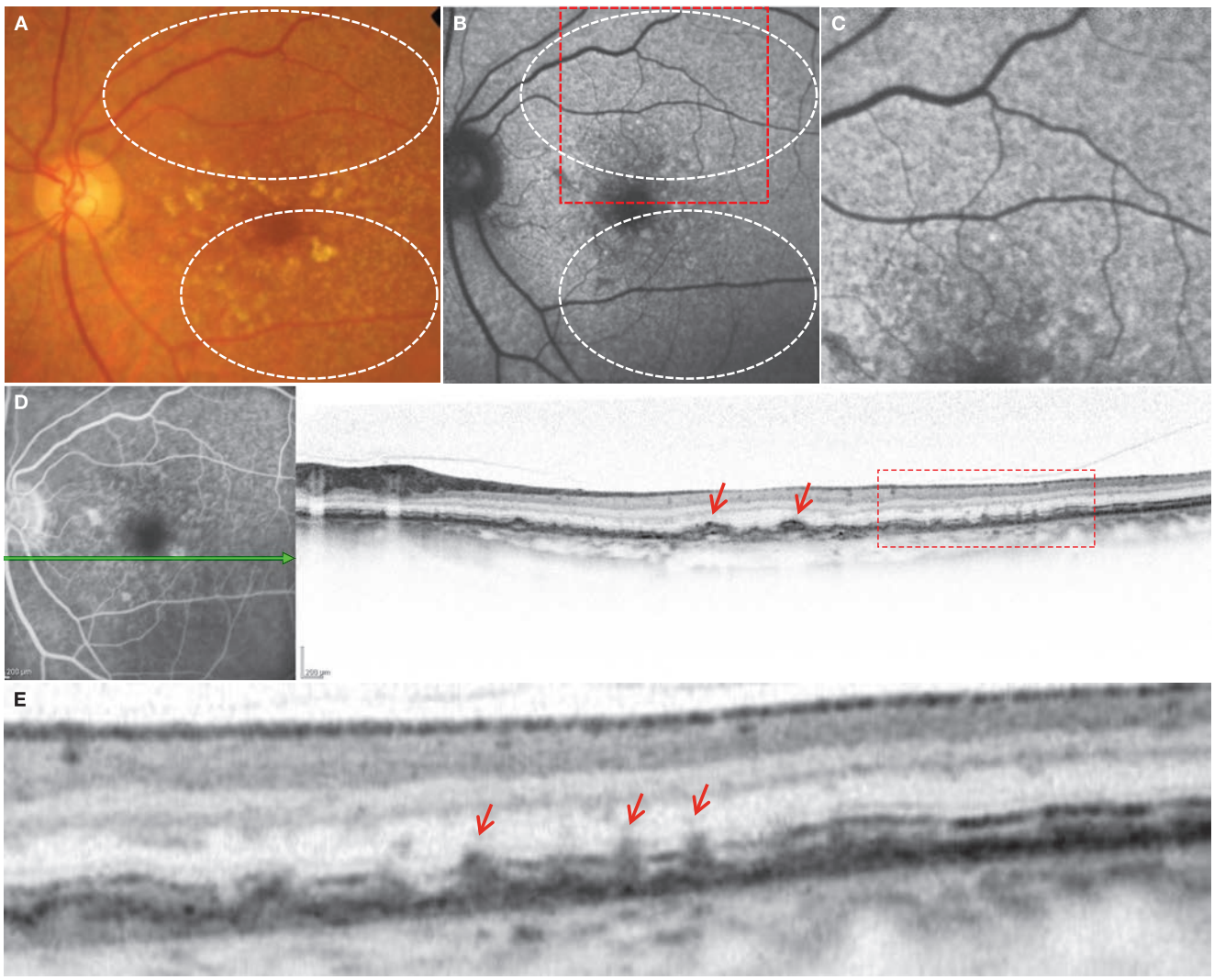

A: Color fundus photograph: Numerous drusen are visible. A reticular pattern is seen in the deep retinal layers within the white dashed circles. **B:** FAF in the left eye: Some drusen are exhibiting hyperfluorescence while others are exhibiting hypofluorescence. Reticular autofluorescence abnormalities can be observed within the white dashed circle in the superotemporal area. **C:** Enlarged version of B [red dashed box]: Hypofluorescence corresponding to reticular pseudodrusen is shown. **D:** FA + OCT horizontal scan of the left eye: Small PED and reactive proliferation of RPE cells is noticeable in the inferior macula (→). Temporal to these lesions, highly reflective features are seen on the RPE to penetrate the ELM line. These are reticular pseudodrusen. **E:** Enlarged version of D [red dashed box]: Stage 2 and 3 reticular pseudodrusen are seen (→).

Image interpretation points

In soft drusen, the RPE protrudes into the retina and deposits can be seen underneath the RPE; by contrast, in reticular pseudodrusen, deposits are characteristically seen on the RPE. Reticular pseudodrusen is a pathological condition that has recently received a lot of attention. While OCT is extremely important for diagnosis, it is important to capture a wide area of posterior pole particularly including the fovea and superotemporal region. Reticular pseudodrusen can also sometimes be seen nasally as well. In this case, RAP was seen in the fellow eye.

Case 84 Reticular pseudodrusen: Case with atrophic age-related macular degeneration (atrophic AMD)

An 84-year-old female, OD, BCVA 0.3

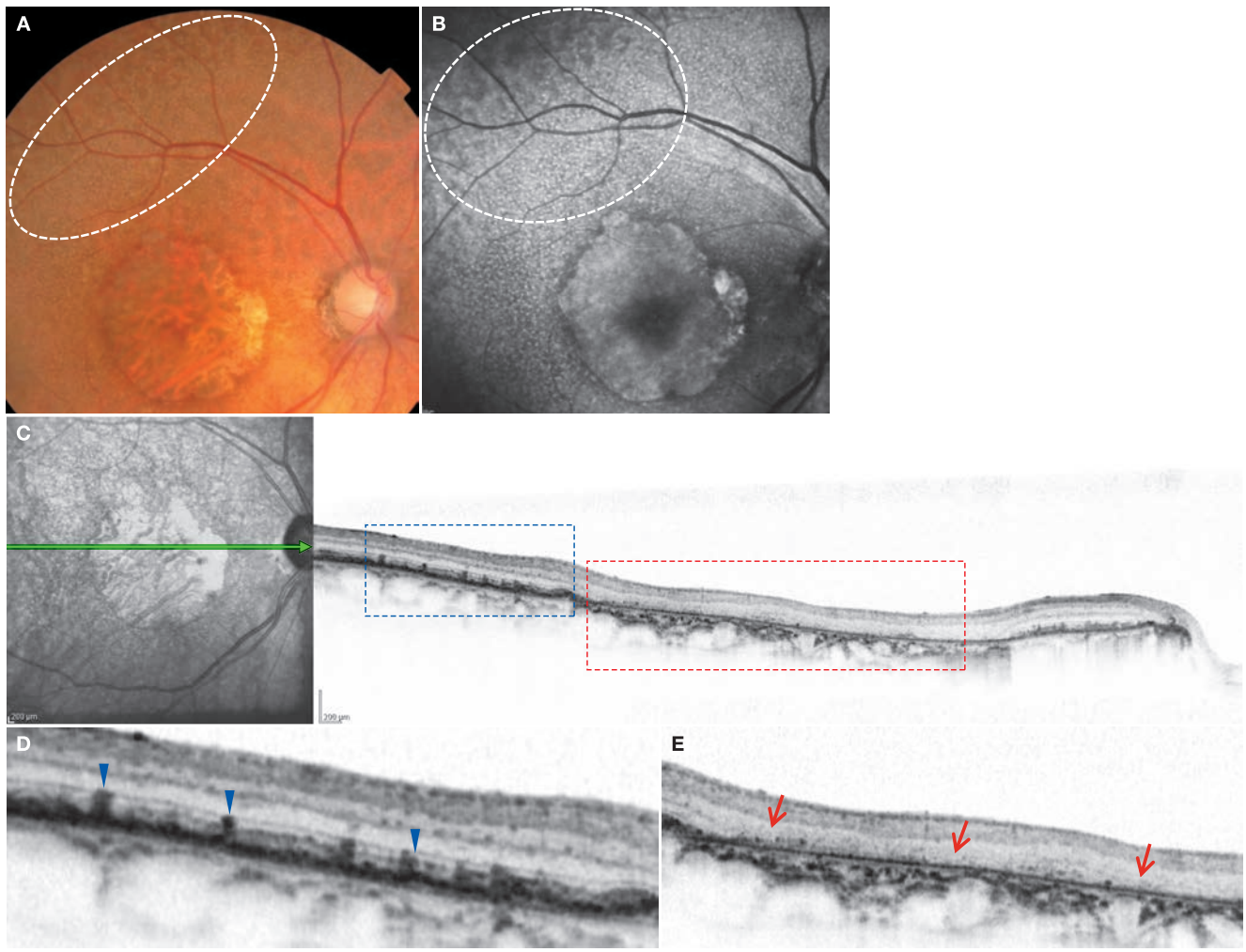

A: Color fundus photograph in the right eye: Large geographic atrophic lesions can be seen in the macula where choroidal macrovessels are fairly translucent. Reticular lesions are exhibited in the white dashed circle. **B:** Red-free imaging in the right eye: A reticular structure is visible in the white dashed circle. White spots are seen around the fovea centralis. **C:** IR + OCT horizontal scan of the right eye: Reticular pseudodrusen can be seen within the blue dashed box. No RPE reflectivity can be seen within the red dashed box. **D:** Enlarged version of C [blue dashed box]: Stage 2 and 3 reticular pseudodrusen are seen (►). **E:** Enlarged version of C [red dashed box]: No significant RPE reflectivity can be seen (➔). In addition, the outer retinal layers are seen to be preserved only on the left margin of the image and the photoreceptor cells have almost entirely disappeared. This is atrophic AMD.

Image interpretation points

This is a case of reticular pseudodrusen accompanying atrophic AMD. When examining the image more closely, reticular pseudodrusen can be found at an unexpectedly high frequency. They often accompany atrophic AMD and RAP, however, it is relatively rare to see them in combination with PCV. Choroidal signal enhancement occurs due to RPE atrophy in the geographic atrophic lesion area where the choroid is seen more clearly.

Case 85 Reticular pseudodrusen and soft drusen

A 74-year-old male, OD, BCVA 1.2

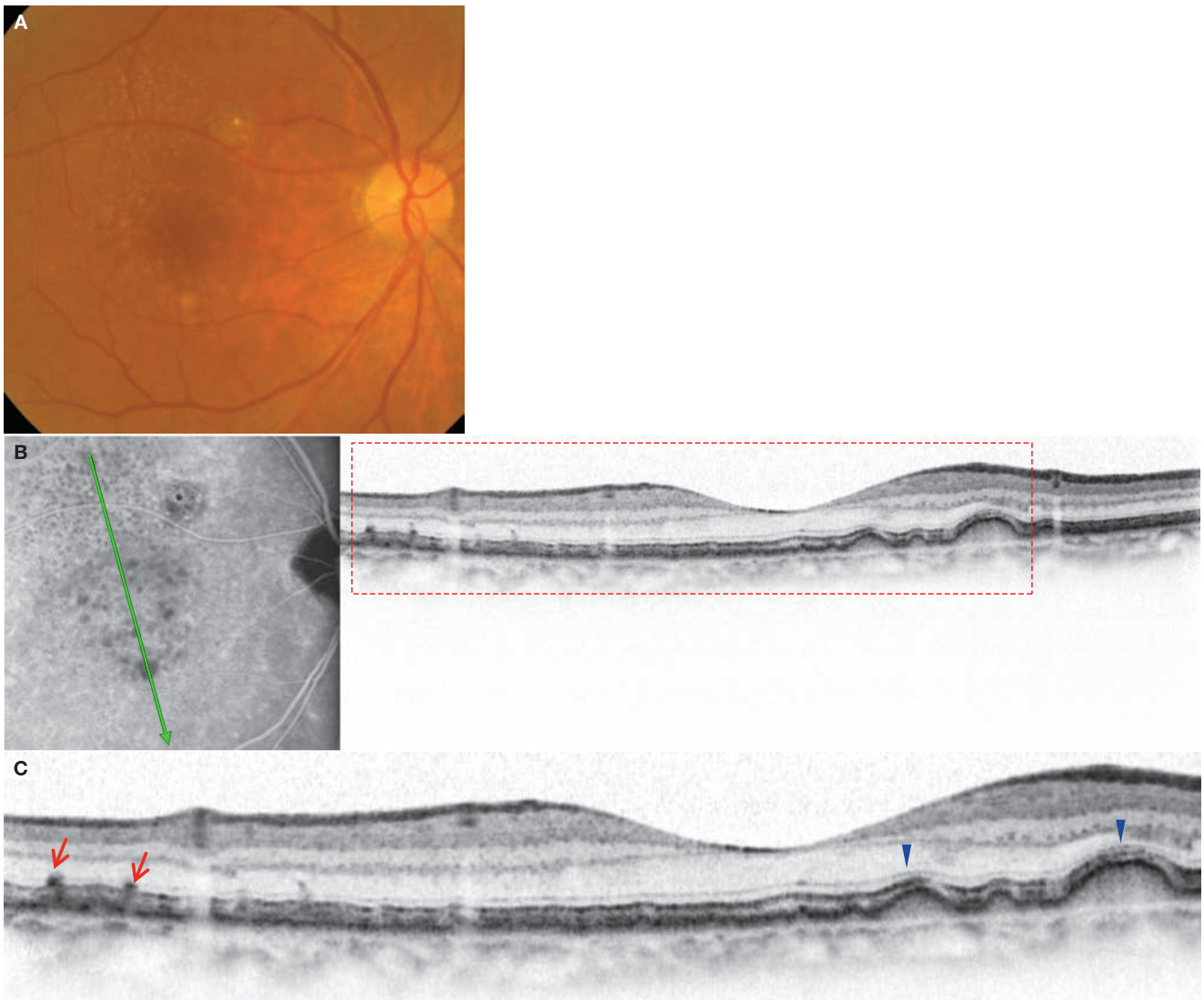

A: Color fundus photograph in the right eye: Soft drusen can be seen in the macular area around the fovea centralis. Drusen up to 250 µm in size are present along with other slightly smaller ones. Relatively small, uniform size of yellowish-white spots are visible superotemporally. These are reticular pseudodrusen. **B:** IA + OCT oblique scan of the right eye: In the late stage IA image, the soft drusen are exhibiting hypofluorescence. The reticular pseudodrusen are also hypofluorescent. In the OCT image, it is clear that the reticular pseudodrusen and soft drusen are coexisting. The coexistence of both drusen is actually common, and not unusual. **C:** Enlarged version of B [red dashed box]: The difference between reticular pseudodrusen (➔) and soft drusen (►) is clear. The two can be distinguished more easily using OCT than with an ophthalmoscope.

Image interpretation points

The OCT findings of reticular pseudodrusen and soft drusen are completely different. The reticular pseudodrusen appear as deposits anterior to the RPE, while soft drusen are deposits posterior to the RPE. In this case, the content of the soft drusen appears moderately reflective, and findings demonstrating CNV cannot be found in this case.

Case 86 Serous pigment epithelial detachment: Case without CNV

A 49-year-old female, OS, BCVA 0.7

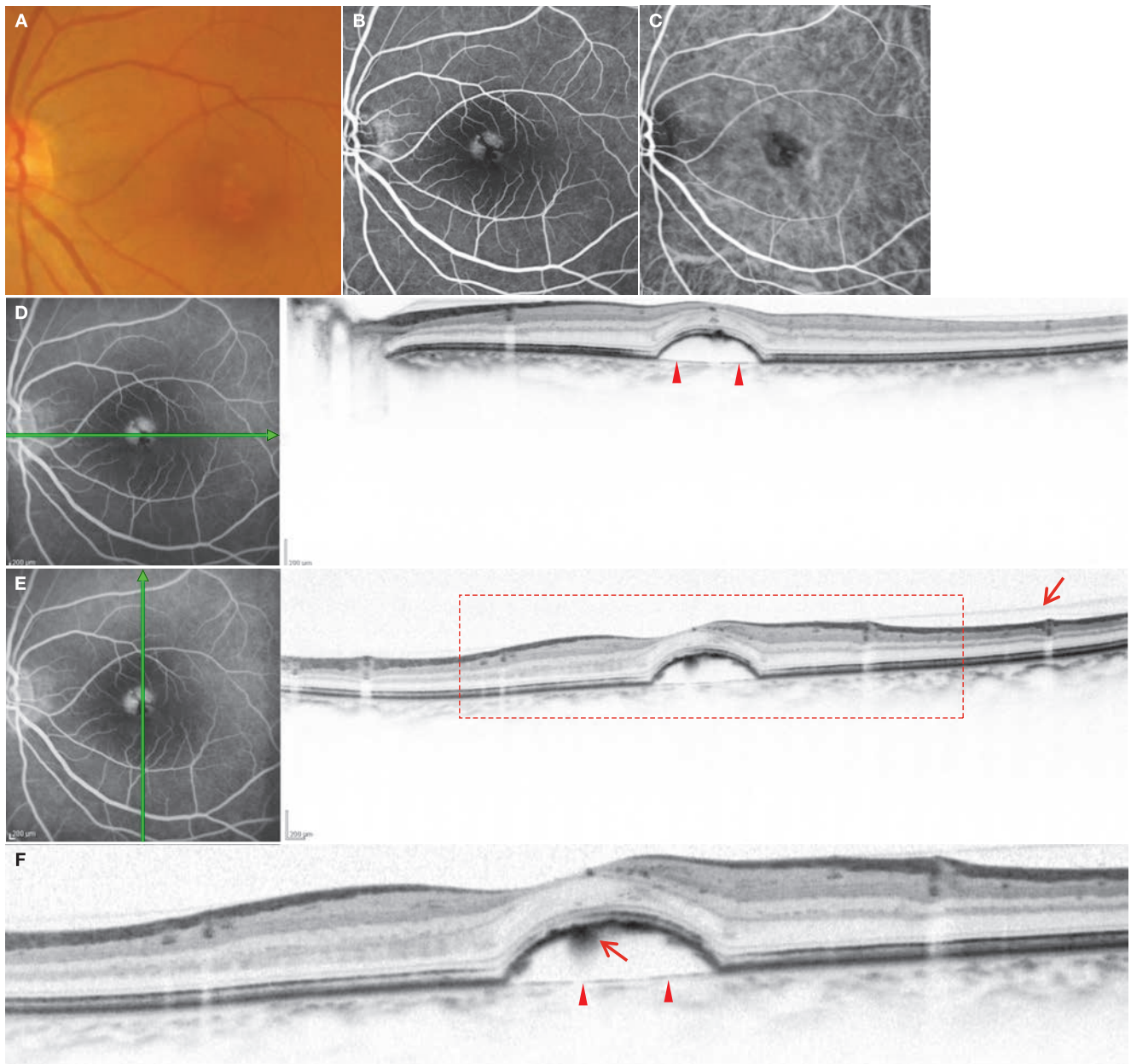

A: Color fundus photograph in the left eye: A PED about 3/4 the diameter of the optic disc is visible. **B:** FA in the left eye (1 minute, 6 seconds): A part of the PED appears hyperfluorescent. **C:** IA in the left eye (1 minute, 6 seconds): CNV cannot be detected. **D:** FA + OCT horizontal scan of the left eye: The content of the PED is weakly reflective and no CNV reflectivity is appreciated. (►) indicates Bruch's membrane. Highly reflective dots, thought to originate from the migrated RPE cells, can be seen in the outer nuclear layer. **E:** FA + OCT vertical scan of the left eye: The posterior vitreous cortex slightly detached from the ILM can be seen (➔). **F:** Enlarged version of E [red dashed box]: Bruch's membrane (►) and a highly reflective feature, likely RPE cell proliferation, (➔) beneath the RPE can be seen.

Image interpretation points

Bruch's membrane is clearly seen at the base of the PED (►). The high reflectivity that can be seen posterior to the PED may be proliferated RPE (➔). The ELM and IS/OS lines above the PED are well preserved.

Case 87 Pigment epithelial detachment: Reactive proliferation of retinal pigment epithelial cells

A 78-year-old female, OD, BCVA 0.9

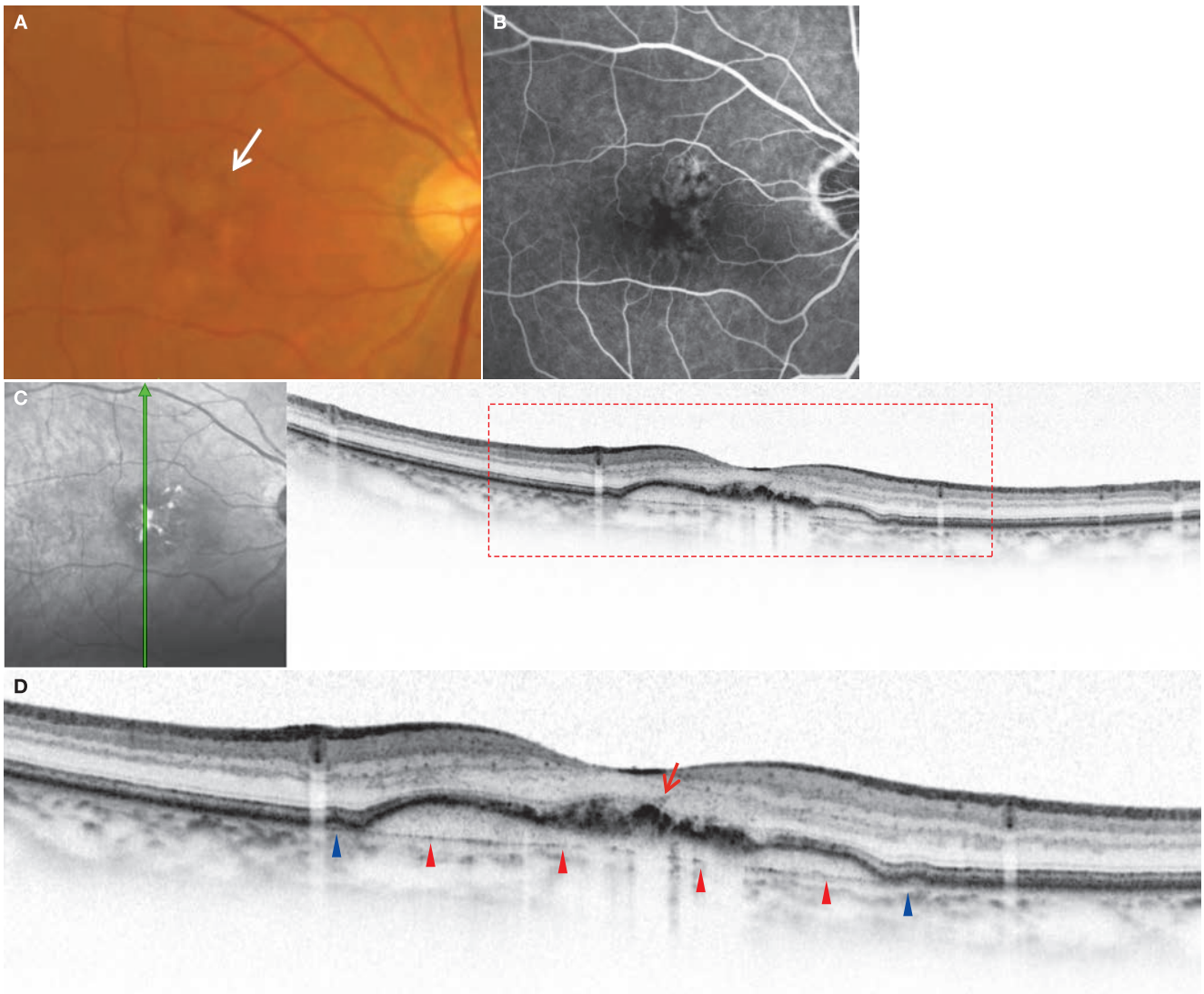

A: A fundus photograph in the right eye: A PED about 1.5 the diameter of the optic disc can be seen (⇛). **B:** in the right eye (1 minute, 4 seconds) FA: A part of the PED appears hyperfluorescent. CNV is not detected on FA. **C:** IR + OCT vertical scan of the right eye: A flat PED can be seen. **D:** Enlarged version of C [red dashed box]: A straight line representing Bruch's membrane can be seen on the posterior aspect of the PED (►). The content of the PED is homogeneous and moderately reflective. Findings showing proliferation of the RPE can be seen in the center of the PED (➔). This kinds of findings are frequently seen in relatively old PED. Small drusen exist adjacent to the PED (►).

Image interpretation points

The »straight highly reflective line« thought to originate from Bruch's membrane cannot be detected unless the RPE detaches from Bruch's membrane. In figure D of this case, this line can only be seen in the area of small drusen (►), and under the large PED. The ELM can be traced almost from end-to-end in figure D, but the IS/OS is not always clearly defined in the area where RPE reactive proliferation has occurred (➔). As a result, we can infer that the sensory retina on the PED undergoes partial damage.

Case 88 Drusenoid PED: Case where CNV is suspected

An 84-year-old male, OS, BCVA 0.9

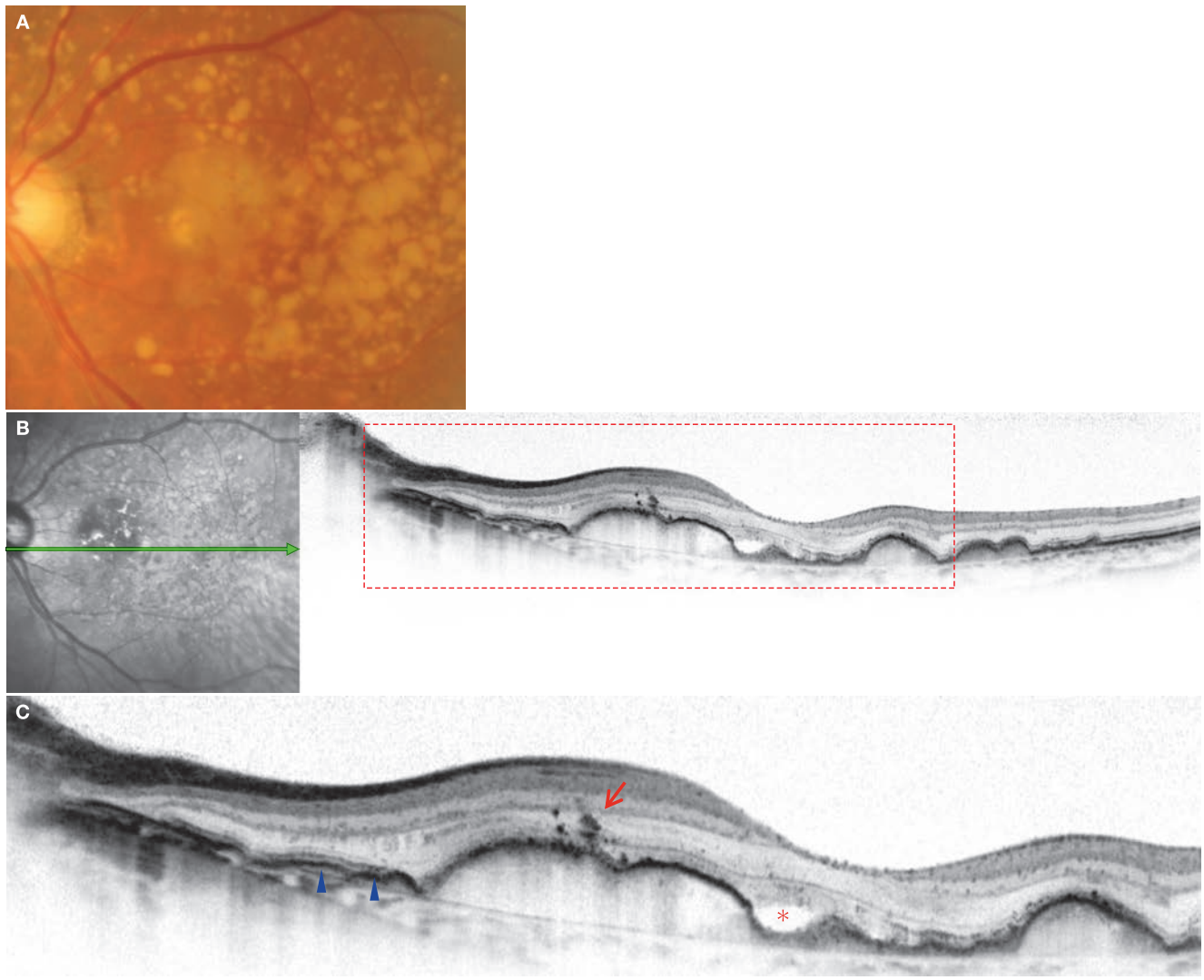

A: Color fundus photograph in the left eye: Soft drusen of various sizes and PED are visible. **B:** IR + OCT horizontal scan of the left eye: The line indicating Bruch's membrane is seen over a wide area from the area near the optic disc to the area temporal to the fovea centralis. The content of the PED and drusen varies from weakly reflective to moderately reflective. **C:** Enlarged version of B [red dashed box]: Flat RPE protrusions with irregular undulation are seen nasal to the large PED (►). This suggests the presence of CNV. High reflectivity due to RPE proliferation anterior to the large PED is exhibited (➔). The reflectivity of the content of the PED is not homogeneous; it is relatively weakly reflective near the fovea centralis. A SRD (*) can be seen in the nasal side of the fovea centralis. The content of the drusen temporally is moderately reflective. These are also findings that suggest the presence of CNV. (Continued on the next page)

Image interpretation points

This is a case where it is difficult to determine if CNV is occurring. Here, exudative changes primarily cannot be seen with an ophthalmoscope. The undulating RPE protrusions near the optic disc and the relatively strong reflectivity between the RPE and Bruch's membrane strongly suggest the presence of CNV. An extremely careful follow-up is necessary in cases like this.

Case 88 17 months later

An 84-year-old male, OS, BCVA 0.4

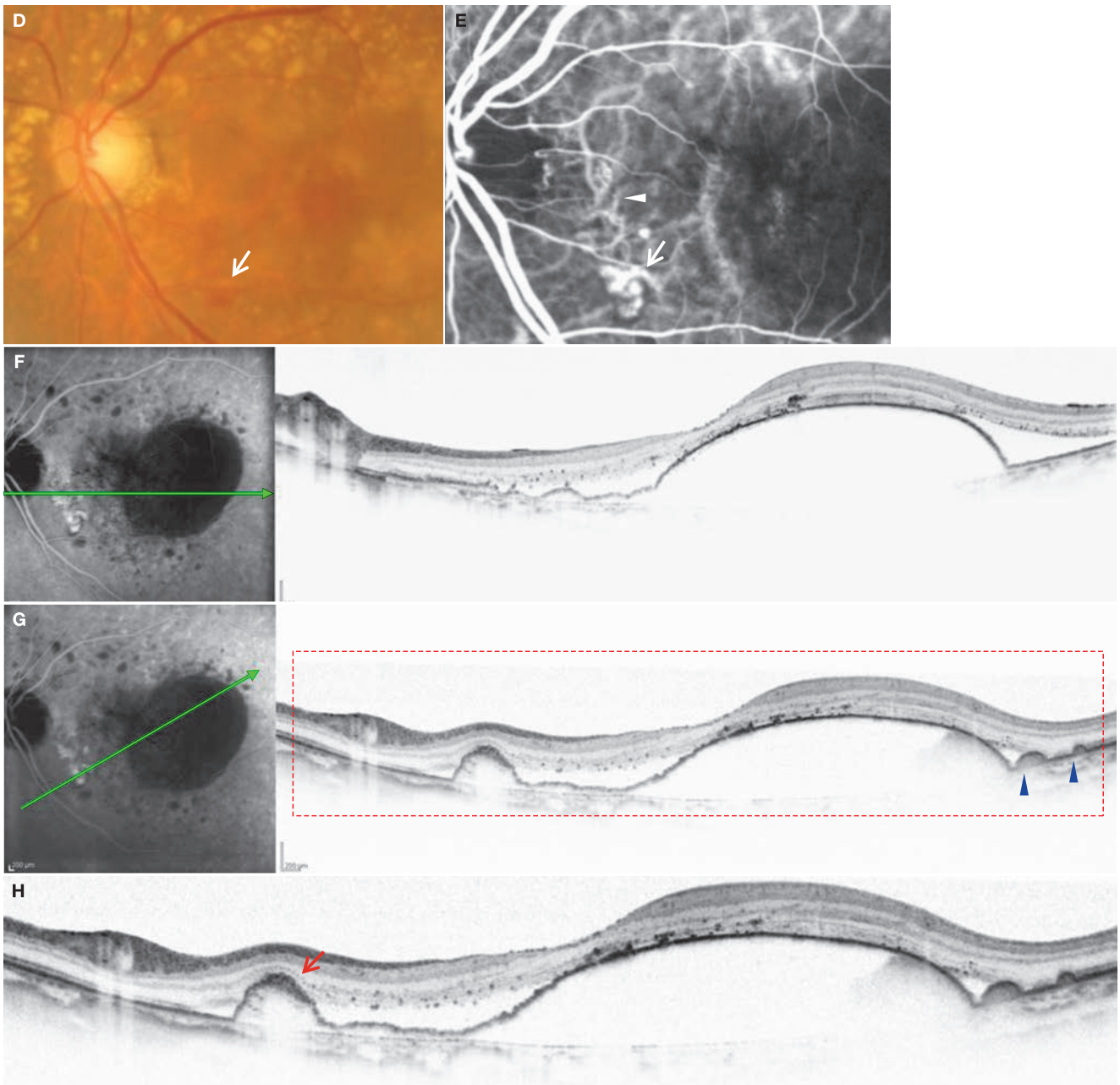

D: Color fundus photograph in the left eye: faint retinal hemorrhage can be seen (⇨). **E:** IA in the left eye: Polypoidal lesions are observed inferotemporal to the optic disc (⇨). In addition, an abnormal vascular network exists superiorly to this (▷). This is a typical image of PCV. **F:** IA + OCT horizontal scan of the left eye: Flat, undulating RPE protrusions are visible in the area corresponding to the abnormal vascular network near the optic disc. This feature is also known as the »double layer sign«, but this term dates back to the era of time-domain OCT. **G:** IA + OCT oblique scan of the left eye: This is a scan passing through polypoidal lesions. Drusen are seen further above temporal to the large PED (►). **H:** Enlarged version of G [red dashed box]: The polypoidal lesions are visible as steep RPE protrusions (➔). The reflectivity of its content differs from the reflectivity of the drusen located superotemporally. We can see that the content of the large PED is not homogeneous.

Image interpretation points

PCV developed 17 months after initial diagnosis. It would be useful to compare the moderate reflectivity of the polypoidal lesions with the weak reflectivity within the large PED superotemporally, and to correlate these features with the CNV area detected on IA.

Case 89 Large pigment epithelial detachment: Case where CNV is suspected

A 76-year-old male, OS, BCVA 0.8

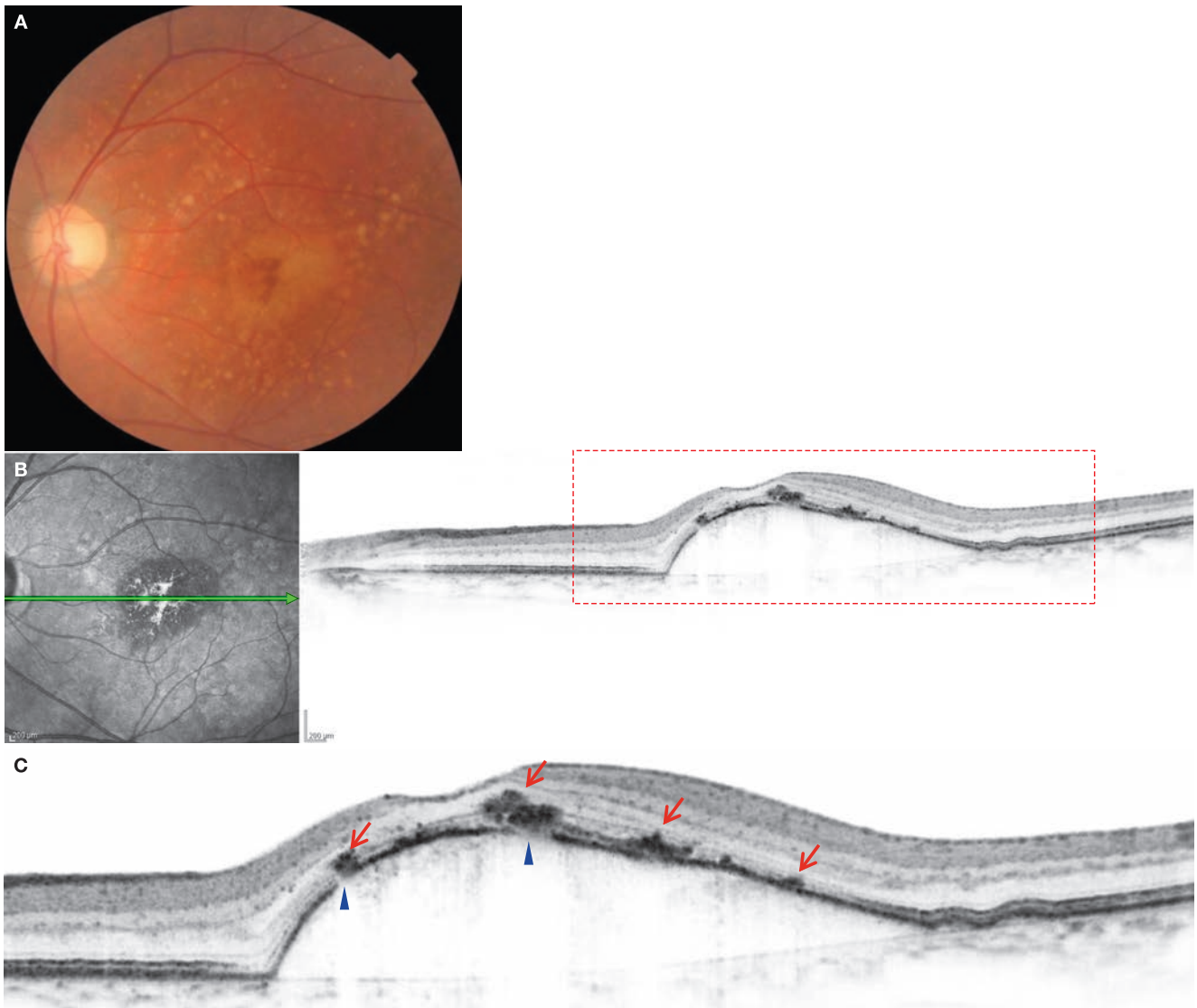

A: Left eye fundus photograph: Large soft drusen are scattered over the entire posterior pole. A large PED is visible in the macular area including the fovea centralis. There is RPE pigmentation in the center of the PED. **B:** IR + OCT horizontal scan of the left eye: A large PED is seen. **C:** Enlarged version of B [red dashed box]: The reactive RPE proliferations are exhibiting high reflectivity in the sensory retina (➔). They are located both anteriorly and posteriorly to the ELM. The structures below these features are not well defined due to high reflectivity. While the RPE appears to be disrupting, this is likely due to shadows caused by RPE proliferations. Although it is a relatively tall PED, but Bruch's membrane can be visualized over almost the entire length. Part of the PED content appears to have a reflective structure suggesting the presence of CNV, but it cannot be confirmed only based on OCT imaging.

Image interpretation points

Highly reflective structures such as blood vessels, hard exudates, and pigmentation, can cause shadows which obscure visualization of other objects below.

Case 90 Pigment epithelial detachment: Case with type 1 CNV ①

A 73-year-old male, OS, BCVA 0.4

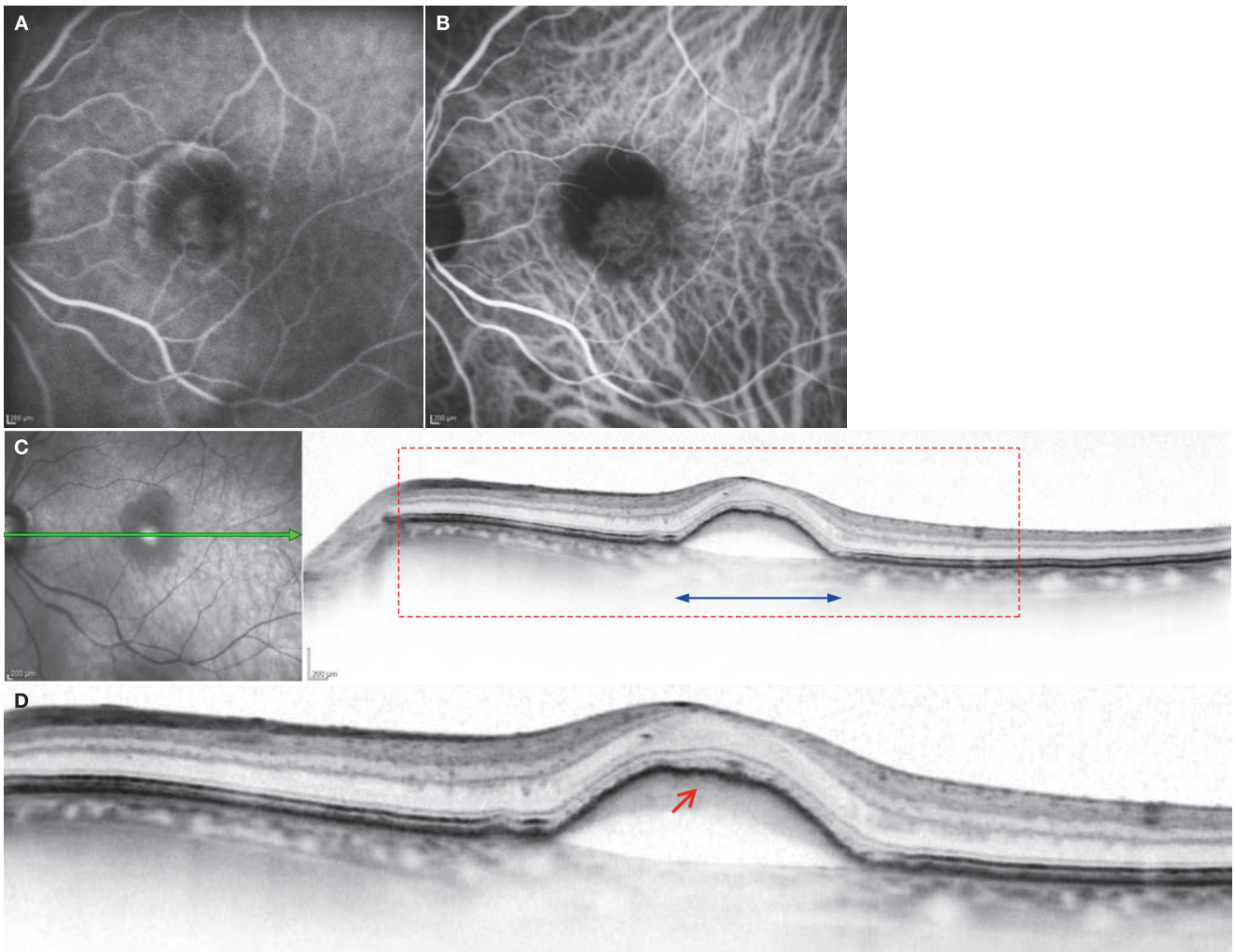

A: FA in the left eye (1 minute, 21 seconds): Annular hyperfluorescent foci along the circumference of the PED about 1.5 times the diameter of the optic disc is observed in and around the fovea centralis. Within this area, there is also hyperfluorescence due to CNV roughly the diameter of the disc. **B:** IA in the left eye (1 minute, 21 seconds): The PED is exhibiting hypofluorescence. Reticular hyperfluorescence representing CNV is clearly seen in the PED. **C:** IR + OCT horizontal scan of the left eye: The PED is clearly visible. The choroid is poorly visible due to a decrease in penetration of OCT probe light in the PED area (⟷). **D:** Enlarged version of C [red dashed box]: The CNV is moderately reflective (➔). The IS/OS is not well visualized in the PED area.

Image interpretation points

This is the case of a Caucasian male patient. There are not many cases of Japanese people where CNV is clearly visible within a PED. Even in PCV, Type 1 CNV typically grows along the posterior surface of the RPE as in this case.
It is useful to correlate disruption of foveal outer retinal structure with visual acuity loss. However, when the retina becomes convex as seen in this case, it is difficult to determine if the IS/OS is actually or if it is obscure just because of the decrease in light reflection/backscattering due to the oblique position of the retina against the OCT probe light.

Case 91 Pigment epithelial detachment: Case with type 1 CNV ②

A 64-year-old female, OD, BCVA 0.7

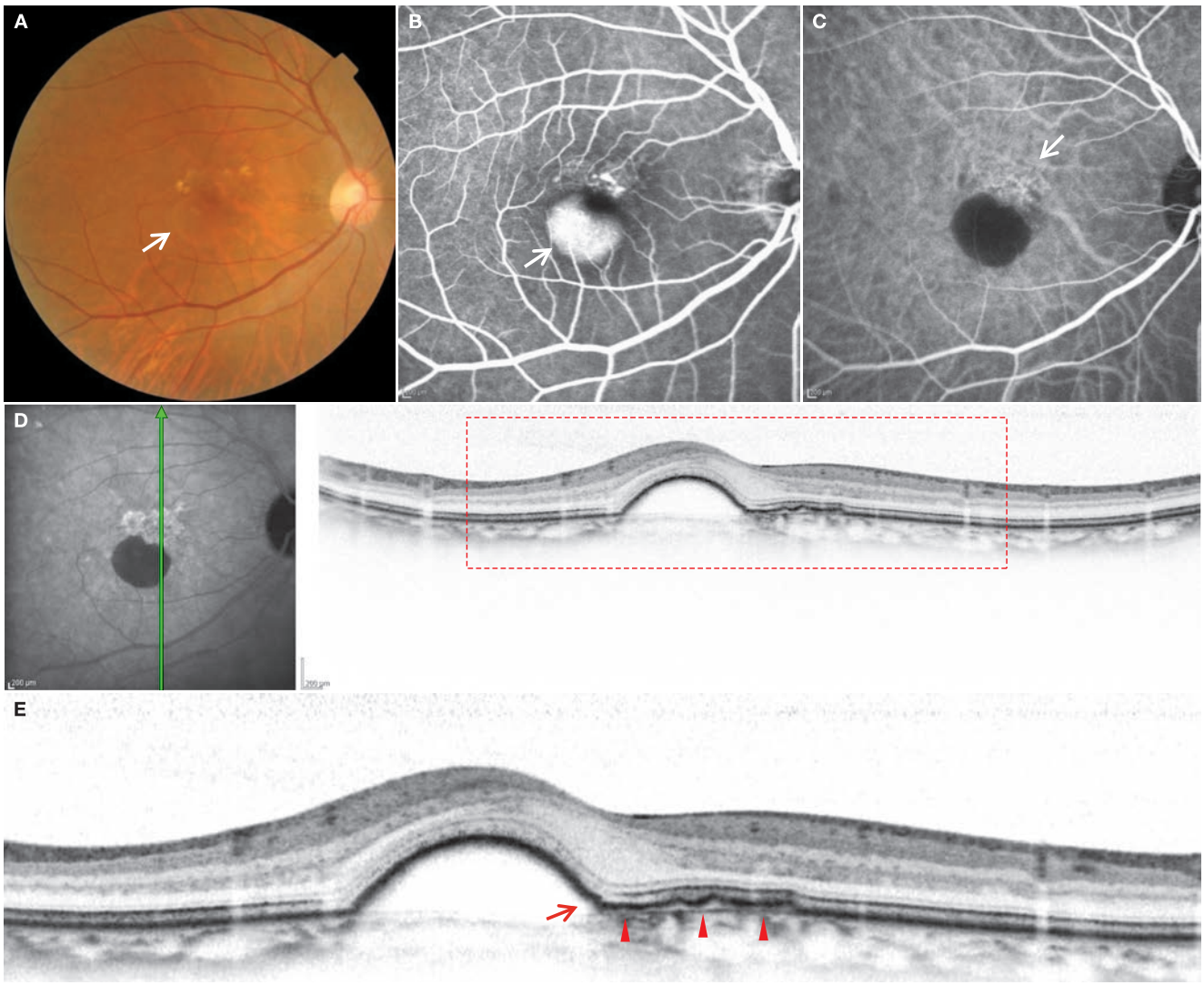

A: Color fundus photograph in the right eye: A PED roughly the diameter of the optic disc is observed in the fovea centralis (⇛). Multiple soft drusen can be seen superior to the PED. Exudative changes in the sensory retina are mild. **B:** FA in the right eye (5 minutes, 30 seconds): Fluorescein has accumulated in the PED, which exhibits hyperfluorescence (⇛). In the superior parafovea, faint hyperfluorescence and a stronger, granular hyperfluorescence is visible. **C:** IA in the right eye (5 minutes, 30 seconds): The PED is hypofluorescent. Branching CNV is seen in the area exhibiting faint hyperfluorescence on FA (⇛). **D:** IA + OCT vertical scan of the right eye: Undulations of the RPE are noticeable at the edge of and superior to the PED. The space between the undulating RPE and Bruch's membrane is moderately reflective. **E:** Enlarged version of D [red dashed box]: Bruch's membrane is clearly visible on the posterior aspect of the abnormal RPE (►). Extension of CNV inside the PED is not clear on this scan (➔).

Image interpretation points

In this case, the IS/OS cannot be seen in the sensory retina above the PED. It is not clear if this represents damage to the outer retinal layers due to pressure from the PED or if this is simply a finding due to optical properties. This image undeniably shows that CNV may be present over entire posterior aspect of the detached RPE.

Case 92 Large pigment epithelial detachment: Case where CNV is present

A 76-year-old male, OS, BCVA 0.6

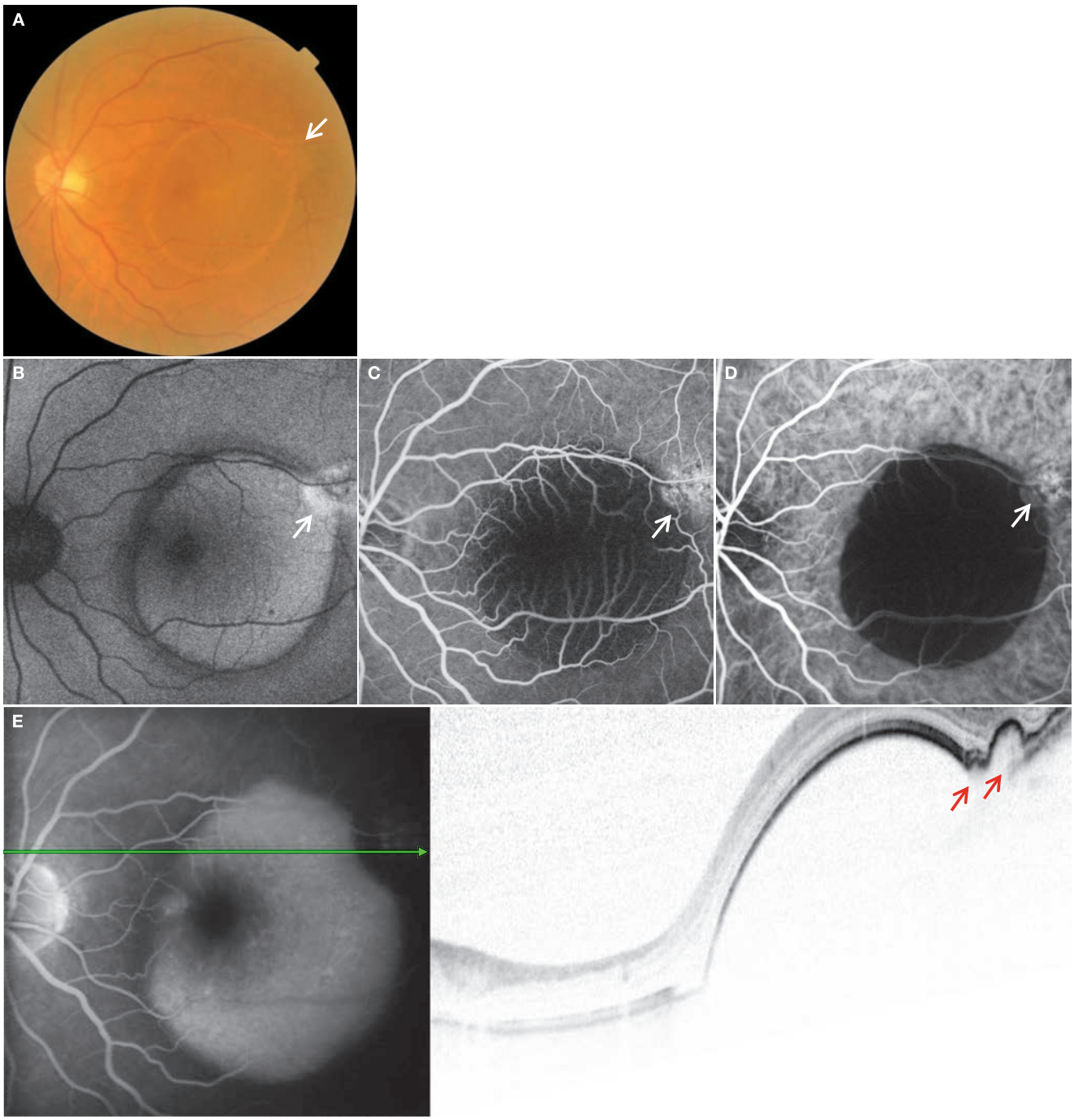

A: Color fundus photograph in the left eye: A large PED about 4 times the diameter of the optic disc is exhibited in the macula. A notch is seen at the superotemporal edge of the PED (⇛). This kind of large PED usually have CNV. **B:** FAF in the left eye: The PED is exhibiting hyperfluorescence. A hypofluorescent ring exists around the PED. The notched area is exhibiting even stronger hyperfluorescence (⇛). **C:** FA in the left eye (31 seconds): The PED is exhibiting hypofluorescence. The notched area is exhibiting granular hyperfluorescence (⇛). **D:** IA in the left eye (31 seconds): The PED is also hypofluorescent on IA, and the notched area is exhibiting hyperfluorescence due to CNV (⇛). **E:** FA + OCT horizontal scan on the left eye: In this late stage FA image, the PED is hyperfluorescent due to fluoroscein pooling. CNV is detected on OCT in the location corresponding to the hyporeflective notch. (➔).
(Continued on the next page)

Case 92 Continuation

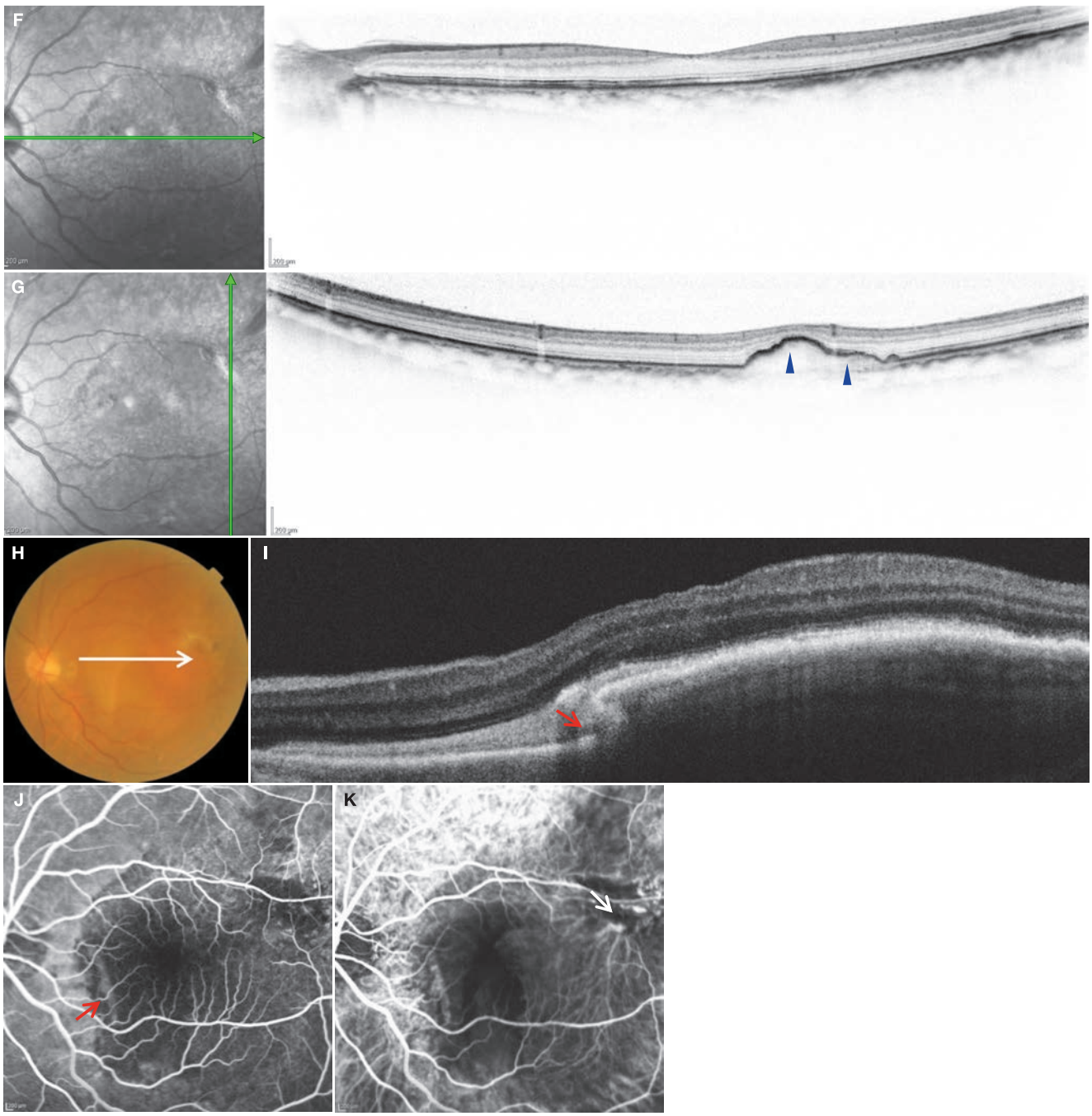

F: IR + OCT horizontal scan of the left eye: 17 months after initial diagnosis. The PED is temporarily flattened as a result of anti-VEGF treatment and sub-Tenon's steroid injection. No abnormal findings can be seen in the OCT image passing through the fovea centralis. **G:** IR + OCT vertical scan of the left eye: The PED and CNV inside the PED (►) is detected on the OCT image passing through the notching in the superotemporal area. **H:** Color fundus photograph in the left eye: Exudative changes are occurring in the sensory retina. The white arrow represents the OCT scan line for figure I. **I:** OCT horizontal scan of the left eye: Two years after initial diagnosis. CNV is present over an extensive area beneath the RPE temporal to the fovea centralis. The gap of the RPE shown in (➔) is an RPE tear. **J:** FA in the left eye (30 seconds): The long vertical hyperfluorescent area represents the RPE tear (➔). K: IA in the left eye (3 seconds): A large CNV originating at the temporal edge of the macula (⇨) is seen.

Image interpretation points

The PED was temporarily flattened as a result of anti-VEGF treatment and sub-Tenon's steroid injection (17 months after initial diagnosis). Cases with a large PED have CNV almost without exception. It is important to detect CNV using FA, IA and OCT.

6.3 Atrophic age-related macular degeneration

Background

Atrophic AMD or dry AMD is a type of age-related macular degeneration (AMD) often seen in Caucasians. The frequency of atrophic AMD used to be very low in Asians, including the Japanese, but this type of AMD has been on the rise in recent years. The most significant factors correlated with the onset of atrophic AMD and exudative AMD are age-related changes in the RPE and Bruch's membrane. Fundus findings such as drusen and RPE pigmentation changes (pigmentation and depigmentation) represent these age-related changes. Thus, atrophic AMD and exudative AMD are not separate diseases; rather exudative changes can occur during atrophic AMD, and exudative AMD can become atrophic during its course.

Recently, the concept of viewing atrophic AMD as one spectrum of reticular pseudodrusen in reticular macular diseases has been proposed (reticular pseudodrusen and exudative AMD are not unrelated and are, in fact, closely related).[1]

OCT findings

OCT images of atrophic AMD show distinctive findings such as atrophy and thinning of the sensory retina, atrophy and loss of the RPE, and choroidal signal enhancement (Fig. 6-6).[2, 3] In addition, RPE cells are migrating within the sensory retina and are seen as highly reflective dots. This feature is also a characteristic.[3] Cystic changes sometimes occur in the sensory retina, and should not be mistaken for exudative changes.[4]

There are detailed reports on OCT findings for atrophic AMD. According to Fleckenstein et al., various changes can be seen around atrophic lesions, as shown in Fig. 6-7.[5] All these changes occur on the RPE and Bruch's membrane level.

The RPE disappears in the atrophic lesion, and the edge of the atrophic change demonstrate several patterns, as shown in Fig. 6-8, indicating the diversity of pathogenesis of atrophic AMD.

The ELM, IS/OS, RPE and outer nuclear layer usually disappear inside the atrophic lesion. In many cases, a relatively thin line thought to be Bruch's membrane remains with debris originating from the outer retinal layers left anteriorly (Fig. 6-9).

While OCT is extremely crucial in the diagnosis of atrophic AMD (Fig. 6-10), useful information can also be obtained from fundus autofluorescence (FAF) imaging. Holz et al. have demonstrated through a large scale of prospective studies that they can predict the rate of progression of atrophic AMD based on FAF image patterns.[6]

There is debate as to whether degeneration of the sensory retina or degeneration of the RPE occurs first in the onset of this disease. While no conclusion has been reached regarding this issue, recent studies suggest that RPE degeneration occurs first.[7, 8]

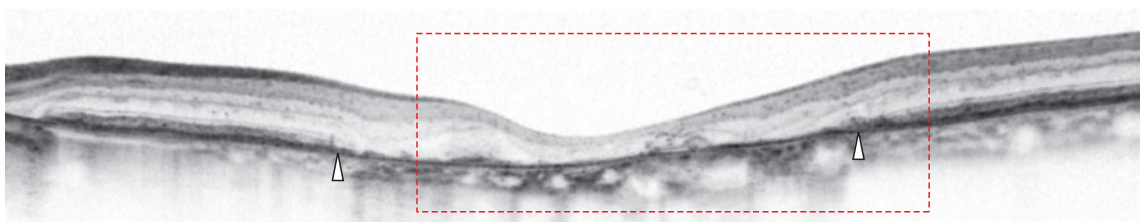

Fig. 6-6 OCT B-scan image for atrophic AMD
The foveal retina is significantly thinned. The RPE is atrophic and lost. In addition, choroidal signal enhancement is seen beneath the atrophied RPE (between ▷◁). See the red dashed box area in Fig. 6-10.

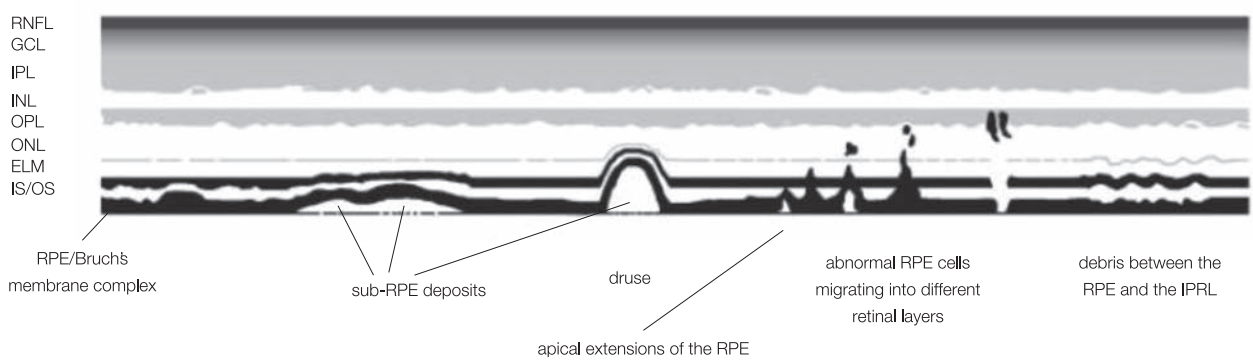

Fig. 6-7 Findings visible around the atrophic lesion of atrophic AMD
Changes in the RPE and Bruch's membrane and subsequent findings can be seen.
RNFL= retinal nerve fiber layer, GCL= ganglion cell layer, IPL= inner plexiform layer, INL= inner nuclear layer, IPRL=interface of inner and outer photoreceptor segment layer, OPL= outer plexiform layer, ONL= outer nuclear layer.
(Modified according to Fleckenstein M, et al. High-resolution spectral domain-OCT imaging in geographic atrophy associated with age-related macular degeneration. Invest Ophthalmol Vis Sci. 2008; 49: 4137-4144)

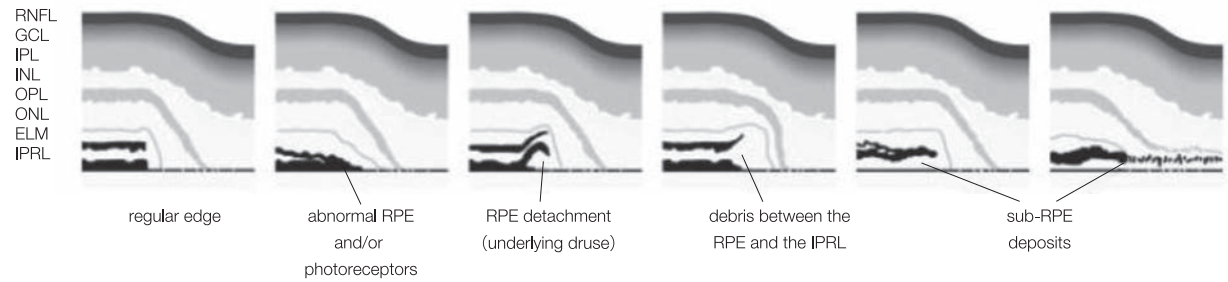

Fig. 6-8 Findings visible at the edge of the atrophic lesion of atrophic AMD
The pattern of RPE loss is not uniform and exhibits varied findings. IPRL = interface of inner and outer photoreceptor segment layer.
(Modified according to Fleckenstein M, et al. High-resolution spectral domain-OCT imaging in geographic atrophy associated with age-related macular degeneration. Invest Ophthalmol Vis Sci. 2008; 49: 4137-4144)

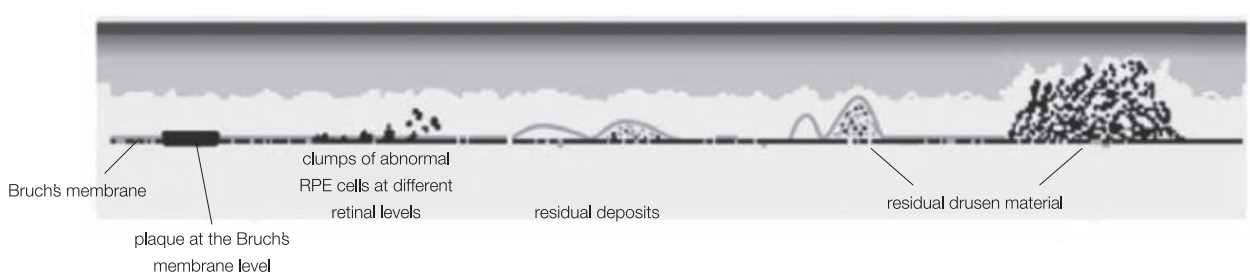

Fig. 6-9 Findings visible in the atrophic lesion of atrophic AMD
The RPE has disappeared and the debris exists on the remaining Bruch's membrane.
(Modified according to Fleckenstein M, et al. High-resolution spectral domain-OCT imaging in geographic atrophy associated with age-related macular degeneration. Invest Ophthalmol Vis Sci. 2008; 49: 4137-4144)

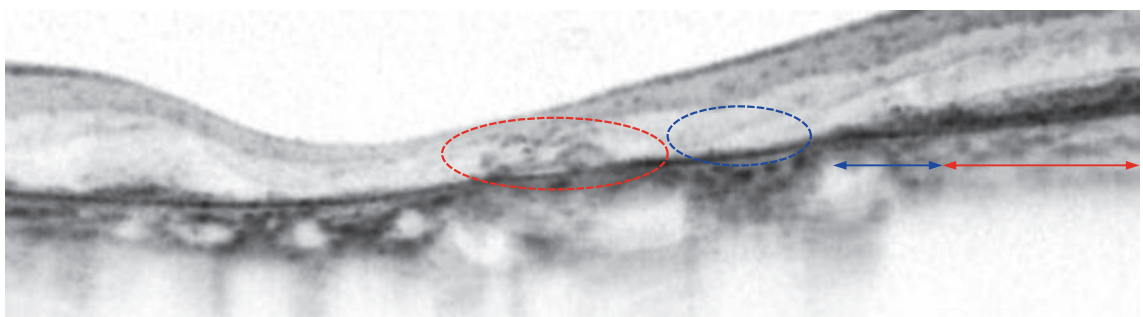

Fig. 6-10 Atrophic lesions on OCT
Enlarged version of Fig. 6-6 [red dashed box]. On the right side, there is an area where the RPE and outer retinal layers are almost normal. In the area indicated by (↔), the RPE, IS/OS and ELM are almost normal but on the foveal side the ELM has disappeared and IS/OS reflectivity is irregular. In the area indicated by (↔) the RPE has partially lost, and the corresponding retinal tissue external to the ELM is disrupted. Moving towards the fovea, the RPE has almost disappeared. In addition, the outer nuclear layer is thinned. In the red dashed circle near the fovea centralis, a structure exhibiting high reflectivity can be seen within the sensory retina. This likely represents migrated RPE cells.

6.3.1 References

1) Smith RT, Sohrab MA, Busuioc M, et al. Reticular macular disease. *Am J Ophthalmol*. 2009; 148:733-743.
2) Ho J, Witkin AJ, Liu J, et al. Duker JS. Documentation of intraretinal retinal pigment epithelium migration via high-speed ultrahigh-resolution optical coherence tomography. *Ophthalmology*. 2011; 118:687-693.
3) Lujian BL, Rosenfeld PJ, Gregori G, et al. Spectral domain optical coherence tomographic imaging of geographic atrophy. *Ophthalmic Surg Lasers Imaging*. 2009; 40:96-101.
4) Cohen SY, Dubois L, Nghiem-Buffet S, et al. Retinal pseudocysts in age-related geographic atrophy. *Am J Ophthalmol*. 2010; 150:211-217.
5) Fleckenstein M, Charbel Issa P, Helb HM, et al. High-resolution spectral domain-OCT imaging in geographic atrophy associated with age-related macular degeneration. *Invest Ophthalmol Vis Sci*. 2008; 49:4137-4144.
6) Holz FG, Bindewald-Wittch A, Fleckenstein M, et al. FAM-Study Group. Progression of geographic atrophy and impact of fundus autofluorescence patterns in age-related macular degeneration. *Am J Ophthalmol*. 2007; 143:463-472.
7) Sayegh RG, Simader C, Scheschy U, et al. A systematic comparison of spectral-domain optical coherence tomography and fundus autofluorescence in patients with geographic atrophy. *Ophthalmology*. 2011; 118:1844-1851.
8) Fleckenstein M, Schmitz-Valckenberg S, Martens C, et al. Fundus autofluorescence and spectral-domain optical coherence tomography characteristics in a rapidly progressing form of geographic atrophy. *Invest Ophthalmol Vis Sci*. 2011; 52:3761-3766.

Case 93 Atrophic age-related macular degeneration: A typical example

A 65-year-old male, OS, BCVA 0.04

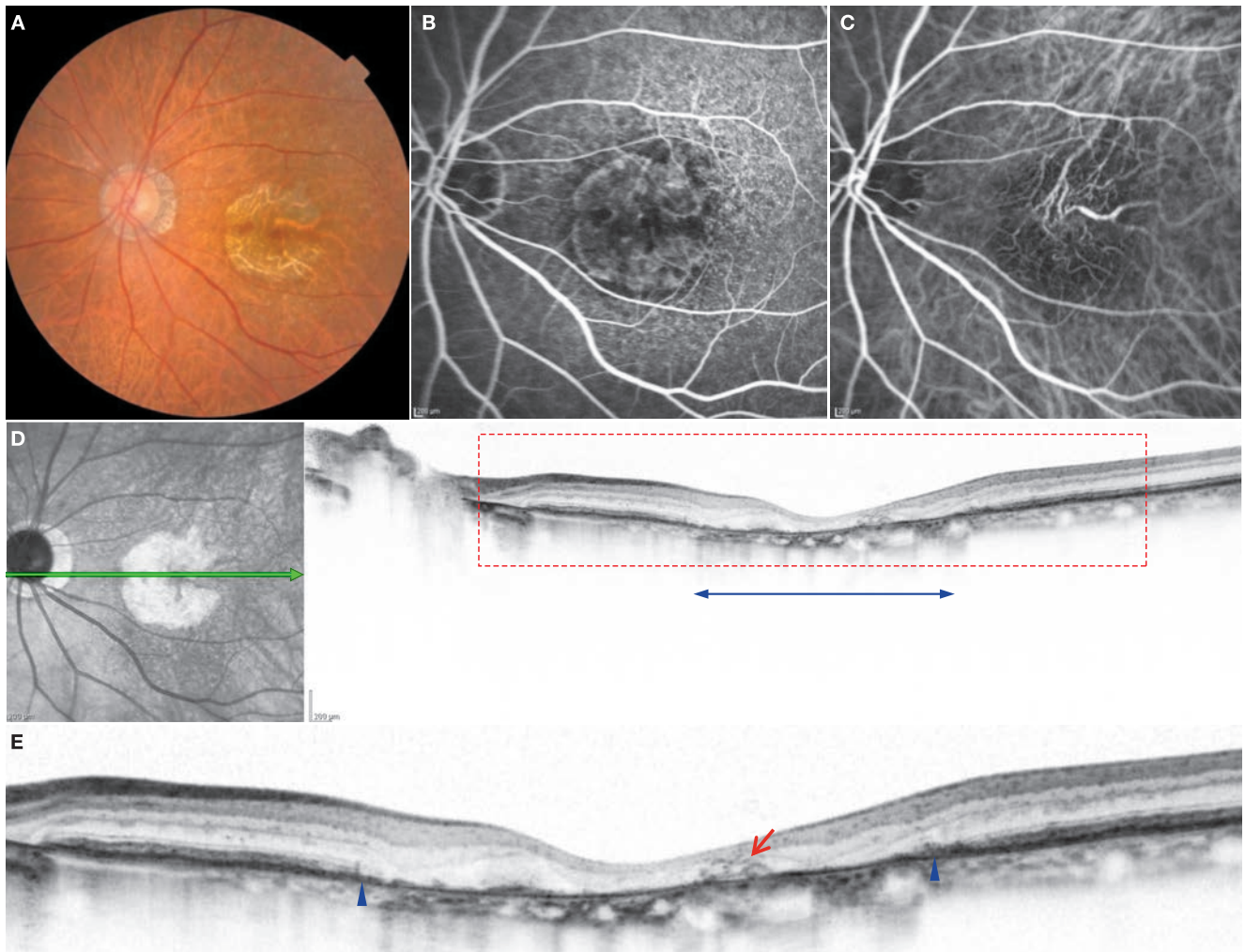

A: Color fundus photograph: A geographic atrophic lesion of about 1.5 disc diameter is visible in the macula. The large blood vessels of the choroid are visible around the atrophic lesion. Relatively small drusen and reticular pseudodrusen are observed. **B:** FA in the left eye (42 seconds): The round atrophic lesion is exhibiting hyperfluorescence due to window defects. Blocked fluorescence is seen in one part of the lesion due to reactive proliferation of the RPE. Multiple drusen can be seen around the atrophic lesion. **C:** IA in the left eye (42 seconds): The large blood vessels of the choroid are clearly visible. The drusen are essentially exhibiting hypofluorescence. **D:** IR + OCT horizontal scan of the left eye: Retinal atrophy is exhibited in the geographic lesion area (◄—►). **E:** Enlarged version of D [red dashed box]: The ELM and IS/OS are not visible between the two (►). The RPE is also lost. As a result, choroidal signal enhancement can be seen. The outer retinal layers are partially visible in a small area. In addition, highly reflective patterns (➔) can be seen within the retina. Reticular pseudodrusen can also be seen.

Image interpretation points

This is atrophic AMD with a typical geographic atrophic lesion. While previously rare in Japanese people, the frequency of these lesions has increased in recent years. The RPE is lost over a wide area, though similar findings are also seen in cone and macular dystrophies. Whether or not various pathological conditions can be differentiated with OCT findings alone is the subject of future investigation.

Case 94 Atrophic age-related macular degeneration: Atrophic lesions of various sizes

A 65-year-old male, OS, BCVA 0.4

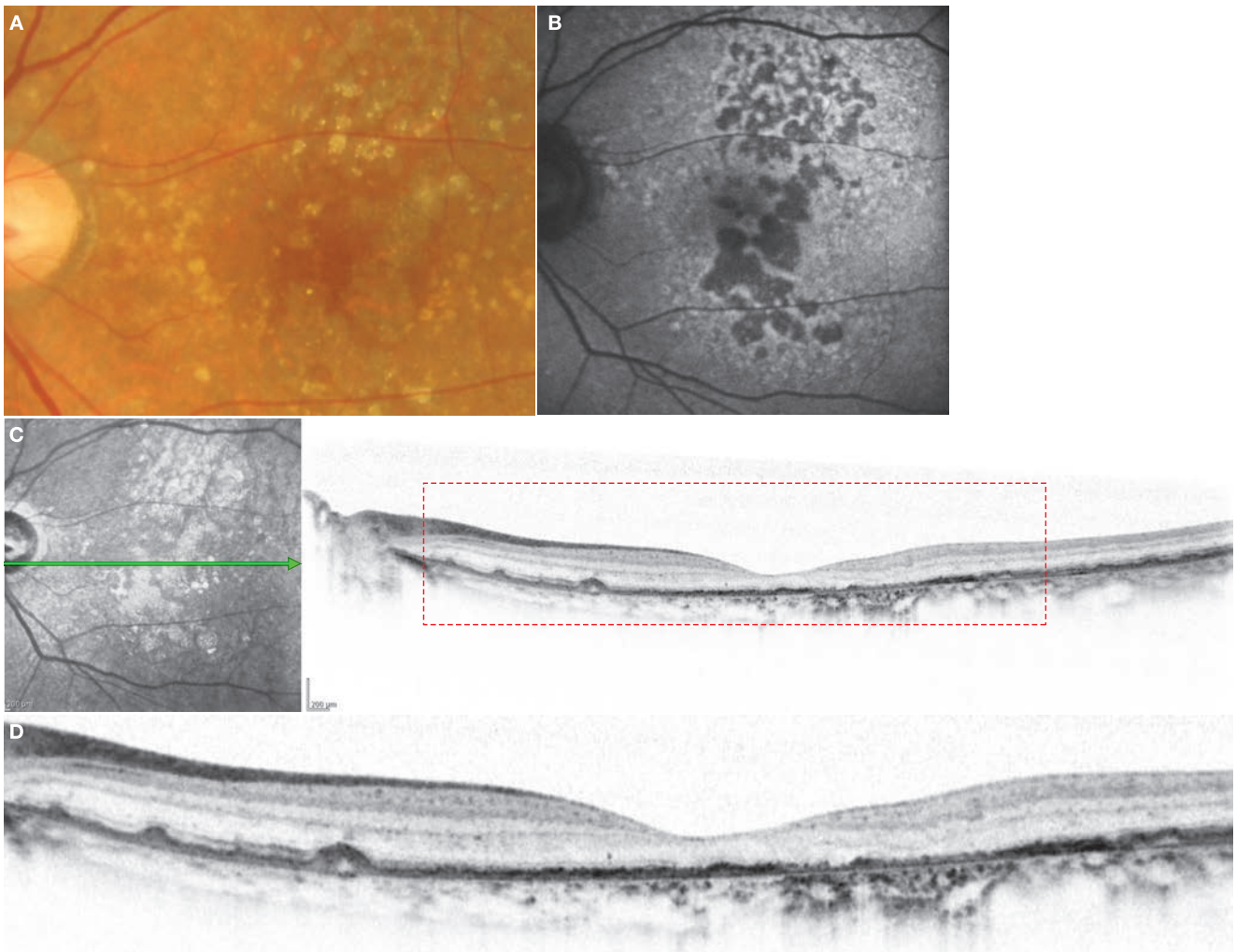

A: Color fundus photograph: Drusen of various sizes and RPE pigmentation changes can be seen over a wide area of the macula. The atrophic lesions present as punctiform patterns. **B:** FAF in the left eye: Relatively large hypofluorescent foci and small hyperfluorescent foci are mixed together. The hypofluorescent foci are bordered by hyperfluorescence. The atrophic lesions are hypofluorescent. **C:** IR + OCT horizontal scan of the left eye: The foveal retina is thinned. **D:** Enlarged version of C [red dashed box]: Loss of the outer retinal layers and RPE is mild and localized. Visual acuity is relatively good. Reticular pseudodrusen can also be seen.

Image interpretation points

This is a case of relatively mild atrophic AMD. Multiple drusen are present but the fundus appearance differs from geographic atrophic lesions. There is a mild visual decline (best-corrected visual acuity 0.4) and the lesions can be diagnosed as atrophic AMD.

Cases where drusen are numerous can develop exudative AMD, or progress to atrophic AMD, as seen in this case. The risk factor for the pattern of progression is an important area of study but there is currently no consensus.

Case 95 Atrophic age-related macular degeneration: Fellow eye of PCV

An 84-year-old male, OD and OS, BCVA 0.4 and 0.6 respectively

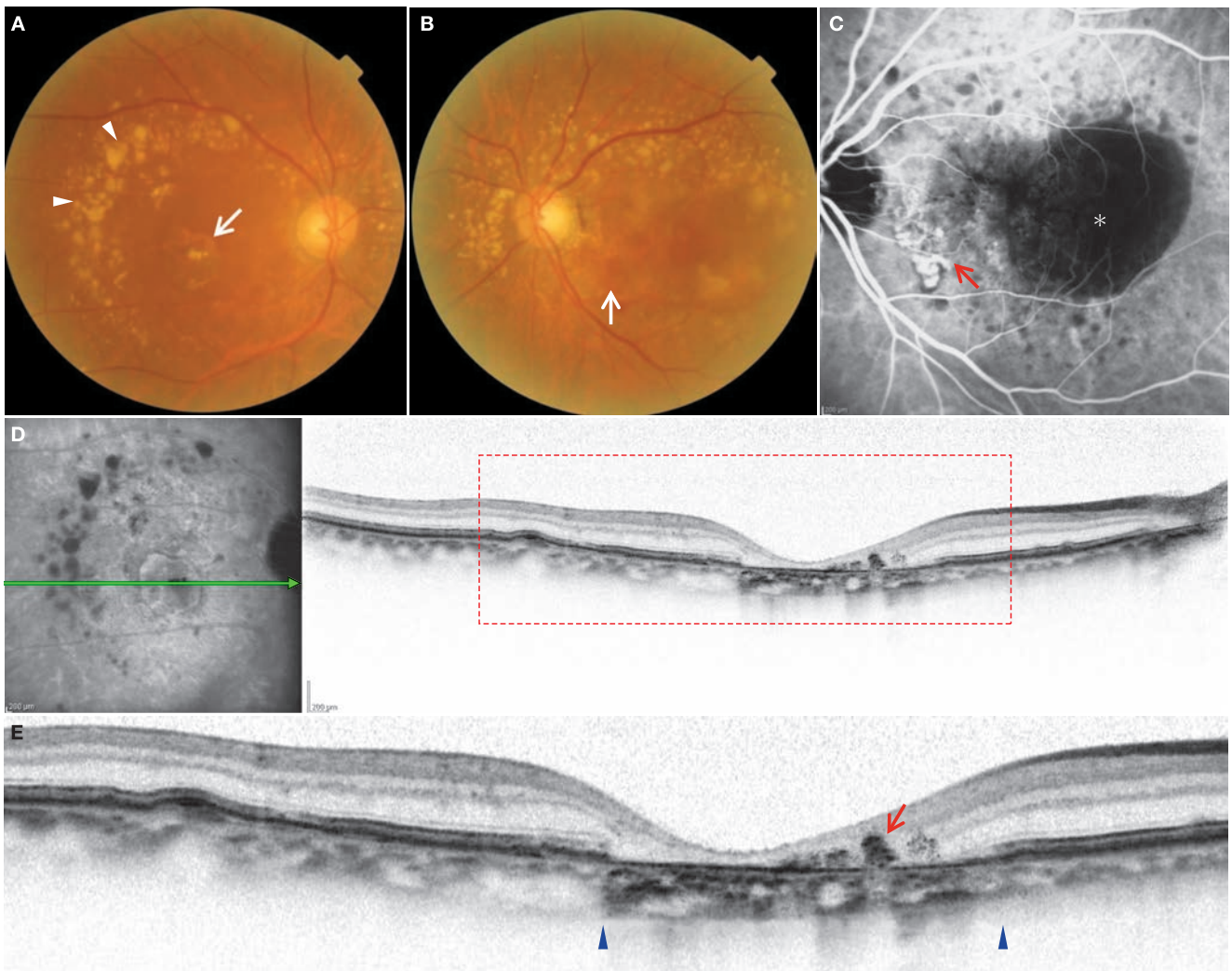

A: Color fundus photograph in the right eye: An atrophic lesion of about 1 disc diameter is observed in the fovea centralis. Multiple large drusen are scattered around the lesion (▷). The atrophic foveal lesion may have developed from a serous PED. **B:** Color fundus photograph in the left eye: A polypoidal lesion is visible inferonasal to the fovea centralis (⇨). It is accompanied by a large PED. **C:** IA in the left eye (40 seconds): A typical polypoidal lesion and an abnormal vascular network (➔) can be seen. The PED is exhibiting hypofluorescence (✻). CNV appears to exist within the PED. **D:** IR + OCT horizontal scan of the right eye: The fovea is significantly thinned. **E:** Enlarged version of D [red dashed box]: The ELM, IS/OS and RPE are not seen in the area indicated by (►). Migrating RPE cells are seen within the sensory retina (➔). Thinning of the fovea is evident.

Image interpretation points

This case is the same as case 88. During initial diagnosis, the right eye exhibited atrophic AMD, and the left eye exhibited drusenoid PED. PCV subsequently occurred in the left eye. This case illustrates the fact that both atrophic and exudative AMD progress from drusen and that PCV falls into the category of exudative AMD.

Cases that progress from serous PED to a geographic atrophic lesion such as in this case appear to be common in Japanese people. In addition, there are cases where prolonged courses of central serous chorioretinopathy progress to geographic atrophy.

6.4 Choroidal neovascularization and exudative age-related macular degeneration

Background

Choroidal neovascularization (CNV) is the state in which new vessel growth originating from the choroid penetrates Bruch's membrane to beneath the RPE or the sensory retina. Terms such as classic or occult CNV are often used to classify CNV (Fig. 6-11). To be strict, these terms, are used to describe findings on FA.[1] FA does not provide detailed information about depth. As a result, this classification system cannot be used to describe the retinal layer structures in which a lesion exists. For example, a label of classic or occult CNV will not discriminate CNV localized beneath the RPE or CNV extending through the RPE.

On the other hand, Gass's classification of Type 1 CNV and Type 2 CNV are also often used[2] (Fig. 6-12). These terms are based on histopathological descriptions where Type 1 CNV is confined to sub-RPE space and Type 2 CNV penetrates the RPE and extends to the subretinal space. Unfortunately, the clinical setting is limited to biomicroscopy, confocal laser ophthalmoscopy, FA, IA, and OCT. Given its ability to obtain tomographic image of lesions, the OCT is an practical option for discriminating Type 1 and Type 2 CNV.

While Type 1 CNV is seen in most cases of exudative AMD, Type 2 CNV is not as common as previously understood.[3] Most cases thought to be Type 2 CNV. During the era of time-domain OCT where resolution was poor were the so-called »mixed type« (a mixture of Type 1 and Type 2 components). Therefore, pure Type 2 CNV is rare in AMD patients. When such cases were seen, secondary causes of CNV had to be considered. Abnormal vascular network of PCV is Type 1 CNV.[4, 5]

Idiopathic CNV and CNV associated with severe myopia are almost without exception Type 2 CNV and they do not have any components of Type 1 CNV.[6] Type 2 CNV often occurs in angioid streaks, as well, where Type 1 CNV is sometimes seen.[7, 8]

Even using the latest spectral-domain OCT, the beam does not sufficiently penetrate the RPE in cases where strong exuda-

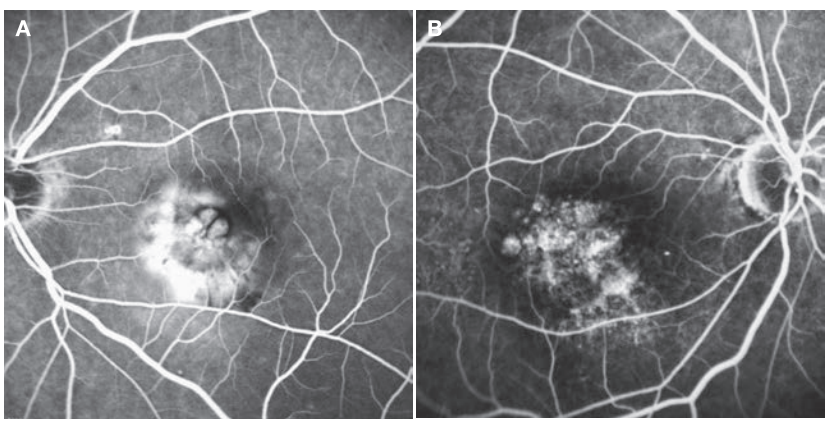

Fig. 6-11 FA of classic CNV and occult CNV
A: Predominantly classic CNV. Strong fluoroscein leakage can be seen from CNV inferonasal to the fovea centralis. **B:** Occult with no classic CNV. The fluoroscein is confined to the sub-RPE space and leakage is weak..

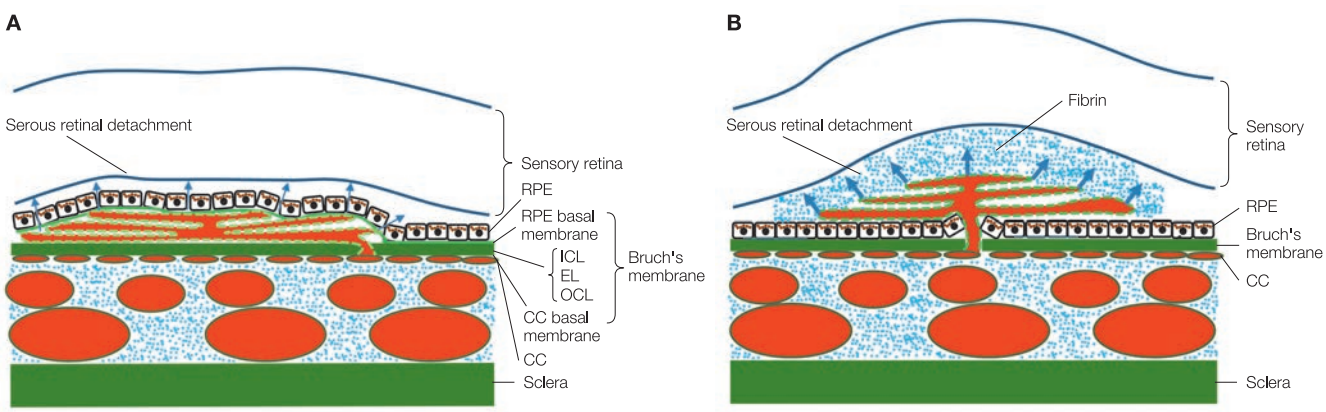

Fig. 6-12 Type 1 CNV and Type 2 CNV
A: Schematic diagram of Type 1 CNV, **B:** Schematic diagram of Type 2 CNV.
Type 1 CNV spreads beneath the RPE, whereas Type 2 CNV breaks through the RPE and extends to beneath the sensory retina. In general, exudative changes in the sensory retina are stronger in Type 2 CNV.
RPE= retinal pigment epithelium, ICL= inner collagenous layer, EL= elastic layer, OCL= outer collagenous layer, CC= choriocapillaris

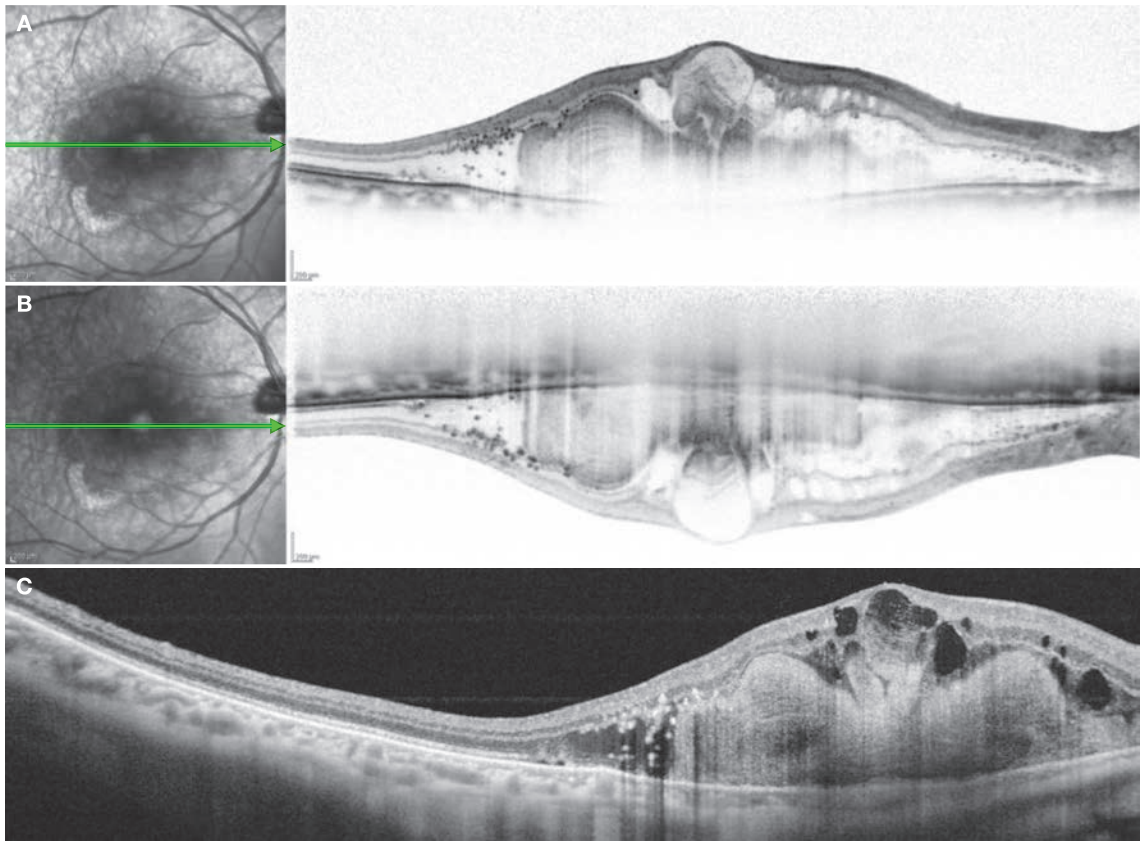

Fig. 6-13 CNV OCT findings
A: Scanning in normal mode. The state of the RPE is difficult to determine due to strong retinal exudative changes and CNV. **B:** Scanning in EDI-OCT. We can clearly see that there is no breakdown in the RPE line. **C:** 1,050 nm SS-OCT image. The state of the RPE is clearly seen as a result of a long-wavelength light source. All the scans are taken from approximately the same site in the same eye.

tive changes are found in the sensory retina. As a result, the type of CNV cannot be reliably determined (Fig. 6-13A). In such cases EDI-OCT images[9] can be useful (Fig. 6-13B). In addition, changes beneath the RPE may be easier to detect using high-penetration OCT (also termed SS-OCT), which is highly likely to spread in the near future (widelly used SD-OCT uses an OCT light source with a central wavelength of about 840 nm, whereas this new SS-OCT uses a scanning light source of 1, 050 nm) (Fig. 6-13C).

6.4.1 References

1) Macular Photocoagulation Study Group. Subfoveal neovascular lesions in age-related macular degeneration. Guidelines for evaluation and treatment in the macular photocoagulation study. *Arch Ophthalmol*. 1991; 109:1242–1257.
2) Gass JM. Biomicroscopic and histopathologic considerations regarding the feasibility of surgical excision of subfoveal neovascular membranes. *Am J Ophthalmol*. 1994; 118:285–298.
3) Coscas F, Coscas G, Souied E, et al. Optical coherence tomography identification of occult choroidal neovascularization in age-related macular degeneration. *Am J Ophthalmol*. 2007; 144:592–599.
4) Freund KB, Zweifel SA, Engelbert M. Do we need a new classification for choroidal neovascularization in age-related macular degeneration? *Retina*. 2010; 30:1333–1349.
5) Imamura Y, Engelbert M, Iida T, et al. Polypoidal choroidal vasculopathy: a review. *Surv Ophthalmol*. 2010; 55:501–515.
6) Gass JDM. Stereoscopic atlas of Macular Diseases. Diagnosis and Treatment. 4th Ed. Mosby, St. Louis, 1997.
7) Sawa M, Gomi F, Tsujikawa M, et al. Long-term results of intravitreal bevacizumab injection for choroidal neovascularization secondary to angioid streaks. *Am J Ophthalmol*. 2009; 148:584–590.
8) Costa RA, Calucci D, Cardillo JA, et al. Selective occlusion of subfoveal choroidal neovascularization in angioid streaks by using a new technique of ingrowth site treatment. *Ophthalmology*. 2003; 110:1192–1203.
9) Spaide RF. Enhanced depth imaging optical coherence tomography of retinal pigment epithelial detachment in age-related macular degeneration. *Am J Ophthalmol*. 2009; 147:644–652.

Case 96 Exudative age-related macular degeneration: Type 1 CNV with a SRD

Right eye of 58 year male with vision corrected to 0.1

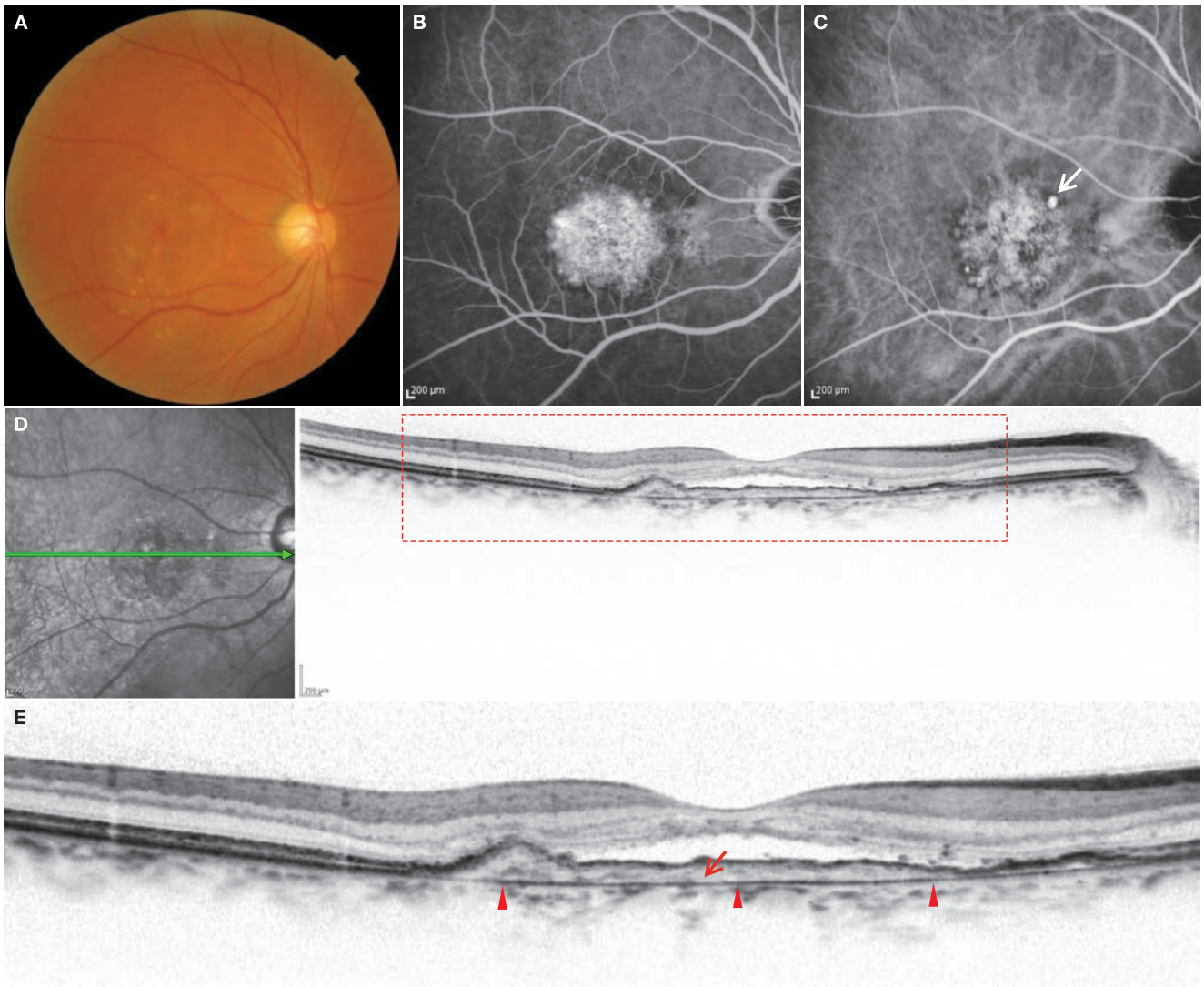

A: Color fundus photograph in the right eye: A SRD of about 1.5 disc diameters is seen in the fovea centralis. Drusen are scattered. No exudative changes such as retinal hemorrhages or hard exudates are visible. **B:** FA in the right eye (3 minutes, 36 seconds): Granular hyperfluorescence is observed in the SRD area. Fluoroscein leakage is mild. **C:** IA in the right eye (3 minutes, 36 seconds): A abnormal vascular network appears to exist on IA. A Hyperfluorescent focus suggestive of polypoidal lesions is seen (⇨). **D:** IR + OCT horizontal scan of the right eye: A flat RPE protrusion and a SRD can be seen on OCT. The area between the RPE and Bruch's membrane is exhibiting moderate reflectivity. **E:** Enlarged version of D [red dashed box]: CNV exhibiting moderate reflectivity is confined to sub-RPE space (➔). Bruch's membrane is depicted as a straight, highly reflective line indicated by (►). The location of Type 1 CNV is always between the RPE and Bruch's membrane. The foveal photoreceptor outer segment is not seen and the fovea centralis is thinned.

Image interpretation points

This is a case where PCV should be considered based on the IA findings. Nevertheless, only a flat protruding fibrovascular PED is seen rather than a steep RPE protrusion. Based on these OCT findings, it may be reasonable to consider this a Type 1 CNV. Also note, Bruch's membrane is easily visible.

Case 97 Exudative age-related macular degeneration: Type 1 CNV with low activity

A 57-year-old male, OS, BCVA 0.4

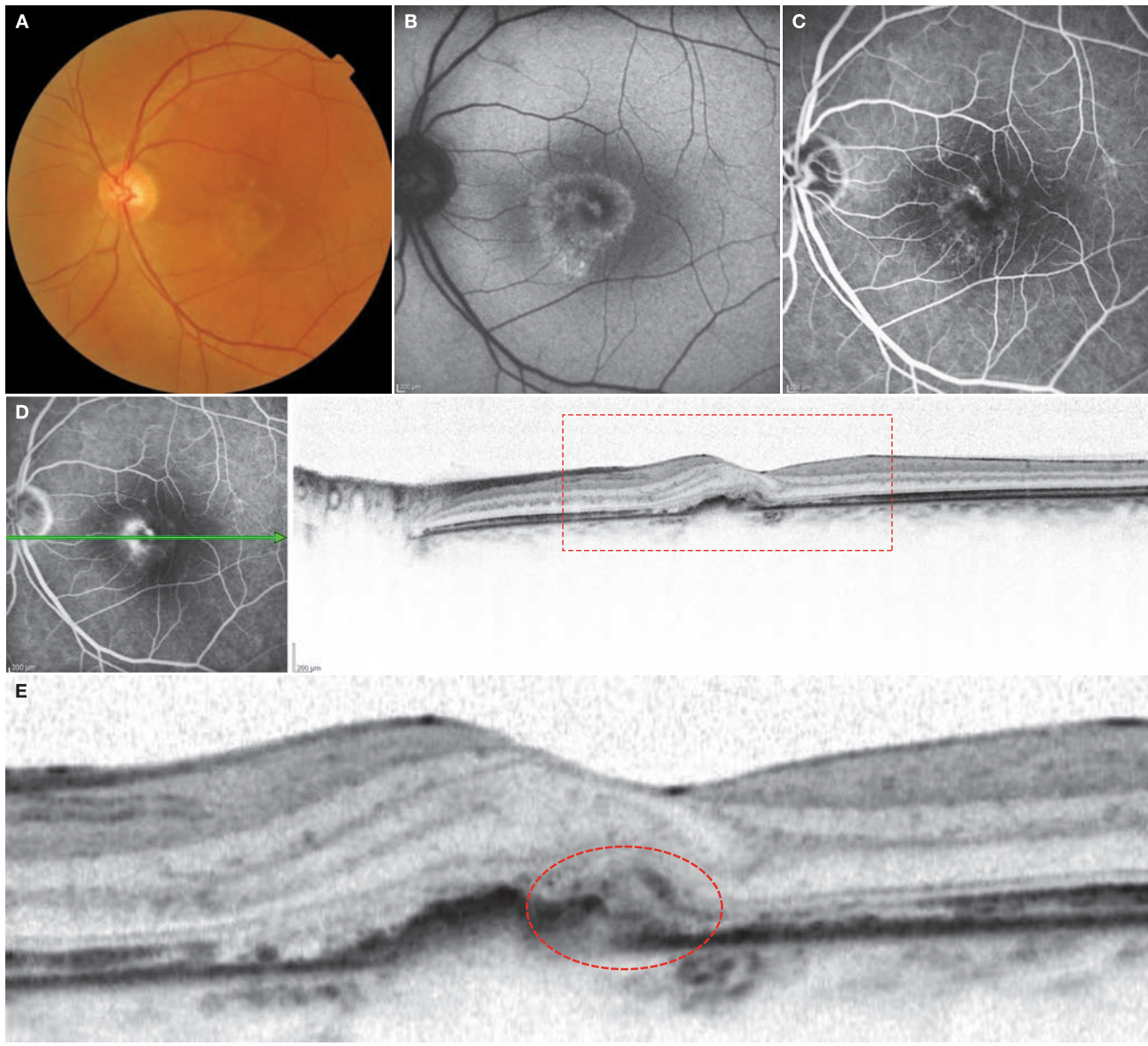

A: Color fundus photograph in the right eye: Annular RPE depigmentation about 1.5 disc diameters is observed in the fovea centralis. **B:** FAF in the left eye: The area of abnormal RPE pigment is exhibiting hyperfluorescence. The surrounding area is slightly hypofluorescent. **C:** FA in the left eye (1 minute, 12 seconds): Faint hyperfluorescence can be seen in the fovea centralis. **D:** FA + OCT horizontal scan of the left eye: A flat RPE protrusion can be seen on OCT. The content of the PED is exhibiting moderate reflectivity. **E:** Enlarged version of D [red dashed box]: The highly reflective line of the PED appears to be breaking down in the site encircled by the red dashed line (red dashed circle). The subfoveal IS/OS is poorly visible.

Image interpretation points

It may be difficult to determine if CNV is present in this case. Even if CNV exists, its activity is low. The structure of the foveal IS/OS is abnormal, consistent with the best-corrected visual acuity of 0.4. Mild edema can be seen in the retina, and it is highly likely that CNV is penetrating slightly below the retina in the area of the red dashed line seen in E.

Case 98 Exudative age-related macular degeneration: Type 1 CNV with relatively strong exudative changes

A 57-year-old male, OD, BCVA 1.2

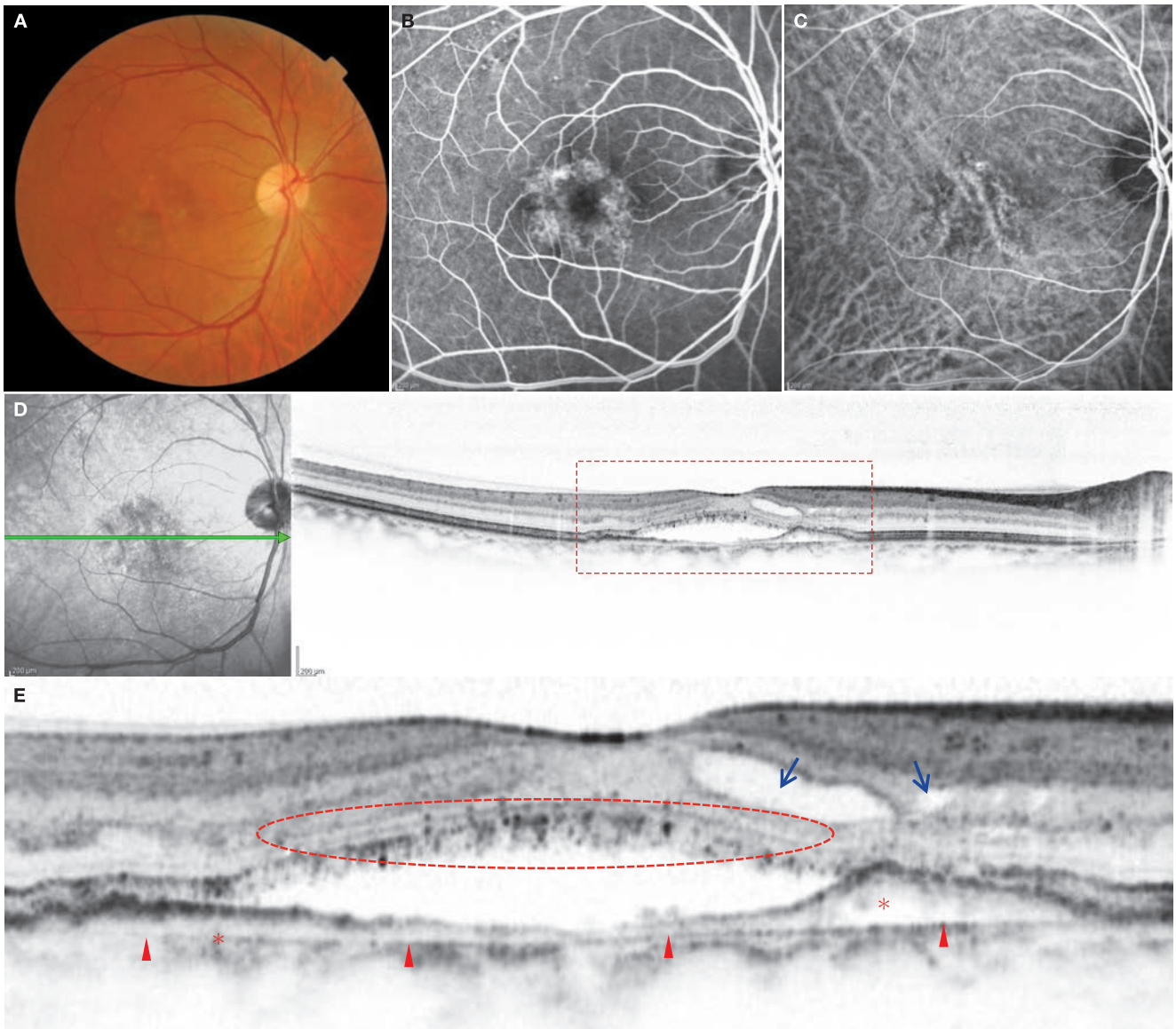

A: Color fundus photograph: Mottled depigmentation can be seen in the RPE in the fovea centralis. A flat SRD is also present. **B:** FA in the right eye (27 seconds): Hyperfluorescence consistent with the site exhibiting the RPE depigmentation is visible. These are findings characteristic to occult CNV. **C:** IA in the right eye (27 seconds): The choroidal vessels can be observed more clearly in the region exhibiting hyperfluorescence on FA. **D:** IR + OCT horizontal scan of the right eye: A SRD is observed in the fovea centralis. Cystic changes can be seen in the sensory retina. **E:** Enlarged version of D [red dashed box]: The flat RPE protrusion is due to CNV (*). The line of Bruch's membrane (►) is clearly visible beneath the RPE. Cystic changes (➔) are exhibited in the sensory retina. The photoreceptor outer segment of the detached retina is slightly elongated. Highly reflective spots are scattered in the outer retinal layers (red dashed circle). These may be penetrated macrophages. (Continued on the next page)

Image interpretation points

This is a case of Type 1 CNV with a few findings indicating PCV on angiography and OCT images. The activity of CNV in this case is relatively strong as evidenced by the exudative changes found in the sensory retina.

Case 98 Six months later

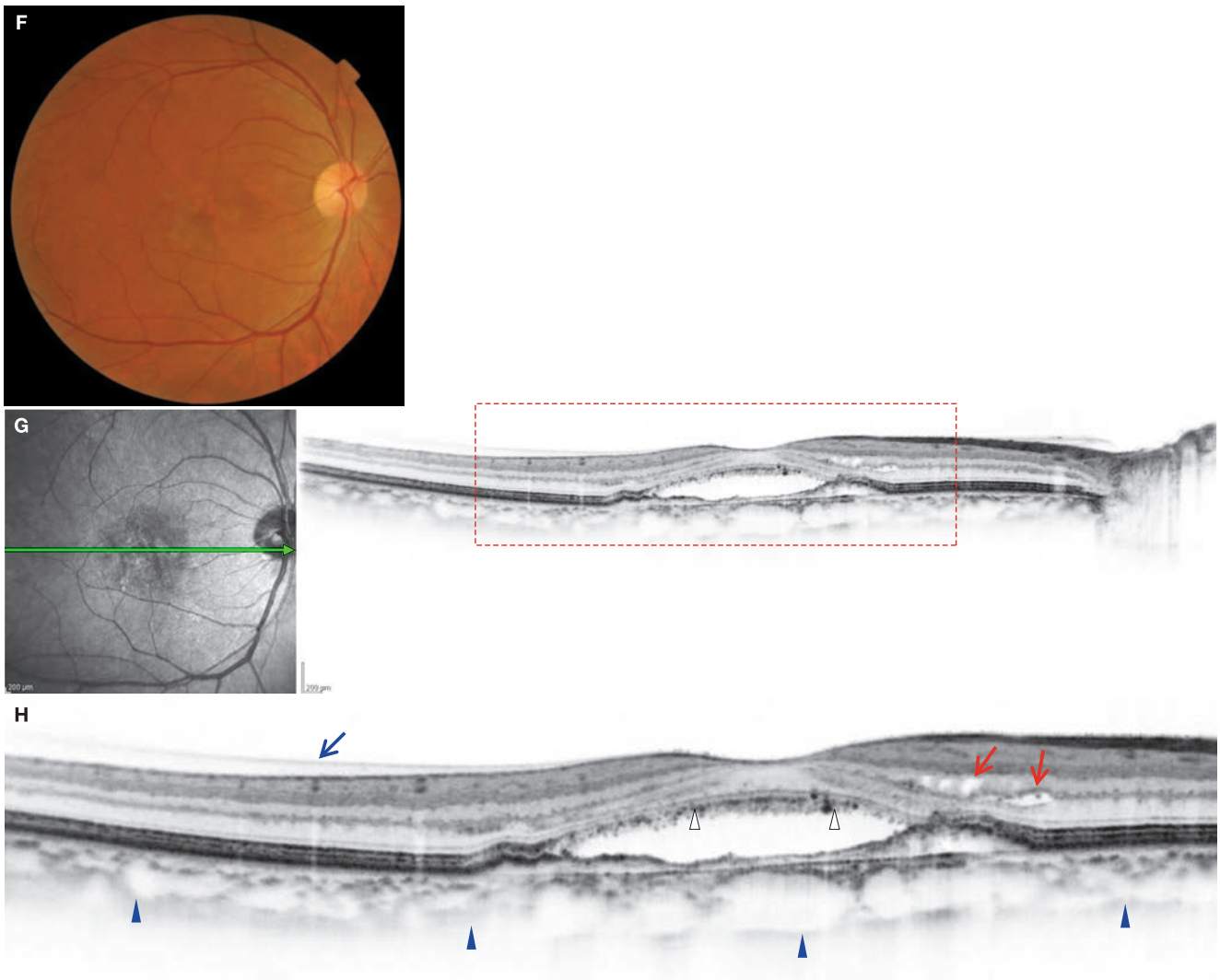

F: Color fundus photograph in the right eye: There is almost no change compared to the fundus photograph from 6 months earlier. **G:** IR + OCT horizontal scan of the right eye: There is almost no change observed in the RPE protrusion and SRD compared with the IR and OCT from 6 months earlier. **H:** Enlarged version of G [red dashed box]: Type 1 CNV is clearly visible. Cystic changes (➔) remain in the sensory retina. Photoreceptor outer segment changes (▷) are insignificant. The detached posterior vitreous cortex (➔) is seen outside the fovea centralis. The line on the outer edge of the choroid can be traced (►) as a result of averaging multiple B-scans at the identical location of interest. Choroidal thickness in this case appears to be normal.

Image interpretation points

This is a case where there was almost no progress in 6 months based on just a follow-up. Differentiation from central serous chorioretinopathy is difficult with biomicroscopic findings, but PEDs larger and taller than this case are not seen in central serous chorioretinopathy.

Case 99 Exudative age-related macular degeneration: Case with extensive Type 1 and 2 CNV exudative changes

A 59-year-old male, OS, BCVA 0.15

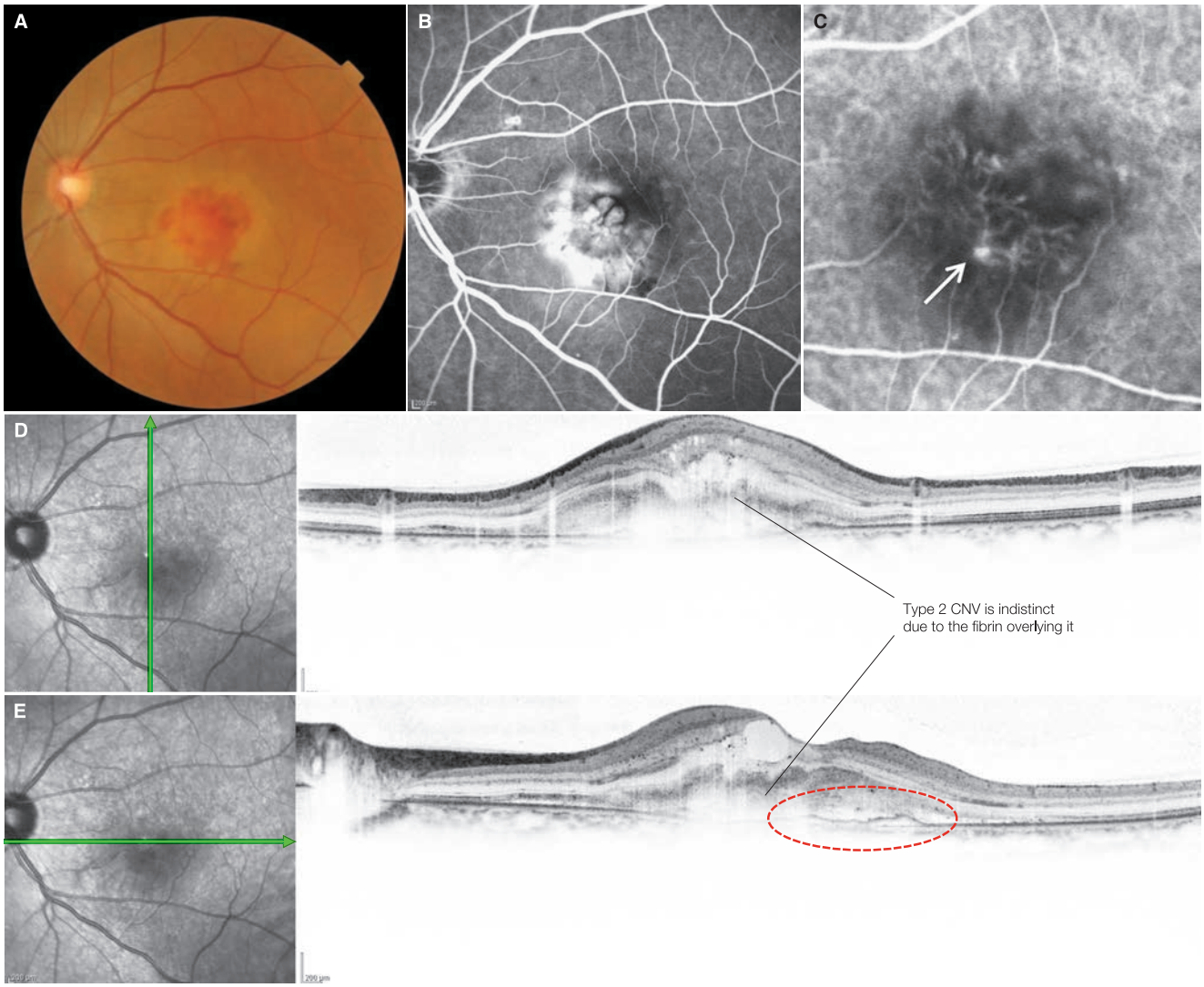

A: Color fundus photograph in the left eye: CNV with retinal hemorrhages is seen in the fovea centralis. Fibrin is seen deposited over the CNV. **B:** FA in the left eye (40 seconds): Intense hyperfluorescence can be seen. CME is also visible. **C:** Enlarged image of IA in the left eye (1 minute, 17 seconds): Reticular pattern of CNV is seen, which is similar to the abnormal vascular network that can be seen in PCV. The CNV appears to originate inferonasally to the fovea centralis (⇨). **D:** IR + OCT vertical scan of left eye: Cystoid spaces are is observed. Although the RPE line is incomplete, it is mostly visible and relatively flat. There are highly reflective clumps above the RPE due to hemorrhages, fibrin and Type 2 CNV. **E:** IR + OCT horizontal scan of left eye: Similar findings as D are noted. In the red dashed circle outside the fovea centralis, there is a flat RPE protrusion corresponding to Type 1 CNV. In the other area, the RPE is flat and visible over the entire length of the scan. (Continued on the next page)

Image interpretation points

Fibrin deposits can be seen on the fundus photograph. A classic CNV pattern is exhibited on FA, and a reticular, branched CNV is seen on IA. Type 2 CNV is not clearly appreciated on OCT; however, since the RPE protrusion is not significant, it may be Type 2 CNV combined with fibrin. Type 1 CNV also exists beneath the RPE in the red dashed circle in E.

Case 99 Six months after treatment with anti-VEGF treatment

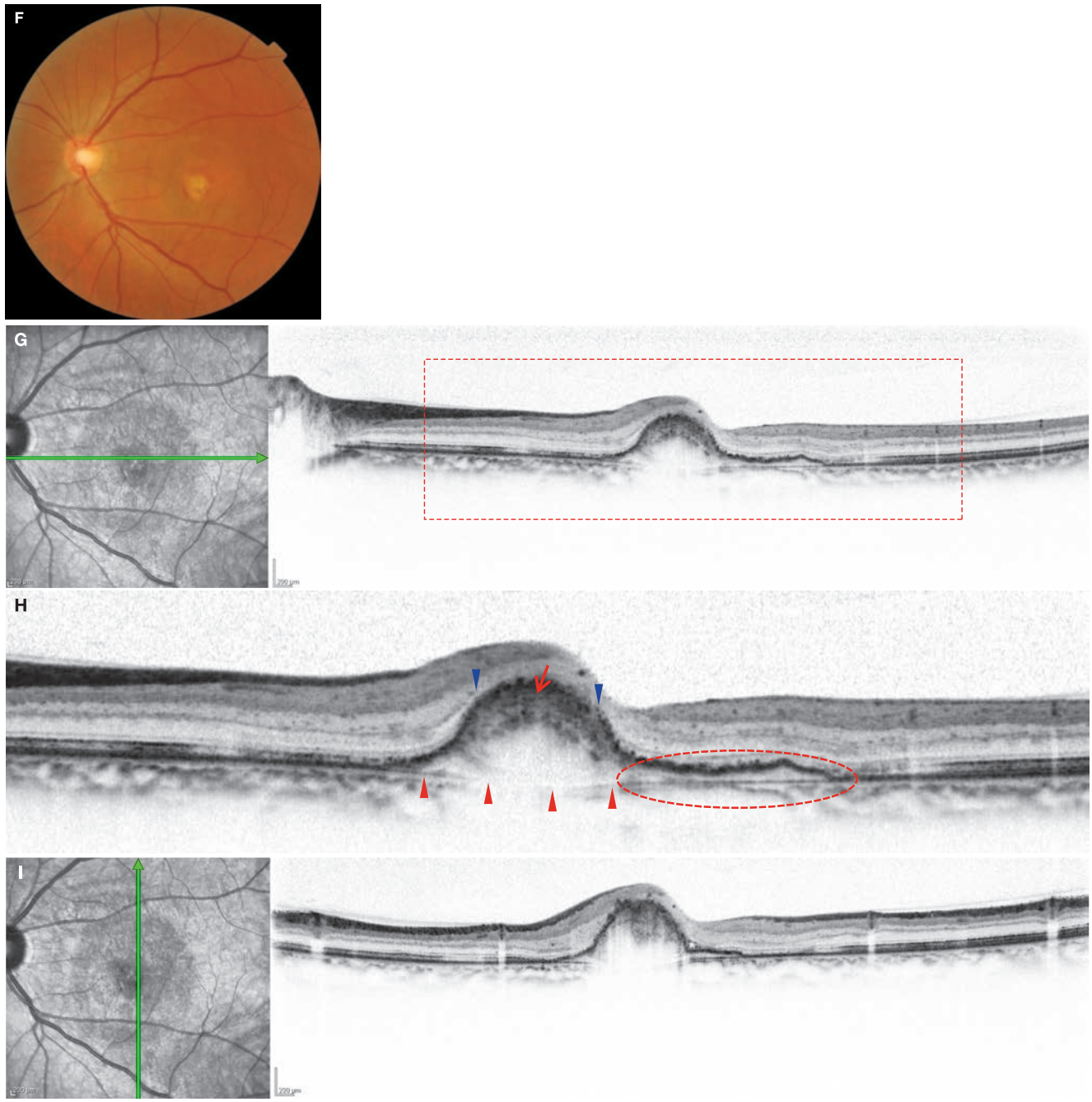

F: Color fundus photograph in the left eye: The exudative changes seen in the fovea centralis has disappeared. Scar formation can be seen. **G:** IR + OCT horizontal scan of the left eye: The CNV has scarred and there is a large RPE protrusion. No exudative changes can be seen in the retina. **H:** Enlarged version of G [red dashed box]: CNV enveloped by the RPE is clearly visible (►). The highly reflective (➔) Bruch's membrane can be traced beneath the scarred CNV (►). Temporally, there is a flat RPE protrusion with Type 1 CNV within the red dashed circle. **I:** IR + OCT vertical scan of the left eye: The internal reflectivity of the scar lesions is relatively high.

Image interpretation points

These are images taken 6 months after intravitreal injection of bevacizumab (Avastin®). We can see that the RPE is enveloping the CNV with resultant scarring. No exudative changes are observed in the sensory retina. Best-corrected visual acuity continues to be 0.15 with no improvement after treatment. There is a flat RPE protrusion (the red dashed circle in C), which indicates that Type 1 CNV remains. Scarred Type 2 CNV also remains beneath the significant RPE protrusion nasal to the fovea centralis.

Case 100 Exudative age-related macular degeneration: Type 1 and 2 CNV with extensive serous retinal detachment

An 87-year-old male, OS, BCVA 0.6

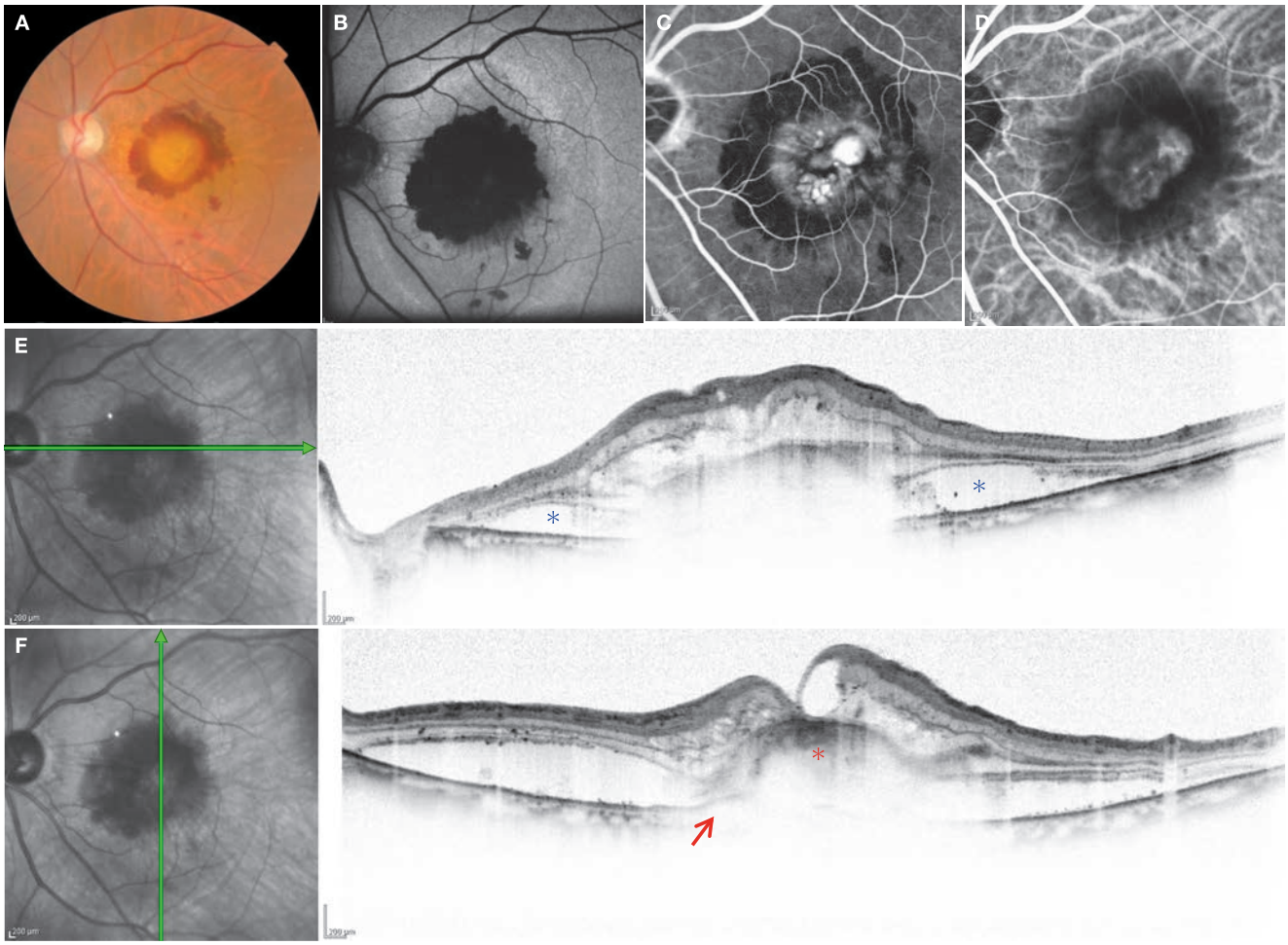

A: Color fundus photograph in the left eye: Large CNV is seen in the fovea centralis and a subretinal hemorrhage exists around it. There are also fibrin deposits. **B:** FAF in the left eye: The CNV and surrounding hemorrhages are exhibiting hypofluorescence. The weak hyperfluorescence around it appears annular. **C:** FA in the left eye (1 minute, 8 seconds): Hyperfluorescence can be seen as a result of fluorescein accumulation in the CNV and cystoid spaces. **D:** IA in the left eye (1 minute, 8 seconds): CNV is easily appreciated on IA. **E:** IR + OCT horizontal scan of the left eye: The RPE is not well defined due to strong exudative changes in the sensory retina. We can see a SRD (*). **F:** IR + OCT vertical scan of left eye: The RPE protrusion can be seen (→). This protrusion indicates Type 1 CNV. The subfoveal lesion is comprised of CNV and fibrin (*).

Image interpretation points

This is a case with large CNV. Significant exudative changes can be seen in the sensory retina. Blocking of OCT probe light by the CNV causes the poor OCT image below it. (*). The RPE line is protruding slightly (→) and Type 1 CNV appears to exist in this area. OCT allows detection of a wider SRD than a biomicroscopy does.

Case 101 Exudative age-related macular degeneration: Type 1 and 2 CNV with cystic changes

A 67-year-old male, OD, BCVA 0.05

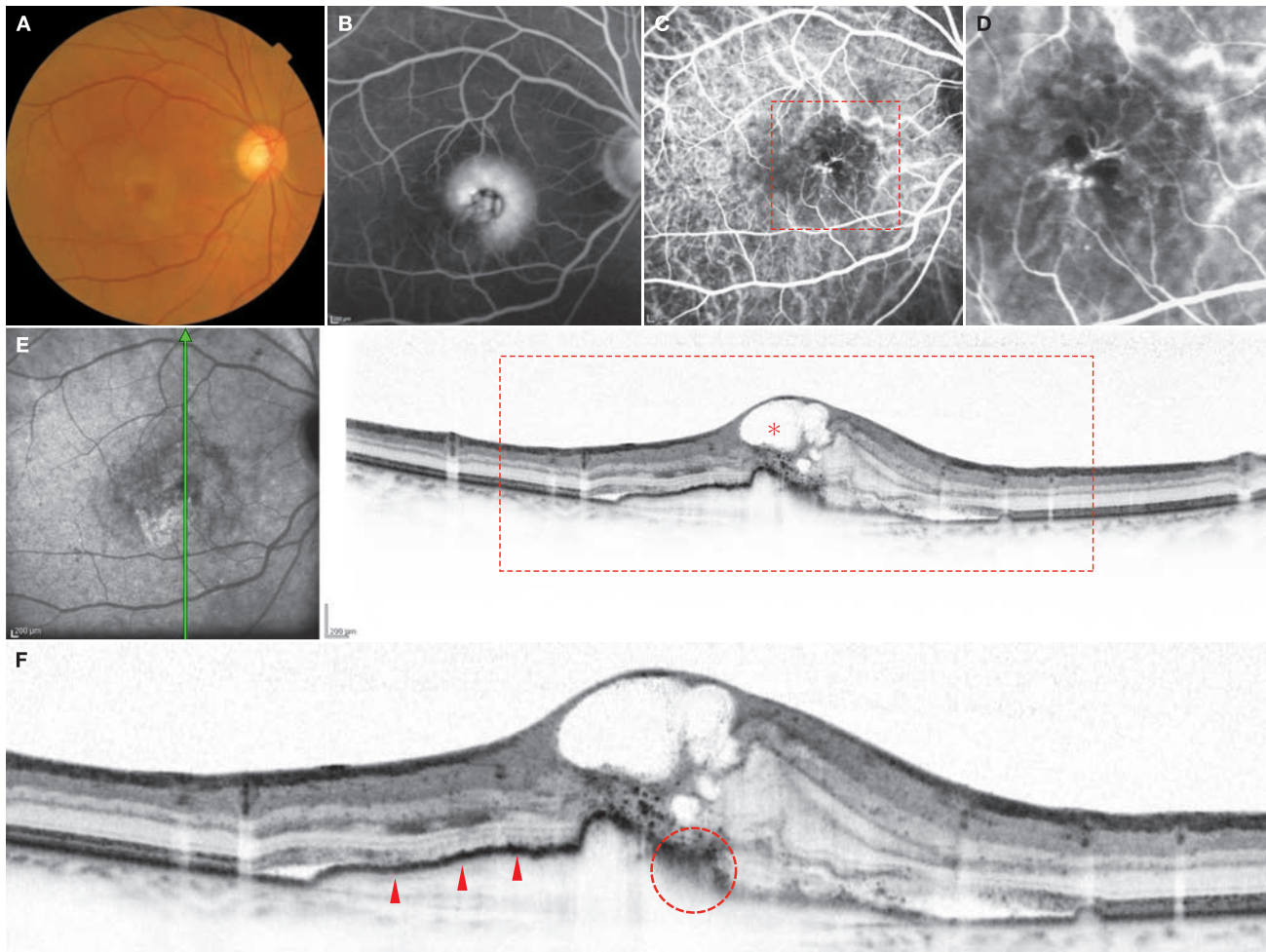

A: Color fundus photograph in the right eye: A flat PED is seen in the fovea centralis. Subfoveal CNV appears to exist. **B:** FA in the right eye (3 minutes): A significant hyperfluorescent focus is visible in the late-stage FA image. **C:** IA in the right eye (52 seconds): The branched CNV is easily seen on IA. **D:** Enlarged version of C [red dashed box]: The CNV root appear to be branching out in a fan shape. **E:** IR + OCT vertical scan of the right eye: A large cystoid space is seen (✻). The large RPE protrusion is clearly visible. **F:** Enlarged version of E [red dashed box]: The cystoid spaces and RPE protrusion (►) are clearly visible. In the area of the irregular RPE line at the superior fovea centralis, Type 2 CNV can be seen extending beneath the sensory retina (red dashed circle).

Image interpretation points

A classic CNV pattern is seen on FA. On OCT, a large RPE protrusion caused by Type 1 CNV can seen. Superior to this, type 2 CNV can be seen penetrating the RPE. The Type 2 CNV seen on OCT corresponds to classic CNV on FA.

Case 102 Exudative age-related macular degeneration: Type 2 CNV localized in the fovea centralis

A 71-year-old female, OD, BCVA 0.05

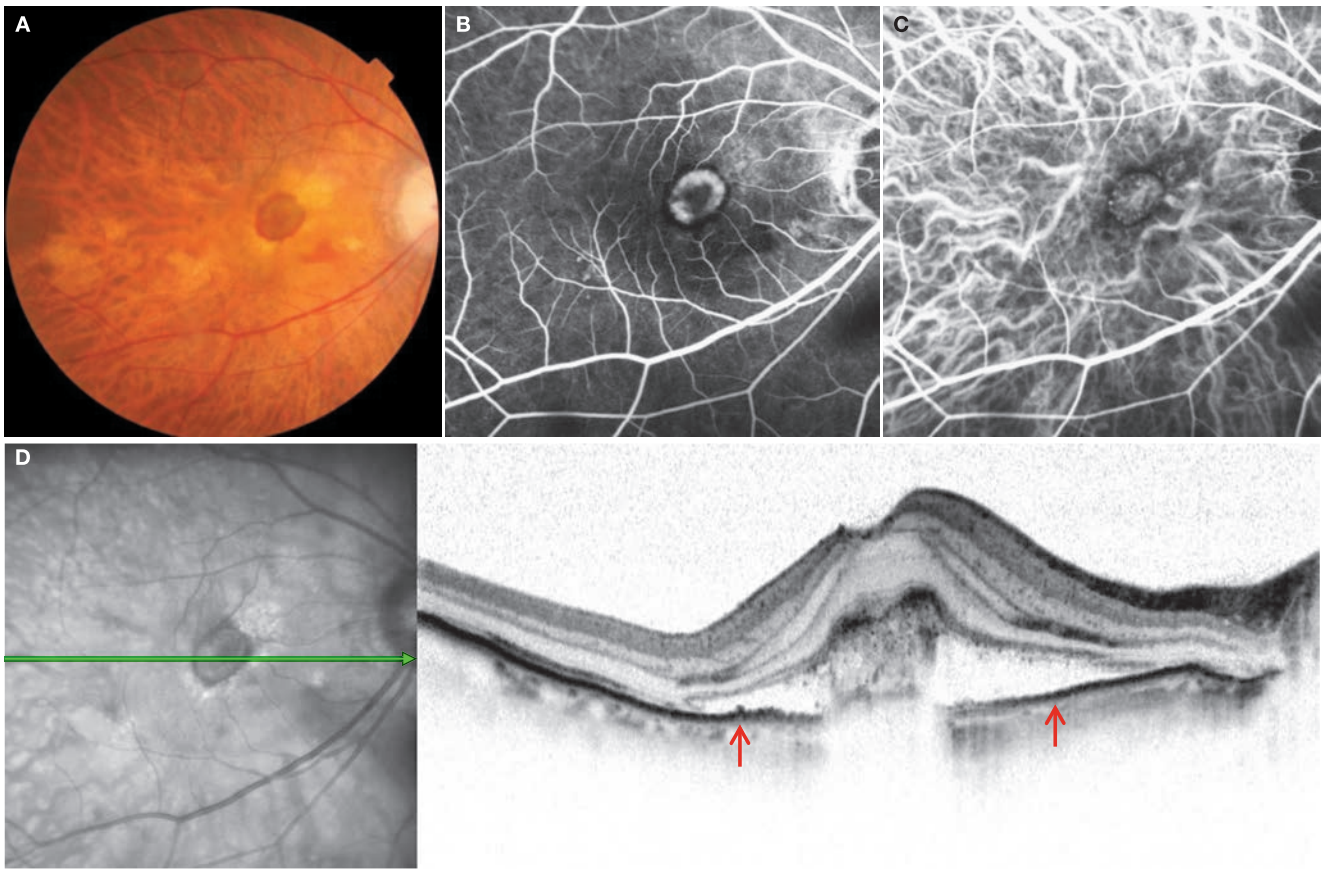

A: Color fundus photograph in the right eye: Well-defined CNV can be seen in the fovea centralis. The tigroid fundus as seen in myopic eyes is observed, but the axial length is 22.63 nm. **B:** FA in the right eye (40 seconds): Typical classic CNV is observed. **C:** IA in the right eye (40 seconds): Reticular CNV is seen. **D:** IR + OCT horizontal scan of the right eye: CNV with high reflectivity is visible beneath the fovea centralis. The high reflectivity in contact with the retina is due to fibrin. Little protrusion can be seen in the RPE (→). No elements of Type 1 CNV can be seen. The choroid is thinned.

Image interpretation points

AMD is accompanied by Type 1 CNV in most cases; in fact, it is rare to see CNV consisting of only Type 2 CNV. It is necessary to consider secondary CNV if only Type 2 CNV was found. The choroid is thinned, which may be due to age-related choroidal atrophy.

Case 103 Exudative age-related macular degeneration: Type 2 CNV with strong exudative changes

Right eye of a 71-year-old male with vision corrected to 0.1

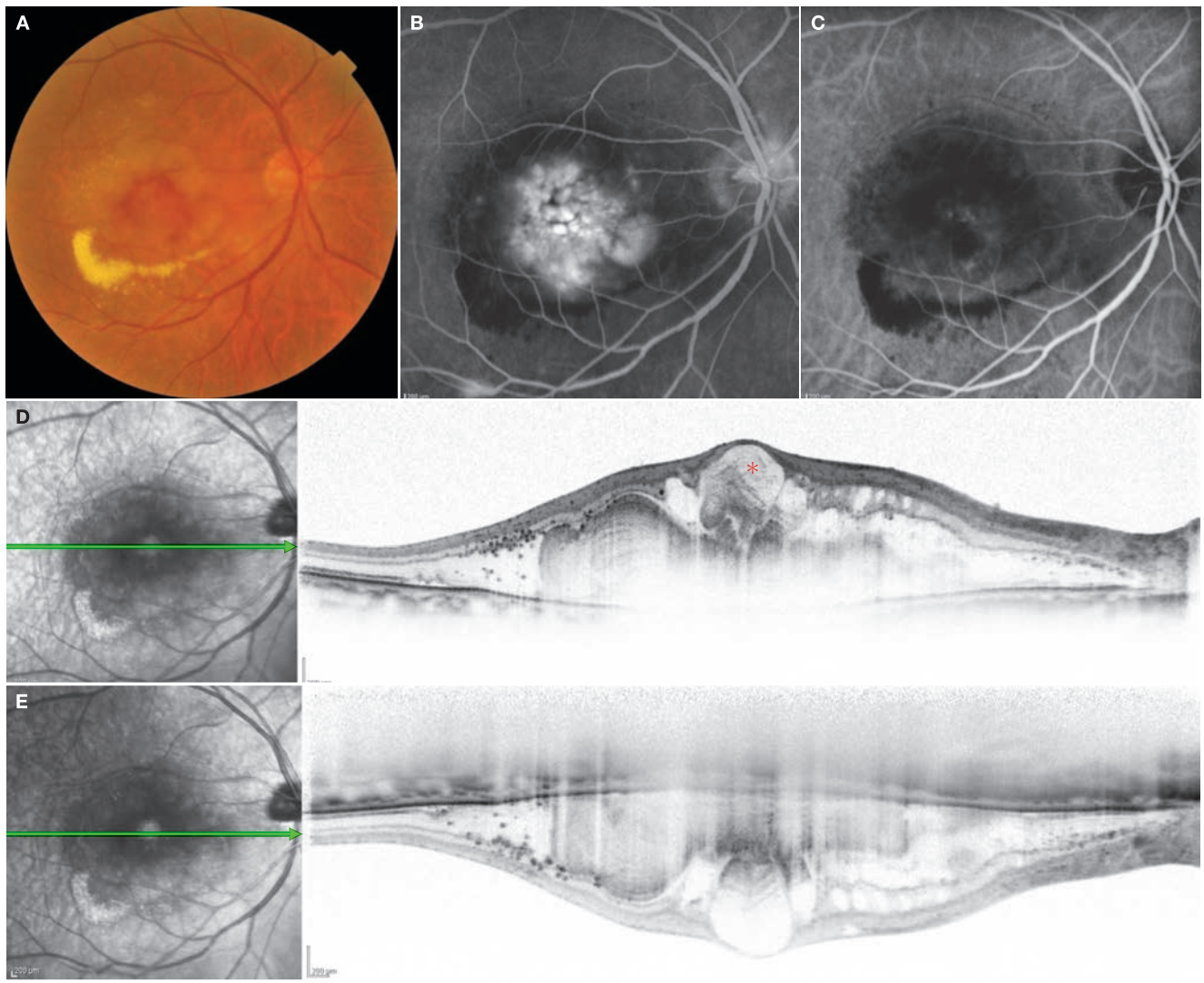

A: Color fundus photograph in the right eye: Retinal whitening is seen in the macula. Hard exudates are seen inferotemporal to the fovea centralis. **B:** FA in the right eye (7 minutes, 26 seconds): Intense hyperfluorescence indicating CME is exhibited. The fluorescence pattern is classic CNV. **C:** IA in the right eye (7 minutes, 26 seconds): CNV shows faint hyperfluorescence. **D:** IR + OCT horizontal scan of the right eye: CME accompanied by a large foveal cystoid space (*) exists over the entire macular area. The RPE line is seen over almost the entire length and appears flat on this scan. There are highly reflective clumps above the RPE, which are due to CNV and fibrin. **E:** IR + EDI-OCT horizontal scan of the right eye: The RPE can be seen more clearly when scanned with EDI-OCT.

Image interpretation points

This is a case where strong exudative changes are observed. The whitened retina reduces the penetration of the OCT beam; as a result, the RPE is not well characterized. Using EDI-OCT, the RPE is more clearly depicted compared to the retinal surface. In this case, the EDI-OCT confirms that there are no RPE protrusions indicative of Type 1 CNV. The highly reflective clumps seen below the sensory retina in the SD-OCT imaging are a complex ofType 2 CNV and the resulting exudates.

6.5 Polypoidal choroidal vasculopathy

Background

Polypoidal choroidal vasculopathy (PCV) is a disease first reported in 1982 by Yannuzzi et al. It was at first thought to be a peculiar disease in black women[1–4] (Fig. 6-14), but subsequent research found it to be one of the phenotypes of AMD that can be seen at a high frequency in Asians including the Japanese.[5, 6] In Japan, about half the cases of exudative AMD are PCV.[7] It is common in men with a history of smoking and is often seen with hypertension. There was heated debate in Japan as to whether PCV is essentially CNV or a choroidal vascular abnormality, but histopathological investigations are not enough to draw a conclusion at present. However, in the Western macular society, PCV is thought to be CNV.[8] While IA is an extremely important tool in the diagnosis of PCV, macular specialists in the West does not perform IA as routinely as those in Japan; as a result, it is highly likely that the disease frequency of PCV is underestimated in the West. PCV is composed of two main elements. The first is branching vascular network vessels in Japan. The second element is a vasodilative lesion known as a polypoidal structure.[9]

OCT findings

Studies up until now using OCT have found that the location of the abnormal vascular network is between the RPE and Bruch's membrane.[10] In addition, it has also become apparent that polypoidal lesions are frequently attached posteriorly to the RPE and detached from Bruch's membrane.[10, 11] Fig. 6-15 shows a schematic diagram of the development of PCV and the corresponding OCT image.

A »double layer sign« is a distinctive OCT finding of PCV. Because of the low axial resolution of time-domain OCT, it cannot resolve the abnormal vascular network, Bruch's membrane and choriocapillaris, which are depicted as a bold single line. A »double layer sign« describes the parallel appearance of the detached RPE line and this bold line derived from the complex.[12] With SD-OCT, however, this term is no longer suitable given the improved resolution. As previously mentioned, PED is a finding frequently seen in this disease. A notch often exists in the periphery of a PED secondary to CNV. CNV is frequently found in this notched edge of the PED. Gass called this phenomenon »notch sign«.[13] On OCT, a notch can be seen in the RPE line consistent with the notch sign on FA. These findings are called »tomographic notch sign«.[14] These signs are often seen in PCV. In recent years, we have been able to depict the choroid more clearly using EDI-OCT.[15] As a result, the relationship between choroidal thickness and various fundus diseases has been gathering attention. For example, we know that choroidal thickness significantly increases in central serous chorioretinopathy.[16] It is also reported that the choroid is thicker in PCV than in typical AMD.[17]

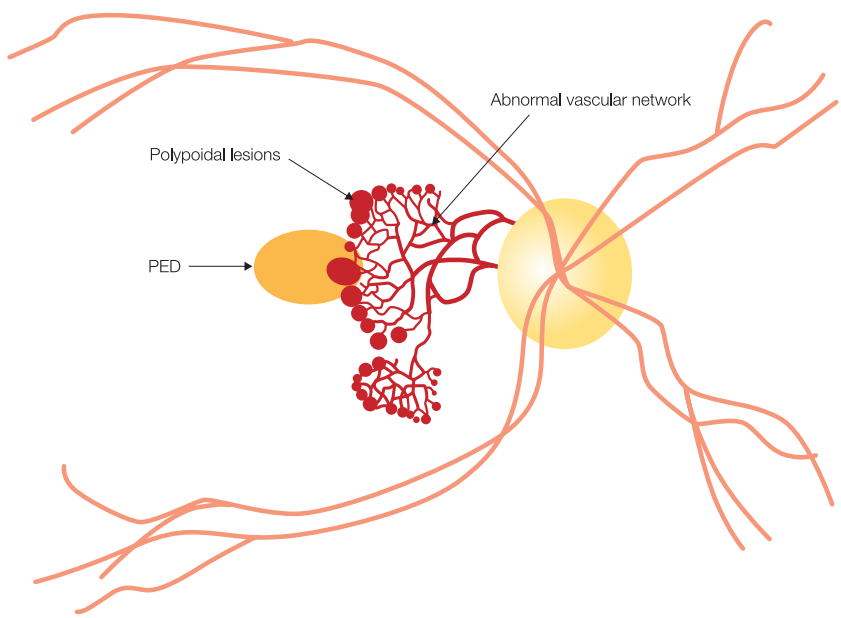

Fig. 6-14 Schematic diagram of PCV
In this figure, the optic disc is depicted as the origin of the abnormal vascular network, but the origin also exists in the macula in the macular type PCV common in Japanese people. Bulging of the tips of the abnormal vascular network forms polypoidal lesions. PEDs are a frequently observed finding. (Modified according to Yannuzzi LA, et al. Indocyanine green angiography. 1997, Mosby-Year Book, p331)

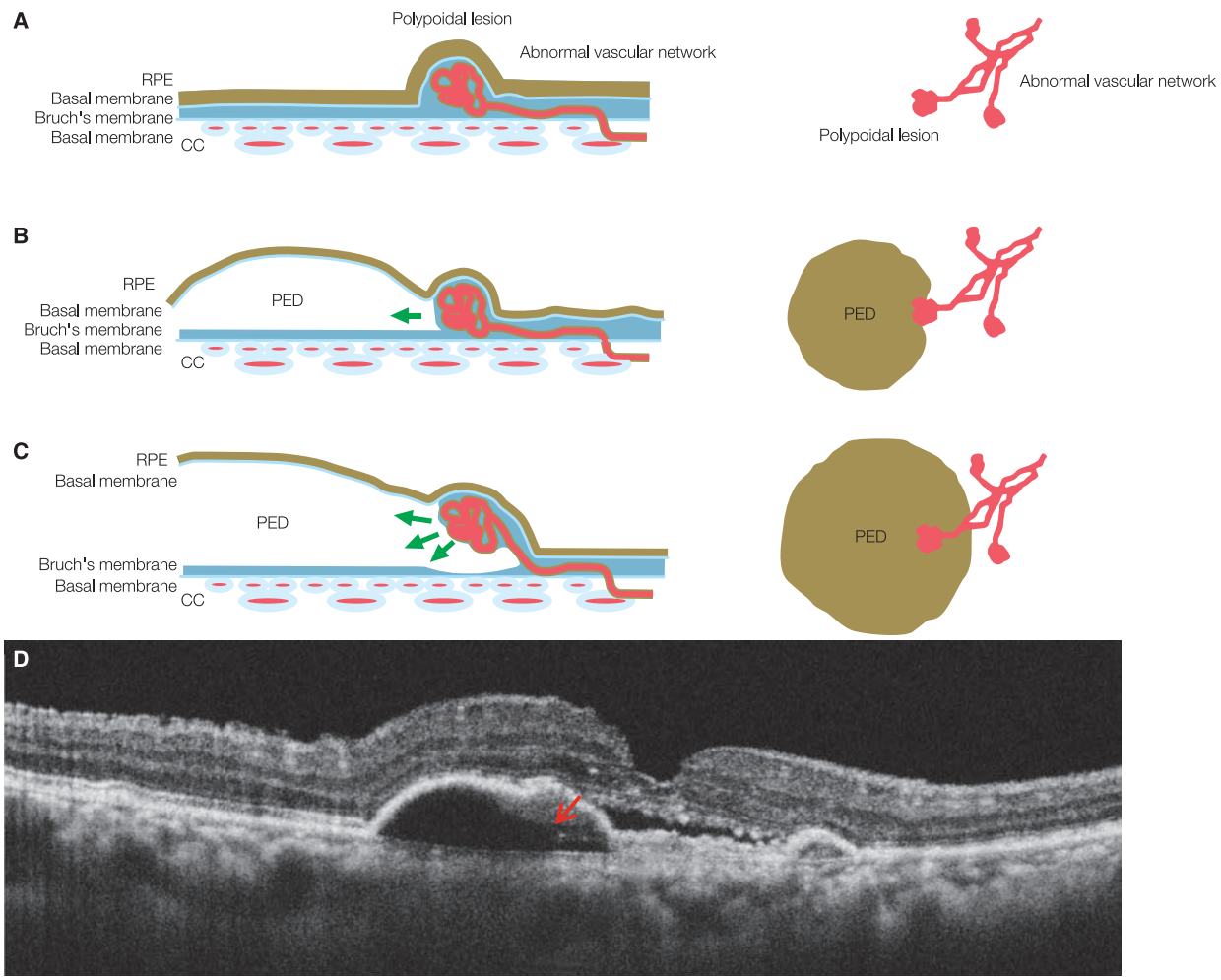

Fig. 6-15 Schematic diagram of the development of PCV
A: The abnormal vascular network exists within Bruch's membrane. **B:** As exudative changes from the polypoidal lesion get stronger, exudate fluid accumulates in the sub-RPE space and a PED develops. **C:** When the exudative changes get even stronger, the polypoidal lesion detaches from Bruch's membrane with their attachment to the posterior aspect of the RPE. **D:** OCT findings. The polypoidal lesion is attached to the posterior aspect of the RPE and is detaching from Bruch's membrane (→). (Modified according to Tsujikawa A, Sasahara M, Otani A, et al. Pigment epithelial detachment in polypoidal choroidal vasculopathy. Am J Ophthalmol. 2007; 143: 102-111)

6.5.1 References

1) Stern RM, Zakov N, Zegarra H, et al. Multiple recurrent serosanguineous retinal pigment epithelial detachments in black women. *Am J Ophthalmol*. 1985; 100:560–569.
2) Yannuzzi LA, Sorenson J, Spaide RF, et al. Idiopathic polypoidal choroidal vasculopathy. *Retina*. 1990; 10:1–8.
3) Kleiner RC, Brucker AJ, Johnston RL. The posterior uveal bleeding syndrome. *Retina*. 1990; 10:9–17.
4) Perkovich BT, Zakov ZN, Berlin LA, et al. An update on multiple recurrent serosanguineous retinal pigment epithelial detachments in black women. *Retina*. 1990; 10:18–26.
5) Uyama M, Wada M, Nagai Y, et al. Polypoidal choroidal vasculopathy: natural history. *Am J Ophthalmol*. 2002; 133:639–648.
6) Sho K, Takahashi K, Yamada H, et al. Polypoidal choroidal vasculopathy: incidence, demographic features, and clinical characteristics. *Arch Ophthalmol*. 2003; 121:1392–1396.
7) Maruko I, Iida T, Saito M, et al. Clinical characteristics of exudative age-related macular degeneration in Japanese patients. *Am J Ophthalmol*. 2007; 144:15–22.
8) Rosa RH Jr, Davis JL, Eifrig CW. Clinicopathologic reports, case reports, and small case series: clinicopathologic correlation of idiopathic polypoidal choroidal vasculopathy. *Arch Ophthalmol*. 2002; 120:502–508.
9) Spaide RF, Yannuzzi LA, Slakter JS, et al. Indocyanine green videoangiography of idiopathic polypoidal choroidal vasculopathy. *Retina*. 1995; 15:100–110.
10) Tsujikawa A, Sasahara M, Otani A, et al. Pigment epithelial detachment in polypoidal choroidal vasculopathy. *Am J Ophthalmol*. 2007; 143:102–111.
11) Ojima Y, Hangai M, Sakamoto A, et al. Improved visualization of polypoidal choroidal vasculopathy lesions using spectral-domain optical coherence tomography. *Retina*. 2009; 29:52–59.
12) Sato T, Kishi S, Watanabe G, et al. Tomographic features of branching vascular networks in polypoidal choroidal vasculopathy. *Retina*. 2007; 27:589–594.
13) Gass JM. Serous retinal pigment epithelial detachment with a notch. A sign of occult choroidal neovascularization. *Retina*. 1984; 4:205–220.
14) Sato T, Iida T, Hagimura N, et al. Correlation of optical coherence tomography with angiography in retinal pigment epithelial detachment associated with age-related macular degeneration. *Retina*. 2004; 24:910–914.
15) Spaide RF, Koizumi H, Pozzoni MC. Enhanced depth imaging spectral-domain optical coherence tomography. *Am J Ophthalmol*. 2008; 146:496–500.
16) Imamura Y, Fujiwara T, Margolis R, et al. Enhanced depth imaging optical coherence tomography of the choroid in central serous chorioretinopathy. *Retina*. 2009; 29:1469–1473.
17) Chung SE, Kang SW, Lee JH, et al. Choroidal thickness in polypoidal choroidal vasculopathy and exudative age-related macular degeneration. *Ophthalmology*. 2011; 118:840–845.

Case 104 Polypoidal choroidal vasculopathy: Small lesions

A 65-year-old male, OS, BCVA 0.1

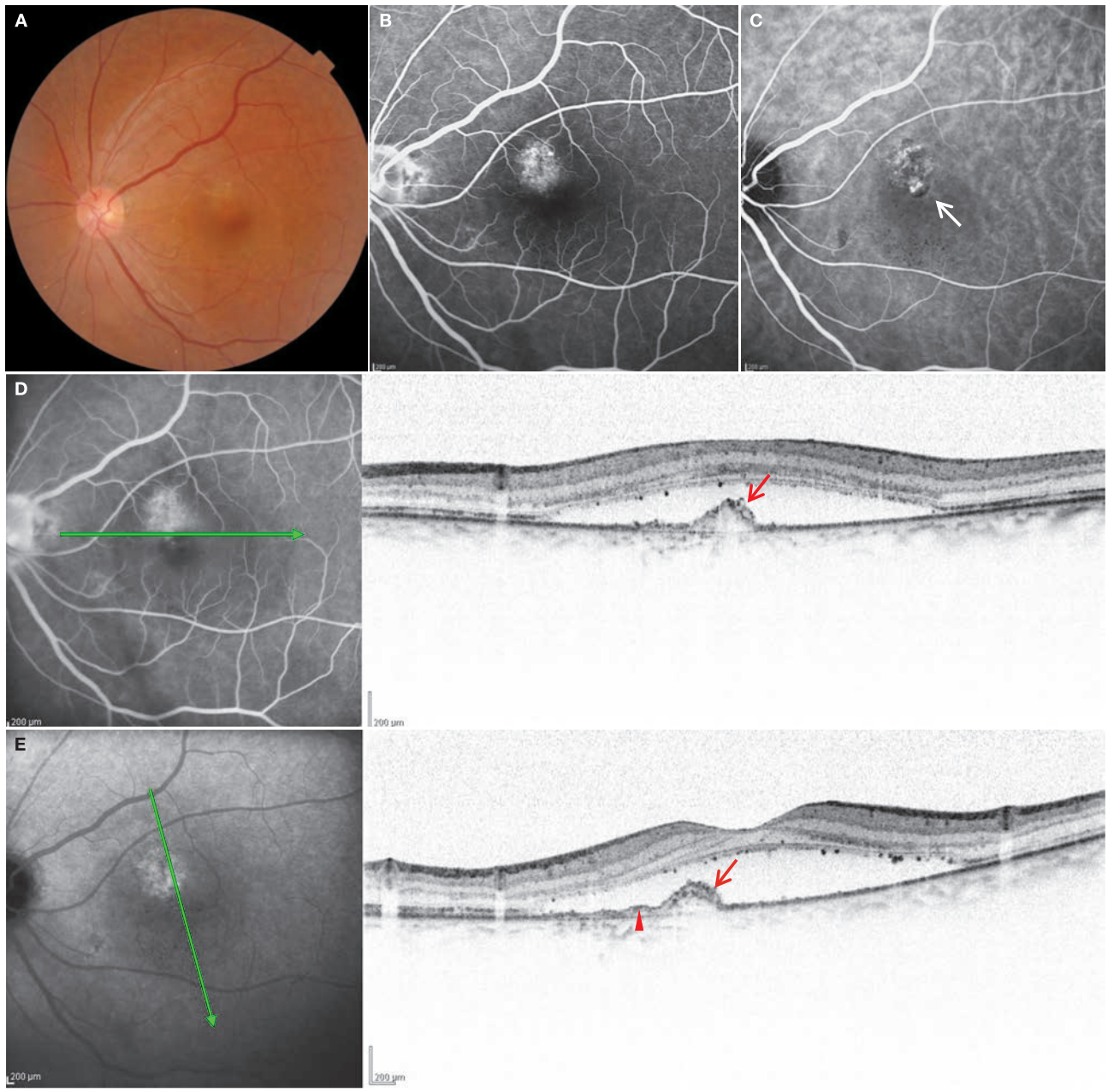

A: Color fundus photograph in the left eye: A small, elevated orange-red lesion is visible superonasal to the fovea centralis, but they are easily overlooked if not observed in detail. A SRD exists in the macula. Drusen are not seen. **B:** FA in the left eye (5 minutes, 10 seconds): The elevated orange-red lesions superonasal to the fovea centralis are exhibiting granular hyperfluorescence. **C:** IA in the left eye (5 minutes, 10 seconds): Small polypoidal lesions are clearly visible on IA (⇒). An abnormal vascular network is observed superior to the polypoidal lesion. **D:** IR + OCT horizontal scan of the left eye: A SRD is seen. A small RPE protrusion can be seen (➔). Bruch's membrane is seen beneath the elevated RPE. **E:** IR + OCT diagonal scan of the left eye: A flat RPE elevation is visible in the area corresponding to the abnormal vascular network (►). The relatively tall protrusion area corresponds to the polypoidal lesions detected on IA (➔).

Image interpretation points

This is a case of PCV with extensive SRD and a small polypoidal lesion.

While differentiation with central serous chorioretinopathy is difficult with ophthalmoscopic findings, but the protruding lesions seen on OCT are typical of PCV.

Case 105 Polypoidal choroidal vasculopathy: Case confused with central serous chorioretinopathy

A 63-year-old female, OS, BCVA 0.4

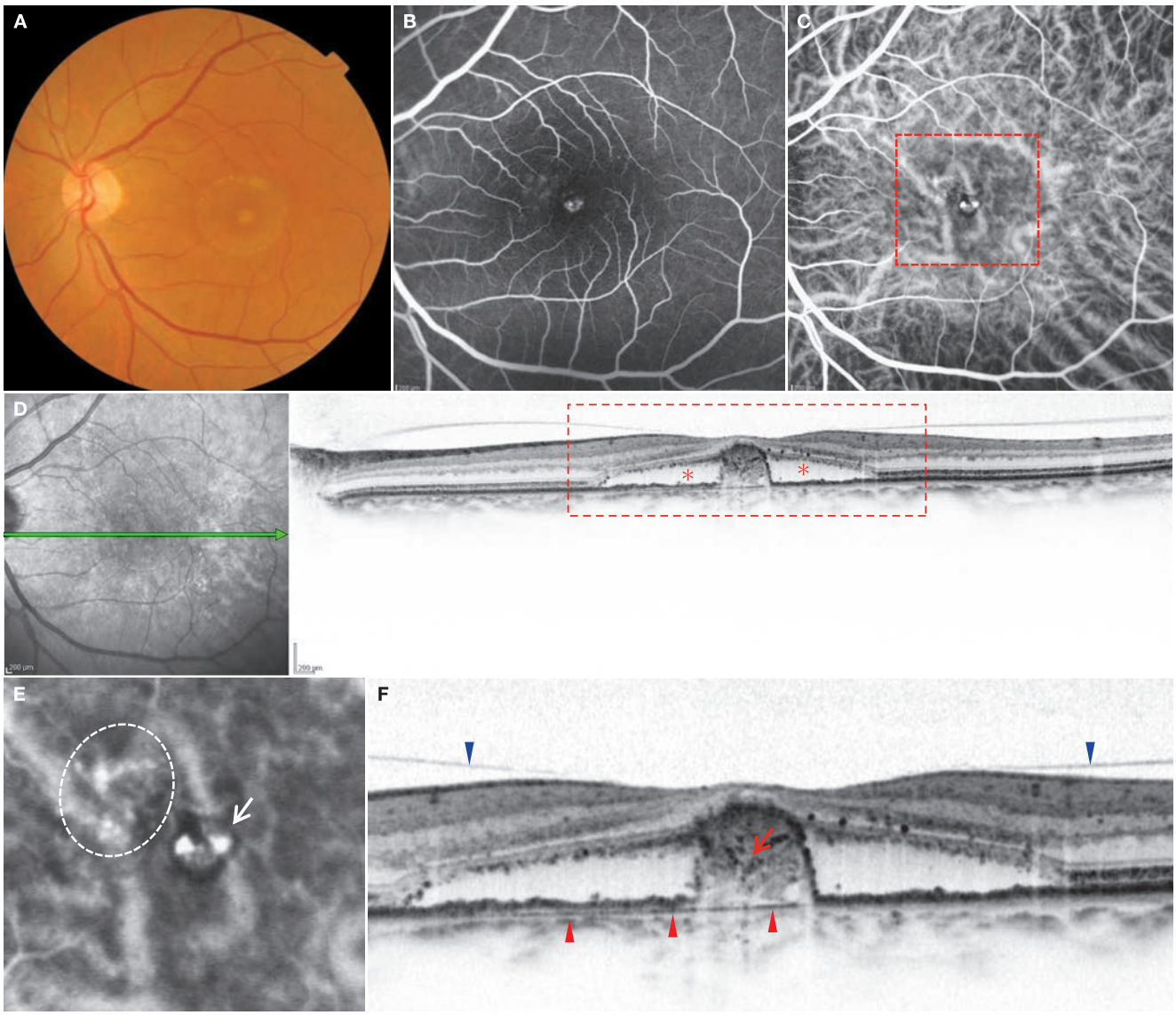

A: Color fundus photograph in the left eye: A SRD about 1.5 disc diameters can be seen in the macula. A white spot is evident in the fovea centralis. This may be fibrin deposits. Drusen are barely visible in the posterior pole. **B:** FA in the left eye (28 seconds): A small, granular hyperfluorescent focus can be seen in the fovea centralis. **C:** IA in the left eye (28 seconds): A small polypoidal lesion is seen on IA. **D:** IR + OCT horizontal scan of the left eye: A SRD can be seen (✻). There is an steep RPE protrusion. **E:** Enlarged version of C [red dashed box]: We can see that two polypoidal lesions (⇛) and an abnormal vascular network exist superonasally (white dashed circle). **F:** Enlarged version of D [red dashed box]: There is moderate reflectivity seen inside the RPE protrusion. This suggests that the content is solid (including fibrovascular components) (➔). A highly reflective structure suggestive of a polypoidal lesion appears to be penetrating the foveal sensory retina, but this may be a fibrin clot. A flat RPE protrusion can be seen nasally adjacent to the steep protrusion. Bruch's membrane is seen (►). We can clearly see that the posterior vitreous cortex is attached to the retinal surface (►). (Continued in the next page)

Image interpretation points

This is a case that can be confused with central serous chorioretinopathy. In addition to the importance of IA, the steep, protruding lesion on OCT is typical of PCV. A characteristic of this case is the highly reflective particulates (probably infiltrating cells) within the protruding lesion.

Case 105 After treatment with anti-VEGF treatment

An 63-year-old female, OS, BCVA 0.6

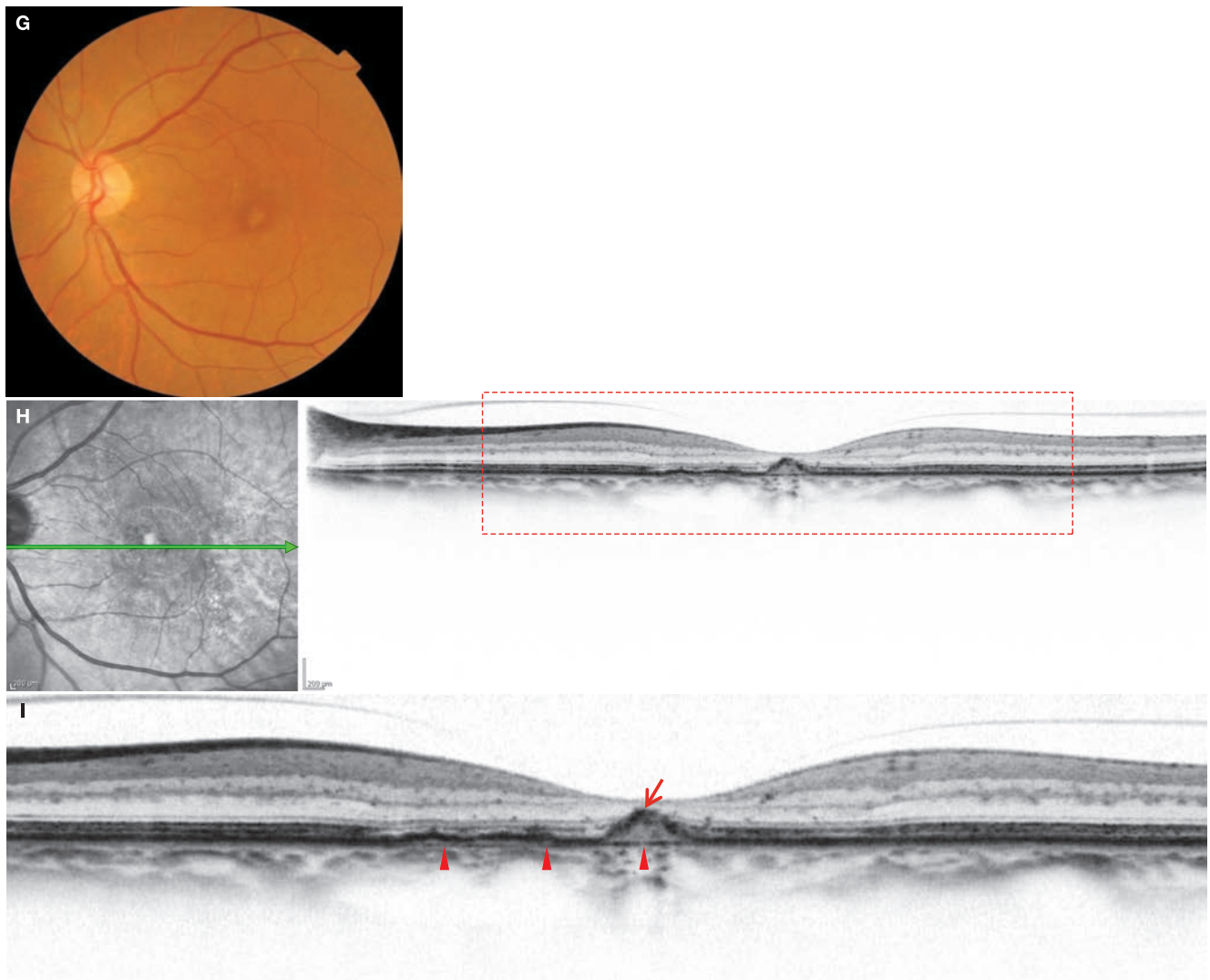

G: Color fundus photograph in the left eye: The SRD in the macula has disappeared, but white spots can still be seen in the center. **H:** IR + OCT horizontal scan of the left eye: The disappearance of the SRD can be confirmed with OCT. The fovea is significantly thinned. The area where the retina had been detached can be seen on the left IR image. **I:** Enlarged version of H [red dashed box]: The protruding lesion that existed before treatment has decreased in size, but remains visible (➔). Moderate internal reflectivity is still visible in the protruding lesion. Bruch's membrane is seen (►). There is a disruption in the structure of the outer retinal layers in the area of the RPE protrusion: the ELM is relatively preserved, but the IS/OS and COST lines cannot be clearly seen.

Image interpretation points

This is a case where the therapeutic value of anti-VEGF treatment is clear. While the SRD has significantly decreased, the CNV remains with partial scarring.

Case 106 Polypoidal choroidal vasculopathy: Fibrin deposits ①

A 77-year-old female, OD, BCVA 0.05

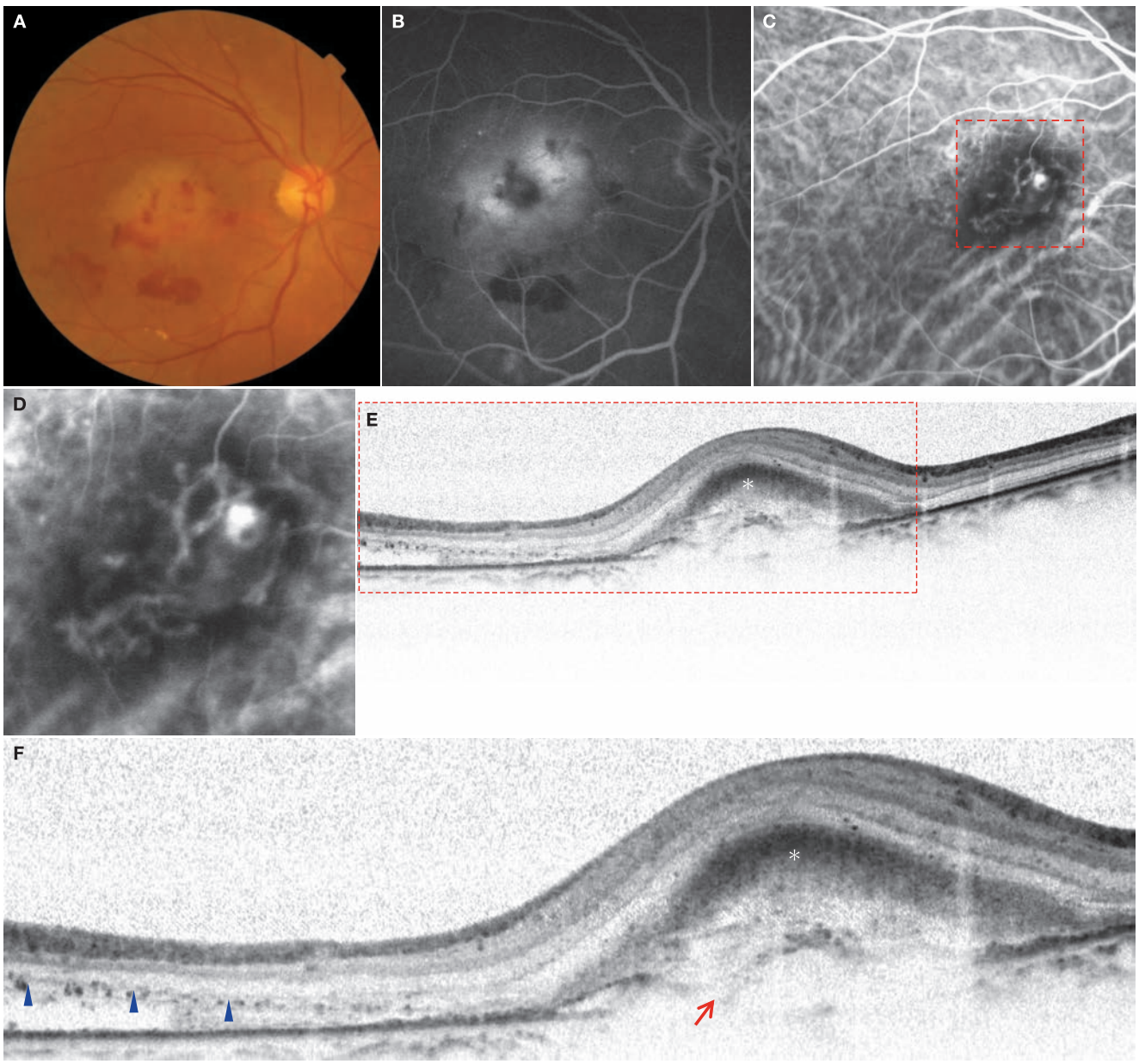

A: Color fundus photograph in the right: Retinal whitening due to fibrin deposits about 2 disc diameters in size are visible in the macular area. Drusen are unremarkable. There are subretinal hemorrhages inferior to the fovea centralis. **B:** FA in the right eye (14 minutes, 55 seconds): The fovea centralis is hypofluorescent, but hyperfluorescence can be seen around it. This is tissue staining due to fibrin. **C:** IA in the right eye (1 minute, 36 seconds): While indistinct on FA, a polypoidal lesion and a abnormal vascular network including relatively thick vesselsare easily seen on IA. **D:** Enlarged version of C [red dashed box]: Polypoidal lesions and an abnormal vascular network resembling a »coil« are clearly visible. **E:** OCT horizontal scan of the right eye: The high reflectivity in the outer retinal layers is due to fibrin (❄). The structure of the inner retinal layers is relatively preserved. **F:** Enlarged version of E [red dashed box]: Fibrin, depicted as highly reflective, appears to be penetrating the outer retinal layers (❄). This may be correlated with the poor visual acuity. While the RPE line is indistinct there appears to be a RPE protrusion (➔). Multiple inflammatory cells can be seen infiltrating the retina (►).

Image interpretation points

On FA, lesions behind fibrin deposits are indistinct due to blocking of OCT beam. In this case, insufficient information can be obtained with OCT, while IA clearly depicts the choroid.

Although both use near-infrared light sources, each modality has different visualization power. It is important to properly use both angiography and OCT in the diagnosis.

Case 107 Polypoidal choroidal vasculopathy: Fibrin deposits ②

A 63-year-old male, OD, BCVA 0.09

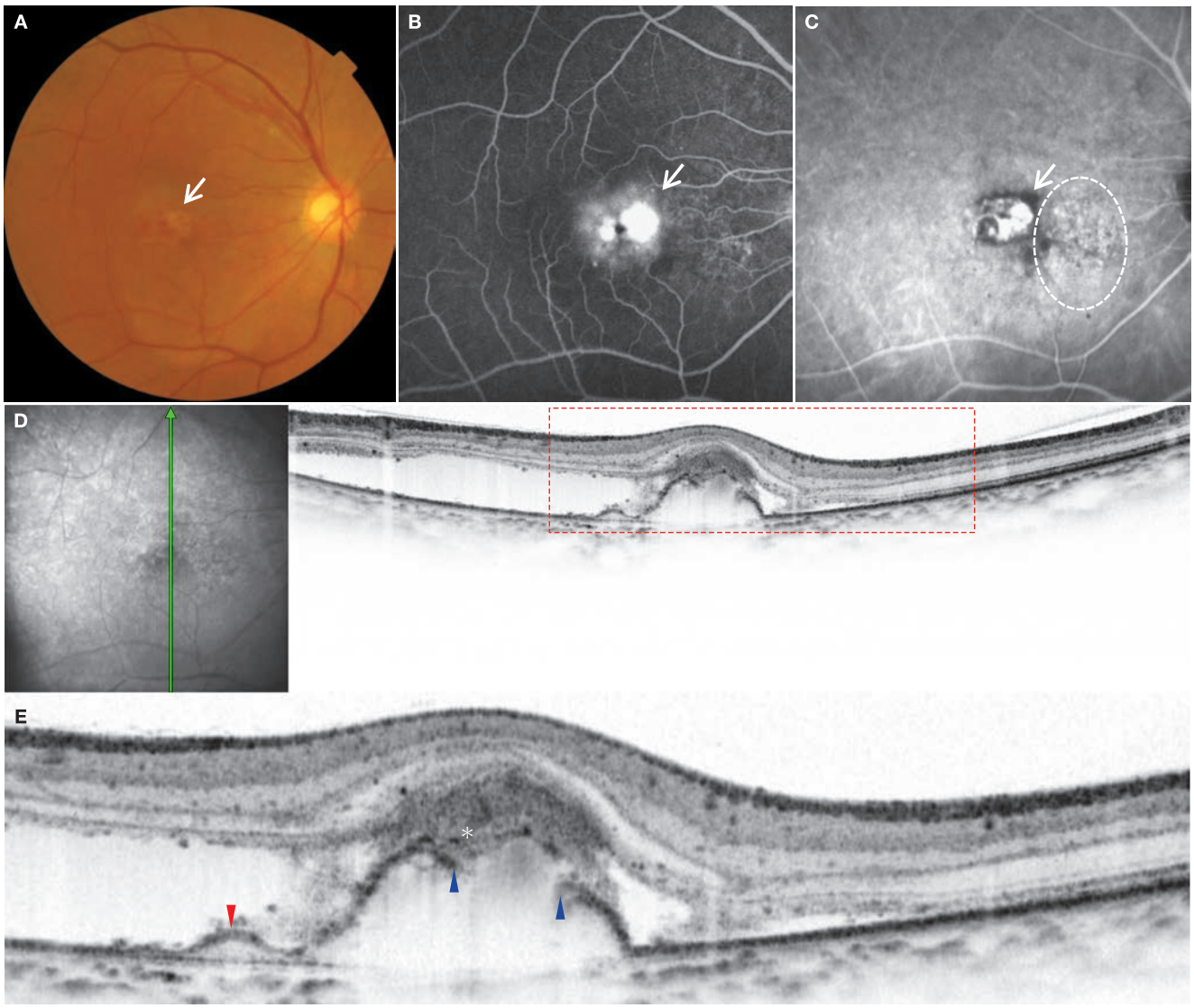

A: Color fundus photograph in the right eye: A elevated orange-red lesion is noticeable below in fovea centralis of the right eye (⇛). A SRD is visible over a wide area from the fovea centralis to the inferior fundus. **B:** FA in the right eye (6 minute, 23 seconds): Intense hyperfluorescent foci can be seen in the fovea centralis and immediately nasally (⇛). **C:** IA in the right eye (6 minutes, 37 seconds): The lesions with hyperfluorescent foci on FA are exhibiting strong hyperfluorescence even on IA. These are polypoidal lesions (⇛). An abnormal vascular network is also seen (white dashed circle). **D:** IR + OCT vertical scan of the right eye: A SRD and a steep RPE protrusion are seen. **E:** Enlarged version of D [red dashed box]: The retina is protruding into the vitreous body due to a protrusion that exists below the fovea centralis. Fibrin deposits in the outer retinal layers are exhibiting moderate to relatively high reflectivity (❄). There appears to be a RPE tear between the two (►). The RPE protrusion indicated by (►) is exhibiting moderate reflectivity and likely includes vascular components.

Image interpretation points

Fibrin deposits are sometimes apparent in PCV. In such case, the pattern of classic CNV can be shown on FA due to staining of fibrin deposits. PCV exhibiting a classic CNV pattern due to fibrin deposits often responds well to treatment.

Case 108 Polypoidal choroidal vasculopathy: A large branching vascular network

A 78-year-old female, OS, BCVA 0.6

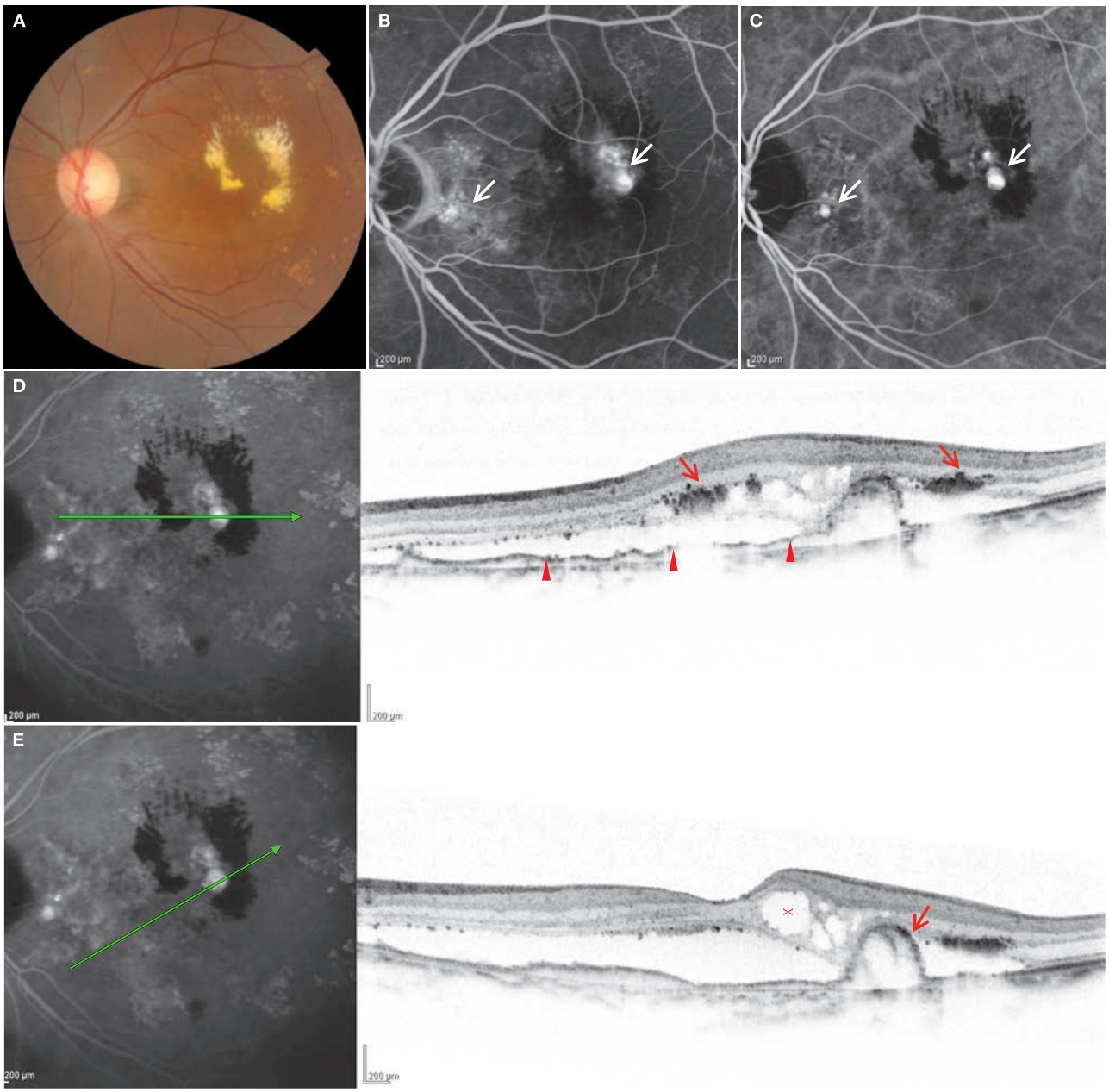

A: Color fundus photograph in the left eye: Circinate hard exudates are observed superotemporal to the fovea centralis of the left eye. No retinal hemorrhages are seen. There are drusen in the temporal macula. **B:** FA in the left eye (1 minute, 10 seconds): Hyperfluorescent foci can be seen temporal to the optic disc and superotemporal to the fovea centralis (⇒). The hard exudates are exhibiting hypofluorescence. **C:** IA in the left eye (1 minute, 10 seconds): The hyperfluorescent lesions on FA are exhibiting hyperfluorescence on IA (⇒). Both are polypoidal lesions. An branching vascular network is visible immediately above the polypoidal lesions temporal to the optic disc. **D:** FA + OCT horizontal scan of the left eye: A SRD can be seen over a wide area. The hard exudates exhibit strong reflectivity (➔). Flat elevation of the RPE is seen representing the branching vascular network (►) in the spot corresponding to the polypoidal lesion. Moderate reflectivity indicating choroidal neovascularization is noticeable between the RPE and Bruch's membrane. **E:** FA + OCT diagonal scan of the left eye: This is a scan passing through polypoidal lesions temporal to the fovea centralis. The polypoidal lesions exhibit a steep rise and are composed of contents of both moderately and weakly reflective contents (➔). Cystoid spaces are seen in the sensory retina (*).

Image interpretation points

We can clearly see that hard exudates exhibit strong reflectivity on OCT images. In this case, a large branching vascular network is seen, which is seen as a flat RPE elevation on OCT.

Case 109 Polypoidal choroidal vasculopathy: Large foveal cystoid space

A 69-year-old female, OD, BCVA 0.06

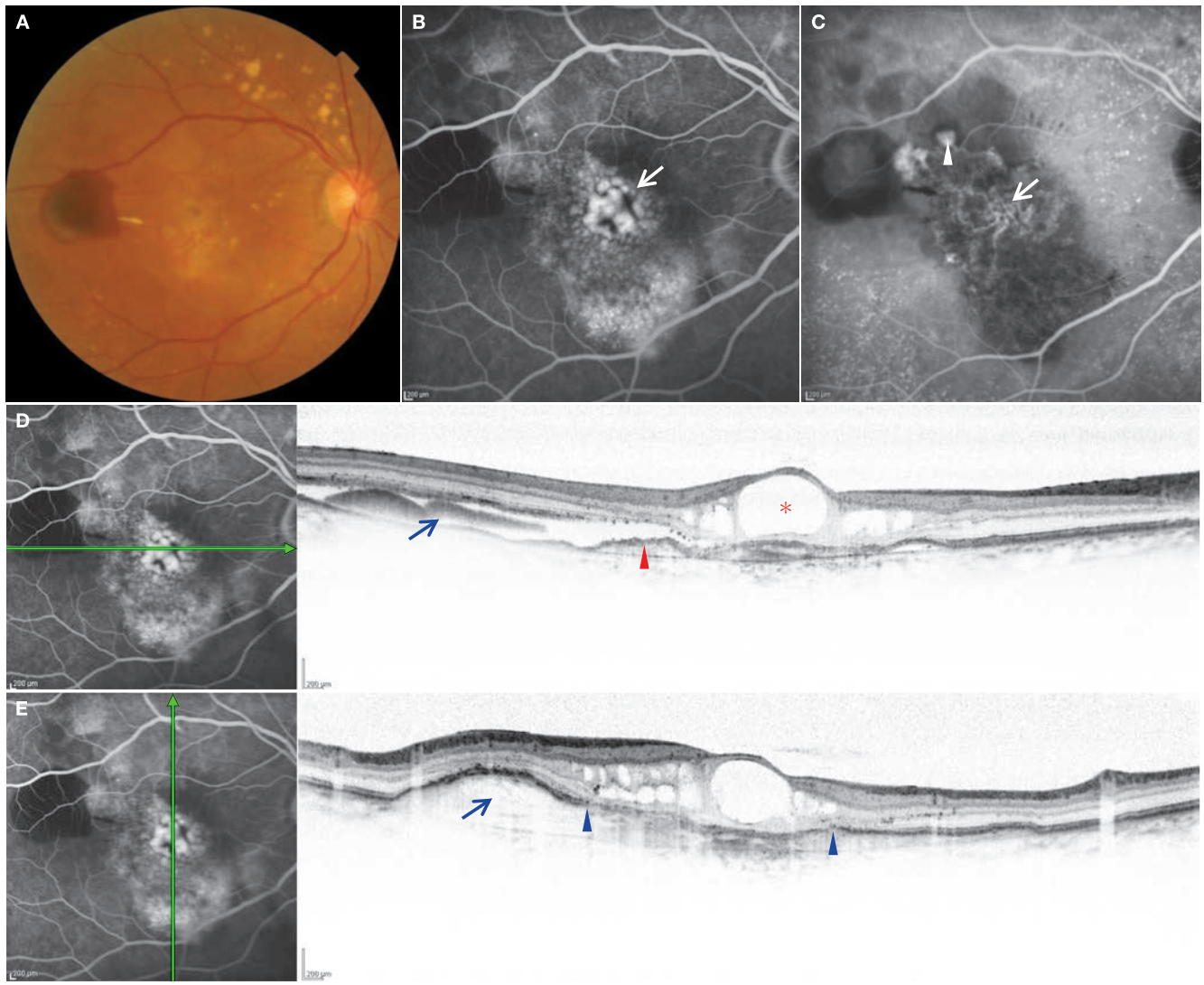

A: Color fundus photograph in the right eye: A subretinal hemorrhage about 1.5 disc diameters in size is visible temporal in the temporal macula of the right eye. The RPE of the fovea centralis appears to be atrophic. Multiple large drusen are seen superior to the optic disc. **B:** FA in the right eye (11 minutes, 30 seconds): Significant CME can be seen (⇨). **C:** IA in the right eye (11 minutes, 30 seconds): A branching vascular network (⇨) not visible on FA has been detected. A polypoidal lesion is seen at the end of this branching vascular network (▷). Drusen can be seen as hyperfluorescent dots. **D:** FA + OCT horizonta l scan of the right eye: A large cystoid space (✻) is seen in the fovea centralis. High reflectivity due to a subretinal hemorrhage is seen temporally (➔). The temporal retina is detaching. A flat RPE elevation is visible immediately temporal to the fovea centralis (►). **E:** FA + OCT vertical scan of the right eye: A large fibrovascular PED with moderately reflective content can be seen (➔). The RPE line below the fovea centralis cannot be accurately traced (between the two ►). This corresponds to RPE atrophy that can be viewed with an ophthalmoscope.
(Continued on the next page)

Image interpretation points

This is a case where a large foveal cystoid space can be seen. RPE atrophy below the cystoid space may be attributed to the existence of the branching vascular network. Both RPE atrophy and the existence of CNV may be associated with the development of CME in this case.

Case 109 Enlargement of hemorrhagic pigment epithelial detachment

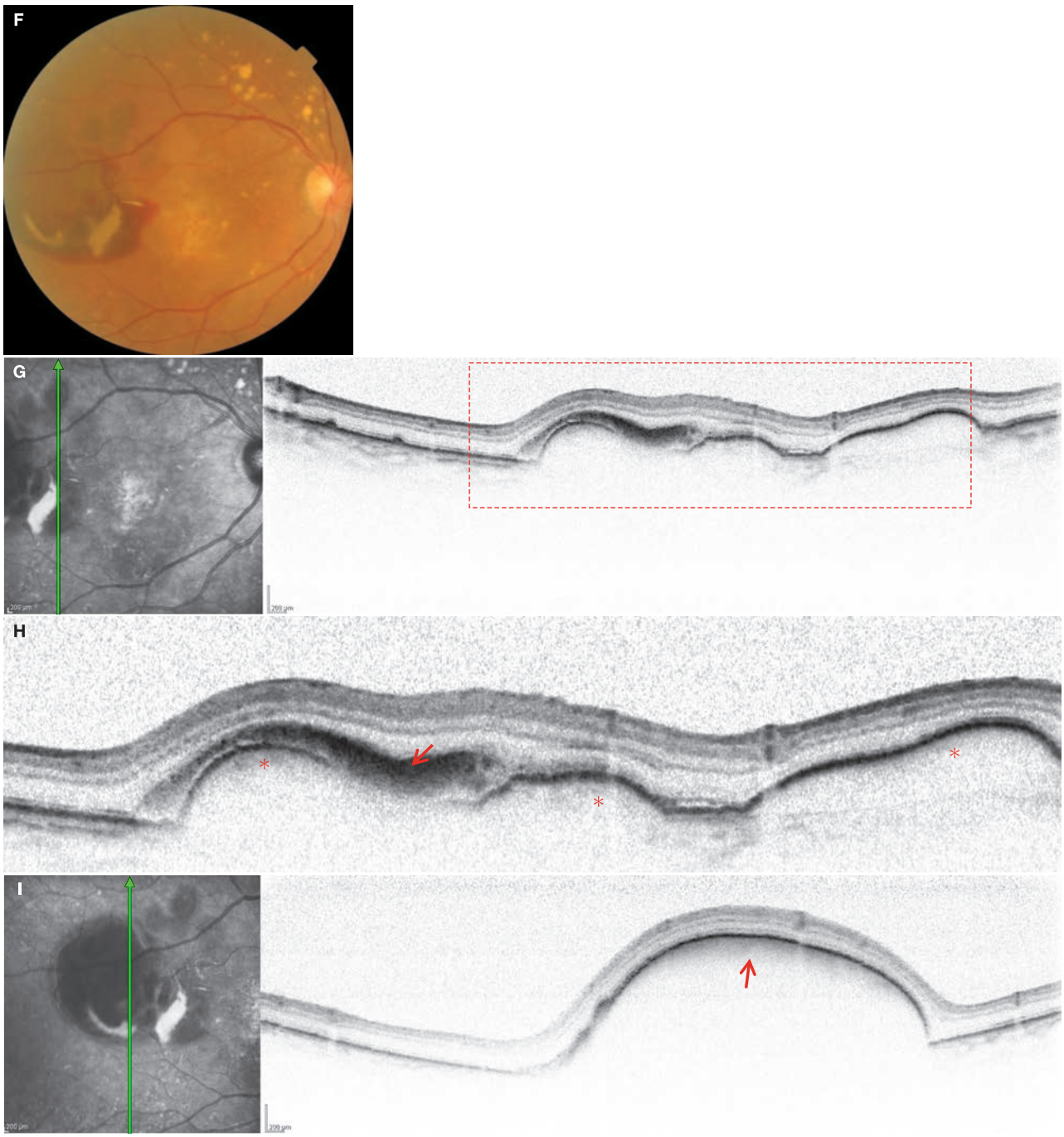

F: Color fundus photograph in the right eye: Subretinal hemorrhage is increasing in size with partial organization. **G:** IR + OCT vertical scan of the right eye: A RPE protrusion and hemorrhages anteriorly can be seen in the scan passing through the polypoidal lesion. **H:** Enlarged version of G [red dashed box]: A tall PED is expanding (*). (→) indicates high reflectivity due to the hemorrhage. **I:** IR + OCT vertical scan of the right eye: A vertical scan even further temporally. A RPE protrusion with a steep rise is visible. While moderate reflectivity (→) is observed immediately below the RPE it is unclear if this is CNV.
(continued on the next page)

Image interpretation points

Two months after initial diagnosis, a large hemorrhagic PED has developed. The highly reflective line of the RPE is partially obscured by blockage of OCT beamdue to hemorrhages, but there does not appear to be an interruption in the line. In this area, there may be CNV confined to the RPE.

Case 109 Enlargement of the abnormal vascular network

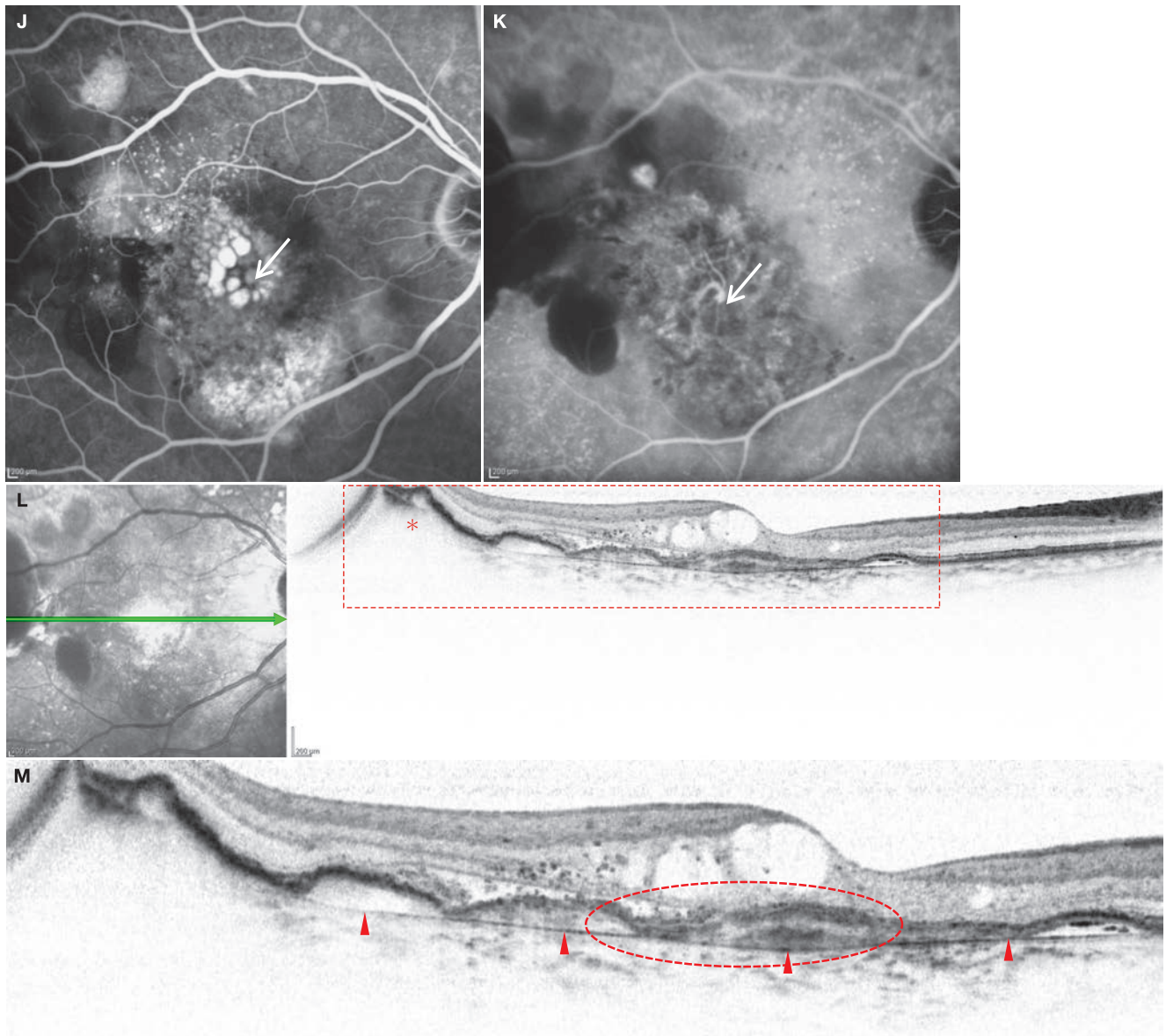

J: FA in the right eye: Fluoroscein accumulation is seen within the cystoid space (⇛). **K:** IA in the right eye (10 minute, 15 seconds): The CNV is expanding and its activity is increasing. Thick neovascular root is visible (⇛). **L:** IR + OCT horizontal scan of the right eye: A tall PED can be seen temporally (✻). **M:** Enlarged version of L [red dashed box]: The cystoid spaces are clearly seen. The straight, thin, highly reflective line is Bruch's membrane (►). The RPE is irregular and indistinct within the red dashed circle. Moderate reflectivity is seen immediately above Bruch's membrane. This is Type 2 CNV.

Image interpretation points

After 1.5 months, CNV has passed through the RPE to form Type 2 and is expanding in the area indicated by the red dashed circle in M. It is highly likely that Type 2 CNV existed from the time of the initial diagnosis. Also, note that Bruch's membrane is clearly defined.

Case 110 Polypoidal choroidal vasculopathy: A large hemorrhagic pigment epithelial detachment ①

A 64-year-old male, OD, BCVA 0.15

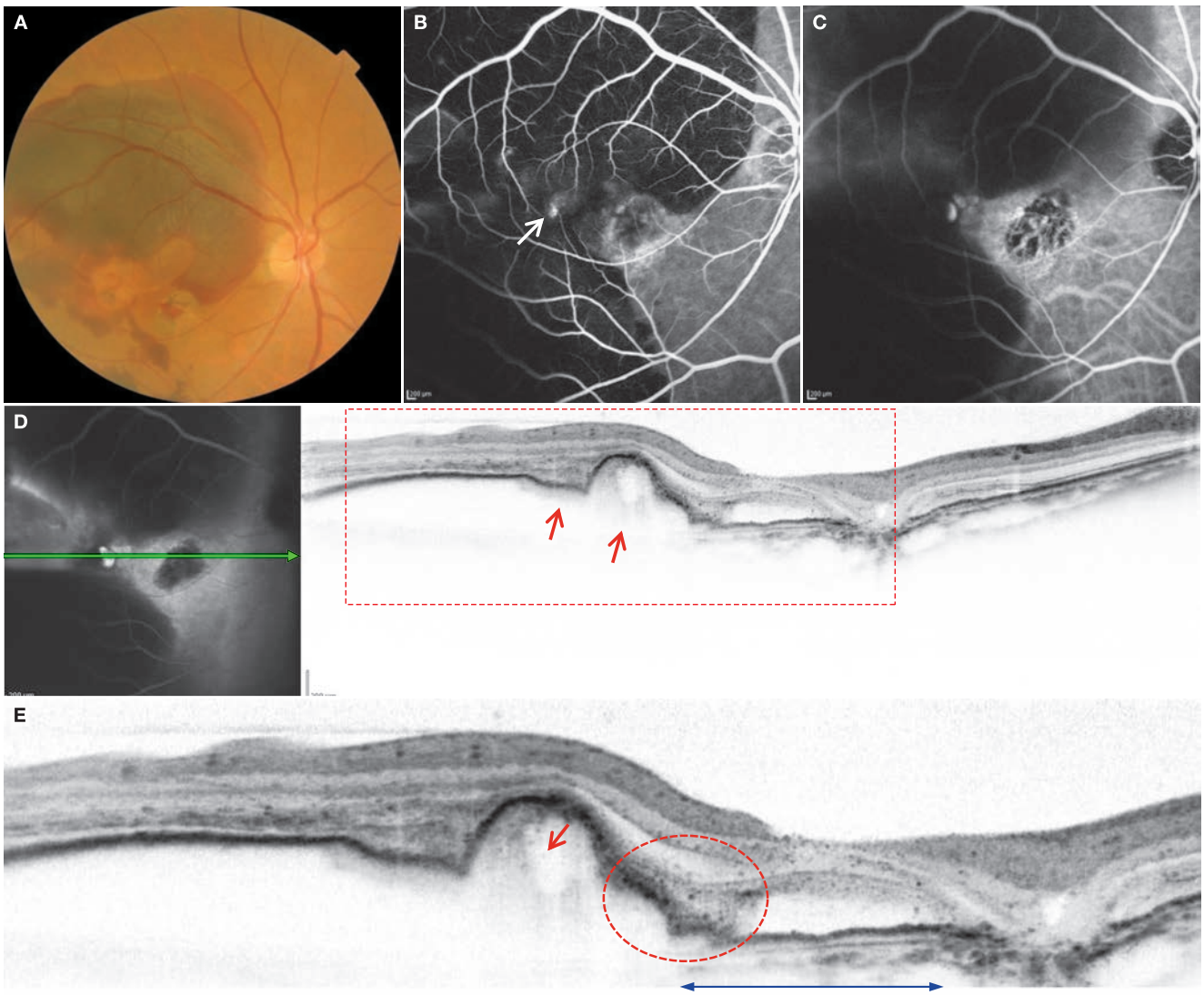

A: Color fundus photograph in the right eye: A large hemorrhagic PED is seen. There is little subretinal hemorrhage in the inferotemporal macula because a tall polypoidal lesion is present in this area. **B:** FA in the right eye (1minute): Fluorescence is blocked due to subretinal hemorrhages, but a hyperfluorescent lesion can be seen temporal to the fovea centralis (⇨). **C:** IA in the right eye (1 minute): The subretinal characteristics are difficult to discern on IA due to thick subretinal hemorrhages. **D:** FA + OCT horizontal scan of the right eye: We can see that CNV is expanding along the posterior surface of the RPE (➔). **E:** Enlarged version of D [red dashed box]: A steep protrusion is seen in the RPE whose content is moderately reflective. A hyporeflective cavity appears to exist within the protrusion (➔). There is a flat RPE protrusion in the (*) area indicated by (⟷) and Bruch's membrane is seen below this protrusion. This corresponds to the area of an branching vascular network. The RPE line is slightly indistinct in the red dashed circle area.

Image interpretation points

This is a typical example of a large hemorrhagic PED associated with PCV. In this case, the thick subretinal hemorrhages obscure the lesions on IA. The OCT findings are, however, suggestive of PCV.

Case 111 Polypoidal choroidal vasculopathy: A large hemorrhagic pigment epithelial detachment ②

A 56-year-old female, OS, BCVA 1.0

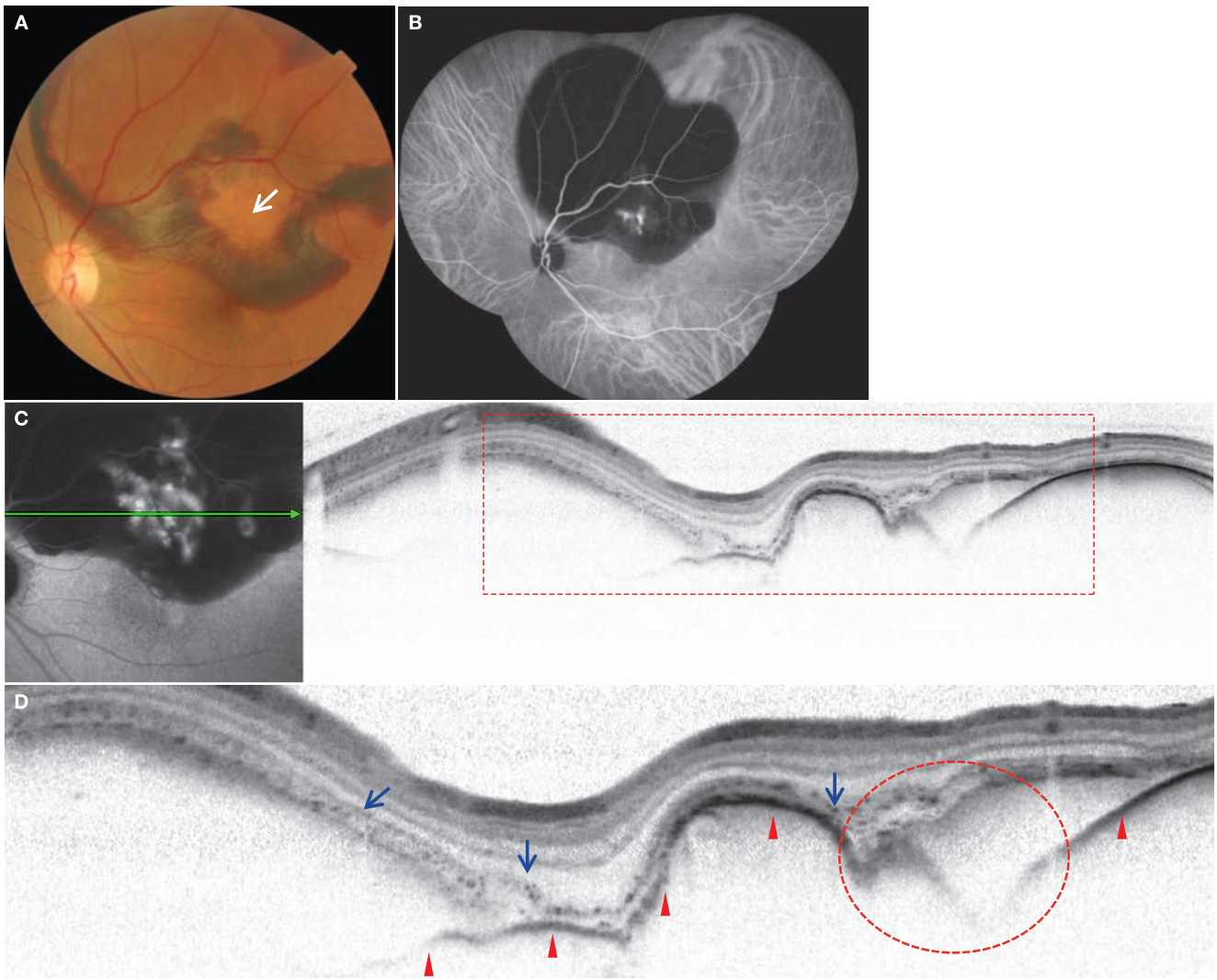

A: Color fundus photograph in the left eye: Subretinal hemorrhages and a hemorrhagic PED can be seen over a wide area from the fovea centralis to above the vascular arcades. A large, elevated, orange-red lesion about 1.5 disc diameters is present superior to the fovea centralis (⇛). **B:** IA montage of the left eye (7 minutes, 3 seconds) in the left eye: Fluorescence is blocked due to thick subretinal hemorrhages and choroidal characteristics cannot be seen in detail. The orange-red lesion superior to the fovea centralis is partially hyperfluorescent. The extent of subretinal hemorrhage and hemorrhagic PED is clearly visible. **C:** FA + OCT horizontal scan of the left eye: The nasal RPE is relatively flat. There is a steep RPE protrusion adjacent to a gently sloping protrusion outside of the fovea centralis. **D:** Enlarged version of C [red dashed box]: The RPE line (►) is becoming partially indistinct temporal to the fovea centralis (red dashed circle). Multiple small highly reflective dots are present in the outer retinal layers (➔). These may represent infiltrating macrophages.
(Continued on the next page)

Image interpretation points

This is also a case of hemorrhagic PED associated with PCV. Visual acuity is well preserved considering the significant fundus findings. This is due to the preservation of the fovea. The highly reflective dots seen in the outer retinal layers are probably infiltrating macrophages.

Case 111 Spontaneous remission

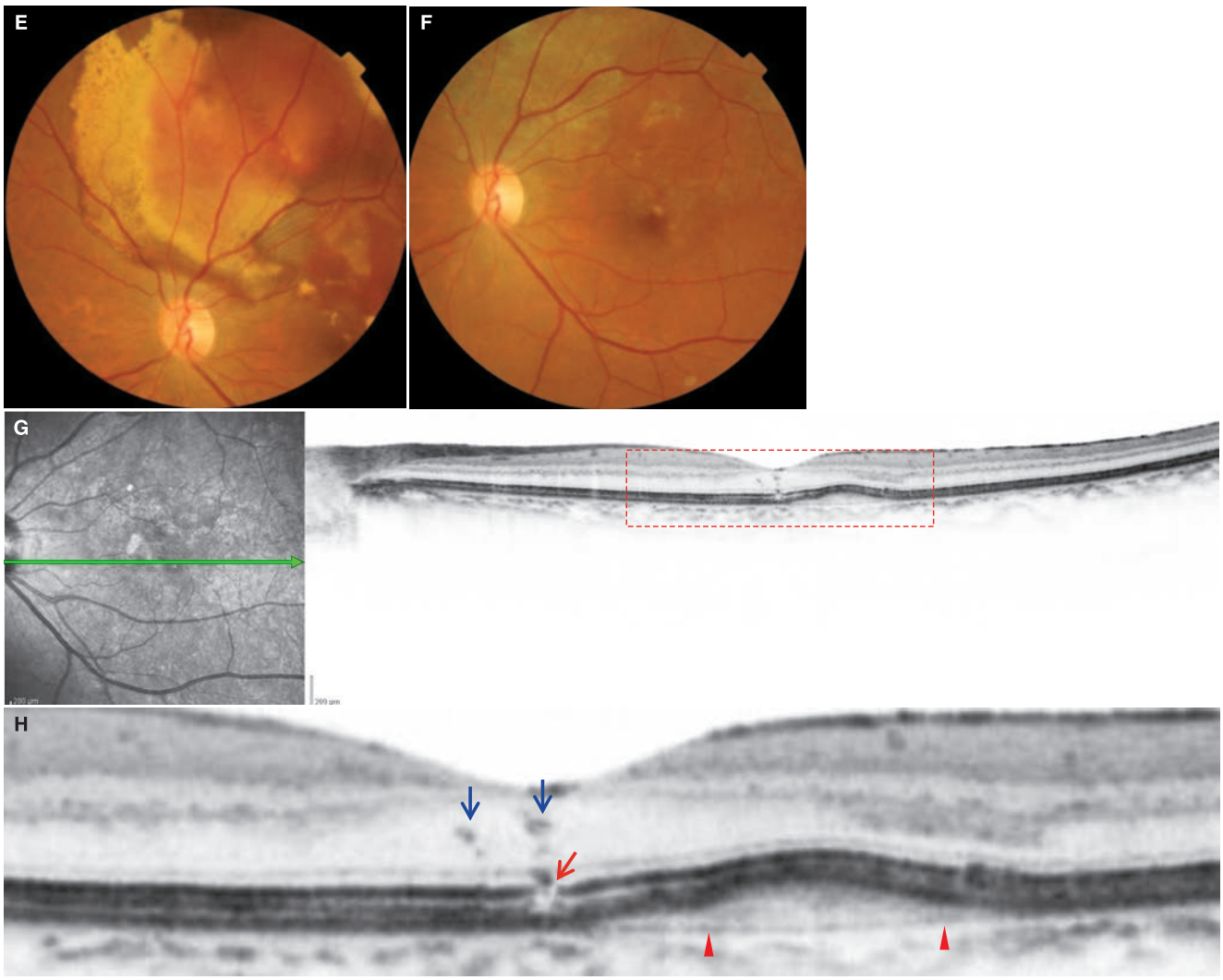

E: Color fundus photograph in the left eye: Six weeks after initial diagnosis. Subretinal and choroidal hemorrhages have organized and are becoming yellow. **F:** Color fundus photograph in the left eye: 22 months after initial diagnosis. The hemorrhages have been absorbed. The previous areas of hemorrhages now exhibit a greyish white appearance. **G:** IR + OCT horizontal scan of the left eye: Image from the same day as F. The retinal contour is close to normal. A mild, flat elevation is seen in the RPE. **H:** Enlarged version of G [red dashed box]: Defects are seen in the outer retinal layers at the fovea centralis. The IS/OS and COST lines are no longer visible (➔). The high reflectivity seen in the foveal outer nuclear layer is reactive RPE migration or macrophages that have phagocytized erythrocytes (➔). Bruch's membrane (►) is clearly visible below the RPE elevation immediately outside the fovea centralis.

Image interpretation points

This case illustrates that there can be significant improvement without treatment despite large hemorrhages in the setting of PCV. Damage can occur to the photoreceptor outer layer in the fovea centralis after the disappearance of hemorrhages regardless of no involvement of the fovea in the hemorrhagic lesions. The mechanism of this is unknown.

Case 112 Polypoidal choroidal vasculopathy: Optic disc type

A 70-year-old male, OD, BCVA 1.2

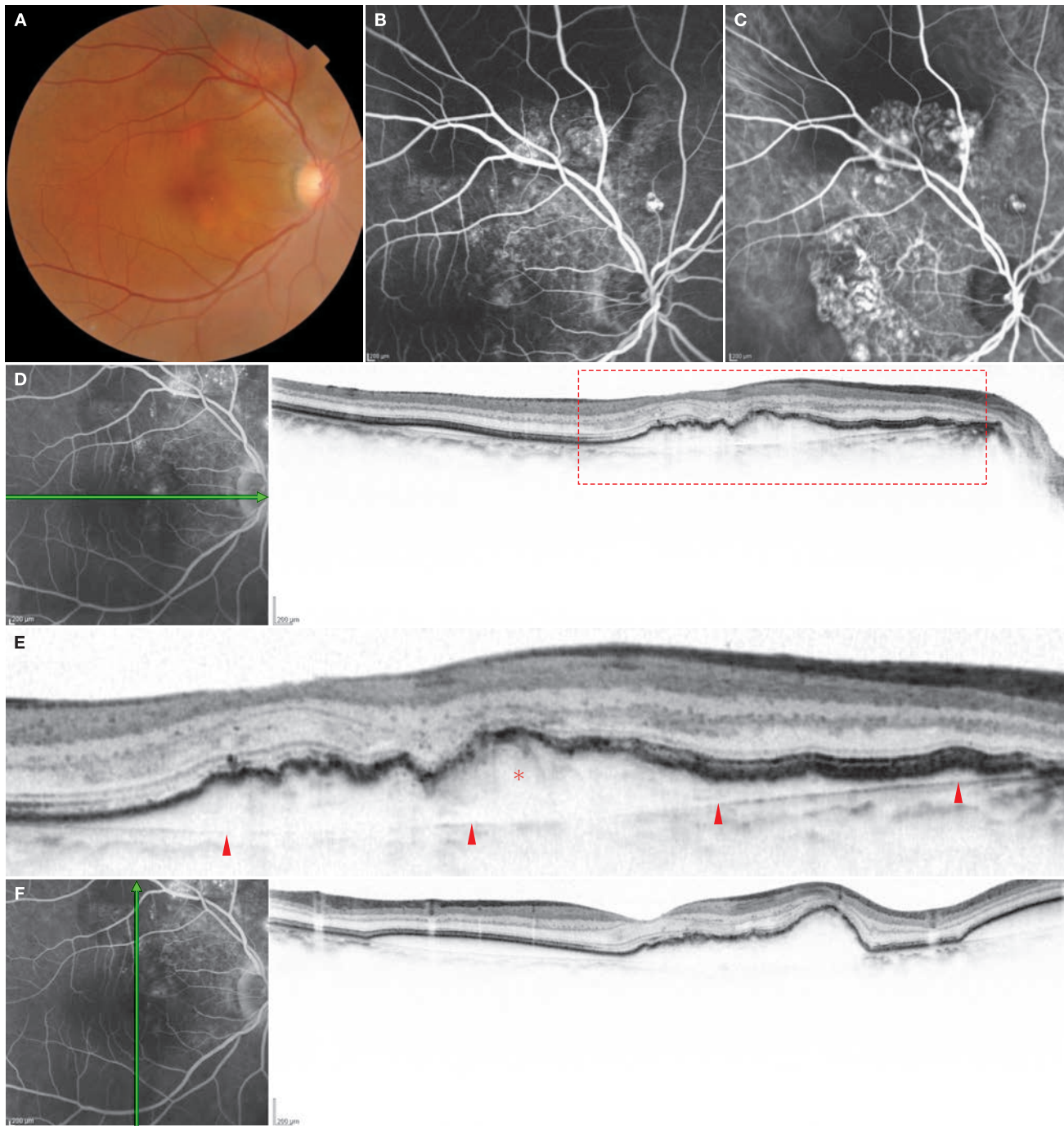

A: Color fundus photograph in the right eye: Elevated orange-red lesions are visible both superior and inferior to the fovea centralis and superiorly outside the vascular arcade. The orange-red lesion superiorly outside the vascular arcade is associated with a hemorrhagic PED. **B:** FA in the right eye (1 minute, 15 seconds): Hyperfluorescent lesions can be seen over a wide area from the fovea centralis to the vascular arcade. The origin of the branching vascular network is adjacent to the optic disc with one part exhibiting intense hyperfluorescence. **C:** IA in the right eye (1 minute, 15 seconds): The hyperfluorescent lesions seen on FA are the a wide area of branching vascular network and polypoidal lesions. **D:** FA + OCT horizontal scan of the right eye: A undulating RPE elevation with moderately reflective contents is seen suggestive of a fibrovascular PED. Bruch's membrane is also seen. The RPE elevation is seen to begin immediately adjacent to the optic disc indicating that the branching vascular network is CNV. **E:** Enlarged version of D [red dashed box]: There is no interruption in the RPE line. The moderate reflectivity below the RPE is due to fibrovascular components (✻). Bruch's membrane (►) is clearly visible. The structure of the sensory retina is relatively preserved. **F:** FA + OCT vertical scan of the right eye: It is clear that CNV exists over a wide area.
(Continued on the next page)

Case 112 Continuation

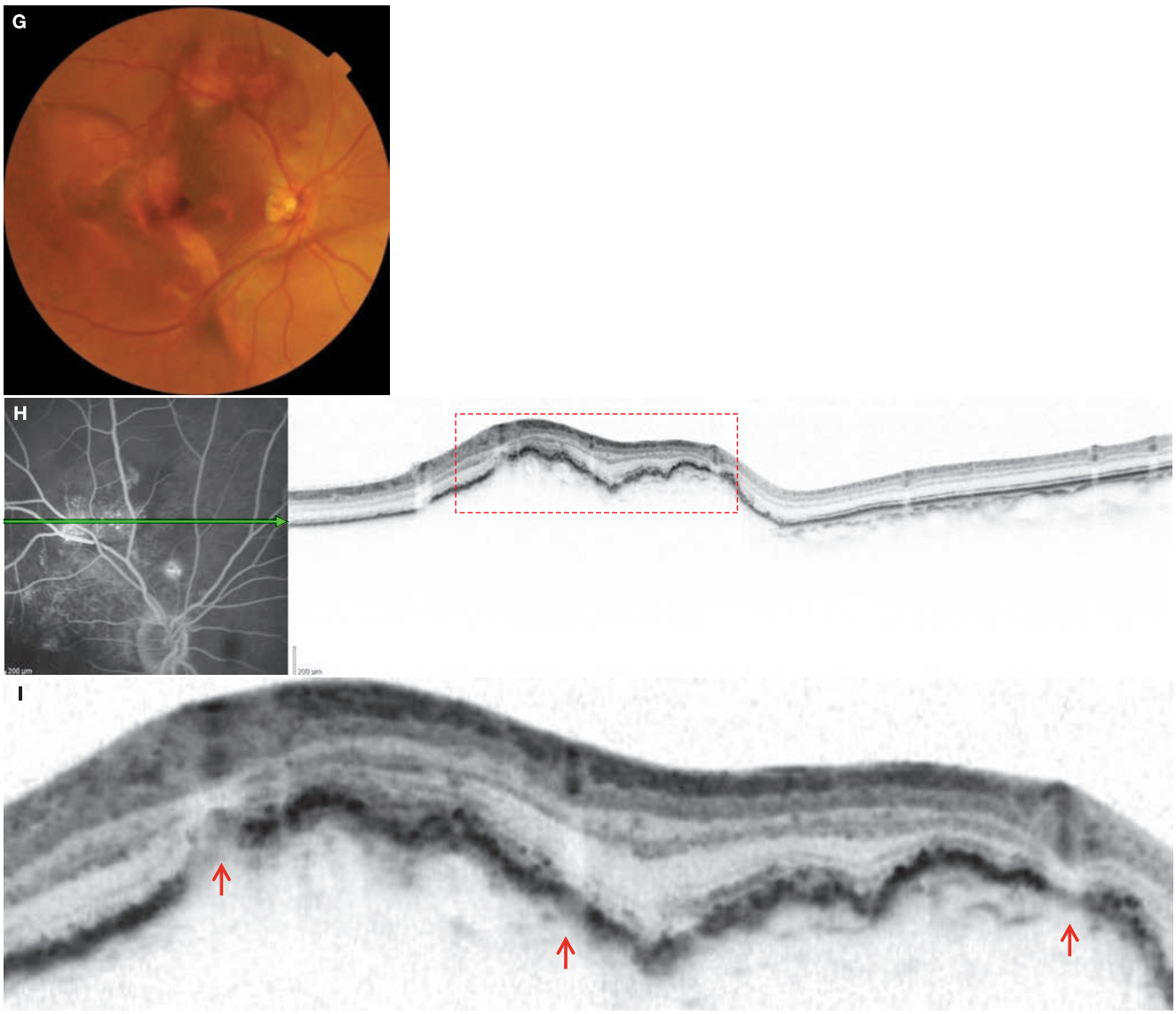

G: Color fundus photograph in the right eye: Eight months after initial diagnosis. Suprachoroidal hemorrhages have. Best-corrected visual acuity is 0.1. **H:** FA + OCT horizontal scan of the right eye: This is a B-scan through the active lesion superior to the optic disc. **I:** Enlarged version of H [red dashed box]: The RPE appears to be disrupted at the sites indicated by (➔), however, these are in fact artifacts resulting from signal blocking due to blood vessels in the sensory retina.

Image interpretation points

In this case, there are large subretinal and suprachoroidal hemorrhages associated with PCV, clearly indicating that PCV lesions are only present in the sub-RPE space.

Case 113 Polypoidal choroidal vasculopathy: Polypoidal lesions and pigment epithelial detachment

A 56-year-old male, OD, BCVA 0.5

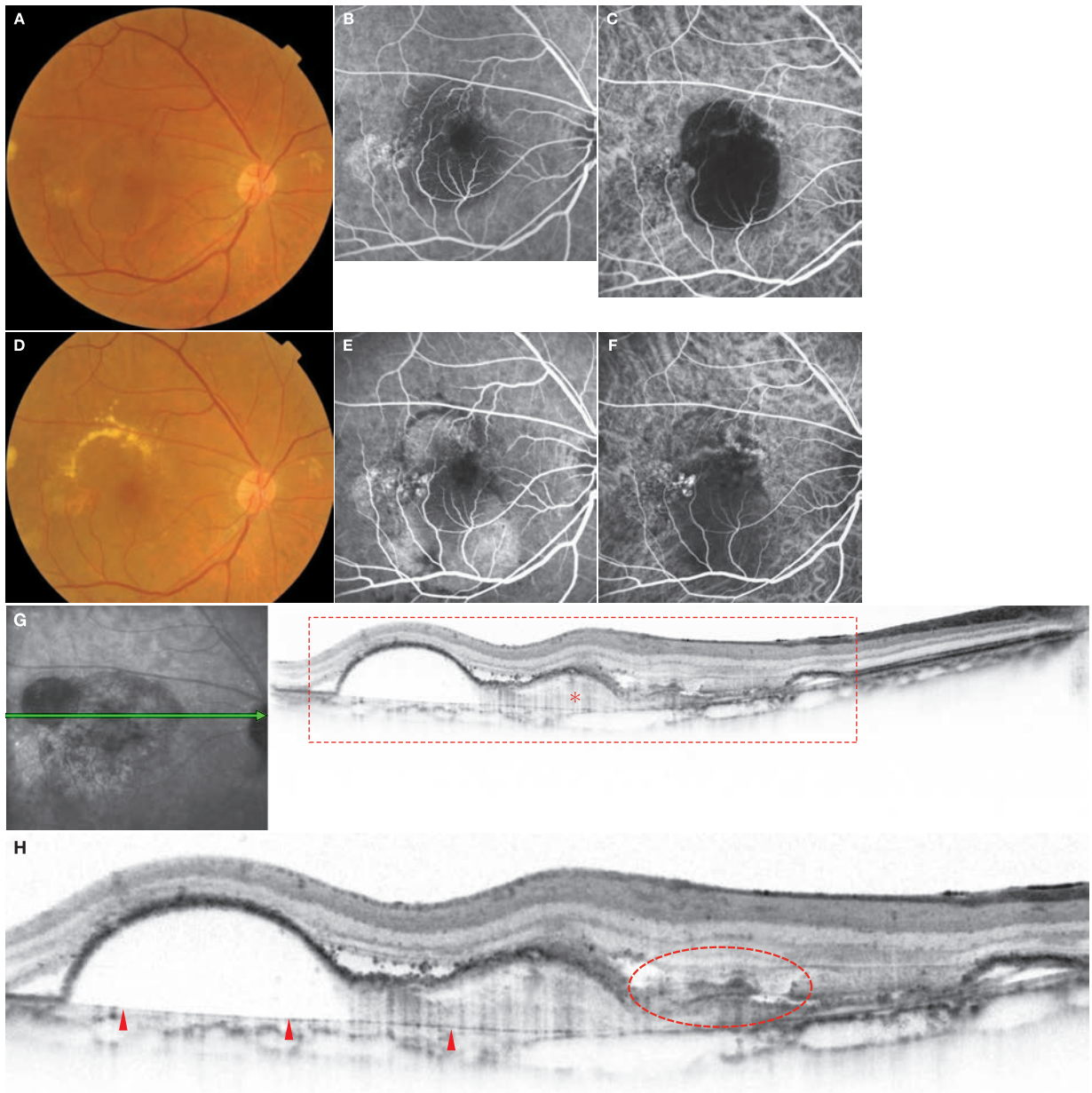

A: Color fundus photograph in the right eye: At initial diagnosis. A relatively new PED is seen seemingly with notches nasally and temporally at the edge of the PED. Best-corrected visual acuity is 0.5. **B:** FA in the right eye (43 seconds): At initial diagnosis. Hyperfluorescent lesions consistent with the notched sites are noticeable. **C:** IA in the right eye (43 seconds): During initial diagnosis. There appears to be polypoidal lesions consistent with the notched sites on IA. **D:** Color fundus photograph in the right eye: Six months after initial diagnosis. The PED has slightly flattened and hard exudates are deposited along its upper margin. The color of the RPE is abnormal on the temporal notch. Best-corrected visual acuity is 0.9. **E:** FA in the right eye (1 minute, 17 seconds): Six months after initial diagnosis. The inside of the PED is hyperfluorescent. **F:** IA in the right eye (1 minute, 17 seconds): Six months after initial diagnosis. The temporal notches exhibit intense fluorescence suggestive of a polypoidal lesion. I also appears to exist nasally. **G:** IA + OCT horizontal scan of the right eye: 1 year, 6 months after initial diagnosis. There are 2 PEDs seen adjacent to the each other in the superotemporal to the fovea centralis. The temporal PED is weakly reflective inside while the nasal PED is moderately reflective. (*). **H:** Enlarged version of G [red dashed box]: Bruch's membrane is clearly seen (►). Type 2 CNV appears to be growing beneath the sensory retina from the RPE defect (red dashed circle).

Image interpretation points

The reflectivity of the two adjacent RPE protrusions differs significantly indicating different contents. The moderate reflectivity of the nasal PED is due to CNV.

Case 114 Polypoidal choroidal vasculopathy: Tomographic notch sign

An 84-year-old female, OD, BCVA 0.5

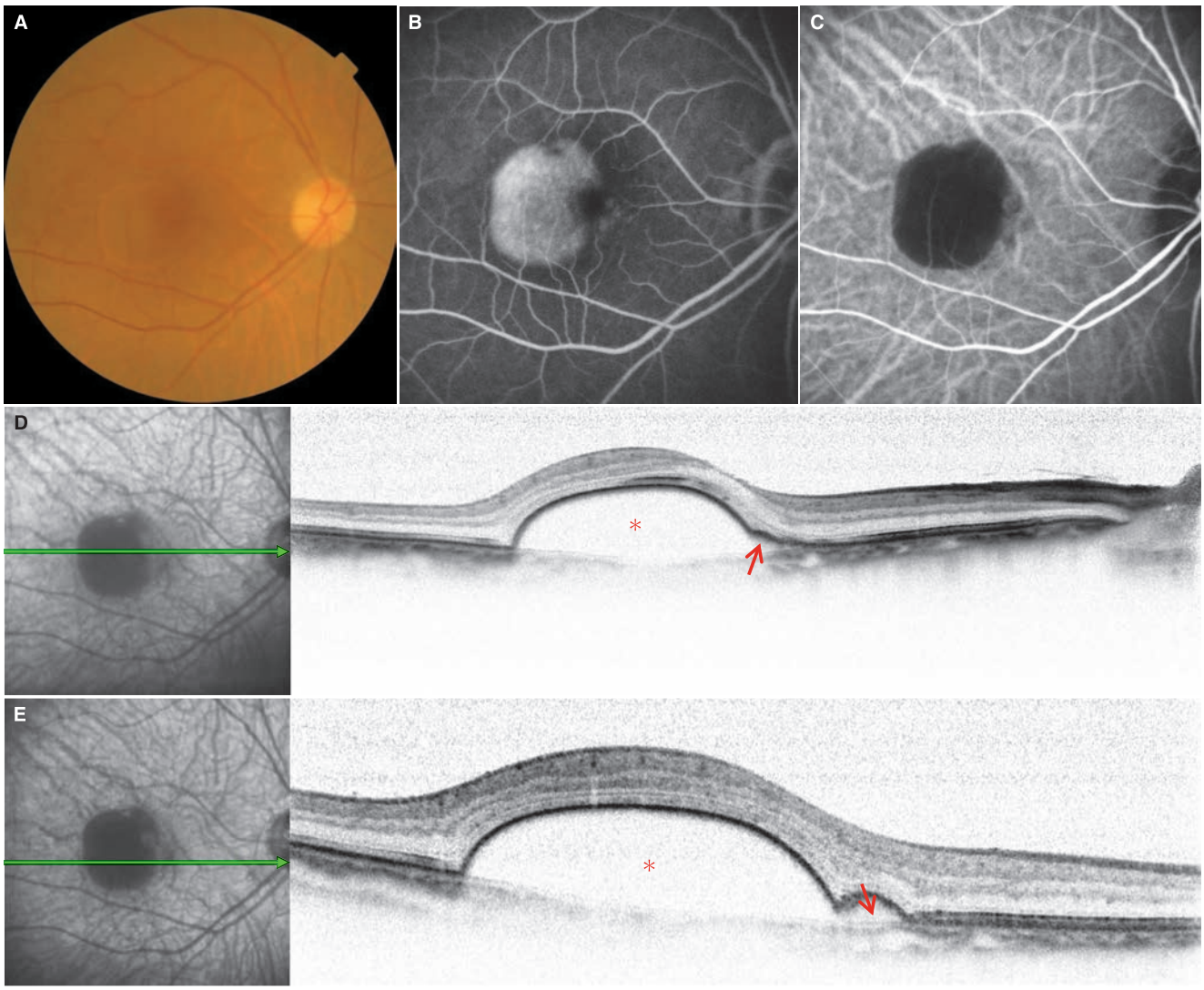

A: Color fundus photograph in the right eye: A serous PED about 1.5 disc diameters is seen temporally and includes the fovea centralis. No retinal hemorrhages or hard exudates are visible. **B:** FA in the right eye (3 minute, 43 seconds): Stronger hyperfluorescence can be seen in the temporal part of the PED. There are notches at the superior and nasal (corresponding to the fovea centralis) margins of the PED. **C:** IA in the right eye (3 minutes, 43 seconds): Slight hyperfluorescence is seen at the sites corresponding to the notches; however, a definitive diagnosis of PCV cannot be made. **D:** IR + OCT horizontal scan of the right eye: A serous PED (*) is observed. A so-called »tomographic notch sign« is seen nasally with moderately reflective contents (➔). This indicates the existence of vascular components. **E:** IR + OCT horizontal scan of the right eye: A serous PED (*) and a »tomographic notch sign« can be seen (➔).

Image interpretation points

This is a case where a serous PED is observed, a notch sign can be seen on angiography, and a »tomographic notch sign« is visible on OCT. While PCV is suspected, the diagnosis of PCV cannot be confirmed with angiography and it is typical to classify this case as AMD.

Case 115 Polypoidal choroidal vasculopathy: Case where the branching vascular network has detached

An 81-year-old male, OD, BCVA 0.04

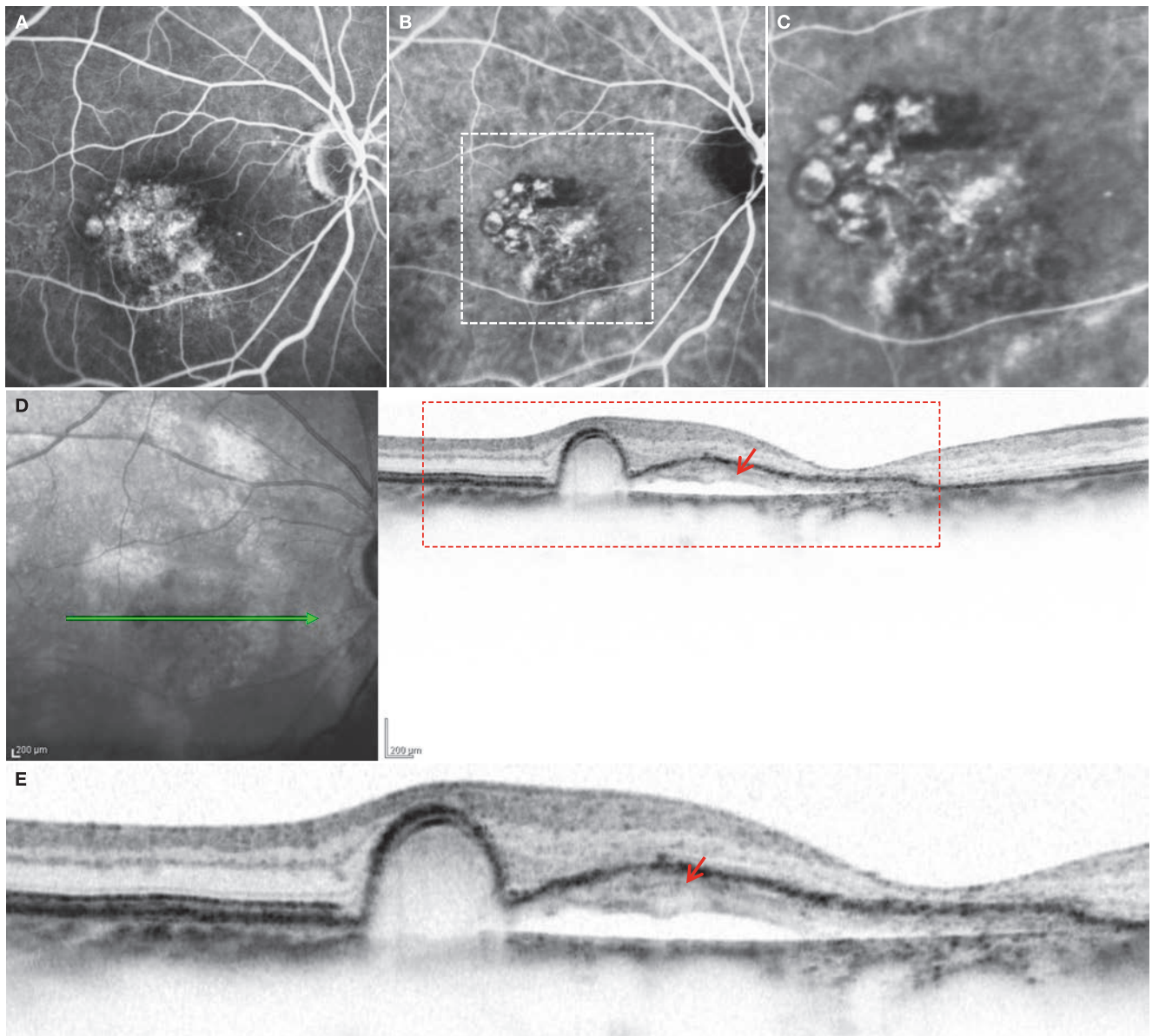

A: FA in the right eye (4 minute, 10 seconds): Irregular hyperfluorescent lesions about 2 disc diameters in size can be seen in the fovea centralis. **B:** IA in the right eye (4 minutes, 10 seconds): An branching vascular network and polypoidal lesions are seen. **C:** Enlarged version of B [white dashed box]: Polypoidal lesions are accumulating in grape-like structures. **D:** IR + OCT horizontal scan of the right eye: The polypoidal lesion is exhibiting steep RPE protrusion. There is moderate reflectivity within the foveal PED. The branching vascular network is detaching from Bruch's membrane (→). **E:** Enlarged version of D [red dashed box]: It is clear that the branching vascular network is detaching from Bruch's membrane (→). The polypoidal lesion and branching vascular network have almost the same reflectivity and are also connected. The foveal sensory retina is significantly thinned, consistent with the patient's poor visual acuity.

Image interpretation points

In this case, the branching vascular network is detaching from Bruch's membrane. Normally, the branching vascular network stably exists between Bruch's membrane and RPE and its detachment is much less frequent than the detachment of polypoidal lesions. As a result, this kind of case is extremely unusual.

Case 116 Polypoidal choroidal vasculopathy: A massive lesion

A 70-year-old male, OD, BCVA 0.1

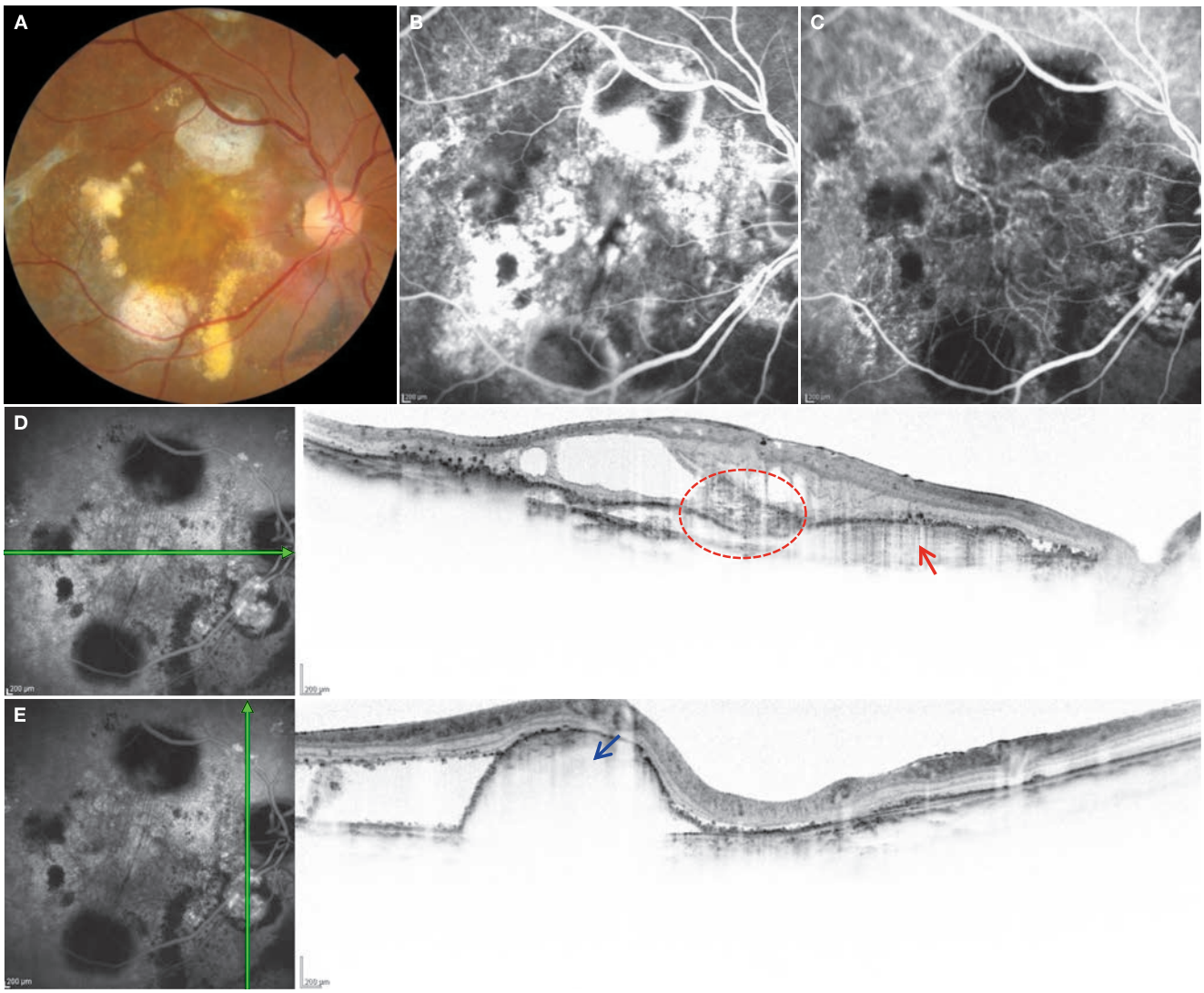

A: Color fundus photograph in the right eye: A large lesion is occupying the posterior pole and the fovea is atrophic. There are also atrophic lesions superior and inferior to the fovea centralis and hard exudates are visible temporal and inferior to the fovea. A large polypoidal lesion, which is still active, is observed immediately inferior to the optic disc. **B:** FA in the right eye (52 seconds): The entire posterior pole of the retina is exhibiting strong hyperfluorescence. **C:** IA in the right eye (52 seconds): A large branching vascular network is seen in the macula. **D:** IA + OCT horizontal scan of the right eye: The branching vascular network can be seen as moderate reflectivity beneath the RPE (→). There is a RPE disruption below the fovea centralis and Type 2 CNV is growing into subretinal space (red dashed circle). **E:** IA + OCT vertical scan of the right eye: This is a scan passing through a large, elevated, orange-red lesion inferior to the optic disc. A large polypoidal lesion is seen. There is moderate reflectivity (→) beneath the RPE at the apex of the polypoidal lesion, suggestive of fibrovascular contents.

Image interpretation points

This is a case of PCV with a large lesion. While the fovea is already atrophic, a highly active, elevated, orange-red lesion exists in the periphery of the large branching vascular network, indicating that exudative changes is still ongoing.

6.6 Retinal angiomatous proliferation

Background

Retinal angiomatous proliferation is a pathological condition that was described by Yannuzzi et al. in 2006[1] (Fig. 6-16). The condition where neovascularization originating from retinal blood vessels occurs has been known for a long time based on ophthalmoscopic findings, so rather than discovering the pathology, it is more appropriate to say this pathology was established based on Yannuzzi's systematic description. Gass proposed the concept of occult chorioretinal anastomosis, which appears contradictory to the disease concept of neovascularization derived from retinal blood vessels.[2] Nevertheless, the concept of RAP being neovascularization derived from retinal blood vessels is more convincing.

Freund et al. contrasted this neovascularization with Type 1 CNV and Type 2 CNV classified by Gass and proposed that it be called Type 3 CNV.[3] The clinical and genetic backgrounds of patients with RAP differ slightly from the narrowly defined AMD and PCV, consistent with the difference in pathological conditions of RAP and the other AMD types.[4]

OCT findings

OCT images of RAP differ according to the stage.[5] In Stage 1, mild intraretinal edema can be seen in the outer plexiform layer. As the disease stage progresses, clear, highly reflective lesion becomes visible in the retina. The highly reflective lesion is thought to represent intraretinal neovascularization. Defects in the RPE corresponding to the intraretinal neovascularization can always be seen, but it is sometimes difficult to ascertain if the disease stage is an early stage. The low frequency at which SRDs are seen in OCT images is a characteristic of RAP cases.

There are few histopathological reports on RAP. In a recent paper by Klein and Wilson, neovascularization derived from retinal blood vessels reportedly passes through the small RPE defect in the PED and appears to spread immediately beneath the RPE.[6] However, there do not yet appear to be any reports demonstrating the correspondence between OCT and histological images. Fig. 6-17 contrasts the histological image in the report by Klein and Wilson with the OCT image from our similar case. We can see that the histological image on the left and OCT image on the right correspond very well.

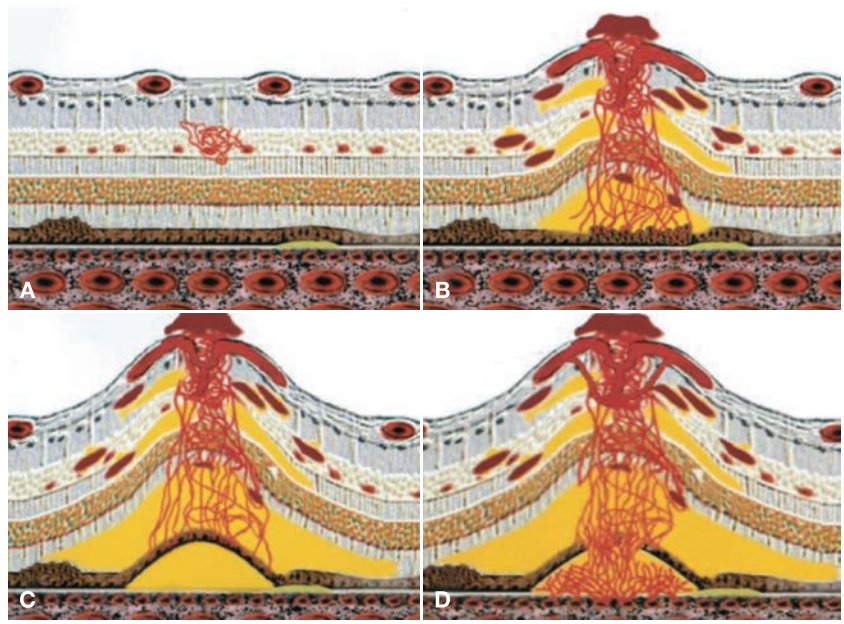

Fig. 6-16 Schematic diagram of RAP
A: Stage 1; Proliferation of the retinal blood vessels occurs. There are no changes beneath the RPE at this point. **B:** Stage 2A; The proliferative neovascularization derived from the retinal blood vessels is growing to all layers of the retina, but no PED is developing. **C:** Stage 2B; A PED develops. **D:** Stage 3; Anastomosis of retinal and choroidal neovascularization is complete. (These images are cited from Yannuzzi LA, Negr .A Nco S, Iida T, Carvalho C, Rodriguez-Coleman H, Slakter J, Freund KB, Sorenson J, Orlock D, Borodoker N. Retinal angiomatous proliferation in age-related macular degeneration. Retina. 2001;21:416–434.)

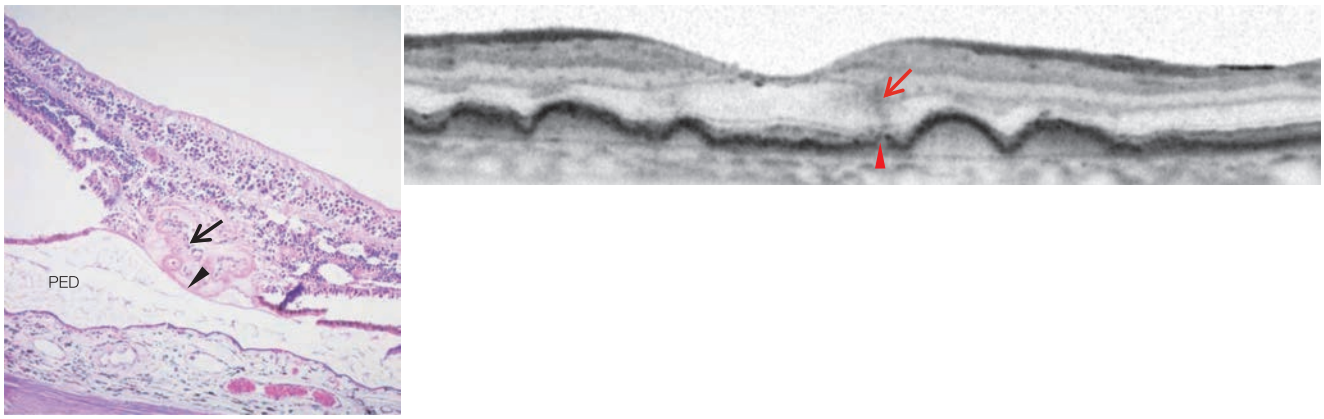

Fig. 6-17 Contrast of a histological image with an OCT image in similar RAP cases
In the histological image on the left, neovascularization is confined to the sensory retina (➔). The PED and neovascularization exist in contact with each other. A partial RPE defect can be seen in the PED (►). In the OCT image on the right, there is spreading of retinal neovascularization, indicated by ➔, toward the RPE defect, indicated by ►. (The histological image on the left is modified according to, Klein ML, Wilson DJ. Clinicopathologic correlation of choroidal and retinal neovascular lesions in age-related macular degeneration. Am J Ophthalmol. 2011; 151: 161–169)

6.6.1 References

1) Yannuzzi LA, Negrao S, Iida T, et al. Retinal angiomatous proliferation in age-related macular degeneration. *Retina*. 2001; 21:416–434.
2) Gass JDM, Agarwal A, Lavina AM, et al. Focal inner retinal hemorrhages in patients with drusen: an early sign of occult choroidal neovascularization and chorioretinal anastomosis. *Retina*. 2003; 23:741–751.
3) Freund KB, Ho IV, Barbazetto IA, et al. Type 3 neovascularization: the expanded spectrum of retinal angiomatous proliferation. *Retina*. 2008; 28:201–211.
4) Matsumoto H, Sato T, Kishi S. Tomographic features of intraretinal neovascularization in retinal angiomatous proliferation. *Retina*. 2010; 30:425–430.
5) Hayashi H, Yamashiro K, Gotoh N, et al. CFH and ARMS2 variations in age-related macular degeneration, polypoidal choroidal vasculopathy, and retinal angiomatous proliferation. *Invest Ophthalmol Vis Sci*. 2010; 51:5914–5919.
6) Klein ML, Wilson DJ. Clinicopathologic correlation of choroidal and retinal neovascular lesions in age-related macular degeneration. *Am J Ophthalmol*. 2011; 151:161–169.

Case 117 Retinal angiomatous proliferation: Stage 1

An 85-year-old male, OS, BCVA 1.2

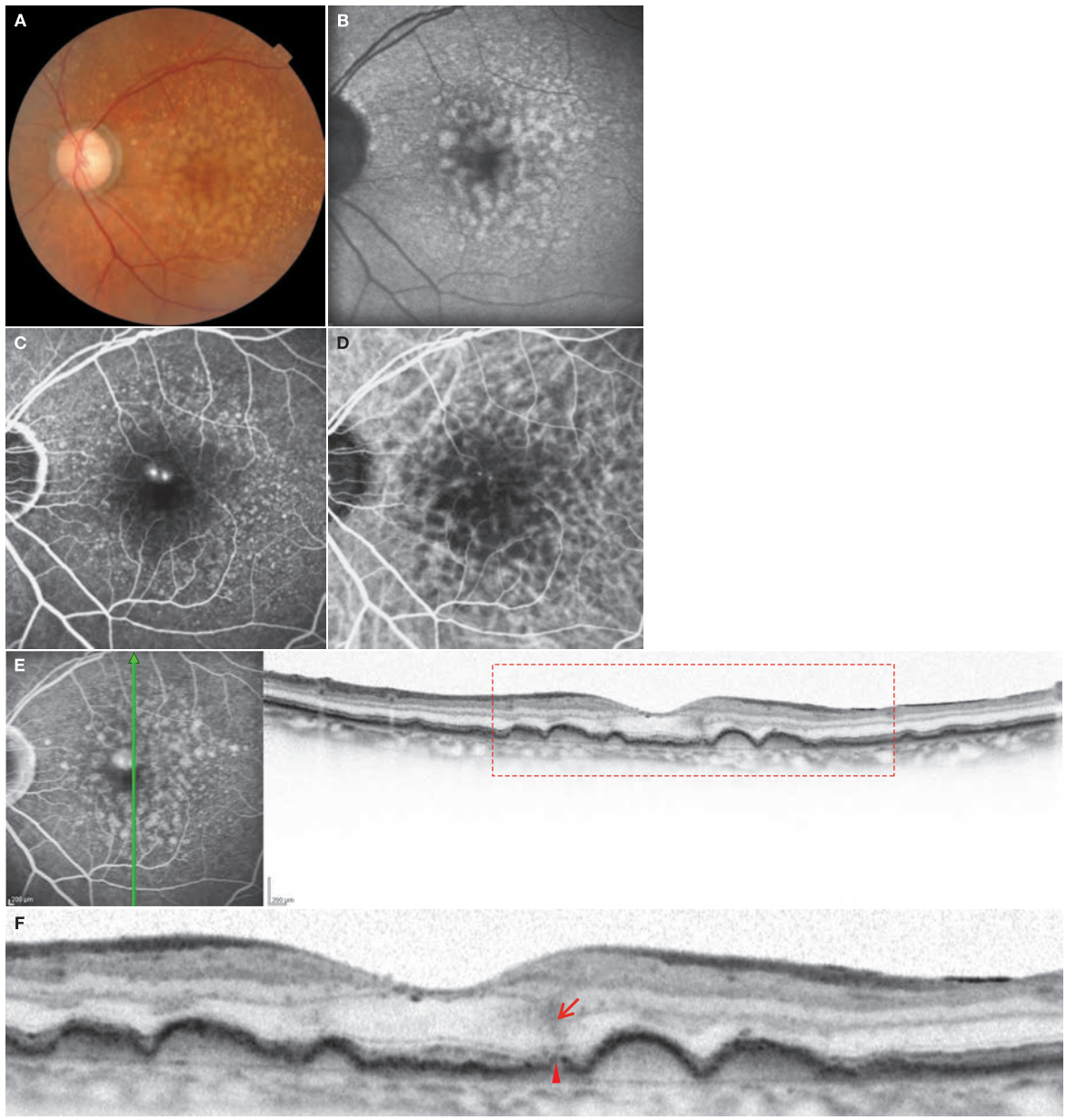

A: Color fundus photograph in the left eye: Multiple soft drusen exist in the macular area. A part of them are drusenoid PED rather than drusen. **B:** FAF in the left eye: The drusenoid PED is exhibiting hyperfluorescence. The punctate hyperfluorescent foci that appear to be surrounding the macula are reticular pseudodrusen. **C:** FA in the left eye (52 seconds): Two lesions exhibiting strong hyperfluorescence are visible. These are due to intraretinal neovascularization (IRN). The drusen are hyperfluorescent even on FA. **D:** IA in the left eye (1 minute, 52 seconds): Different from FA, the drusen are exhibiting hypofluorescence. IRN is seen. **E:** FA + OCT horizontal scan of the left eye: RPE protrusions as a result of drusen can be seen. The content of the drusen is exhibiting moderate reflectivity. **F:** Enlarged version of E [red dashed box]: Moderate reflectivity extending in a longitudinal direction can be seen within the retina (➔). This appears to be IRN when pieced together with other findings. Small defects in the RPE can be seen immediately below the IRN (►).

Image interpretation points

This is Stage 1 RAP. The intraretinal neovascularization (IRN) is clearly visible. There appear to be small defects in the RPE corresponding to IRN. RAP is often binocular and Stage 1 cases are often discovered in the fellow eye of advanced RAP.

Notably, Bruch's membrane is depicted as a thin, straight, highly reflective line at the base of the drusen. The content of the drusen exhibits moderate reflectivity, and the ELM and IS/OS of the sensory retina immediately above the drusen is not depicted.

Case 118 Retinal angiomatous proliferation: Stage 2A

An 81-year-old male, OD, BCVA 0.15

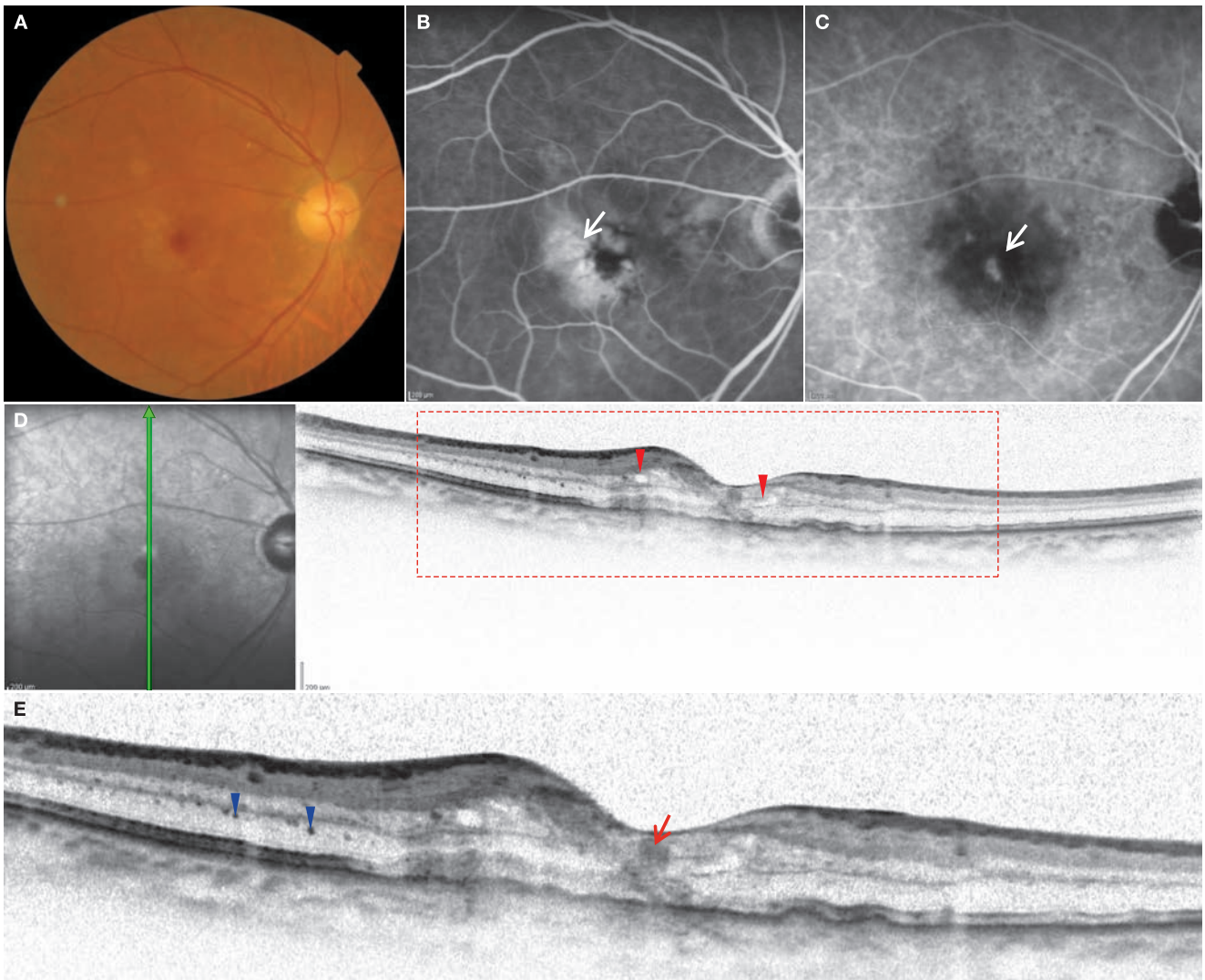

A: Color fundus photograph: Macular edema can be seen temporal to the fovea centralis, but the changes that can be seen with an biomicroscopy are relatively mild. Drusen are scattered. **B:** FA in the right eye (12 minutes, 26 seconds): Strong hyperfluorescent lesion can be seen temporal to the fovea centralis (⇒). **C:** IA in the right eye (12 minutes, 26 seconds): Hyperfluorescence due to IRN can be seen (⇒). **D:** IR + OCT vertical scan of the right eye: Cystoid spaces (►) can be seen superior and inferior to the fovea centralis **E:** Enlarged version of D [red dashed box]: Moderate reflectivity extending longitudinally across retinal layers can be seen (➔). This is IRN. The RPE line is continuous and no clear defect can be seen. Particulates exhibiting high reflectivity are seen in the outer nuclear layer (►).

Image interpretation points

This is Stage 2A RAP. IRN is seen. The RPE line is flat and is not accompanied by a PED. It should be noted that the RAP stage classification does not necessarily represent disease development. Rather, it would be best to consider the system as a useful method of categorization.

Some researchers believe the highly reflective dots visible in the outer nuclear layer are macrophages. The existence of these punctiform highly reflective dots is generally thought to reflect a highly active clinical picture.

Case 119 Retinal angiomatous proliferation: Stage 2B ①

A 71-year-old female, OS, BCVA 1.0

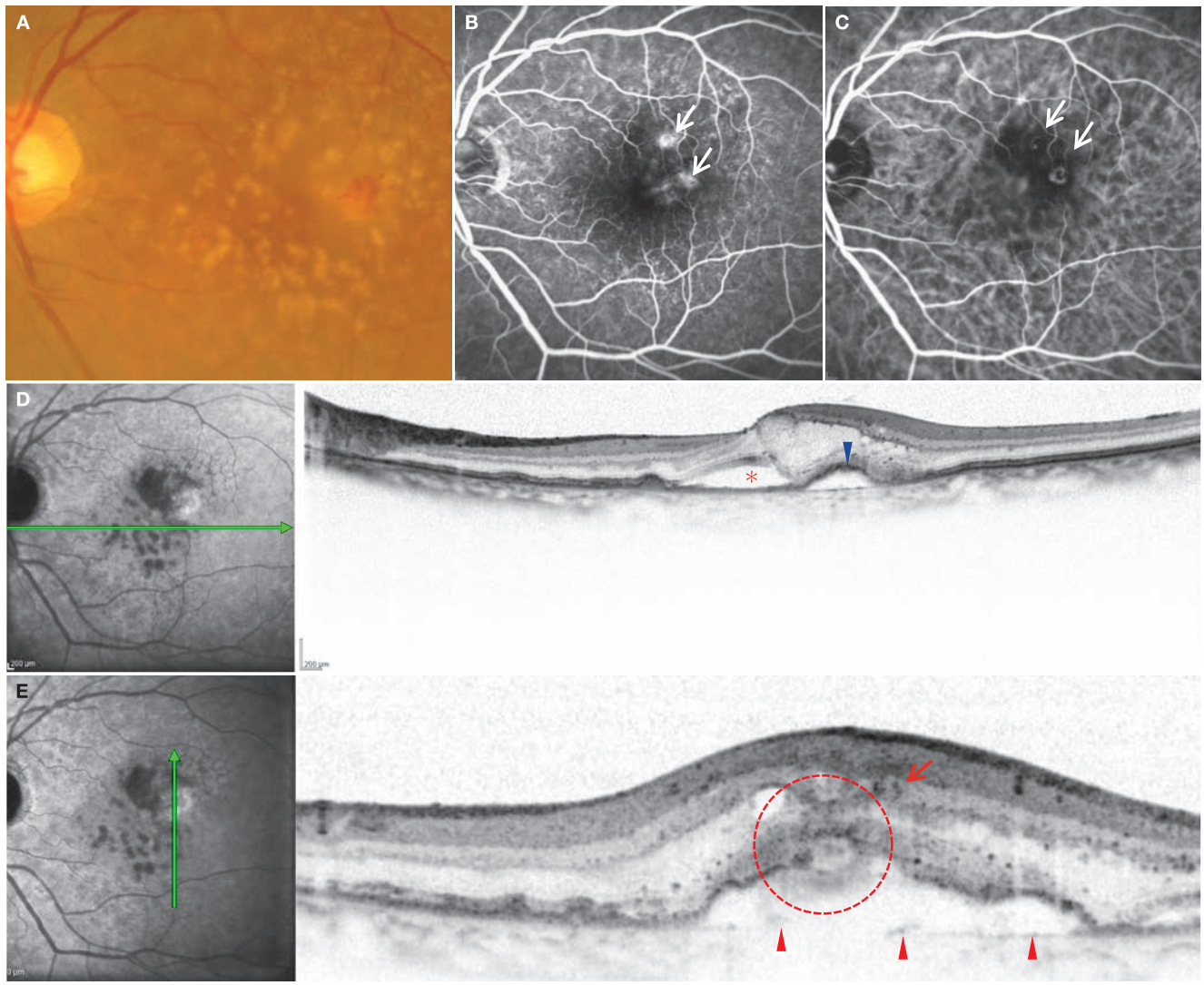

A: Color fundus photograph in the left eye: Multiple soft drusen can be seen in the macula. Preretinal hemorrhages and a few fibrin deposits are visible slightly temporal to the fovea centralis. Good visual acuity is achieved since foveal changes are mild. **B:** FA in the left eye (46 seconds): Hyperfluorescent lesions are seen superotemporal to the fovea centralis (⇛). **C:** IAin the left eye (1 minute, 55 seconds): The hyperfluorescent lesions seen on FA can be confirmed as chorioretinal anastomosis (⇛). **D:** IA + OCT horizontal scan of the left eye: A B-scan image passing through the fovea centralis. A subfoveal SRD is seen (✻). Cystoid spaces are seen in the sensory retina temporal to the fovea centralis. A PED exists temporally (►). **E:** IA + OCT vertical scan of the left eye: This is a B-scan passing through the area of chorioretinal anastomosis. Multiple infiltrating cells can be seen in the sensory retina (➔). The intraretinal neovascularization appears to be growing down within the PED through the RPE break (red dashed circle). Bruch's membrane is seen at the base of the PED (►).

Image interpretation points

This is Stage 2B or Stage 3 RAP. Due to difficulty in determining the internal state of PEDs on OCT, it is difficult to confirm anastomosis of the choroidal and retinal blood vessels (chorioretinal anastomosis) on OCT.

Case 120 Retinal angiomatous proliferation: Stage 2B ②

An 84-year-old male, OD, BCVA 0.4

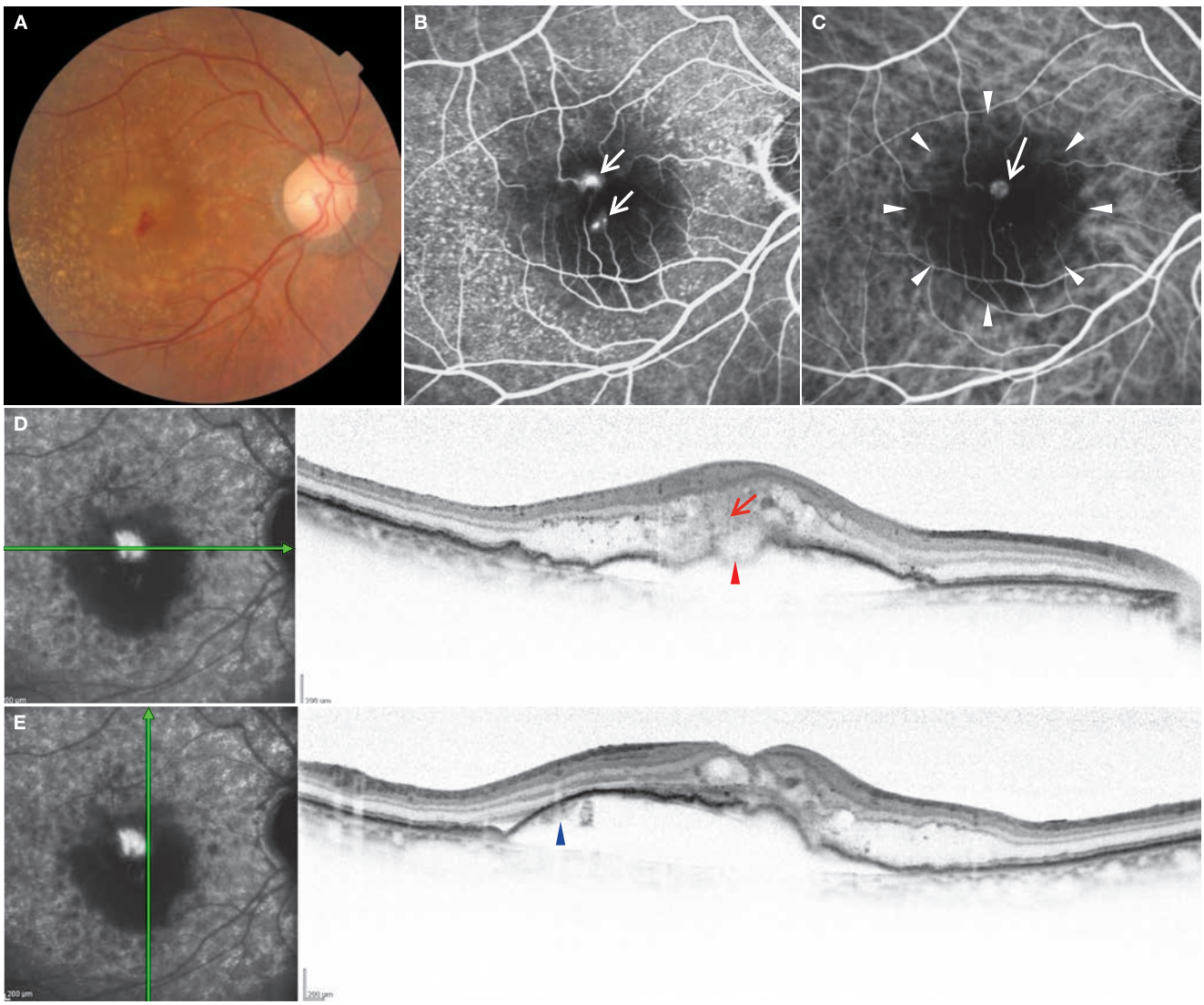

A: Color fundus photograph in the right eye: Retinal hemorrhages as well as fibrin deposits are visible in the fovea centralis. Multiple drusen are seen in the macular area. **B:** FA in the right eye (1 minute, 24 seconds): Two strong hyperfluorescent foci are visible (⇨). The drusen are also exhibiting strong hyperfluorescence. **C:** IA in the right eye (1 minute, 24 seconds): Chorioretinal anastomosis is clearly seen (⇨). The PED is hypofluorescent on IA (▷ area). **D:** IA + OCT horizontal scan of the right eye: A large PED can be seen. A break is noticeable in the RPE (►). Such findings are sometimes referred to as »bump sign«. Moderate reflectivity due to fibrin deposits and IRN is visible anterior to the RPE break (➔). Exudative changes can be seen in the retina. **E:** IA + OCT vertical scan of the right eye: A large PED is visible. The high reflectivity (►) observed on the posterior surface of the RPE may be neovascularization that has grown into the PED, but it could also be exudate. Cystoid spaces can be seen in the sensory retina.

Image interpretation points

In this case, a large PED is seen suggesting RAP Stage 2B. Neovascularization can be seen growing into the PED through the RPE break represented by the partial disruption in the RPE line.

Most spectral-domain OCT devices currently on the market use a light source with a center wavelength of about 840 nm. Since this wavelength does not allow the OCT beam to sufficiently reach below the RPE, it is difficult to determine the contents of the PED. Even with the development of OCT using 1 µm band light sources, it is not easy to determine the contents of the PED.

Case 121 Retinal angiomatous proliferation: Stage 3

A 72-year-old female, OS, BCVA 0.2

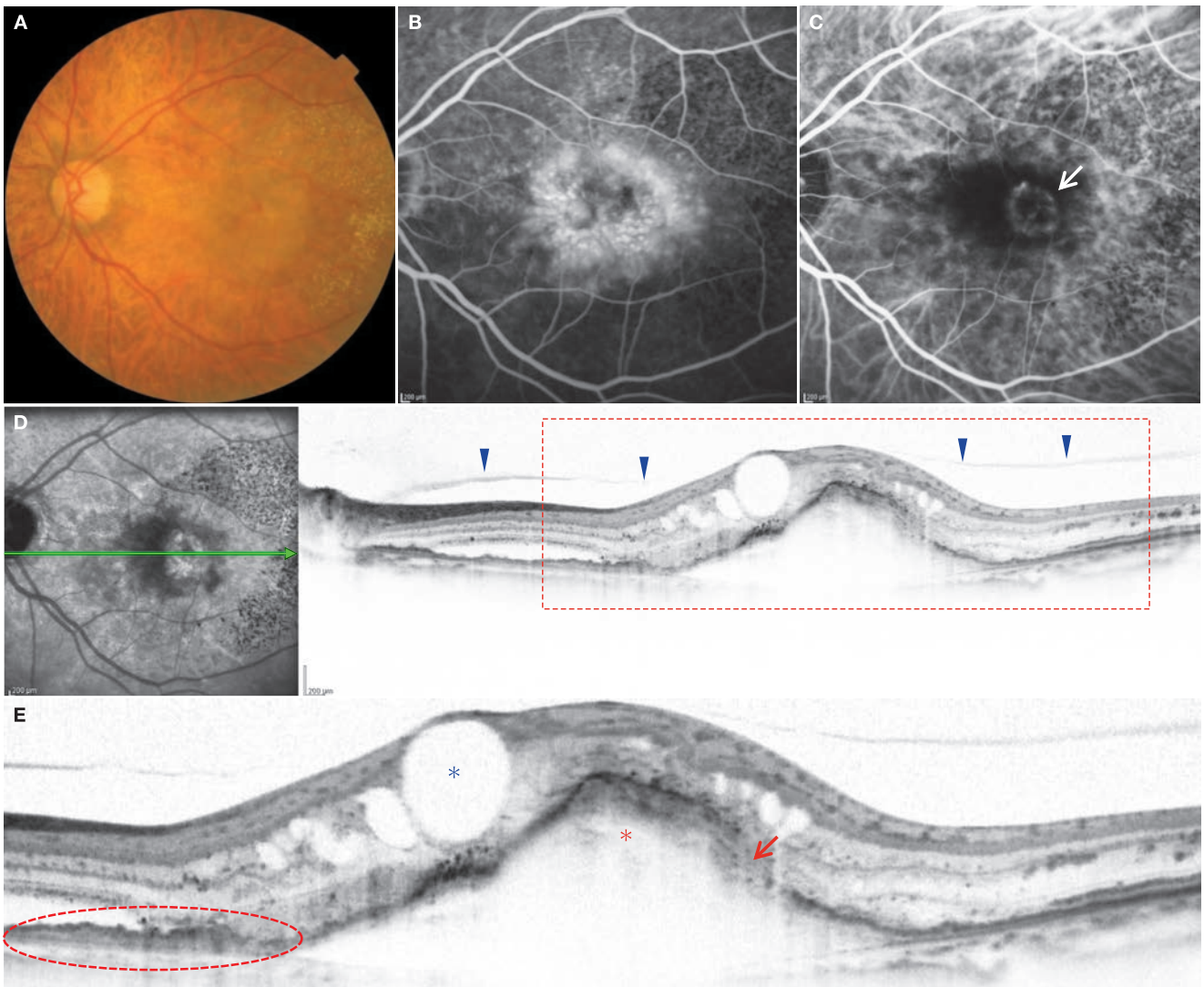

A: Color fundus photograph in the left eye: Multiple drusen can be seen mainly in the temporal macula. A portion of them are reticular pseudodrusen. A large PED is seen at the fovea centralis. Tiny retinal hemorrhages are also visible. **B:** FA in the left eye (3 minutes, 18 seconds): A CME is appreciated. **C:** IA in the left eye (3 minutes, 18 seconds) : The PED is exhibiting hypofluorescence. CNV is seen (⇨). **D:** IA + OCT horizontal scan of the left eye: A large PED can be seen. The RPE line is disrupted. Cystoid spaces are observed in the sensory retina and a SRD is visible between the fovea centralis and optic disc. Traction as exerted by the posterior vitreous cortex is also present (►). **E:** Enlarged version of D [red dashed box]: Moderate reflectivity is seen within the PED (✻). This is a fibrovascular PED. The RPE line is disrupted (➔). The neovascularization from the retina appears to be growing posterior to the RPE through the RPE break temporal to the fovea centralis. The reflectivity intensity of the lesions anterior and inferior to the RPE break appears constant, suggesting this is continuous tissue. Multiple cystoid spaces (✻) are seen within the sensory retina. The RPE nasal to the PED is gently elevated (red dashed circle). CNV appears to exist in this area.

(Continued on the next page)

Image interpretation points

This is a case of typical Stage 3 RAP. The retinal neovascularization can be seen passing through the RPE tear and anastomosing with CNV. The RPE nasal to the lesions is gently sloping and CNV appears to exist below this.

Case 121 After treatment with anti-VEGF treatment

A 72-year-old female, OS, BCVA 0.1

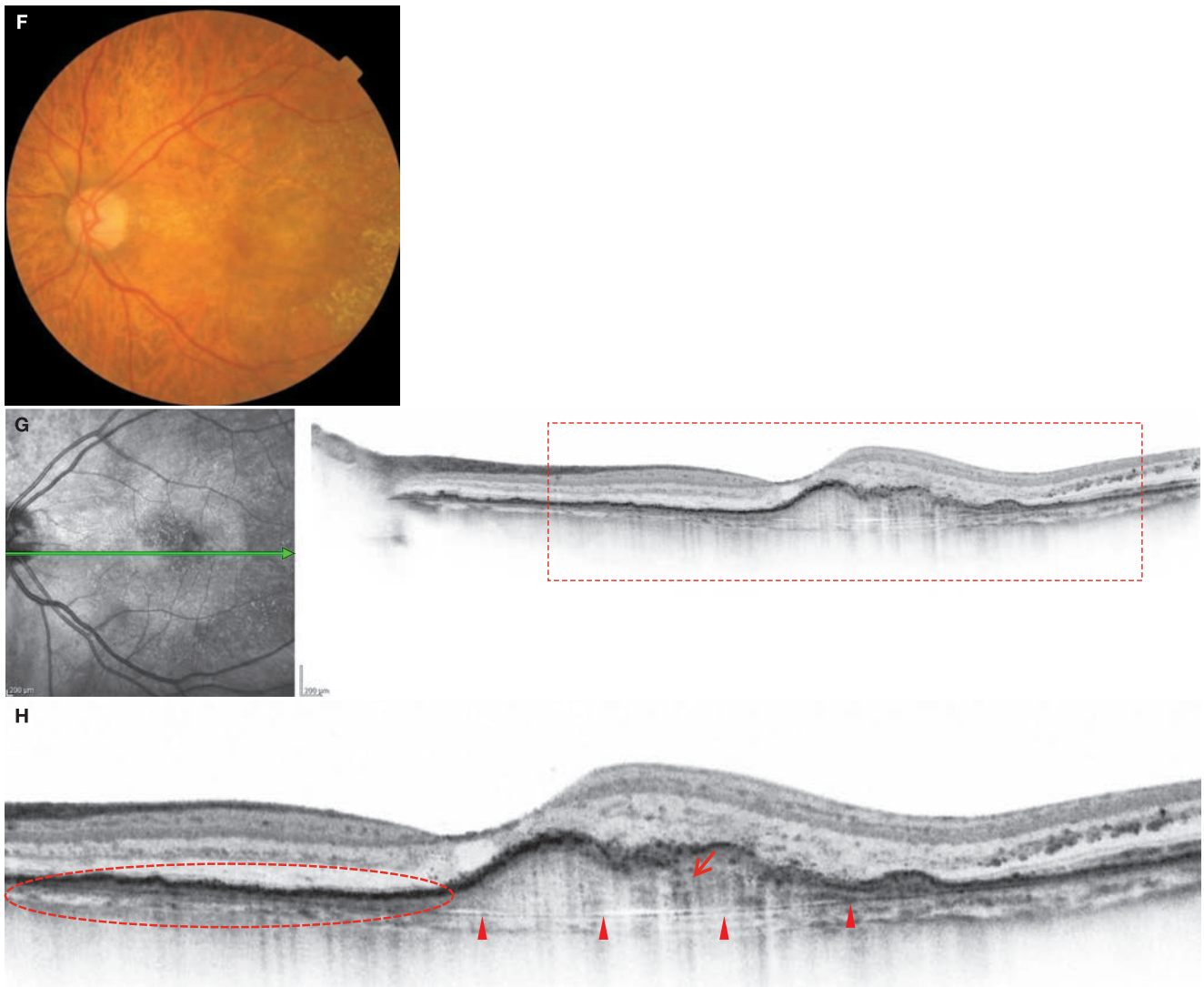

F: Color fundus photograph in the left eye: Exudative changes in the macular area are receding. Retinal hemorrhages are no longer seen. **G:** IR + OCT horizontal scan of the left eye: The cystoid spaces have also almost disappeared on OCT. The internal reflectivity of the PED is actually increasing, indicating the existence of a fibrovascular PED. **H:** Enlarged version of G [red dashed box]: Moderate reflectivity is observed within the PED (→). Bruch's membrane is clearly seen at the base of the PED (►). The CNV below the RPE that was seen before treatment remains (red dashed circle).

Image interpretation points

It is clear that exudative changes in the retina are receding as a result of treatment with anti-VEGF treatment.

When there is an RPE protrusion as in this case, neovascularization may be present on the choroidal side of the RPE. Thus, it is important to closely observe the features in the choroidal side of the RPE line.

6.7 Malattia leventinese

Background

Malattia leventinese is a rare disease with a dominant form of hereditary characterized by juvenile binocular onset and radially arranged drusen. Drusen in the vicinity of the fovea centralis are large, have a strong tendency to become confluent, and those in the periphery often exhibit a typical radial array. This disease is sometimes referred to by the disease names of familial drusen or Doyne's honeycomb retinal dystrophy. It is known that genetic abnormalities in Fibulin-3 (EFEMP1) are associated with this disease.[1]

OCT findings

Patients with malattia leventinese characteristically maintain good visual acuity despite the prominent abnormalities in the fundus. Since previous reports on histopathological findings for malattia leventinese have not been enough, the reason for this is not entirely understood. However, based on a small number of reports on OCT findings, visual acuity may be maintained due to relatively mild changes in the sensory retina. One report using time-domain OCT stated that while the RPE and Bruch's membrane appeared thick, the sensory retina was relatively well preserved.[2] However, according to a report using spectral-domain OCT, damage to the IS/OS can be seen.[3]

6.7.1 References

1) Stone EM, Lotery AJ, Munier FL, et al. A single EFEMP1 mutation associated with both Malattia Leventinese and Doyne honeycomb retinal dystrophy. Nat Genet. 1999; 22:199–202.
2) Souied EH, Leveziel N, Letien V, et al. Optical coherent tomography features of malattia leventinese. Am J Ophthalmol. 2006; 141:404–407.
3) Gerth C, Zawadzki RJ, Werner JS, et al. Retinal microstructure in patients with EFEMP1 retinal dystrophy evaluated by Fourier domain OCT. Eye (Lond). 2009; 23:480–483.

Case 122 Malattia leventinese: A typical example

A 39-year-old male, OD and OS, BCVA 1.5 and 1.5 respectively

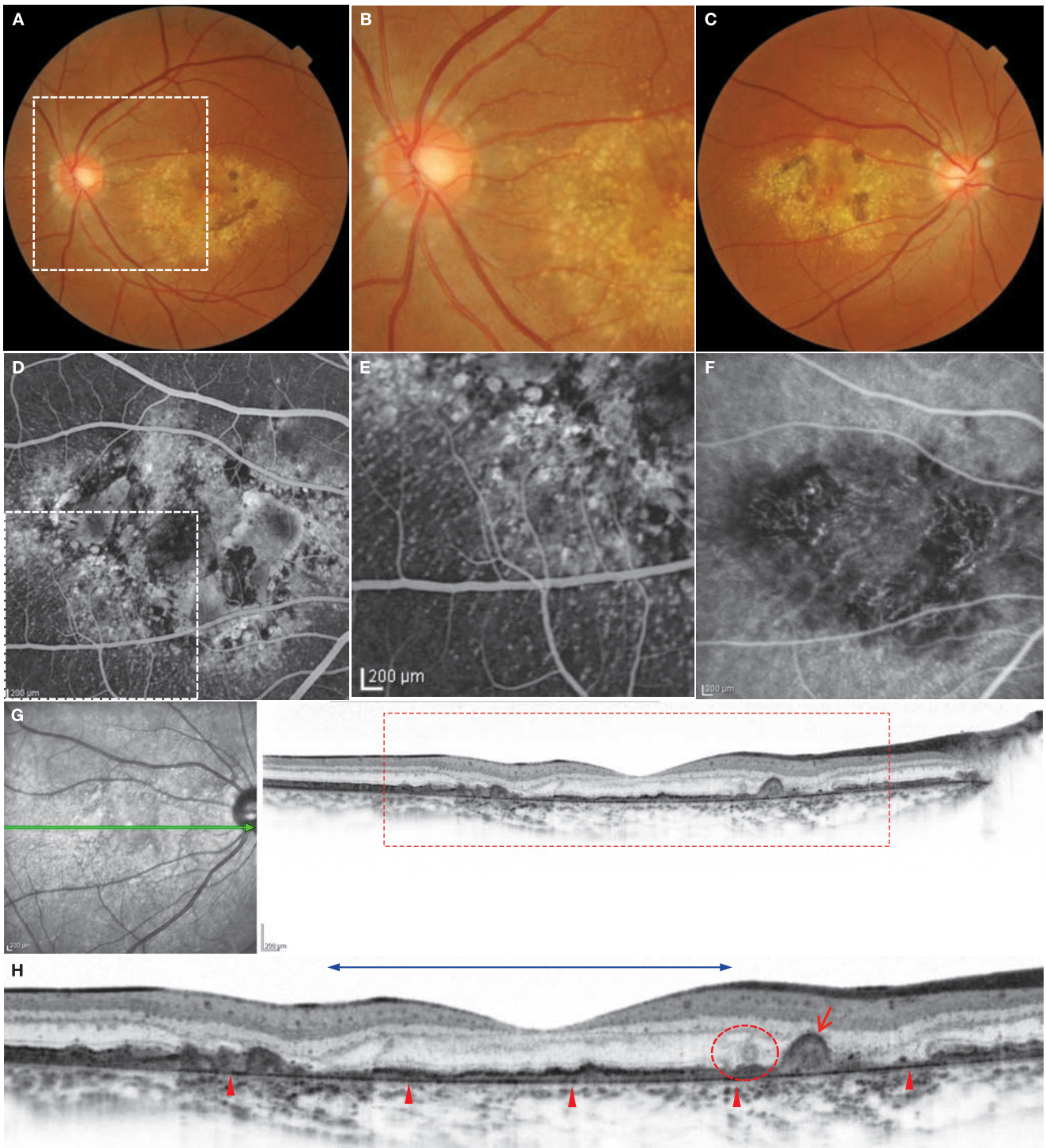

A: Color fundus photograph in the left eye: There is a large number of drusen over a wide area of the macula. Drusen can also be seen near the optic disc. **B:** Enlarged version of A [white dashed box]: Drusen surrounding the optic disc are clearly visible. Most of the drusen near the fovea centralis are confluent. **C:** Color fundus photograph: The same findings as the left eye are seen. RPE pigment changes are also present. **D:** FA in the right eye (1 minute, 42 seconds): The RPE pigment changes near the fovea centralis are exhibiting hypofluorescence. Multiple drusen forming a radial pattern can be seen temporal to the fovea centralis. **E:** Enlarged version of D [white dashed box]: Drusen forming a radial pattern are clearly visible. **F:** IA in the right eye (1 minute, 42 seconds): The small drusen are also exhibiting hyperfluorescence on IA. No CNV can be seen. **G:** IR + OCT horizontal scan of the right eye: The subfoveal RPE is gently elevated. The retinal structure is largely preserved. **H:** Enlarged version of G [red dashed box]: The ELM can be traced in the area indicated by (↔). The photoreceptor inner segment is disrupted on the nasal and temporal side of the area indicated by (↔). A relatively tall PED is seen nasally (→). In the red dashed circle area, an outer retinal tubulation is seen. Reflectivity of Bruch's membrane appears to be increasing (►).

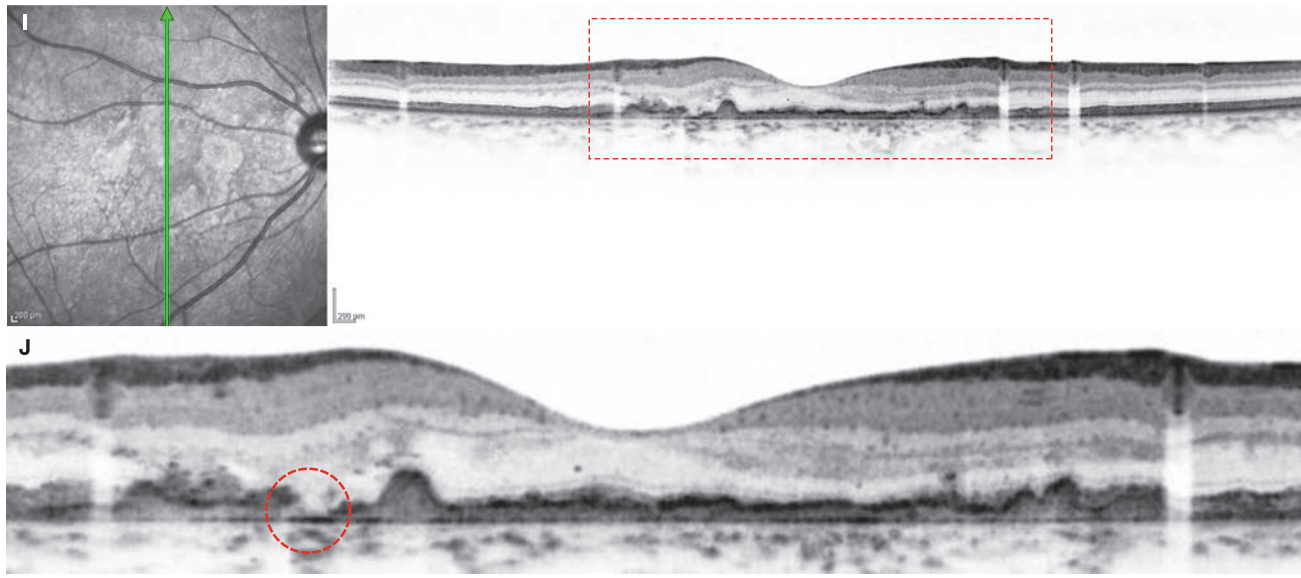

I: IR + OCT vertical scan of the right eye: The retinal structure is well preserved. **J:** Enlarged version of I [red dashed box]: The RPE is slightly elevated from Bruch's membrane, and deposits with moderate reflectivity are seen between the RPE and Bruch's membrane. Reflectivity of Bruch's membrane appears stronger than normal on this scan as well. The ELM line can be traced. There is a RPE break in the red dashed circle area.

Image interpretation points

Malattia leventinese is a relatively rare disease. As with typical drusen, the drusen are located beneath the RPE. Mutated proteins (EFEMP1) are known to be deposited in sub-RPE space in this disease. The moderate reflectivity between the RPE and Bruch's membrane is thought to be due to these mutated protein deposits. While older reports state that there is histological thickening of Bruch's membrane, further studies will be necessary to determine if Bruch's membrane does indeed have increased reflectivity indicating the thickened Bruch's membrane.

6.8 Idiopathic choroidal neovascularization

Background

Idiopathic choroidal neovascularization (idiopathic CNV) is a disease often seen in relatively young women, mostly occuring in moderately myopic eyes.[1] The diagnosis of idiopathic CNV can only be applied once all other factors that cause CNV have been excluded. Presumed ocular histoplasmosis is one disease that requires differentiation, although it is believed that this disease does not exist in Japan. The biggest challenge in clinical settings, however, is differentiation from myopic CNV.[2] Whereas idiopathic CNV primarily occurs in patients under 50, myopic CNV rarely occurs in patients under 50.

Punctate inner choroidopathy (PIC) is also cited as a disease requiring differentiation. Please refer to »Chapter 7 Retinal degeneration« for PIC (► p. 238–241).

OCT findings

CNV seen in this disease is Type 2 CNV. Tall, cone-shaped CNV is seen in the active stage, but as the disease progresses, CNV is enveloped by the RPE, making the borders of the RPE and CNV indistinct. As a result, this disease often looks like Type 1 CNV on OCT.[3]

6.8.1 References

1) Cleasby GW. Idiopathic focal subretinal neovascularization. Am J Ophthalmol. 1976; 81:590–599.
2) Machida S, Hasegawa Y, Kondo M, et al. High prevalence of myopia in Japanese patients with idiopathic focal subretinal neovascularization. Retina. 2006; 26:170–175.
3) Iida T, Hagimura N, Sato T, et al. Optical coherence tomographic features of idiopathic submacular choroidal neovascularization. Am J Ophthalmol. 2000; 130:763–768.

Case 123 Idiopathic choroidal neovascularization: A fresh case

A 33-year-old female, OS, BCVA 0.6, refraction –4.75D, axial length 25.96 mm

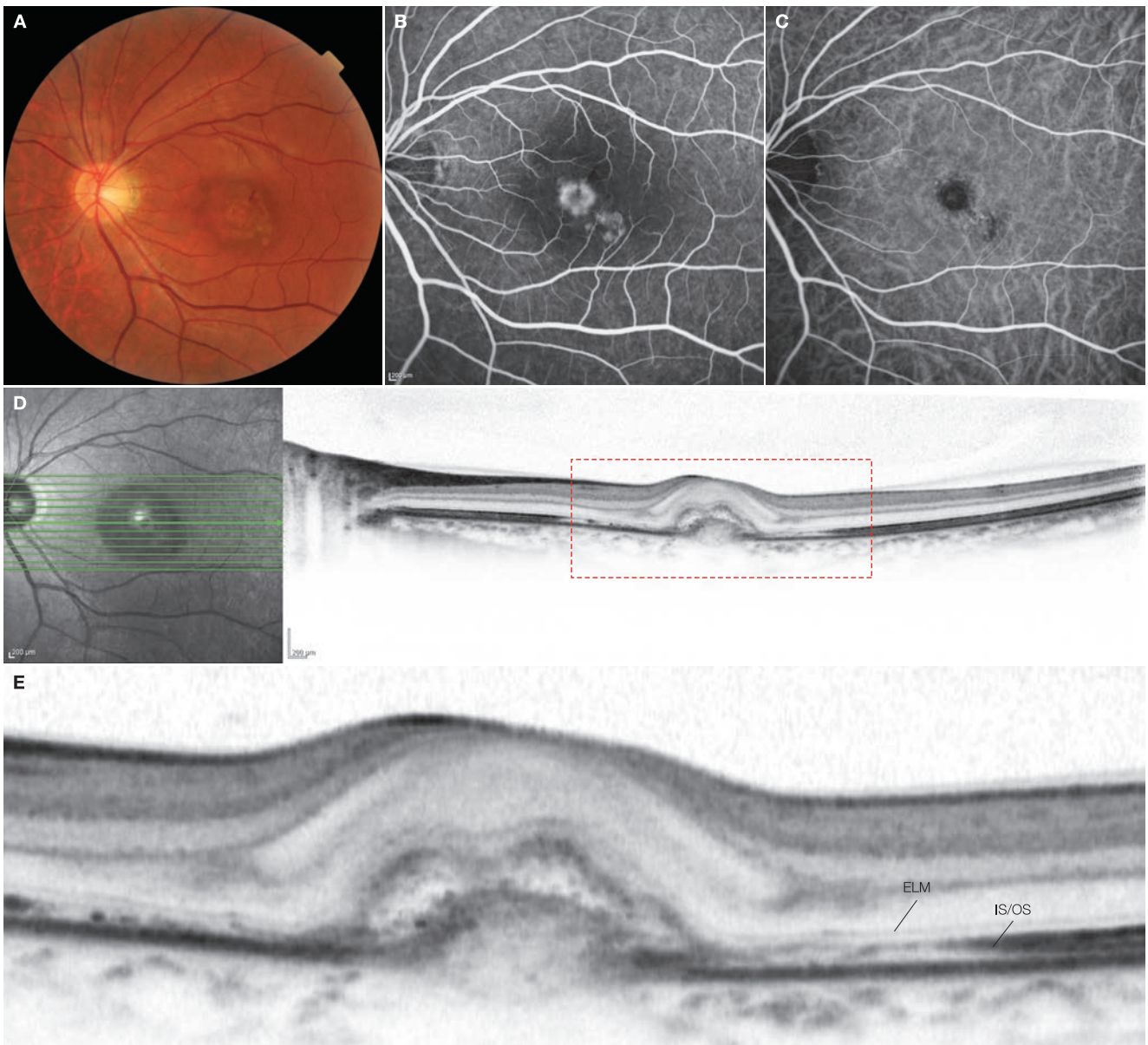

A: Color fundus photograph in the left eye: This is a tigroid fundus. Annular CNV can be seen at the fovea centralis. Thin subretinal hemorrhages are present around the CNV. **B:** FA in the left eye (1 minute, 31 seconds): Annular hyperfluorescence due to fluorescein leakage from CNV is visible. Hyperfluorescent lesions due to window defects are seen inferotemporal to the CNV. **C:** IA in the left eye (1 minute, 31 seconds): Annular hypofluorescent lesion is exhibited on the CNV at the fovea centralis on IA. **D:** IR + OCT horizontal scan of the left eye: CNV at the fovea centralis is seen. There is also a very thin SRD. The RPE line is disrupted as a result of CNV. **E:** Enlarged version of D [red dashed box]: While the ELM line is seen over almost the entire length of the scan, the IS/OS line is disrupted near the CNV.

Image interpretation points

This is Type 2 CNV that has occurred in a relatively young female with moderate myopia. As these images were taken soon after disease onset, the characteristics of Type 2 CNV are evident. The RPE line is disrupted as a result of CNV and envelopment of CNV by the RPE has not yet been completed.

Case 124 Idiopathic choroidal neovascularization: Envelopment by RPE cells

A 36-year-old male, OD, BCVA 0.4, refraction –7.0D, axial length 27.12 mm

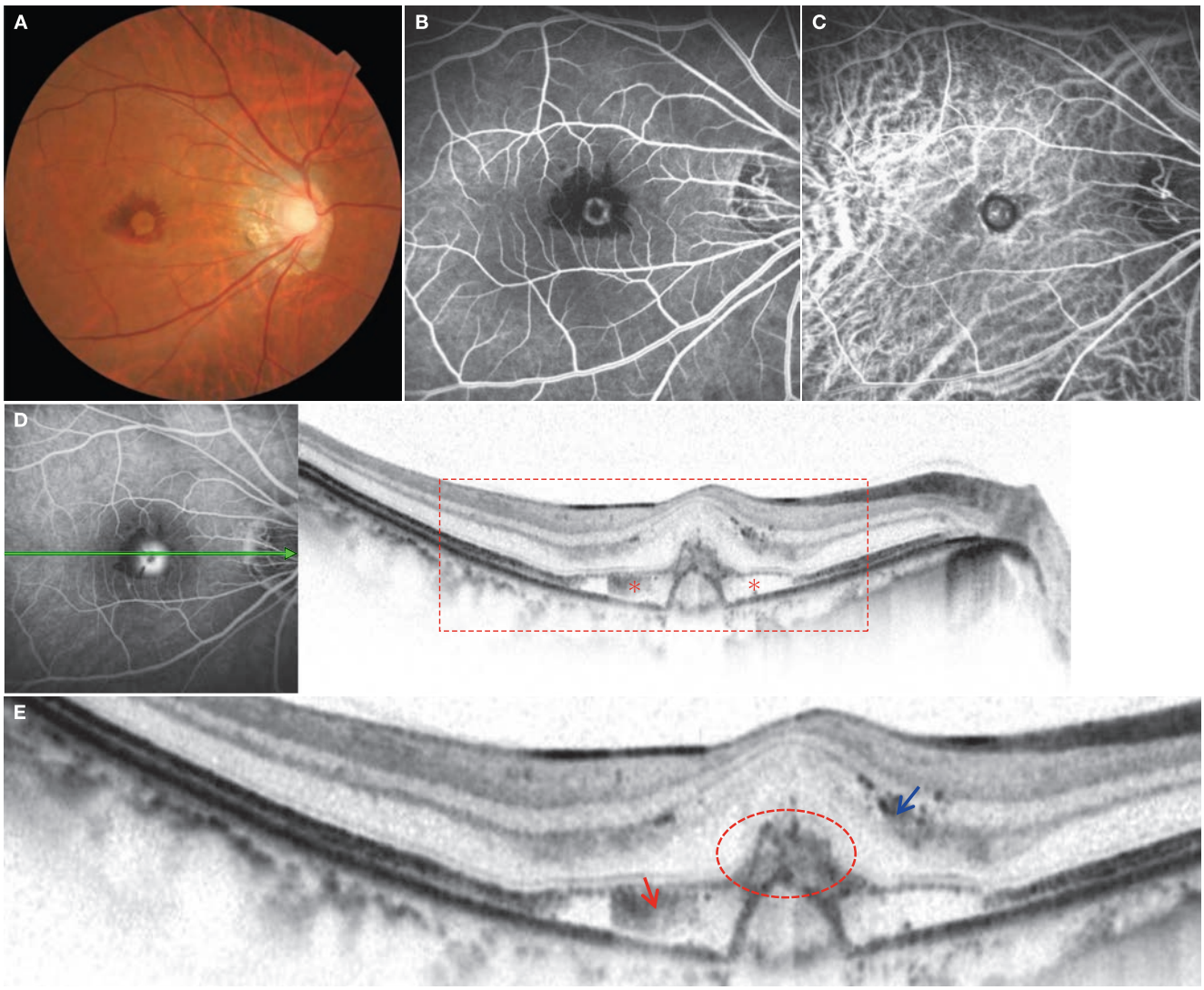

A: Color fundus photograph in the right eye: This is a tigroid fundus. Annular CNV can be seen beneath the fovea centralis. Thin subretinal hemorrhages are present around the CNV. **B:** FA in the right eye (23 seconds): Annular hyperfluorescence due to fluorescein leakage from CNV is seen. Around this, there is hypofluorescence due to subretinal hemorrhages. **C:** IA in the right eye (23 seconds): The hypofluorescent area is smaller on IA than on FA. This finding indicates that the hypofluorescence on FA is not only due to retinal hemorrhages, but also due to a combination of two elements. The infrared light in IA can pass through the hemorrhages. The hypofluorescence surrounding the CNV on IA is due to the RPE cells enveloping the CNV. **D:** FA + OCT horizontal scan of the right eye: Type 2 CNV is enveloped by the RPE. A thin SRD (*) is present around the CNV. **E:** Enlarged version of D [red dashed box]: Subretinal hemorrhages (→), CNV with moderate reflectivity anteriorly (red dashed circle), as well as cells infiltrating into the sensory retina can be seen (→). (Continued on the next page)

Image interpretation points

While idiopathic CNV generally occurs in women with moderate myopia, this is Type 2 CNV that has occurred in a relatviely young male with high myopia. While the possibility cannot be excluded that this is a case of myopic CNV, this disease entity rarely occurs in the 4th decade of life. This case may have been typical Type 2 CNV, but the scarring mechanism had already started at initial diagnosis. Moderate reflectivity thought to be due to infiltrating cells can be seen immediately anterior to the CNV, and the border region between the outer plexiform layer and the outer nuclear layer. While it is natural to assume these represent reactive proliferations of RPE cells and macrophages that have phagocytized erythrocytes, there is not enough evidence to support this claim.

Case 124 After treatment with anti-VEGF treatment

A 36-year-old male, OD, BCVA 0.8

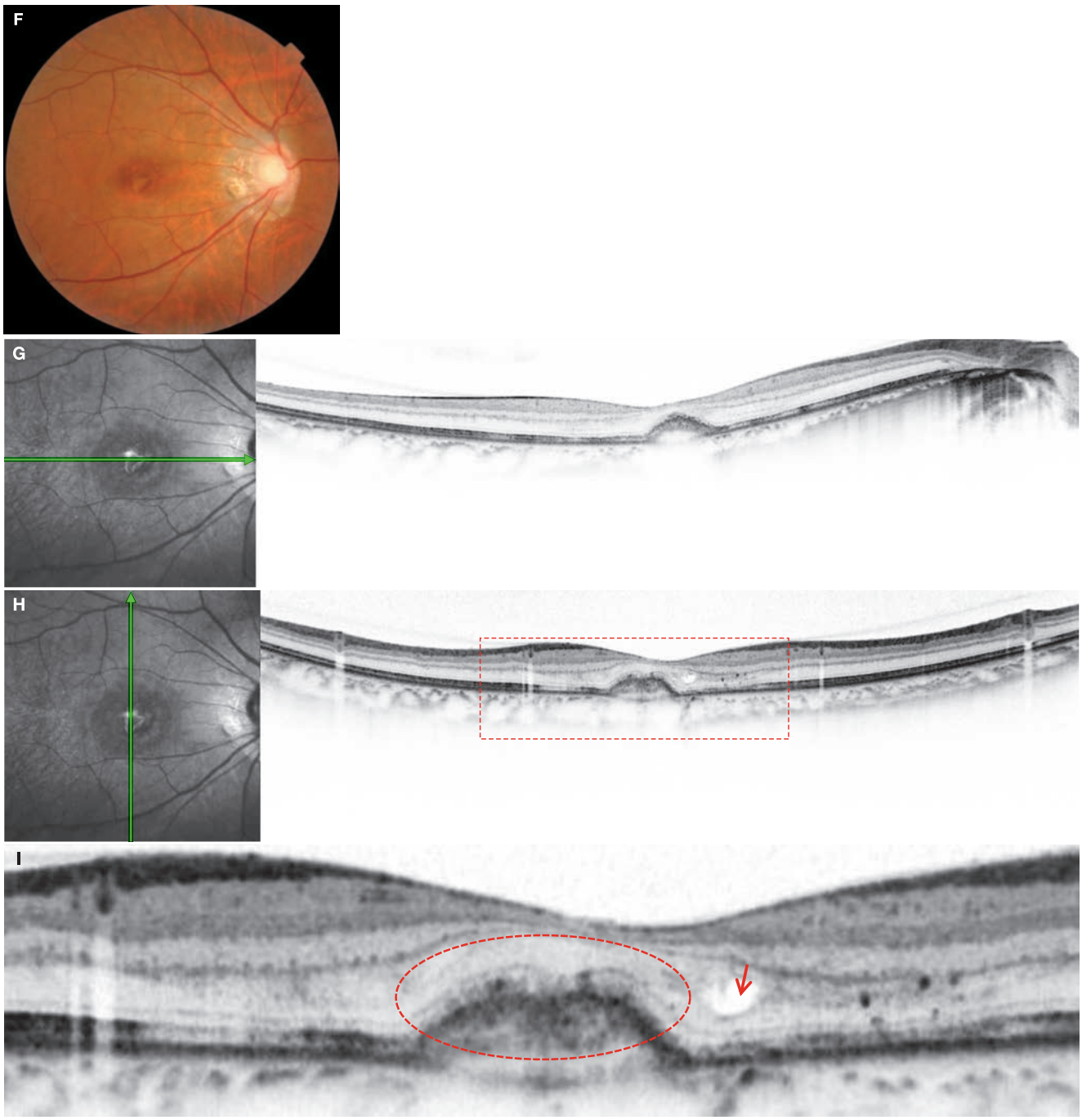

F: Color fundus photograph in the right eye: There is a scar forming beneath the fovea centralis. The hemorrhages has disappeared. **G:** IR + OCT horizontal scan of the right eye: A RPE protrusion is seen beneath the fovea centralis. No SRD can be seen. **H:** IR + OCT vertical scan of the right eye: Cystoid spaces are seen at the superior part of the fovea. **I:** Enlarged version of H [red dashed box]: A cystoid space (➔) is present in the Henle's fibrous layer of the outer plexiform layer. The ELM is seen almost entirely uninterrupted (red dashed circle). The IS/OS is difficult to distinguish. However, if closely observed, the irregular ELM and IS/OS lines can just barely be seen (red dashed circle). Infiltrating cells are scattered in the retina.

Image interpretation points

Vitreous injection of bevacizumab (Avastin®) was successful. The retinal structure is relatively well preserved and visual acuity has improved. The CNV has scarred enveloped by the RPE. The SRD has disappeared.

Case 125 Idiopathic choroidal neovascularization: The scarring process

A 38-year-old female, OD, BCVA 0.8, refraction –12.5D, axial length 27.65 mm

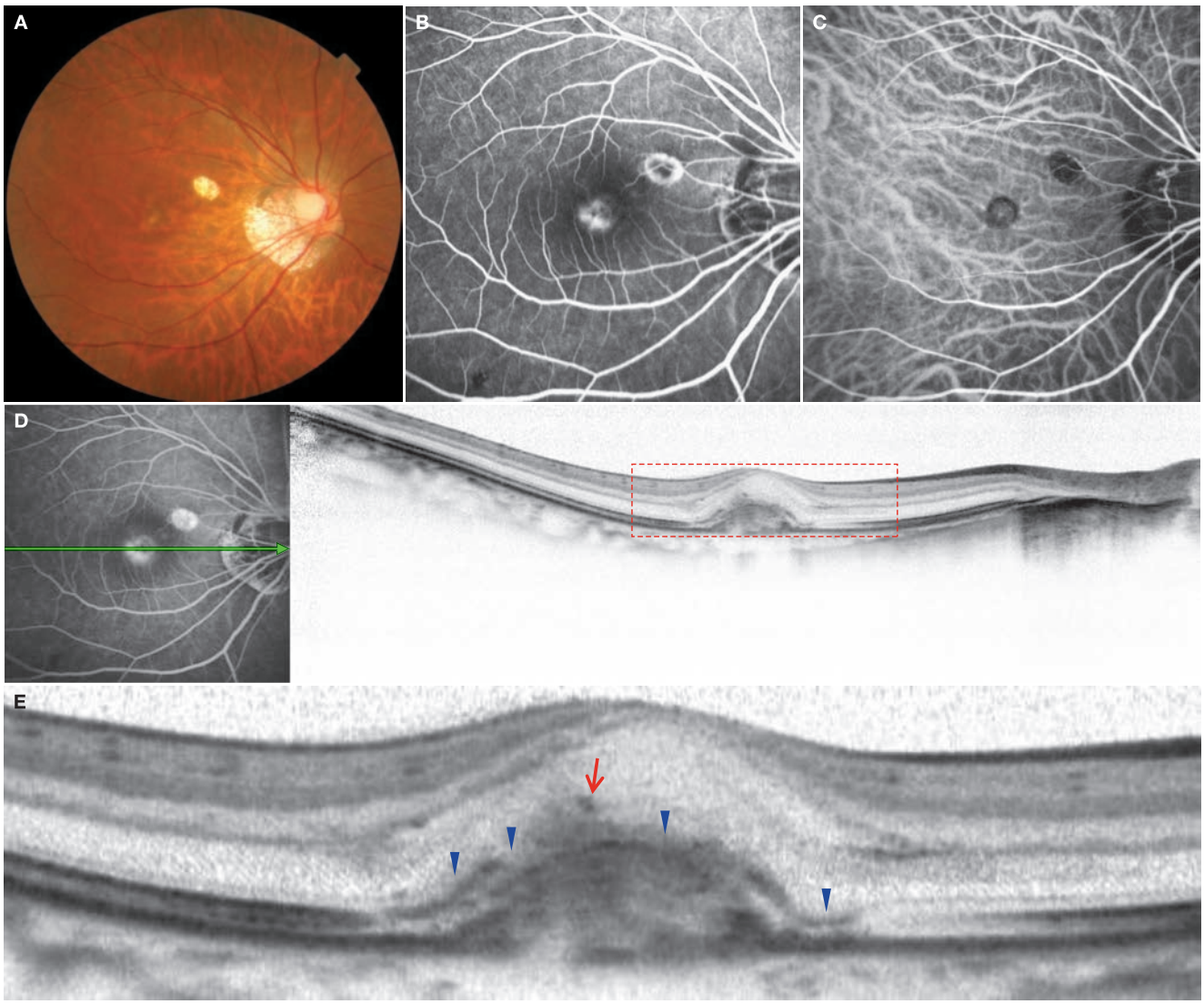

A: Color fundus photograph in the right eye: The optic disc is tilted. There is an atrophic lesion between the optic disc and fovea centralis. CNV probably occurred at this location in the past and spontaneously receded. Still active CNV can be seen beneath the fovea centralis. **B:** FA in the right eye (3 minutes, 2 seconds): Hyperfluorescence due to fluorescien leakage from CNV is seen with relatively indistinct border. The atrophic lesion is also exhibiting hyperfluorescence with distinct border. **C:** IA in the right eye (3 minutes, 2 seconds): A hypofluorescent ring is seen around the CNV. This may be due to the proliferative reaction of the RPE cells as seen in case 124. **D:** FA + OCT horizontal scan of the right eye: Type 2 CNV can be seen. Retinal changes are not pronounced. The SRD is essentially not seen. **E:** Enlarged version of D [red dashed box]: CNV growing past the RPE is seen. The line thought to be the IS/OS is somewhat traceable, but is partially indistinct (►). High reflectivity due to infiltrating cells can be seen in the retina (➔). (Continued on the next page)

Image interpretation points

There is a scar lesion superonasally outside the fovea centralis. It should be taken into consideration that this case might be accompanied by punctate inner choroidopathy. Although the CNV is still active, the RPE has already begun to envelope it.

Case 125 Course without treatment

A 38-year-old female, OD, BCVA 1.2, refraction –12.5D, axial length 27.65 mm

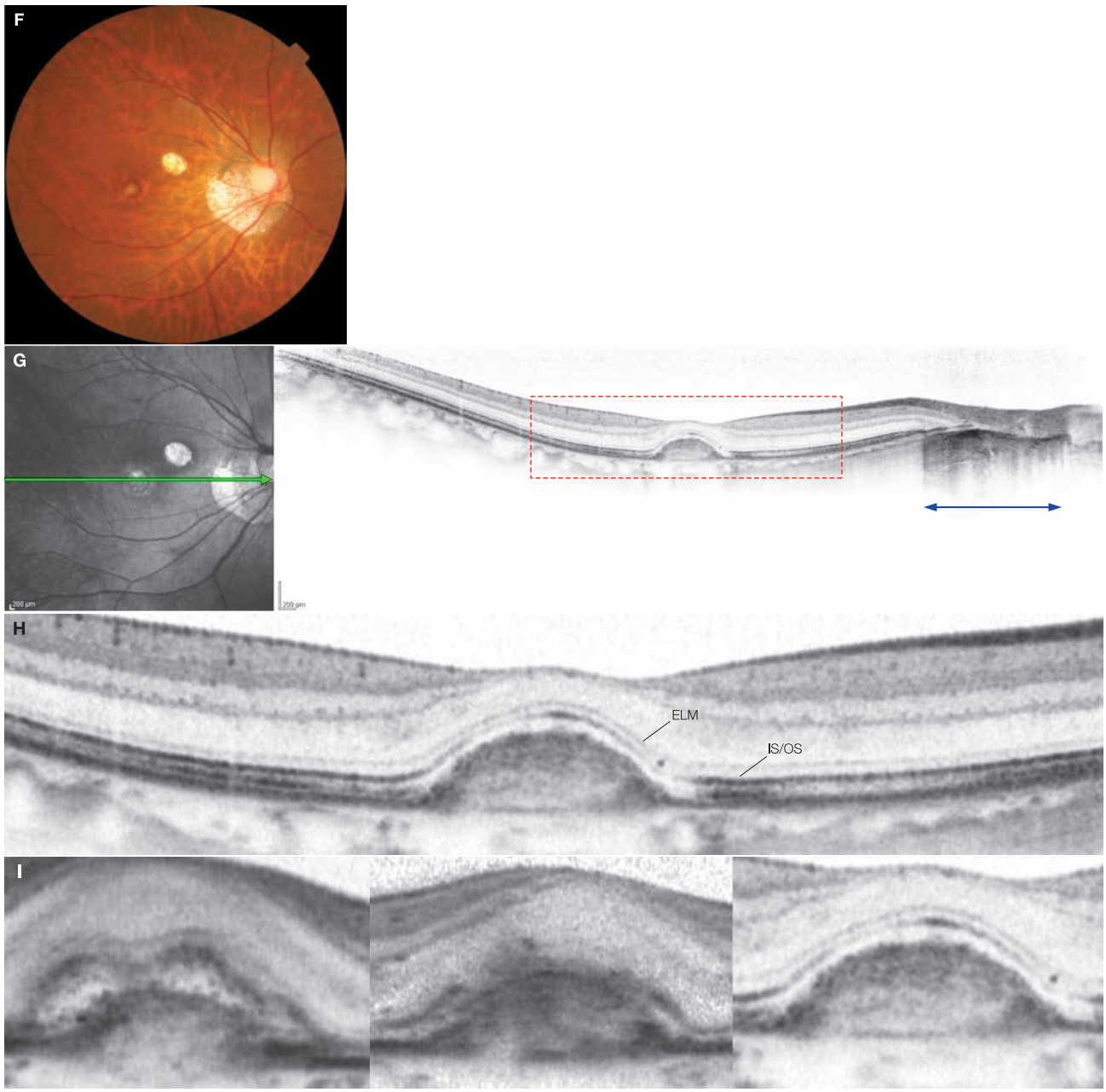

F: Color fundus photograph in the right eye: A small scar lesion is seen beneath the fovea centralis. **G:** IR + OCT horizontal scan of the right eye: A gently sloping RPE protrusion due to envelopment by RPE cells is seen beneath the fovea centralis. In the area of peripapillary atrophy (◄►), the reflectivity of the underlying sclera is enhanced by the excessive measurement beam penetration due to the RPE defects and choroidal atrophy. **H:** Enlarged version of G [red dashed box]: The proliferated RPE cells and scar tissue beneath the fovea centralis has similar reflectivity, making the RPE line indistinct. The structure of the outer retinal layers is preserved and the ELM line has been almost completely restored. The IS/OS line can also be mostly traced. **I:** Time-course of OCT horizontal scan images of the right eye: From the left, images of relatively fresh CNV, scarring in progress (at initial diagnosis), and scarring upon completion (1 year after initial diagnosis, enlarged version of H) are shown side-by-side.

Image interpretation points

Since the patient declined treatment, a follow up was performed without treatment for one year after intial diagnosis.

The scarring process of Type 2 CNV was observed and the natural progression of the disease can be appreciated.

Retinal degeneration

7.1 Multiple evanescent white dot syndrome – 232
References – 232

Case 126 Multiple evanescent white dot syndrome: A typical example – 233, 234

7.2 Acute zonal occult outer retinopathy – 235
References – 235

Case 127 Acute zonal occult outer retinopathy: Eye with a history of MEWDS – 236

7.3 Punctate inner choroidopathy – 238
References – 238

Case 128 Punctate inner choroidopathy: Atrophic pigmented scars – 239

Case 129 Punctate inner choroidopathy: Case complicated by CNV (fellow eye of case 128) – 240

Case 130 Punctate inner choroidopathy: Yellowish-white spots and CNV – 241

7.4 X-linked juvenile retinoschisis – 242
References – 242

Case 131 X-linked juvenile retinoschisis: Retinoschisis over a wide area – 243, 244

Case 132 X-Linked juvenile retinoschisis: Retinoschisis confined to the macula – 245

7.5 Stargardt disease – 246
References – 246

Case 133 Stargardt disease: A typical example – 247, 248

7.6 Vitelliform macular dystrophy and adult-onset foveomacular vitelliform dystrophy – 249
References – 250

Case 134 Adult-onset foveomacular vitelliform dystrophy: Vitelliform stage – 251

Case 135 Adult-onset foveomacular vitelliform dystrophy: Pseudohypopyon stage – 252

Case 136 Adult-onset foveomacular vitelliform dystrophy: The course – 253

7.7 Pseudoxanthoma elasticum – 254

References – 254

Case 137 Pseudoxanthoma elasticum: A case of Type 1 CNV – 255

Case 138 Pseudoxanthoma elasticum: A case of Type 2 CNV – 256

Case 139 Pseudoxanthoma elasticum: A case of polypoidal lesions – 257

Case 140 Pseudoxanthoma elasticum: Outer retinal tubulation – 258

7.8 Cancer-associated retinopathy – 259

References – 259

Case 141 Cancer-associated retinopathy: Damage to the outer retinal layers – 260

Case 142 Cancer-associated retinopathy: Retinal vasculitis – 261

7.9 Bietti crystalline dystrophy – 262

References – 262

Case 143 Bietti crystalline dystrophy: A typical example – 263

Case 144 Bietti crystalline dystrophy: Outer retinal tubulation – 264

7.10 Retinitis pigmentosa – 265

References – 266

Case 145 Retinitis pigmentosa: A typical example – 267, 268

Case 146 Retinitis pigmentosa: Cystoid macular edema – 269

Case 147 Retinitis pigmentosa: Vitreomacular traction syndrome – 270

7.11 Fundus albipunctatus – 271

References – 271

Case 148 Fundus albipunctatus: A typical example – 272

7.12 Oguchi disease – 274

References – 274

Case 149 Oguchi disease: A typical example – 275

Case 150 Oguchi disease: Cystoid space formation and golden sheen fundus reflex (fellow eye of case 149) – 276

7.1 Multiple evanescent white dot syndrome

Background

Multiple evanescent white dot syndrome (MEWDS) was first reported by Jampol in 1984.[1, 2] It typically affects young women, is unilateral, causes rapid visual decline, and sometimes results in complaints of visual field defects and photopsia. The pathogenesis is unclear, but precursory flu-like symptoms suggest a viral infection. Various grey-white to yellowish-white patches ranging from 100 to 200 µm in size frequently occur between the deep layers of the retina and RPE mainly in the posterior pole. In particular, yellow to orange granularity is visible in the fovea centralis. The fundus findings disappear in the early stage of the disease and are sometimes not visible during initial diagnosis. Hyperfluorescent dots that are described as »wreathlike« can be seen during the early phase on FA. Most of these hyperfluorescent dots are consistent with yellowish-white spots although they are not entirely identical. Fluorescein staining of these lesions can be seen in the late phase FA.[3–7] Distinctive hypofluorescent spots can be seen in the late phase on IA. These hypofluorescent spots can be observed with a biomicroscopy even when the white spots are indistinct.[3–7]

The symptoms of MEWDS and fundus findings spontaneously recede within approximately 1 to 3 months, and it is considered a disease with good visual prognosis. However, there are cases where visual acuity only recovers to 0.6–0.7 or recurs. These cases are thought to be an intermediate type of MEWDS and acute zonal occult outer retinopathy (AZOOR), which has a relatively poor prognosis. MEWDS is considered part of a wide disease concept known as AZOOR complex syndrome.[8–10]

OCT findings

The IS/OS line focally disappears in the acute phase and is known to recover in the recovery phase.[11–14] This IS/OS defect area is reportedly consistent with white dots or hypofluorescent spots on IA,[11] but this consistency is only during the acute phase.[14] In the acute phase, moderately reflective lesions extending from the RPE to the outer nuclear layer via the disrupted IS/OS level, consistent with the disrupted part of the IS/OS, can be observed (the IS/OS line defects and hypofluorescent spots on IA are consistent during this phase).[13, 14] These moderately reflective lesions take on an impressive columnar or patchy form particularly in the fovea centralis. The IS/OS line eventually disappears over a wide area, and the moderately reflective lesions becomes smaller and concurrently increases in number. These moderately reflective lesions at the later phase are still consistent with hypofluorescent spots on IA.[14] The moderately reflective lesions eventually disappear, and the IS/OS line is restored to almost normal over the course of 1 to 3 months, but irregularities occasionally remain.

References

1) Jampol LM, Sieving PA, Pugh D, et al. Multiple evanescent white dot syndrome. I. Clinical findings. *Arch Ophthalmol*. 1984; 102:671–674.
2) Sieving PA, Fishman GA, Jampol LM, et al. Multiple evanescent white dot syndrome. II. Electrophysiology of the photoreceptors during retinal pigment epithelial disease. *Arch Ophthalmol*. 1984; 102:675–679.
3) Ikeda N, Ikeda T, Nagata M, et al. Location of lesions in multiple evanescent white dot syndrome and the cause of the hypofluorescent spots observed by indocyanine green angiography. *Graefes Arch Clin Exp Ophthalmol*. 2001; 239:242–247.
4) Ie D, Glaser BM, Murphy RP, Gordon LW, et al. Indocyanine green angiography in multiple evanescent white-dot syndrome. *Am J Ophthalmol*. 1994; 117:7–12.
5) Obana A, Kusumi M, Miki T. Indocyanine green angiographic aspects of multiple evanescent white dot syndrome. *Retina*. 1996; 16:97–104.
6) Barile GR, Reppucci VS, Schiff WM, et al. Circumpapillary chorioretinopathy in multiple evanescent white-dot syndrome. *Retina*. 1997; 17:75–77.
7) Gross NE, Yannuzzi LA, Freund KB, et al. Multiple evanescent white dot syndrome. *Arch Ophthalmol*. 2006; 124:493–500.
8) Spaide RF, Koizumi H, Freund KB. Photoreceptor outer segment abnormalities as a cause of blind spot enlargement in acute zonal occult outer retinopathy-complex diseases. *Am J Ophthalmol*. 2008; 146:111–120.
9) Bryan RG, Freund KB, Yannuzzi LA, et al. Multiple evanescent white dot syndrome in patients with multifocal choroiditis. *Retina*. 2002; 22:317–322.
10) Fine HF, Spaide RF, Ryan EH Jr, et al. Acute zonal occult outer retinopathy in patients with multiple evanescent white dot syndrome. *Arch Ophthalmol*. 2009; 127:66–70.
11) Nguyen MH, Witkin AJ, Reichel E, et al. Microstructural abnormalities in MEWDS demonstrated by ultrahigh resolution optical coherence tomography. Retina. 2007; 27:414–418.
12) Sikorski BL, Wojtkowski M, Kaluzny JJ, et al. Correlation of spectral optical coherence tomography with fluorescein and indocyanine green angiography in multiple evanescent white dot syndrome. *Br J Ophthalmol*. 2008; 92:1552–1557.
13) Li D, Kishi S. Restored photoreceptor outer segment damage in multiple evanescent white dot syndrome. *Ophthalmology*. 2009; 116:762–770.
14) Hangai M, Fujimoto M, Yoshimura N. Features and function of multiple evanescent white dot syndrome. *Arch Ophthalmol*. 2009; 127:1307–1313.

Case 126 Multiple evanescent white dot syndrome: A typical example

A 35-year-old female, OS, BCVA 1.5

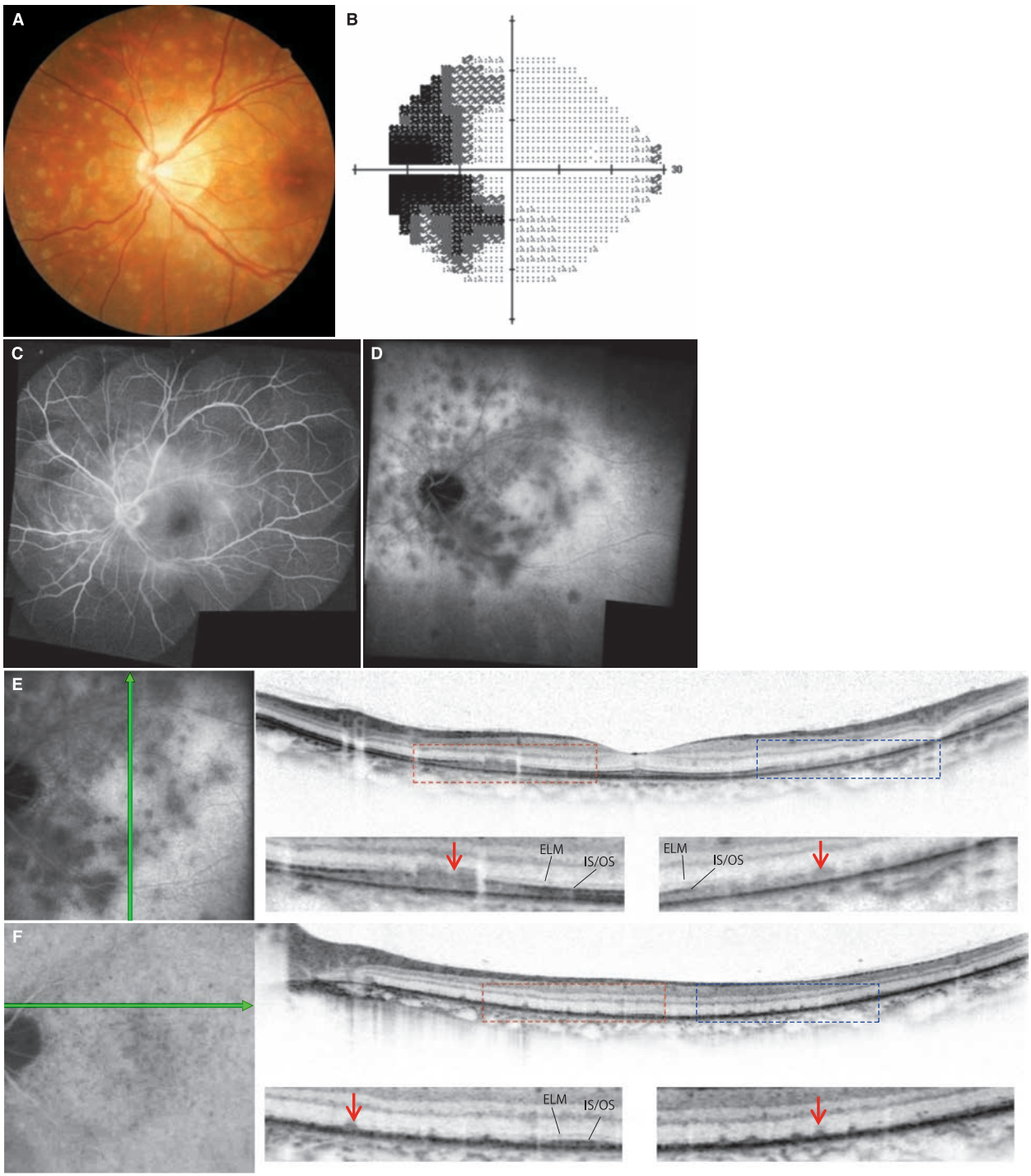

A: Color fundus photograph in the left eye: At initial diagnosis. Multiple grey-white or yellowish-white spots of various sizes are visible around the optic disc. The large spots are annular and hollow in the middle. **B:** Static automated perimetry in the left eye: At initial diagnosis. Enlargement of Mariotte's blind spot is significant. **C:** FA montage of the left eye (7 minutes): At initial diagnosis. The white spots exhibit hyperfluorescence. **D:** IA montage of the left eye (15 minutes): At initial diagnosis. The white spots become distinct hypofluorescent spots in the IA late stage. Weak hypofluorescence is evident around the optic disc and arcade vessels. **E:** IA + OCT horizontal scan of the left eye + enlarged version [red and blue dashed box]: At initial diagnosis. Moderately reflective lesions (➔) consistent with hypofluorescent spots on IA are seen to extend from the RPE to the outer nuclear layer. **F:** IA + OCT vertical scan of the left eye + enlarged version [red and blue dashed box]: Two weeks after initial diagnosis. Best-corrected visual acuity declined to 0.7. The hyporeflective spots on IA has decreased in size and increased in number. (➔). Small moderately reflective lesions on OCT corresponds with these hyporeflective spots on IA, and has decreased in height and width. The IS/OS line in the the area with these findings is missing.

(Continued on the next page)

Case 126 Continuation

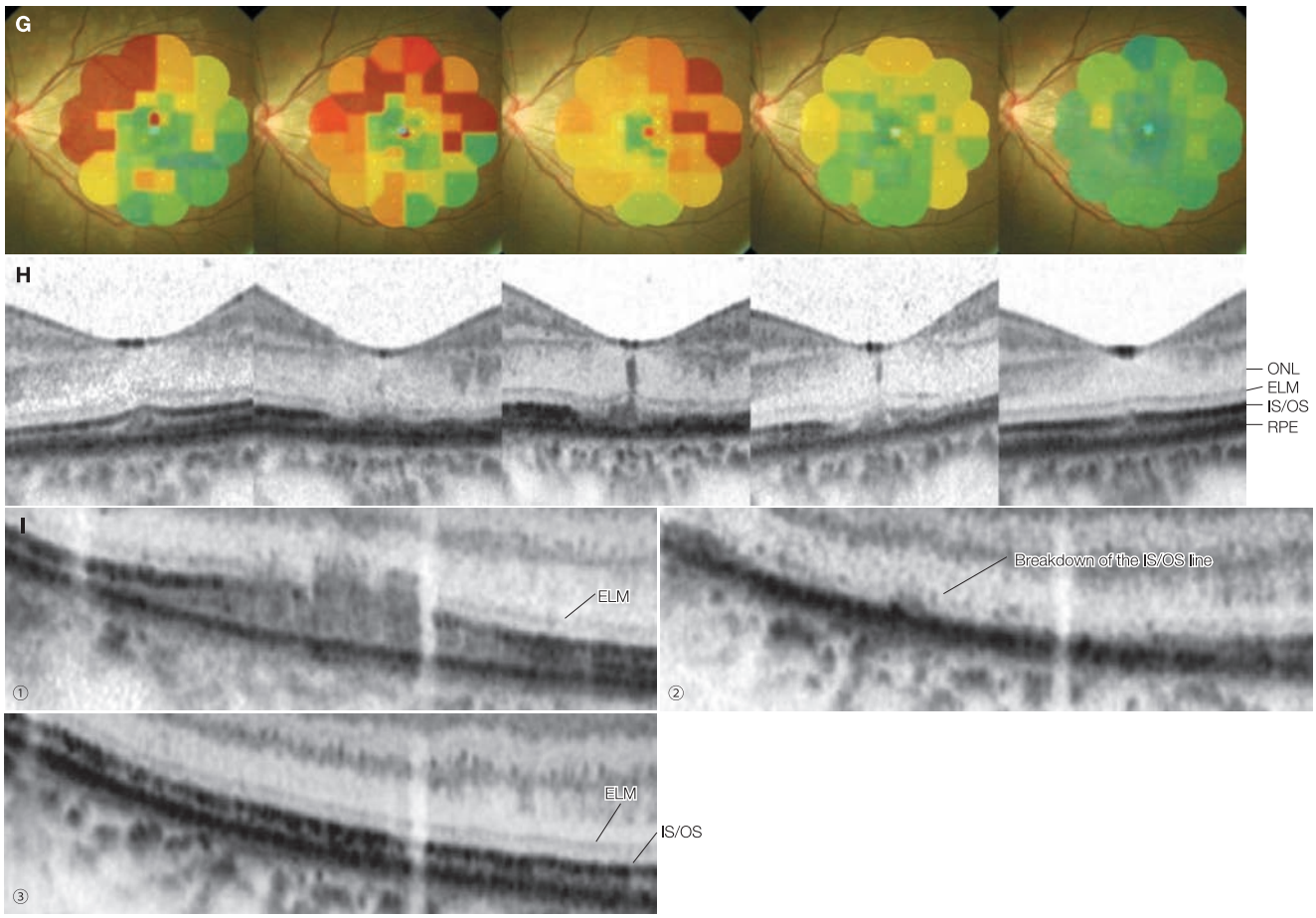

G: Microperimetry-1 (MP-1) of the left eye: Temporal changes are shown. From the left, the number of days from initial visit (best-corrected visual acuity) is: initial visit (1.5), 4 days (0.5), 13 days (0.5), 20 days (0.7), and 34 days (1.2). Scotomas appear to be shifting from the nasal side to the temporal side.
H: Enlarged version of the OCT horizontal scan of the fovea centralis in the left eye: Figures are arranged corresponding to the MP-1 results in the time after initial visit. The IS/OS of the fovea centralis disappeared, and the columnar moderate reflectivity extending from the RPE to the outer nuclear layer at the foveola has appeared and then disappeared, after which the IS/OS has restored. Retinal sensitivity decrease on MP-1 seems to correspond to these OCT findings. **I:** Enlarged version of the OCT vertical scan of the extrafoveal region in the left eye: Images ① at initial diagnosis, ② 4 days later, and ③ 34 days later. The moderately reflective lesions in the inferior macula became smaller, and eventually disappeared. The IS/OS line is almost completely restored. (Modified according to Hangai M, et al. Features and functions of multiple evanescent white dot syndrome *Arch Ophthalmol*. 2009; 127: 1307–1313)

Image interpretation points

This is a typical case of MEWDS. The patient consulted us 4 days after becoming aware of visual field defects in her right eye. Enlargement of Mariotte's blind spot was observed at initial diagnosis, but there was no visual acuity impairment. After 4 days, best-corrected visual acuity had declined to 0.5, but it spontaneously improved to 1.2 after 34 days. Irregularity and disruption of the foveal IS/OS line corresponding to the visual acuity decline were noted, followed by the development of a columnar, moderately reflective lesions spreading from the RPE to all foveal layers. These abnormal findings disappeared together with visual acuity improvement about one month after initial diagnosis. During initial diagnosis, a severe decline in retinal sensitivity was mainly observed in the vicinity of the optic disc on the MP-1, but this gradually shifted to the temporal side and had almost resolved about one month later. On OCT, moderately reflective lesions spreading from the RPE to the outer nuclear layer and disruption of the surrounding IS/OS line, could be seen in the region corresponding to that of the decreased retinal sensitivity. During the disease course, a decrease in size of moderately reflective findings and enlargement of the disrupted IS/OS line were observed. Eventually, the IS/OS line was restored associated with improvement of retinal sensitivity. The moderately reflective lesions at the photoreceptor level were consistent with hypofluorescent spots on IA and were considered distinctive MEWDS findings.

7.2 Acute zonal occult outer retinopathy

Background

Acute zonal occult outer retinopathy (AZOOR) is a disease first reported by Gass in 1994.[1] It typically affects one or both eyes of young women with moderate to high myopia, no clear abnormalities are exhibited on ophthalmoscopy or fluorescein fundus angiography, and patients become aware of rapid visual acuity decline, visual field defects, and photopsia. Visual acuity is preserved at 0.5 or above in roughly 70% of cases, but AZOOR can cause severer visual impairment in rare cases.[2] Central scotomas are common visual field defects.

Differences from MEWDS include no clear abnormalities on biomicroscopy or fluorescein fundus angiography, visual impairment recovering only about 1/4, and visual field defects being hard to cure. Narrowing of retinitis pigmentosa-like retinal blood vessels and RPE depigmentation spots can be seen in some cases. Diseases where the clinical symptoms overlap include AZOOR, MEWDS, acute idiopathic blind spot enlargement, punctate inner choroidopathy (PIC), and multifocal choroiditis and panuveitis. These diseases are thought to belong in the same broader category and are known as the »AZOOR complex diseases«.[3, 4] In addition, AZOOR can occur in eyes affected by MEWDS.[5] Photoreceptor abnormalities can be identified on multifocal ERG and OCT tests even in cases where there are no biomicroscopic abnormalities in the fundus, and the diagnostic value of conducted comparisons of abnormalities in these tests is high. There is also diagnostic value to the lateral difference in ERG.

OCT findings

The characteristics of AZOOR are IS/OS line defects or indistinctiveness on OCT despite normal appearance with a biomicroscopy.[4, 6–9] The areas of IS/OS line abnormalities have distinct margins and are comparable with visual field defect areas and decreased response areas of multifocal ERG. Moderately reflective spots seen in MEWDS or other abnormal features suggestive of inflammatory responses are not evident in AZOOR. As the disease progresses, the outer segment is damaged, the outer nuclear layer thins, and the retinal layer structure becomes irregular. IS/OS abnormalities heal to a certain extent, but do not completely heal as in MEWDS, so it is common for irreversible damage such as outer nuclear layer thinning to remain.

References

1) Gass JD. Acute zonal occult outer retinopathy. Donders Lecture: The Netherlands Ophthalmological Society, Maastricht, Holland, June 19, 1992. *J Clin Neuroophthalmol*. 1993; 13:79–97.
2) Gass JD, Agarwal A, Scott IU. Acute zonal occult outer retinopathy: a long-term follow-up study. *Am J Ophthalmol*. 2002; 134:329–339.
3) Gass JD. Are acute zonal occult outer retinopathy and the white spot syndromes (AZOOR complex) specific autoimmune diseases? *Am J Ophthalmol*. 2003; 135:380–381.
4) Spaide RF, Koizumi H, Freund KB. Photoreceptor outer segment abnormalities as a cause of blind spot enlargement in acute zonal occult outer retinopathy-complex diseases. *Am J Ophthalmol*. 2008; 146:111–120.
5) Fine HF, Spaide RF, Ryan EH Jr, Matsumoto Y, Yannuzzi LA. Acute zonal occult outer retinopathy in patients with multiple evanescent white dot syndrome. *Arch Ophthalmol*. 2009; 127:66–70.
6) Li D, Kishi S. Loss of photoreceptor outer segment in acute zonal occult outer retinopathy. *Arch Ophthalmol*. 2007; 125:1194–1200.
7) Zibrandtsen N, Munch IC, Klemp K, Jørgensen TM, Sander B, Larsen M. Photoreceptor atrophy in acute zonal occult outer retinopathy. *Acta Ophthalmol*. 2008; 86:913–916.
8) Takai Y, Ishiko S, Kagokawa H, Fukui K, Takahashi A, Yoshida A. Morphological study of acute zonal occult outer retinopathy (AZOOR) by multiplanar optical coherence tomography. *Acta Ophthalmol*. 2009; 87:408–418.
9) Fujiwara T, Imamura Y, Giovinazzo VJ, Spaide RF. Fundus autofluorescence and optical coherence tomographic findings in acute zonal occult outer retinopathy. *Retina*. 2010; 30:1206–1216.

Case 127 Acute zonal occult outer retinopathy: Eye with a history of MEWDS

A 45-year-old female, OD, BCVA 0.08, refraction -11.5 D, axial length 27.43 mm

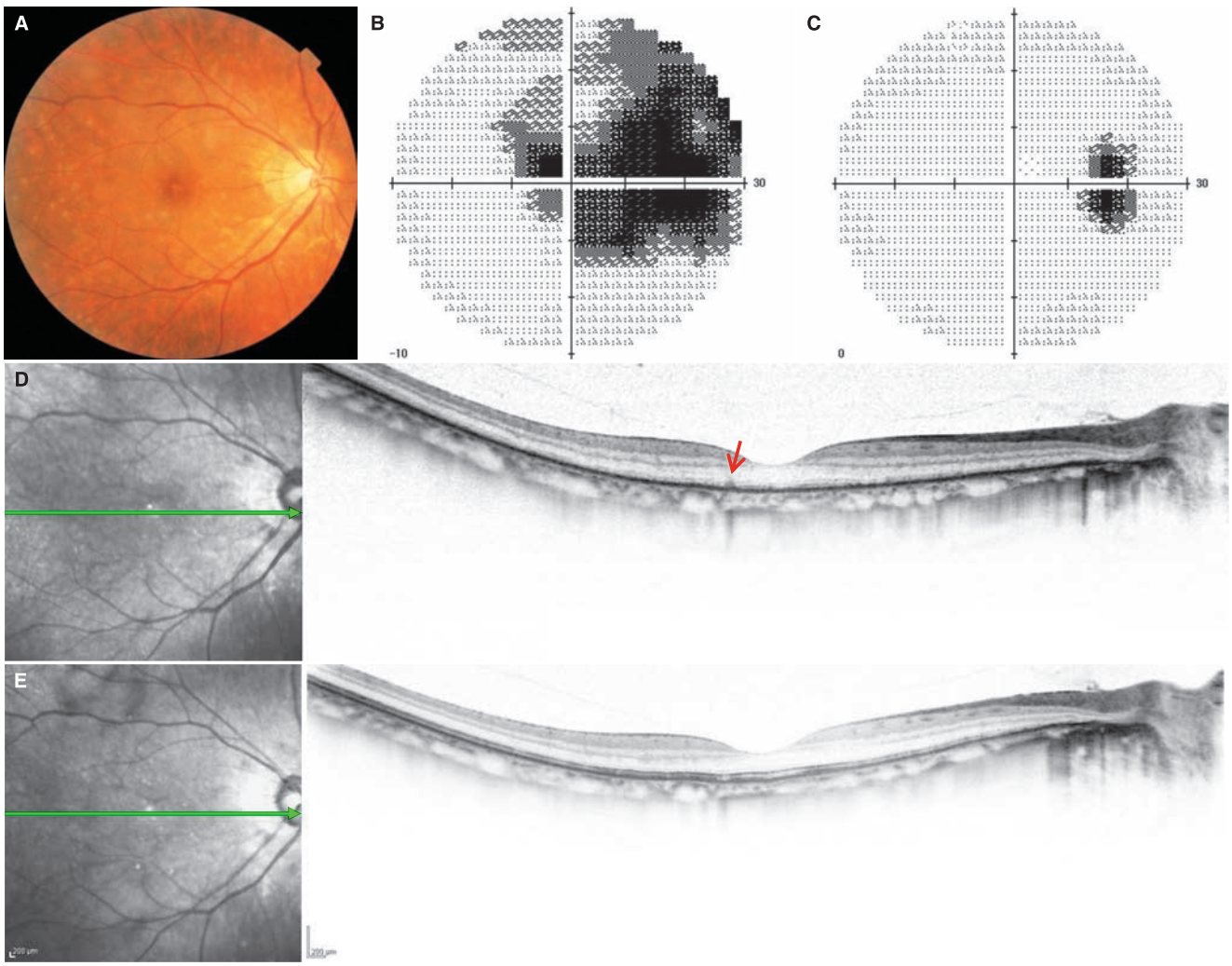

A: Color fundus photograph in the right eye: At initial diagnosis. Relatively large, uniform white spots can be seen. **B:** Static automated perimetry in the right eye: At initial diagnosis. A central scotoma and enlargement of Mariotte's blind spot is evident. **C:** Static automated perimetry in the right eye: After 5 months. Best-corrected visual acuity has improved to 0.6. A central scotoma and enlargement of Mariotte's blind spot has improved. **D:** FA + OCT horizontal scan of right eye: Two weeks after initial diagnosis. Best-corrected visual acuity is 0.3. Decreased, defective or irregular IS/OS line is seen over the entire posterior pole. Moderately reflective lesions can be seen from the RPE to the outer nuclear layer (→). **E:** IA + OCT horizontal scan of the right eye: Five months after initial diagnosis. The IS/OS line has almost been restored to normal. The COST line remains partially defective.

(Continued on the next page)

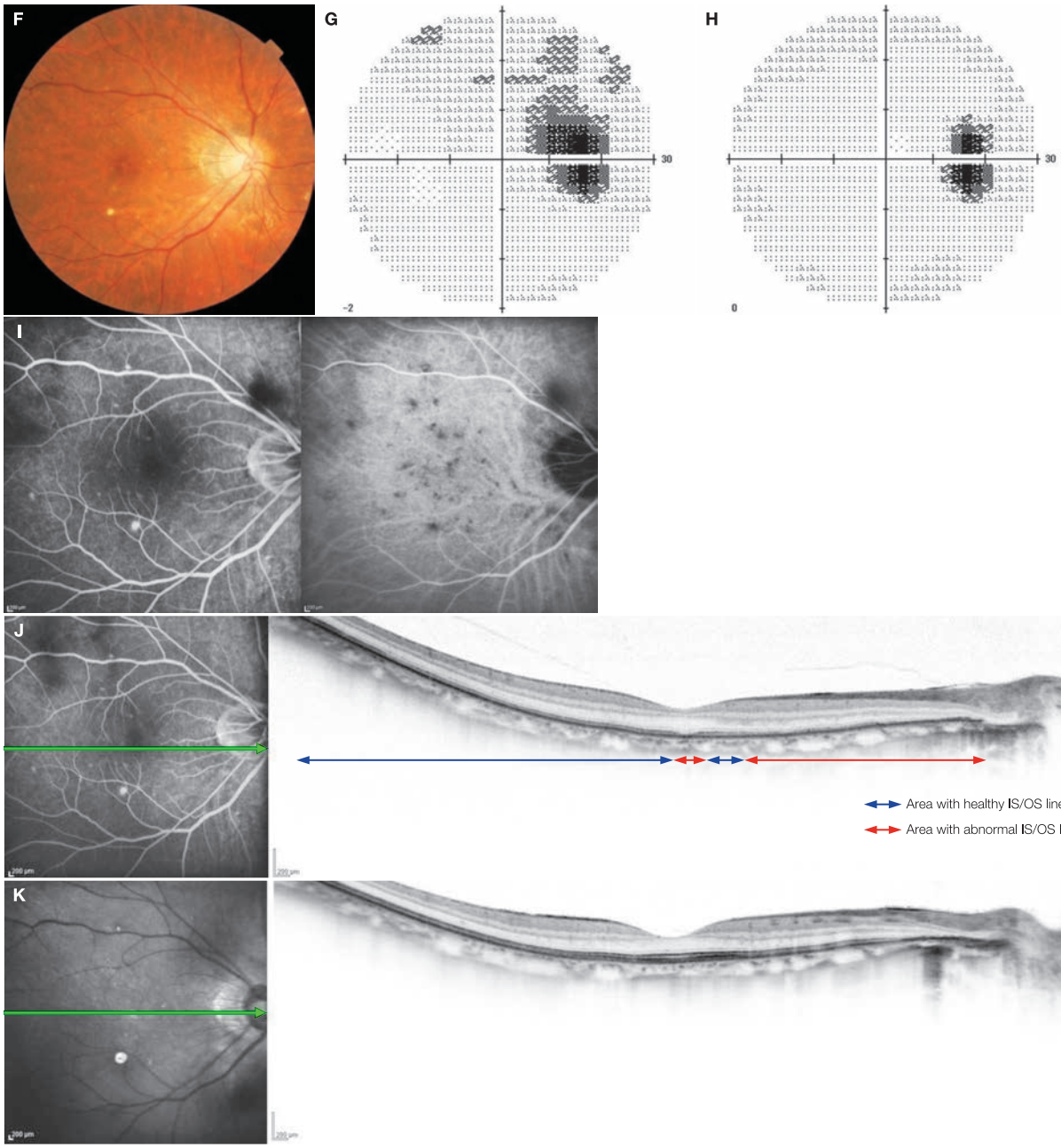

F: Color fundus photograph: Nine months after initial diagnosis. Depigmentation of the RPE is visible in the macula and around the optic disc. **G:** Static automated perimetry in the right eye: Nine months after initial diagnosis. Best-corrected visual acuity has decreased to 0.4. Enlargement of Mariotte's blind spot can once again be seen, but central scotomas are not apparent. **H:** Static automated perimetry in the right eye: 20 months after initial diagnosis. Best-corrected visual acuity has improved to 0.7. Enlargement of Mariotte's blind spot has improved. **I:** FA + IA in the right eye (13 minutes): Nine months after initial diagnosis. Multiple IA hypofluorescent spots containing FA hyperfluorescence consistent with RPE depigmentation spots are depicted. **J:** FA + OCT horizontal scan of the right eye: Nine months after initial diagnosis. IS/OS line irregularity can be seen from the optic disc to the parafovea and at the fovea centralis. **K:** FA + OCT horizontal scan of the right eye: 20 months after initial diagnosis. The IS/OS line has almost recovered.

Image interpretation points

This patient became aware of visual field defects one week prior to their initial consultation. The patient was diagnosed with MEWDS after visual field and visual acuity spontaneously improved approximately 2 months later based on fundus findings, visual field testing, and OCT findings. Nine months after initial diagnosis, enlargement of Mariotte's blind spot and visual acuity decline occurred once again. RPE depigmentation spots as seen in punctate inner choroidopathy (PIC) were seen, and abnormal reflectivity of the IS/OS line around the optic disc corresponding to the visual field abnormality was detected. The patient was diagnosed with AZOOR. This is a case where the pathologies of MEWDS, AZOOR and possibly PIC are considered to overlap.

7.3 Punctate inner choroidopathy

Background

Punctate inner choroidopathy (PIC) typically affects both eyes of women with moderate myopia. Patients become aware of blurred vision, photopsia, and scotomas. A the early phase, multiple yellowish-white lesions are observed in the posterior pole. As the condition regresses, these lesions change to characteristic atrophic pigmented scars .[1–4] Those with similar lesions in a wider area than posterior pole accompanied by uveitis are known as multifocal choroiditis and panuveitis (MCP) and is believed to be part of the same disease spectrum.[5,6] Atrophic pigmented scars are similar to the lesions of ocular toxoplasmosis (POHS). Viral infection and autoimmunity are suspected to be involved in the onset although the details are unclear. Inflammation at the photoreceptor cell, RPE, and choroidal levels appears to be involved in the disease process.

On FA, the yellowish-white lesions are hyperfluorescent and become hypofluorescent after pigmented scarring, but hyperfluorescence or faint leakage can be seen in the hypofluorescent margins. On IA, the both yellowish-white lesions and atrophic pigmented scars exhibit hypofluorescence. This is thought to be due to a blockage by inflamed lesions or filling defects on the choroidal level. Normal visual acuity is maintained in half of the cases. CNV develops subsequently in 40% of cases, which is the primary cause of poor visual prognosis.[7]

OCT findings

RPE atrophy and increased choroidal reflectivity due to excessive measurement beam penetration, undulating irregularities of the IS/OS line, and thinning of the outer nuclear layer are observed consistent with early stage, yellowish-white lesions. Consistent with atrophic pigmented scars, RPE defects or irregularities and even severer thinning of the outer retinal layers can be seen; and the atrophic lesions of the outer retinal layers exhibit characteristic features, as if the outer retina is being drawn into the RPE defect. The disruption of Bruch‹s membrane is sometimes detected, and severe retraction of the retina into the disrupted site is noticeable. This is probably due to severe localized and rapid atrophy in the outer retinal layers. Increased choroidal reflectivity and posterior bending of Bruch's membrane can sometimes be seen. CNV secondary to PIC is essentially Type 2, but multiple CNV lesions can sometimes be observed.

References

1) Watzke RC, Packer AJ, Folk JC, et al. Punctate inner choroidopathy. *Am J Ophthalmol*. 1984; 98:572–584.
2) Amer R, Lois N. Punctate inner choroidopathy. *Surv Ophthalmol*. 2011; 56:36–53.
3) Patel KH, Birnbaum AD, Tessler HH, et al. Presentation and outcome of patients with punctate inner choroidopathy at a tertiary referral center. *Retina*. 2011; 31:1387–1391.
4) Essex RW, Wong J, Fraser-Bell S, et al. Punctate inner choroidopathy: clinical features and outcomes. *Arch Ophthalmol*. 2010; 128:982–987.
5) Archer DB, Maguire CJ. Multifocal choroiditis. *Trans Ophthalmol Soc U K*. 1975; 95:184–191.
6) Watzke RC, Claussen RW. The long-term course of multifocal choroiditis (presumed ocular histoplasmosis) . *Am J Ophthalmol*. 1981; 91:750–760.
7) Amer R, Lois N. Punctate inner choroidopathy. *Surv Ophthalmol*. 2011; 56:36–53.

Case 128 Punctate inner choroidopathy: Atrophic pigmented scars

A 31-year-old female, OS, BCVA 1.5, refraction -5.0 D

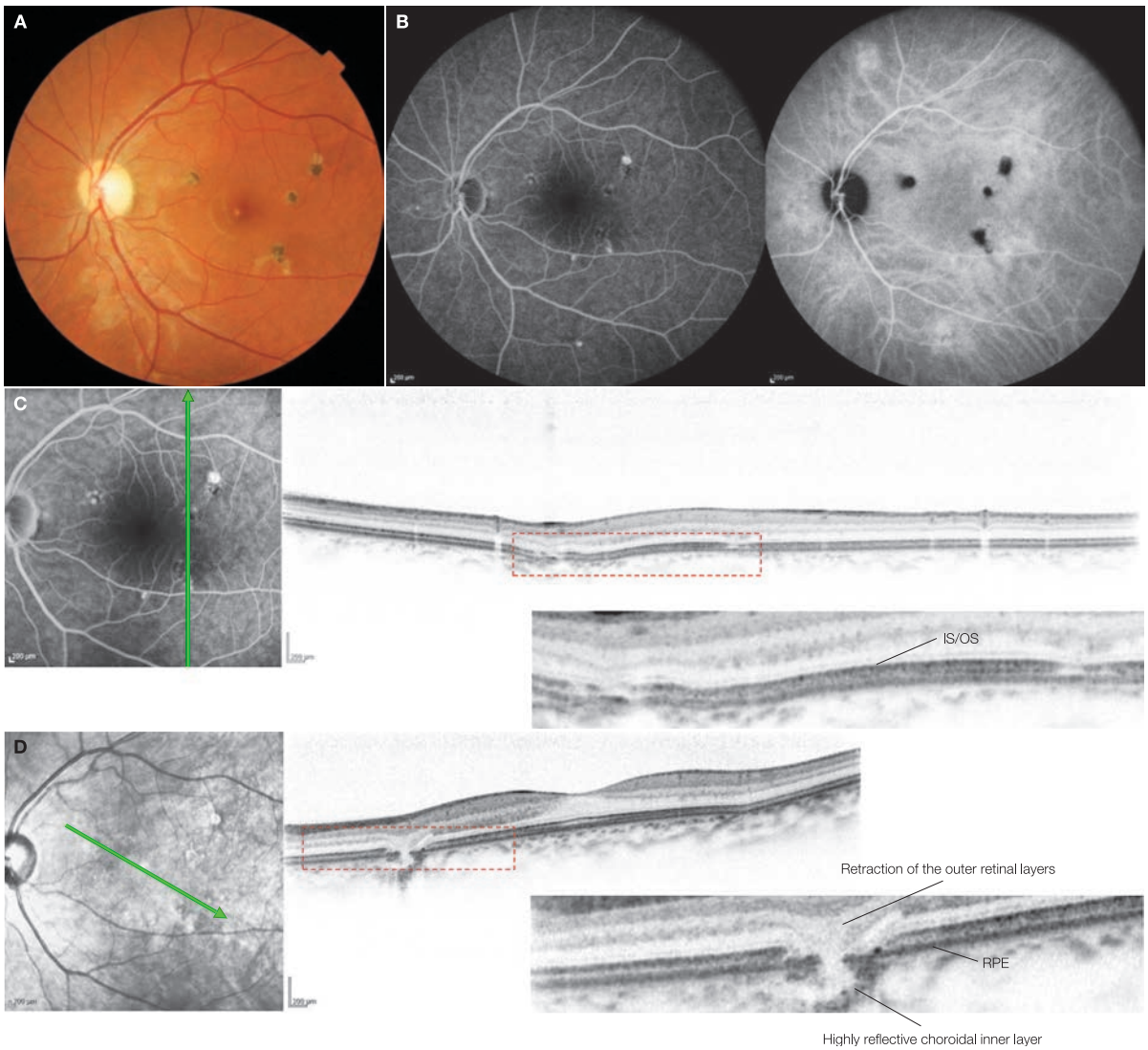

A: Color fundus photograph in the left eye: Yellowish-white spots and adjacent atrophic pigmented scars are depicted in 4 locations in the peripheral macula. **B:** FA + IA in the left eye (9 minutes): The yellowish-white spots are hyperfluorescent, and atrophic pigmented scars hypofluorescent on FA. Both are hypofluorescent on IA. **C:** FA + OCT vertical scan of the left eye + enlarged version [red dashed box]: RPE and IS/OS irregularities consistent with yellowish-white spots and atrophic pigmented scars are visible. **D:** IR + OCT oblique scan of the left eye + enlarged version [red dashed box]: A disruption in Bruch's membrane is consistent with the atrophic pigmented scar, and significant atrophy of the outer retinal layers that is being retracted into that disruption can be seen. Increased reflectivity is noted in the inner layers of the choroid in the vicinity of the RPE and Bruch's membrane disruption. This is different from the increased reflectivity as a result of excessive measurement beam penetration due to RPE atrophy because the high reflectivity is limited to a certain axial level. There are no foveal abnormalities.

Image interpretation points

The patient became aware of metamorphopsia in her right eye two weeks before visiting their local doctor. She was diagnosed with ocular toxoplasmosis and administered acetylspiramycin, but her condition did not improve so they were referred to us. Hemorrhages due to CNV and a serous retinal detachment were observed in the yellowish-white spot area of the right eye (case 129). The yellowish-white spots as an early lesion and atrophic pigmented scars were both present in the left eye (this case).

Both lesions exhibits hyperfluorescence and hypofluorescence, respectively, on FA, whereas both are hypofluorescent on IA. The latter was thought to be due to a blockage of as a result of inflamed lesions or a filling defect on the choroidal level. A break-down of the outer retinal layers could be seen involving the choroid and RPE, consistent with the yellowish-white spots and atrophic pigmented scars.

Case 129 Punctate inner choroidopathy: Case complicated by CNV (fellow eye of case 128)

A 31-year-old female, OD, BCVA 0.4, refraction -6.0 D

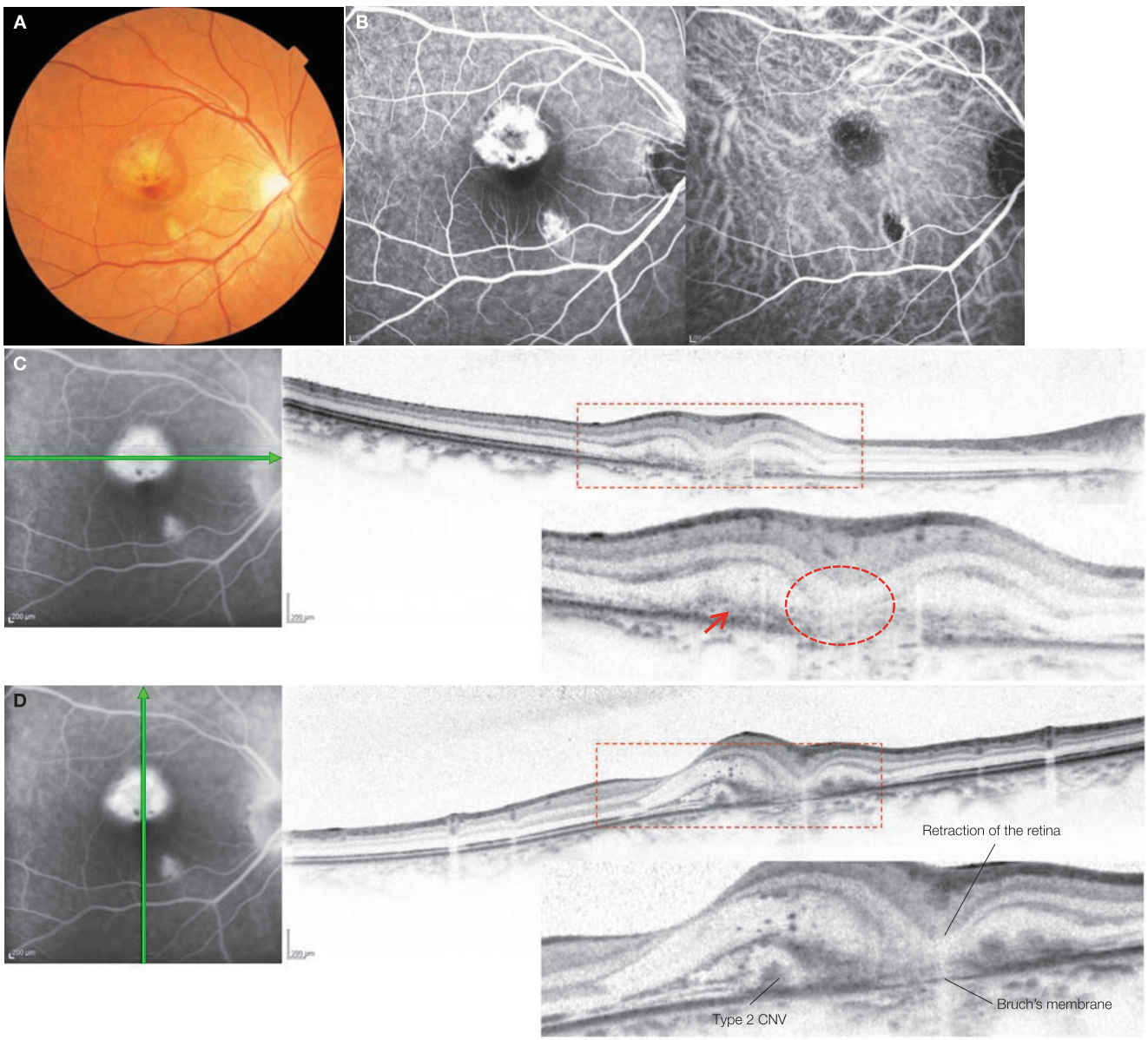

A: Color fundus photograph in the right eye: A greyish-white fibrin over the CNV lesion and accompanying retinal hemorrhages are exhibited slightly superior to the fovea centralis. A small fresh lesion is visible inferior to the fovea centralis. **B:** FA + IA in the right eye (1 minute, 20 seconds): Significant leakage can be seen from the CNV on FA, indicating classic CNV. **C:** FA + OCT horizontal scan on the right eye + enlarged version [red dashed box]: Bruch's membrane consistent with the yellowish-white spot is indistinct and prominent retraction of the retina is noted (red dashed circle). The RPE line protrusion is barely visible, indicating Type 2 CNV (→). **D:** FA + OCT vertical scan of the right eye + enlarged version [red dashed box]: Type 2 CNV is depicted in the parafovea, and RPE elevation and retinal retraction is noticeable in the area consistent with the yellowish-white spots immediately superior to the parafovea.

Image interpretation points

This case is considered early PIC without atrophic pigmented scar lesions. Type 2 CNV is occurring in the parafovea, which is the cause of visual acuity decline. Retinal retraction (rapid and localized atrophy of the outer retinal layers) can be seen in the yellowish-white spots on OCT. Highly reflective intraretinal deposits can also be seen. The yellowish-white spots have scarred 3 months after initial diagnosis. The presence of hyperfluorescent, yellowish-white spots on FA, which are hypofluorescent on IA, in both eyes and atrophic pigmented scars in the fellow eye suggest a diagnosis of PIC. The distinctive retinal retraction on OCT is also helpful.

Case 130 Punctate inner choroidopathy: Yellowish-white spots and CNV

A 26-year-old female, OD and OS, BCVA 1.5 and 0.9, respectively, right refraction -0.25 D and left refraction -1.25 D

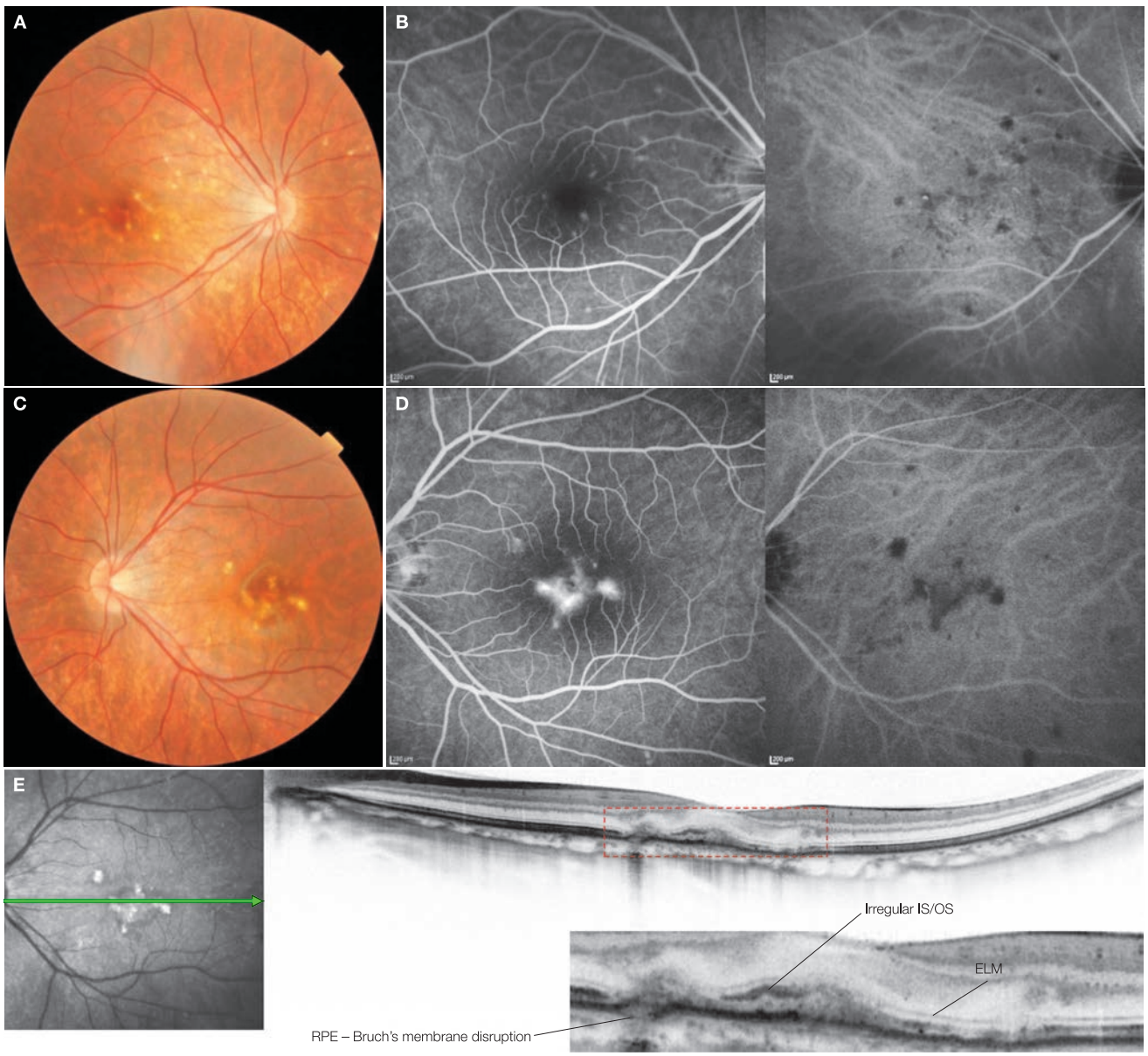

A: Right eye fundus photograph: Multiple small, yellowish-white spots can be seen in the macula and the retina nasal to the optic disc. **B:** FA + IA in the right eye (11 minutes): The yellowish-white spots are hyperfluorescent on FA and hypofluorescent on IA. **C:** Color fundus photograph in the left eye: Several small, yellowish-white spots are observed in the macula. **D:** FA + IA in the left eye (10 minutes): Fluorescein leakage is seen in the yellowish-white spots around the fovea centralis. The yellowish-white spots exhibit hypofluorescence on IA, and hypofluorescence can also be seen in the areas without evident yellowish-white spots. **E:** IR + OCT horizontal scan of left eye + enlarged version [red dashed box]: A disruption is visible in Bruch's membrane. RPE irregularity, unique IS/OS irregularities, and moderate reflectivity in front of the RPE are exhibited.

Image interpretation points

The patient had become aware of metamorphopsia in their left eye 5 months earlier. Yellowish-white spots were observed in both eyes and exhibited hyperfluorescence on FA and hypofluorescence on IA. This characteristic is similar to the yellowish-white spots in MEWDS. However, MEWDS is mostly unilateral, and CNV rarely occurs. Furthermore, disruption in Bruch's membrane as seen in this case are considered specific findings in PIC where significant inflammation occurs from the RPE to the inner layers of the choroid.

7.4 X-linked juvenile retinoschisis

Background

X-linked juvenile retinoschisis is a disease that has been well described.[1] Characteristic, radiating inner retinal cystoid spaces associated with retinoschisis can be seen in the fovea centralis of both eyes in almost all cases, and peripheral retinoschisis occurs in about half of patients.

This disease is known to occur due to the mutation of the *RS1* gene located in the short arm of the X chromosome (Xp22).[2] This anomaly causes the mutation of amino acids in retinoschisin, which is a gene product of *RS1*. Retinoschisin is a protein expressed in photoreceptor cells (both cones and rods) and bipolar cells, and is a factor of cell adhesion.[3] This disease is thought to due to this protein mutation resulting in abnormal retinal cell adhesion. However, not all X-linked retinoschisis patients carry the *RS1* genetic mutation, and this disease reportedly has genetic diversity.[4]

OCT findings

Classic reports on the histopathology of this disease describe the retinal nerve fiber layer schisis that can be seen in advanced cases, but there are no mentions of foveal lesions.[5, 6] There have been many reports on what retinal layers the lesions of this disease occur in based on time-domain OCT, but the depth resolution this device is insufficient and does not always show satisfactory results.[7–9] In recent years, we have come to understand that schisis occurs in the nerve fiber layer, inner nuclear layer, outer nuclear layer, and outer plexiform layer in the fovea based on spectral-domain OCT.[10–12] It was also demonstrated that retinoschisis occurs in the inner nuclear layer in the intermediate periphery. Schisis in this intermediate periphery was named lamellar schisis by Prenner et al.[9]

X-linked juvenile retinoschisis is a disease, which has become more apparent owing to advancements in OCT rather than the histopathology that we had relied on up until now and did not necessarily represent the actual state of the disease. However, it has also been reported that retinal disorders depicted by OCT and visual function are not necessarily correlated;[13] and although OCT is no doubt useful in understanding the pathology, OCT alone is not sufficient.

References

1) Haas J. über das Zusammenvorkommen von Veränderungen der Retina und Choroidea. *Arch Augenheilkd*. 1898; 37:343–348.
2) Sauer CG, Gehrig A, Warneke-Wittstock R. et al. Positional cloning of the gene associated with X-linked juvenile retinoschisis. *Nat Genet*. 1997; 17:164–170.
3) Molday LL, Wu WW, Molday RS. Retinoschisin(RS1) , the protein encoded by X-linked retinoschisis gene, is anchored to the surface of retinal photoreceptor and bipolar cells through its interactions with a Na/K APTase-SARM1 complex. *J Biol Chem*. 2007; 282:32792–32801.
4) Hayashi T, Omoto S, Takeuchi T, et al. Four Japanese male patients with juvenile retinoschisis: only three have mutations in the RS1 gene. *Am J Ophthalmol*. 2004; 38:788–798.
5) Yanoff M, Kertesz Rahn E, Zimmerman LE. Histopathology of juvenile retinoschisis. *Arch Ophthalmol*. 1968; 79:49–53.
6) Manschot W. Pathology of hereditary juvenile retinoschisis. *Arch Ophthalmol*. 1972; 88:131–138.
7) Gao H, Kusumi R, Yung, CW. Optical coherence tomographic findings in X-linked juvenile retinoschisis. *Arch Ophthalmol*. 2005; 123:1006–1008.
8) Minami Y, Ishiko S, Takai Y, et al. Retinal changes in juvenile X linked retinoschisis using three dimensional optical coherence tomography. *Br J Ophthalmol*. 2005; 89:1663–1664.
9) Prenner JL, Capone A Jr, Ciaccia S, et al. Congenital X-linked retinoschisis classification system. *Retina*. 2006; 26:S61–S64.
10) Gerth C, Zawadzki RJ, Werner JS, et al. Retinal morphological changes of patients with X-linked retinoschisis evaluated by Fourier-domain optical coherence tomography. *Arch Ophthalmol*. 2008; 126:807–811.
11) Gregori NZ, Berrocal AM, Gregori G, et al. Macular spectral-domain optical coherence tomography in patients with X linked retinoschisis. *Br J Ophthalmol*. 2009; 93:373–378.
12) Yu J, Ni Y, Keane PA, et al. Foveomacular schisis in juvenile X-linked retinoschisis: an optical coherence tomography study. *Am J Ophthalmol*. 2010; 149:973–978.
13) Apushkin MA, Fishman GA, Janowicz MJ. Correlation of optical coherence tomography findings with visual acuity and macular lesions in patients with X-linked retinoschisis. *Ophthalmology*. 2005; 112:495–501.

Case 131 X-linked juvenile retinoschisis: Retinoschisis over a wide area

A 19-year-old male, OD and OS, BCVA 0.3 and 0.6, respectively

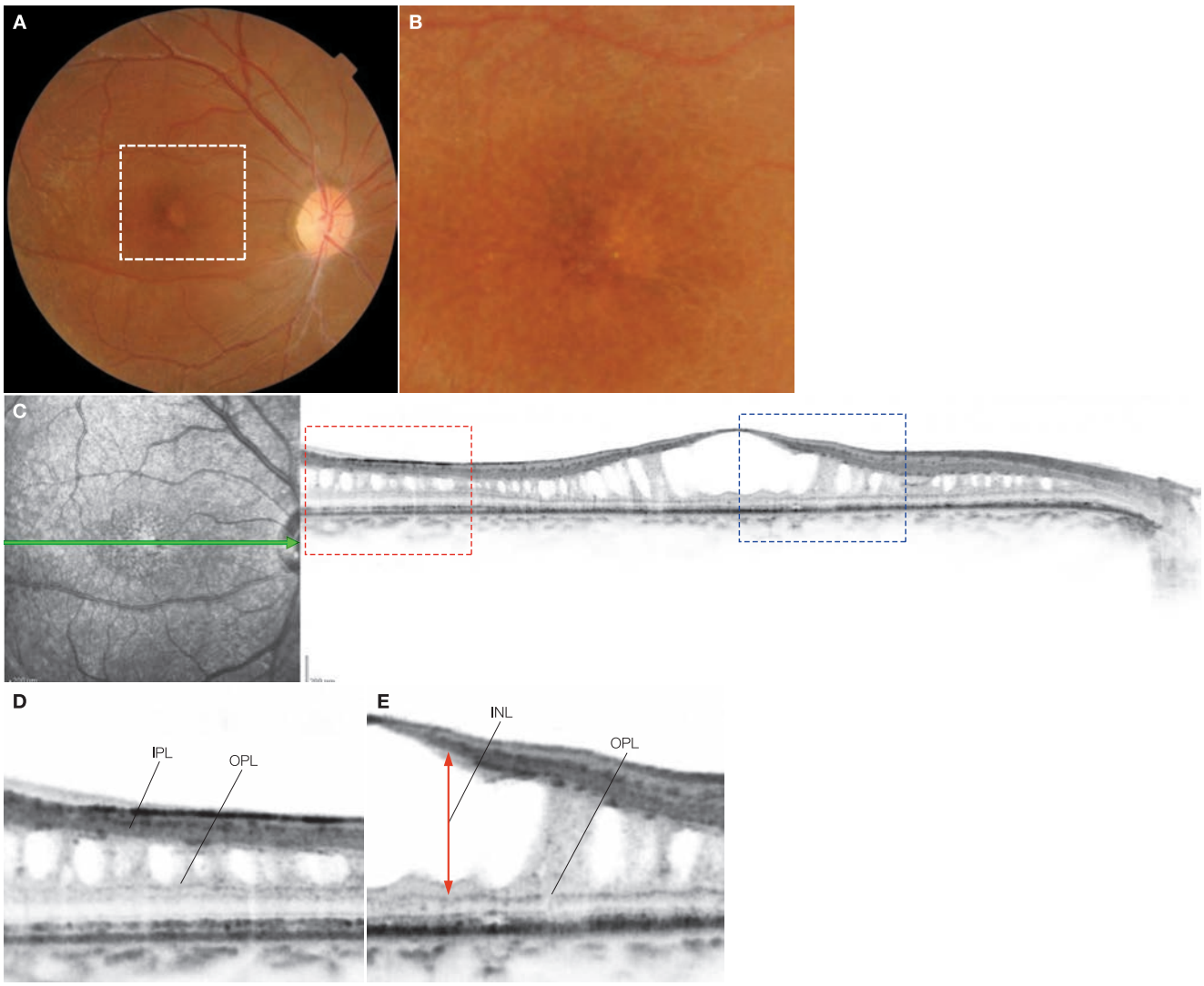

A: Color fundus photograph in the right eye: Radiating inner retinal cystoid spaces associated with retinoschisis can be seen in the fovea centralis. **B:** Enlarged version of A [white dashed box]: Radiating inner retinal cystoid spaces is apparent. **C:** IR + OCT horizontal scan of the left eye: A large retinoschisis cavity is visible in the macula. Retinoschisis is exhibited in the throughout the posterior pole. The retinoschisis is divided by columnar structures. **D:** Enlarged version of C [red dashed box]: Retinoschisis is located in the inner nuclear layer. **E:** Enlarged version of C [blue dashed box]: Retinoschisis is depicted in the inner nuclear layer.

(Continued on the next page)

Case 131 Continuation

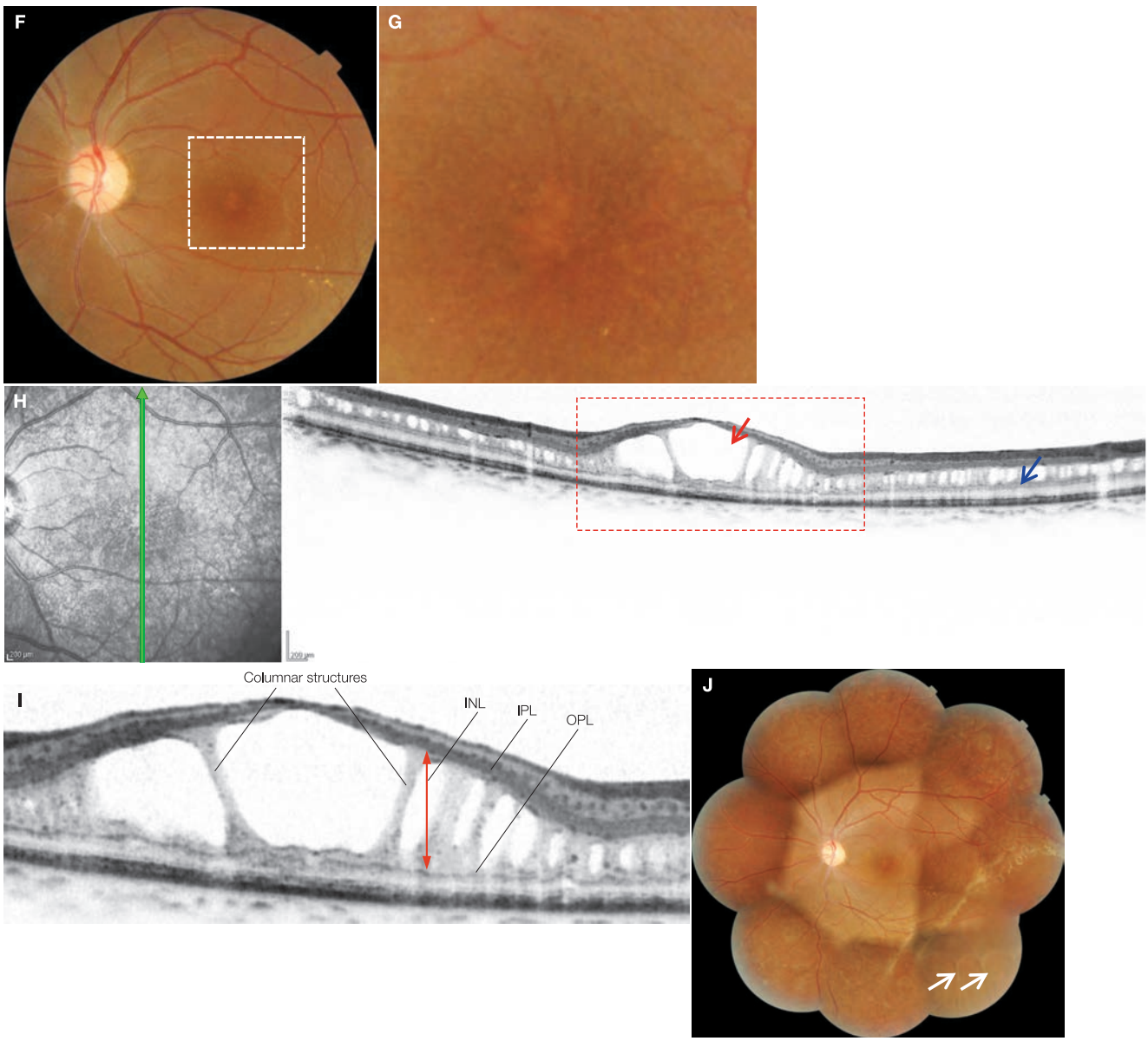

F: Color fundus photograph in the right eye: Radiating inner retinal cystoid spaces associated with retinoschisis can be seen in the fovea centralis. Yellow spots that are visible on the inferior, temporal side of the macula are derived from exudative changes due to retinoschisis in the periphery. **G:** Enlarged version of F [white dashed box]: Radiating inner retinal cystoid spaces is apparent. **H:** IR + macular OCT vertical scan of the left eye: A large retinoschisis cavity is depicted (➔). Retinoschisis can be seen throughout the posterior pole (➔). **I:** Enlarged version of H [red dashed box]: The foveal schisis cavity appears to be divided by thick columnar structures. The cystoid spaces are located in the inner nuclear layer. Cystic changes in the peripheral macula are also visible in the inner nuclear layer. **J:** Color fundus photograph montage of the left eye: Holes (⇛) in the inner retinal layers are visible in the inferior, temporal periphery.

Image interpretation points

Retinoschisis appears to mainly be present in the inner nuclear layer in this case. Retinoschisis seems to mostly be located in the inner nuclear layer, but it is reported that schisis also occurs in the retinal nerve fiber layer, outer nuclear layer, and outer plexiform layer. Schisis was seen in the intermediate periphery in 82% of cases in a report by Prenner et al.

Case 132 X-Linked juvenile retinoschisis: Retinoschisis confined to the macula

A 17-year-old male, OD, BCVA 0.15

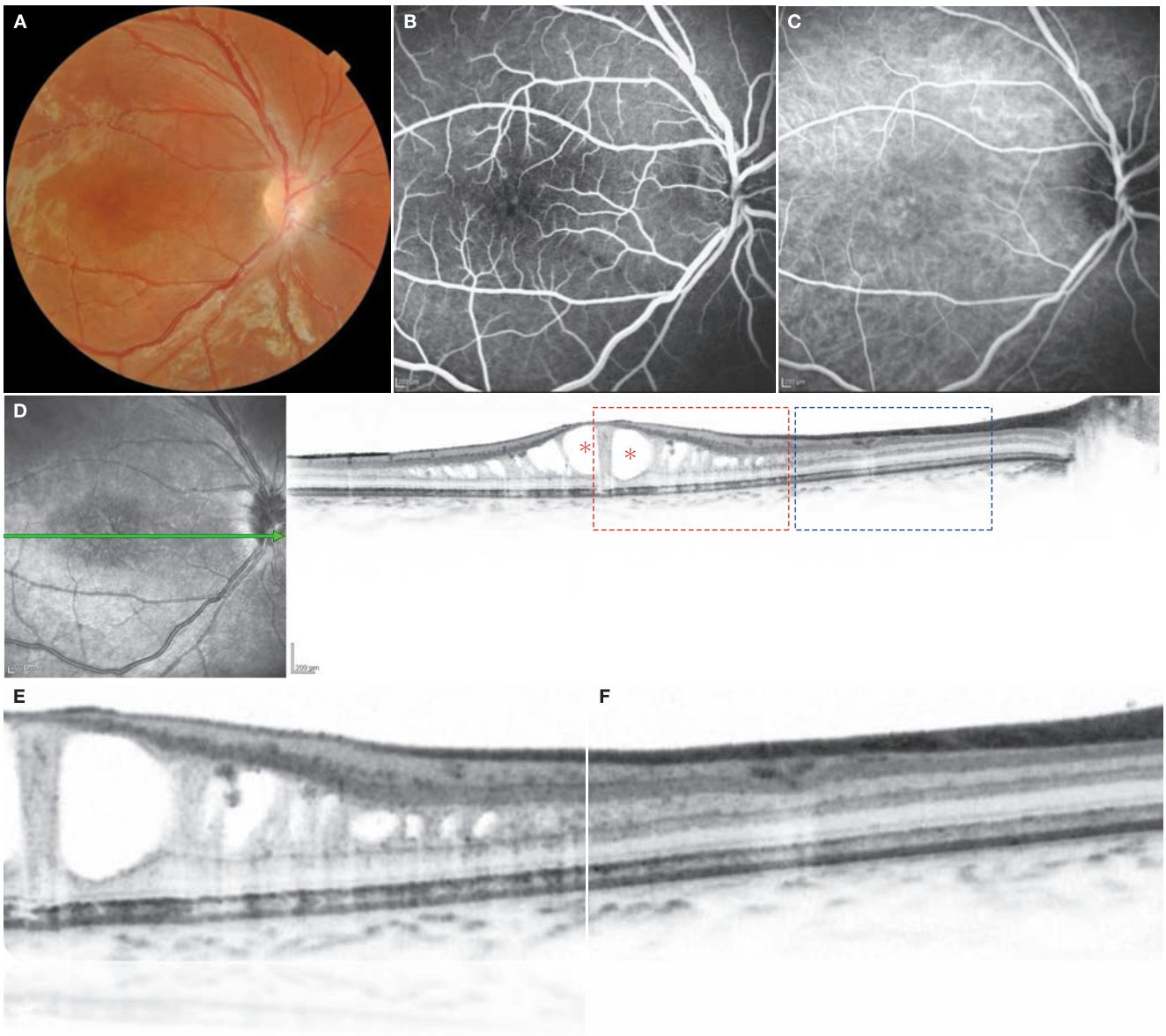

A: Color fundus photograph in the right eye: Radiating inner retinal cystoid spaces associated with retinoschisis can be seen in the fovea centralis.
B: FA in the right eye (18 seconds): Faint hyperfluorescence is visible in the fovea centralis. There appears to be dye leakage from the retinal blood vessels.
C: IA in the right eye (18 seconds): There are few particular findings. **D:** IR + OCT horizontal scan of the right eye: A large cystoid space is seen in the fovea centralis (*). The intermediate periphery is relatively normal. **E:** Enlarged version of D [red dashed box]: Retinoschisis is evident in the inner nuclear layer.
F: Enlarged version of D [blue dashed box]: The retinal structure in the intermediate area of the fovea centralis and optic disc is also relatively normal.

Image interpretation points

In this case, retinoschisis is confined to the vicinity of the fovea centralis and retinoschisis is located in the inner nuclear layer. In this disease, retinoschisis tends to easily occur in this layer in retinoschisis.

7.5 Stargardt disease

Background

Stargardt disease, also known as fundus flavimaculatus, is a bilateral, progressive hereditary form of macular dystrophy. In the Western world, it is the most frequent macular dystrophy and develops in relatively young patients in their teens and 20s. The frequency of this disease in Japan is unknown, but it is considerably lower compared with the Western world. It is autosomal recessive. There are also reports of genealogies exhibiting a dominant mode of inheritance, but these should be differentiated as Stargardt-like diseases. *ABCA4* (ATP binding cassette transporter A4) is well known as the genetic abnormality.[1] According to reports from the Western world, this genetic abnormality is present in close to 80% of Stargardt disease cases, although ELOVL 4 (elongation of very long chain fatty acids protein 4)[2] and PROM1 (prominin 1)[3] are also reported as causative genes. However, these genetic abnormalities do not necessarily result in Stargardt disease, and abnormalities in *ABCA4* are also associated with the onset of cone-rod dystrophy and retinitis pigmentosa.

Fundus findings in Stargardt disease are extremely varied. Fundus findings change as the disease stage progresses. A dark choroid is a well-known clinical finding on FA. However, this finding is not unique to Stargardt disease and is not seen in all cases of the disease. The detection frequency varies according to the disease stage, and when FA was performed with a confocal laser ophthalmoscopy, the ability of this device to adjust fluorescence gains make it difficult to detect dark choroid.

OCT findings

There are several reports on OCT findings for Stargardt disease. An earliest report showed that changes were greater in the outer retinal layers than in the inner layers,[4] and a more detailed examination is currently being conducted. Yellow spots are thought to be due to lipofuscin deposited on the RPE.[5] It is proposed that the yellow spots can be divided into 5 stages based on their positional relationship with the RPE and IS/OS.[6] In addition, it has been reported that retinal nerve fiber layer thickness around the optic disc is thicker than normal eyes, similar to retinitis pigmentosa.[7] The tomographic features of this disease include loss of photoreceptor and RPE cells and subsequent choroidal signal enhancement, which is similar to other degenerative diseases or atrophic form of age-related macular degeneration. Furthermore, reactive proliferation of the RPE cells can be seen in conjunction with these changes.

Currently, there are ongoing Phase I and Phase II clinical trials on stem cell therapy. As a representative retinal degenerative condition, detailed comparative studies between visual function and structure have been conducted in Stargardt disease. One topic being addressed is the detailed study of the state of photoreceptor cells using adaptive optics confocal scanning laser ophthalmoscopy.[8]

References

1) Allikmets R, Singh N, Sun H, et al. A photoreceptor cell-specific ATP-binding transporter gene (ABCR) is mutated in recessive Stargardt macular dystrophy. *Nature Genet*. 1997; 15: 236–246.
2) Bernstein PS, Tammur J, Singh N, et al. Diverse macular dystrophy phenotype caused by a novel complex mutation in the ELOVL4 gene. *Invest Ophthal Vis Sci*. 2001; 42: 3331–3336.
3) Yang Z, Chen Y, Lillo C, et al. Mutant prominin 1 found in patients with macular degeneration disrupts photoreceptor disk morphogenesis in mice. *J Clin Invest*. 2008; 118: 2908–2916.
4) Lim JI, Tan O, Fawzi AA, et al. A pilot study of Fourier-domain optical coherence tomography of retinal dystrophy patients. *Am J Ophthalmol*. 2008; 146:417–426.
5) Birnbach CD, Järveläinen M, Possin DE, et al. Histopathology and immunocytochemistry of the neurosensory retina in fundus flavimaculatus. *Ophthalmology*. 1994; 101:1211–1219.
6) Voigt M, Querques G, Atmani K, et al. Analysis of retinal flecks in fundus flavimaculatus using high-definition spectral-domain optical coherence tomography. *Am J Ophthalmol*. 2010; 150:330–337.
7) Genead MA, Fishman GA, Anastasakis A. Spectral-domain OCT peripapillary retinal nerve fiber layer thickness measurements in patients with Stargardt disease. *Br J Ophthalmol*. 2011; 95:689–693.
8) Chen Y, Ratnam K, Sundquist SM, et al. Cone photoreceptor abnormalities correlate with vision loss in patients with Stargardt disease. *Invest Ophthalmol Vis Sci*. 2011; 52:3281–3292.

Case 133 Stargardt disease: A typical example

A 43-year-old female, OD, BCVA 0.1

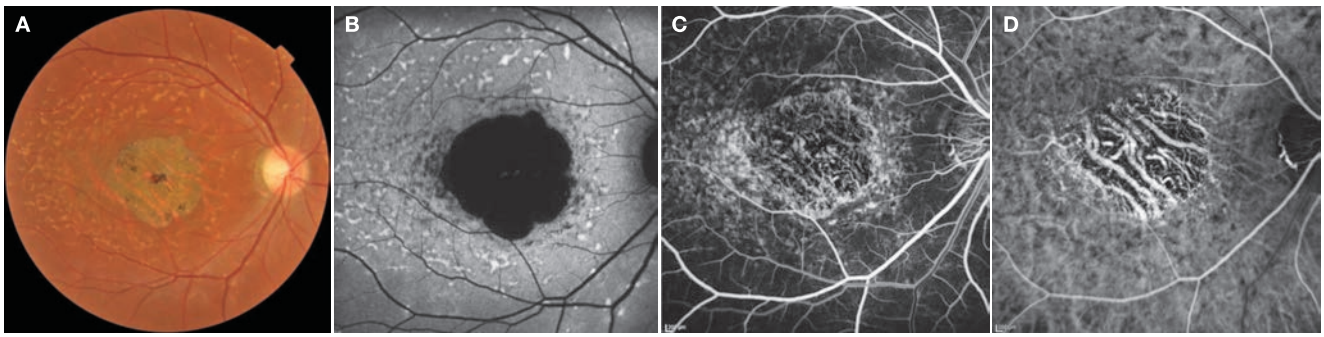

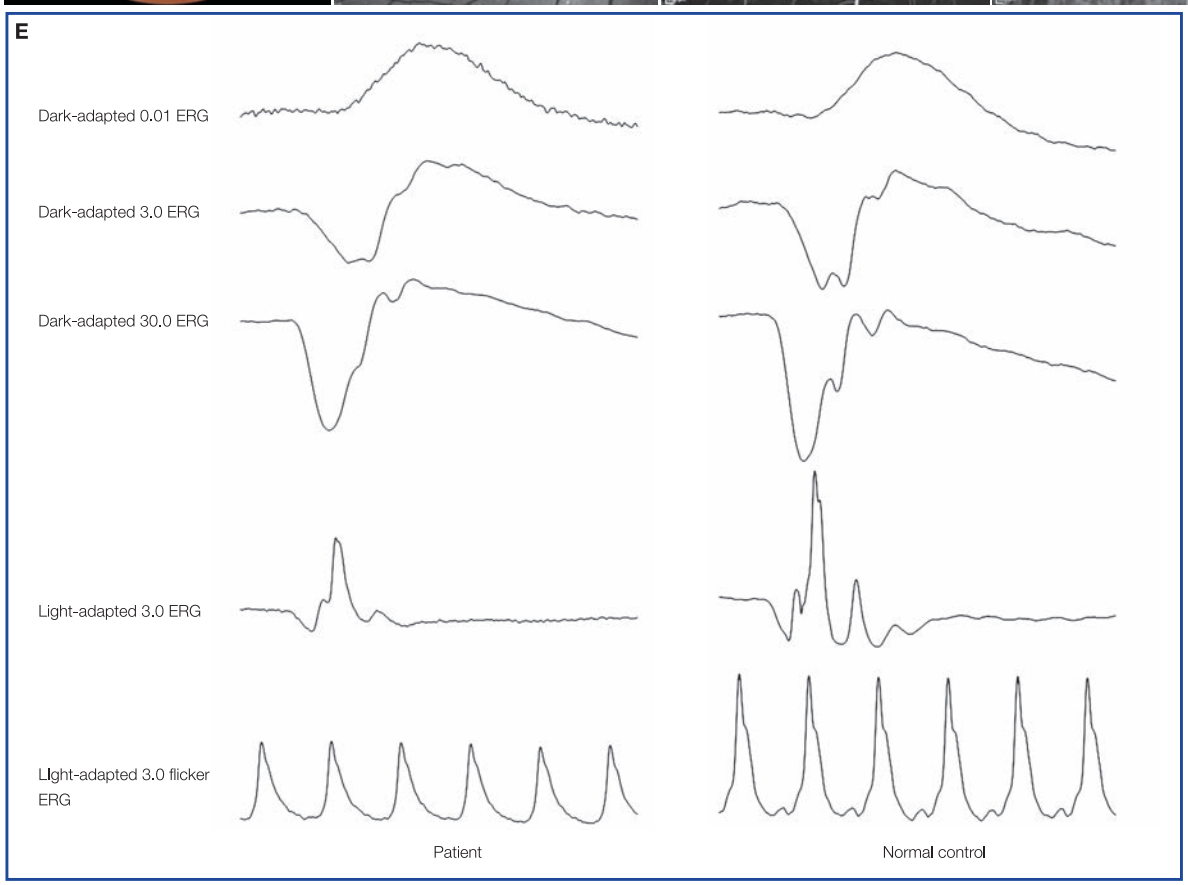

A: Color fundus photograph in the right eye: An atrophic lesion of about 2 disc diameters is seen in the fovea centralis. Yellow spots are visible over the entire posterior pole. **B:** FAF in the right eye: There is significant hyopfluorescence within the atrophic lesion. Small hypofluorescent spots are scattered around the atrophic lesion. The yellow spots are exhibiting hyperfluorescence. **C:** FA in the right eye (18 seconds): Background fluorescence is low, which as a typical dark choroid. The atrophic lesion in the macula is exhibiting hyperfluorescence due to window defects. The pigmentation inside this area is significantly hypofluorescence. **D:** IA in the right eye (18 seconds): The large choroidal vessels are seen through the translucent atrophic lesion even on IA. Mottled hypofluorescence is exhibited around the atrophic lesion. **E:** Electroretinogram (ERG) in the right eye: Recorded according to International Society for Clinical Electrophysiology of Vision (ISCEV) criteria. Both cone and rod responses are relatively well preserved. The state of the left eye is almost the same as the right eye.

(Continued on the next page)

Case 133 Continuation

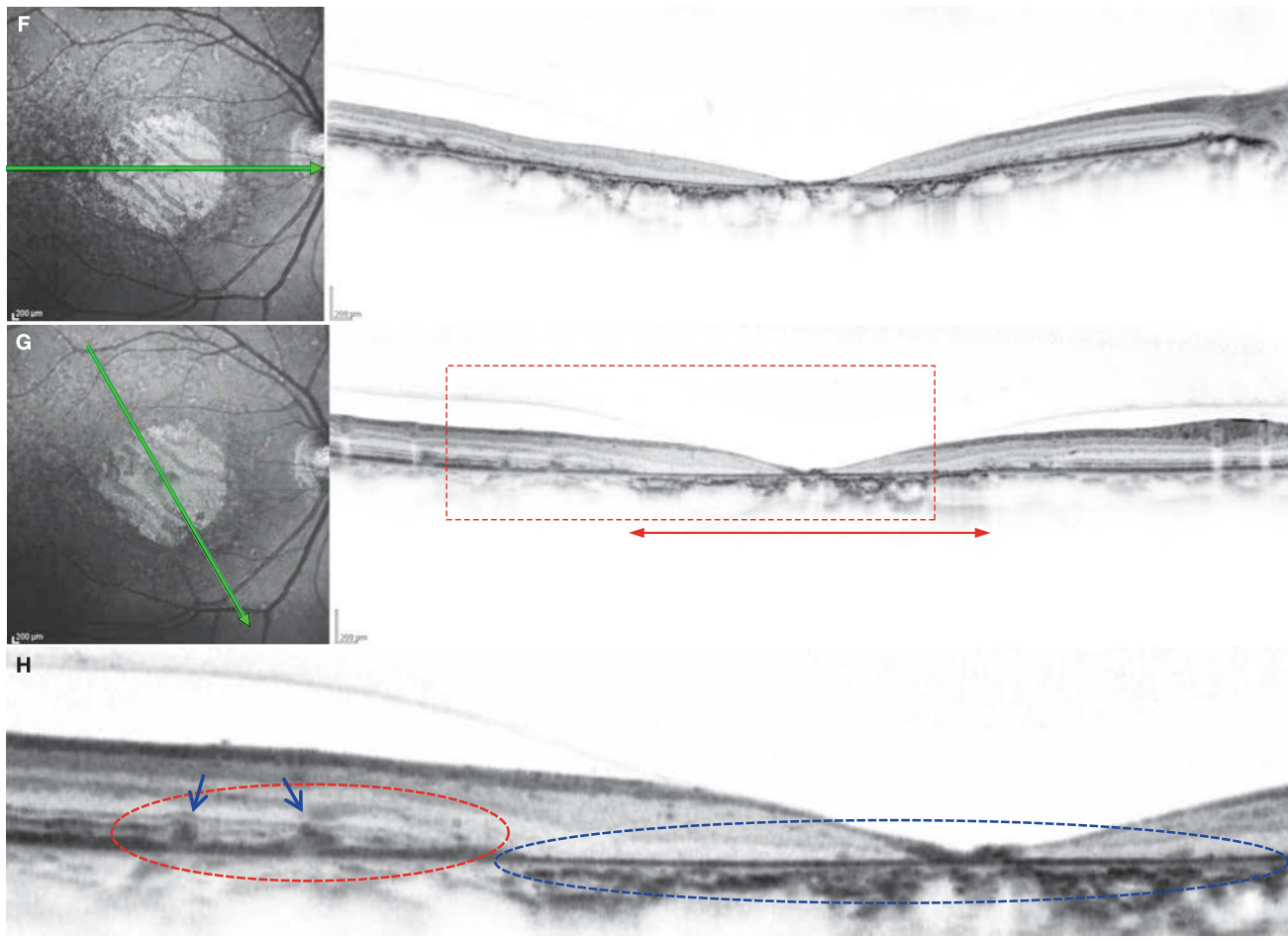

F: IR + OCT horizontal scan of the right eye: The retina in the macula is significantly thin. **G:** IR + OCT oblique scan of the right eye: The yellow spots scattered around the atrophic lesion are visible as protrusions in the RPE. The choroidal signal enhancement (↔) is visible due to loss of the RPE within the atrophic lesion. **H:** Enlarged version of G [red dashed box]: We can see that the loss of the RPE is more apparent the closer it gets to the center of the atrophic lesion (blue dashed circle). The RPE is relatively well preserved around the atrophic lesion, but the photoreceptor inner and outer segment junction line is interrupted, and the ELM line in the intermediate area (between the two) appears to be »bowing« downwards (red dashed circle). The yellow spots can mainly be seen as highly reflective lesions between the ELM and RPE (→).

Image interpretation points

In this case, c2798A>T and c4195G>A compound heterozygote mutations were detected in the *ABCA4* gene. This is typical Stargardt disease where the dark choroid can be seen on FA.

This disease does not appear to have specific OCT findings, although it does exhibit findings very similar to cone dystrophy and atrophic AMD.

7.6 Vitelliform macular dystrophy and adult-onset foveomacular vitelliform dystrophy

Background

Vitelliform macular dystrophy (VMD), or Best disease, was first reported over 100 years ago by Best in 1905.[1] This disease has an autosomal dominant form of inheritance and is caused by a mutation of the *VMD2* gene.[2] The *VMD2* gene is located on 11q13 of the long arm of chromosome 11 and its gene product is known as bestrophin. Bestrophin is a Ca^{2+} dependent chloride channel protein localized in the cell membrane at the base of RPE cells.[3, 4]

Vitelliform macular dystrophy is essentially a bilateral disease (and unilateral in rare cases). This disease typically affects children aged 6 to 12 years, often results in relatively mild visual dysfunction, is sometimes only discovered on fundus examinations, and maintains relatively good visual function until middle-age. A typical finding of VMD is a decrease in the length to diameter ratio (L/D ratio) in electrooculography (EOG), although it is – difficult to conduct EOG tests during childhood. Fundus findings of this disease are known to change with age. Moehler and Fine proposed dividing this disease into 5 stages from 0 to IV; Stage 0, the subclinical stage; Stage I, the vitelliform stage; Stage II, the pseudohypopyon stage; Stage III, the vitelliruptive stage; and Stage IV, the atrophic stage.[5]

In contrast, adult-onset foveomacular vitelliform dystrophy (AOFVD) was first described by Gass in 1974.[6] This disease is a type of pattern dystrophy and often develops in those in their 40s and 50s. Fundus findings are very similar to VMD, but lesions are often small compared with VMD. This disease includes unilateral cases. EOG test results are generally normal but there are also cases where the L/D ratio decreases. The hereditary form is autosomal dominant with a low penetration rate. Peripherin/RDS mutations are reported in AOFVD, although there are also cases in which *VMD2* genetic mutations can be found.[7] Visual dysfunction is also mild in this disease.

The clinical features of these two diseases are similar, and the differences are not well understood. Neither disease has been recorded in recent years, and only fragmented histopathological information is available. In addition, it has recently become a topic that impaired RPE phagocytosis of the photoreceptor outer segments as a result of various causes leads to development of vitelliform lesions. Gass et al. reported on vitelliform lesions associated with cuticular drusen in 1985,[8] but impaired photoreceptor outer segment phagocytosis and subsequent development of vitelliform lesions actually occurs with chronic foveal detachment. This occurs in diseases such as reticular drusen,[9] vitreoretinal traction syndrome, and central serous chorioretinopathy. Freund et al. referred to this state as »acquired vitelliform lesions«.[10]

With characteristic fundus findings, the diagnosis of VMD is straightforward; however, diagnosis can be difficult in cases that have entered the atrophic stage. FA (corona sign), fundus autofluorescence (hyperfluorescence) and OCT findings are useful for diagnosis, with a unique hyperreflective feature in fundus autofluorescence being particularly useful. In the most advanced stage of the disease, however, the hyperfluorescence on autofluorescence attenuates and the diagnostic value decreases.[11]

OCT findings

Known OCT findings for VMD and AOFVD are shown in ◘ Table 7-1.[12–15] However, there are no reports comparing the OCT findings between the two diseases; as a result, it is unknown if there are essential differences between the two. Additionally, a very recent report on the genetic analysis of numerous cases was published in France. According to this report, age of onset was the biggest factor in differentiating both diseases, whereas the L/D ratio of EOG tests is apparently not a good index for differentiation.[16]

◘ **Table 7-1** OCT findings in vitelliform macular dystrophy and adult-onset foveomacular vitelliform dystrophy.

Subclinical stage or vitelliform stage	Partial disruption of the IS/OS line The COST line is more clearly depicted than usual Amorphous material deposits are visible between the sensory retina and RPE
Pseudohypopyon stage	The optically empty zone in the superior fovea (area of low reflectivity) Highly reflective deposits in the inferior fovea
Vitelliruptive stage	Optical empty zone Enhanced reflectivity of the RPE Partial disruption of the IS/OS line
Atrophic stage	Thinning of all retinal layers Complete disappearance of the IS/OS line Reactive proliferation of the RPE cells

The current consensus is that subfoveal deposits can be seen between the sensory retina and RPE in VMD. In the previous era of time-domain OCT, deposits were seen to be located beneath the RPE due to low depth resolution, but it is clear that such previous interpretation was wrong after the introduction of high resolution spectral-domain OCT.

References

1) Best F. Über eine hereditäre Maculaaffektion. Beiträg zur Vererbungslhere. *Z Augenheilkd*. 1905; 13:199–212.
2) Petrunkhin K, Koisti MJ, Bakall B, et al. Identification of the gene responsible for Best macular dystrophy. *Nat Genet*. 1998; 19:241–247.
3) Marmorstein AD, Marmostein LY, Rayborn M, et al. Bestrophin, the product of the Best vitelliform macular dystrophy gene (VMD2), localizes to the basolateral plasma membrane of the retinal pigment epithelium. *Proc Natl Acad Sci USA*. 2000; 97:12758–12763.
4) Sun H, Tsunenari T, Yau KW, et al. The vitelliform macular dystrophy protein defines a new family of chloride channels. *Proc Natl Acad Sci USA*. 2002; 99:4008–4013.
5) Moehler CW, Fine SL. Long-term evaluation of patients with Best's vitelliform dystrophy. *Ophthalmology*. 1981; 88:688–692.
6) Gass JDM. A clinicopathologic study of a peculiar foveomacular dystrophy. *Trans Am Ophthalmol Soc*. 1974; 72:139–156.
7) Seddon JM, Afshari MA, Sharma S, et al. Assessment of mutations in the Best macular dystrophy (VMD2)gene in patients with adult-onset foveomacular vitelliform dystrophy, age-related maculopathy, and bull's eye maculopathy. *Ophthalmology*. 2001; 108:2060–2067.
8) Gass JDM, Jallow S, Davis B. Adult vitelliform macular detachment occurring in patients with basal laminar drusen. *Am J Ophthalmol*. 1985; 99:445–459.
9) Zweifel SA, Spaide RF, Yannuzzi LA. Acquired vitelliform detachment in patients with subretinal drusenoid deposits (reticular pseudodrusen). *Retina*. 2011; 31:229–234.
10) Freund KB, Laud K, Lima LH, et al. Acquired vitelliform lesions. Correlation of clinical findings and multiple imaging analyses. *Retina*. 2011; 31:13–25.
11) Spaide RF, Noble K, Morgan A, et al. Vitelliform macular dystrophy. *Ophthalmology*. 2006; 113:1392–1400.
12) Ferrara DC. Costa RA, Tsang S, et al. Multimodal fundus imaging in Best vitelliform macular dystrophy. *Graefes Arch Clin Exp Ophthalmol*. 2010; 248:1377–1386.
13) Puche N, Querques G, Benhamou N, et al. High-resolution spectral domain optical coherence tomography features in adult onset foveomacular vitelliform dystrophy. *Br J Ophthalmol*. 2010; 94:1190–1196.
14) Querques G, Bux AV, Prato R, et al. Correlation of visual function impairment and optical coherence tomography findings in patients with adult-onset foveomacular vitelliform macular dystrophy. *Am J Ophthalmol*. 2008; 146:135–142.
15) Querques G, Regenbogen M, Quijano C, et al. High-definition optical coherence tomography features in vitelliform macular dystrophy. *Am J Ophthalmol*. 2008; 146:501–507.
16) Meunier I, Sénéchal A, Dhaenens CM, et al. Systemic screening of BEST1 and PRPH2 in juvenile and adult vitelliform macular dystrophies: a rationale for molecular analysis. *Ophthalmology*. 2011; 118:1130–1136.

Case 134 Adult-onset foveomacular vitelliform dystrophy: Vitelliform stage

Right and left eye of a 60-year-old male, OD and OS, BCVA 0.8 and 1.2, respectively

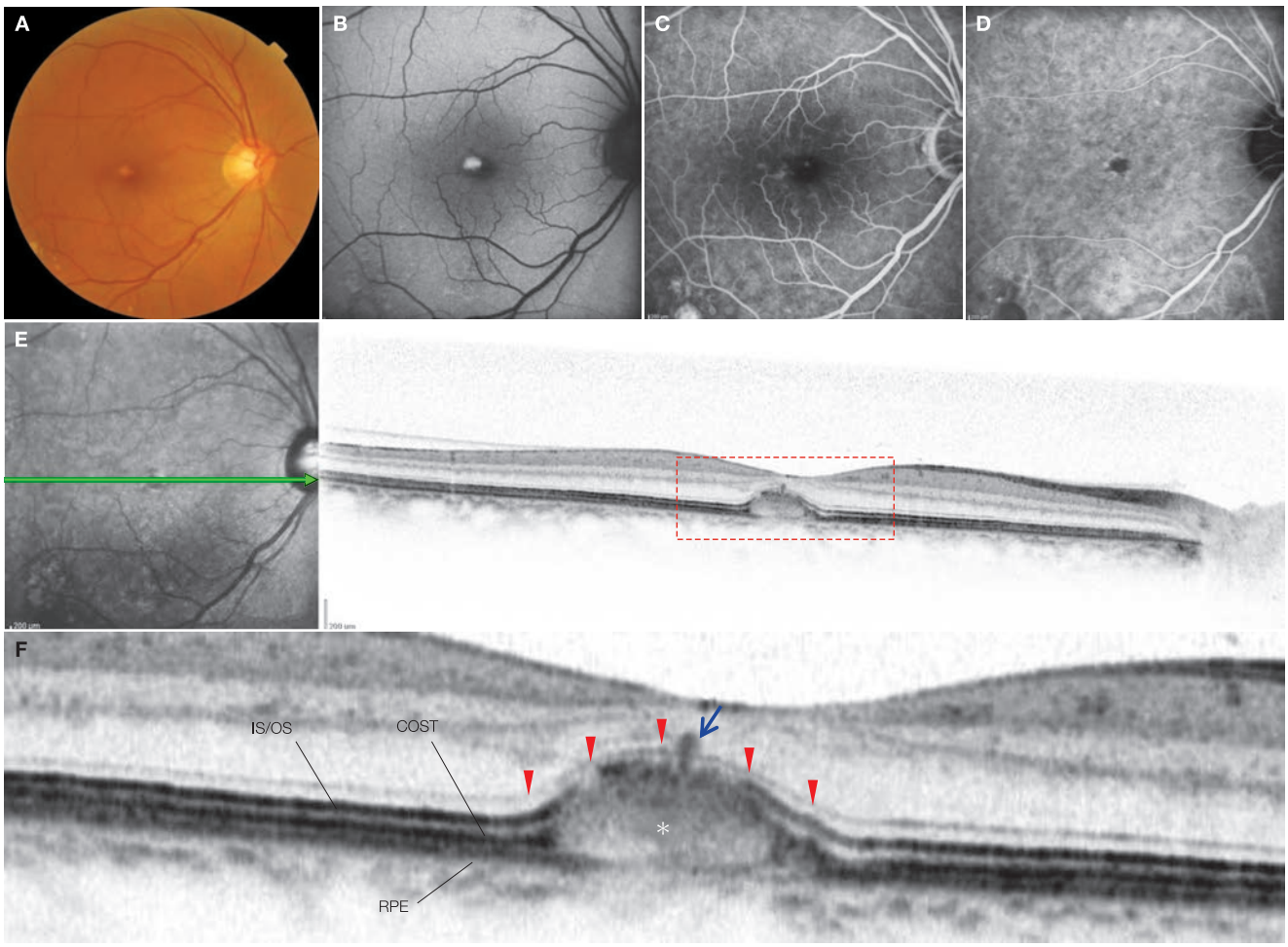

A: Color fundus photograph in the right eye: A yellowish-white spot is visible in the fovea centralis. A yellowish-white spots is also seen near the inferotemporal vascular arcade. **B:** FAF in the right eye: Intense hyperfluorescence is noted in the fovea centralis and its surroundings are slightly hypofluorescent. **C:** FA in the right eye (4 minutes, 32 seconds): Very faint hyperfluorescence can be seen around the fovea centralis. The yellowish-white spot inferotemporally also appears to be exhibiting hyperfluorescence. **D:** IA in the right eye (4minutes, 32 seconds): The fovea centralis is exhibiting hypofluorescence. **E:** IR + OCT horizontal scan of the right eye: Moderately reflective deposits are seen beneath the fovea centralis. **F:** Enlarged version of E [red dashed box]: The subfoveal deposits (❄) are amorphous. Both the RPE line and ELM (▶) are continuous and the COST line is as clearly seen as IS/OS line. This appears to be typical of this disease. Reactive proliferation of the RPE cells can be seen (➔). The IS/OS line is intermittently visible.

Image interpretation points

Based on the patient's medical history and fundus findings, this is unmistakably AOFVD. Intense autofluorescence on FAF is useful for diagnosis. Subfoveal deposits exist between the sensory retina and RPE. The COST line is clearly seen outside of the lesion site. Such an enhanced COST line also present in the fellow eye.

Case 135 Adult-onset foveomacular vitelliform dystrophy: Pseudohypopyon stage

A 59-year-old female, OS, BCVA 0.6

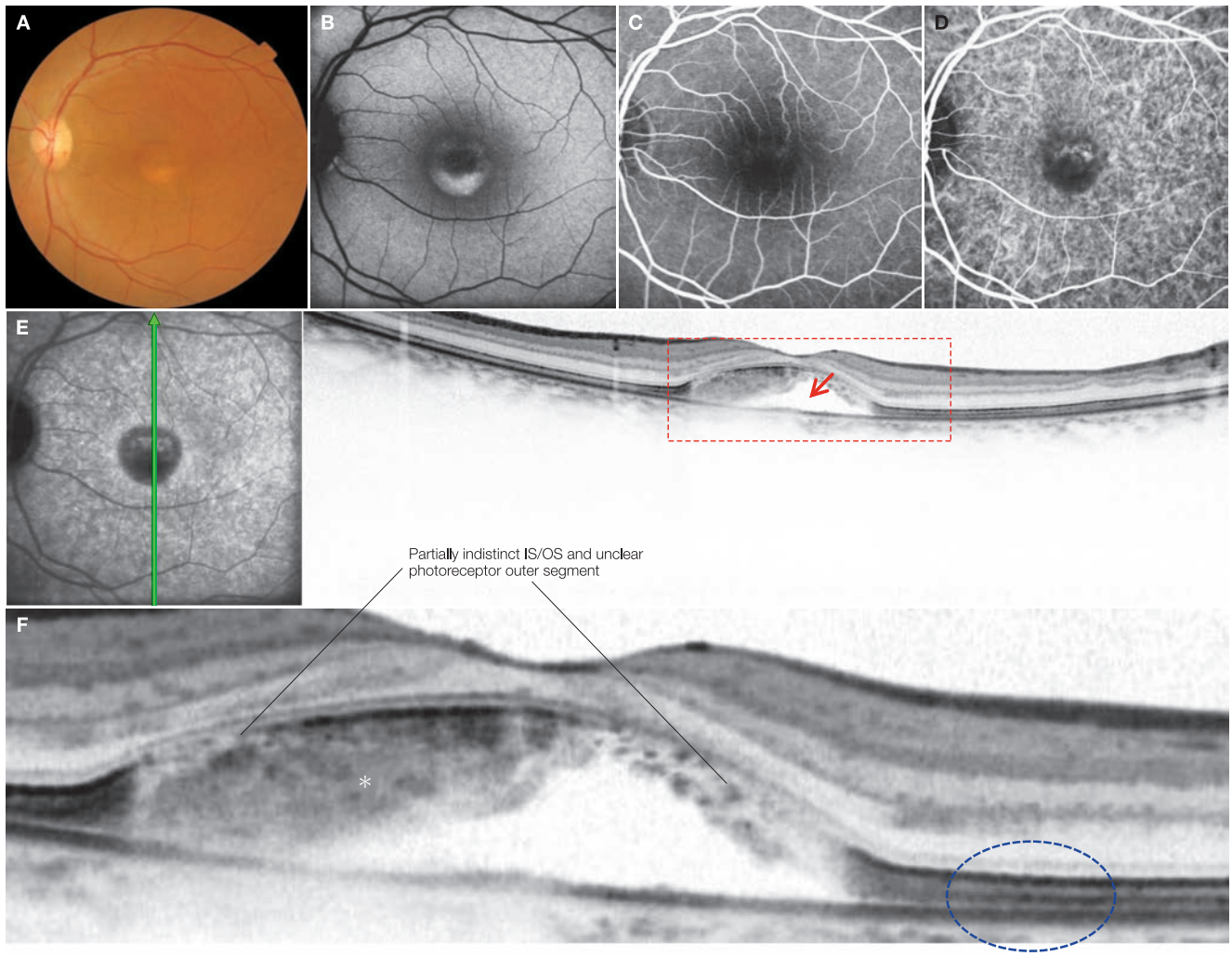

A: Color fundus photograph in the left eye: A lesion of about 1 disc diameter is visible in the fovea centralis and a yellowish-white spot exhibiting a niveau pattern can be seen inferiorly. The yellow color is weak above this area. **B:** FAF in the left eye: Significant hyperfluorescence is seen in the inferior fovea. **C:** FA in the left eye (29 seconds): The superior fovea is slightly hyperfluorescent. The inferior fovea with the yellowish-white lesion is hypofluorescent. **D:** IA in the left eye (29 seconds): The superior fovea is hyperfluorescent, while the inferior fovea with the yellowish-white lesion is hypofluorescent. **E:** IA + OCT vertical scan of the left eye: A so-called vitelliform detachment (➔) is visible below the fovea centralis. Moderate reflectivity from vitelliform deposits is visible below the detached retina. **F:** Enlarged version of E [red dashed box]: The vitelliform deposits are clearly visible (❄). The IS/OS is partially indistinct in the detached area of the retina. In addition, the photoreceptor outer segment has merged with the vitelliform deposits and cannot be distinguished. The structure of the outer retinal layers is well preserved in the area without retinal detachment (blue dashed circle). The RPE is flat.

Image interpretation points

This is a case of pseudohypopyon stage AOFVD. It is clear that the vitelliform deposits are located between the sensory retina and RPE. The vitelliform detachment is also clearly visible.

Case 136 Adult-onset foveomacular vitelliform dystrophy: The course

Course of the right eye of a 59-year-old female (fellow eye of case 135)

A, B, C: Color fundus photographs in the right eye: At initial diagnosis A, 1 year and 2 months after initial diagnosis B, and 2 years and 8 months after initial diagnosis C. The subfoveal yellowish-white lesion is becoming indistinct over time. Best-corrected visual acuity of the left eye is 0.8 in A, 0.6 in B and 0.4 in C. **D, E, F:** OCT horizontal scans of the right eye: The same course is shown: At initial diagnosis D, 1 year and 2 months after initial diagnosis E, and 2 years and 8 months after initial diagnosis F. Subfoveal vitelliform deposits get smaller and eventually disappear leaving behind a foveal detachment. **G:** Enlarged version of D [red dashed box]: **H:** Enlarged version of F [blue dashed box]: The ELM and IS/OS (red dashed circle) are preserved in G where visual acuity is relatively good. The IS/OS is becoming indistinct with the degeneration of the outer retinal layers in H (→) and highly reflective patterns (blue dashed circle) thought to be reactive proliferation of the RPE cells in the foveal retina are visible.

Image interpretation points

This is the fellow eye of case 135. Subretinal deposits can be seen on OCT when vitelliform lesions are clearly visibly with an ophthalmoscopy. The deposits disappear with time followed by atrophic degeneration of the outer retinal layers with remaining foveal detachment.

7.7 Pseudoxanthoma elasticum

Background

Pseudoxanthoma elasticum (PXE) is a relatively rare systemic disease. Lesions occur in the skin, gastrointestinal tract, cardiovascular system and the eyes.[1] A mutation of ABCC6 gene that exists in p13.1 of chromosome 16 is believed to cause tearing and degeneration of systemic elastic fibers.[2] Changes seen in the fundus include angioid streaks (AS), peau d'orange fundus, crystalline bodies, optic disc drusen, comet lesions and CNV.[1] AS are radiating, jaggy, and tapering streaks (clefts) spreading from the peripapillary region that are caused by tears in Bruch's membrane due to elastic fiber abnormalities. In addition to PXE, AS can be seen in patients with Ehlers-Danlos syndrome, Paget's disease and Marfan syndrome.[1]

OCT findings

OCT findings vary. Since abnormalities in the elastic fibers that compose Bruch's membrane are the basis of the disease, abnormal features on OCT are found primarily in the outer retinal layers. Disruption in Bruch's membrane in the sites corresponding to AS and decreased reflectivity of the RPE and Bruch's membrane corresponding to peau d'orange fundus are known to occur prior to the onset of CNV.[3] As the disease progresses, undulating Bruch's membrane appears and round, ovoid or tubular structures known as outer retinal tubulations are formed in the outer nuclear layer.[3, 4] Pathologically, these structures are thought to to be proliferated RPE,[5] the details of which are unclear. So-called Type 2 CNV is often seen, although Type 1 CNV can also develop.

Finally, vitelliform detachment and reticular pseudodrusen-like changes have also been reported in AS.[6]

References

1) Finger RP, Charbel Issa P, Ladewig MS, et al. Pseudoxanthoma elasticum: genetics, clinical manifestations and therapeutic approaches. *Surv Ophthalmol*. 2009; 54:272–285.
2) Le Saux O, Urban Z, Tschuch C, et al. Mutations in a gene encoding an ABC transporter cause pseudoxanthoma elasticum. *Nat Genet*. 2000; 25:223–227.
3) Charbel Issa GP, Finger RP, Holz FG, et al. Multimodal imaging including spectral domain OCT and confocal near infrared reflectance for characterization of outer retinal pathology in pseudoxanthoma elasticum. *Invest Ophthalmol Vis Sci*. 2009; 50:5913–5918.
4) Zweifel SA, Engelbert M, Laud K, et al. Outer retinal tubulation: a novel optical coherence tomography finding. *Arch Ophthalmol*. 2009; 127:1596–1602.
5) Dreyer R, Green WR. The pathology of angioid streaks:a study of twenty-one cases. *Trans Pa Acad Ophthalmol Otolaryngol*. 1978; 31:158–167.
6) Zweifel SA, Imamura Y, Freund KB, et al. Multimodal fundus imaging of pseudoxanthoma elasticum. *Retina*. 2011; 31:482–491.

Case 137 Pseudoxanthoma elasticum: A case of Type 1 CNV

A 63-year-old male, OD, BCVA 0.5

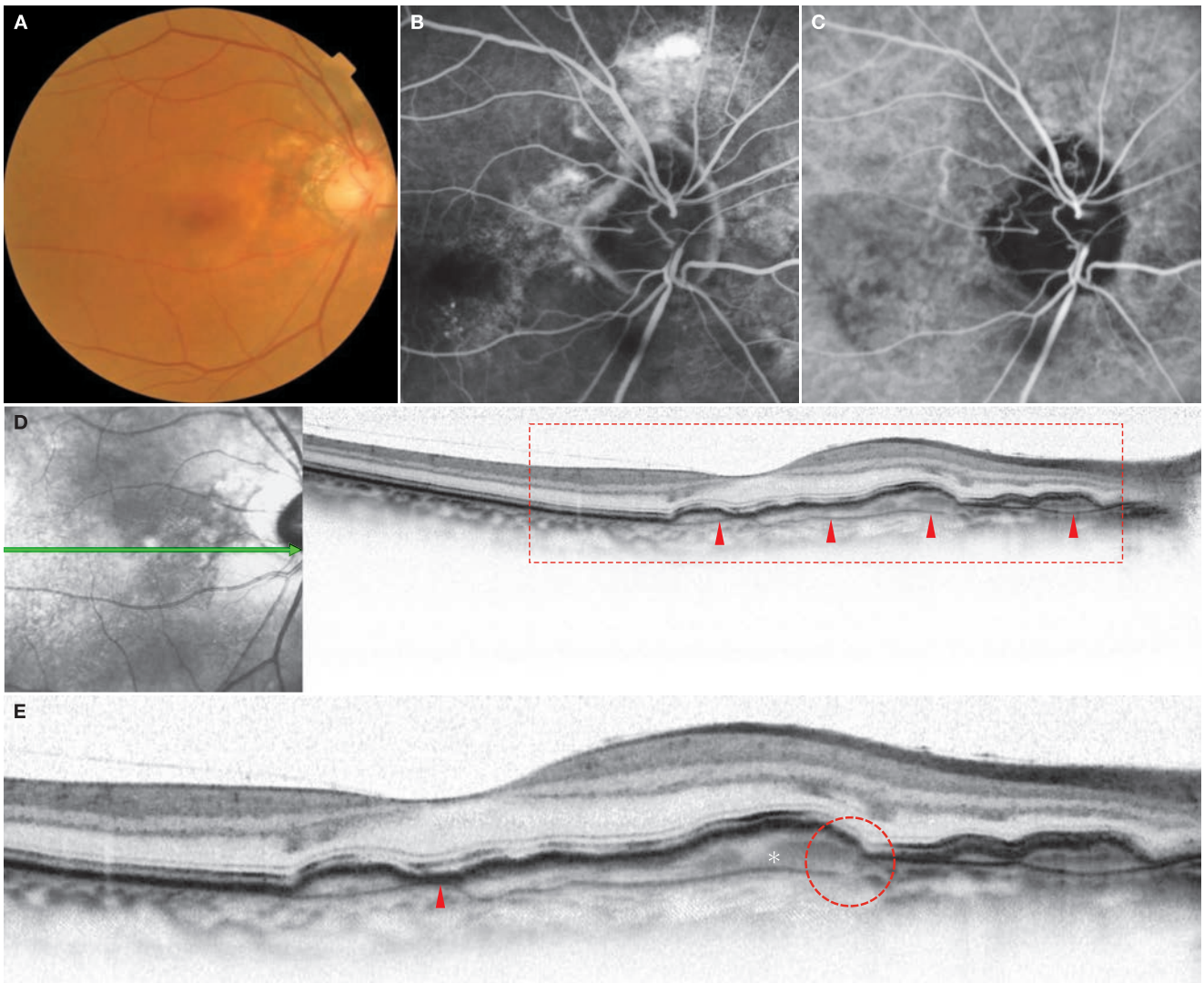

A: Color fundus photograph in the right eye: ASs are visible around the optic disc. **B:** FA in the right eye (7 minutes, 15 seconds): Relatively intense hyperfluorescence can be seen superior to the optic disc. Mild hyperfluorescence is visible temporal to the optic disc. The fovea centralis is hypofluorescent. **C:** IA in the right eye (7 minutes, 15 seconds): CNV appears to be present over a wide area immediately temporal to the optic disc. **D:** IR + OCT horizontal scan of the right eye: CNV is present over a wide area below the RPE from the optic disc to slightly temporal to the fovea centralis. The undulation of Bruch's membrane is clearly seen (►). **E:** Enlarged version of D [red dashed box]: The undulation of Bruch's membrane (►) and the disruption in Bruch's membrane (red dashed circle) are clearly visible. Moderate reflectivity is visible between the RPE and Bruch's membrane where Type 1 CNV (❄) is present.

Image interpretation points

Type 1 CNV has occurred in this case. The undulation of Bruch's membrane and the disruption in Bruch's membrane are typical findings of PXE.

Case 138 Pseudoxanthoma elasticum: A case of Type 2 CNV

A 58-year-old female, OD, BCVA 1.5

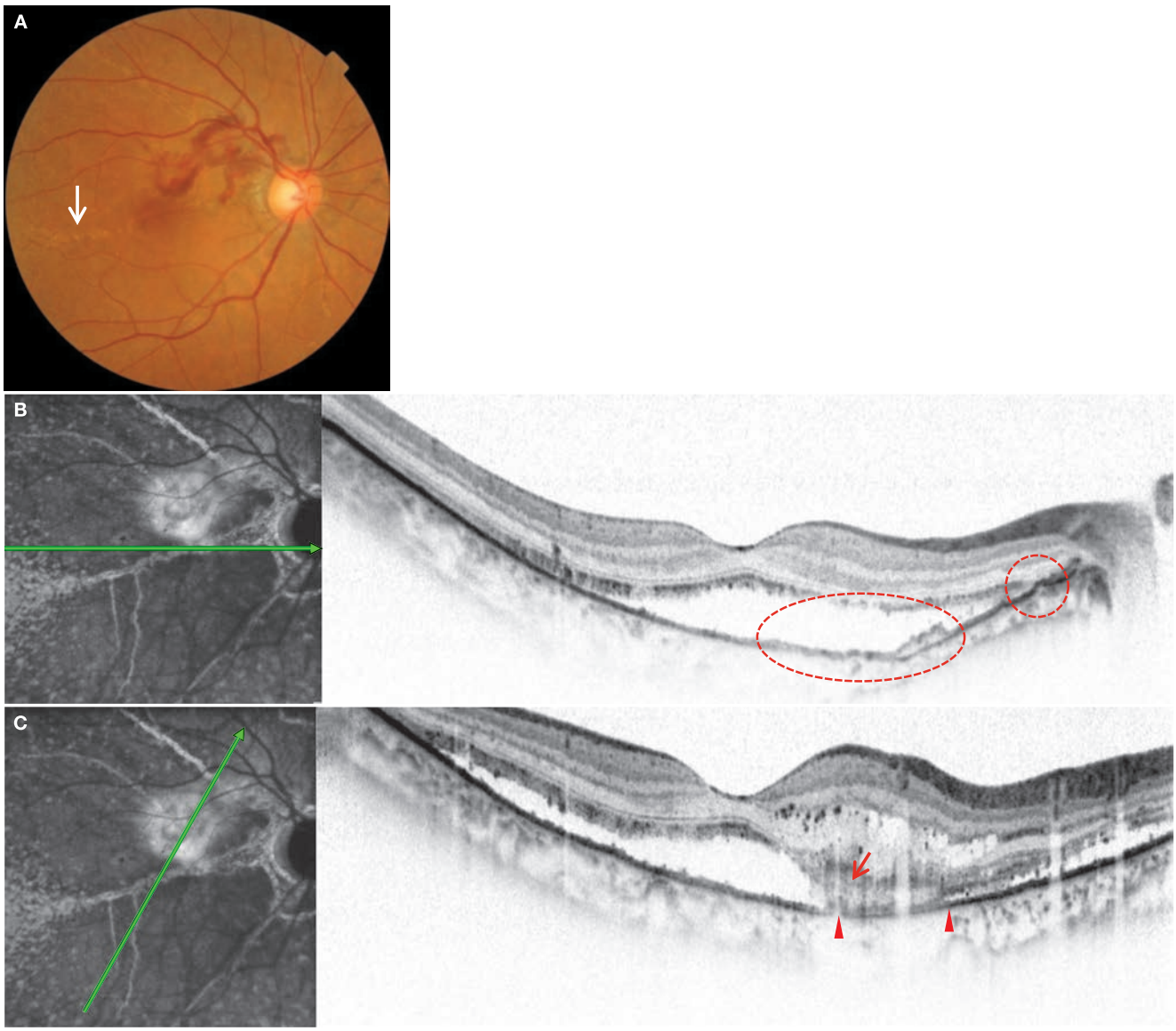

A: Color fundus photograph in the right eye: CNV with hemorrhages can be seen between the optic disc and the fovea centralis. ⇨ indicates AS in the temporal macula. ASs are also present nasal to the optic disc. **B:** FA + OCT horizontal scan of the right eye: This is a horizontal scan of the area inferior to the CNV. The two red dashed circles both correspond to ASs, as seen in the left FA image. Bending of Bruch's membrane is occurring in the AS area. A SRD is visible. **C:** FA + OCT diagonal scan of the right eye: This is a scan passing through the CNV. We can see that Type 2 CNV is present (➔). Below the CNV, Bruch's membrane is flat without disruption (►). Cystoid spaces are visible in the outer plexiform layer. The granular, highly reflective dots inside the neural retina are either lipid deposits or macrophages that have phagocytized erythrocytes and deposited lipids.

Image interpretation points

This is a case of typical PXE with thick AS. Bending of Bruch's membrane can be seen in the AS site. A PED exists nasal to the the bent Bruch's membrane in the AS site close to the fovea centralis in B. Type 2 CNV is visible in C. While it is typical for Type 2 CNV to occur in this disease, Type 1 CNV can also develop.

Case 139 Pseudoxanthoma elasticum: A case of polypoidal lesions

A 71-year-old male, OD and OS, BCVA 1.5 and 0.7, respectively

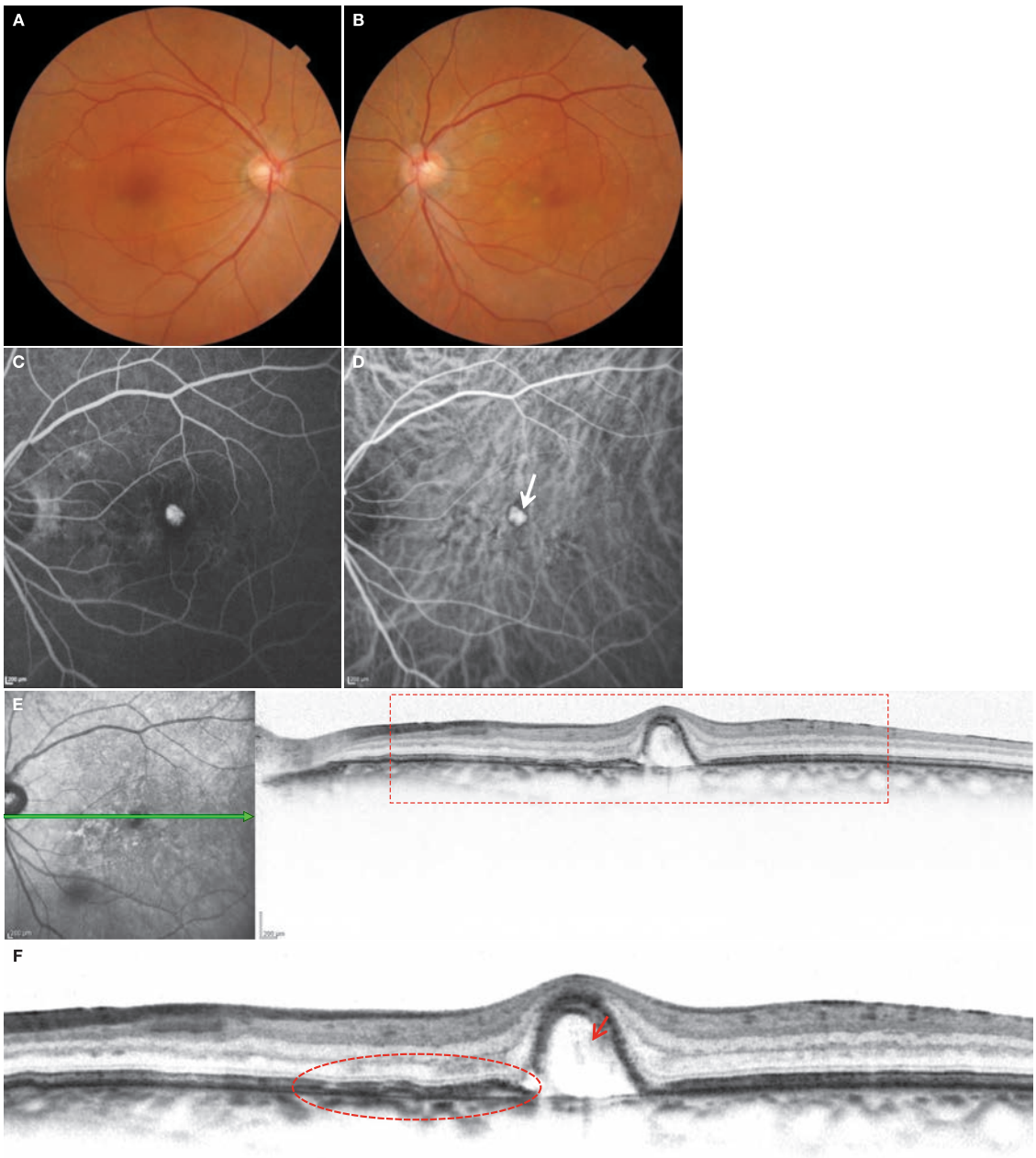

A: Color fundus photograph in the right eye: ASs are visible around the optic disc. **B:** Color fundus photograph in the left eye: ASs are visible, similar to the right eye. **C:** FA in the left eye (42 seconds): A round hyperfluorescent spot is seen superonasal to the fovea centralis. **D:** IA in the left eye (42 seconds): On IA, this appears to be a polypoidal lesion (⇨). An abnormal vascular network is also seen inferonasally. **E:** IR + OCT horizontal scan of the left eye: A RPE protrusion exhibiting a steep elevation is visible. **F:** Enlarged version of E [red dashed box]: Mild reflective lesions are seen within the polypoidal lesion (➔). The RPE on the immediately nasal to the polypoidal lesion is gently sloping away from Bruch's membrane (red dashed circle). This corresponds with the abnormal vascular network.

Image interpretation points

Although rare, PXE can be seen in combination with polypoidal choroidal vasculopathy (PCV). This combination questions the basic pathogenesis of PCV.

Case 140 Pseudoxanthoma elasticum: Outer retinal tubulation

A 54-year-old male, OS, BCVA 0.15

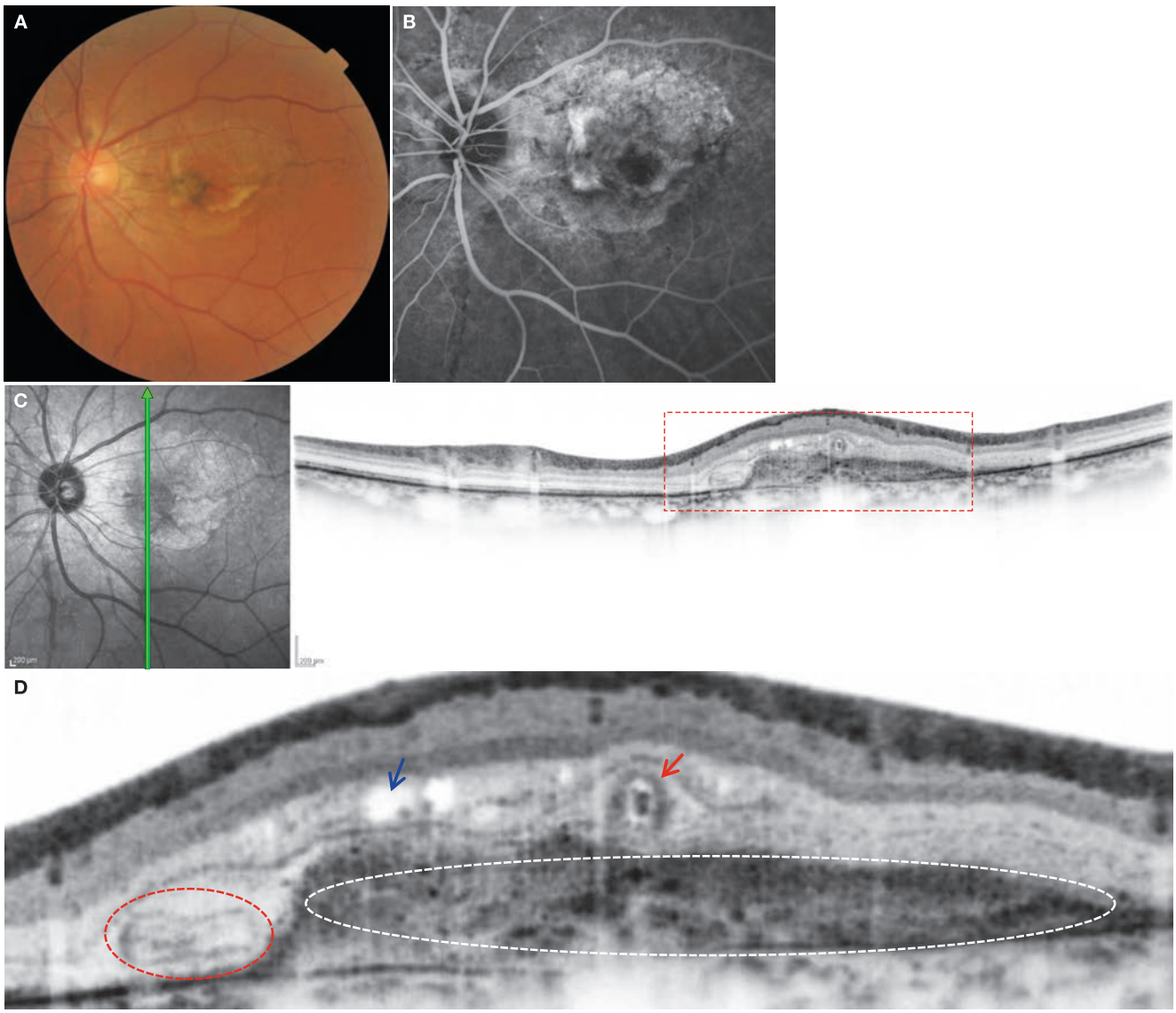

A: Color fundus photograph in the left eye: ASs are visible around the optic disc. CNV with pigmentation can be seen in the fovea. **B:** FA in the left eye (48 seconds): There is a thick rodlike structure exhibiting significant hyperfluorescence nasal to the fovea centralis. **C:** IR + OCT vertical scan of the left eye: Scan of the thick rodlike structure area in B. Type 2 CNV is visible. **D:** Enlarged version of C [red dashed box]: A structure (→) enveloped by a moderately reflective ring known as an outer retinal tubulation is seen between the CNV and outer plexiform layer. Another tubulation cut longitudinally (red dashed circle) is shown nasal to the CNV (white dashed circle). The outer retinal tubulation is often exhibiting a small highly reflective dot in its center. Cystoid spaces (→) are visible in the sensory retina of the CNV.

Image interpretation points

The biological explanation of outer retinal tubulation is unclear. It appears to be a reactive change originating from the RPE or outer retinal layers in which the RPE and photoreceptor cells undergo damage. It may resemble rosettes similar to those seen in retinoblastoma. Outer retinal tubulations have a tubular-shaped structure which exhibit a staining pattern on FA. Refer to the page on crystalline retinopathy (▶ pages 262–264).

7.8 Cancer-associated retinopathy

Background

Cancer-associated retinopathy (CAR)[1] is a relatively rare disease classified as an autoimmune retinopathy. In CAR, autoantibodies to protein expressed in the retina form in the serum of cancer patients and cause damage to the retinal photoreceptor cells.[2] Small cell lung cancer is well known as an underlying disease, and there are also reports citing endometrial cancer and thymoma. The antigen proteins recognized by the autoantibodies are diverse. Since not all patients with CAR have autoantibodies to recoverin, the lack of anti-recoverin antibodies does not exclude the diagnosis of CAR.

Symptoms are progressive and often follow a relatively acute or subacute course, although cases with gradual progression are also encountered.[3] Diagnosis is not straightforward, as antiretinal autoantibodies and progressive retinal degeneration need to be verified. As mentioned above, a negative anti-recoverin antibody test cannot rule out this disease; in these cases, more specific laboratory tests are required to determine the presence or absence of autoantibodies for other retinal antigens. OCT is useful for the verification of retinal degeneration. CAR is unlikely in cases where damage to the outer retinal layers cannot be verified with OCT. Supplementary tests other than OCT include visual field tests (perimetry), attenuation of rod and cone response with ERG, fundus autofluorescence and fluorescein fundus angiography.

OCT findings

OCT findings for CAR vary depending on the stage of disease progression. Thinning of the entire retina is evident in advanced cases. In such cases, evaluation with a retinal thickness map is useful for diagnosis.[4] Damage to the inner retinal layers in the intermediate periphery has also been reported. CME can also be seen, similar to retinitis pigmentosa. There are very few reporting the findings of the inner retinal layers on OCT from early stages of disease. These early cases primarily involve changes in the outer retinal layers, starting with the disappearance of the IS/OS line. The sample size is insufficient to examine the differences with retinitis pigmentosa.

References

1) Sawyer RA, Selhorst JB, Zimmerman LE, et al. Blindness caused by photoreceptor degeneration as a remote effect of cancer. *Am J Ophthalmol*. 1976; 81:606–613.
2) Thirkill CE, Roth AM, Keltner JL. Cancer-associated retinopathy. *Arch Ophthalmol*. 1987; 105:372–375.
3) Saito W, Kase S, Ohguro H, et al. Slowly progressive cancer-associated retinopathy. *Arch Ophthalmol*. 2007; 125:1431–1433.
4) Mohamed Q, Harper CA. Acute optical coherence tomographic findings in cancer-associated retinopathy. *Arch Ophthalmol*. 2007; 125:1132–1133.

Case 141 Cancer-associated retinopathy: Damage to the outer retinal layers

A 77-year-old female, OD, BCVA 1.0

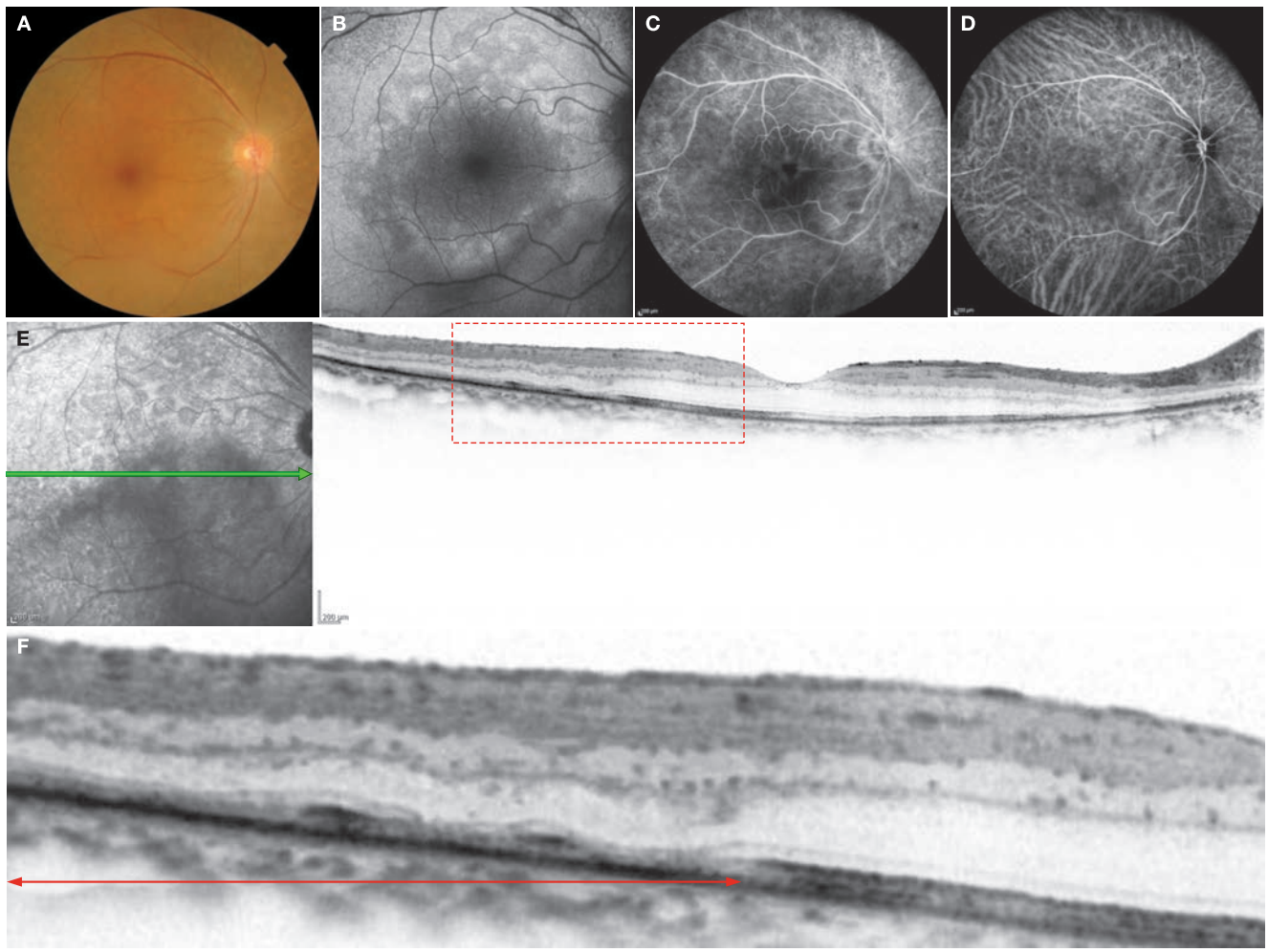

A: Color fundus photograph in the right eye: Narrowing of the retinal artery is evident. The retina around the vascular arcade is pale. **B:** FAF in the right eye: The macular area is hypofluorescent and its surroundings are exhibiting hyperfluorescence. Islets of hypofluorescent foci are visible. **C:** FA in the right eye (40 seconds): Mild fluoroscein leakage is seen from the retinal blood vessels. Choroidal background fluorescence is mottled and has a salt-and-pepper appearance. **D:** IA in the right eye (40 seconds): There are scattered small hypofluorescent spots. **E:** IR + OCT horizontal scan of the right eye: The outer retinal layers in the intermediate periphery are damaged. **F:** Enlarged version of E [red dashed box]: The IS/OS is disrupted and ELM is »bowing« in ⟷. It is unclear whether this is an inherent pattern for this condition or whether these are secondary changes.

Image interpretation points

In this case, the patient had significant bilateral concentric visual field contraction. The diagnosis of CAR was made based on the degeneration of the outer retinal layers evident on OCT.

Case 142 Cancer-associated retinopathy: Retinal vasculitis

A 54-year-old female, OD, BCVA 0.4

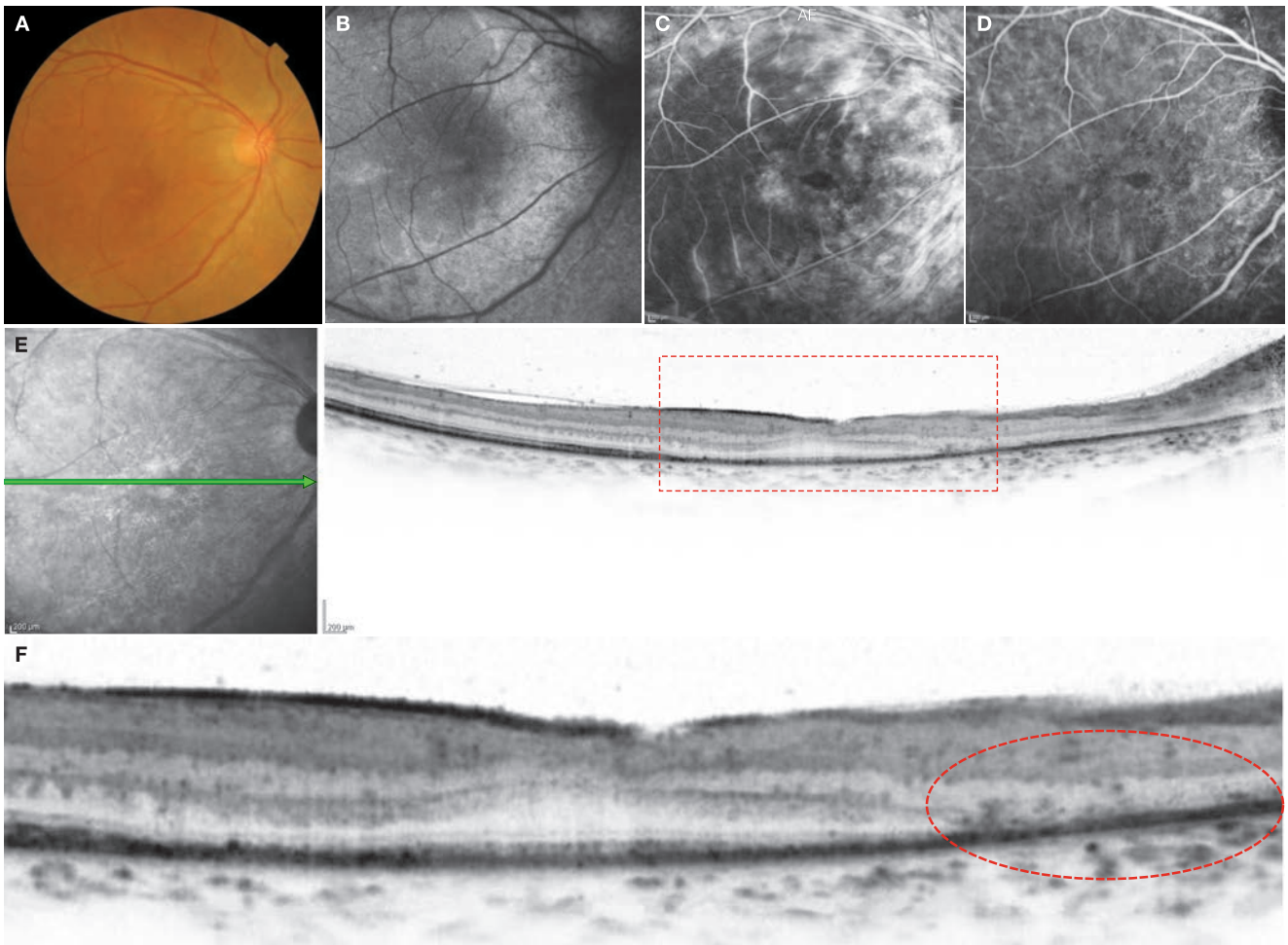

A: Color fundus photograph in the right eye: Retinal hemorrhages are seen immediately superior to the vascular arcade. The fundus is otherwise relatively unremarkable. **B:** FAF in the right eye: Hyperfluorescence is seen along the vascular arcades. **C:** FA in the right eye (47 seconds): Significant fluoroscein leakage from the retinal blood vessels is seen. The area of hyperfluorescence corresponds to the hyperfluorescent area on fundus autofluorescence. The fovea centralis is hypofluorescent. **D:** IA in the right eye (47 seconds): A oblong hypofluorescence in the fovea centralis can be seen on IA. **E:** IR + OCT horizontal scan of right eye: Damage to the outer retinal layers is visible. **F:** Enlarged version of E [red dashed box]: Loss or irregularity of the IS/OS line is seen. The outer nuclear layer and photoreceptor IS/OS are lost nasal to the fovea centralis (red dashed circle).

Image interpretation points

This is a case of CAR in conjunction with retinal vasculitis in a patient with small cell lung cancer.

In this case, testing for anti-recoverin antibodies was positive.

7.9 Bietti crystalline dystrophy

Background

Bietti crystalline dystrophy is a hereditary retinal degenerative disease with an autosomal recessive mode of inheritance discovered by the Italian ophthalmologist Bietti in 1937.[1] Although it can be confused with typical retinitis pigmentosa, this disease is characterized by multiple yellowish-white deposits known as crystalline bodies. These deposits can sometimes be found in the peripheral cornea. These findings allow for a clear diagnosis. In the majority of cases, night blindness and tunnel vision gradually progress between the age of 20 and 50.[2]

The frequency of crystalline dystrophy is known to have an ethnic difference and is seen at a relatively high frequency in Japanese and Chinese people.[2] *CYP4V2* is well known as a causative gene of this disease.[3, 4] This gene product belongs to the cytochrome P450 superfamily and is also associated with lipid metabolism.

OCT findings

There are few reports on the retinal histopathological findings of this disease and there are no established OCT findings. In studies using EDI-OCT, choroidal thickness is thinned significiantly.[5] In our studies, crystalline bodies were mainly seen on the RPE or Bruch's membrane after the RPE had been lost.[6] Typical findings of this disease are round or funicular structures visible in the retinal outer nuclear layer. These structures are thought to be outer retinal layer structures[7] reported as outer retinal tubulations. In our cases, outer retinal tubulation was seen in all cases of crystalline dystrophy.[8]

References

1) Bietti G. Ueber familiares Vorkommen von Retinitis punctata albescence (Verbunden mit»Dystrophia marginalis cristallinea cornea«) . Glitzen des Glaskopers und andeen degenerativen Augenveranderungen. *Klin Mbl Augenhelik*. 1937; 99:737–756.
2) Kaiser-Kupfer MI, Chan CC, Markello TC, et al. Clinical biochemical and pathologic correlations in Bietti's crystalline dystrophy. *Am J Ophthalmol*. 1994; 118:569–582.
3) Li A, Jiao X, Munier FL, et al. Bietti crystalline corneoretinal dystrophy is caused by mutations in the novel gene CYP4V2. *Am J Hum Genet*. 2004; 74:817–826.
4) Lin J, Nishiguchi KM, Nakamura M, et al. Recessive mutations in the CYP4V2 gene in East Asian and Middle Eastern patients with Bietti crystalline corneoretinal dystrophy. *J Med Genet*. 2005; 42:e38.
5) Yeoh J, Rahman W, Chen F, et al. Choroidal imaging in inherited retinal disease using the technique of enhanced depth imaging optical coherence tomography. *Graefes Arch Clin Exp Ophthalmol*. 2010; 248:1719–1728.
6) Pennesi ME, Weleber RG. High-resolution optical coherence tomography shows new aspects of Bietti crystalline retinopathy. *Retina*. 2010; 30:531–532.
7) Zweifel SA, Engelbert M, Laud K, et al. Outer retinal tubulation; a novel optical coherence tomography finding. *Arch Ophthalmol*. 2009; 127:1596–1602.
8) Kojima H, Otani A, Ogino K, et al. Outer retinal circular structures in patients with Bietti crystalline retinopathy. *Br J Ophthalmol*. 2012:in press.

Case 143 Bietti crystalline dystrophy: A typical example

A 53-year-old female with, OS, BCVA 1.5

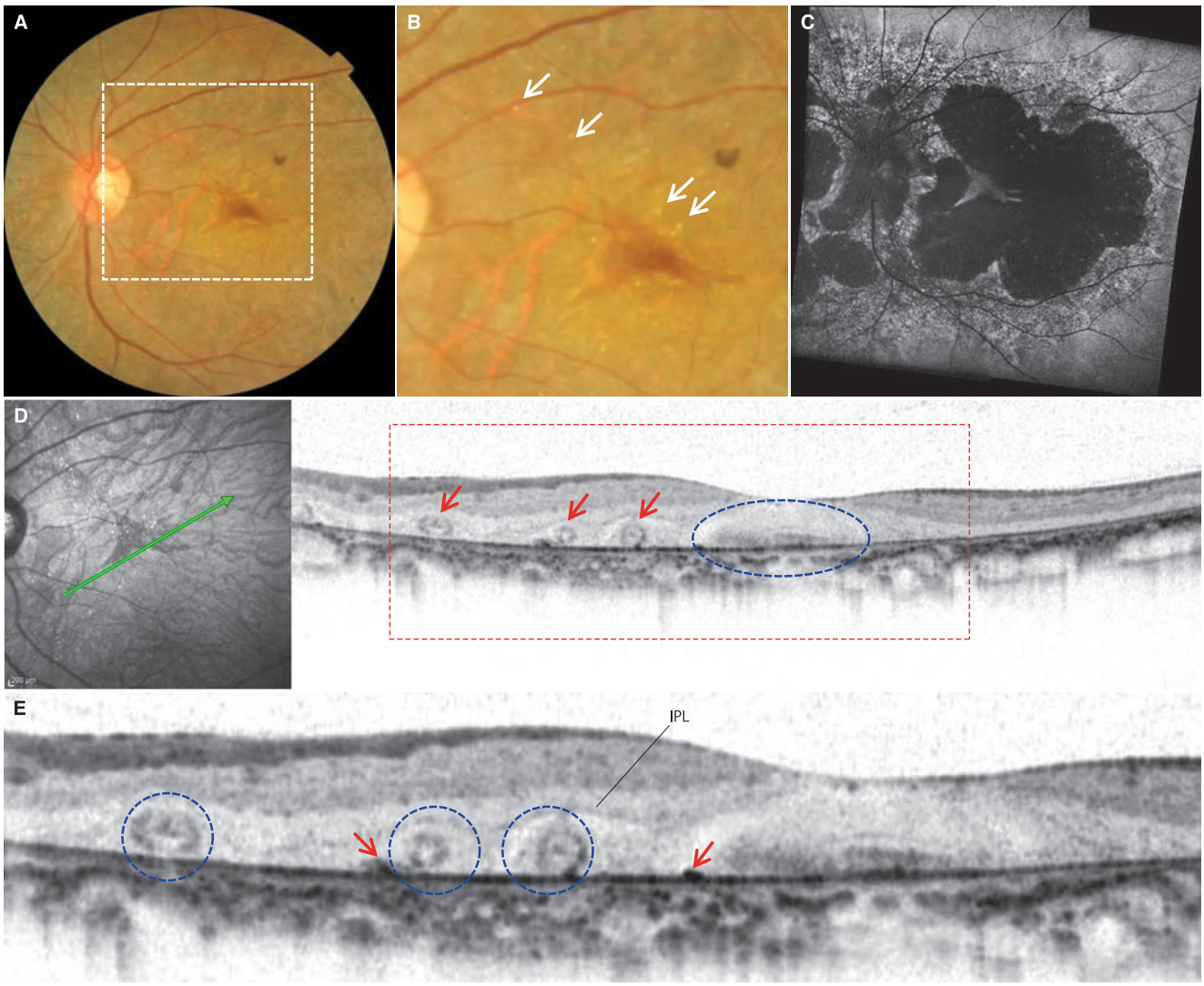

A: Color fundus photograph in the left eye: Extensive degeneration is visible in the posterior pole of the retina. There is no optic disc atrophy and narrowing of the retinal artery is insignificant. **B:** Enlarged version of A [white dashed box]: Small yellowish-white deposits are visible (⇨). The foveal retina is relatively close to normal in color. **C:** FAF in the left eye: A wide area temporal to the fovea centralis is exhibiting hypofluorescence. There is an area of almost normal autofluorescence that corresponds to the foveal area of relatively normal retinal color in the fundus photograph. Around the area of extensive hypofluorescence, there is an mixed appearance of hypofluorescence and normal fluorescence exhibiting in a granular mottled appearance. **D:** IR + OCT oblique scan of the left eye: The ELM and IS/OS lines are partially seen in the fovea centralis (blue dashed circle). Three round or ovoid structures are seen in a line inferonasal to the fovea centralis (→). **E:** Enlarged version of D [red dashed box]: Crystalline bodies appear to be in contact with the anterior aspect of Bruch's membrane after the RPE has shed (→). Round or ovoid structures (outer retinal tubulation) can be seen in the outer nuclear layer (blue dashed circles). There is extensive atrophy and loss of the RPE.

Image interpretation points

There is no significant difference between the degeneration of the outer retinal layers seen in this example and that seen in typical retinal degenerative diseases. Outer retinal tubulation, however, is more commonly found in Bietti crystalline dystrophy. Depending on the direction of the OCT scans, structures in outer retinal tubulation are not round, but elongated. Nevertheless, the structures in this case appeared round or ovoid regardless of the OCT scan, perhaps because they are almost spherical. The basic pathogenesis of these structures is unknown, but they can be seen in various degenerative diseases with variable frequency.

Case 144 Bietti crystalline dystrophy: Outer retinal tubulation

A 42-year-old female, OD, BCVA 0.8

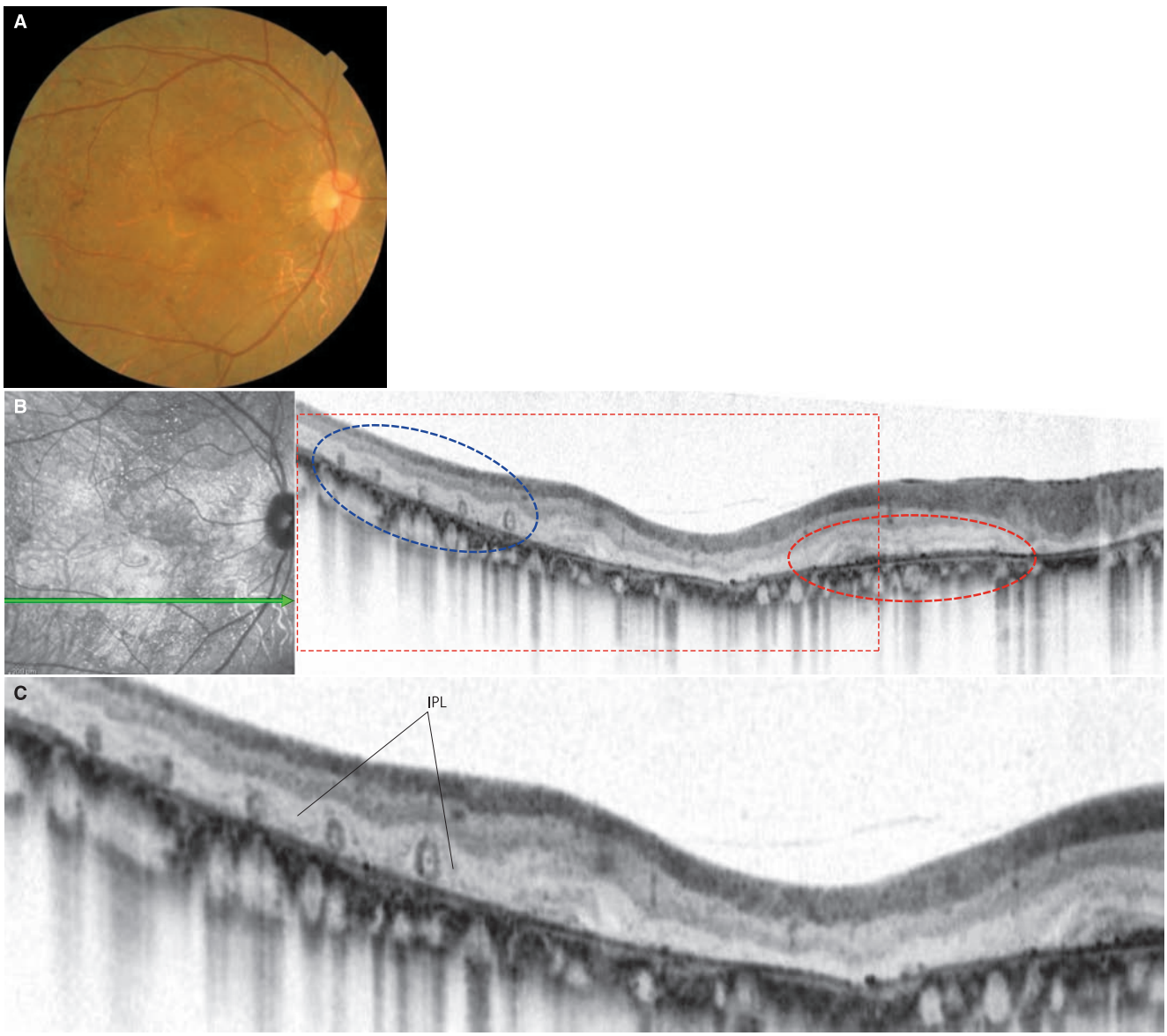

A: Color fundus photograph in the right eye: Extensive degeneration is visible in the posterior pole of the retina. There is no optic disc atrophy and narrowing of the retinal artery is insignificant. Crystalline bodies are unremarkable. **B:** IR + subfoveal OCT horizontal scan of the right eye: The RPE is lost extensively and Bruch's membrane is seen. The RPE is partially visible in the area of the red dashed circle. The ELM is also depicted with an irregular pattern in this area. Cross-sections of outer retinal tubulation are lined up consecutively in the area indicated by the blue dashed circle. The reflectivity immediately beneath the RPE representing choriocapillaris is not seen, indicating loss of choriocapillaris. **C:** Enlarged version of B [red dashed box]: Damages in the outer retinal layers and loss of the RPE is evident. Outer retinal tubulation is present in the outer nuclear layer as well.

Image interpretation points

When examined closely, small, a highly reflective punctiform structures can be seen in the center of the outer retinal tubulation. While it is unclear what these represent, they may be similar to retinal rosette formations.

7.10 Retinitis pigmentosa

Background

Retinitis pigmentosa (RP) is a collective term for diseases that cause hereditary and progressive degeneration of the photoreceptor cells (rods are damaged first) and the RPE. One in every 4,000 suffers from RP. Frequent symptoms include night blindness, dark adaptation impairment and photophobia. As it progresses, tunnel vision typically advances from the intermediate periphery to the periphery, eventually leading to loss of central vision.

The mode of inheritance is typically divided into autosomal dominant, autosomal recessive, sex-linked, digenic and sporadic. In Japan, there are a few cases of RP exhibiting a dominant mode of inheritance, but autosomal recessive inheritance and sporadic cases account for the majority. Cases that exhibit systemic symptoms in addition to ocular fundus abnormalities have specific disease names (e.g. Usher syndrome).

It is well known that mutations in rhodopsin and peripherin induce RP. However, as mentioned above, there are few cases in Japan that exhibit a dominant inheritance and less information is available on RP mutations in the Japanese.

OCT findings

Reports on the retinal nerve fiber layer (RNFL) thickness in RP vary considerably.[1–3] Originally, thinning of the RNFL was reported; however, subsequent studies cite thickening of the RNFL using SD-OCT. In comparison, there was no significant difference between the thickness of the retinal ganglion cell layer in eyes with RP and normal eyes.[3] The cause of RNFL thickening is unclear, although the proliferation of retinal glial cells is thought to be a factor.[2]

CME is also frequently seen in RP. There are significant differences in the rate of detection depending on the type of OCT and imaging method used, with detection rates as low as 10%[4, 5] and as high as 40%.[6] One report states that there is no significant correlation between the frequency of detection of CME and mode of inheritance,[6] while another report of high frequency of CME in cases of dominant inheritance is available.[7] Another report claims that examining whether or not the IS/OS is depicted is better correlated with visual acuity than examining the spread of CME horizontally or vertically on OCT.[8] There does not appear to be a strong correlation between the presence or absence of CME and visual function in RP patients.

Epiretinal membranes (ERM) and vitreomacular traction syndromes are seen at a high frequency in RP. Figures are diverse; one report claims to have seen ERMs in 64.3% of cases[9] while another claims it occurs in less than 1%.[3]

The basic pathology of RP is apoptosis of the photoreceptor cells.[10] Retinal degeneration starts from the intermediate periphery since apoptosis of the rods precedes apoptosis of the cones. As a result, changes in the outer retinal layers in the intermediate periphery occur first on OCT where the IS/OS line can no longer be detected.

The RPE undergoes reactive changes and partial migration of reactive RPE cells can be seen towards the inner sensory retina. The retinal structure near the fovea centralis is often relatively well preserved. In contrast in cone dystrophy, the retinal structure of the intermediate periphery is often well preserved since degeneration starts near the fovea centralis. Thus, OCT images of both diseases show opposing findings. Hood et al. studied OCT findings for boundaries between areas of RP degeneration and relatively healthy areas, and noted that damage to the photoreceptor outer segment occurs first, followed by thinning of the outer nuclear layer and outer plexiform layer. There is continued loss of the photoreceptor outer segment, finally resulting in further thinning of the outer nuclear layer and outer plexiform layer.[11] As expected, foveal retinal thickness and visual acuity are strongly correlated.[12]

There are many reports on comparisons between photoreceptor damage as detected on OCT and visual function or other test findings such as with FAF testing. One report found that OCT findings and visual function were strongly correlated upon examining macular OCT features of RP patients divided into normal, CME, vitreoretinal traction syndrome, and macular atrophy groups.[13] The depiction of the IS/OS on OCT is also strongly correlated with visual function.[14, 15] A comparison of IS/OS findings, FAF and visual field tests suggested that there were multiple patterns that could represent the progression of visual dysfunction in RP.[16]

References

1) Walia S, Fishman GA, Edward DP, et al. Retinal nerve fiber layer defects in RP patients. *Invest Ophthalmol Vis Sci.* 2007; 48:4748–4752.
2) Walia S, Fishman GA. Retinal nerve fiber layer analysis in RP patients using Fourier-domain OCT. *Invest Ophthalmol Vis Sci*. 2008; 49:3525–3528.
3) Hood RC, Lin CE, Lazow MA, et al. Thickness of receptor and post-receptor retinal layers in patients with retinitis pigmentosa measured with frequency-domain optical coherence tomography. *Invest Ophthalmol Vis Sci*. 2009; 50:2328–2336.
4) Hagiwara A, Yamamoto S, Ogata K, et al. Macular abnormalities in patients with retinitis pigmentosa: prevalence on OCT examination and outcomes of vitreoretinal surgery. *Acta Ophthalmol*. 2011; 89:e122–125.
5) Hirakawa H, Iijima H, Gohdo T, et al. Optical coherence tomography of cystoid macular edema associated with retinitis pigmentosa. *Am J Ophthalmol*. 1999; 128:185–191.
6) Hajali M, Fishman GA, Anderson RJ. The prevalence of cystoid macular oedema in retinitis pigmentosa patients determined by optical coherence tomography. *Br J Ophthalmol*. 2008; 92:1065–1068.
7) Sandberg MA, Brockhurst RJ, Gaudio AR, et al. Visual acuity is related to parafoveal retinal thickness in patients with retinitis pigmentosa and macular cysts. *Invest Ophthalmol Vis Sci*. 2008; 49:4568–4572.
8) Oishi A, Otani A, Sasahara M, et al. Photoreceptor integrity and visual acuity in cystoid macular oedema associated with retinitis pigmentosa. *Eye* (*Lond*) . 2009; 23:1411–1416.
9) Grigoropoulos VG, Emfietzoglou J, Nikolaidis P, et al. Optical coherence tomography findings in patients with retinitis pigmentosa and low visual acuity. *Ophthalmic Surg Lasers Imaging*. 2010; 41:35–39.
10) Adler R. Mechanisms of photoreceptor death in retinal degenerations. From the cell biology of the 1990s to the ophthalmology of the 21st century? *Arch Ophthalmol*. 1996; 114:79–83. Review.
11) Hood DC, Lazow MA, Locke KG, et al. The transition zone between healthy and diseased retina in patients with retinitis pigmentosa. *Invest Ophthalmol Vis Sci*. 2011; 52:101–108.
12) Sandberg MA, Brockhurst RJ, Gaudio AR, et al. The association between visual acuity and central retinal thickness in retinitis pigmentosa. *Invest Ophthalmol Vis Sci.* 2005; 46:3349–3354.
13) Aleman TS, Cideciyan AV, Sumaroka A, et al. Retinal laminar architecture in human retinitis pigmentosa caused by Rhodopsin gene mutations. *Invest Ophthalmol Vis Sci*. 2008; 49:1580–1590.
14) Aizawa S, Mitamura Y, Baba T, et al. Correlation between visual function and photoreceptor inner/outer segment junction in patients with retinitis pigmentosa. *Eye* (*Lond*) . 2009; 23:304–308.
15) Oishi A, Nakamura H, Tatsumi I, et al. Optical coherence tomographic pattern and focal electroretinogram in patients with retinitis pigmentosa. *Eye* (*Lond*) . 2009; 23:299–303.
16) Murakami T, Akimoto M, Ooto S, et al. Association between abnormal autofluorescence and photoreceptor disorganization in retinitis pigmentosa. *Am J Ophthalmol*. 2008; 145:687–694.

Case 145 Retinitis pigmentosa: A typical example

A 45-year-old male, OD, BCVA 1.0

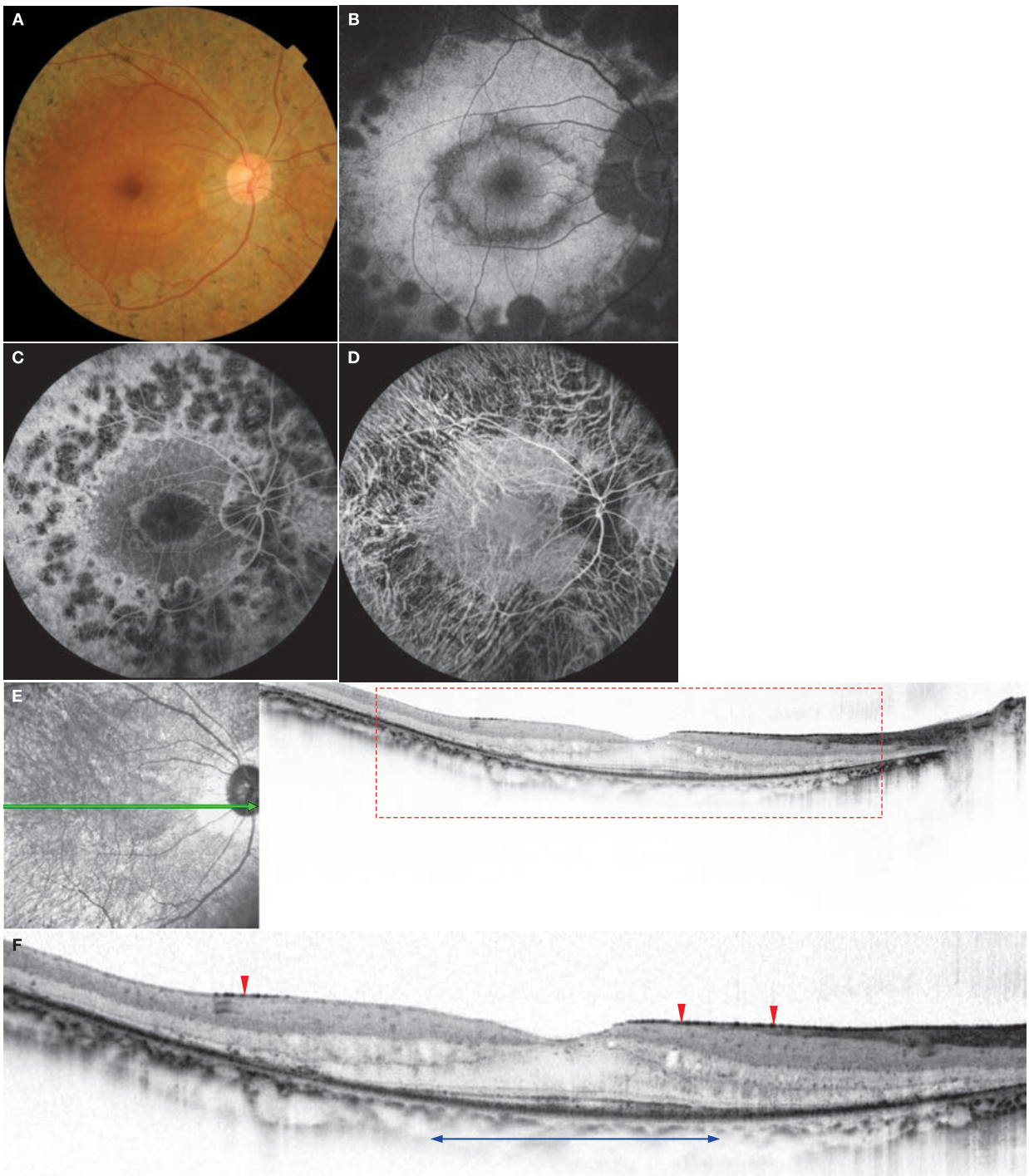

A: Color fundus photograph: The optic disc normal in color. The retinal arteries are narrowed. Degeneration is apparent peripheral to the vascular arcade. Bone spicule pigmentation is also present. **B:** FAF in the right eye: Annular hypofluorescence is visible around the fovea centralis. Autofluorescence is increasing around the fovea centralis. **C:** FA in the right eye (2 minutes, 5 seconds): The fovea centralis is exhibiting significant hypofluorescence and there is a slightly hypofluorescent area surrounding it. Multiple, relatively large, patchy hypofluorescent foci are visible peripheral to the vascular arcade. **D:** IA in the right eye (2 minutes, 5 seconds): The large choroidal vessels are clearly seen in the area of retinal atrophy peripheral to the vascular arcade. Choroidal background fluorescence appears almost normal where the retinal color is also normal. **E:** IR + OCT horizontal scan of the right eye: The structure of the fovea is almost normal. **F:** Enlarged version of E [red dashed box]: Small cystoid spaces are visible near the fovea. The outer retinal layer structure is relatively well preserved in the area indicated by ◄►. The outer retinal layer structure peripheral to this area is damaged. Best-corrected visual acuity is good at 1.0 since the foveal structure is maintained. ► indicates mild ERM.

(Continued on the next page)

Case 145 Continuation

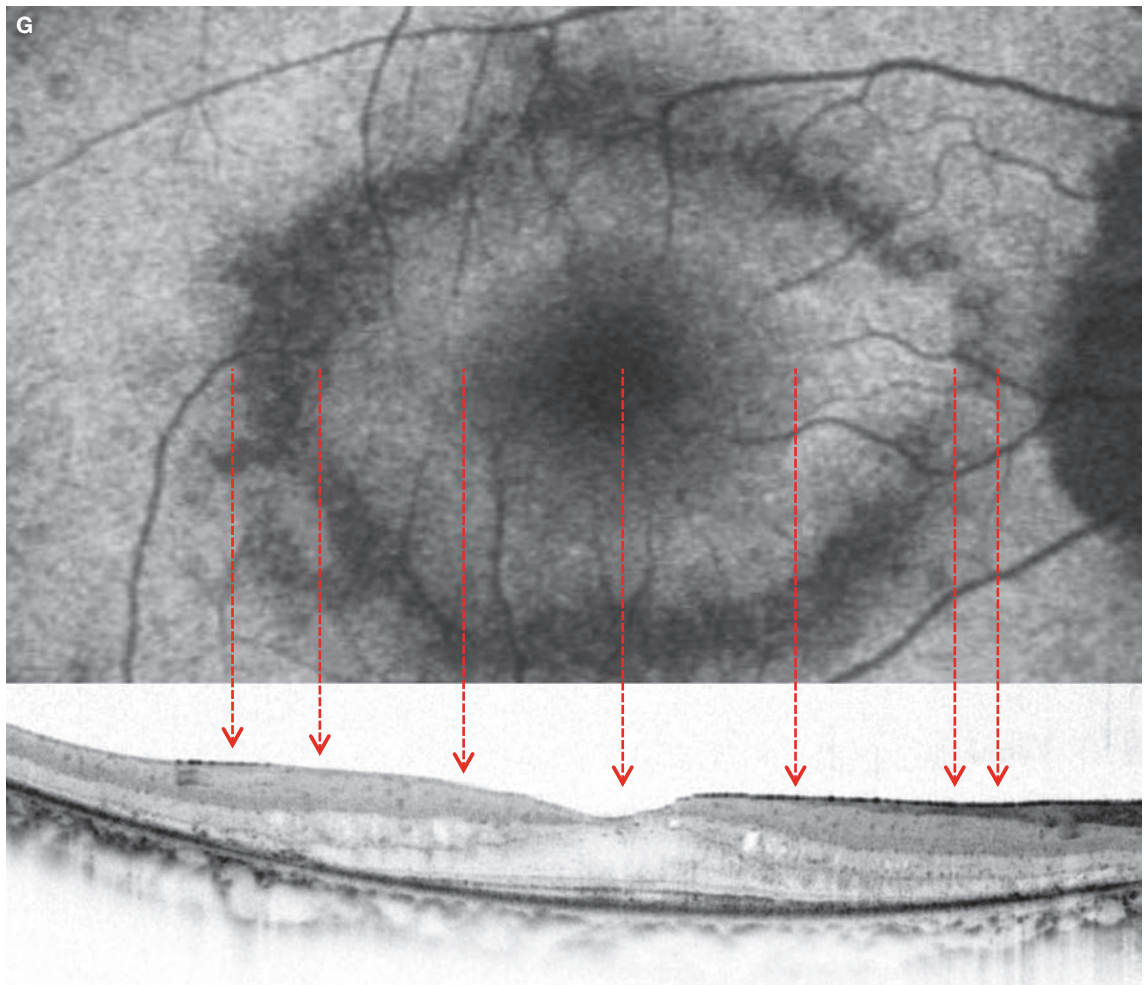

G: FAF and corresponding OCT horizontal scan in the right eye: Comparison of FAF and OCT images. On the FAF, the fovea centralis is exhibiting relatively intense hypofluorescence. Around this, there is a region of weaker hypofluorescence. Mild hyperfluorescence surrounds this region which is itself surrounded by another region of hypofluorescence forming a ring-shape. The area outside the annular hypofluorescence shows hyperfluorescence. On OCT, the RPE and outer retinal layer structure is relatively well preserved in the hypofluorescent area near the fovea centralis. The RPE is also fairly well preserved in the hyperfluorescent area around this, but neither the ELM nor the IS/OS are visible. Damage to the RPE appears severe (particularly temporally), looking as if it is »fuzzy«, in the hypofluorescent ring area around this. In addition, only a small part of the outer nuclear layer appears to be remaining. The outer retinal layer structure has completely disappeared even further peripherally. RPE reflectivity appears normal at first glance.

Image interpretation points

This is a typical case of RP. There is damage to the outer retinal layers in the periphery and the structure near the fovea centralis is relatively well preserved. Interestingly, there are characteristic RPE abnormalities between these areas. Good correspondence between FAF and OCT images provides important information.

Case 146 Retinitis pigmentosa: Cystoid macular edema

A 18-year-old male, OD, BCVA 0.6

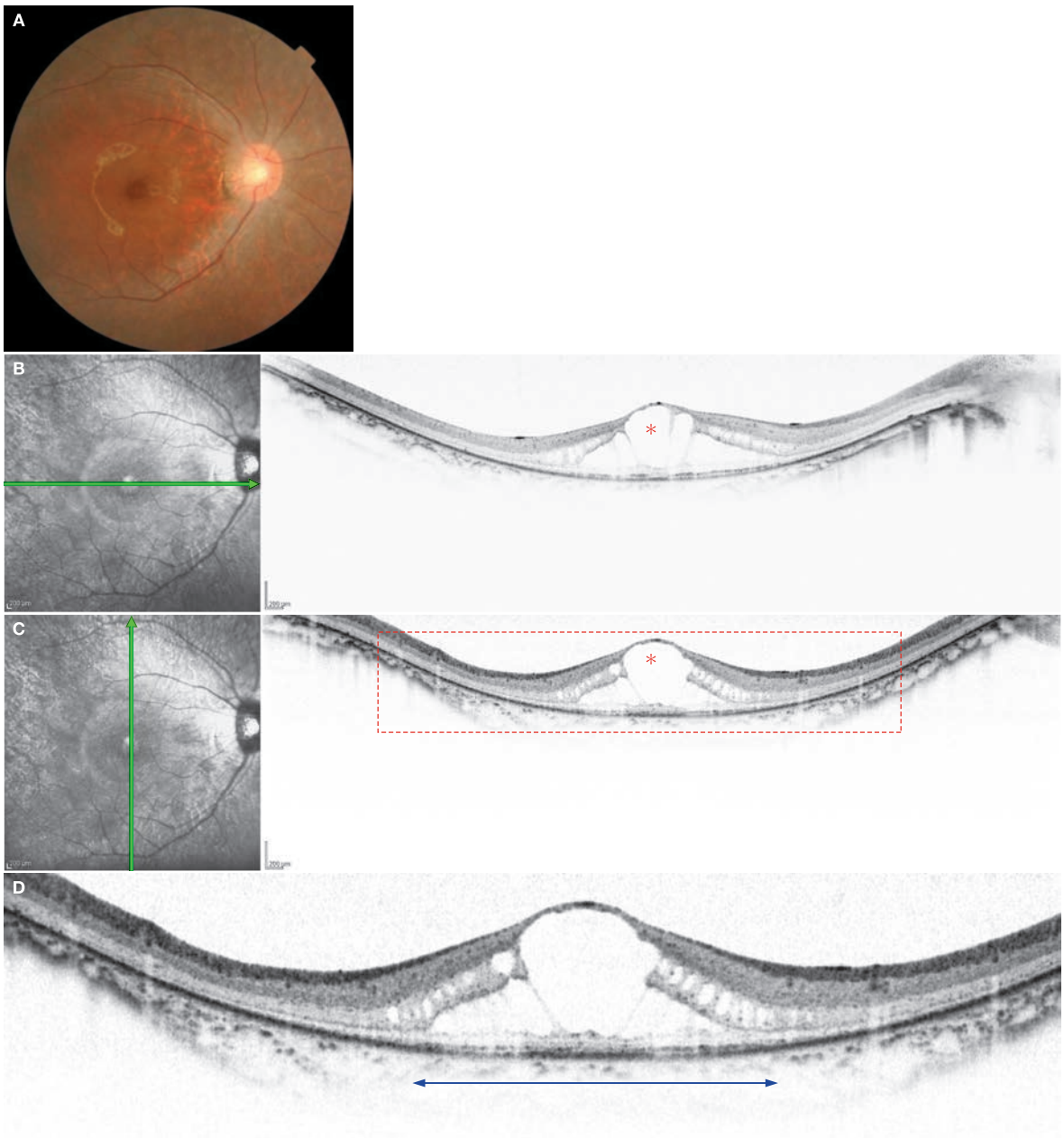

A: Color fundus photograph in the right eye: A fundus reflex unique to young people is apparent. The color of the macula is relatively normal, but the the area peripheral to the vascular arcades is degenerative and exhibiting a grey appearance. **B:** IR + OCT horizontal scan of the right eye: A large cystoid space (*) is visible in the fovea centralis. **C:** IR + OCT vertical scan of the right eye: A large cystoid space (*) is also noticeable in the fovea centralis in this vertical scan. Cystoid spaces are seen side by side in the inner nuclear layer and outer plexiform layer peripheral to the large cystoid space. **D:** Enlarged version of B [red dashed box]: The ELM and IS/OS, although indistinct, are seen in the foveal outer retinal layers (↔). There is significant damage to the outer retinal layers outside of this area, and the IS/OS line cannot be seen. The retinal nerve fiber layer is preserved.

Image interpretation points

This is a case of RP in a relatively young patient. A large cystoid space is seen in the fovea centralis. Damage to the outer retinal layers is more pronounced peripheral to the vascular arcades and, although the outer plexiform layer is visible, the IS/OS line is not seen. Since this is a young patient, an ERM is not visible. The RNFL is well preserved, although retinal nerve fiber layer can reportedly be thicker than normal in RP.

Case 147 Retinitis pigmentosa: Vitreomacular traction syndrome

A 57-year-old female, OD, BCVA 0.3

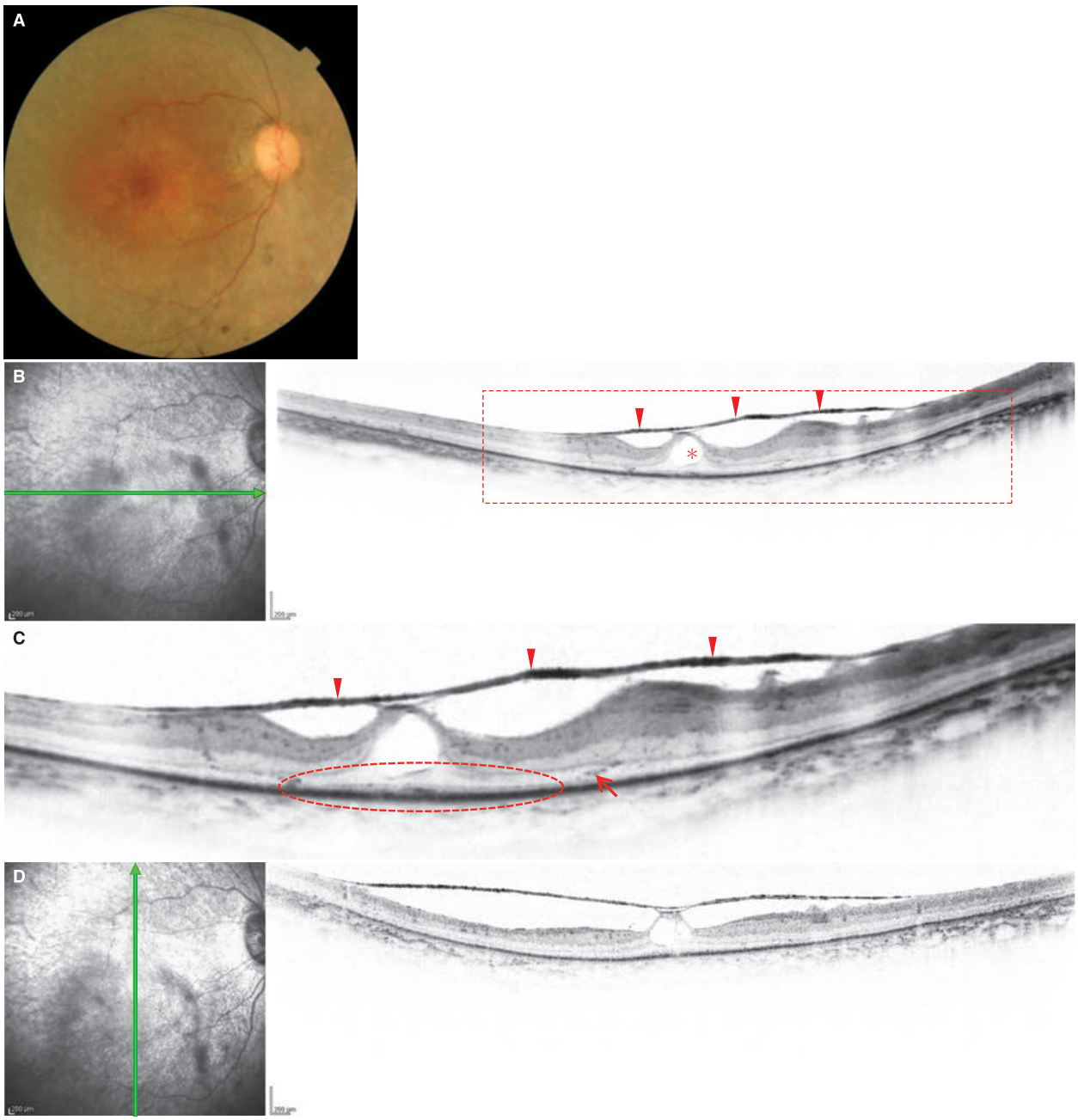

A: Color fundus photograph in the right eye: The optic disc is pale and there is significant narrowing of the retinal arteries. The color of the macular retina is relatively normal. Degeneration is apparent in the area peripheral to the vascular arcades. Bone spicule pigmentation is present inferior to the vascular arcades. **B:** IR + OCT horizontal scan of the right eye: The fovea centralis is elevated as a result of the traction by the considerably thickened posterior vitreous cortex (▶). Cystoid spaces can be seen in the fovea centralis (✻). **C:** Enlarged version of B [red dashed box]: The ELM and partially remaining IS/OS are visible in the fovea centralis (red dashed circle). The outer retinal layer structure peripheral to the fovea centralis has almost disappeared. Small highly reflective dots are visible in the outer nuclear layer, which may be derived from the RPE (➔). **D:** IR + OCT vertical scan of the right eye: Traction to the fovea is clearly visible.

Image interpretation points

This is a case of RP in conjunction with vitreomacular traction syndrome. A thickened posterior vitreous cortex is a typical feature. These findings are common in older patients. There is limited information available on the outcomes of vitreous surgery in these cases.

7.11 Fundus albipunctatus

Background

Fundus albipunctatus is a disease that exhibits an autosomal recessive mode of inheritance and was first reported by Lauber.[1] Typical ophthalmoscopic findings include white dots visible from the posterior pole to the intermediate periphery of the fundus. This disease typically involves stationary night blindness with electrophysiological abnormalities in both rods and cones in the setting of good visual acuity. This disease has been classified as stationary night blindness; however, cases of progressive visual dysfunction have been reported in recent years.[2]

Mutations in retinol dehydrogenase (*RDH5*) are known to be a cause of fundus albipunctatus.[3] Currently, at least 25 mutations have been reported. The majority of these reports come from Japan, where this disease is frequently seen in Japanese people. *RPE65* is also reported as a causative gene.[4]

OCT findings

There are a number of miscellaneous reports on spectral-domain OCT findings.[5–8] The white dots in the ocular fundus tend to become less noticeable as the disease stage progresses and OCT findings may change in accordance with this. Nevertheless, there are only a few reports that have conducted detailed follow-ups of multiple cases. The white dots can be seen as protruding, dome-shaped, highly reflective structures extending from Bruch's membrane to the ELM. They can sometimes be accompanied by cone dystrophy and a decrease in foveal thickness. In addition, highly reflective deposits are visible posterior to the ELM in elderly patients as well as loss of the photoreceptor outer segment.

References

1) Lauber H. Die sogenannter retinitis punctata albescens. *Klin Monatsbl Augenheilkd*. 1910; 48:133–148.
2) Niwa Y, Kondo M, Ueno S, et al. Cone and rod dysfunction in fundus albipunctatus with RDH5 mutation: an electrophysiological study. *Invest Ophthalmol Vis Sci*. 2005; 46:1480–1485.
3) Yamamoto H, Simon A, Eriksson U, et al. Mutations in the gene encoding 11-cis retinol dehydrogenase cause delayed dark adaptation and fundus albipunctatus. *Nat Genet*. 1999; 22:188–191.
4) Schatz P, Preising M, Lorenz B, et al. Fundus albipunctatus associated with compound heterozygous mutations in RPE65. *Ophthalmology*. 2011; 118:888–894.
5) Querques G, Carrillo P, Querques L, et al. High-definition optical coherence tomographic visualization of photoreceptor layer and retinal flecks in fundus albipunctatus associated with cone dystrophy. *Arch Ophthalmol*. 2009; 127:703–706.
6) Schatz P, Preising M, Lorenz B, et al. Lack of autofluorescence in fundus albipunctatus associated with mutations in RDH5. *Retina*. 2010; 30:1704–1713.
7) Genead MA, Fishman GA, Lindeman M. Spectral-domain optical coherence tomography and fundus autofluorescence characteristics in patients with fundus albipunctatus and retinitis punctata albescens. *Ophthalmic Genet*. 2010; 31:66–72.
8) Sergouniotis PI, Sohn EH, Li Z, et al. Phenotypic variability in RDH5 retinopathy (Fundus Albipunctatus) . *Ophthalmology*. 2011 ; 118 : 1661–1670.

Case 148 Fundus albipunctatus: A typical example

An 18-year-old female, OD, BCVA 0.9

A: Color fundus photograph in the right eye: Although unremarkable in the macula, characteristic white dots are visible peripheral to the vascular arcades and nasal to the optic disc. **B:** Enlarged version of A [white dashed box]: White dots are clearly visible. **C:** IR + OCT vertical scan of the right eye: This is a scan passing through the fovea centralis. The IS/OS in the fovea centralis is disrupted. **D:** Enlarged version of C [red dashed box]: Disruption in the IS/OS of the fovea centralis is clearly visible. Faint highly reflective images are present in the foveal ELM, which appears to be changes that have occurred as a consequence of photoreceptor cell loss. The IS/OS line exhibits the same thickness as the RPE.

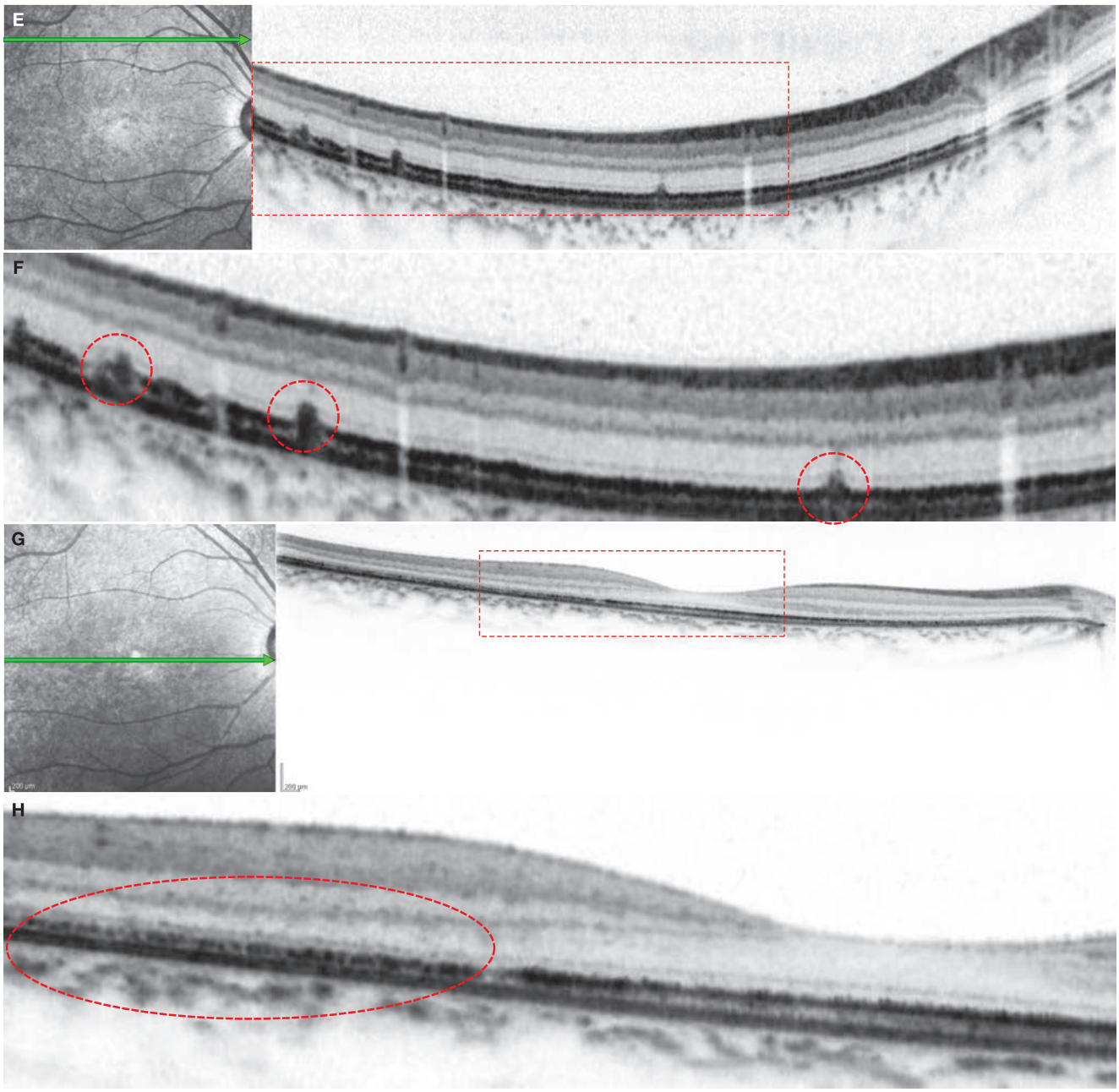

E: IR + OCT horizontal scan of the right eye: This is a horizontal scan superior to the fovea centralis. Highly reflective structures extending from the RPE to the ELM are seen to partially penetrate the ELM. Small, highly reflective dots are visible in the outer nuclear layer immediately anterior to these structures. **F:** Enlarged version of E [red dashed box]: The highly reflective structures appear to be extending to just inside the ELM (red dashed circle). **G:** IR + OCT horizontal scan of the right eye: This is a scan passing through the area immediately above the fovea centralis. No IS/OS defects are evident in this image. **H:** Enlarged version of G [red dashed box]: The IS/OS line temporal to the fovea centralis is depicted as a discontinuous line (red dashed circle)

Image interpretation points

This case presents OCT findings typical of fundus albipunctatus. The white dots are described as dome-shaped, highly reflective structures that appear to pass through the ELM from the RPE level or Bruch's membrane. However, upon closer observation these structures do not appear to be in contact with the RPE. The poorly visible COST and IS/OS lines may be a characteristic of fundus albipunctatus, but further study of multiple cases is required to confirm this. A comparison study with the *RDH5* mutation is, of course, necessary.

7.12 Oguchi disease

Background

Oguchi disease is a disease first reported by Chuta Oguchi in 1907.[1] It exhibits a typical retinal color expressed as a »golden sheen«, which can be restored to its normal color through prolonged dark adaptation (Mizuo-Nakamura phenomenon). Oguchi disease is a type of congenital stationary night blindness that exhibits an autosomal recessive mode of inheritance where mutations of arrestin (SAG)[2] and rhodopsin kinase (GRK1)[3] are reportedly associated with the onset of this disease. Arrestin and rhodopsin kinase are proteins that act to render activated rhodopsin inactive. In Oguchi disease, the activity of these proteins is decreased causing the rhodopsin present in the rod outer segments to remain active. As a result, a prolonged time course is required for dark adaptation of the rods.[4] Historically, Oguchi disease has been classified as stationary night blindness; however, there are cases where progressive tunnel vision and cone dysfunction is seen.[5]

OCT findings

Very little information has been available on OCT findings for Oguchi disease. There are three studies from Japan; however, each only reports one case. According to these reports, the parafoveal IS/OS line becomes clearly visible when the Mizuo-Nakamura phenomenon occurs[6] and the photoreceptor outer segment is shortened in the area where a golden sheen fundus reflex is visible.[7] In this area, the IS/OS line, COST line, and RPE line are depicted as a highly reflective thick line in bright conditions and the fused 3 lines becomes separated into three lines when the Mizuo-Nakamura phenomenon occurs.[8]

References

1) Oguchi C. Types of night blindness. *Japanese Journal of Ophthalmology* 1907; 11: 123–134.
2) Fuchs S, Nakazawa M, Maw M, et al. A homozygous 1-base pair deletion in the arrestin gene is a frequent cause of Oguchi disease in Japanese. *Nat Genet*. 1995; 10:360–362.
3) Yamamoto S, Sippel KC, Berson E, et al. Defects in the rhodopsin kinase gene in the Oguchi form of stationary night blindness. *Nat Genet*. 1997; 15:175–178.
4) Dryja TP. Molecular genetics of Oguchi disease, Fundus albipunctatus, and other forms of stationary night blindness: LVII Edward Jackson Memorial Lecture. *Am J Ophthalmol*. 2000; 130:547–563.
5) Hayashi T, Gekka T, Takeuchi T, et al. A novel homozygous GRK1 mutation (P391H) in 2 siblings with Oguchi disease with markedly reduced cone responses. *Ophthalmology*. 2007; 114:134–141.
6) Yamada K, Motomura Y, Matsumoto CS, et al. Optical coherence tomographic evaluation of the outer retinal architecture in Oguchi disease. *Jpn J Ophthalmol*. 2009; 53:449–451.
7) Hashimoto H, Kishi S. Shortening of the rod outer segment in Oguchi disease. *Graefes Arch Clin Exp Ophthalmol*. 2009; 247:1561–1563.
8) Takada M, Otani A, Ogino K, et al. Spectral-domain optical coherence tomography findings in the Mizuo-Nakamura Phenomenon of Oguchi disease. *Retina*. 2011; 31:626–628.

Case 149 Oguchi disease: A typical example

A 51-year-old male, OD, BCVA 1.2

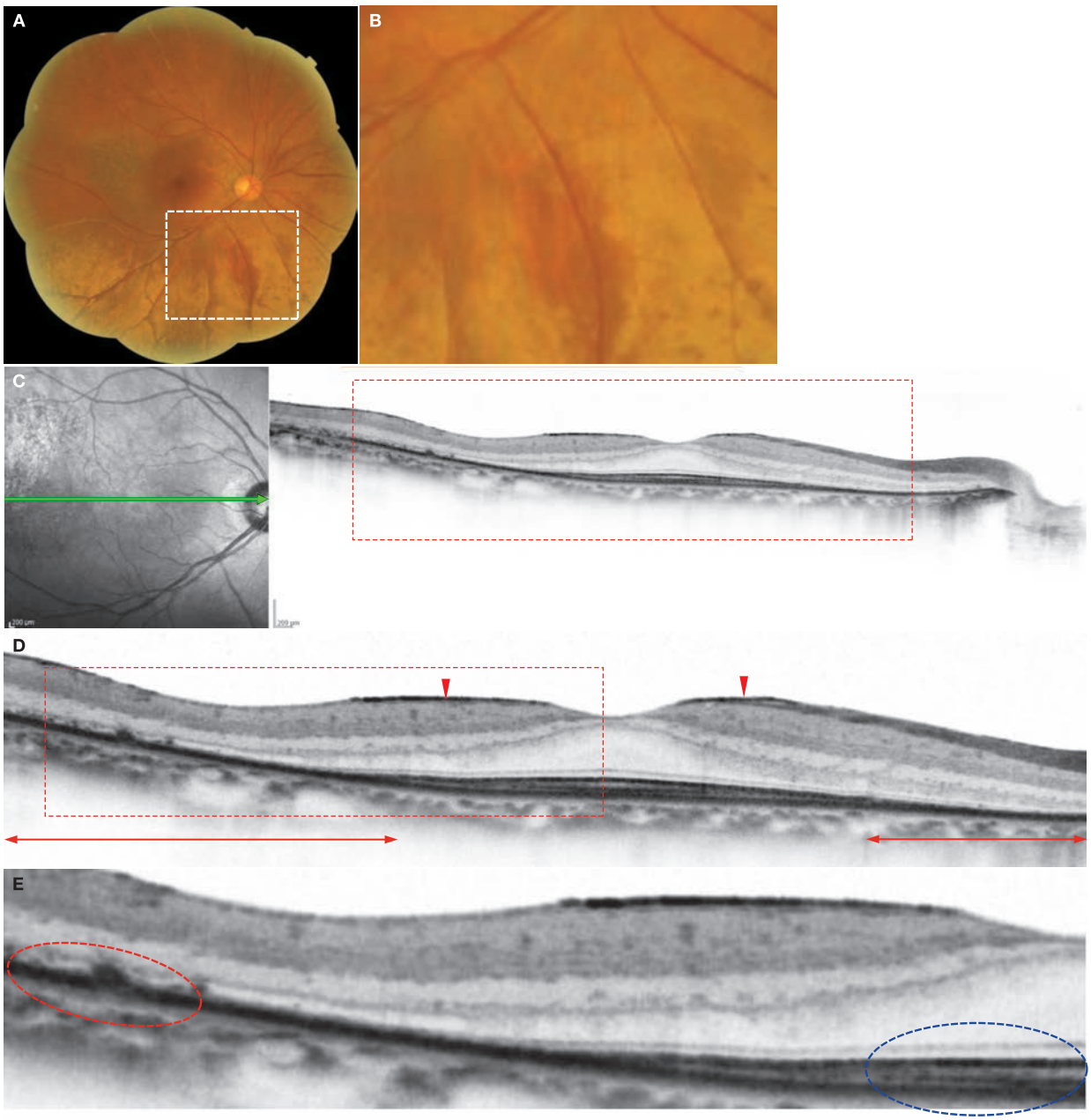

A: Color fundus photograph in the right eye: A golden sheen fundus reflex is visible in the inferior retina. **B:** Enlarged version of A [white dashed box]: We can see the golden sheen appearance and normal retinal color around the blood vessels. **C:** IR + OCT horizontal scan of the right eye: Foveal retinal thickness is preserved, but thinning is evident in the outer retinal layers both temporally and near the optic nerve. **D:** Enlarged version of C [red dashed box]: The retinal structure near the fovea centralis appears normal. A thin ERM is visible (►). The ELM and IS/OS are indistinct in the peripheral areas indicated by ◄►. **E:** Enlarged version of D [red dashed box]: The outer retinal layer structure near the fovea centralis including the ELM, IS/OS and COST lines appears almost normal (blue dashed circle). Temporally, the ELM is approaching to the RPE, the IS/OS line is disappearing, and the outer nuclear layer is thinning and is almost completely lost at the most temporal area (red dashed circle).

Image interpretation points

There are only a few reports on SD-OCT findings in Oguchi disease. While the macular structure is preserved in this case, there is thinning of the ELM, IS/OS, and COST lines in the periphery of the macula. Even further peripherally, RPE stratification and disappearance of the outer nuclear layer is observed.

Case 150 Oguchi disease: Cystoid space formation and golden sheen fundus reflex (fellow eye of case 149)

A 51-year-old male, OS, BCVA 1.0

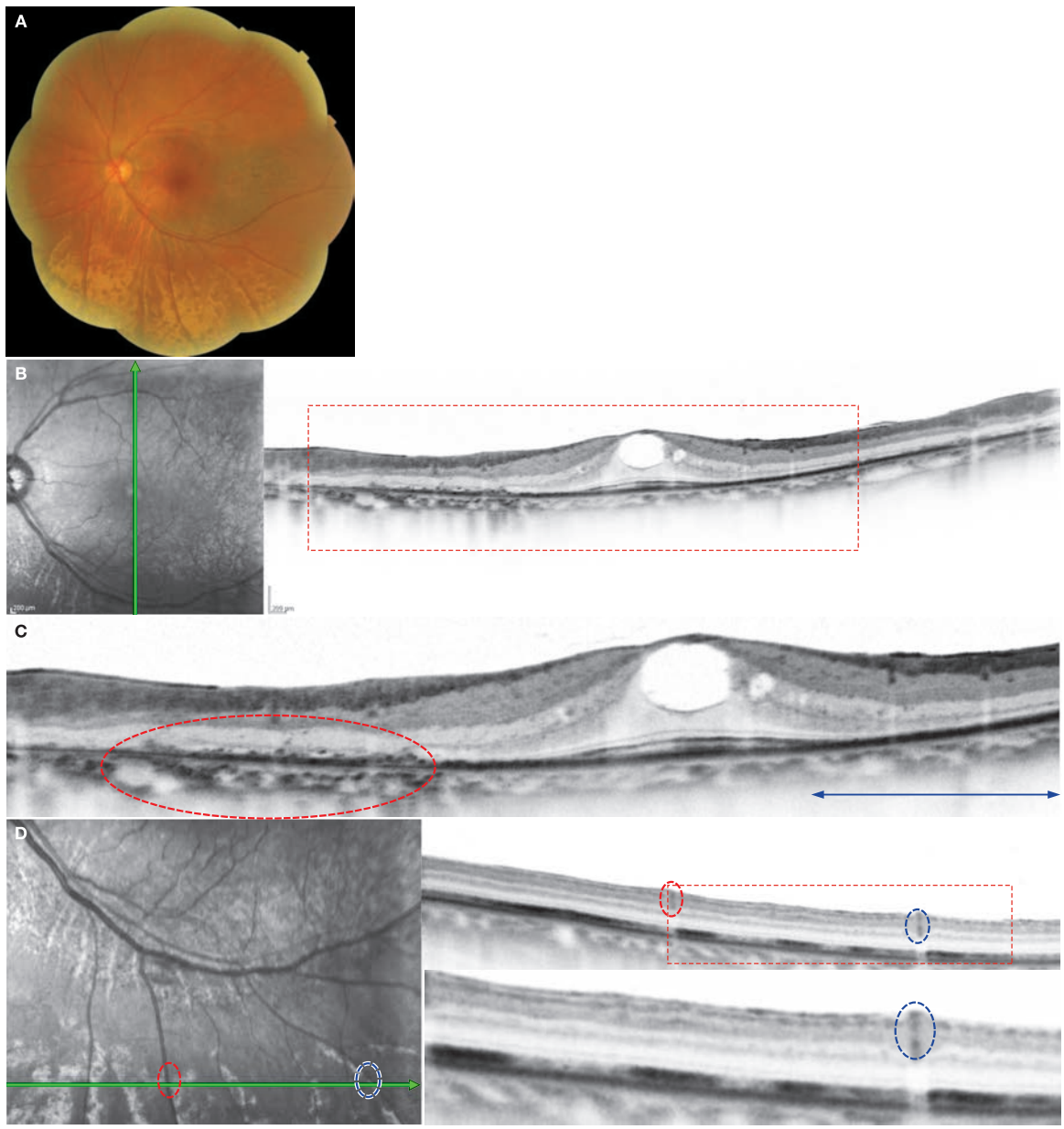

A: Color fundus photograph in the left eye: A golden sheen fundus reflex is visible in the inferior retina similar to the right eye. **B:** IR + OCT vertical scan of left eye: A foveal cystoid space is seen. The superior RPE is exhibiting high reflectivity. Damage to the outer retinal layers of the inferior macula is significant when compared the the superior macula. **C:** Enlarged version of B [red dashed box]: Loss of the RPE and photoreceptor layer is evident in the area indicated by the red dashed circle. Choroidal signal enhancement is visible consistent with this damaged area. The foveal outer retinal layer structure is relatively well preserved, consistent with the patient's good visual acuity (1.0). High RPE reflectivity is noted superior to the fovea centralis (↔). The outer nuclear layer is severely thinned in this area too. **D:** IR + OCT horizontal scan of the left eye golden sheen fundus reflex area + enlarged version [red dashed box]: The red and blue dashed circles indicate the corresponding retinal blood vessels. We can see that the IS/OS line is a thick line in the area exhibiting a golden sheen fundus reflex. The ELM line is normal and there is no obvious thinning of the photoreceptor inner and outer segments. (D was modified according to Takada M, et al. Spectral-domain optical coherence tomography findings in the Mizuo-Nakamura phenomenon of Oguchi disease. *Retina*. 2011; 31: 626–628)

Image interpretation points

In this case, the RPE and IS/OS lines are depicted separately as a result of prolonged dark adaptation. With limited case reports, it is unclear whether these findings are characteristic of Oguchi disease.

Uveitis

8.1 Behçet disease – 278
References – 278

Case 151 Behçet disease: Cystoid edema and foveal detachment – 279

Case 152 Behçet disease: Retinal atrophy – 280

Case 153 Behçet disease: Acute attack – 281

8.2 Sarcoidosis – 282
References – 282

Case 154 Sarcoidosis: Cystoid macular edema – 283

Case 155 Sarcoidosis: Foveal detachment – 284

8.3 Vogt-Koyanagi-Harada disease – 285
References – 286

Case 156 Vogt-Koyanagi-Harada disease: Large foveal cystoid space – 287

Case 156 Continuation – 288

Case 157 Vogt-Koyanagi-Harada disease: Prominent choroidal thickening – 289

Case 157 Continuation – 290

Case 158 Vogt-Koyanagi-Harada disease: Reattachment process – 291

Case 158 Continuation – 292

Case 159 Vogt-Koyanagi-Harada disease: Choroidal folds – 293

Case 159 Continuation – 294

8.4 Sympathetic ophthalmia – 295
References – 295

Case 160 Sympathetic ophthalmia: After vitreous surgery – 296

8.5 Toxocariasis – 297
References – 297

Case 161 Toxocariasis: Proliferative membrane – 298

8.6 Acute retinal necrosis (Kirisawa-type uveitis) – 299
References – 299

Case 162 Acute retinal necrosis (Kirisawa-type uveitis): A typical example – 300

8.1 Behçet disease

Background

Behçet disease is a disease characterized by four main symptoms: recurrent aphthous ulcer of the oral mucosa, skin manifestations, intraocular inflammation, and vulvar ulcer. The prevalence of HLA-B51 is high. Ninety % of eye symptoms are bilateral acute uveitis that occurs repeatedly. This disease is nongranulomatous uveitis, and hypopyon sometimes occurs. The sudden, violent occurrence of inflammation is called an acute attack. Repeated acute attacks accompanied by retinal perivasculitis with hemorrhages, patchy retinal whitening, macular edema, and optic disc edema cause macular degeneration and optic nerve atrophy resulting in a poor visual prognosis. Topical therapy with triamcinolone is reported to be effective for macular edema. The use of colchicine and cyclosporine is effective as a systemic therapy, but systemic administration of steroids is contraindicated. Recently, intravenous treatment with the anti-human TNF-α monoclonal antibody infliximab (Remicade®) has been confirmed as more effective than traditional therapies.

OCT findings

Behçet disease develops macular edema accompanied by foveal detachment, which characterized by the intraretinal and subretinal infiltration of leukocytes. Repeated acute attacks cause the retina to thin and leads to poor visual acuity.[1, 2] Thinning of the outer retinal layers in the macular area is directly linked to visual acuity decline. Retinal vasculitis and retinal edema can occur significantly in the extensive area where both the inner and outer layers of the retina thin.

References

1) Unoki N, Nishijima K, Kita M, et al. Structural changes of fovea during remission of Behçet's disease as imaged by spectral domain optical coherence tomography. *Eye (Lond)*. 2010; 24: 969–975.
2) Takeuchi M, Iwasaki T, Kezuka T, et al. Functional and morphological changes in the eyes of Behçet's patients with uveitis. *Acta Ophthalmol*. 2010; 88: 257–262.

Case 151 Behçet disease: Cystoid edema and foveal detachment

A 30-year-old female, OD and OS, BCVA 0.02 and 0.2, respectively

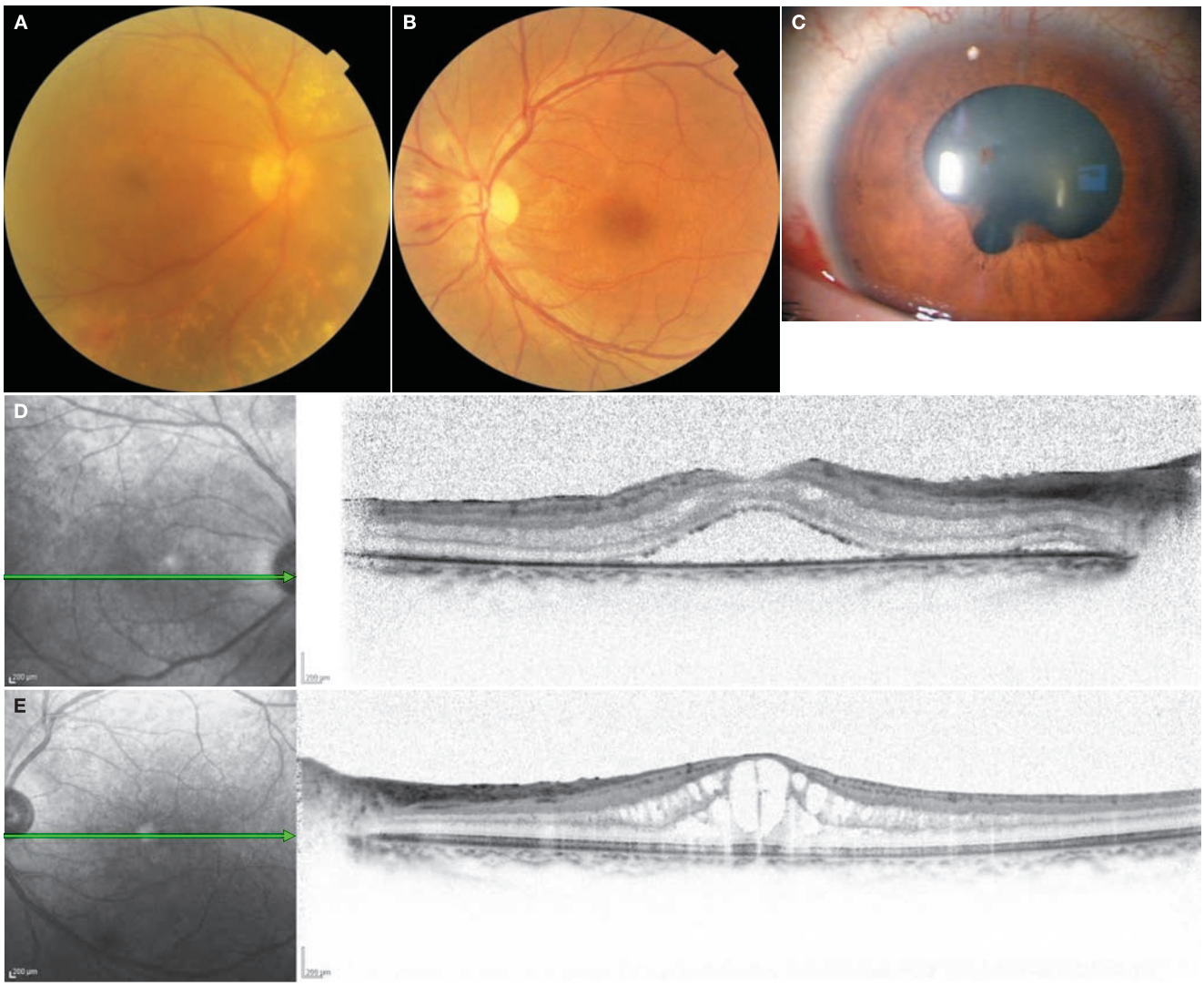

A: Color fundus photograph in the right eye: There is clouding of the vitreous body. RPE atrophy is evident inferior and nasal to the optic disc, and retinal hemorrhages and focal accumulations of yellow-white deep retinal exudates are visible. **B:** Color fundus photograph in the left eye: Retinal hemorrhages and patchy retinal whitening noticeable. CME is also visible. **C:** Anterior segment photograph: A posterior synechia is seen. **D:** IR + OCT horizontal scan of the right eye: A foveal detachment and a SRD in the vicinity of the optic disc can be seen. **E:** IR + OCT horizontal scan of the left eye: A typical image of CME is visible.

Image interpretation points

The patient became aware of blurred vision and reduced visual acuity 6 months earlier and visited their local doctor. Only topical steroid therapy was initiated since she was pregnant. At initial diagnosis, a foveal detachment was seen in her right eye, and typical CME was seen in her left eye. This was an incomplete form of Behçet disease. In this case, infiltration of neutrophils into the retina or vitreous cavity was not evident.

Case 152 Behçet disease: Retinal atrophy

A 51-year-old male, OD, BCVA 0.7

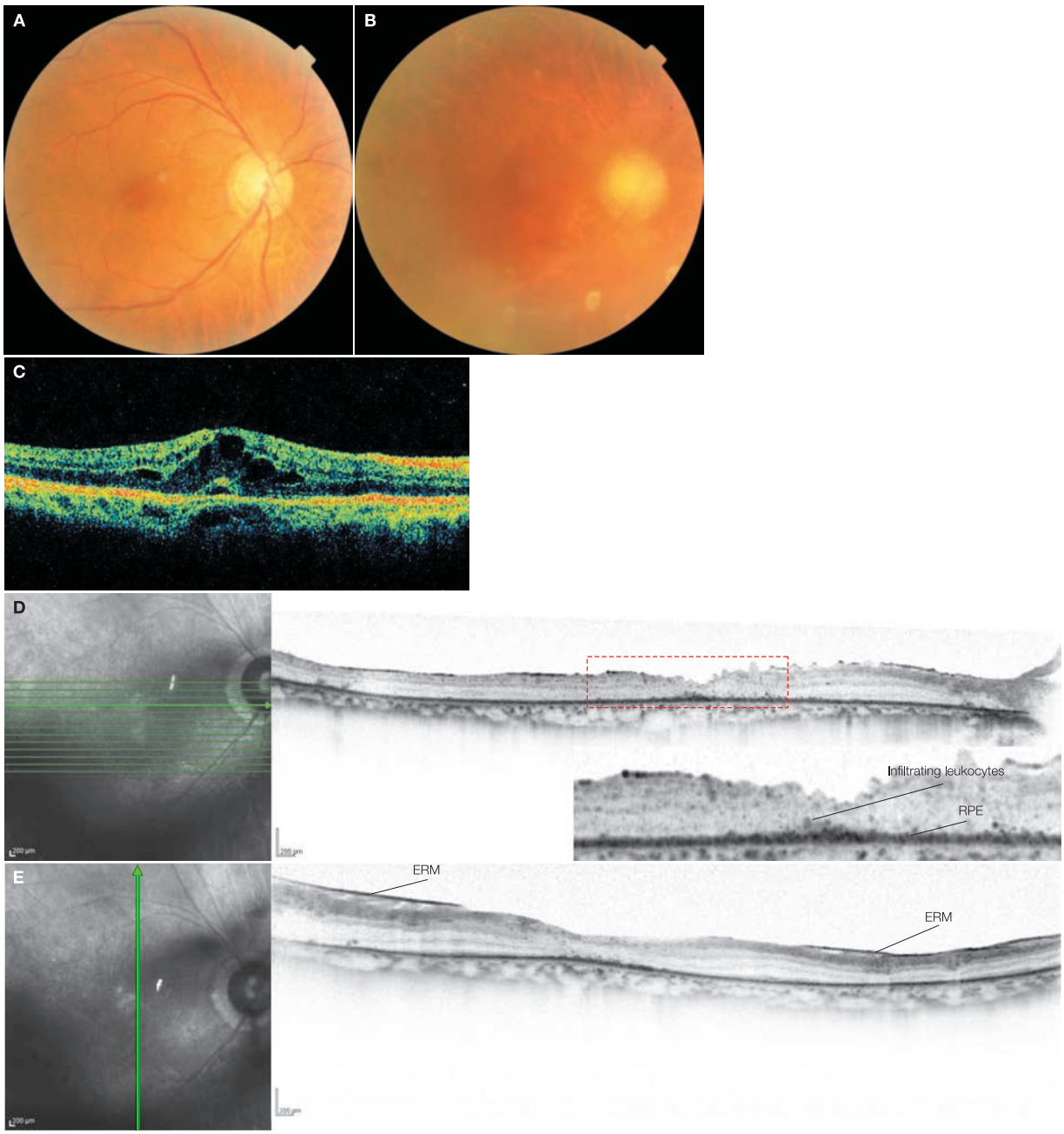

A: Color fundus photograph in the right eye: At initial diagnosis. CME is visible. **B:** Color fundus photograph in the right eye: 3 years and 5 months after initial diagnosis. Best-corrected visual acuity has declined to 0.05. The vitreous is cloudy. Narrowing of retinal blood vessels and optic nerve atrophy are apparent. **C:** OCT horizontal scan of the right eye: At initial diagnosis. Time-domain OCT image. CME and a foveal detachment are noted. **D:** IR + OCT horizontal scan of the right eye + enlarged version [red dashed box]: 3 years and 5 months after initial diagnosis. The entire retina is thin. The structure of layers within the fovea centralis in particular is indistinct, and infiltration of leukocytes and RPE stratification is visible. **E:** IR + OCT vertical scan of the right eye: 3 years and 5 months after initial diagnosis. Foveal atrophy is significant and the infiltration of leukocytes, and RPE stratification is exhibited. ERM is seen.

Image interpretation points

The patient became aware of blurred vision in their right eye 3 months earlier and was referred to our hospital. At initial diagnosis, CME accompanied by a foveal detachment was seen. After the third acute attack that occured 3 years and 5 months after initial diagnosis, retinal atrophy had occurred over a wide area.

Case 153 Behçet disease: Acute attack

A 48-year-old female, OD and OS, 0.5 and 0.1, respectively

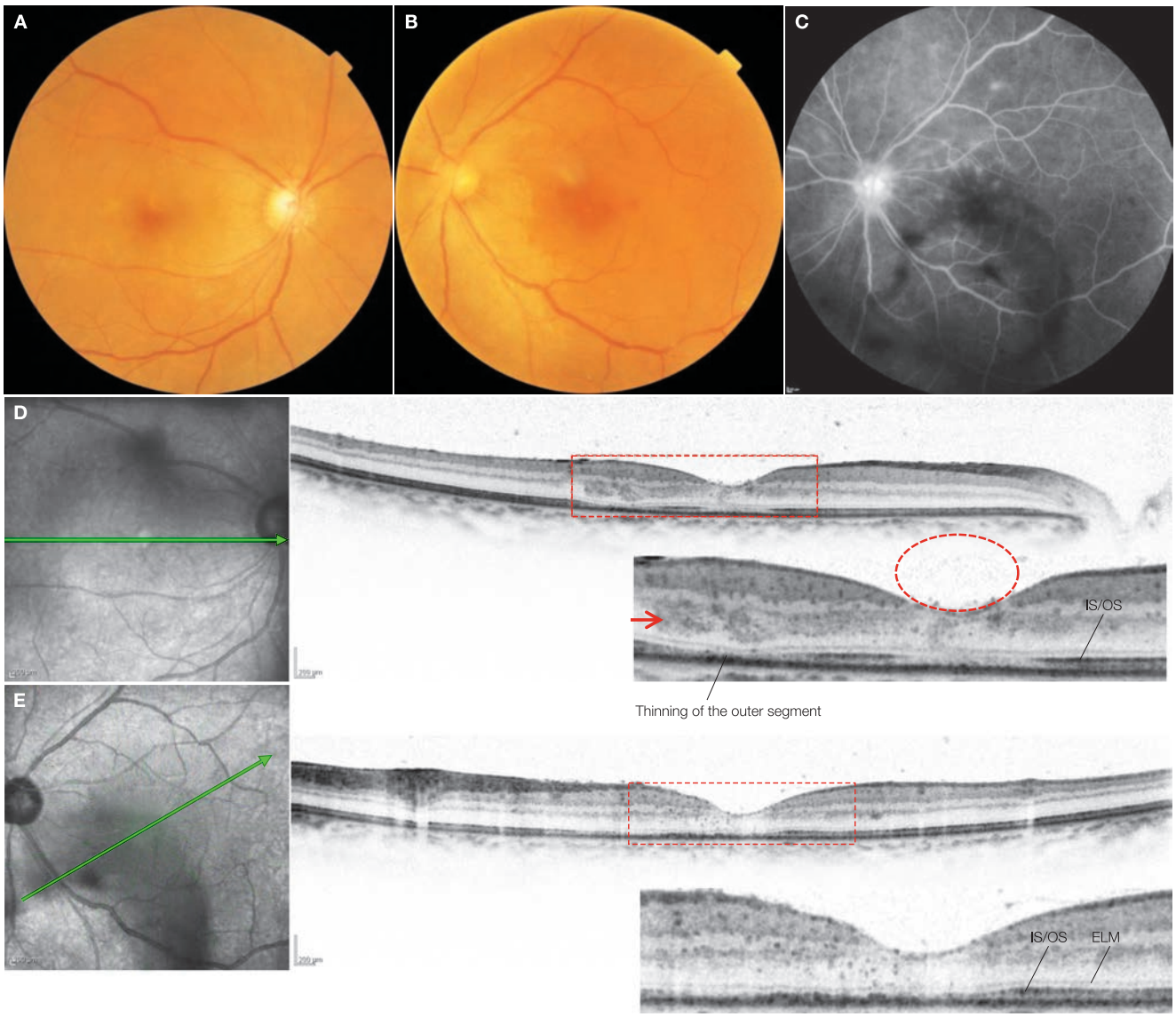

A: Color fundus photograph in the right eye: During an acute attack of the right eye. **B:** Color fundus photograph in the left eye: During an acute attack of the left eye that occurred 14 months after A. Best-corrected visual acuity declined to 0.1 (1.2 at initial diagnosis). Patchy retinal whitening is evident in the macular area of both eyes. **C:** FA in the left eye (8 minutes): Left eye during an acute attack. Leakage from retinal capillaries in the macular area is visible beyond the vitreous opacity. **D:** IR + OCT horizontal scan of the right eye + enlarged version [red dashed box]: During an acute attack of the right eye. Moderate reflectivity (➔) due to accumulating infiltrated leukocytes is apparent. Infiltrated leukocytes can also be seen in the vitreous cavity (red dashed circle). The foveal IS/OS line has disappeared and the outer segment on the temporal side of the fovea centralis is thin. **E:** IR + OCT oblique scan of the left eye + enlarged version [red dashed box]: During an acute attack of the left eye. Infiltrated leukocytes and thinning of the foveal outer segment is exhibited.

Image interpretation points

The first acute attack had occurred in the right eye 4 years prior, and a follow-up was continued after symptoms receded with therapy using colchicine and cyclosporine. Patchy retinal whitening was visible in the macula in both eyes during acute attacks, and leukocyte infiltration was seen on OCT in the same area. No cystoid edema or SRDs could be seen. Irregularities and disappearance of the IS/OS line and thinning of the outer segment were seen in both eyes, which were the cause of visual impairment.

8.2 Sarcoidosis

Background

Sarcoidosis is a systemic, noncaseating granulomatous disease that affects multiple organs starting with the lungs, eyes, lymph nodes, and skin. It is characterized by noncaseating, epithelioid granuloma (sarcoid nodules) and is accompanied by granulomatous angiitis and microangiopathy.[1] The incidence is twice higher in women than in men and is common in women in their 20s and 60s and men in their 20s. The frequency of ocular lesions in Japan is high at 60–80%. Prognosis is relatively good, although death as a result of cardiac lesions etc. has been reported in 10–20% of the cases, so diagnosis is important.

Ocular lesions include granulomatous anterior uveitis, trabecular nodules, tent-like adhesion of the peripheral iris, vitreous clouding (snowball-like, beaded, lump-like, and particle-like), retinal perivasculitis (particularly periphlebitis), exudative chorioretinal spots, and chorioretinal atrophic lesions. Periphlebitis, perivenous tubercles, and sometimes, a nonperfusion area are visible on FA.

OCT findings

CME is a typical finding in sarcoidosis.[2] Retinal granulomatous lesions appear to occupy the inner retinal layers.[3] Although Behçet disease is accompanied by the intraretinal and subretinal infiltration of leukocytes this is not seen in sarcoidosis.

References

1) Uyama M. Uveitis in sarcoidosis. *Int Ophthalmol Clin*. 2002; 42: 143–150.
2) Larsson J, Hvarfner C, Skarin A. Intravitreal triamcinolone in two patients with refractory macular oedema in sarcoid uveitis. *Acta Ophthalmol Scand*. 2005; 83: 618–619.
3) Wong M, Janowicz M, Tessler HH, et al. High-resolution optical coherence tomography of presumed sarcoid retinal granulomas. *Retina*. 2009; 29: 1545–1546.

Case 154 Sarcoidosis: Cystoid macular edema

A 76-year-old female, OD and OS, BCVA 0.3 and 0.2, respectively

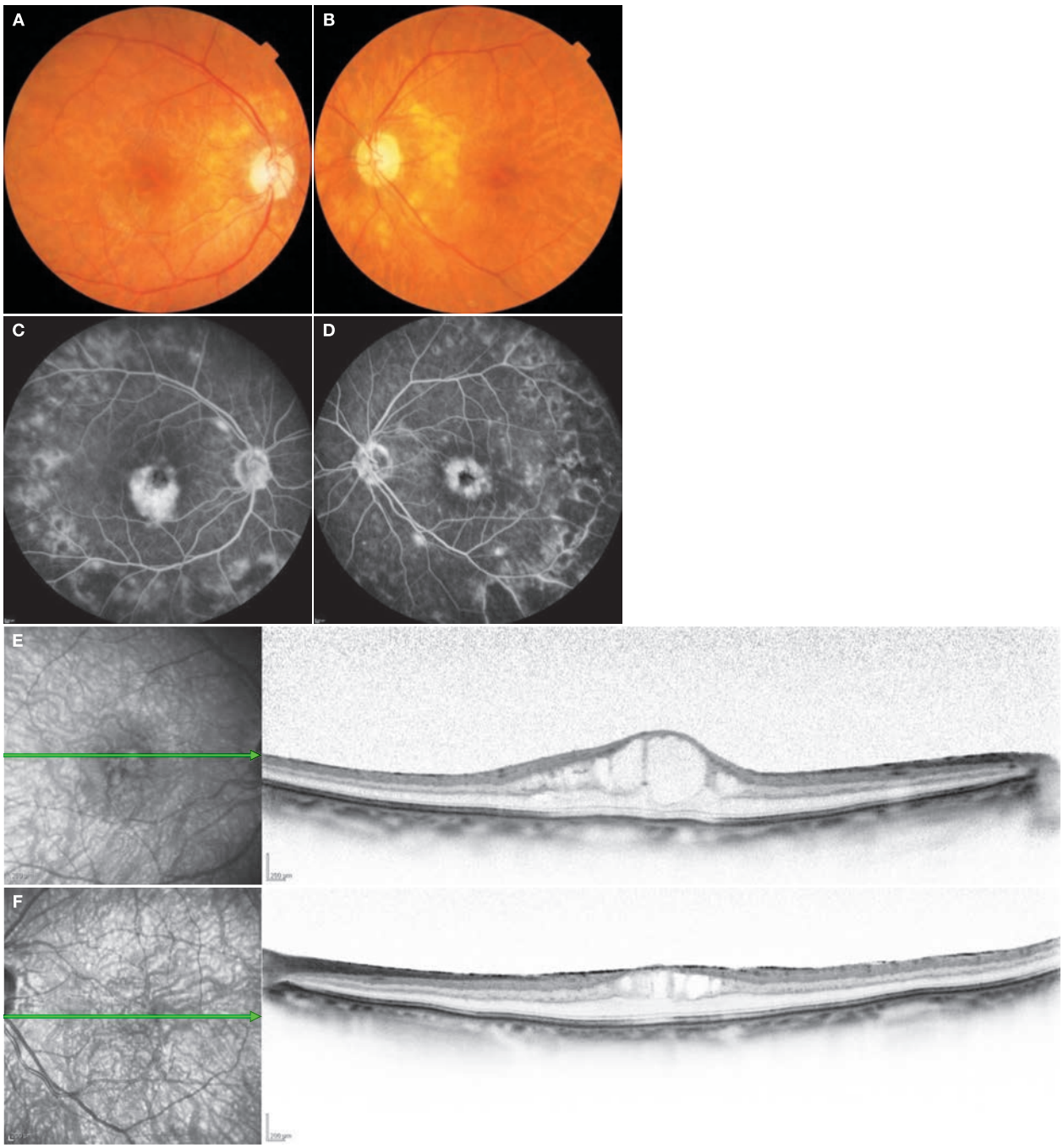

A: Color fundus photograph in the right eye, **B:** Color fundus photograph in the left eye. CME is visible. Patchy choroidal atrophy is evident around the optic disc. **C:** FA in the right eye (6 minutes), **D:** FA in the left eye (4 minutes). CME can be seen in both eyes. Retinal periphlebitis and the formation of a nonperfusion area are noted outside the arcade vessels. **E:** IA + OCT horizontal scan of the right eye, **F:** IA + OCT horizontal scan of the left eye: CME is visible in both eyes.

Image interpretation points

The patient became aware of reduced visual acuity in both eyes 15 months before visiting her local doctor who diagnosed her with uveitis and gave her eye drops. CME exacerbated and the patient was referred to us. CME was visible in both eyes on FA and OCT, but no findings consistent with retinal periphlebitis outside the macula could be seen on OCT.

Case 155 Sarcoidosis: Foveal detachment

A 60-year-old female, OS, BCVA 0.5

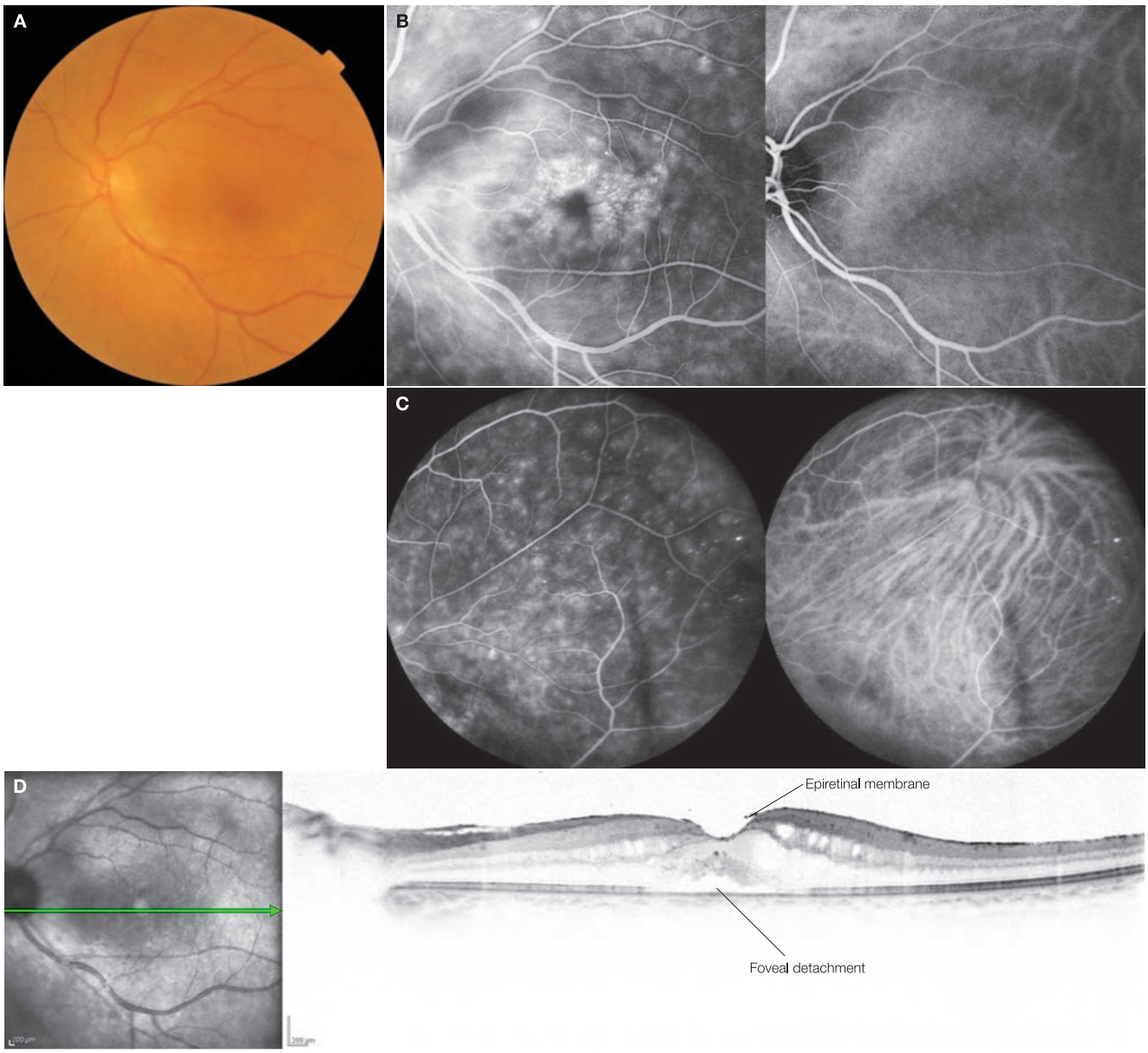

A: Color fundus photograph in the left eye: Edema is evident around the optic disc and in the macular area. **B:** FA + IA in the left eye (5 minutes): On FA, CME is visible in the posterior pole, and retinal periphlebitis and exudative chorioretinal spots are noted around the arcade vessels. Small, hypofluorescent lesions are scattered above the arcade vessels on IA. Macular choroidal vessels are not sufficiently depicted due to macular edema. **C:** FA + IA in the left eye (6 minutes): Multiple patchy hyperfluorescent lesions corresponding to exudative chorioretinal spots are depicted in the equatorial area on FA. Hypofluorescent spots are visible on IA, but they are not consistent with the multiple, patchy hyperfluorescent lesions on FA. **D:** IA + OCT horizontal scan of the left eye: CME accompanied by a foveal detachment is visible.

Image interpretation points

After being diagnosed with uveitis, the patient continued steroid eye drop instillation; nevertheless, vitreous clouding and CME developed one year later. CME is evident on FA and OCT. ERM not including the fovea centralis and a foveal detachment are visible on OCT and progressing to a macular pseudohole.

8.3 Vogt-Koyanagi-Harada disease

Background

Vogt-Koyanagi-Harada disease (VKH) is characterized by bilateral serous retinal detachments (SRDs). Patients become aware of rapid visual decline as a result. This disease is common in Asians and is considered a systemic autoimmune disease toward melanocytes. Typical eye symptoms, increased cerebrospinal fluid cell count, and typical extraocular symptoms are useful for diagnosis. Five to seven days before eye symptoms occur, premonitory signs such as flu-like symptoms, headache, nausea, fatigue, hair hyperesthesia, tinnitus, and dizziness manifest in roughly one-third of cases. During the recovery phase, choroidal depigmentation develops in the eyes and over the entire body. The eyes exhibit a sunset glow fundus appearance and skin depigmentation spots; whitening of the hair, eyebrows, and eyelashes occurs over the entire body.[1]

Disease types

This disease can be divided into the following two types based on the main lesion site.

Harada type

Mainly characterized by lesions in the posterior pole of the fundus. A typical multilobular SRD occurs in the posterior pole. A yellowish-white rim is often observed around the foveal SRD. Choroidal folds can also occur. There is also a papilledema type consisting mainly of redness and swelling of the optic disc. About 2 months after onset, the SRD starts to disappear radial retinal folds develops, choroidal depigmentation progresses, and a typical sunset glow fundus is finally formed.

Vogt-Koyanagi type

Mainly characterized by inflammation of the anterior segment. Granulomatous iridocyclitis occurs causing inflammatory cells in the anterior chamber, iris nodules, and keratic precipitate. The anterior chamber becomes shallow as a result of swelling of the ciliary body, and supraciliary effusions in eyes with severe inflammation.

Fluorescein fundus angiography

- **FA**

Multiple punctate leaking points are visible at the early phase, and multilobular fluorescent accumulation is visible during the late phase. A weakly reflective border known as a dark rim can be seen around the foveal fluorescent accumulation.[2]

- **IA**

A choroidal filling delay is evident. Hypofluorescence is seen consistent with a SRD.

OCT findings

- **Sensory retina**

Typical OCT findings include membranous structures (also called septa) that partition the subretinal space. Exactly what this membranous structure is has become the subject of debate. One theory states that this membranous structure is part of the retina,[3, 4] and another states that it is fibrin membrane.[5]

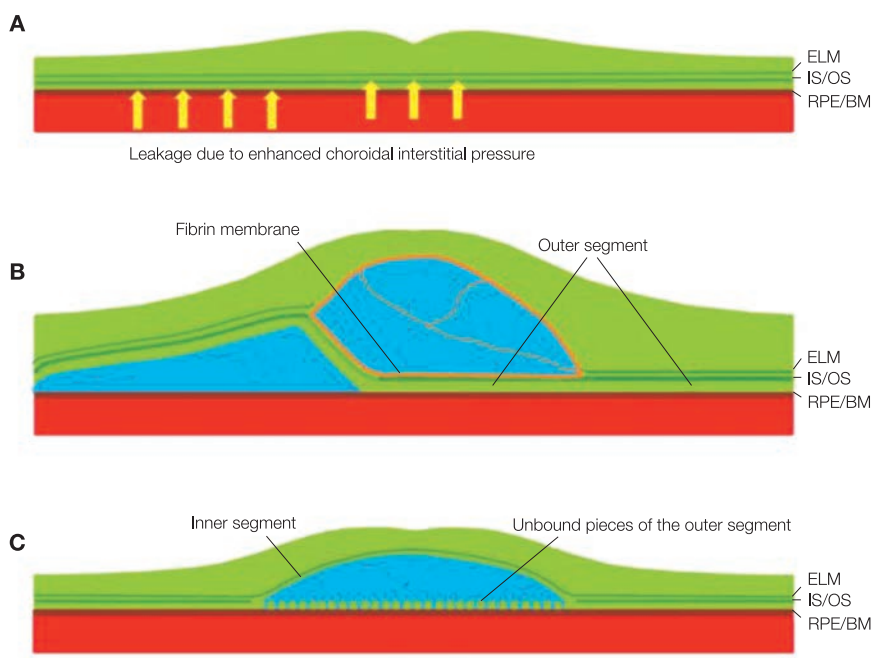

Fig. 8-1 Schematic diagram showing how the membranous structure characteristic of acute VKH disease form and, with high-dose steroid therapy, resolve. **A:** Choroidal interstitial pressure is enhanced, and subretinal or intraretinal leakages occur from the failed junctions between RPE cells. **B:** Fluid exudates accumulate subretinally, causing serous retinal detachment, and within the retina, forming a cystoid space between photoreceptor inner and outer segment. The leakage fluid contains fibrin, and the intraretinal cystoid space is lined with a fibrin membrane. The fibrin also binds the detached outer segments to form the membranous structure . **C:** Fibrin rapidly disappears with the administration of steroids, and consequently the outer segment loses its adhesive forces to each other and resulting unbound pieces of the outer segment collapse on the RPE (Modified according to Ishihara K, et al. Acute Vogt-Koyanagi-Harada disease in enhanced spectral-domain optical coherence tomography. Ophthalmology. 2009; 116: 1799–1807)

However, when observed on images with speckle noise removed, ① a IS/OS line in continuity with the IS/OS line in the attached retina is visible in the membranous structure , ② and fluid space can sometimes be seen anterior to the IS/OS line. Furthermore, ③ the width of the membranous structure is uniform in each eye and similar between cases, and ④ the membranous structure immediately disappears with steroid therapy and instead granular structures accumulate on the RPE (clearly visible on IR images). This can be interpreted as exudate containing a lot of fibrin accumulated in the space between the photoreceptor inner and outer segments forming a cystoid space. This cystoid space is then lined with a fibrin membrane, and the outer segment, which originally has no adhesive force to each other, becomes a membranous structure with the adhesive force of the fibrin (Fig. 8-1).[6] In practice, reflectivity with amorphous structure that differs from the membranous structure is seen within the cystoid space, which appears to be fibrin alone. The granular structures seen after steroid therapy are thought to be unbound pieces of the outer segments that has collapsed onto the RPE as a result of dissolution of the fibrin that binded them.

The choroid

Thickening of the choroid first became evident on ultrasonography.[7] When observed with EDI-OCT and SS-OCT, prominent choroidal thickening and obscuration of the choroidal striation pattern are evident.[8] Sometimes, the choroid exhibits significant undulations.[9, 10] On steroid therapy, choroidal thickening recedes faster than the SRD disappears.[7, 8]

References

1) Moorthy RS, Inomata H, Rao NA.Vogt-Koyanagi-Harada syndrome. *Surv Ophthalmol*. 1995; 39: 265–292.
2) Gass JDM. Harada's disease. Stereoscopic atlas of macular diseases. Diagnosis and treatment 4th ed., CV Mosby, St. Louis, 1997. pp176–180.
3) Maruyama Y, Kishi S. Tomographic features of serous retinal detachment in Vogt-Koyanagi-Harada syndrome. *Ophthalmic Surg Lasers Imaging*. 2004; 35: 239–242.
4) Tsujikawa A, Yamashiro K, Yamamoto K, et al. Retinal cystoid spaces in acute Vogt-Koyanagi-Harada syndrome. *Am J Ophthalmol*. 2005; 139: 670–677.
5) Yamaguchi Y, Otani T, Kishi S. Tomographic features of serous retinal detachment with multilobular dye pooling in acute Vogt-Koyanagi-Harada disease. *Am J Ophthalmol*. 2007; 144: 260–265.
6) Ishihara K, Hangai M, Kita M, et al. Acute Vogt-Koyanagi-Harada disease in enhanced spectral-domain optical coherence tomography. *Ophthalmology*. 2009; 116: 1799–1807.
7) Forster DJ, Cano MR, Green RL, et al. Echographic features of the Vogt-Koyanagi-Harada syndrome. *Arch Ophthalmol*. 1990; 108: 1421–1426.
8) Maruko I, Iida T, Sugano Y, et al. Subfoveal choroidal thickness after treatment of Vogt-Koyanagi-Harada disease. *Retina*. 2011; 31: 510–517.
9) Wu W, Wen F, Huang S, et al. Choroidal folds in Vogt-Koyanagi-Harada disease. *Am J Ophthalmol*. 2007; 143: 900–901.
10) Gupta V, Gupta A, Gupta P, et al. Spectral-domain cirrus optical coherence tomography of choroidal striations seen in the acute stage of Vogt-Koyanagi-Harada disease. *Am J Ophthalmol*. 2009; 147: 148–153.e2.

Case 156 Vogt-Koyanagi-Harada disease: Large foveal cystoid space

A 24-year-old female, OD, BCVA 0.5

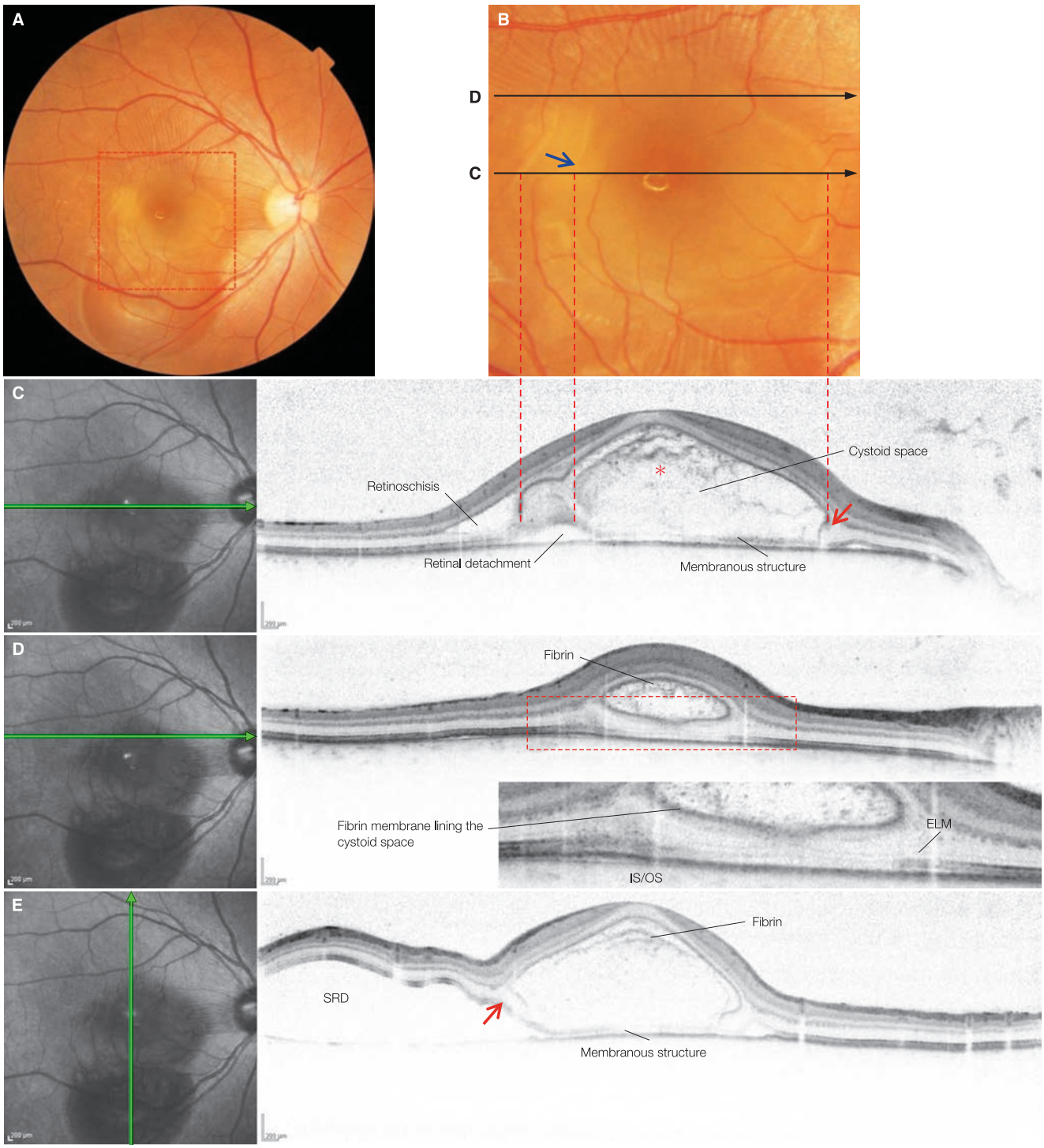

A: Color fundus photograph in the right eye, **B:** Enlarged version of A [red dashed box]: A multilobular SRD is visible. The foveal SRD is large, and partially encompassed by a double yellow rims. Fibrin is visible on the temporal side (➔). **C:** IR + OCT horizontal scan of right eye: A scan along the lower arrow in B. Membranous structure uniform in width on the RPE can be seen at the bottom of the cystoid space. Amorphous reflectivity (✻) corresponding to fibrin is observed inside. The outer retinal layers (➔) stretched out tongue-like and visible in the border of the foveal cystoid space correspond to the yellow rim. Retinoschisis is evident in part of the posterior border of the outer plexiform layer. **D:** IR + OCT horizontal scan of the right eye + enlarged version [red dashed box]: A scan along the upper arrow in B. The bottom of the cystoid space is formed anterior to the ELM, that is to say, it has formed within the outer nuclear layer. **E:** IR + OCT vertical scan of the right eye: The cystoid space and SRD are partitioned by the outer retinal layers (➔) stretching out in a tongue-like form and membranous structure continuing from it.

(Continued on the next page)

Case 156 Continuation

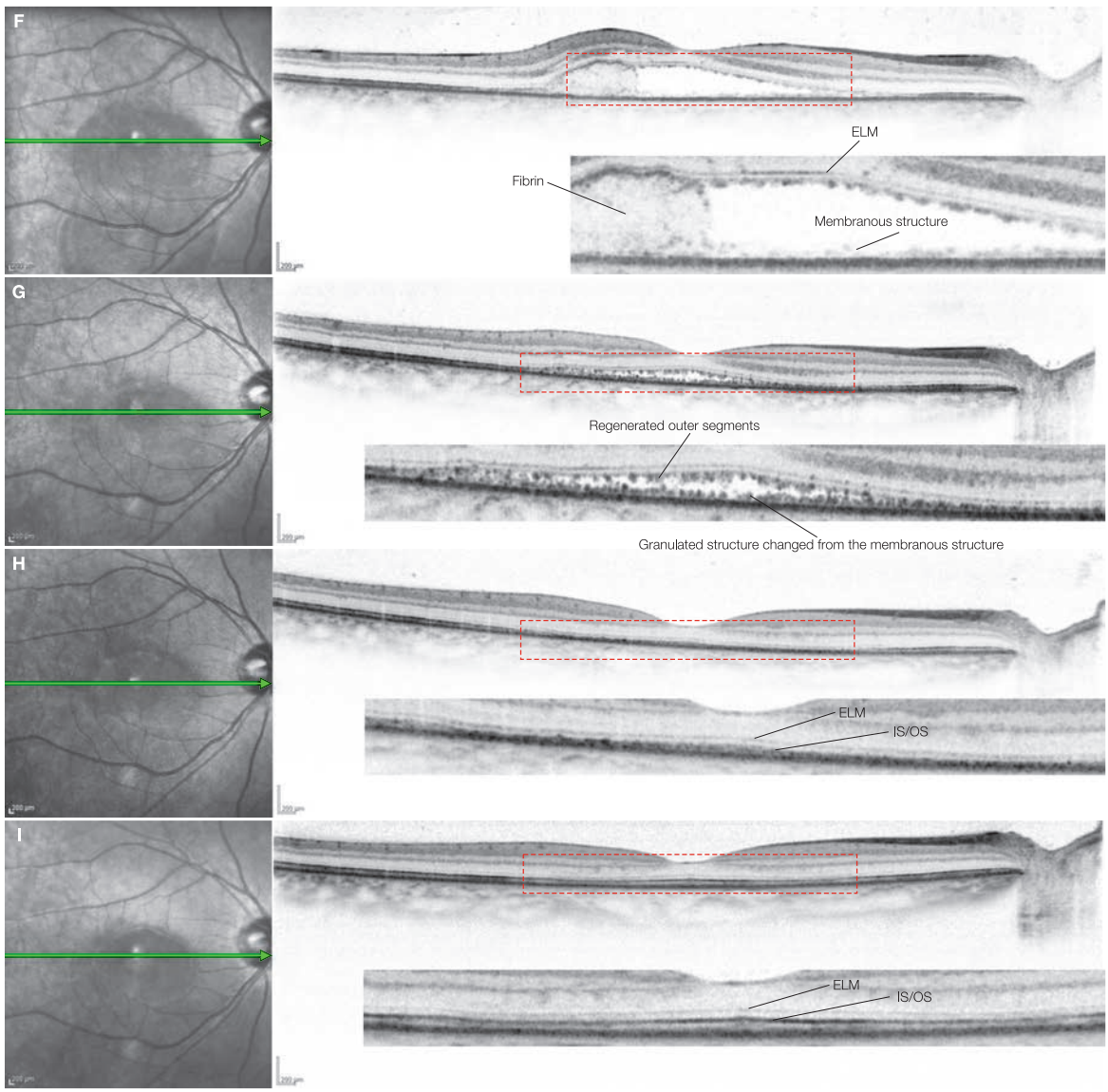

F: IR + OCT horizontal scan of the right eye + enlarged version [red dashed box]: Third day after starting steroid therapy. Best-corrected visual acuity is 0.15. The height of the cystoid space is decreasing, fibrin is decreasing, and the membranous structure is becoming irregular. **G:** IR + OCT horizontal scan of the right eye + enlarged version [red dashed box]: Seventh day after starting steroid therapy. Best-corrected visual acuity is 0.4. The membranous structure on the RPE is undergoing granular changes. Fibrin has disappeared. The newly formed outer segments becoming partially elongated, but they are highly reflective and irregular. **H:** IR + OCT horizontal scan of the right eye + enlarged version [red dashed box]: Tenth day after starting steroid therapy. The retina is reattached, but the IS/OS is irregular, and the outer segment is thin. **I:** IR + OCT horizontal scan of the right eye + enlarged version [red dashed box]: 32nd day after starting steroid therapy. Best-corrected visual acuity has improved to 1.2. IS/OS and outer segment thickness has almost normalized.

Image interpretation points

We wish to understand the specific structures visible in the color fundus photo in VKH syndrome through comparisons between the ocular fundus and OCT. The area encompassed by the yellow rim is the cystoid space, which has a wall composed of membranous structure. Fibrin precipitated in the cystoid space is lining the cystoid space. It is thought that outer segments becomes bound by the fibrin, and acts as membranous structure. The cystoid space and fibrin recede rapidly with steroid therapy and the membranous structure undergoes granular changes on the RPE during this process. This observation can be interpreted as the outer segment bound by fibrin becoming scattered with the disappearance of the fibrin and each of the scattered outer segments corresponding to the granular structure. The IS/OS line is irregular, and the photoreceptor outer segment is thin immediately after reattachment, but this usually normalizes in around 2 weeks.

Case 157 Vogt-Koyanagi-Harada disease: Prominent choroidal thickening

A 42-year-old female, OS, BCVA 1.2

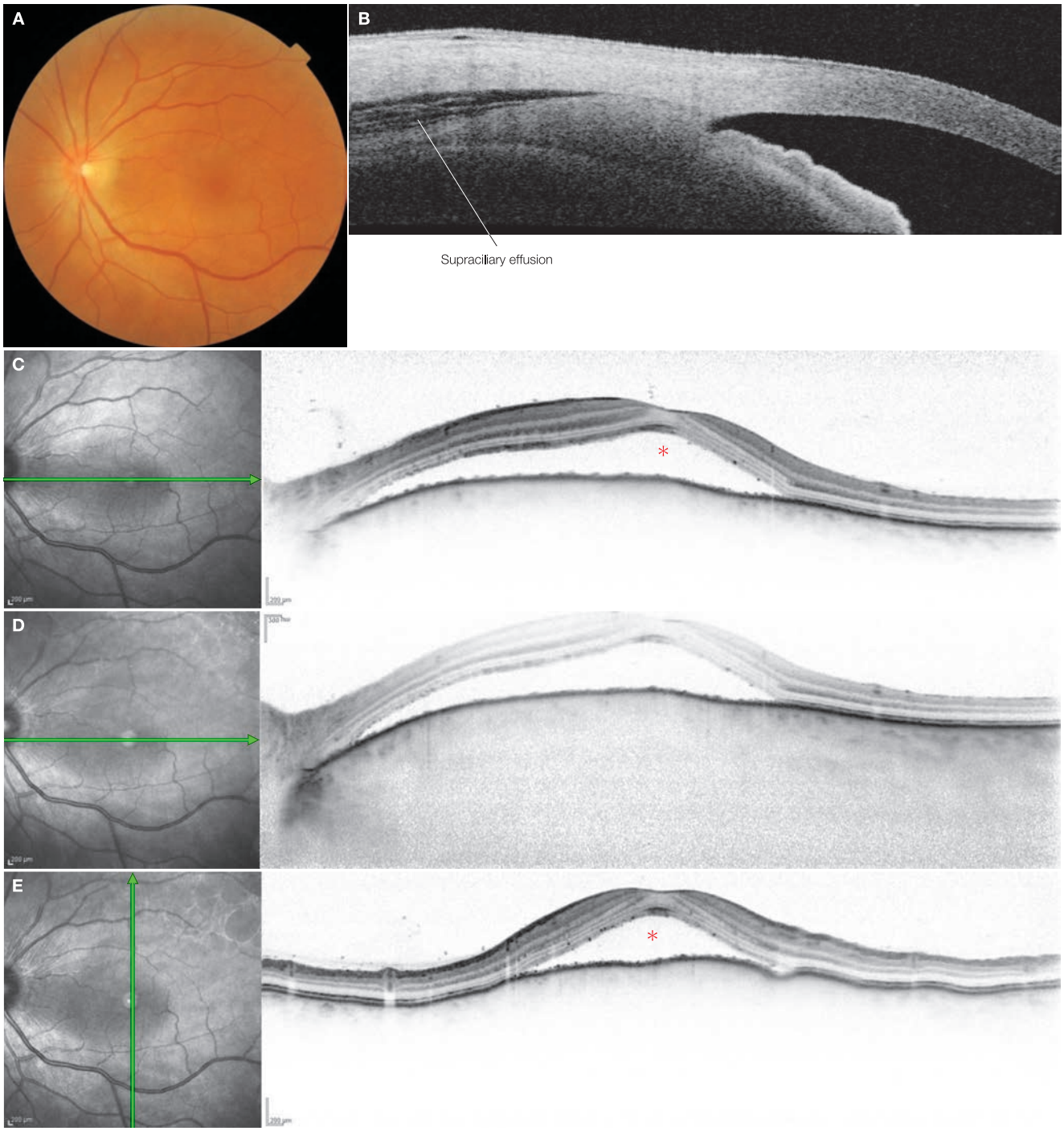

A: Color fundus photograph in the left eye: A SRD is seen. Retinal whitening can be seen around the optic disc and following the arcade vessels. **B:** Anterior segment OCT image of the left eye: A supraciliary effusion and consequent shallow anterior chamber is seen. **C:** IR + OCT horizontal scan of the left eye: A SRD (*) is noted. The RPE is protruding forward, and loss of the choroidal striation pattern is apparent. The shed outer segments are noticeable on the RPE. **D:** IR + EDI-OCT horizontal scan of the left eye: Choroidal thickening is prominent, and the sclera is not depicted on EDI-OCT. The choroidal striation pattern is blurred. **E:** IR + OCT vertical scan of left eye: A SRD (*) and RPE undulation is exhibited.

(Continued on the next page)

Case 157 Continuation

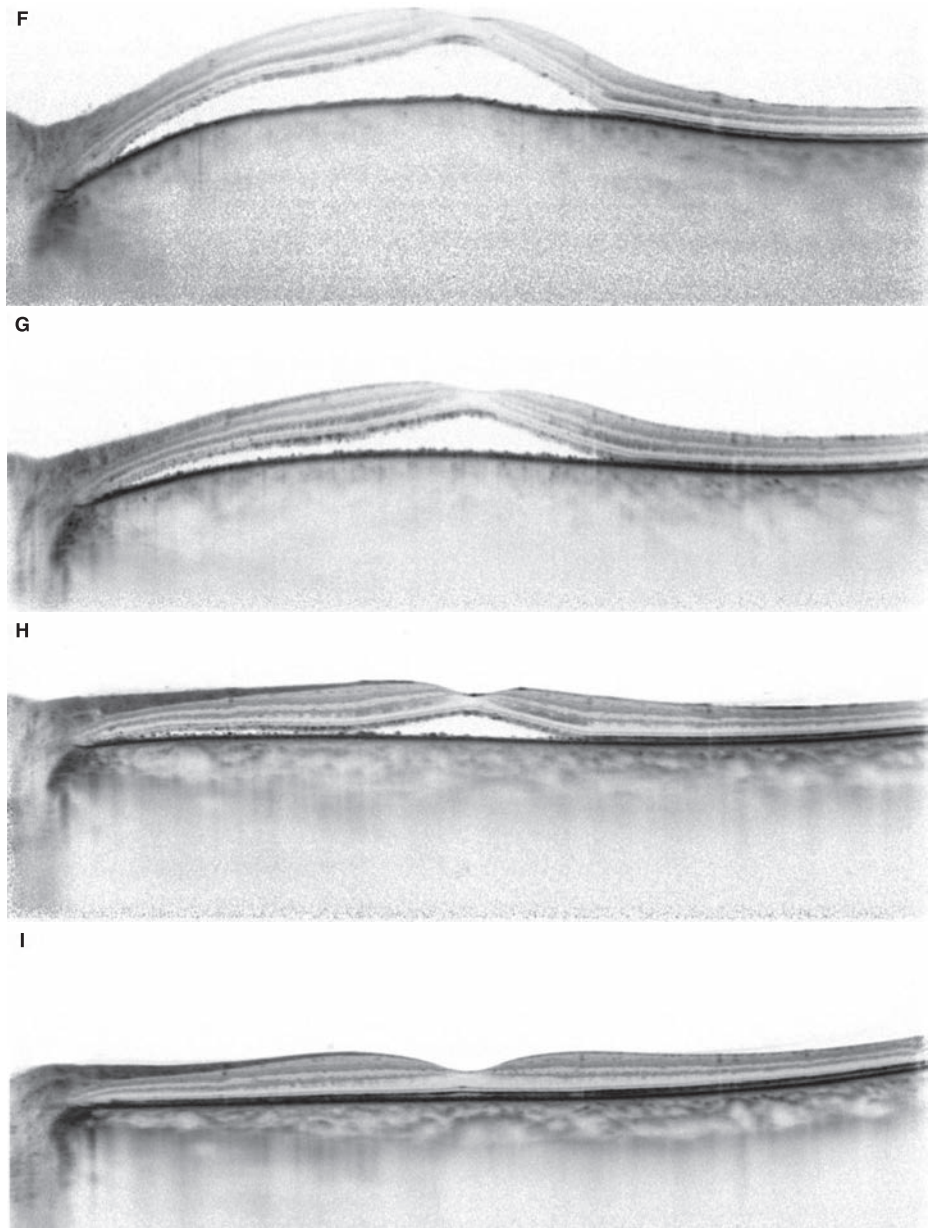

F: IR + EDI-OCT horizontal scan of the left eye: At initial diagnosis. **G:** IR + EDI-OCT horizontal scan of the left eye: First day after starting steroid therapy. The SRD and RPE protrusion are receding, but choroidal thickening is still significant, and the sclera is not visible. **H:** IR + EDI-OCT horizontal scan of the left eye: Fifth day after starting steroid therapy. Choroidal thickening has receded significantly, and the sclera can be seen. The choroidal striation pattern is being restored. **I:** IR + EDI-OCT horizontal scan of the left eye: 28th day after starting steroid therapy. The thickness and pattern of the choroid have almost normalized. The sensory retina has almost normalized.

Image interpretation points

The patient became aware of reduced visual acuity in both eyes 2 weeks earlier and visited our hospital. The patient was aware of dizziness, hearing loss, and headache. Keratic precipitates and inflammation of the anterior chamber were observed. Supraciliary effusion was seen on anterior segment OCT, but the depth of the anterior chamber was normal. There was a SRD, but not any cystoid spaces. At initial diagnosis, prominent choroidal thickening and blurring of the choroidal striation pattern was observed on EDI-OCT, and the scleral border could not be seen. Choroidal abnormalities and the SRD quickly resolved with steroid mass therapy and had almost normalized about one month later. These findings suggest that severe inflammation of the choroid occurs in VKH syndrome.

Case 158 Vogt-Koyanagi-Harada disease: Reattachment process

Right eye of a 26-year-old male with vision corrected to 0.6

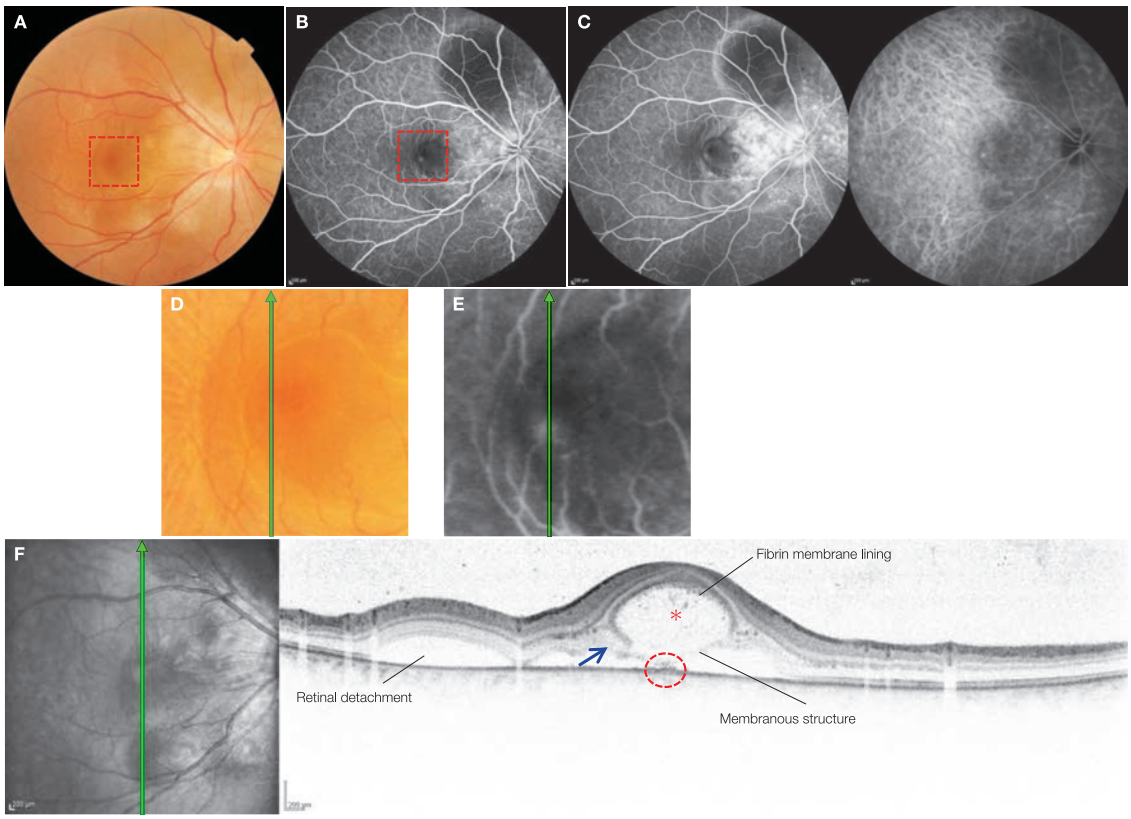

A: Color fundus photograph in the right eye. **B:** FA in the right eye (3 minutes), During initial diagnosis. Multiple punctate leaking points are seen, particularly around the optic disc. **C:** FA + IA in the right eye (10 minutes): Multilobular fluorescein accumulation is exhibited. The foveal lobule has a dark rim. The area of the SRD is hypofluorescent on IA. **D:** Enlarged version of A [red dashed box]: The foveal cystoid space of one disc diameter is encompassed by a yellow rim. Retinal folds are noted. **E:** Enlarged version of B [red dashed box]: Dye leakage can be seen into the foveal lobule. **F:** IR + OCT vertical scan of the right eye: A high reflectivity thought to be due to a fibrin membrane lining is observed in the the inner wall of the foveal cystoid space, (*) and membranous structure is visible at the bottom. Amorphous reflectivity corresponding to fibrin can be seen inside. The outer retinal layers (➔) are stretched out in a tongue-like form in the border of the cystoid space corresponding to the yellow rim on the fundus photograph. A slight RPE elevation is depicted in the leakage site on FA (red dashed circle)

G: IR + OCT vertical scan of the right eye + enlarged version [red dashed box]: Second day after starting steroid therapy. Membranous structure (➔) of uniform thickness is noted extending from the outer segment. The structure posterior to the ELM is thinned in the area where membranous structure can be seen. **H:** IR + OCT vertical scan of the right eye + enlarged version [red dashed box]: Third day after starting steroid therapy. **I:** IR + OCT vertical scan of the right eye + enlarged version [red dashed box]: Fourth day after starting steroid therapy. **J:** IR + OCT vertical scan of the right eye + enlarged version [red dashed box]: Fifth day after starting steroid therapy. I to K show the process where membranous structure dissolves and disappears, leaving behind just granular high reflectivity. **K:** IR + OCT vertical scan of the right eye + enlarged version [red dashed box]: One month after starting steroid therapy. Best-corrected visual acuity has improved to 0.9. The outer segment is elongated and the IS/OS line is almost restored.

(Continued on the next page)

Image interpretation points

There is a yellow rim on fundus photo and a dark rim on FA along the SRD margin, which OCT reveals to be a cystoid space. The outer retinal layers is stretched out in a tongue-like form along the border of the cystoid space, which corresponds to this rim. Membranous structure can be seen at the bottom of the cystoid space (on the RPE), but after starting steroid therapy we can see that this membranous structure continues on from the outer segment and has a uniform thickness. Afterwards, it gradually splits into a relatively weakly reflective membranous structure and granular high reflectivity, and the membranous structure eventually disappears, leaving behind just granular high reflectivity. This membranous structure is thought to be the outer segment solidified with fibrin. The structure posterior to the ELM is thin in the area where membranous structure can be seen. This is because only the inner segment remains as a layer in this area with regenerating outer segments appearing as a highly reflective dots beneath the inner segment. One month after starting steroid therapy, the retina is reattached and the outer segment is almost restored to its former state.

Case 158 Continuation

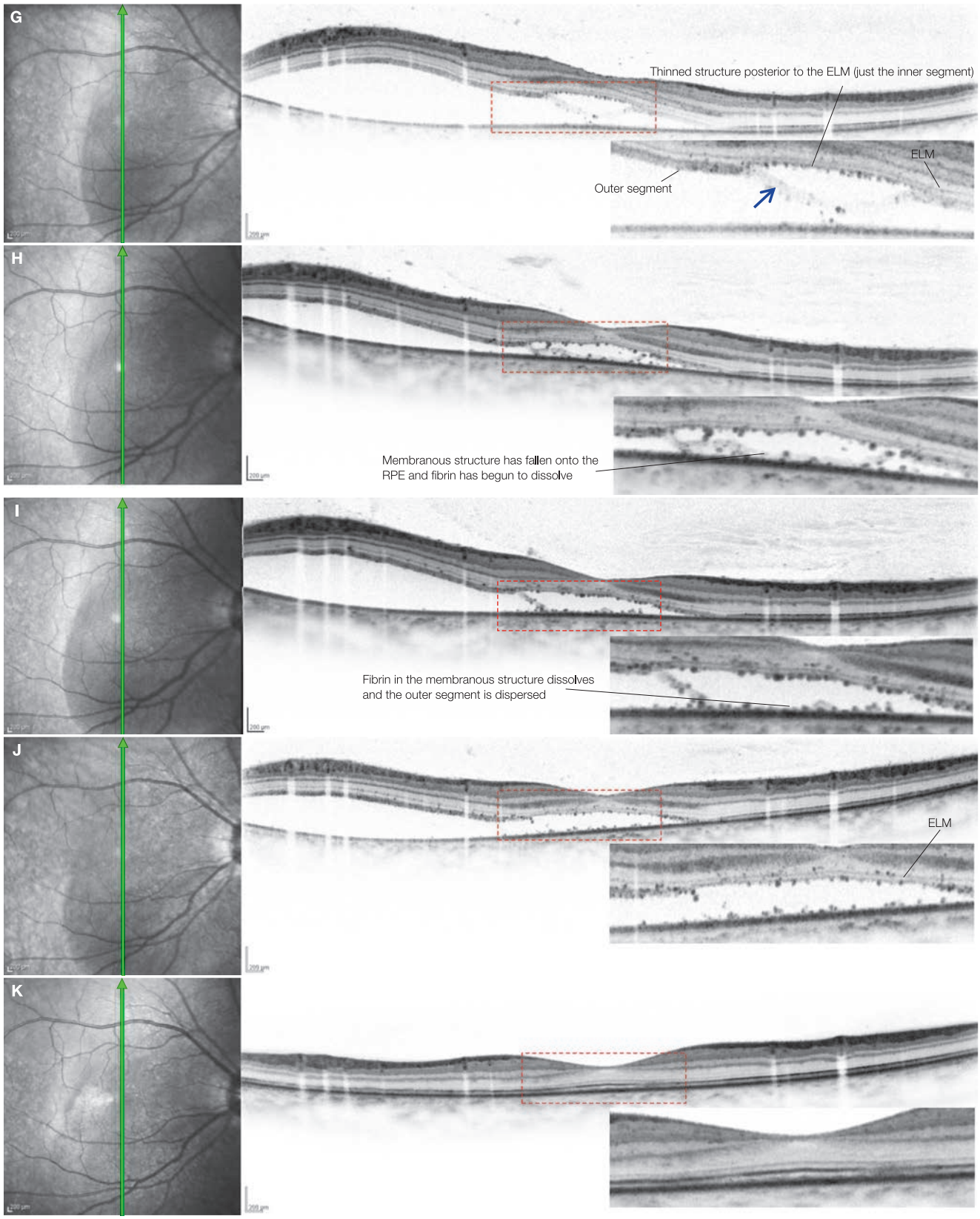

G–K: IR + OCT vertical scan of the right eye + enlarged version [red dashed box]

Case 159 Vogt-Koyanagi-Harada disease: Choroidal folds

A 68-year-old male, OD, BCVA 0.7

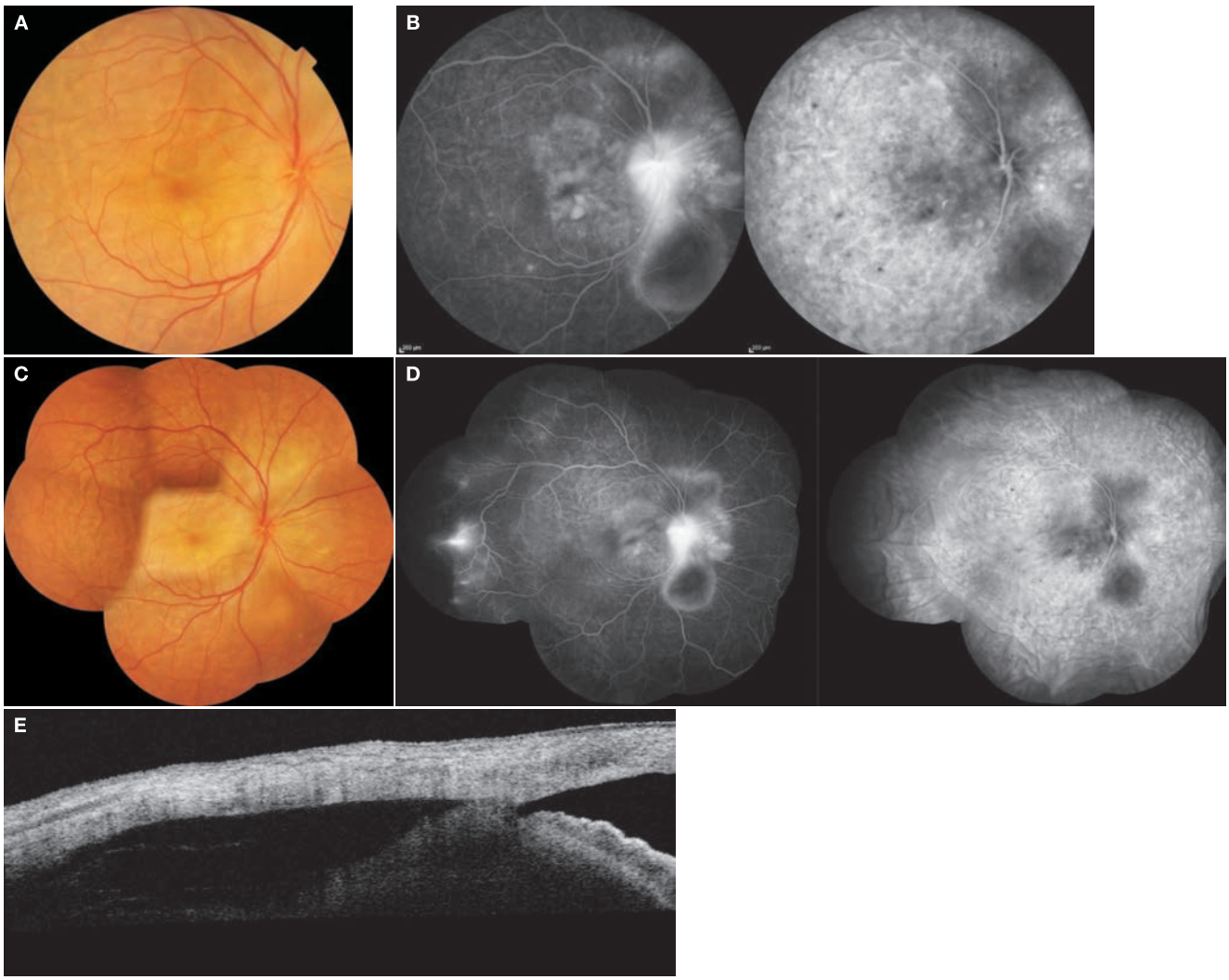

A: Color fundus photograph in the right eye: At initial diagnosis. Choroidal folds and papilledema are visible. **B:** FA + IA in the right eye (15 minutes): At initial diagnosis. Significant fluorescein leakage is noted in the optic disc, and multiple lobular dye accumulations are observed around the optic disc. **C:** Color fundus photo montage in the right eye: At initial diagnosis. Choroidal folds are seen over the entire fundus and choroidal detachments in the periphery. **D:** FA + IA montages in the right eye (20 minutes): At initial diagnosis. Fluorescein leakage is also apparent around the temporal side. **E:** Anterior segmentOCT image of the right eye: At initial diagnosis. A supraciliary effusion is visible.

F: IR + OCT vertical scan of the right eye: At initial diagnosis. Significant undulation is evident in the RPE, and SRDs (*) are visible in and superior to the fovea centralis. **G:** IR + OCT horizontal scan of the right eye + enlarged version [red dashed box]: Cystoid spaces existing in different layers are exhibited in the lower macular area. The cystoid space nasal to the fovea can be seen within the Henle's fibrous layer of the outer plexiform layer. **H:** IR + OCT vertical scan of the right eye + enlarged version [red dashed box]: Two weeks after starting steroid therapy. Best-corrected visual acuity is 0.6. The significant undulation in the RPE and the SRDs (*) appear to be worse with the gradual tapering of steroids. The outer segment undergoing shedding is depicted. **I:** IR + OCT vertical scan of the right eye + enlarged version [red dashed box]: Three weeks after starting steroid therapy. Best-corrected visual acuity is 0.6. The RPE undulation and SRDs are finally receding. The photoreceptor outer segment layer is mostly gone.

(Continued on the next page)

Case 159 Continuation

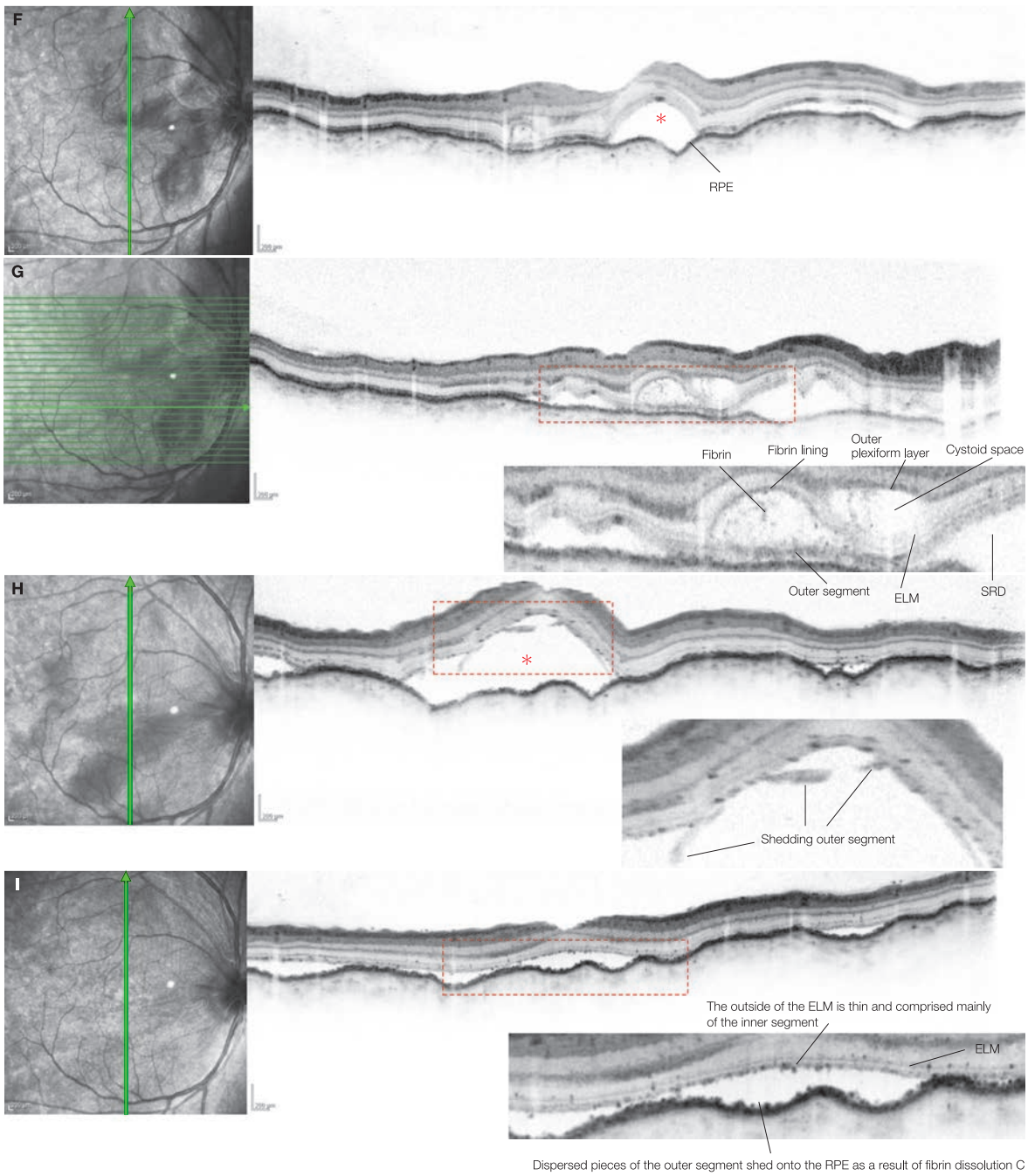

F: IR + OCT vertical scan of the right eye, **G:** IR + OCT horizontal scan of the right eye + enlarged version [red dashed box], **H, I:** IR + OCT vertical scan of the right eye + enlarged version [red dashed box]

Image interpretation points

The patient became aware of metamorphopsia and ocular pain in both eyes the day before being diagnosed. Choroidal fold formation was significant, and a choroidal detachment was visible in the periphery of the fundus. A supraciliary effusion was seen on an anterior segment OCT image. The patient was resistant to steroid therapy, and it took approximately 6 months for the RPE undulation and SRDs to recede. On OCT, in addition to the commonly seen foveal cystoid spaces, significant RPE undulation and an unusual cystoid space formation in the outer plexiform layer were exhibited. Shedding of the outer segments was seen during the therapy.

8.4 Sympathetic ophthalmia

Background

Sympathetic ophthalmia is bilateral panuveitis that occurs between 3 weeks and 6 months after a perforating ocular injury accompanied by uveal damage orintraocular surgery. Excluding a history of trauma or intraocular surgery, the onset mechanism is thought to be an autoimmune mechanism, similar to VKH syndrome. Eye symptoms such as ocular pain, photophobia, blurred vision, metamorphopsia, and reduced visual acuity can be accompanied by extraocular symptoms such as headache, fever, sensorineural hearing loss, and tinnitus. Similar to VKH syndrome, HLA-DR4 and HLA-DR53 are found in most cases, implying a genetic predisposition. Punctate or patchy leakages can be seen from the RPE and multilobular fluorescein accumulations are visible on FA. There are few reports on OCT, but cystoid space-like SRDs can be exhibited and findings similar to VKH syndrome are sometimes seen,[1] although this does not apply to all cases.[2]

References

1) Gupta V, Gupta A, Dogra MR, et al. Reversible retinal changes in the acute stage of sympathetic ophthalmia seen on spectral domain optical coherence tomography. *Int Ophthalmol*. 2011; 31: 105–110.
2) Gallagher MJ, Yilmaz T, Cervantes-Castañeda RA, et al. The characteristic features of optical coherence tomography in posterior uveitis. *Br J Ophthalmol*. 2007; 91: 1680–1685.

Case 160 Sympathetic ophthalmia: After vitreous surgery

A 41-year-old female, OD and OS, BCVA 0.1 and 1.0, respectively

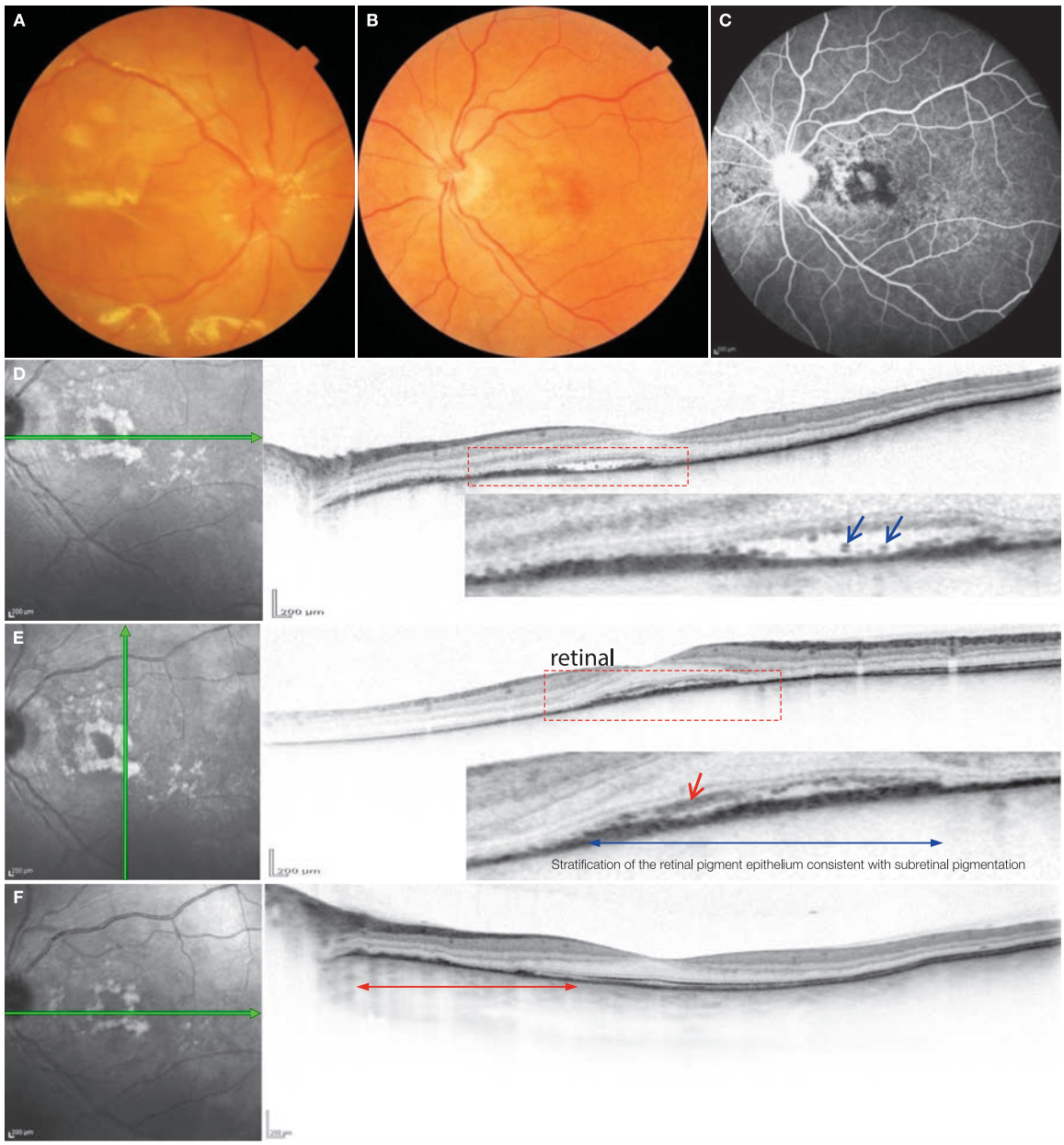

A: Color fundus photograph in the right eye: Eye with silicone oil tamponade after retinal detachment surgery. There is significant hyperemia of the optic disc. **B:** Color fundus photograph in the left eye: Pigmentation, greyish-white lesions, and a flat foveal retinal detachment are visible in the macula and around the optic disc. **C:** FA in the left eye (8 minutes): Fluorescein leakage can be seen from the optic disc and hypofluorescent lesions due to the occlusion of the choriocapillaris are seen in the macula and around the optic disc. **D:** IR + OCT horizontal scan of the left eye + enlarged version [red dashed box], **E:** IR + OCT vertical scan of the left eye + enlarged version [red dashed box]: Thickening of the RPE line consistent with pigmentation is depicted (↔). The photoreceptor outer segment of the detached area is becoming highly reflective (→) and is partially shedding as highly reflective granules. (→). **F:** IR + OCT horizontal scan of the left eye: Three months after starting steroid therapy. Best-corrected visual acuity is 1.2. The foveal IS/OS line is restored. IS/OS line defects remain in the area temporal to the optic disc the optic disc (↔)

Image interpretation points

The patient was hospitalized 4 months earlier to undergo vitreous surgery for a rhegmatogenous retinal detachment in the right eye, and 25 days later developed blurred vision in the left eye. Sympathetic ophthalmia was diagnosed and the patient underwent pulse steroid therapy, but this was ineffective. The SRD receded with combination therapy of cyclosporine and steroids.

8.5 Toxocariasis

Background

Toxocariasis occurs as a result of the ocular invasion by the larvae of Toxocara canis and Toxocara cati. It is common in ages 6 to 14 and differentiation from retinoblastoma is important since it exhibits leukocoria. Recently, this condition has developed into uveitis in adults due to the increase in number of pets and gourmet dining. Isolated, white elevated granulomatous lesions with blurred borders occur in the macular area and on the temporal side of the optic disc, and the scar contraction of the lesions causes retinal traction.

OCT findings

A mite body can be seen as a highly reflective lesion protruding into the vitreous body from the RNFL.[1] There are localized inflammatory findings in the early stages of activity including highly reflective lesions in the inner retinal layers, retinal edema, and highly reflective dots corresponding to inflammatory cells in the vitreous body and retina. Furthermore, as this condition progresses, a thick granulomatous membrane is formed in the macular area and around the optic disc, and significant retinal thickening and retinal folds can be seen.[2, 3]

References

1) Suzuki T, Joko T, Akao N, et al. Following the migration of a Toxocara larva in the retina by optical coherence tomography and fluorescein angiography. *Jpn J Ophthalmol*. 2005; 49: 159–161.
2) Higashide T, Akao N, Shirao E, et al. Optical coherence tomographic and angiographic findings of a case with subretinal toxocara granuloma. *Am J Ophthalmol*. 2003; 136: 188–190.
3) Shimizu Y, Imai M, Fukasawa A, et al. Premacular membrane peeling without removal of subretinal granuloma in an eye with ocular toxocariasis. *Acta Ophthalmol Scand*. 2005; 83: 395–396

Case 161 Toxocariasis: Proliferative membrane

A 33-year-old female, OD, BCVA 0.1

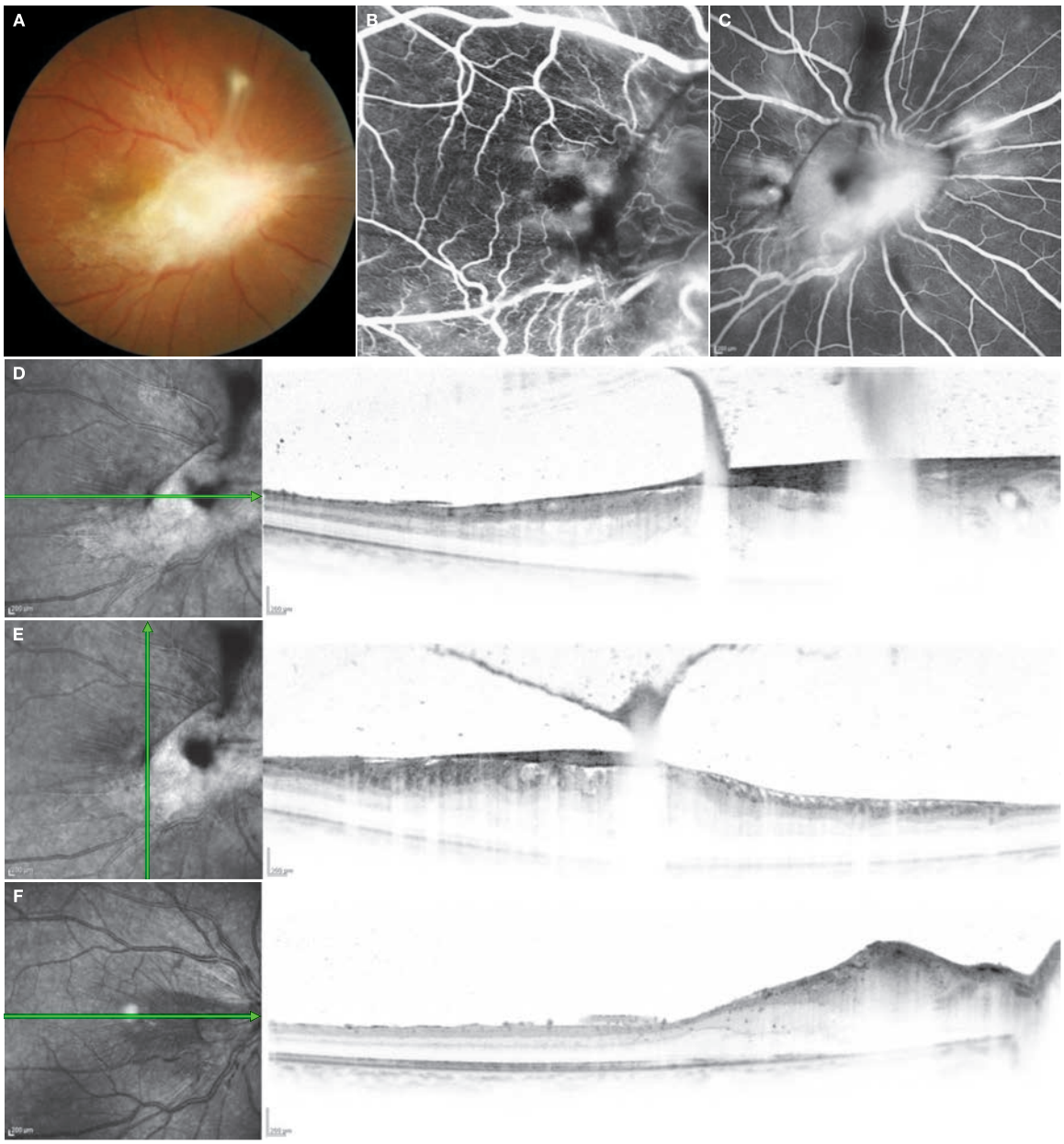

A: Color fundus photograph in the right eye: An isolated, white elevated granulomatous lesion is visible from the optic disc to the macula. Retinal folds can be observed as a result of scar contraction. **B:** FA in the right eye (2 minutes), **C:** FA in the right eye (16 minutes): Retinal capillary abnormalities and leakages are seen as a result of traction. CME is also visible. Leakages are also noticeable from the adhesion site of the granulomatous lesions and retinal blood vessels. **D:** IR + OCT horizontal scan of the right eye, **E:** IR + OCT vertical scan of the right eye: Thick proliferative membrane is exhibited on the surface of the retina and appears elevated into the vitreous body. Folds in the retinal surface layer can be seen as a result of contractile traction. **F:** IR + OCT horizontal scan of right eye: One month after vitreous surgery. Best-corrected visual acuity has improved to 0.3. The proliferative membrane has been almost completely removed. Retinal thickening remains in the vicinity of the optic disc

Image interpretation points

The patient became aware of rapid visual decline in the right eye 3 months before visiting her local doctor. A white, membrane-like structure had developed in the vitreous body and the patient was referred to us. The patient had a history of eating raw liver. Vitreous samples collected during surgery were positive for Toxocara canis and Ascaris suum antibodies. Final best-corrected visual acuity was 0.6.

8.6 Acute retinal necrosis (Kirisawa-type uveitis)

Background

Acute retinal necrosis is acute panuveitis that occurs in one or both eyes of healthy individuals of all ages as a result of a localized infection of the eye with the varicella-zoster virus (VZV) or herpes simplex virus (HSV). This disease progresses rapidly and has a high risk of blindness due to phthisis bulbi, optic neuropathy and/or CRAO.[1, 2] Early detection is important, and if acute iridocyclitis accompanied by mutton-fat keratic precipitates and ocular hypertension is seen, it is important not to overlook yellowish-white patches in the periphery of the retina, retinal periarteritis, and hyperemia of the optic disc. The yellowish-white patches indicate retinal necrotic lesions, and the yellowish-white patchy lesions in the early phase become confluent resulting in geographic lesions. Vasculitis also occurs in the acute phase with perivascular hemorrhages, sheathing, and terminal obliteration of arterioles. During the quiescent phase, in approximately 90% of cases, a rhegmatogenous retinal detachment occurs in the peripheral retinal necrotic area. An average of two main branches of the retinal artery are occluded during the quiescent phase. Hydatoid polymerase chain reaction (PCR) is the most sensitive and specific for a definitive diagnosis.

OCT findings

During the acute phase, multiple highly reflective dots corresponding to inflammatory cells can be seen mainly in the vitreous body, and the inner retinal layers become highly reflective consistent with yellowish-white patchy lesions. This is sometimes accompanied by subretinal fluid and exudation. Irregular thinning of the retina, cystoid space formation, and obscuration of the retinal layer structure progresses as the retina gradually breaks down.[3, 4] During the remission phase, significant retinal thinning consistent with the sites of severe necrosis and retinal detachment is visible.

References

1) Usui Y, Goto H. Overview and diagnosis of acute retinal necrosis syndrome. *Semin Ophthalmol*. 2008; 23: 275–283.
2) Kawaguchi T, Spencer DB, Mochizuki M. Therapy for acute retinal necrosis. *Semin Ophthalmol*. 2008; 23: 285–290.
3) Suzuki J, Goto H, Minoda H, et al. Analysis of retinal findings of acute retinal necrosis using optical coherence tomography. *Ocul Immunol Inflamm*. 2006; 14: 165–170.
4) Blair MP, Goldstein DA, Shapiro MJ. Optical coherence tomography of progressive outer retinal necrosis. *Retina*. 2007; 27: 1313–1314.

Case 162 Acute retinal necrosis (Kirisawa-type uveitis): A typical example

A 28-year-old female, OD, BCVA 0.4

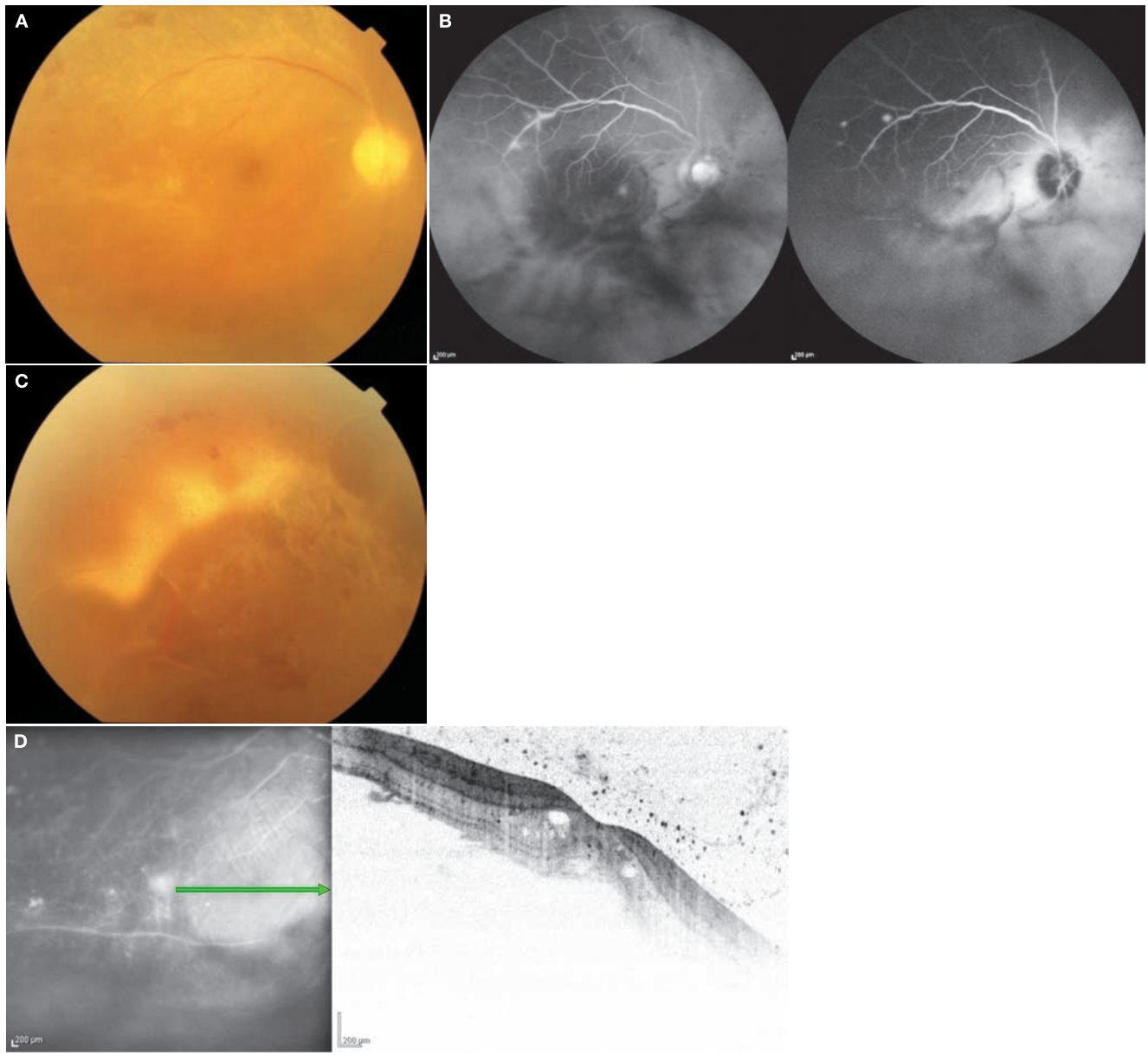

A: Color fundus photograph in the right eye: At initial diagnosis. In the posterior pole, retinal detachment accompanied by retinal hemorrhages and effusive retinal whitening, sheathed retinal artery, vitreous clouding, and a pale optic disc are seen. **B:** FA + IA in the right eye (14 minutes): The lower half of the retinal blood vessels cannot be seen due to vitreous clouding. **C:** Color fundus photograph in the right eye: At initial diagnosis. Upper temporal periphery of the fundus. Yellowish-white patchy lesions, retinal breaks, retinal hemorrhages, thinned retina, and sheathed retinal blood vessels are visible. **D:** IR + OCT horizontal scan of the right eye: A retinal detachment accompanied by a foveal cystoid spaces is observed. Multiple infiltrating cells can be seen in the vitreous cavity.

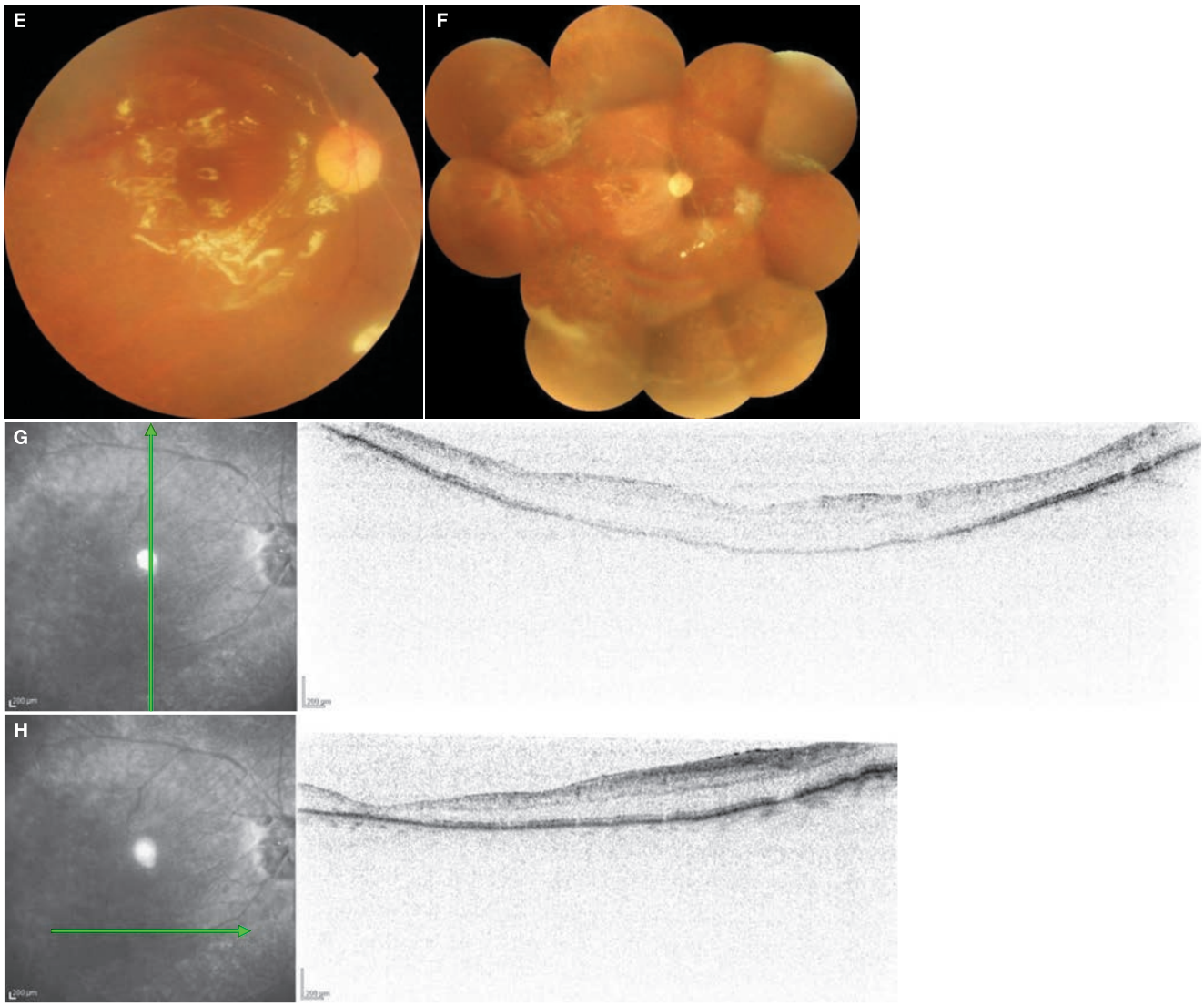

E: Color fundus photograph in the right eye, **F:** Color photograph montage in the right eye: One month after surgery. Best-corrected visual acuity 0.2. The retina is reattached under silicone oil tamponade. Three sheathed retinal blood vessels are visible. **G:** IR + OCT vertical scan of the right eye, **H:** IR + OCT horizontal scan of the right eye: The retina is reattached, but the retina is significantly thin.

Image interpretation points

The patient was diagnosed with acute retinal necrosis in the right eye by her local doctor 20 days earlier and underwent combination therapy with acyclovir, interferon, and steroids. A bullous, retinal detachment had developed several days prior, and the patient was referred to us. The patient exhibited rapid progression including peripheral retinal necrosis with retinal hemorrhages and clouding, sheathing of the retinal blood vessels, and vitreous inflammation. The patient tested strongly positive for VZV. Once again, a combination therapy of acyclovir, valacyclovir hydrochloride, and steroids was administered.
The retina was reattached by vitreous surgery and a silicone oil tamponade, but breakdown of the retina was significant.

Pathologic myopia and related diseases

9.1 Myopia – 304
References – 307
Case 163 Intrachoroidal cavitation: A Typical example – 308
Case 164 Intrachoroidal cavitation: Connection with the vitreous cavity – 309
Case 165 Lacquer cracks: A typical example – 310
Case 166 Lacquer cracks: A mild case – 311
Case 167 ILM detachment: Case without foveoschisis – 312
Case 168 Myopic foveoschisis: Case without foveal detachment – 313
Case 169 Myopic foveoschisis: Case with foveal detachment – 314, 315
Case 170 Myopic foveoschisis: Case with macular retinal detachment – 316
Case 170 Two and a half years after surgery – 317
Case 171 Myopic foveoschisis: Traction from the thickened posterior vitreous cortex – 318
Case 172 Myopic foveoschisis: Macular hole formation – 319
Case 173 Myopic foveoschisis: MHRD – 320
Case 174 Myopic foveoschisis: Before and after surgery for MHRD – 321
Case 175 Myopic subretinal hemorrhages: A typical example – 322, 323
Case 176 Myopic choroidal neovascularization: A typical example – 324
Case 177 Myopic choroidal neovascularization: Small CNV – 325
Case 177 After anti-VEGF treatment – 326
Case 178 Myopic choroidal neovascularization: Large CNV – 327
Case 179 Myopic choroidal neovascularization: A young example – 328, 329
Case 180 Myopic choroidal neovascularization: Foveoschisis – 330
9.2 Dome-shaped macula and inferior staphyloma – 331
References – 331
Case 181 Dome-shaped macula: A typical example – 332
Case 182 Inferior staphyloma: Serous retinal detachment – 333, 334

9.1 Myopia

Background

Myopia is a disease seen at a high frequency in Asians. It is more common in women than men and results in various fundus changes from 30 years of age. Myopia that develops fundus changes such as posterior staphyloma in the posterior pole or chorioretinal atrophic lesions is known as pathologic myopia or degenerative myopia. The basic element of degenerative myopia is elongation of the axial length with the sclera stretching posteriorly. Ocular axial lengths of normally about 22 to 24 mm are sometimes seen to stretch beyond 30 mm.

Elongation of the sclera is not uniform and in particular, significant elongation occurs in the posterior pole. This condition is called a posterior staphyloma (Fig. 9-1). In posterior staphyloma, the sclera (eyeball wall) protrudes posteriorly in various areas of the posterior pole and can also exhibit complex forms. Curtin classified posterior staphyloma into 10 types ranging from I to X [1] (Fig. 9-2). This classification is based on binocular indirect ophthalmoscopy findings and is not necessarily based on precise evaluation of the ocular configuration. According to Hsiang et al., Type II of the Curtin classification is the most common posterior staphyloma seen in myopia of Japanese people and accounts for over 50% throughout all ages. Type II decreases with age and Type IX, which features ridge-like anteriorly protruding curvature of the sclera along vertical direction of the fundus between the optic disc and fovea centralis, increases. This kind of uneven deformation of the sclera is thought

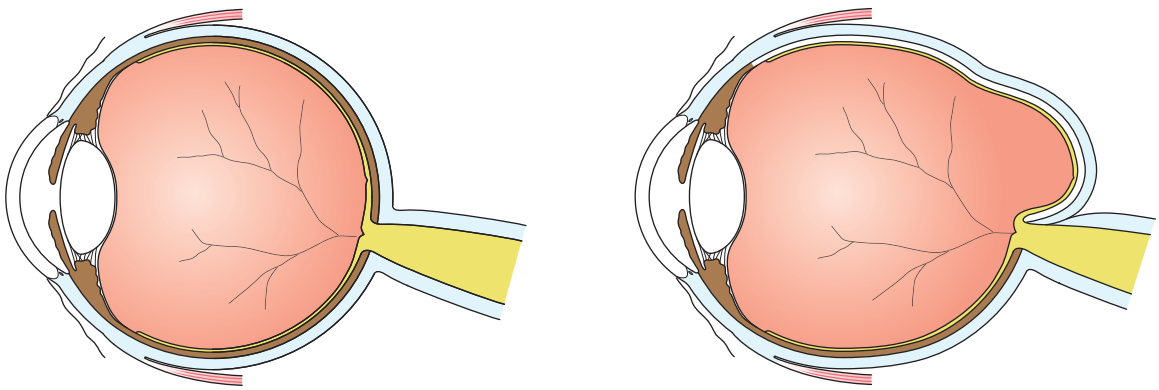

Fig. 9-1 Schematic diagram of posterior staphyloma
Compared with a normal eye (**A**), in a highly myopic eye the axial length is extended and the posterior pole of the fundus protrudes backwards (**B**)

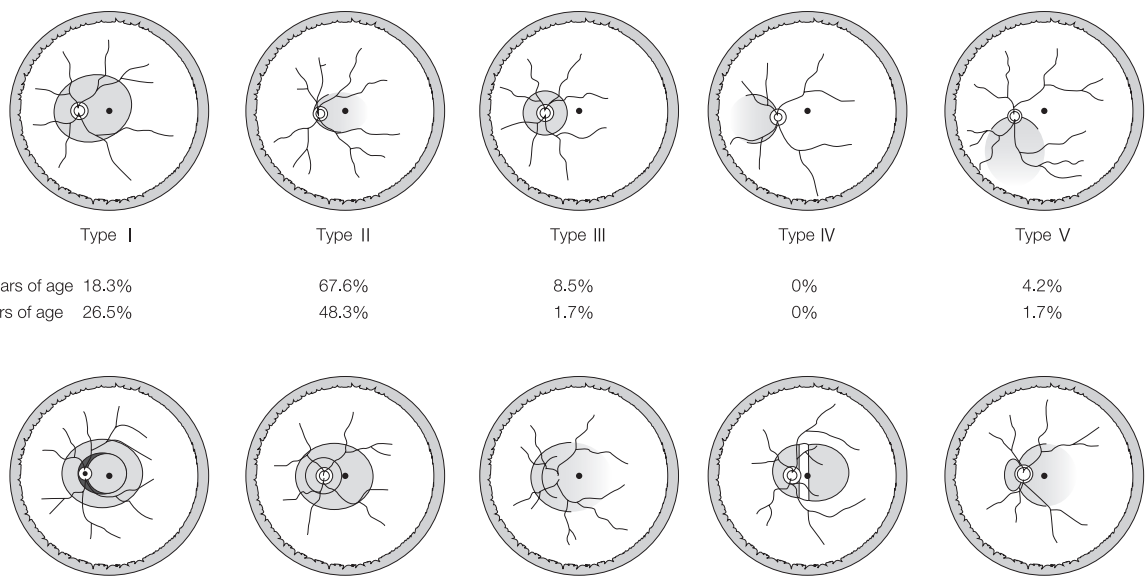

Fig. 9-2 Curtin classification and frequency of each type of posterior staphyloma in highly myopic eyes of Japanese people.
Type II decreases and Type IX increases with age.
(Modified according to Hsiang HW, et al. Clinical characteristics of posterior staphyloma in eyes with pathologic myopia. *Am J Ophthalmol*. 2008; 146: 102–110)

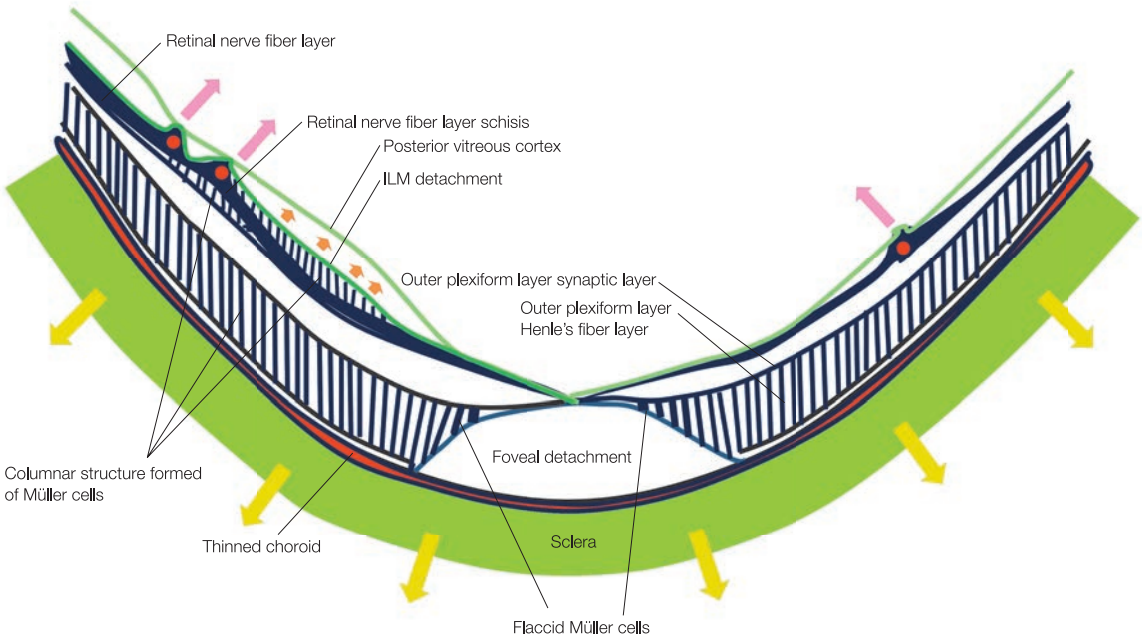

Fig. 9-3 Chorioretinal and scleral changes visible in high myopia
Various chorioretinal and scleral changes occurs in conjunction with the posterior elongation of the ocular length in highly myopic eyes.
: Forward traction towards the inner retinal layers by retinal blood vessels resulting from posterior scleral elongation
: Forward traction towards the inner retinal layers by the ILM resulting from posterior scleral elongation
: Backward traction towards the outer retinal layers due to posterior scleral elongation

to play a large role in the onset of complications seen in degenerative myopia.[2]

An important element to understand pathogenesis of the fundus lesions that occur in degenerative myopia is the presence of tissue that is easily stretched, and tissue that is difficult to stretch that comprise the eyeball. When the sclera extends posteriorly, traction to soft tissue is generated if there are differences in the extensibility of the intraocular tissues. Specifically, the thickened posterior vitreous cortex, ILM, retinal blood vessels, and Bruch's membrane, which are relatively inelastic cannot be so severely elongated posteriorly as the sclera, thus causing various changes such as ILM detachment, retinal nerve fiber layer separation, retinoschisis, and lacquer cracks (Fig. 9-3).

Typical fundus findings seen in degenerative myopia and their OCT images

Intrachoroidal cavitation (ICC)

These are cavity-like findings in the choroid seen around the optic disc. This was formerly known as peripapillary detachment in pathologic myopia (PDPM).[3] It was originally supposed to be a PED,[4] but this interpretation was found to be incorrect based on examinations with high resolution OCT. The detection frequency is 5–10% in myopic eyes of -8D or above.[5, 6] A large cavity in ICC develops in the choroid. Some believe that the content of this cavity is vitreous humor.[7] ICC can exhibit visual field defects that are indistinguishable from glaucoma.[5, 6]

Lacquer cracks

Breaks spontaneously occur in Bruch's membrane with the elongation of the axial length. These breaks are observed as linear lesions, often radially, in the fundus.[8] They are depicted as abnormalities at the level of Bruch's membrane and photoreceptor inner and outer segment junction (IS/OS) on OCT.

Myopic foveoschisis or myopic macular retinoschisis

This is a pathological condition resulting in retinoschisis as first reported by Takano and Kishi in 1999.[9] It was identified as retinal detachment during the era without OCT, but the true pathology has been revealed by OCT. In highly myopic eyes, retinal detachment can occur without the formation of retinal breaks before the onset of macular hole retinal detachment (MHRD). This condition is seen in 10–34% of highly myopic eyes.[9, 10] Various findings, such as IS/OS abnormalities, ERM formation, macular holes, retinal fold formation, and ILM detachment are seen on SD-OCT imaging at a high frequency.[11] Columnar structures traversing the retina in the longitudinal direction thought to be Müller cells are detected in the retinoschisis.[12]

Lower extensibility of the retinal blood vessels and ILM, than other sensory retinal tissues play an important role in the onset of myopic foveoschisis.[13] That is to say, the sensory retina is elongated posteriorly with posterior staphyloma formation, but the retinal blood vessels and ILM cannot follow the elongation of the sensory retina closely because of their poor extensibility, and consequently the superficial layer of the retina is pulled in the longitudinal direction causing retinoschisis (Fig. 9-3). MHRD is thought to develop from myopic foveoschisis. Thus, myopic foveaschisis is a progressive disease.[14] Visual acuity tend to

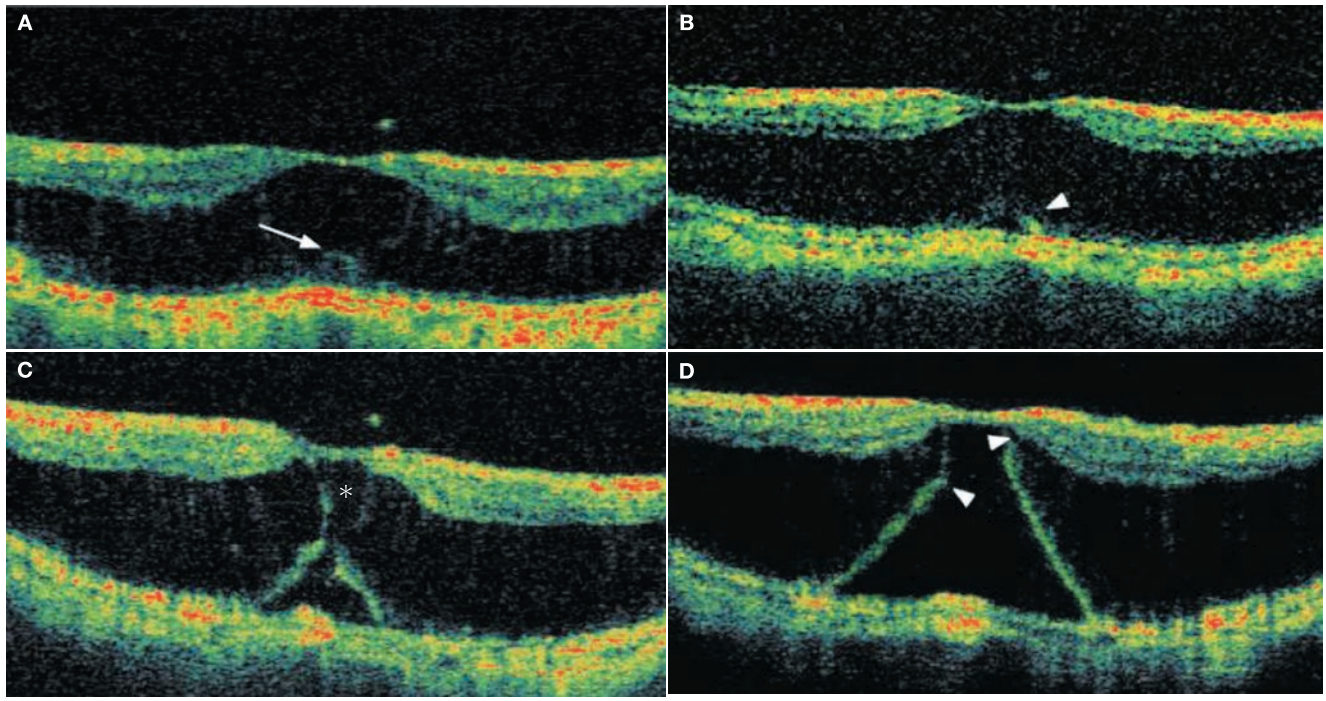

Fig. 9-4 An example of the formation process of a macular hole in high myopia
A: Stage 1, high reflectivity associated with the focal elevation of outer retinal layers can be seen (⇨). **B:** Stage 2, outer lamellar hole formation (▷). **C:** Inward expansion of the outer lamellar hole and progression of retinoschisis (❋). **D:** The outer lamellar hole progresses forward and comes in contact with the retinoschisis (▷).
(Modified according to Shimada N, et al. Progression from macular retinoschisis to retinal detachment in highly myopic eyes in associated with outer lamellar hole formation. *Br J Ophthalmol* 2008; 92: 762–764.)

decrease in the cases that not only undergo intraretinal changes, but also vitreoretinal interface-related changes such as ERM formation, macular hole formation, and ILM detachment. Cases with foveal detachment often develop macular holes.[15] Currently, vitreous surgery in combination with ILM peeling is a standard treatment for cases of myopic foveoschisis with foveal detachment.[15–17]

Myopic subretinal hemorrhages

Highly myopic eyes in which hemorrhages are seen at the fovea centralis require the differentiation of myopic subretinal hemorrhages from hemorrhages with choroidal neovascularization (CNV). Myopic subretinal hemorrhages develop without the presence of CNV and are caused by breaks in Bruch's membrane and choroid that occurs with axial length elongation. The incidence is reportedly 3% in highly myopic eyes.[18] Lacquer cracks are known to appear after myopic subretinal hemorrhages have subsided.[19] The visual prognosis for myopic subretinal hemorrhages is generally good, but prognosis is poor in cases of poor visual acuity at initial diagnosis, cases where the IS/OS is not depicted on OCT imaging at initial diagnosis, and cases where there is hypofluorescence on fundus autofluorescence.[20]

Macular hole

Macular holes in highly myopic eyes result from a variety of mechanisms including those similar to idiopathic macular holes, those which develop from myopic foveoschisis, and those which develop from vitreomacular traction syndrome.[21, 22] Shimada et al. report that the progression from myopic foveoschisis to foveal retinal detachment can be divided into 4 stages based on OCT findings.

Stage 1 involves the localized elevation of the foveal outer retinal layers and the increased reflectivity in these layers. In Stage 2, a outer lamellar hole (a foveal detachment on OCT) develops in the fovea centralis and parafovea. Stage 3 comprises the inward expansion of the lamellar hole into the retina. In Stage 4, the inner border of the outer lamellar hole extends until it comes into contact with the innermost layer of the separated retina and retinal detachment has expanded[22] (Fig. 9-4).

Paravascular retinal cysts

Paravascular retinal cysts were initially described as changes in retinal thinning around retinal blood vessels,[23] but Shimada et al. paravascular retinal cysts to be intraretinal cavities around the blood vessels on OCT images.[24] These changes are detected in 49.5% of highly myopic eyes. Rupture of the inner walls of paravascular retinal cysts can result in the development of paravascular lamellar holes and can contribute to changes in the vitreoretinal interface (ILM detachment, ERM etc.) observed in eyes with degenerative myopia.[24]

Vascular microfolds

Vascular microfolds are findings that are also seen frequently in highly myopic eyes. Because the tissue extensibility of retinal blood vessels is low compared with the sensory retina, the superficial retinal layer is elevated by the blood vessels. These features

are termed vascular microfolds, and initially were reported as findings seen after vitreous surgery in combination with ILM peeling,[25] but they are unrelated to surgery[26] and are evident in 20–44.6% of highly myopic eyes.[25, 27]

ILM detachment

The ILM is seen to be separated from the retinal nerve fiber layer in 2.4–6% of highly myopic eyes, which is termed ILM detachment.[27, 28] Based on the fact that myopic foveoschisis occurs in the majority of cases with ILM detachment, there is thought to be a close relationship between ILM detachment and myopic foveoschisis.[2, 28] The onset mechanism of ILM detachment is not necessarily fully understood, but the posterior vitreous cortex that remains on the retinal surface is thought to play a role.

This feature needs to be differentiated from RNFL detachment, which is caused by the inwards traction of the retinal blood vessels to the RNFL.

Myopic CNV

CNV is a complication seen in 4–11% of highly myopic eyes.[29–31] Its natural course is extremely poor, and according to long-term follow-up reports, best-corrected visual acuity becomes less than 0.1 in almost all cases.[32] The CNV is type 2 CNV, and patchy chorioretinal atrophy and lacquer cracks are important in the onset of neovascularization.[33] CNV becomes an atrophic lesion (Fuchs' spot) over time, and macular holes frequently develop in cases where the chorioretinal atrophic lesion is larger than 1 disc diameter.[33] Photocoagulation and photodynamic therapy can be used in the treatment of myopic CNV,[34, 35] but results in expansion of atrophic lesions. Therefore, anti-VEGF therapy is currently the first choice.[36] However, its long-term outcome still remains unclear.

References

1) Curtin BJ. The posterior staphyloma of pathologic myopia. *Trans Am Ophthal Soc*. 1997; 75: 67–86.
2) Hsiang HW, Ohno-Matsui K, Shimada N, et al. Clinical characteristics of posterior staphyloma in eyes with pathologic myopia. *Am J Ophthalmol*. 2008; 146: 102–110.
3) Toranzo J, Cohen SY, Erginay A, et al. Peripapillary intrachoroidal cavitation in myopia. *Am J Ophthalmol*. 2005; 140: 731–732.
4) Freund KB, Ciardella AP, Yannuzzi LA, et al. Peripapillary detachment in pathologic myopia. *Arch Ophthalmol*. 2003; 121: 197–204.
5) Shimada N, Ohno-Matsui K, Nishimuta A, et al. Characteristics of peripapillary detachment in pathologic myopia. *Arch Ophthalmol*. 2006; 124: 46–52.
6) Shimada N, Ohno-Matsui K, Nishimuta A, et al. Peripapillary changes detected by optical coherence tomography in eyes with high myopia. *Ophthalmology*. 2007; 114: 2070–2076.
7) Wei YH, Yang CM, Chen MS, et al. Peripapillary intrachoroidal cavitation in high myopia : reappraisal. *Eye* (*Lond*). 2009; 23: 141–144.
8) Klein RM, Curtin BJ. Lacquer crack lesions in pathologic myopia. *Am J Ophthalmol*. 1975; 79: 386–392.
9) Takano M, Kishi S. Foveal retinoschisis and retinal detachment in severely myopic eyes with posterior staphyloma. *Am J Ophthalmol*. 1999; 128: 472–476.
10) Baba T, Ohno-Matsui K, Futagami S, et al. Prevalence and characteristics of foveal retinal detachment without macular hole in high myopia. *Am J Ophthalmol*. 2003; 135: 338–342.
11) Sayanagi K, Morimoto Y, Ikuno Y, et al. Spectral-domain optical coherence tomographic findings in myopic foveoschisis. *Retina*. 2010; 30: 623–628.
12) Fujimoto M, Hangai M, Suda K, et al. Features associated with foveal retinal detachment in myopic macular retinoschisis. *Am J Ophthalmol*. 2010; 150: 863–870.
13) Shimada N, Ohno-Matsui K, Baba T, et al. Natural course of macular retinoschisis in highly myopic eyes without macular hole or retinal detachment. *Am J Ophthalmol*. 2006; 142: 497–500.
14) Gaucher D, Haouchine B, Tadayoni R, et al. Long-term follow-up of high myopic foveoschisis : natural course and surgical outcome. *Am J Ophthalmol*. 2007; 143: 455–462.
15) Kobayashi H, Kishi S. Vitreous surgery for highly myopic eyes with foveal detachment and retinoschisis. *Ophthalmology*. 2003; 110: 1702–1707.
16) Ikuno Y, Sayanagi K, Ohji M, et al. Vitrectomy and internal limiting membrane peeling for myopic foveoschisis. *Am J Ophthalmol*. 2004; 137: 719–724.
17) Scott IU, Moshfeghi AA, Flynn HW Jr. Surgical management of macular retinoschisis associated with high myopia. *Arch Ophthalmol*. 2006; 124: 1197–1199.
18) Tokoro T. Explanatory factors of chorioretinal atrophy. In : Tokoro T, ed. Atlas of Posterior Fundus Changes in Pathologic Myopia. Tokyo, Japan, Springer-Verlag, 1998. pp23–54.
19) Ohno-Matsui K, Ito M, Tokoro T. Subretinal bleeding without choroidal neovascularization in pathologic myopia. A sign of new lacquer crack formation. *Retina*. 1996; 16: 196–202.
20) Moriyama M, Ohno-Matsui K, Shimada N, et al. Correlation between visual prognosis and fundus autofluorescence and optical coherence tomographic findings in highly myopic eyes with submacular hemorrhage and without choroidal neovascularization. *Retina*. 2011; 31: 74–80.
21) Smiddy WE, Kim SS, Lujan BJ, et al. Myopic traction maculopathy : spectral domain optical coherence tomographic imaging and a hypothesized mechanism. *Ophthalmic Surg Lasers Imaging*. 2009; 40: 169–173.
22) Shimada N, Ohno-Matsui K, Yoshida T, et al. Progression from macular retinoschisis to retinal detachment in highly myopic eyes is associated with outer lamellar hole formation. *Br J Ophthalmol*. 2008; 92: 762–764.
23) Spencer LM, Foos RY. Paravascular vitreoretinal attachments. Role in retinal tears. *Arch Ophthalmol*. 1970; 84: 557–564.
24) Shimada N, Ohno-Matsui K, Nishimuta A, et al. Detection of paravascular lamellar holes and other paravascular abnormalities by optical coherence tomography in eyes with high myopia. *Ophthalmology*. 2008; 115: 708–717.
25) Ikuno Y, Gomi F, Tano Y. Potent retinal arteriolar traction as a possible cause of myopic foveoschisis. *Am J Ophthalmol*. 2005; 139: 462–467.
26) Sayanagi K, Ikuno Y, Gomi F, et al. Retinal vascular microfolds in highly myopic eyes. *Am J Ophthalmol*. 2005; 139: 658–663.
27) Forte R, Cennamo G, Pascotto F, et al. En face optical coherence tomography of the posterior pole in high myopia. *Am J Ophthalmol*. 2008; 145: 281–288.
28) Sayanagi K, Ikuno Y, Tano Y. Tractional internal limiting membrane detachment in highly myopic eyes. *Am J Ophthalmol*. 2006; 142: 850–852.
29) Curtin BJ, Karlin BD. Axial length measurements and fundus changes of the myopic eyes. *Am J Ophthalmol*. 1971; 71: 42–50.
30) Grossniklaus HE, Green WR. Pathologic findings in pathologic myopia. *Retina*. 1992; 12: 127–133.
31) Hotchkiss ML, Fine SL. Pathologic myopia and choroidal neovascularization. *Am J Ophthalmol*. 1981; 91: 177–183.
32) Yoshida T, Ohno-Matsui K, Yasuzumi K, et al. Myopic choroidal neovascularization : a 10-year follow-up. *Ophthalmology*. 2003; 110: 1297–1305.
33) Shimada N, Ohno-Matsui K, Yoshida T, et al. Development of macular hole and macular retinoschisis in eyes with myopic choroidal neovascularization. *Am J Ophthalmol*. 2008; 145: 155–161.
34) Chan WM, Ohji M, Lai TY, et al. Choroidal neovascularisation in pathological myopia : an update in management. *Br J Ophthalmol*. 2005; 89: 1522–1528.
35) Hayashi K, Ohno-Matsui K, Shimada N, et al. Long-term results of photodynamic therapy for choroidal neovascularization in Japanese patients with pathologic myopia. *Am J Ophthalmol*. 2011; 151: 137–147.
36) Gharbiya M, Giustolisi R, Allievi F, et al. Choroidal neovascularization in pathologic myopia : intravitreal ranibizumab versus bevacizumab – a randomized controlled trial. *Am J Ophthalmol*. 2010; 149: 458–464.

Case 163 Intrachoroidal cavitation: A Typical example

A 40-year-old male, OS, BCVA 1.2, an axial length 29.46 mm

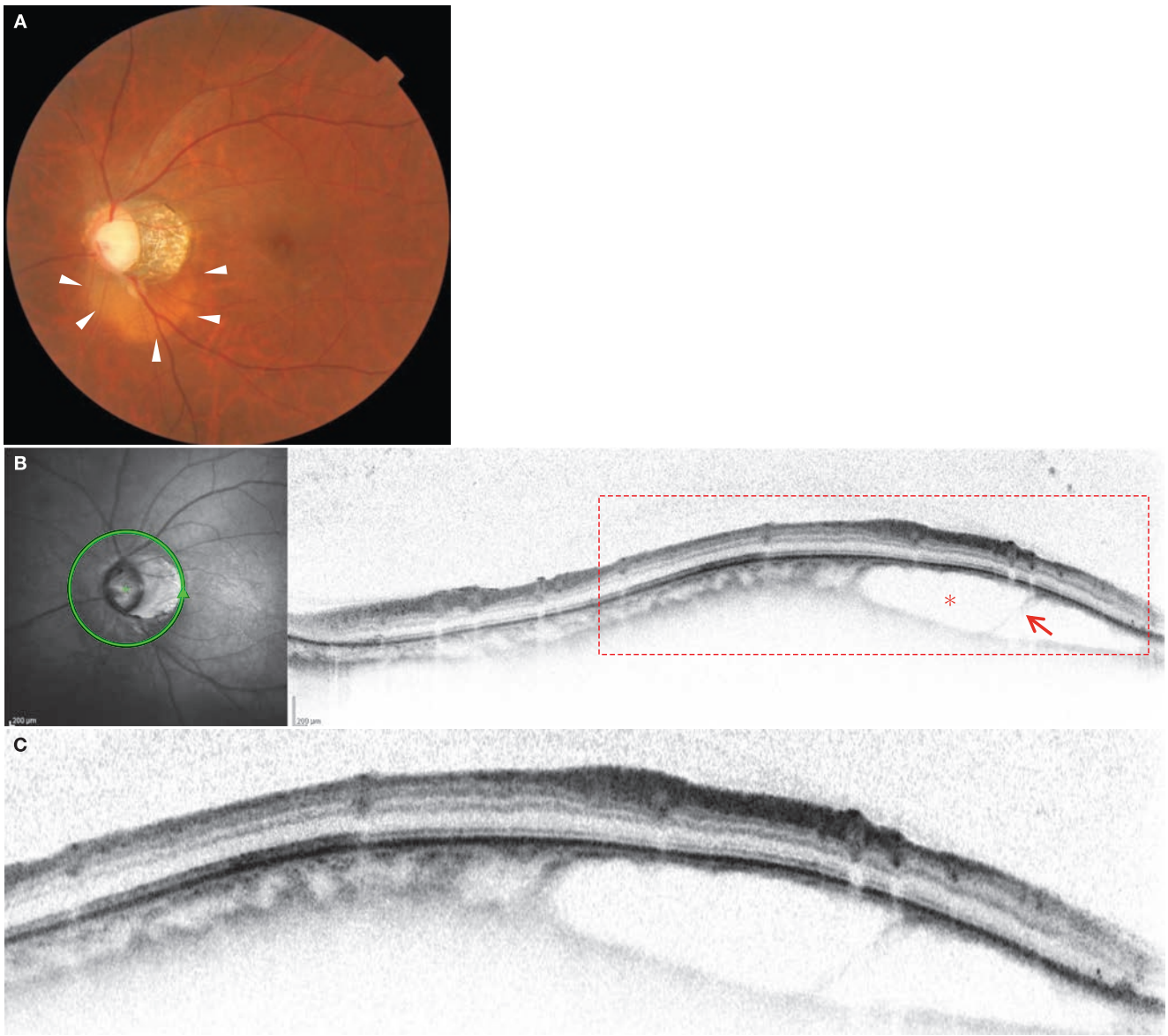

A: Color fundus photograph in the left eye: The optic disc cupping is large, suggesting glaucoma is present. Extensive peripapillary atrophy (PPA) is present. Typical intrachoroidal cavitation is visible inferior to the optic disc (▷). **B:** IR + OCT circle scan of the left eye: A circle scan of the area around the optic disc. Extensive intrachoroidal cavitation (✻) is evident. Thin choroidal tissue appears to remain immediately beneath the retinal pigment epithelium. A septum is present in the cavity (➔). **C:** Enlarged version of B [red dashed box]: We can see that intrachoroidal cavitation is a cavity inside the choroid and not a PED. The cavity is clearly depicted in B, and on the enlarged image, the remaining thin choroidal tissue on the choroidal side of the highly reflective retinal pigment epithelium is more apparent.

Image interpretation points

This is a case of extensive intrachoroidal cavitation. This was formerly reported under the name of peripapillary detachment in pathologic myopia (PDPM), but intrachoroidal cavitation (ICC) better reflects the pathologic condition. There is insufficient research on the relationship between ICC and visual dysfunction, which is the topic of future studies.

Case 164 Intrachoroidal cavitation: Connection with the vitreous cavity

A 59-year-old female, OS, BCVA 1.5, an axial length 27.90 mm

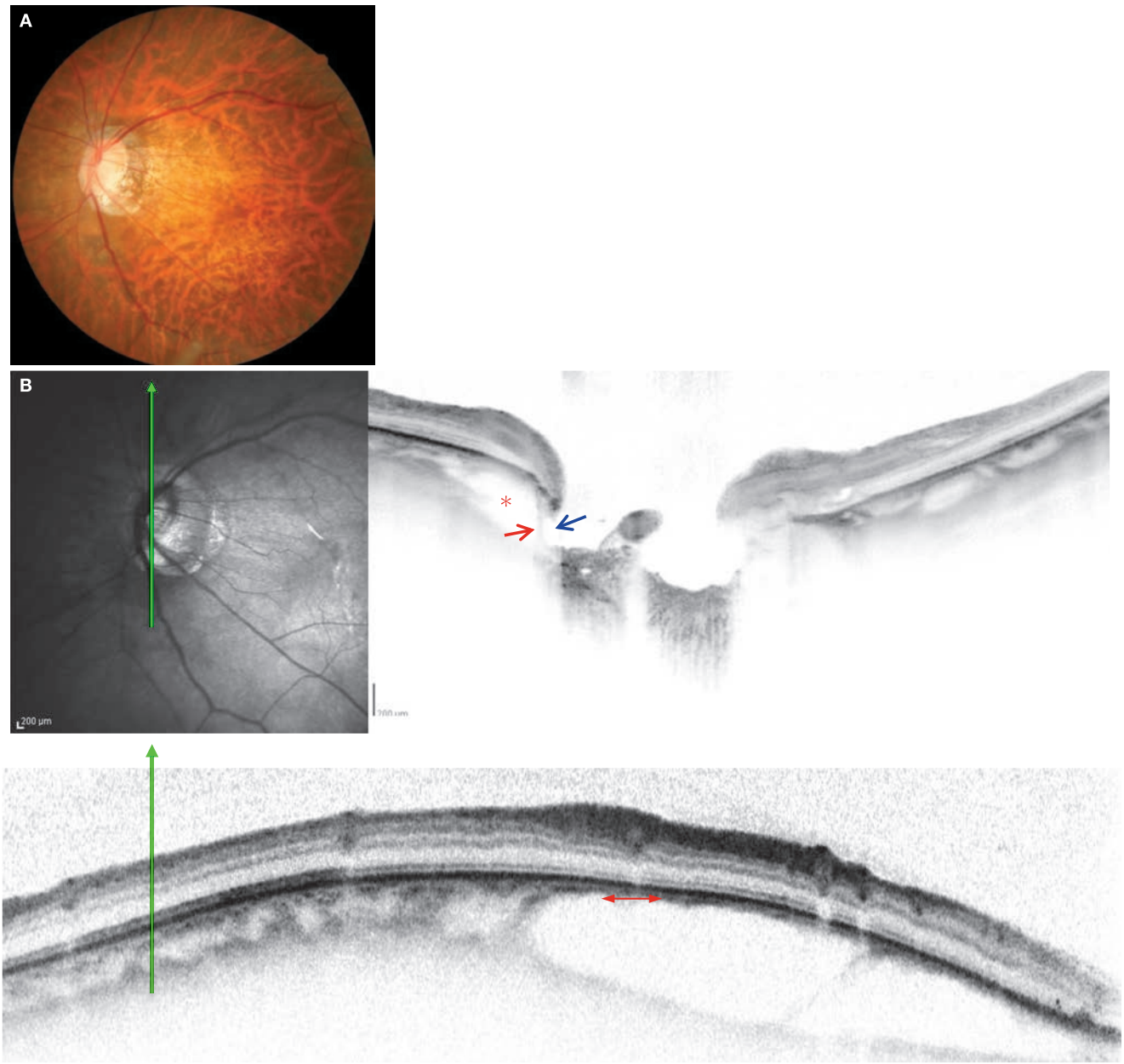

A: Color fundus photograph in the left eye: The ICC is not as clear as case 163 on photo. **B:** IR + OCT vertical scan of the left eye: Scan passing through the optic disc. Small ICC (✻) can be seen immediately inferior to the optic disc. A very thin septum exists between the ICC and vitreous cavity (→). The sensory retina is disrupted (→). **C:** IR + OCT vertical scan of the left eye: Scan of the area immediately nasal to the scan in B. We can see that there is an intersection between the ICC and vitreous body (↔). In such cases, the neural retina may become disrupted and the retinal nerve fibers rupture.

Image interpretation points

Some believe that the content of ICC is derived from the vitreous fluid. In this case, there is a clear connection between the ICC and vitreous cavity.

Case 165 Lacquer cracks: A typical example

A 67-year-old male, OS, BCVA 0.4, an axial length 28.22 mm

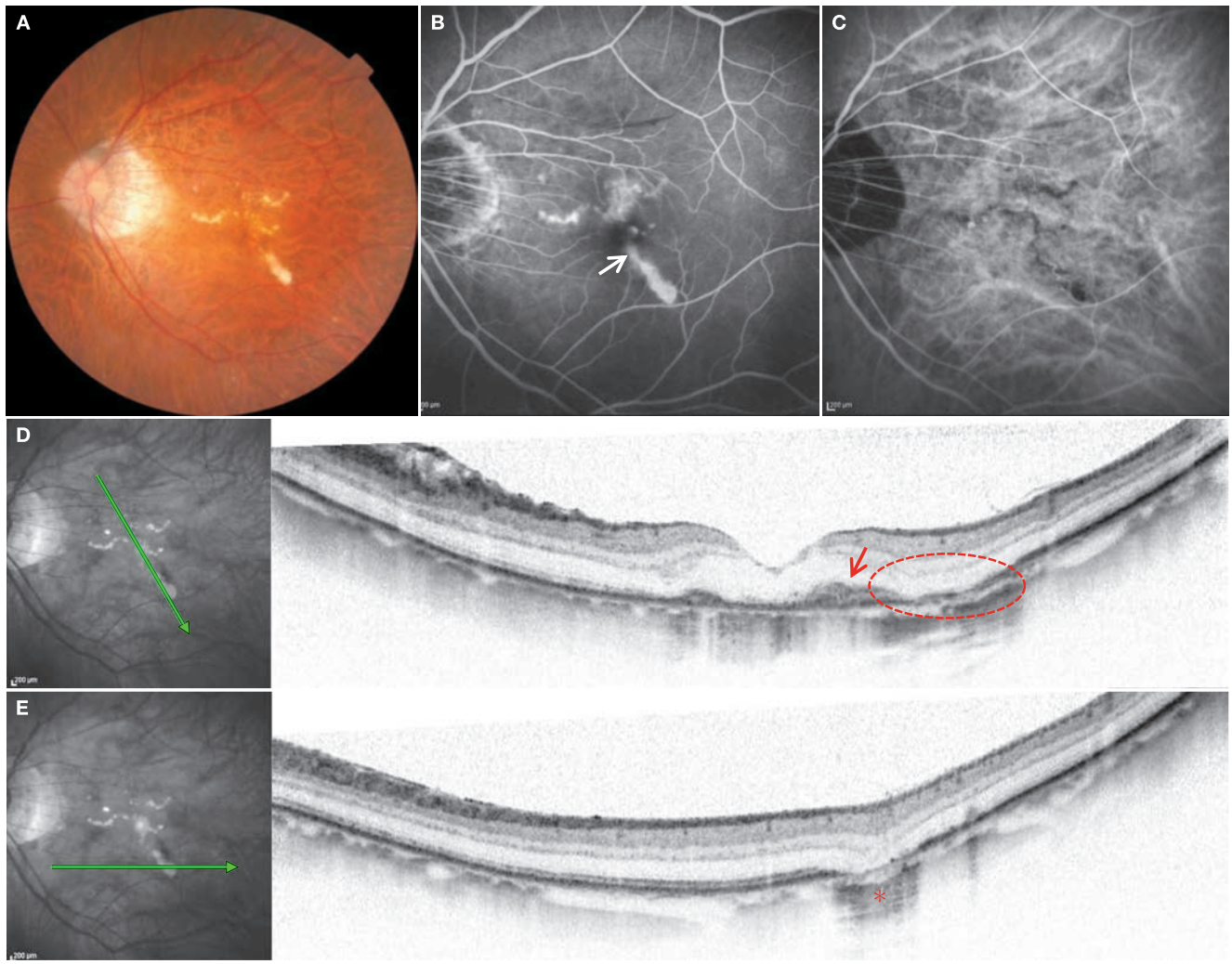

A: Color fundus photograph in the left eye: Multiple lacquer cracks can be clearly seen in the macular area. B: FA in the left eye (11 minutes, 10 seconds): The lacquer cracks are depicted as hyperfluorescent lesions in late phase FA imaging. Small CNV is present in the inferior macula (⇨). **C:** IA in the left eye (11 minutes, 10 seconds): The lacquer cracks are exhibited as hypofluorescent lines in late phase IA imaging. **D:** IR + OCT oblique scan of the left eye: Scan mostly passing through the fovea centralis. CNV is noted (➔). The RPE, IS/OS, and ELM are all defective in the lacquer cracks area (red dashed circle). The choroid is thin. **E:** IR + OCT horizontal scan of the left eye: Scan passing through the lacquer crack area. Mild outward retraction of the inner retinal layer structure and RPE defects as seen in atrophic AMD, degenerative disease, and PIC are visible. The sclera is significantly visible due to RPE defects (*).

Image interpretation points

Lacquer cracks are one of the initial changes seen in highly myopic eyes. This case is accompanied by myopic CNV. Lacquer cracks are a risk factor in the onset of CNV.

Case 166 Lacquer cracks: A mild case

A 36-year-old male, OS, BCVA 0.9, an axial length 31.66 mm

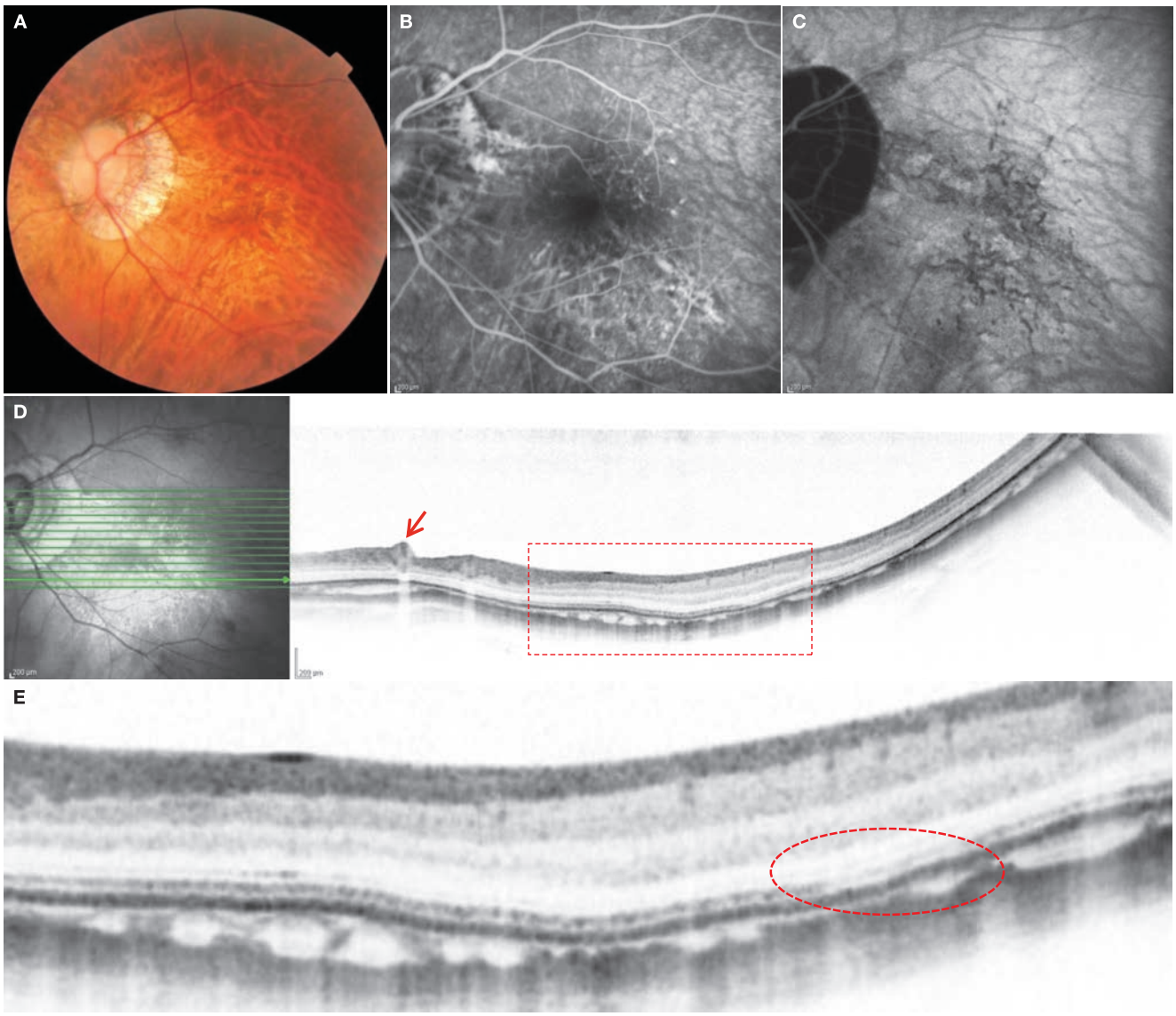

A: Color fundus photograph in the left eye: In contrast to case 165, the lacquer cracks are not clear on an biomicroscopic examination. **B:** FA in the left eye (15 minutes, 54 seconds): The lacquer cracks are depicted as hyperfluorescent lesions in late phase FA imaging. No CNV is present. **C:** IA in the left eye (15 minutes, 54 seconds): There are hypofluorescent lesions both consistent and inconsistent with the hyperfluorescent lesions on FA on late phase IA imaging. Not all of these hypofluorescent lesions are lacquer cracks. **D:** IR + OCT horizontal scan of the left eye: Vascular microfolds are apparent (➔). Choroidal thinning is clearly exhibited. **E:** Enlarged version of D [red dashed box]: The ELM and IS/OS line are becoming indistinct in the hypofluorescent area on IA (red dashed circle). This change is very mild consistent with the lack of clear lacquer cracks on biomicroscopy.

Image interpretation points

In contrast with case 165, only very mild structural changes are evident in the outer retinal layers associated with lacquer cracks. There are few biomicroscopic findings. The mild change in reflectivity of ELM and IS/IS lines corresponds to the linear lesions seen on angiographic imaging (particularly late phase IA imaging). To be strict, the lacquer cracks are detected liner lesions on biomicroscopy and hypofluorescent lesions on FA. The hypofluorescent lesions seen only on late phase IA imaging may develop into lacquer cracks in the future, but it is inappropriate to call the lesions themselves lacquer cracks.

Case 167 ILM detachment: Case without foveoschisis

A 68-year-old male, OS, BCVA 1.2, an axial length 27.91 mm

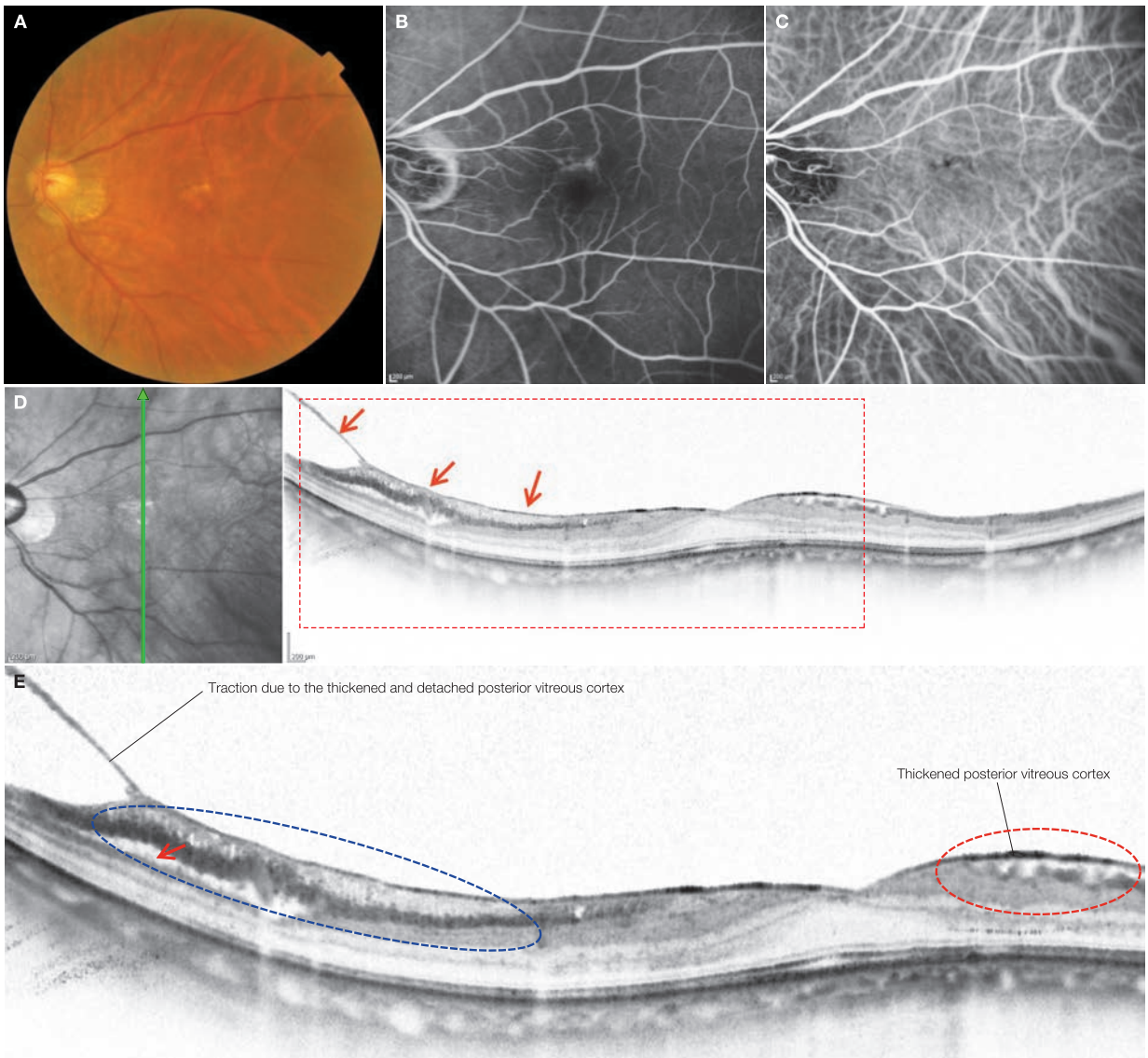

A: Color fundus photograph in the left eye: A tilted optic disc with cyclotorsion and PPA are visible. A lacquer crack is evident superior to the fovea centralis. **B:** FA in the left eye (1 minute, 52 seconds): Hyperfluorescence as a result of a lacquer crack is noted superior to the fovea centralis. **C:** IA in the left eye (1 minute, 52 seconds): The lacquer crack is exhibiting hypofluorescence on IA. **D:** IR + OCT vertical scan of the left eye: Traction from the thickened posterior vitreous cortex is evident below the macula in the inferior posterior pole (➔). **E:** Enlarged version of D [red dashed box]: The posterior vitreous cortex has been detached inferiorly and in continuity with this the ILM and the thickened posterior vitreous cortex are detached from the retinal nerve fiber layer together, with a columnar structure of Müller cells in the gap (blue dashed circle). Schisis (➔) can also be seen between the retinal nerve fiber layer and ganglion cell layer. Compared with the inferior portion, the upper portion of the retinal nerve fiber layer is undulating, and the columnar structure is not visible (red dashed circle). This is similar to findings seen in ERM.

Image interpretation points

This is a case of a highly myopic eye in which the posterior vitreous cortex and ILM are responsible for multiple lesions in the vitreoretinal interface. The state of the lesions is easy to assess from findings in the gap between the posterior vitreous cortex and retinal nerve fiber layer. It is also important to note the membrane formation as a result of cell migration and extracellular matrix production (refer to page 60 for idiopathic ERM). The thick and detached posterior vitreous cortex and bridging membrane in the upper macula are thought to be generated by cell migration and extracellular matrix production with the posterior vitreous cortex as scaffolding similar to the pathogenesis of idiopathic ERM. The lesion in the inferior macula is known as ILM detachment.

Case 168 Myopic foveoschisis: Case without foveal detachment

A 66-year-old female, OD, BCVA 1.5, an axial length 30.31 mm

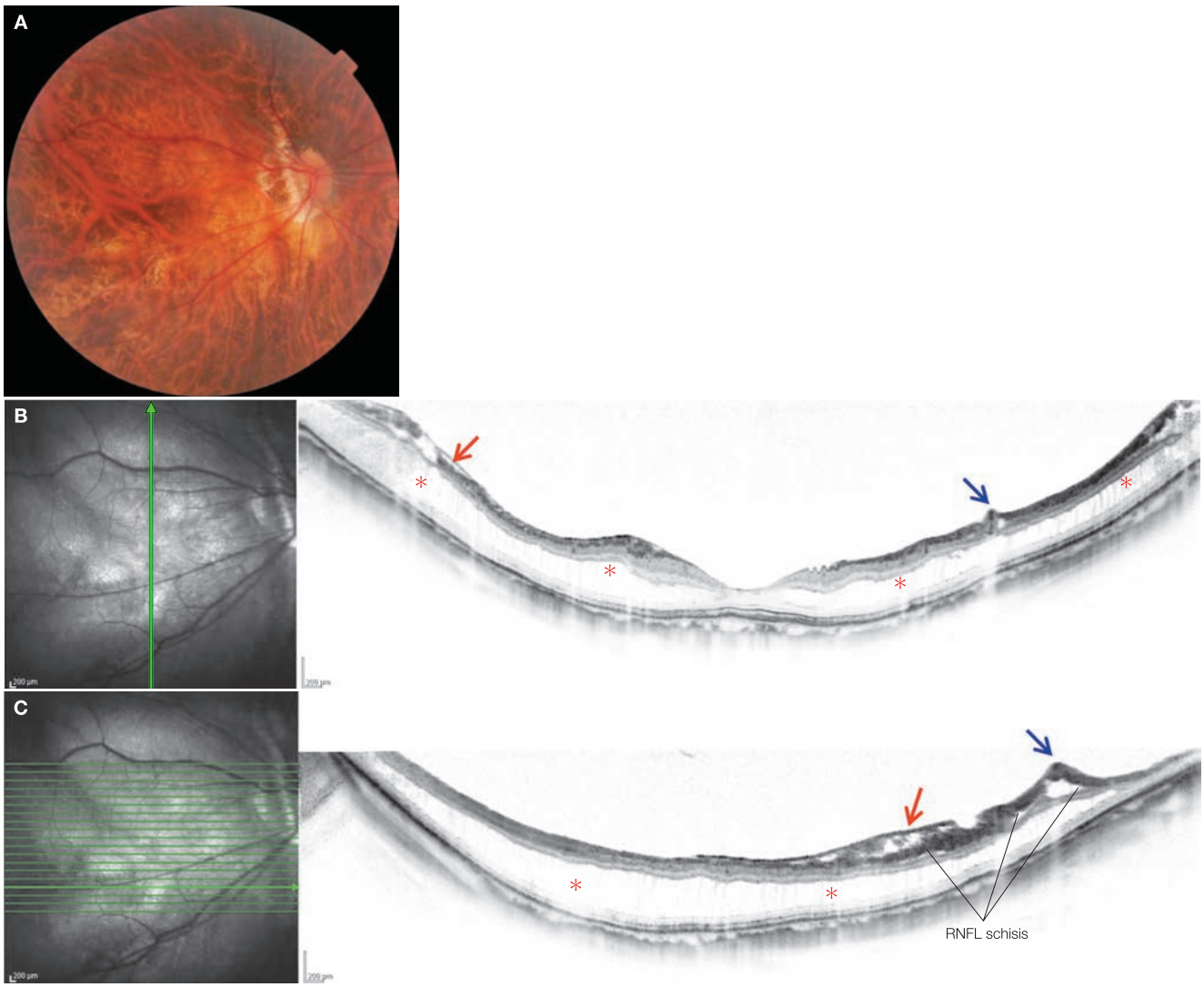

A: Color fundus photograph in the right eye: The optic disc is tilted and the anteriorly protruding scleral curvature is seen the immediate temporal margin of the optic disc. The large blood vessels of the choroid are visible. ICC is present inferior to the optic disc. **B:** IR + OCT vertical scan of the right eye: ILM detachment (➔) is observed in the left side of the OCT image. Retinoschisis is apparent over a wide area (*). Vascular microfolds that have developed as a result of poor extensibility of the retinal blood vessels are evident in the superior macula (➔). The choroid is thinned. The extensibility of the retinal blood vessels themselves is poor, which is thought to be the cause of traction on other retinal tissues. **C:** IR + OCT horizontal scan of the right eye: A vascular microfold is depicted (➔). ILM detachment is present immediately temporal to the ILM detachment this (➔). RNFL schisis is also seen in association with the vascular microfold and ILM detachment. Retinoschisis is also clearly depicted on this scan (*). The choroid is extremely thin.

Image interpretation points

A variety of changes occur simultaneously in highly myopic eyes. In this case, ILM detachment, vascular microfolds, and retinoschisis including RNFL schisis are occurring simultaneously. Complex changes occur at the same time due to traction that occurs between tissue that stretches easily (sensory retina), and tissue that is difficult to stretch (ILM, retinal blood vessels) when posterior scleral elongation occurs. These pathologic myopic changes are frequently seen.

Case 169 Myopic foveoschisis: Case with foveal detachment

A 50-year-old female, OS, BCVA 0.4, an axial length 29.45 mm

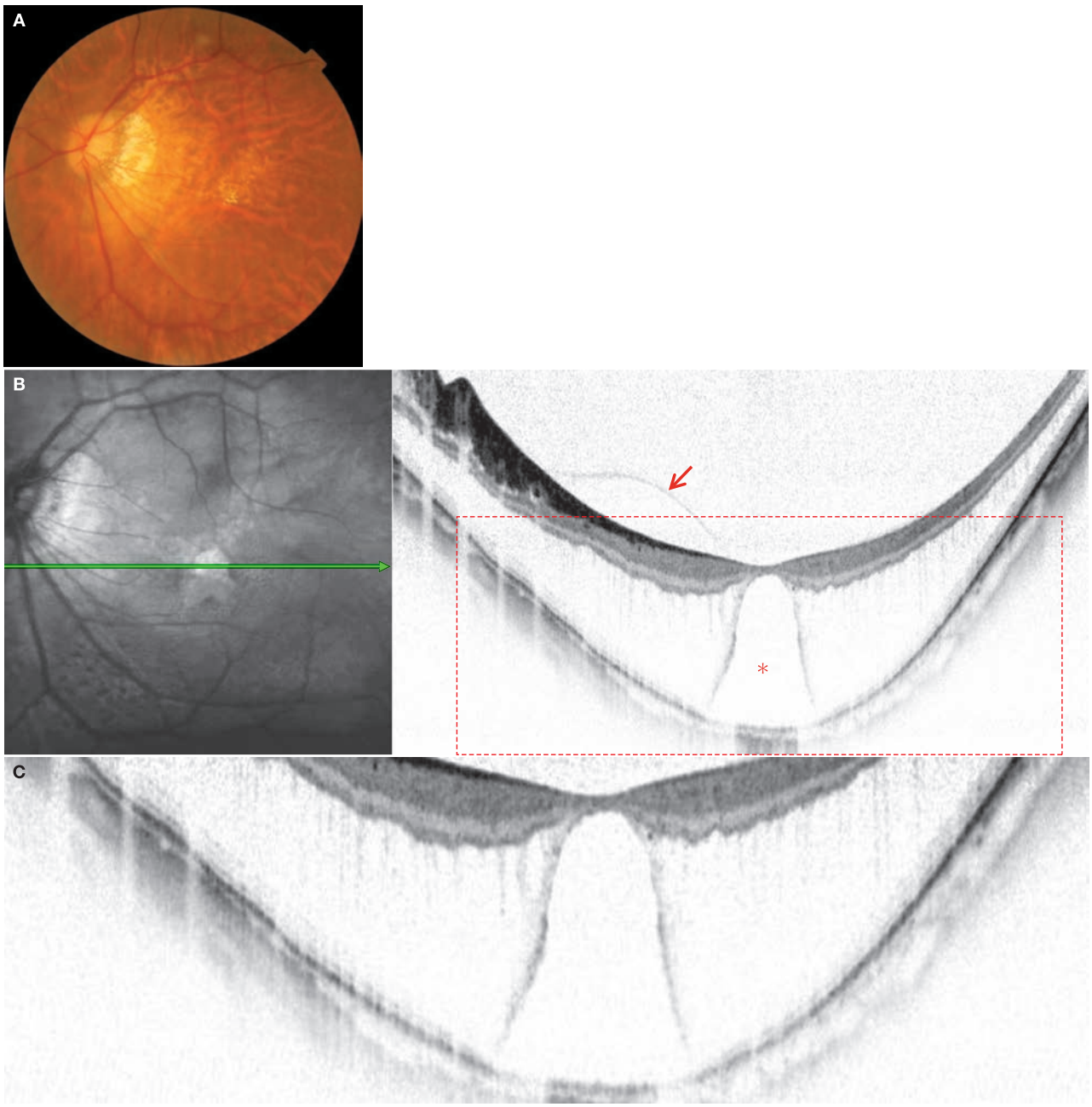

A: Color fundus photograph in the left eye: The optic disc is tilted. Extensive PPA is visible. Foveal retinoschisis is not clear on the fundus photograph. However, the presence of retinoschisis in the vicinity of the lower arcade vessels is evident. **B:** IR + OCT horizontal scan of the left eye: Extensive retinoschisis is evident in the macular area. Retinal detachment (*) is also seen in the fovea centralis. The posterior vitreous cortex is exhibited on the nasal side of the fovea centralis (➔). **C:** Enlarged version of B [red dashed box]: Foveal detachment is clearly depicted. The vertical (longitudinal direction of the eyeball) columnar structure in the area of retinoschisis is likely Müller cells.

Image interpretation points

This is an example of retinoschisis and foveal detachment that can be seen in highly myopic eyes. In this case, traction from the posterior vitreous cortex was observed, which may have partially contributed to the development of retinoschisis.

Other factors causing traction of the retina include inelastic retinal arterioles and the ILM. This patient complained of visual decline and a foveal detachment was found; so vitreous surgery in combination with ILM peeling was performed.

Case 169 One year after surgery

A 50-year-old female, OS, BCVA 1.2, an axial length 29.45 mm

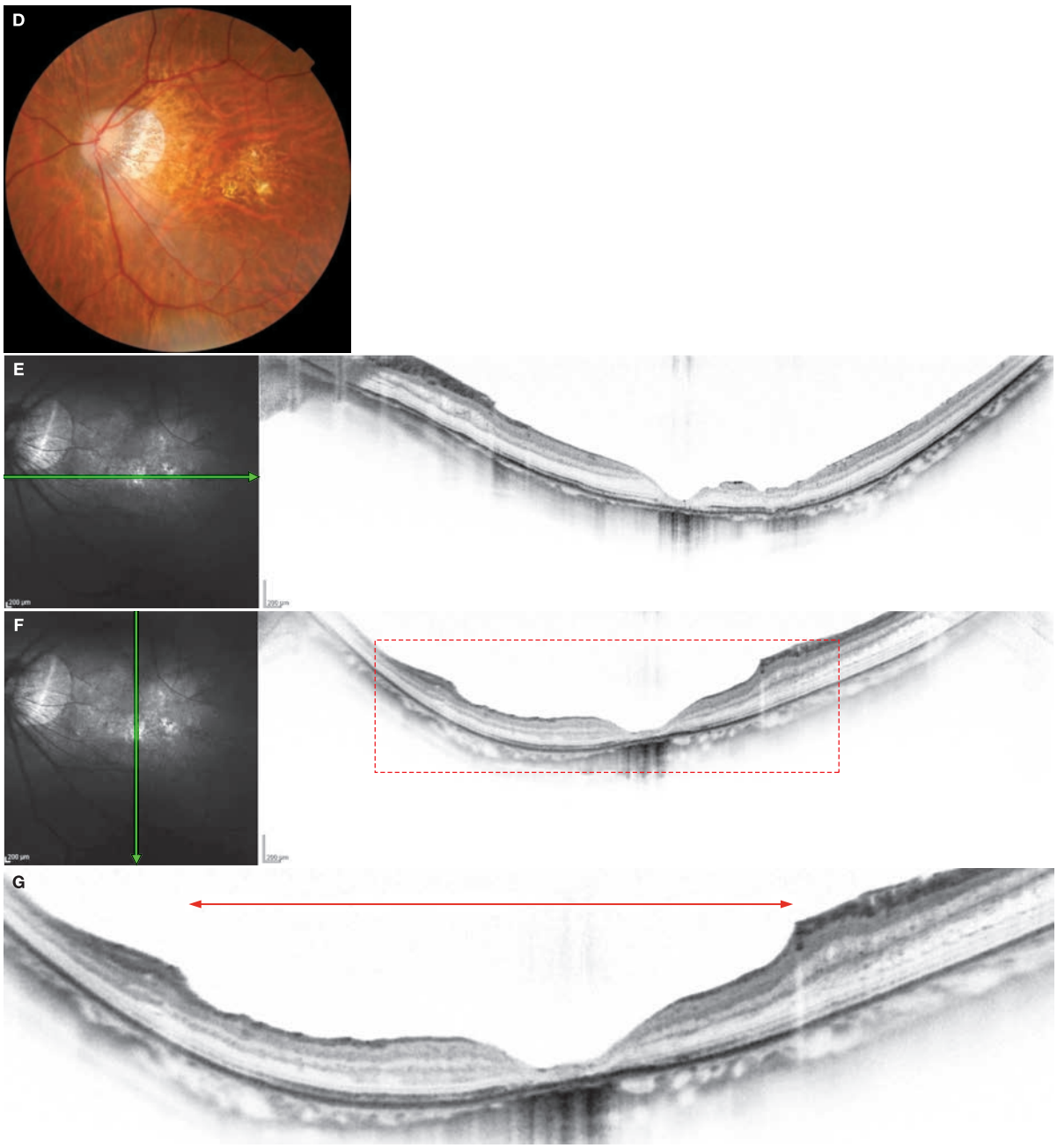

D: Color fundus photograph in the left eye: The results of surgery are not evident on the fundus photograph. Subfoveal atrophic lesions appear to be more clearly depicted. Additionally, atrophic lesions appear to have progressed on the temporal side of the macula. **E:** IR + OCT horizontal scan of the left eye: The detachment in the fovea centralis had disappeared and retinoschisis is also mostly resolved. **F:** IR + OCT vertical scan of the left eye: The fovea is thin. The high reflectivity in the choroid and sclera below the fovea is due to foveal RPE atrophy. **G:** Enlarged version of F [red dashed box]: The area of ILM peeling is clearly visible as an area with thinned RNFL (⟷). Traction to the ILM and RNFL is evident in the site where the ILM has not been peeled. The RNFL appears to be thin in the site of ILM peeling. Additionally, the IS/OS line is lost in the fovea with RPE atrophy, but is clearly exhibited in the other area.

Image interpretation points

The area where vitreous surgery in combination with ILM peeling was performed is clearly visible. Significant changes were observed in the structures of the inner retinal layers in the area where ILM peeling was performed compared with the site where it was not performed. Foveal retinal thinning is well depicted.

Case 170 Myopic foveoschisis: Case with macular retinal detachment

A 70-year-old female, OD, BCVA 0.4, an axial length 28.20 mm

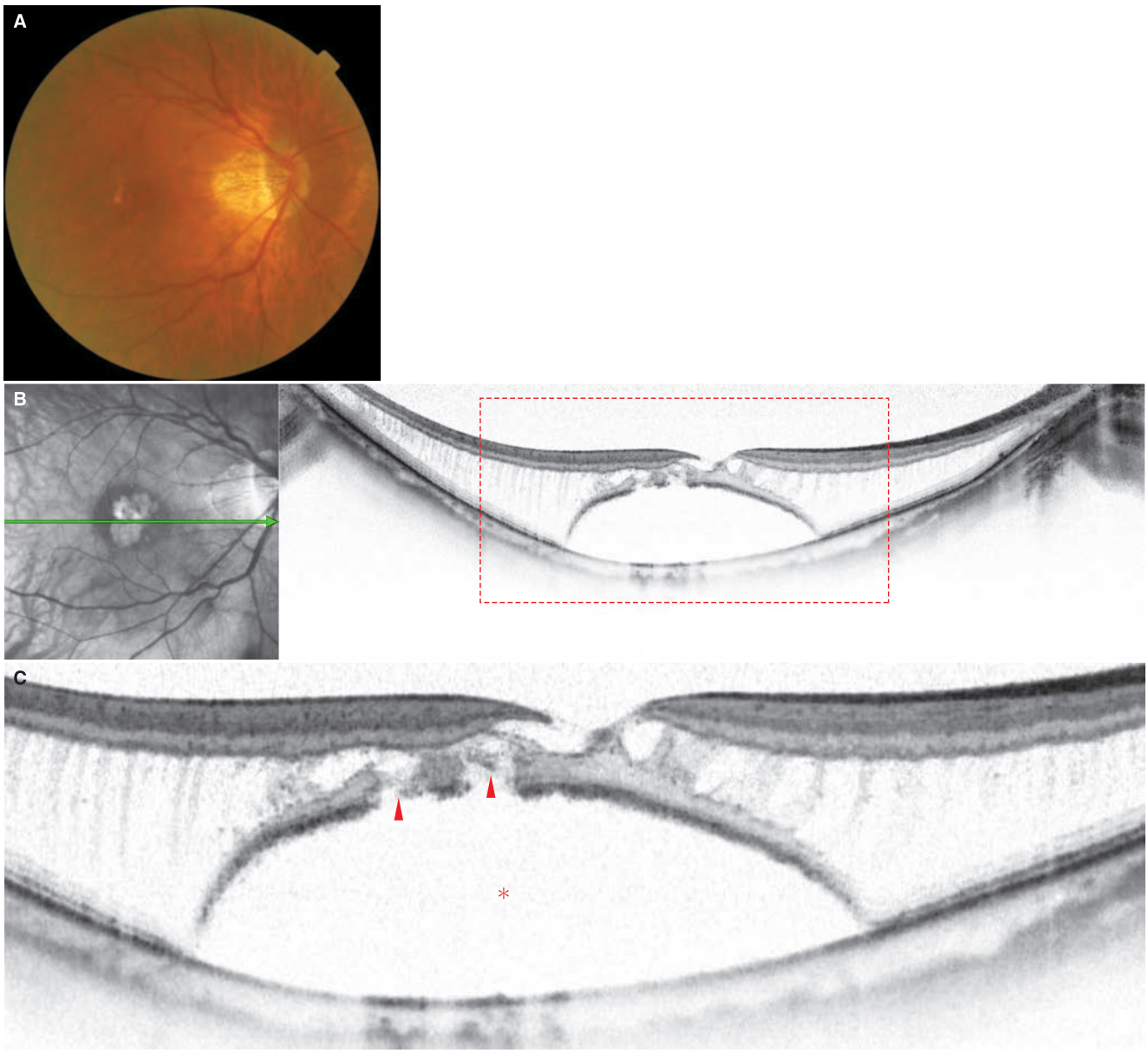

A: Color fundus photograph in the right eye: The optic disc is tilted horizontally. A large PPA is evident on the temporal side. Foveal retinoschisis is not evident on the fundus photograph. **B:** IR + OCT horizontal scan of the right eye: Retinoschisis with macular retinal detachment is evident. The choroid is extremely thin. **C:** Enlarged version of B [red dashed box]: Retinoschisis and retinal detachment (*) are clearly exhibited. Defects can be seen within the photoreceptor layer (►). The ELM is partially depicted. The moderately reflective columnar structure running in the longitudinal direction of the retina is likely composed of Müller cells.

Image interpretation points

These images clearly reveal the characteristics of myopic foveoschisis with macular retinal detachment. No particular tractional factors pulling the retina were found in these images. We can clearly see that the photoreceptor outer segment of the detached retina (the ELM is partially depicted) possess defects like nicks in a saw blade.

Case 170 Two and a half years after surgery

A 70-year-old female, OD, BCVA 0.9, an axial length 28.20 mm

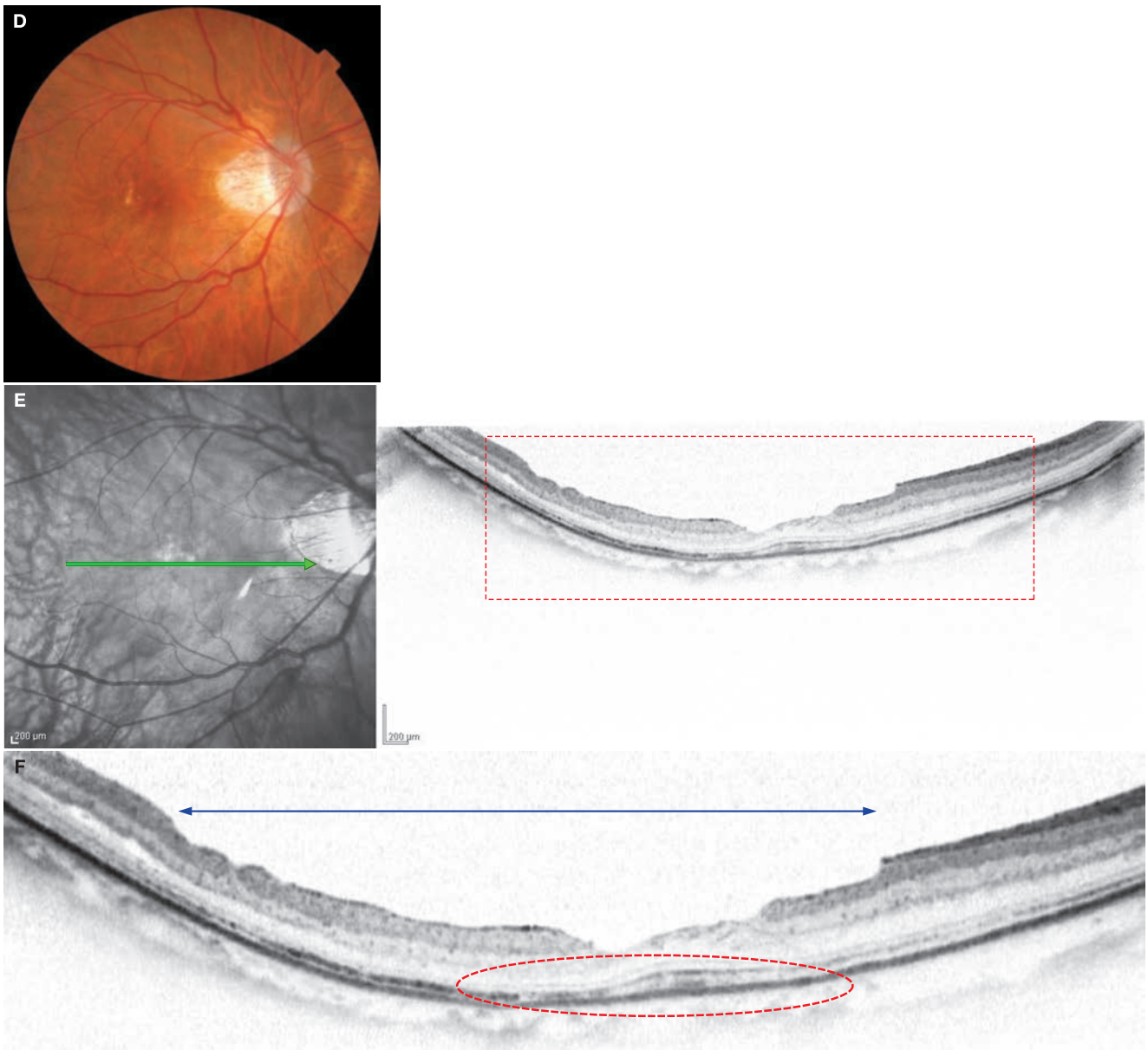

D: Color fundus photograph in the right eye: Fundus visibility is improved since cataract surgery was performed at the same time. **E:** IR + OCT horizontal scan of the left eye: Retinoschisis has mostly disappeared. **F:** Enlarged version of E [red dashed box]: The area that underwent ILM peeling is indicated by (⟷). Thinning of the retinal nerve fiber layer is evident in this area. The foveal outer retinal layer structure (ELM and IS/OS lines) has almost returned to normal (red dashed circle). This is consistent with good postoperative visual acuity.

Image interpretation points

This is a case where vitreous surgery combined with ILM peeling was effective. The retinal nerve fiber layer is thin in the area that underwent ILM peeling, but the significant changes in the retinal nerve fiber layer are not necessarily consistent with good postoperative visual acuity.

Case 171 Myopic foveoschisis: Traction from the thickened posterior vitreous cortex

A 67-year-old female, OS, BCVA 0.6, an axial length 27.92 mm

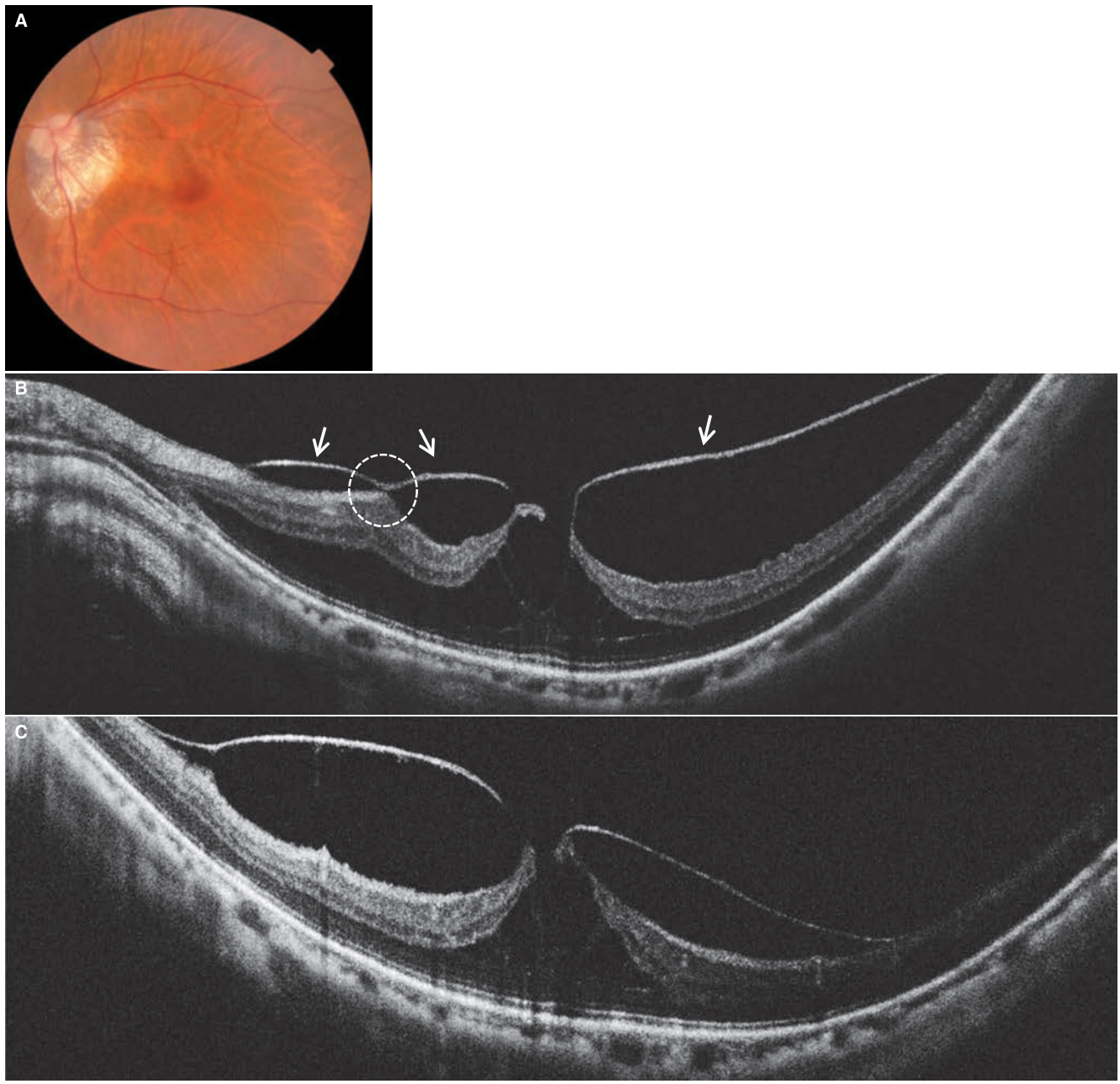

A: Color fundus photograph in the left eye: Traction to the fovea centralis is unclear in this photograph. **B:** OCT horizontal scan of the left eye: We can clearly see that the sensory retina is being pulled towards the vitreous cavity by the posterior vitreous cortex (⇨). There is a site where the posterior vitreous cortex is attached to the retinal surface on the nasal side of the fovea centralis (white dashed circle), and the retina appears to be projecting anteriorly as a result of traction. The fovea centralis is thickened, and the internal state of the retina is unclear, but the IS/OS is depicted as almost normal. **C:** OCT vertical scan of the left eye: Retinal traction due to the posterior vitreous cortex is clearly visible.
(A is modified according to Fujimoto M, et al. Features associated with foveal retinal detachment in myopic macular retinoschisis. *Am J Ophthalmol*. 2010; 150: 863–870)

Image interpretation points

Retinal traction due to the thickened posterior vitreous cortex is clearly depicted. Myopic foveoschisis includes cases such as this one with retinal traction due to the posterior vitreous cortex as well as cases without traction by posterior vitreous cortex such as case 170. This case may be on the same spectrum as vitreomacular traction syndrome.

Case 172 Myopic foveoschisis: Macular hole formation

A 48-year-old male, OD, BCVA 0.7, an axial length 32.03 mm

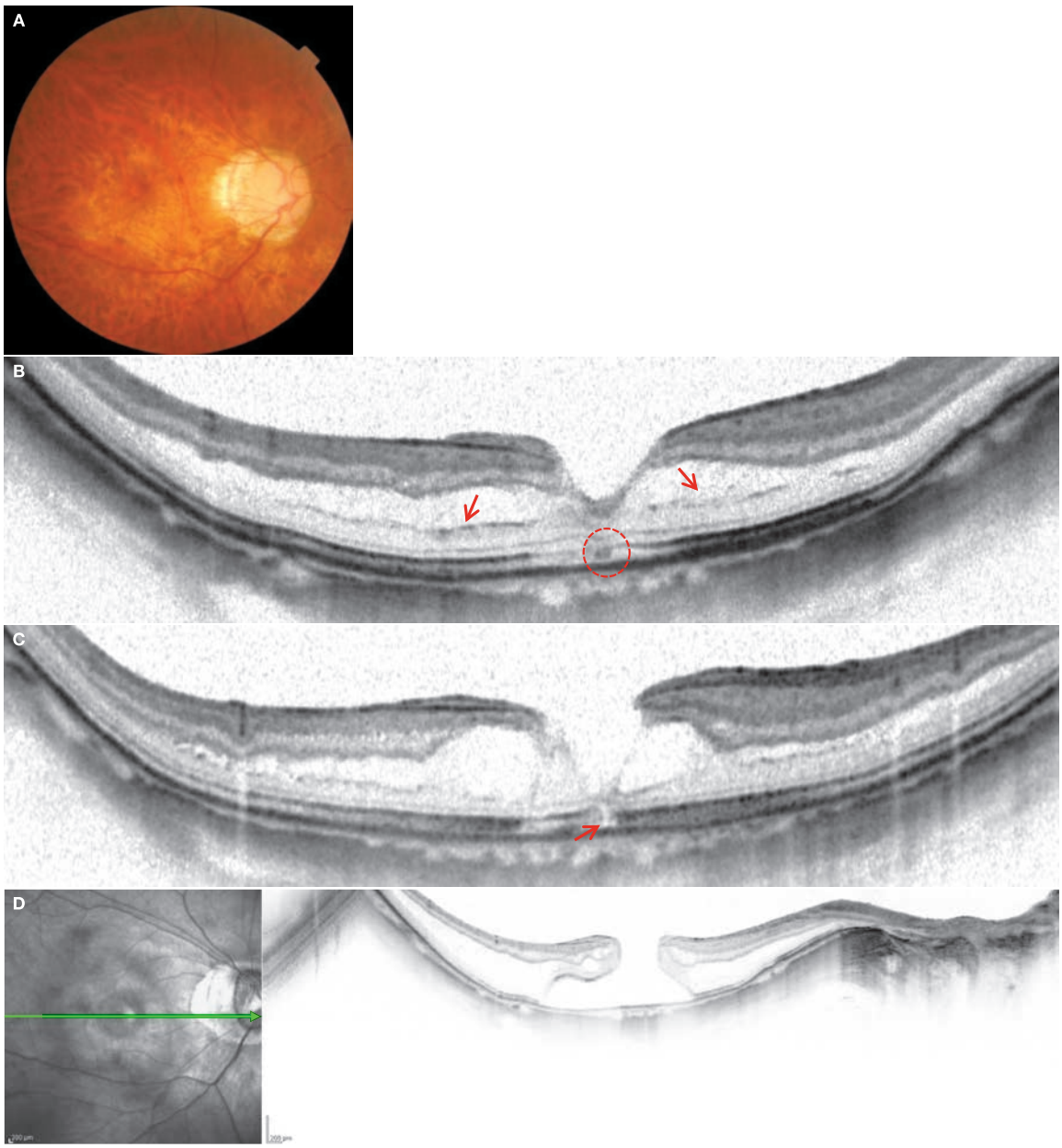

A: Color fundus photograph in the right eye: This is a tigroid fundus with diffuse atrophy, a large PPA, and a ridge temporal to the optic disc in the posterior pole. **B:** OCT horizontal scan of the right eye: Retinoschisis is evident (→). The IS/OS line in the fovea centralis is not sufficiently depicted. In addition, small, a highly reflective lesion is exhibited in the fovea centralis (red dashed circle). **C:** OCT horizontal scan of the right eye: State of the eye 4 months from B. Retinoschisis is progressing. A slit shaped cleft is forming in the foveal photoreceptor inner and outer segment (→). Best-corrected visual acuity at this time is 0.7 and has not declined. **D:** IR + OCT horizontal scan of right eye: State of the eye after a further 13 months. A macular hole has formed, around which retinal detachment is evident. Best-corrected visual acuity at this time is 0.3 and has declined.

Image interpretation points

These are images capturing the process of MHRD development in high myopia. MHRD in this case has developed without undergoing foveal detachment (outer layer lamellar hole). The process leading from foveal photoreceptor cell dehiscence to macular hole formation may have a similar mechanism to the formation process of idiopathic macular holes. Macular hole formation cannot be explained by a single mechanism alone, but instead, a variety of processes underlies the development of macular holes in high myopia.

Case 173 Myopic foveoschisis: MHRD

A 74-year-old female, OD, BCVA 0.5, an axial length 28.72 mm

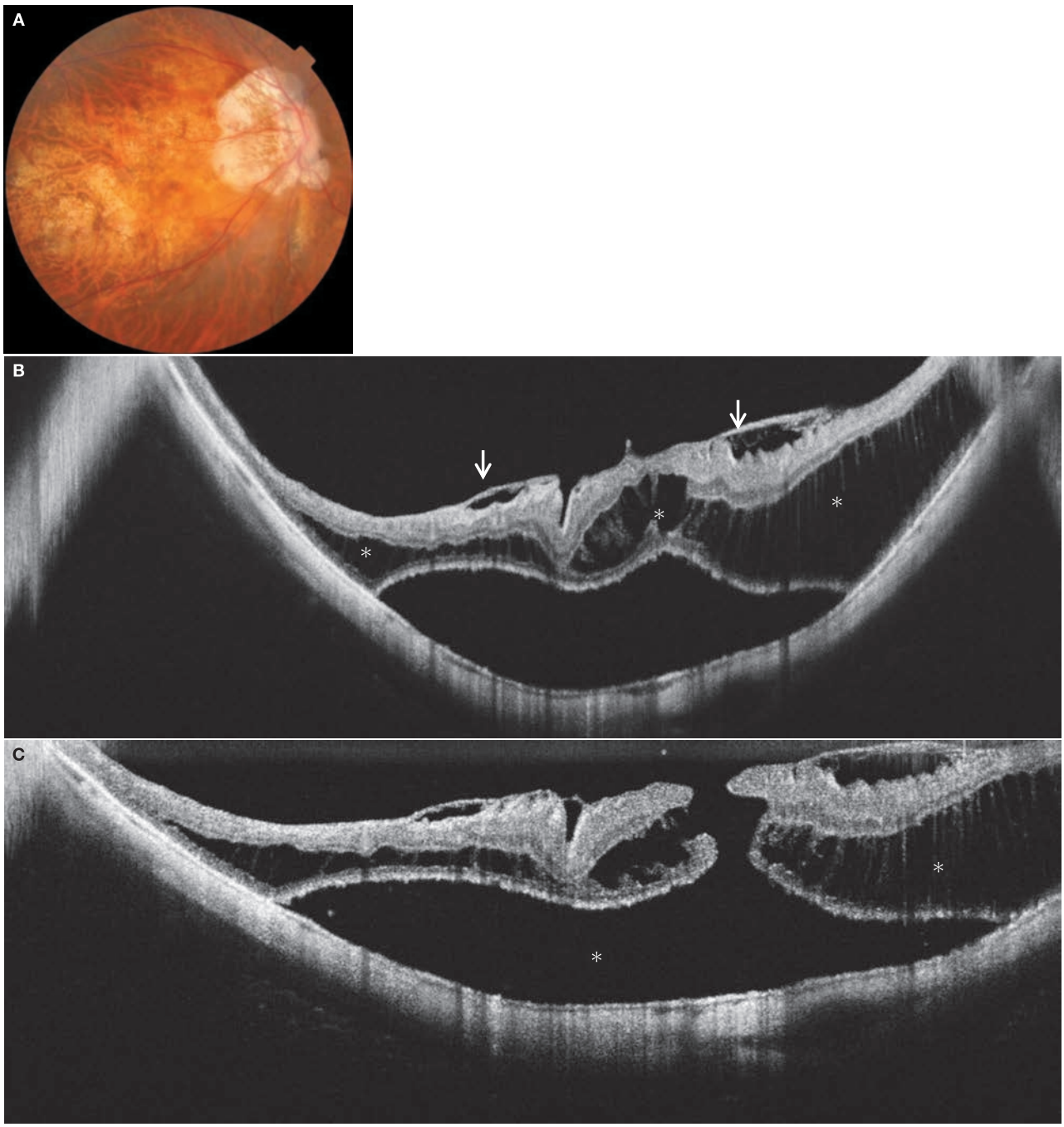

A: Color fundus photograph in the right eye: Diffuse choroidal atrophy is significant. A large temporal PPA and a ridge are evident. Retinal whitening due to retinal detachment was biomicroscopically evident around the fovea centralis, which is unclear on this fundus photograph. **B:** OCT horizontal scan of the right eye: The thickened posterior vitreous cortex (⇨), retinoschisis (❄), and macular detachment are visible. The macular hole is not depicted. **C:** OCT vertical scan of the right eye: The macular hole is depicted. Retinal detachment (❄) is evident in the posterior staphyloma.

Image interpretation points

The eye already exhibited MHRD at initial diagnosis.
Retinal traction due to the posterior vitreous cortex as well as retinoschisis and retinal detachment are clearly depicted.

Case 174 Myopic foveoschisis: Before and after surgery for MHRD

A 77-year-old female, OD, preoperative BCVA 0.2 and postoperative BCVA 0.2, an axial length 28.42 mm

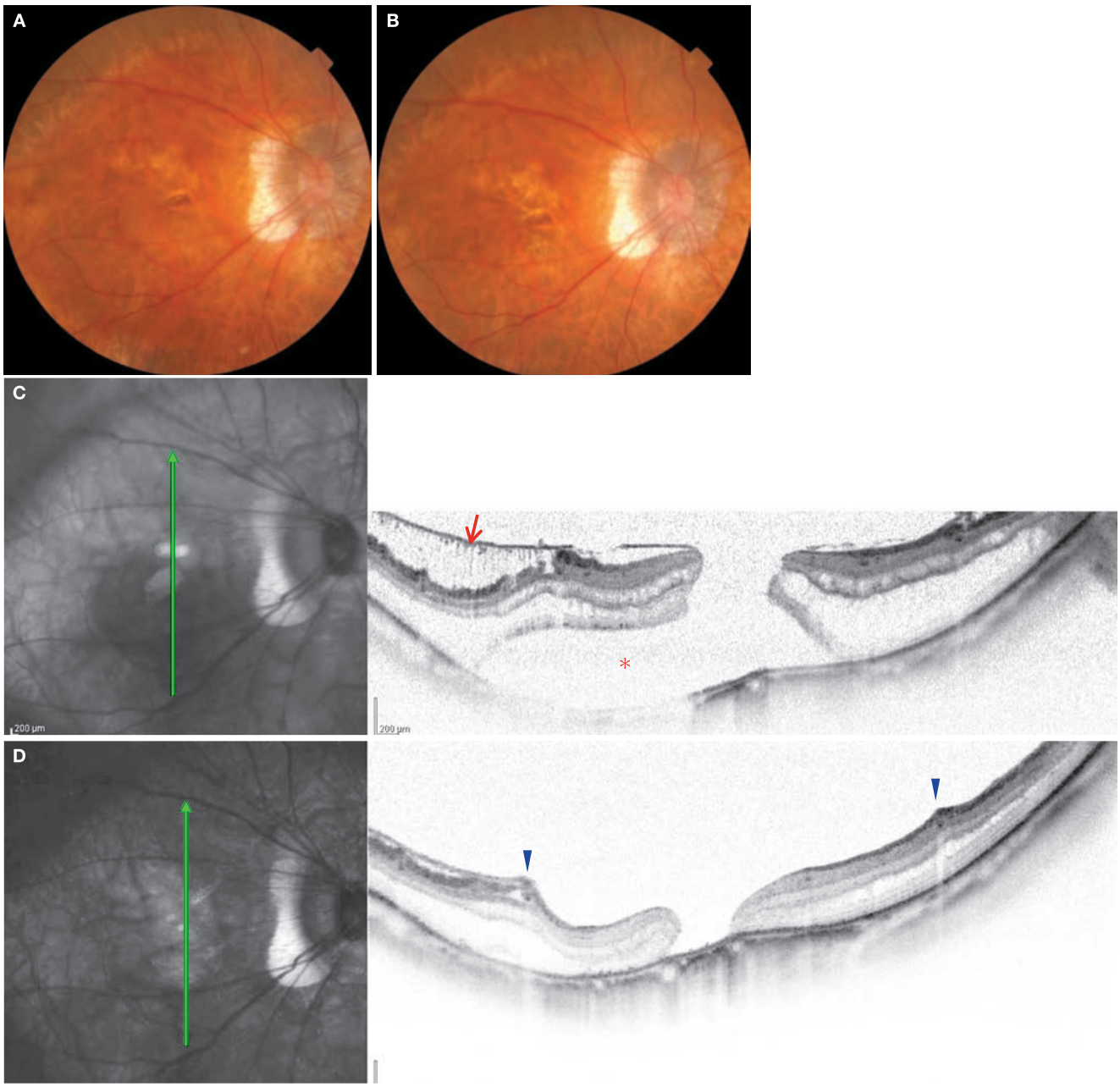

A: Color fundus photograph in the right eye: An elliptical macular hole and surrounding retinal detachment are evident. **B:** Color fundus photograph in the right eye: 7 months after surgery. The macular hole is indistinct. Retinal detachment is also unclear. **C:** Preoperative IR + OCT vertical scan of the right eye: Retinoschisis and a retinal detachment (*) are visible. The macular hole is also depicted. Extensive ILM detachment (→) is apparent. A columnar structure is visible in the gap, which let us know that the lesion is ILM detachment. **D:** Postoperative IR + OCT vertical scan of the right eye: Vitreous surgery combined with ILM peeling was performed in the area between the points indicated by (►). Retinoschisis has become less severe in the area that underwent ILM peeling surgery. The ILM detachment remains inferior to the lower arcade vessels, and traction to the vessels (vascular microfolds) is still observed. The macular hole remains. The superior margin of the macular hole is flattened, but the inferior portion remains elevated.

Image interpretation points

Macular hole closure sometimes cannot be achieved when the retinal detachment area is narrow even after vitreous surgery combined with ILM peeling. ILM peeling in the wider area may have been required.

Case 175 Myopic subretinal hemorrhages: A typical example

A 48-year-old male, OD, BCVA 0.4, an axial length 30.75 mm

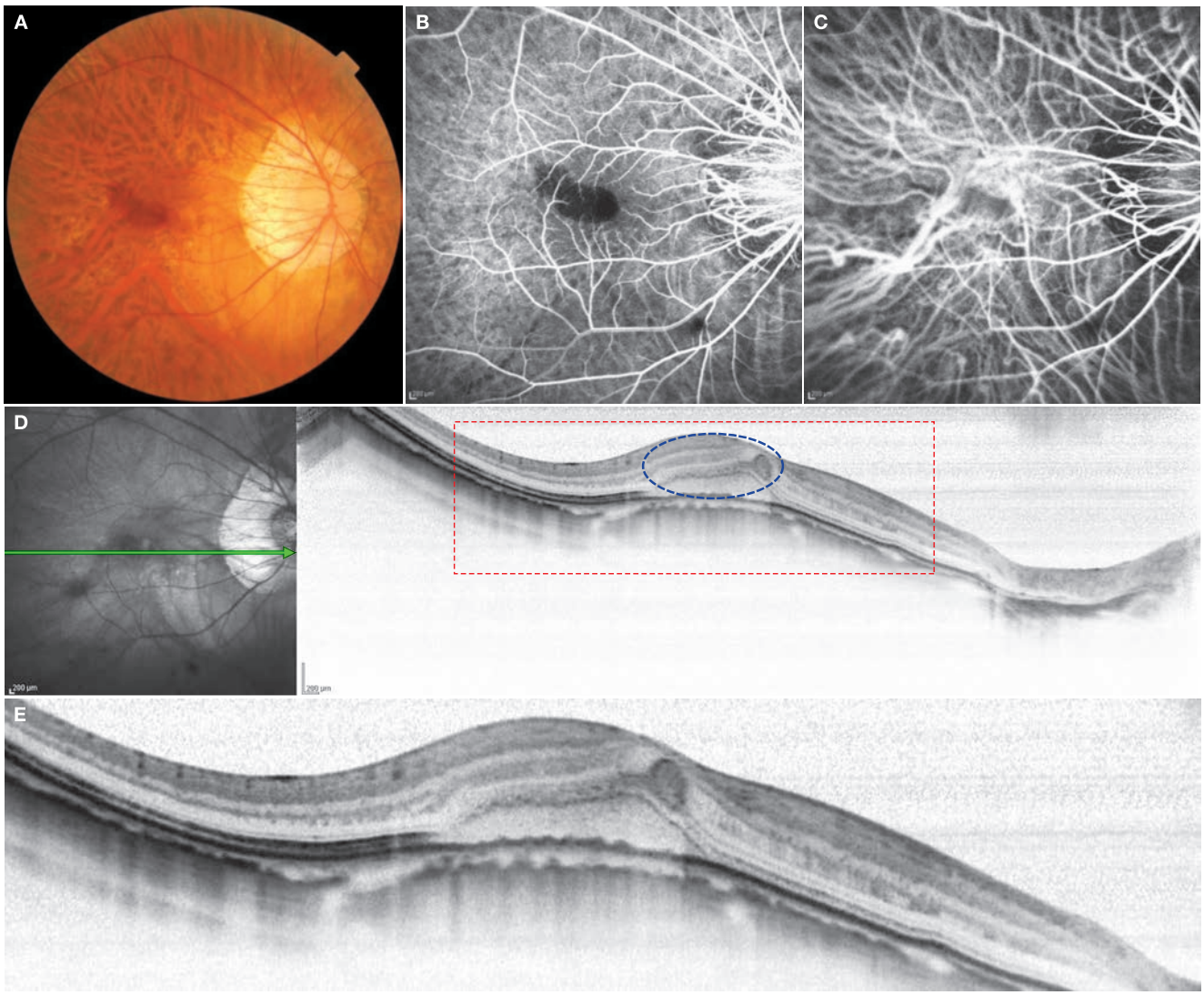

A: Color fundus photograph in the right eye: A faint retinal hemorrhage is visible somewhat to the temporal side of the fovea centralis. This is a case with a large circumferential PPA. **B:** FA in the right eye (26 seconds): A blockage due to the retinal hemorrhage is evident on FA imaging. **C:** IA in the right eye (26 seconds): CNV is not detected even on IA imaging. **D:** IR + OCT horizontal scan of the right eye: A moderately reflective lesion is apparent in the sensory retina (blue dashed circle). **E:** Enlarged version of D [red dashed box]: The moderately reflective lesion is seen as an elliptical shape and a liner one continuous to it. The IS/OS line is disrupted. The RPE line is irregul ar. Subretinal hemorrhages exhibit weakly reflective lesions in the subretinal space.

Image interpretation points

This is a case of myopic subretinal hemorrhages that have developed without CNV in a highly myopic eye. When hemorrhages spreads into the sensory retina, and consequently cause damages to the foveal outer retinal layer as seen in this case, often not as good as generally believed. The changes in the RPE may be secondary to hemorrhages, although it is unclear exactly why they occur.

Case 175 Four months later

A 48-year-old male, OD, BCVA 1.0, an axial length 30.75 mm

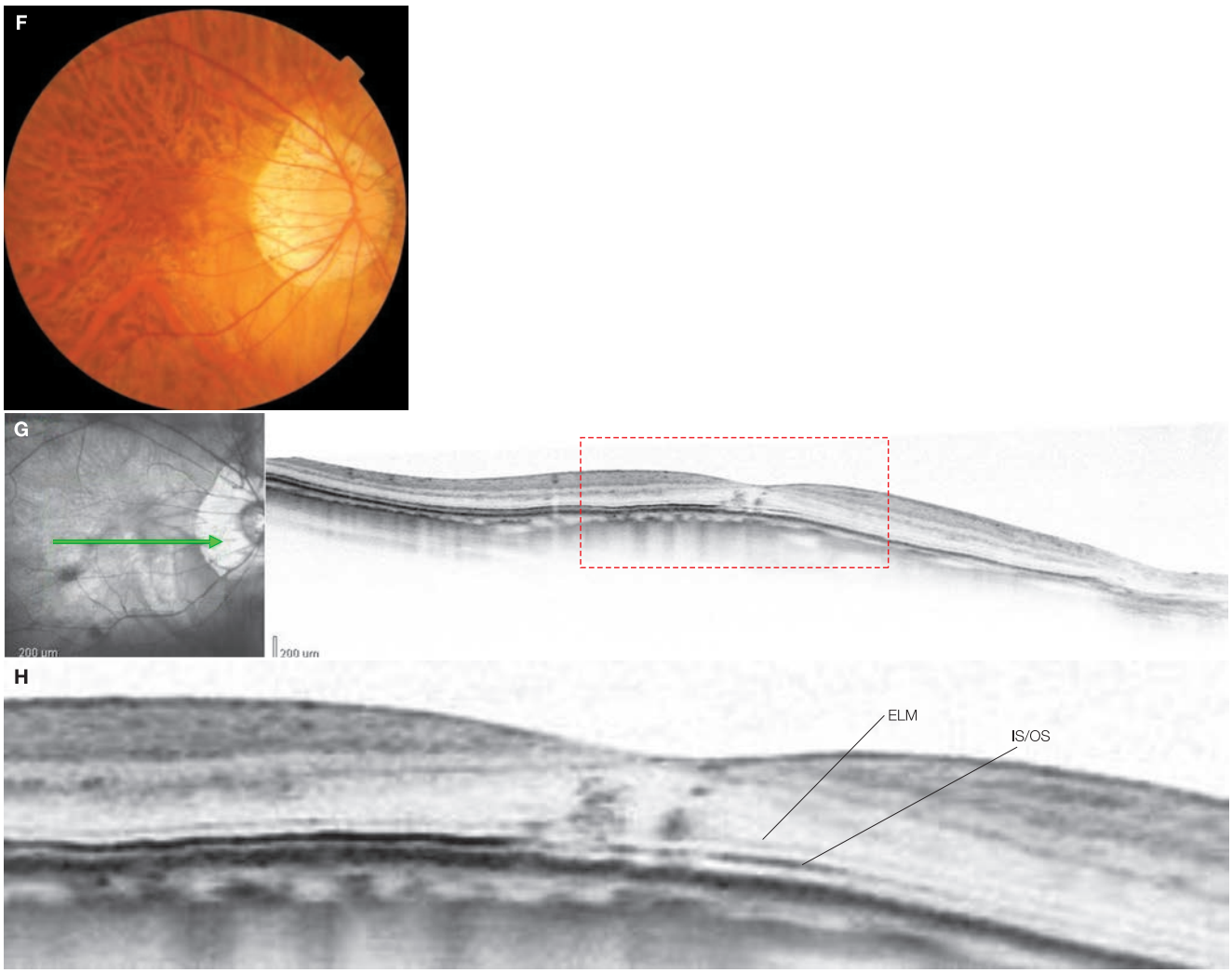

F: Color fundus photograph in the right eye: Retinal hemorrhages has disappeared and best-corrected visual acuity has improved to 1.0. **G:** IR + OCT horizontal scan of the right eye: Irregular, highly reflective lesions are visible in the foveal outer retinal layers. **H:** Enlarged version of G [red dashed box]: RPE line irregularities observed at initial diagnosis have mostly disappeared. The ELM and IS/OS lines have also been restored, although not completely. The irregular, highly reflective lesions visible in the outer retinal layers are likely macrophages that have phagocytized erythrocytes.

Image interpretation points

Myopic subretinal hemorrhages generally have a good visual prognosis. In this case, changes in the outer retinal layers were significant at initial diagnosis but resolved with time, and good visual acuity was eventually restored without treatment.

Case 176 Myopic choroidal neovascularization: A typical example

A 61-year-old female, OD, BCVA 0.3, an axial length 29.43 mm

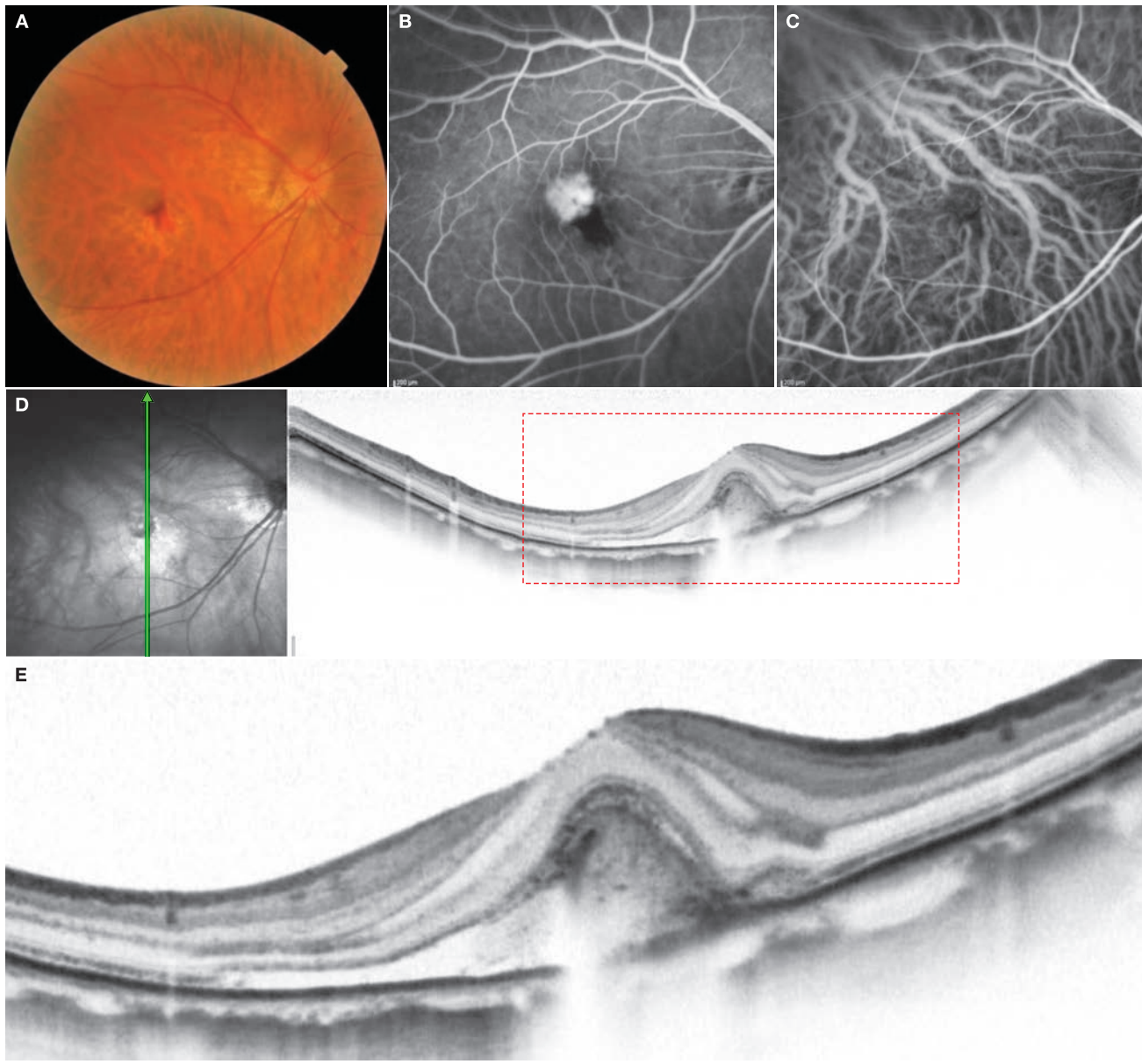

A: Color fundus photograph in the right eye: CNV of about half a disc diameter is visible in the upper temporal side of the fovea centralis. **B:** FA in the right eye (46 seconds): Classic CNV is seen. **C:** IA in the right eye (1 minute, 46 seconds): CNV is hardly seen on IA. **D:** IR + OCT vertical scan of the right eye: Extensive CNV is evident. **E:** Enlarged version of D [red dashed box]: The RPE line is mostly smooth. The retinal structure above the CNV is relatively well preserved based on the observation that the ELM line is exhibited. A SRD is visible in the inferior macula and appears to be continuing from the fovea centralis.

Image interpretation points

This is typical type 2 CNV or otherwise known as classic CNV based on FA classification. A good visual prognosis is expected since the foveal structure is relatively well preserved.

Case 177 Myopic choroidal neovascularization: Small CNV

A 76-year-old male, OD, BCVA 0.1, an axial length 30.14 mm

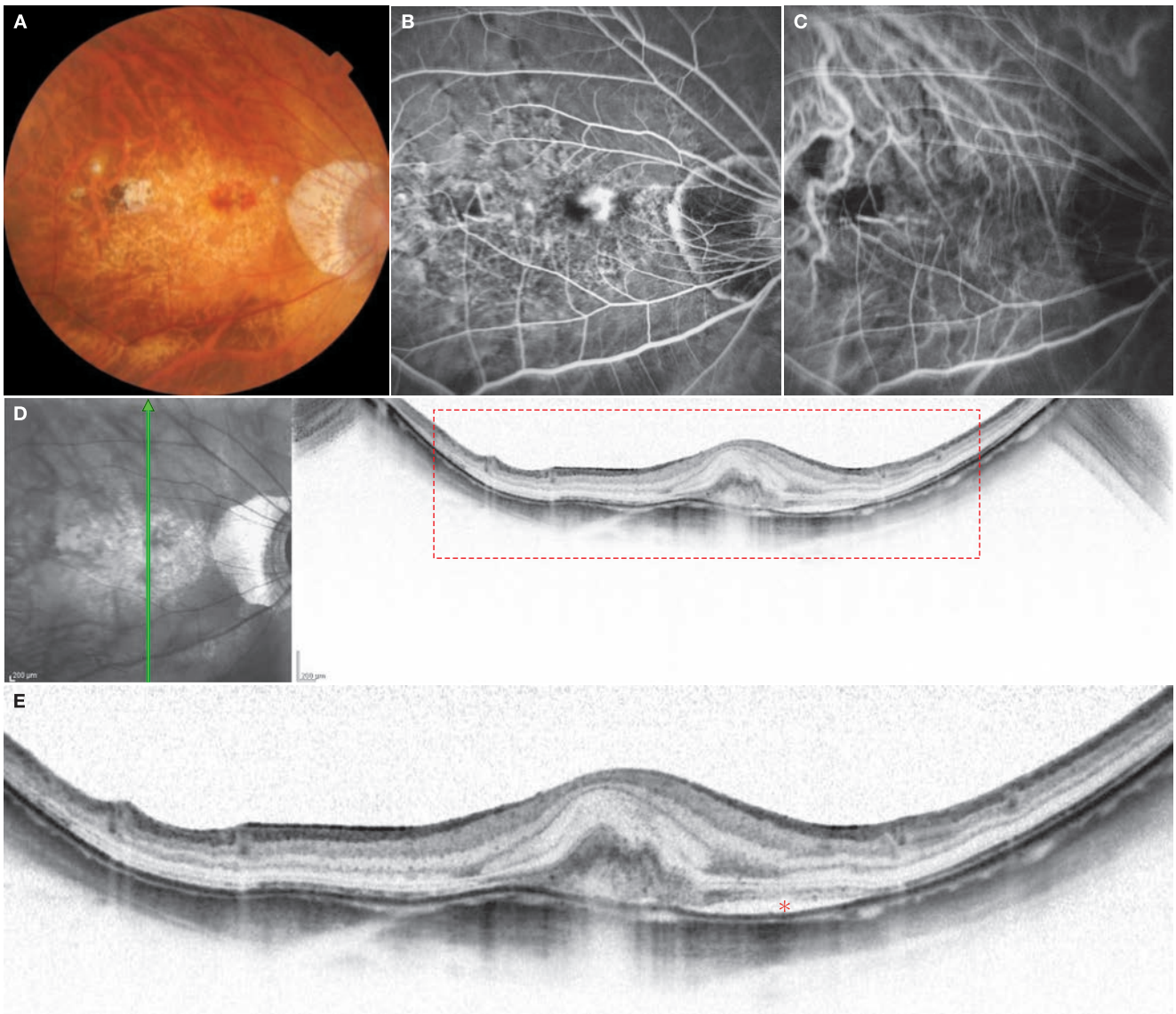

A: Color fundus photograph in the right eye: At initial diagnosis. An elliptical retinal hemorrhage exists in the nasal side of the fovea centralis, in the center of which CNV is visible. Pigmentation in the temporal macula and atrophic lesions immediately to the pigmentation may be old CNV. The edge of posterior staphyloma is evident near the lower arcade vessels. **B:** FA in the right eye (4 minutes, 48 seconds): A strongly hyperfluorescent lesion is noticeable on the nasal side of the fovea centralis. **C:** IA in the right eye (4 minutes, 48 seconds): CNV is harder to detect on IA. **D:** IR + OCT vertical scan of the right eye: Triangular CNV can be seen below the fovea centralis. **E:** Enlarged version of D [red dashed box]: No protrusions are visible in the RPE line. This is Type 2 CNV. A very flat SRD is apparent in the superior macula (*). We can see significant thinning of the choroid.

(Continued on the next page)

Image interpretation points

This is typical myopic CNV. The RPE is slightly undulating, but no protrusions are visible. This is type 2 CNV. The structure of the foveal outer retinal layers is indistinct, but not thinned.

Case 177 After anti-VEGF treatment

A 76-year-old male, OD, BCVA 0.9, an axial length 30.14 mm

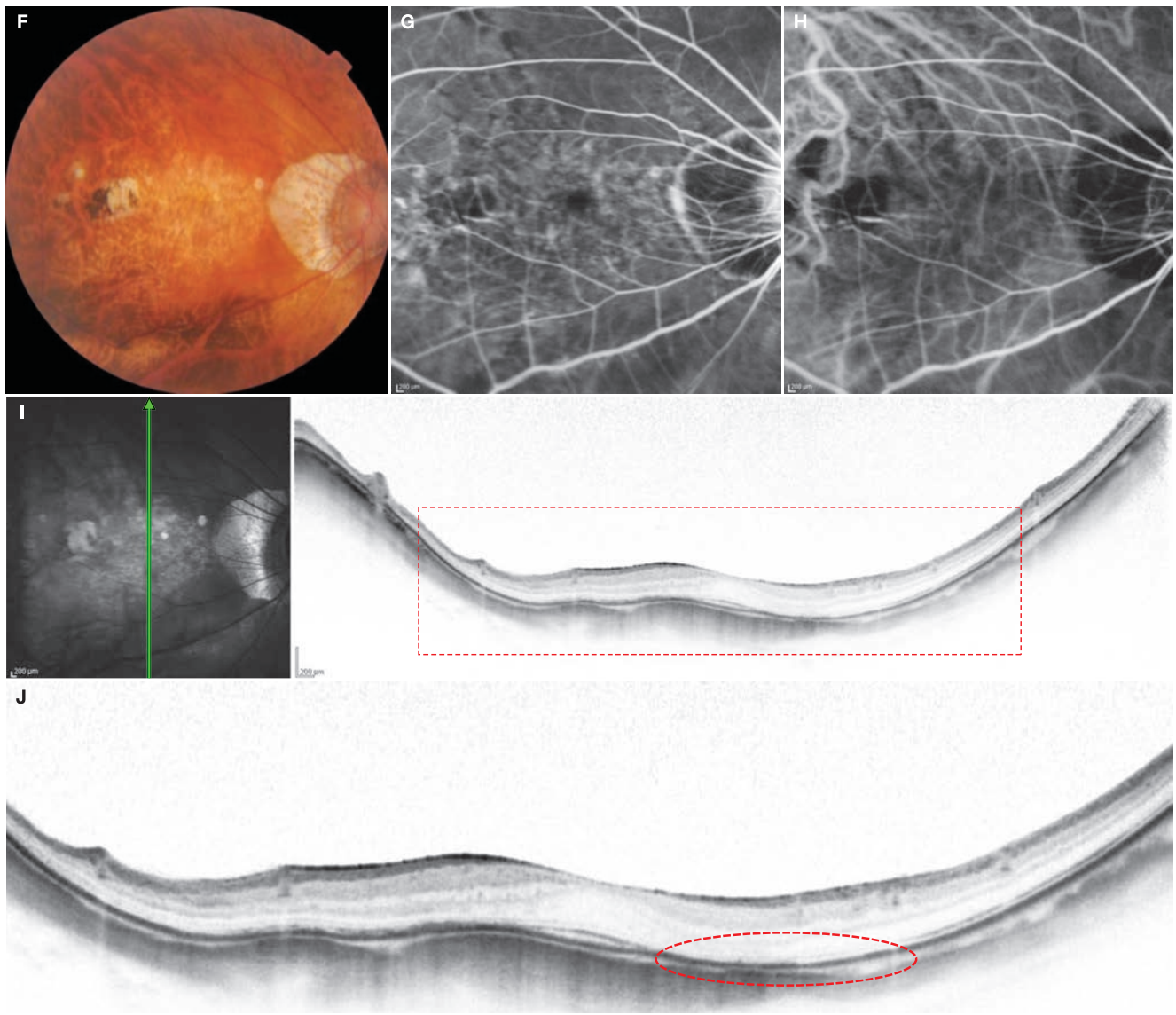

F: Color fundus photograph in the right eye: CNV seen at initial diagnosis has disappeared. There is a faint retinal hemorrhage inferior to the fovea centralis. **G:** FA in the right eye (4 minutes, 2 seconds): The hyperfluorescent lesion seen at initial diagnosis has disappeared. **H:** IA in the right eye (4 minutes, 2 seconds): CNV is not detected on IA. **I:** IR + OCT vertical scan of the right eye: Subfoveal CNV cannot be detected. **J:** Enlarged version of I [red dashed box]: Scan of the somewhat nasal side of the fovea centralis. The foveal shape is almost normal, but the IS/OS line in the superior macula macula where the SRD was present is missing (red dashed circle).

Image interpretation points

This is a case where anti-VEGF treatment was remarkably effective. Best-corrected visual acuity is also greatly improved.

Anti-VEGF treatment generally seems to have a high therapeutic effect in cases with small CNV.

Case 178 Myopic choroidal neovascularization: Large CNV

A 52-year-old female, OS, BCVA 0.06, an axial length 29.04 mm

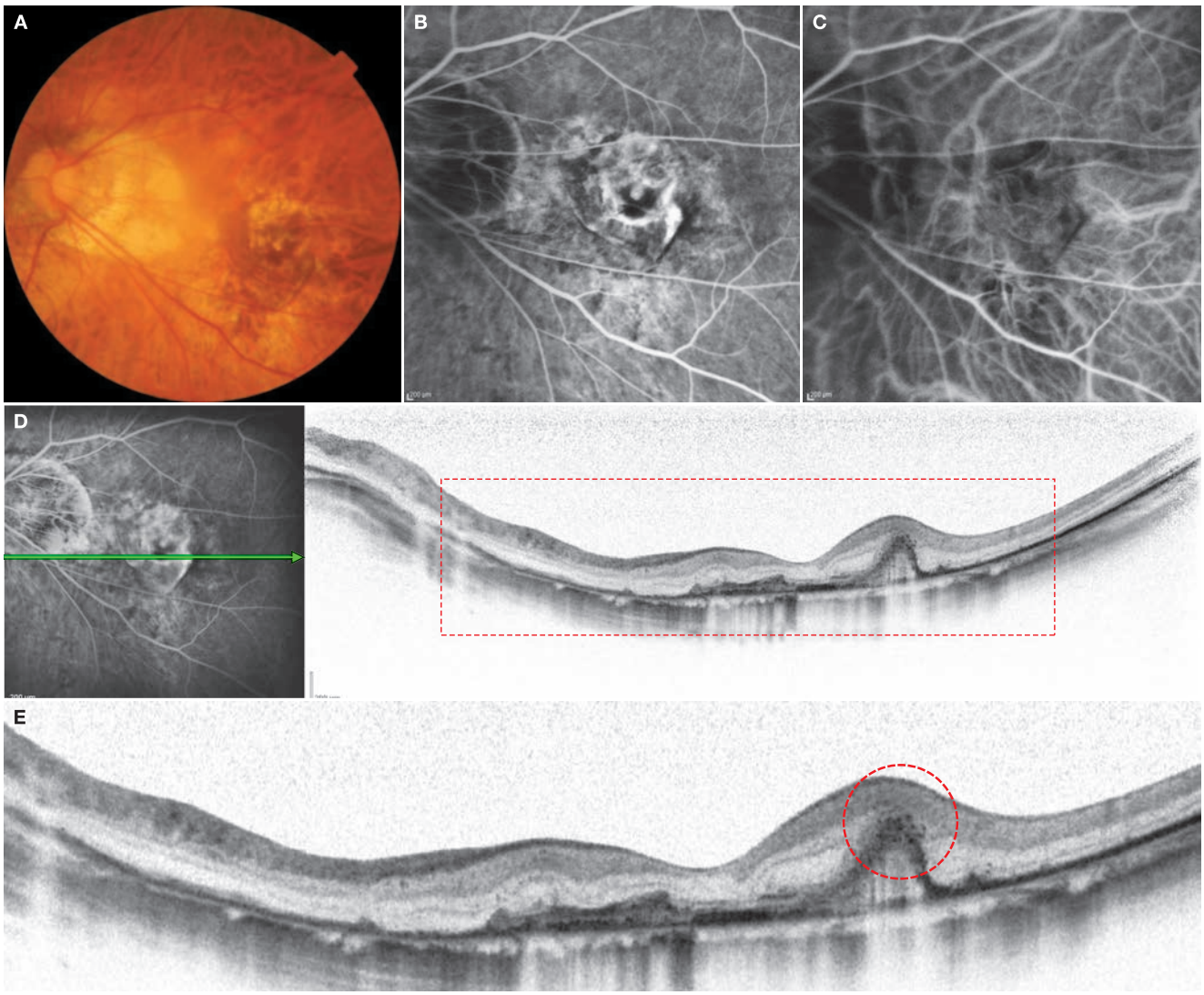

A: Color fundus photograph in the left eye: This is a case with a large temporal PPA. The CNV appears to be quite old. **B:** FA in the left eye (4 minutes, 6 seconds): Irregular hyperfluorescent lesions are evident, and thus CNV is noted as classic CNV. **C:** IA in the left eye (4 minutes, 6 seconds): CNV is depicted although it is not so hyperfluorescent as in FA. **D:** FA + OCT horizontal scan of the left eye: Extensive subfoveal CNV can be seen. The temporal side CNV exhibits a tall protrusion and spreads out flatly on the nasal side. This is Type 2 CNV. **E:** Enlarged version of D [red dashed box]: The temporal side CNV still appears to be active based on the observation that multiple intraretinal highly reflective dots are visible (red dashed circle). The RPE is smooth and no protrusions are apparent.

Image interpretation points

This is CNV observed in a relatively young patient. Elderly people generally tend to have more extensive CNV, although in this case, extensive CNV occurred despite the patient being relatively young.

Case 179 Myopic choroidal neovascularization: A young example

A 46-year-old female, OS, BCVA 0.6, an axial length 30.05 mm

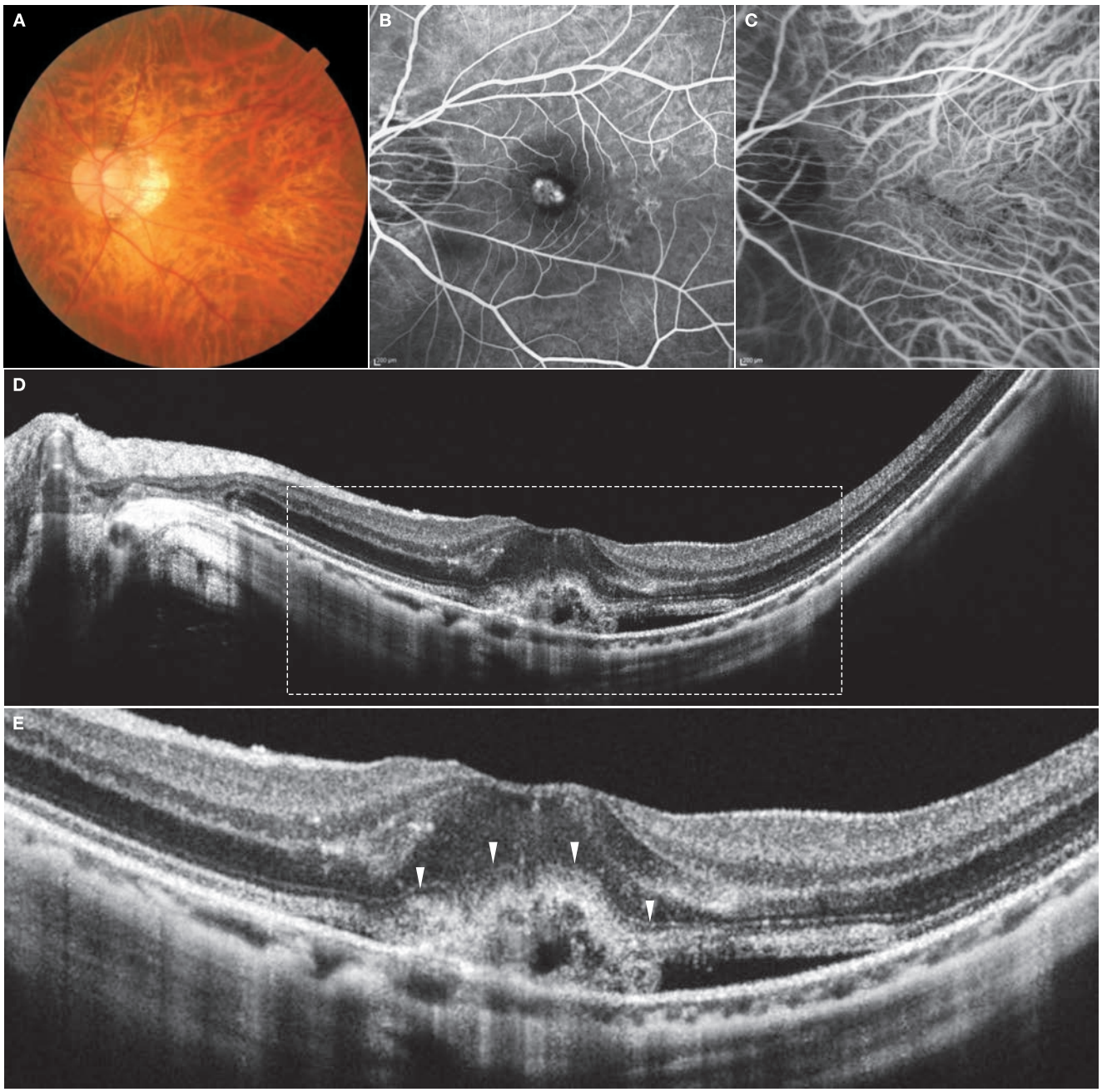

A: Color fundus photograph in the left eye: CNV of about a third of a disc diameter is visible in the fovea centralis. Subretinal hemorrhages are present. **B:** FA in the left eye (1 minute, 17 seconds): Classic CNV is depicted. **C:** IA in the left eye (1 minute, 17 seconds): CNV is only slightly noted on IA. **D:** OCT horizontal scan of the left eye: Type 2 CNV is clearly exhibited. **E:** Enlarged version of D [red dashed box]: The RPE line is smooth. This is a typical finding of type 2 CNV. A thin SRD is apparent in the temporal macula. The ELM line can somehow be traced above the CNV (▷).

Image interpretation points

This is CNV seen in a 46-year-old patient. Myopic CNV is usually rare in patients under 50 years of age. Differentiation from idiopathic CNV (see pages ▶ 223–227) is difficult. This case may actually fall under idiopathic CNV.

Case 179 One year after anti-VEGF treatment

A 46-year-old female, OS, BCVA 1.5, an axial length 30.05 mm

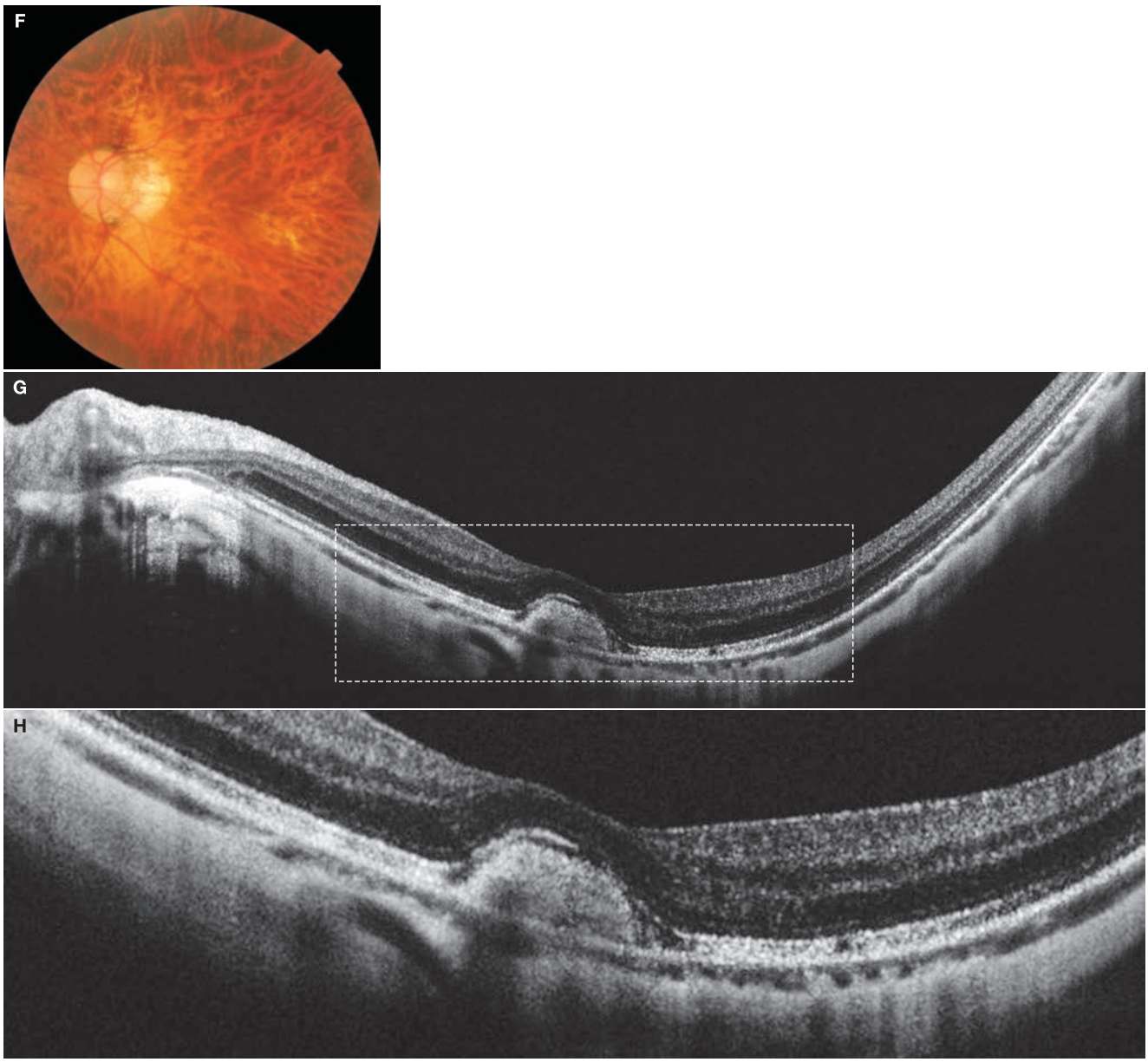

F: Color fundus photograph in the left eye: The CNV is less extensive. **G:** OCT horizontal scan of the left eye: Scarred CNV in a trapezoidal shape is visible in the nasal side of the fovea centralis. **H:** Enlarged version of G [white dashed box]: The RPE and IS/OS lines are mostly depicted. No SRD is visible in the retina.

Image interpretation points

An intravitreal injection of anti-VEGF treatment was successful, and best-corrected visual acuity improved to 1.5 about a year later. Scarring of CNV remained after treatment, but good visual acuity was achieved since there were few retinal changes.

Case 180 Myopic choroidal neovascularization: Foveoschisis

A 61-year-old female, OD, BCVA 0.3, an axial length 28.07 mm

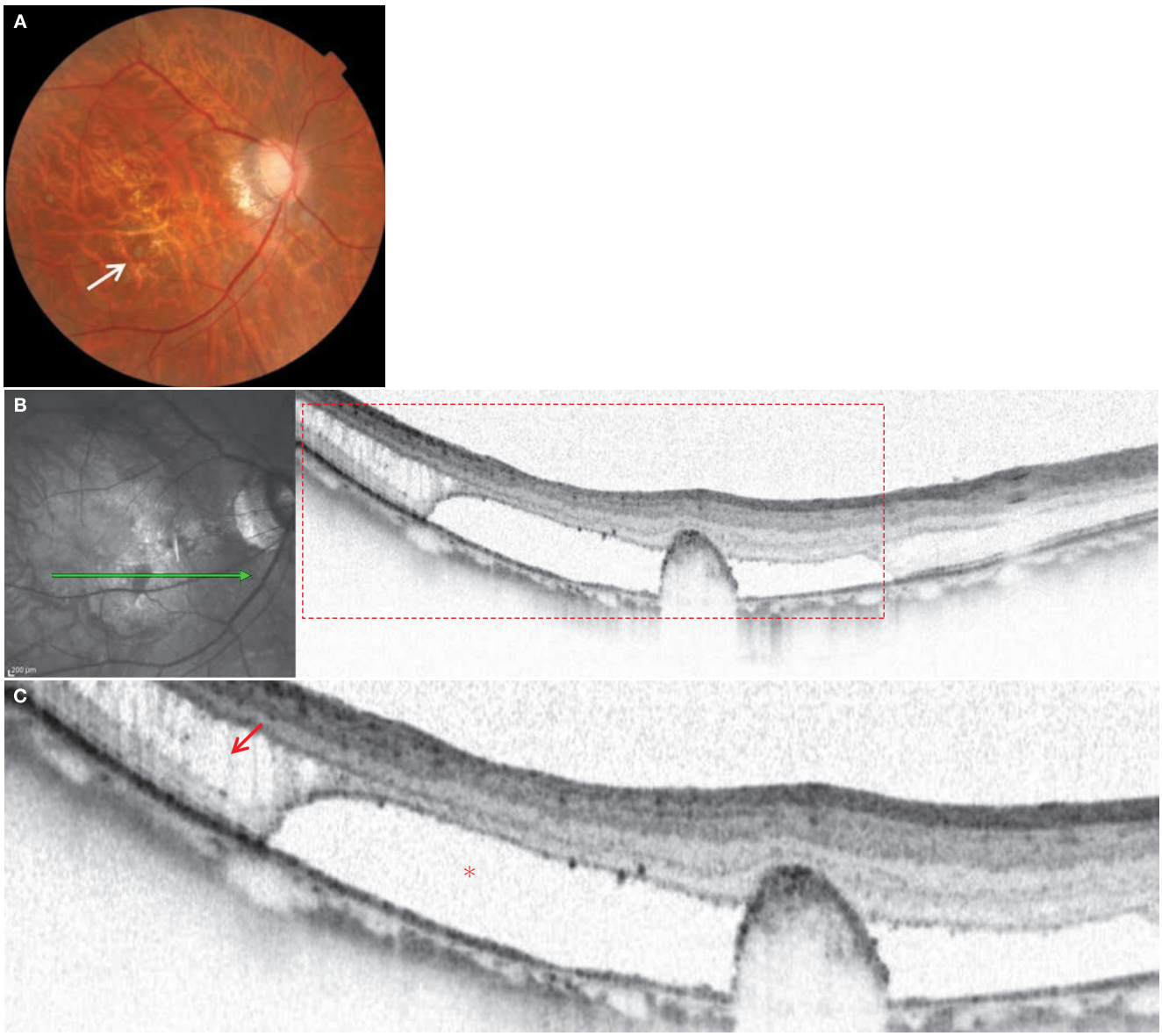

A: Color fundus photograph in the right eye: CNV is visible in the lower macula (⇨). Lacquer cracks are evident. **B:** IR + OCT horizontal scan of the right eye: Scan passing through the CNV. Type 2 CNV exhibiting a sharp elevation is depicted. There is retinal detachment around the CNV, and retinoschisis is evident on the temporal side. **C:** Enlarged version of B [red dashed box]: Type 2 CNV, retinal detachment (*) and retinoschisis (➔) are clearly visible. The CNV is being enveloped by the RPE

Image interpretation points

It is unusual that myopic CNV is accompanied by a large retinal detachment.

This case also includes foveoschisis, and it is unclear to what extent CNV is involved in the onset of retinal detachment.

9.2 Dome-shaped macula and inferior staphyloma

Background

Dome-shaped macula is a particular type of myopic posterior staphyloma reported by Gaucher in 2008.[1] The Curtin classification is well known as a classification for posterior staphyloma,[2] but dome-shaped macula exhibits morphological abnormalities that do not correspond to any of the Curtin classifications. Posterior staphyloma exhibits a posterior projection of the sclera, but dome-shaped macula is the anterior projection of the scleral surface in the vicinity of the fovea centralis (◘ Fig. 9-5). Dome-shaped macula causes macular lesions.

Various macular lesions also develop in the macular area in cases of tilted disc syndrome where the inferior staphyloma margin overlaps in the macular area.[3] For example, chorioretinal atrophy,[4] CNV,[5,6] localized SRD,[7] and PCV[8] are reported to develop. In terms of the disease concept, dome-shaped macula and tilted disc syndrome accompanied by inferior staphyloma are entirely different, but both diseases result in similar complications, and therefore may have similar onset mechanisms.

There are also cases where differentiation between the two is not necessarily easy. The points of differentiation are basically in the form of the posterior staphyloma. In dome-shaped macula, a anterior projecting area is visible in the posterior staphyloma, whereas only a posterior projection is visible in inferior staphyloma. However, cases diagnosed with dome-shaped macula do not always appear to exhibit a single anterior projection pattern. Future studies on the classification of the patterns are needed.

OCT findings

Dome-shaped macula is not rare. In particular, cases that exhibit a dome-shaped macula on OCT without lesions in the macular area are frequent. When a SRD similar to central serous chorioretinopathy (CSC) is found, but dye leakages cannot be found on FA in myopic eyes, a dome-shaped macula or tilted disc syndrome accompanied by inferior staphyloma need to be suspected. In such cases, it is important to capture vertical scans passing through the fovea centralis.

There are many unclear points in the mechanism for the formation of dome-shaped macula. Choroidal thickening was initially considered, to which recent reports are contradictory. Based on EDI-OCT imaging, Imamura et al. suggested that in cases of dome-shaped macula localized thickening of the subfoveal sclera leads to a chorioretinal anterior projection.[9] However, the precise mechanisms remain unclear because full-thickness sclera cannot be depicted in all eyes by EDI-OCT imaging.

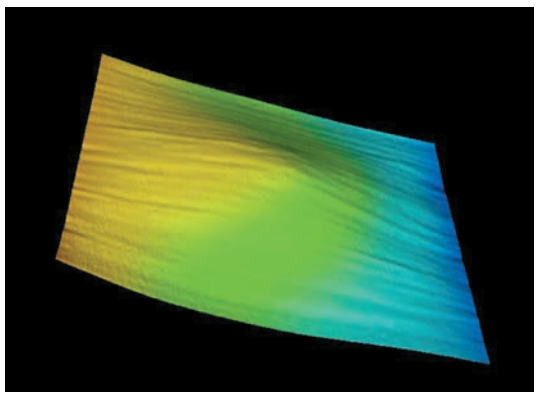

◘ **Fig. 9-5** Three-dimensional RPE reconstructed image of the macular area in a case of dome-shaped macula. We can see that the macular area is projecting forward

References

1) Gaucher D, Erginay A, Lecleire-Collet A, et al. Dome-shaped macula in eyes with myopic posterior staphyloma. *Am J Ophthalmol*. 2008; 145: 909–914.
2) Curtin BJ. The posterior staphyloma of pathologic myopia. *Trans Am Ophthalmol Soc*. 1977; 75: 67–86.
3) Nakanishi H, Tsujikawa A, Gotoh N, et al. Macular complications on the border of an inferior staphyloma associated with tilted disc syndrome. *Retina*. 2008; 28: 1493–1501.
4) Guiffre G. Chorioretinal degenerative changes in the tilted disc syndrome. *Int Ophthalmol*. 1991; 15: 1–7.
5) Tsuboi S, Uchihori Y, Manabe R. Subretinal neovascularisation in eyes with localised inferior posterior staphylomas. *Br J Ophthalmol*. 1984; 68: 869–872.
6) Stur M. Congenital tilted disk syndrome associated with parafoveal subretinal neovascularization. *Am J Ophthalmol*. 1988; 105: 98–99.
7) Cohen SY, Quentel G. Guiberteau B, et al. Macular serous retinal detachment caused by subretinal leakage in tilted disc syndrome. *Ophthalmology*. 1998; 105: 1831–1834.
8) Mauget-Faÿsse M, Cornut PL, Quaranta El-Maftouhi M, et al. Polypoidal choroidal vasculopathy in tilted disk syndrome and high myopia with staphyloma. *Am J Ophthalmol*. 2006; 142: 970–975.
9) Imamura Y, Fujiwara T, Margolis R, et al. Enhanced depth imaging optical coherence tomography of the choroid in central serous chorioretinopathy. *Retina*. 2011; 151: 297–302.

Case 181 Dome-shaped macula: A typical example

A 39-year-old female, OD, BCVA 0.8, an axial length 29.25 mm

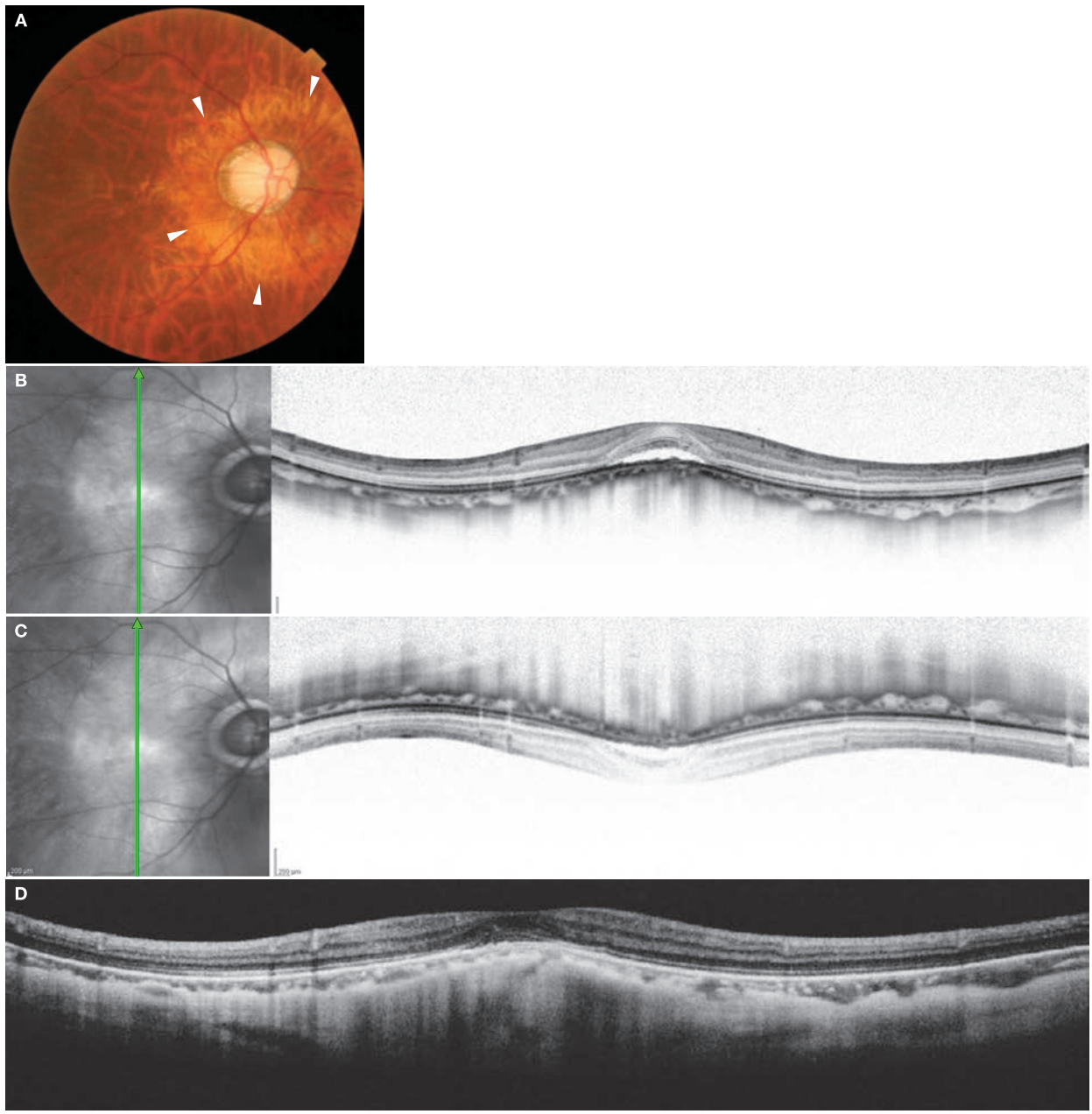

A: Color fundus photograph in the right eye: The optic disc is not tilted. Ring-shaped atrophy is evident around the optic disc (▷), suggesting the Curtin's type 3 staphyloma. **B:** IR + OCT vertical scan of the right eye: A SRD is visible in the fovea centralis. The RPE line is projecting anteriorly. The choroid is thin. The choroid is thinnest at the apex of the dome-shaped macula. **C:** IR + EDI-OCT vertical scan of the right eye: Scleral thickness is relatively well preserved at the apex of the dome-shaped macular, which was unclear using standard OCT imaging. **D:** SS-OCT vertical scan of the right eye: Image of a 12 mm-long scan. We can clearly see that part of the backward projecting posterior staphyloma is projecting anteriorly forming a dome-shaped macula.

Image interpretation points

Dome-shaped macula and tilted disc syndrome with inferior staphyloma are two different diseases. Differentiation of the two is not necessarily clear, but the fundamental difference is that part of the backward projecting posterior staphyloma projects anteriorly in dome-shaped macula, whereas no anterior projection is evident in inferior staphyloma.

Case 182 Inferior staphyloma: Serous retinal detachment

A 45-year-old male, OS, BCVA 1.2, refraction -4.75 D

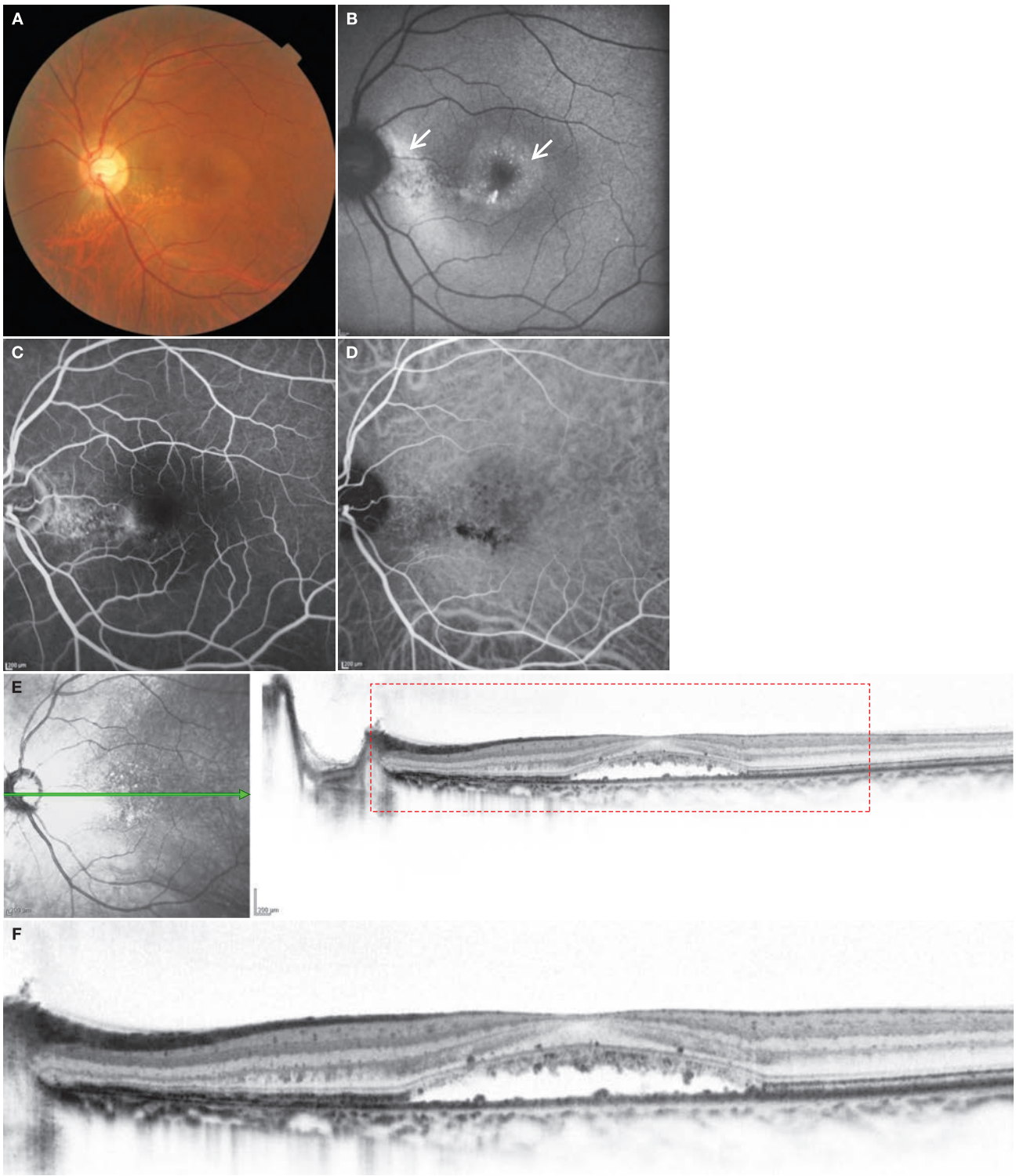

A: Color fundus photograph: A subfoveal SRD is visible. The optic disc exhibits no deformation. The choroidal vessels in the lower fundus are clearly in this area. **B:** FAF in the left eye: The parafoveal and temporal peripapillary areas exhibit hyperfluorescence (⇨). **C:** FA in the left eye (33 seconds): Hyperfluorescence is visible between the optic disc and fovea centralis. Fluorescein leakage spots are indistinct. **D:** IA in the left eye (33 seconds): The hyperfluorescent area on FA exhibits hypofluorescence on IA. **E:** IR + OCT horizontal scan of the left eye: A SRD is depicted in the macula. **F:** Enlarged version of E [red dashed box]: This is very similar with OCT findings in CSC. Foveal thickness is well preserved. Elongation of the photoreceptor outer segment is seen.

(Continued on the next page)

Case 182 Continuation

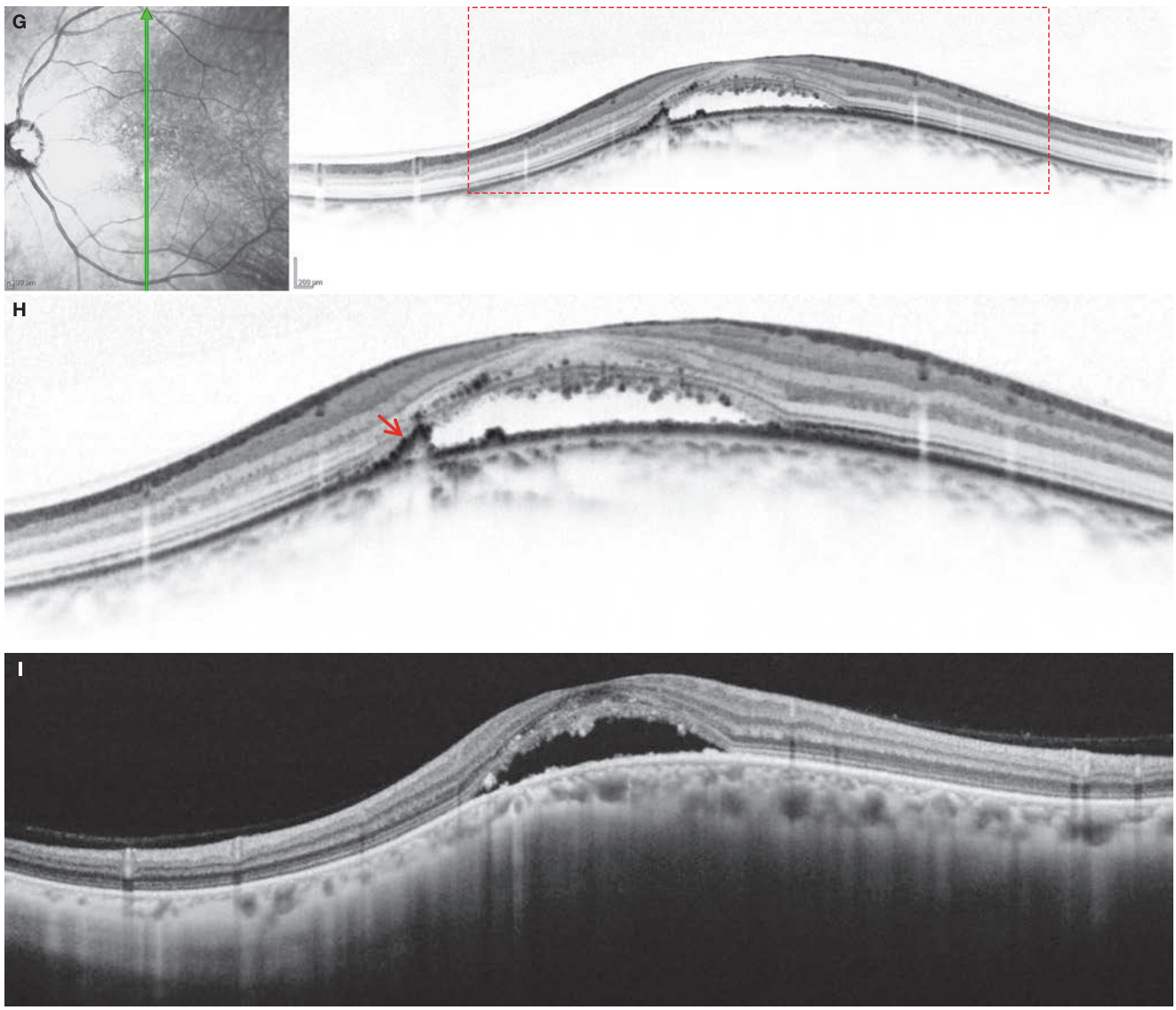

G: IR + OCT vertical scan of the left eye: The RPE line consistent with the hyperfluorescent area on FA and hypofluorescent area on IA is steeply elevated. Such elevation of the RPE is not evident on the horizontal scan shown in E. The white reflective spots on the IR image is the shed photoreceptor outer segments. **H:** Enlarged version of G [red dashed box]: A small RPE protrusion is evident (➔). Intraretinal, granular, highly reflective findings are visible. **I:** SS-OCT vertical scan: Image of a 12 mm-long scan (prototype SS-OCT). We can clearly see the presence of inferior staphyloma. The choroid is thin in the area of staphyloma.

Image interpretation points

This is a case that was difficult to differentiate from CSC. Abnormal shape of the eyeball may have resulted in damage to choroidal circulation leading to the development of SRD, but the combination of CSC and inferior staphyloma is undeniable. However, choroidal thickening suggestive of CSC is not apparent. A small RPE protrusion is visible, but it is a common finding in this disease. It is unclear if this has any pathological significance.

Retinal detachment

10.1 Rhegmatogenous retinal detachment – 336
References – 336

Case 183 Rhegmatogenous retinal detachment: A case where retinal detachment has stopped at the fovea centralis – 337

Case 184 Rhegmatogenous retinal detachment: Macular detachment – 338

Case 185 Rhegmatogenous retinal detachment: Foveal inner segment defects – 339

Case 186 Optic disc pit maculopathy – 340

10.1 Rhegmatogenous retinal detachment

Background

Many cases of rhegmatogenous retinal detachment (RRD) in young people are caused by atrophic retinal holes and progress slowly. In contrast, RRD in middle-aged to elderly patients progress rapidly due to flap retinal tears and retinal breaks along the lattice degeneration caused by acute PVD. Preoperative risk factors resulting in a poor visual prognosis include the presence and extent of foveal detachment, time to foveal reattachment, area of retinal detachment, vitreous hemorrhages, ocular hypotension, presence of choroidal detachment, unidentified retinal breaks, existence of giant tears, and onset of proliferative vitreoretinopathy.[1] Postoperative development of foveal cystoid spaces, ERM and macular pucker, which occur regardless of the presence of preoperative foveal detachment, can be the cause of poor postoperative visual prognosis.[1] OCT allowed us to find that there are residual subretinal fluid and abnormal retinal findings despite the retina appearing to be completely reattached on an ophthalmoscope.

OCT findings for detached retinas

Bullous retinal detachment with the fovea centralis detached is not always sufficiently visible in cases of RRD where the retinal detachment is so high that the detached retina is out of the OCT imaging frame. However, there are many cases where useful information can be obtained by successfully scanning the the fovea centralis.

Foveal detachment is clinically important since it may result in postoperative visual impairment or metamorphopsia. Although it can sometimes be hard to identify with an biomicroscopy, its presence can be easily determined with OCT. In RRD, retinal detachment often appears to temporarily stop once it has reached the fovea centralis before progressing to full detachment.

Separation of the outer retinal layers (known as »intraretinal separation«) is a typical finding seen in detached retinas. This finding can be considered to be cystoid spaces that have formed in the Henle's fibrous layer of the outer plexiform layer, and is actually closer to retinoschisis.[2–5]

Additionally, cystoid space formation in the inner nuclear layer [5, 6] and severe undulations in the photoreceptor layer (outer nuclear layer, photoreceptor inner and outer segments) [2–5] are also typical findings of RRD. As these findings are not seen in CSC, a typical form of SRD, their presence is helpful in diagnosis for cases where it is difficult to determine whether retinal detachment is rhegmatogenous or serous. The formation of intraretinal separation is unrelated to the length of the detachment period.[2]

Defects in foveal photoreceptor inner segment can be detected with SD-OCT.[5] These findings are irreversible since the inner segment does not regenerate. Findings associated with a poor postoperative visual prognosis after reattachment include outer retinal layer cystoid spaces,[2] the height of the foveal detachment,[2, 4, 5, 7] foveal photoreceptor inner and outer segment defects,[5] and foveal[5] or parafoveal[7] outer nuclear layer thinning. In contrast, »intraretinal separation« is reportedly unrelated to postoperative visual acuity.[3, 5]

OCT findings for reattached retinas

There are many cases where although the retina appears to be biomicroscopy after surgery foveal detachment is found on OCT and subsides 6–12 months postoperatively.[3, 8–11] There are reports that claim that the prolongation of foveal detachment after surgery is a cause of poor visual prognosis,[3] while there are also reports claiming that it is unrelated.[9, 11] Lamellar macular hole-like foveal abnormalities can remain postoperatively,[8, 9] and cystoid macular edema can persist or develop halfway through and be prolonged.[8, 10] There are also cases where ERM or macular pucker occurs after surgery.[8] All these findings can be the cause of poor visual acuity. The IS/OS and COST lines that become indistinct immediately after surgery are generally restored months later, but cases without recovery of these lines have a poor visual prognosis.[6, 8–15] Foveal outer nuclear layer thinning measured by SD-OCT is related to a poor postoperative prognosis.[14, 15]

References

1) Williams GA and Aaberg Jr TM. Techniques of scleral buckling. In: Ryan SJ, ed. Retina. 4th ed. Vol 3 Mosby Elsevier Inc, PA, 2006: 2035–2070.
2) Hagimura N, Suto K, Iida T, et al. Optical coherence tomography of the neurosensory retina in rhegmatogenous retinal detachment. *Am J Ophthalmol*. 2000; 129: 186–190.
3) Wolfensberger TJ, Gonvers M. Optical coherence tomography in the evaluation of incomplete visual acuity recovery after macula-off retinal detachments. *Graefes Arch Clin Exp Ophthalmol*. 2002; 240: 85–89.
4) Lecleire-Collet A, Muraine M, Menard JF, et al. Predictive visual outcome after macula-off retinal detachment surgery using optical coherence tomography. *Retina*. 2005; 25: 44–53.
5) Nakanishi H, Hangai M, Unoki N, et al. Spectral-domain optical coherence tomography imaging of the detached macula in rhegmatogenous retinal detachment. *Retina*. 2009; 29: 232–242.
6) Lecleire-Collet A, Muraine M, Ménard JF, et al. Evaluation of macular changes before and after successful retinal detachment surgery using stratus-optical coherence tomography. *Am J Ophthalmol*. 2006; 142: 176–179.
7) Maruko I, Iida T, Sekiryu T, et al. Morphologic changes in the outer layer of the detached retina in rhegmatogenous retinal detachment and central serous chorioretinopathy. *Am J Ophthalmol*. 2009; 147: 489–494.e1.
8) Schocket LS, Witkin AJ, Fujimoto JG, et al. Ultrahigh-resolution optical coherence tomography in patients with decreased visual acuity after retinal detachment repair. *Ophthalmology*. 2006; 113: 666–672.
9) Smith AJ, Telander DG, Zawadzki RJ, et al. High-resolution Fourier-domain optical coherence tomography and microperimetric findings after macula-off retinal detachment repair. *Ophthalmology*. 2008; 115: 1923–1929.
10) Wakabayashi T, Oshima Y, Fujimoto H, et al. Foveal microstructure and visual acuity after retinal detachment repair: imaging analysis by Fourier-domain optical coherence tomography. *Ophthalmology*. 2009; 116: 519–528.
11) Shimoda Y, Sano M, Hashimoto H, et al. Restoration of photoreceptor outer segment after vitrectomy for retinal detachment. *Am J Ophthalmol*. 2010; 149: 284–290.
12) Lai WW, Leung GY, Chan CW, et al. Simultaneous spectral domain OCT and fundus autofluorescence imaging of the macula and microperimetric correspondence after successful repair of rhegmatogenous retinal detachment. *Br J Ophthalmol*. 2010; 94: 311–318.
13) Sheth S, Dabir S, Natarajan S, et al. Spectral domain-optical coherence tomography study of retinas with a normal foveal contour and thickness after retinal detachment surgery. *Retina*. 2010; 30: 724–732.
14) Gharbiya M, Grandinetti F, Scavella V, et al. Correlation between spectral-domain optical coherence tomography findings and visual outcome after primary rhegmatogenous retinal detachment repair. *Retina* 2012; 32: 43–53.
15) Delolme MP, Dugas B, Nicot F, et al. Anatomical and functional macular changes after rhegmatogenous retinal detachment with macula off. *Am J Ophthalmol*. 2012; 153: 128–136.

Case 183 Rhegmatogenous retinal detachment: A case where retinal detachment has stopped at the fovea centralis

A 59-year-old male, OD, BCVA 0.7

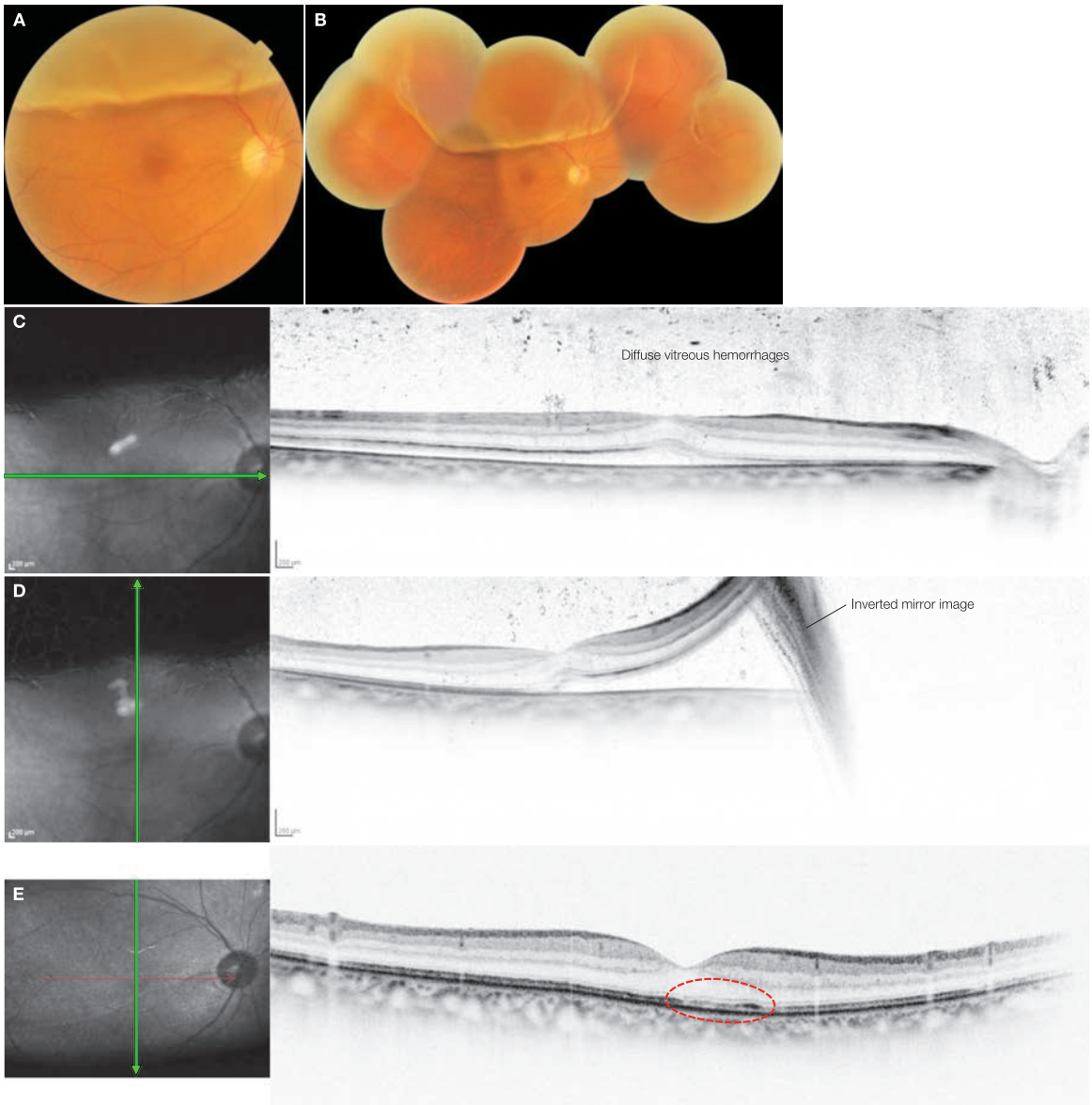

A: Color fundus photograph in the right eye. **B:** Fundus photograph montage in the right eye: At initial diagnosis. A bullous retinal detachment due to a superonasal retinal tearcan be seen in the superior fundus. The retinal detachment is extending towards the fovea centralis. The detached retina has few folds. **C:** FA + OCT horizontal scan of the right eye: At initial diagnosis. A flat retinal detachment is visible from the temporal area to the fovea. Diffuse vitreous hemorrhages thought to have occurred during retinal tear formation is apparent in the vitreous cavity. **D:** FA + OCT vertical scan of the right eye: At initial diagnosis. The retinal detachment is spreading right up to the fovea centralis. The elevation of the superior detached retina is significant. The mirror image of the detached retina that was out of the imaging flame is seen as an inverted image. **E:** IR + OCT vertical scan of the right eye: One month after surgery. Best-corrected visual acuity has improved to 1.0. The retina has been reattached, and the foveal shape has almost been restored to normal. The IS/OS line in the superior fovea centralis is weakly reflective and irregular (red dashed circle).

Image interpretation points

As in this case, patients often see a doctor when the retinal detachment has reached the fovea centralis. The detachment often appears to stop here temporarily. Once it passes this area, it may rapidly advance to macular detachment. OCT findings reveal few changes in the detached retina. This is consistent with the lack of folds in the detached retina on fundus photographs. If the RRD is discovered at this stage and treated by surgery, the visual prognosis is generally good.

Case 184 Rhegmatogenous retinal detachment: Macular detachment

A 61-year-old male, OD, BCVA 0.5

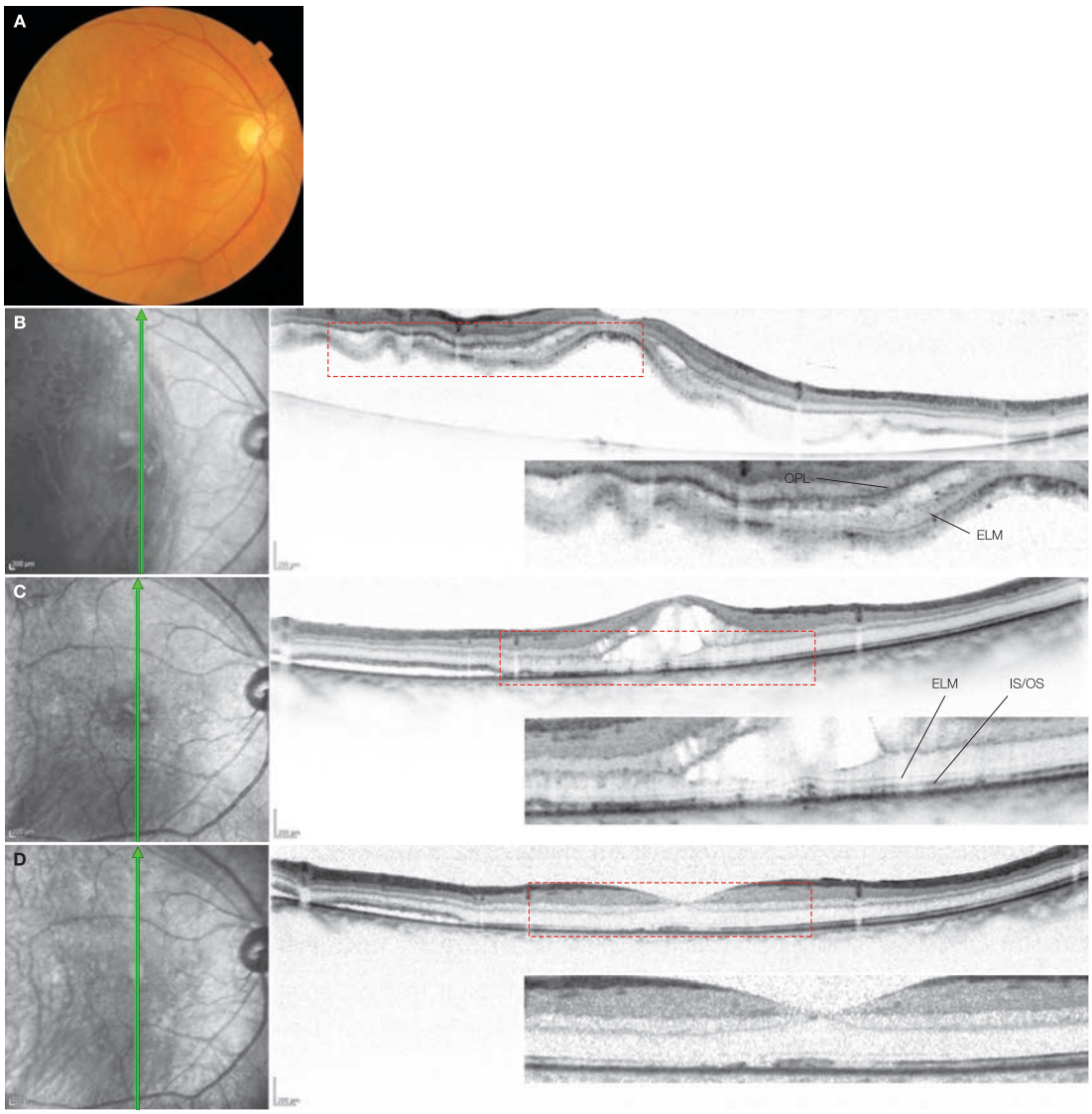

A: Color fundus photograph in the right eye: At initial diagnosis. A retinal detachment including the macula and folds of detached retina are visible. A retinal tear in the temporal fundus led to the retinal detachment. **B:** FA + OCT vertical scan of the right eye + enlarged version [red dashed box]: At initial diagnosis. There are seen in the detached retina intraretinal separation in the Henle's fiber layer of the outer plexiform layer and undulating outer nuclear layer (outer nuclear layer and photoreceptor inner and outer segments, which are findings characteristic to rhegmatogenous retinal detachment. Small inner nuclear layer cystoid spaces are depicted. **C:** IR + OCT vertical scan of right eye + enlarged version [red dashed box]: Two months after surgery. Best-corrected visual acuity is 0.6. There is a flat retinal detachment remaining in the inferior posterior pole. This was indistinct on an biomicroscopy. A typical CME is also seen. The ELM and IS/OS lines are visible in the fovea centralis, but the latter is irregular. **D:** IR + OCT vertical scan of right eye + enlarged version [red dashed box]: Five months after surgery. Best-corrected visual acuity has improved to 1.2. CME has disappeared. Foveal IS/OS reflectivity is partially attenuated. The extent of the residual retinal detachment in the inferior posterior pole is smaller, and thus the detachment is resolving.

Image interpretation points

Characteristic retinal folds are often observed in RRD. On OCT, retinoschisis in the Henle's fiber layer (HFL) of the outer plexiform layer (intraretinal separation) occurs, and the retina outer to the retinoschisis is undulating. This retinal undulation corresponds to the retinal folds on photo. Cystoid spaces can sometimes be seen in the inner nuclear layer. These findings are typical of RRD and are hardly seen in SRDs such as CSC. Vitreous surgery was performed for this patient, and the retina appeared to be reattached on an biomicroscopy; but OCT revealed a residual shallow retinal detachment. CME occurred two months postoperatively, although this subsided by the fifth postoperative month. Thus, OCT allows detection of abnormal features not evident on an biomicroscopy.

Case 185 Rhegmatogenous retinal detachment: Foveal inner segment defects

A 46-year-old male, OD, BCVA 0.1

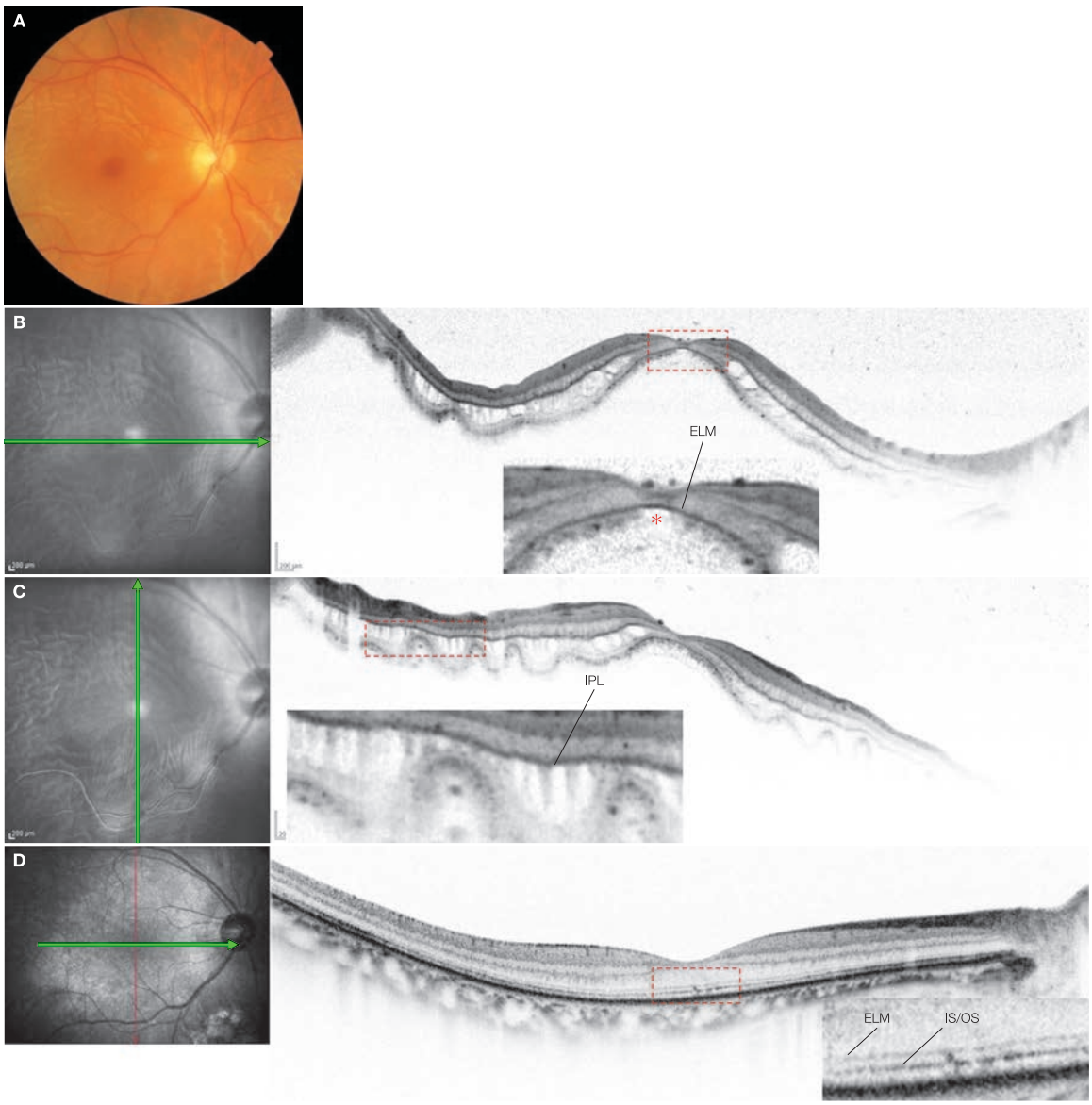

A: Color fundus photograph in the right eye: At initial diagnosis. A retinal detachment is seen in the inferior half of the fundus and the macula. This is due to a retinal tear in the superotemporal periphery. Horizontal retinal folds are seen in the macula. **B:** FA + OCT horizontal scan of the right eye + enlarged version [red dashed box]: At initial diagnosis. Retinal features characteristic to RRD, such as retinoschisis in the Henle's fiber layer of the outer nuclear layer and undulations of the outer retinal layers (outer nuclear layer and photoreceptor inner and outer segments) can be seen in the detached retina. A columnar structure thought to be composed of Müller cells is apparent. Note that no reflectivity is evident outside the ELM in the foveola, which may be due to damage to the inner segment (✻). Insignificant inner nuclear layer cystoid spaces are noted. **C:** FA + OCT vertical scan of the right eye + enlarged version [red dashed box]: At initial diagnosis. Similar findings to B can be seen, but outer retinal folding is more severe. **D:** IR + OCT horizontal scan of the right eye + enlarged version [red dashed box]: 13 months after surgery. IS/OS abnormal reflectivity is visible only in the foveola. Despite the successful retinal detachment surgery, best-corrected visual acuity better than 0.6 has not been achieved.

Image interpretation points

Retinal folds in RRD are consistent with undulations of the retina outer to the retinoschisis of the Henle's fiber layer of the outer plexiform layer as depicted on OCT. Close observation of the foveola reveals loss of the reflectivity outside of the ELM line. This suggests the disappearance of the inner segment, which is irreversible damage. These findings can be seen in cases where foveal detachment is high or many days have passed before surgery and often result in a poor visual prognosis. This patient was diagnosed one week after becoming aware of visual acuity decline.

Case 186 Optic disc pit maculopathy

A 23-year-old male, OS, BCVA 0.4

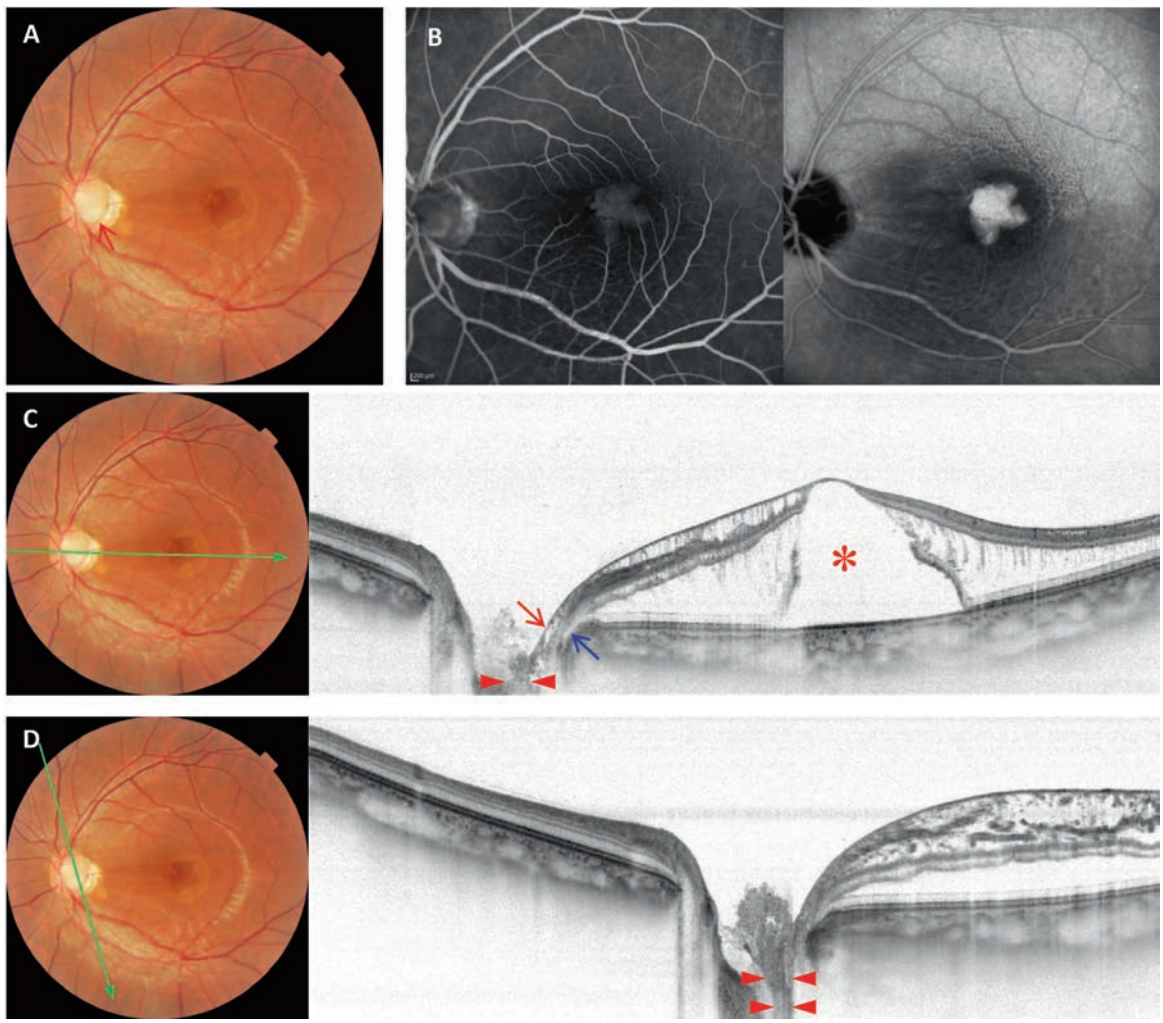

A: Color fundus photograph in the left eye: At initial diagnosis. An elliptical pit is visible on the inferior temporal part of the optic disc (➔). Retinal nerve fiber layer defect-like findings are apparent in the papillomacular bundles and are linked to a macular SRD. **B:** FA/IA in the left eye (14 minutes): No fluorescein leakage is evident in the pit, and no retinal or choroidal vessel hyperpermeability findings can be found. The fovea centralis exhibits hyperfluorescence at the early to late phase of both FA and IA imaging, but this hyperfluorescence is thought to be due to depigmentation of the retina pigment epithelium layer as a result of prolonged detachment. **C:** Color fundus photograph + 1 μm SS-OCT horizontal scan of the left eye: Scan passing through the pit (➔) and fovea centralis. A SRD is visible in the macula, and the foveal photoreceptor layer is dehisced. Retinoschisis is significant in the retinal nerve fiber layer and in the Henle's fiber layer of the outer plexiform layer and appears to be connected to the pit through hyporeflective vacuole or slit spaces in the optic disc rim (➔) and in the deep portion of the optic disc rim (➔). Vacuoles are also visible in the ganglion cell layer and inner nuclear layer. **D:** Color fundus photograph + 1 μm SS-OCT horizontal scan of the left eye: Scan passing through the pit. Highly reflective tissue appears to be filling the pit. The outline of the pit is clearly visible as a result of this tissue, and we can see that the lamina cribrosa is defective.

Image interpretation points

An optic disc pit is thought to be a congenital anomaly where a round or elliptical pit forms in the temporal part of the optic disc. The lamina cribrosa is defective in the pit area, which is filled with abundant collagen. A pit can be seen on the temporal side of the optic disc in this case. This SS-OCT image succeeds in depicting the pit filled with highly reflective fibrous tissue. 25% to 75% of eyes with an optic disc pit subsequently develop a SRD in the macular area, which results in visual decline. This is known as optic disc pit maculopathy. This is always accompanied by retinoschisis in the inner and/or outer retinal layers. The laminar fluid in the gap has been speculated to derive either from cerebrospinal fluid, retinal blood vessels, or the vitreous fluid. However, according to recent observational studies using OCT, cerebrospinal fluid passes through the pit and then inner and/or outer retinal layers to accumulate subretinally in the macular area. SS-OCT images reveal that vacuoles inside the sensory retina and the optic disc rim connect and communicate with the pit.

Lesion morphology index based on OCT

Vitreoretinal interface lesions

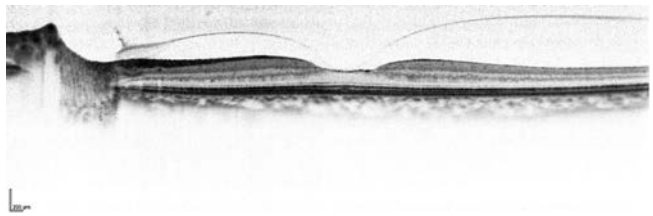

Perifoveal PVD with foveal deformation
(Case 2C, page 30)

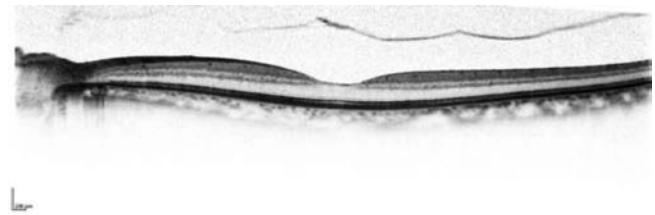

Macular PVD resulting in foveal deformation
(Case 1C, page 29)

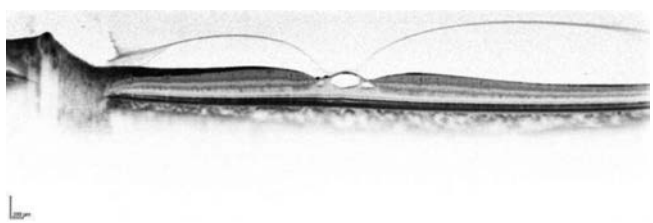

Stage 1 idiopathic macular hole
(Case 2D, page 30)

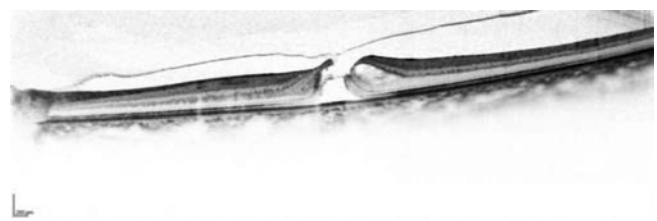

Stage 2 idiopathic macular hole
(Case 8C, page 36)

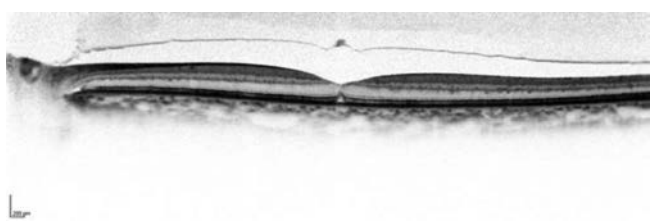

Macular PVD resulting in a macular microhole
(Case 23C, page 57)

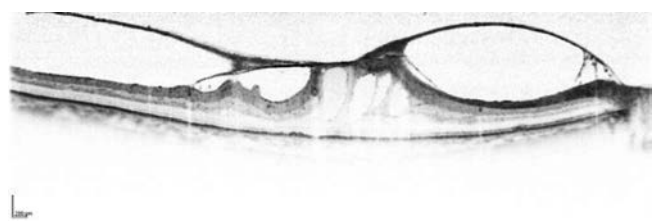

Vitreomacular traction syndrome
(Case 35E, page 74)

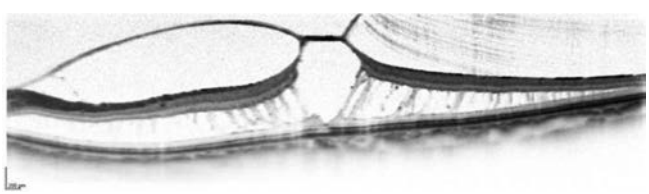

Myopic foveoschisis
(Case 37C, page 76)

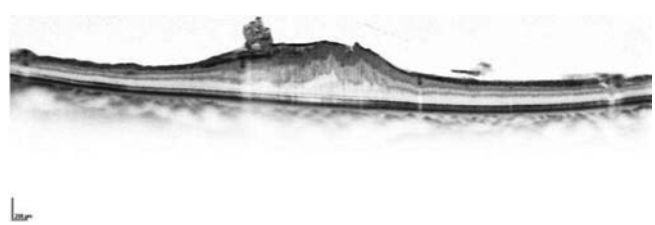

Epiretinal membrane with PVD
(Case 27D, page 64)

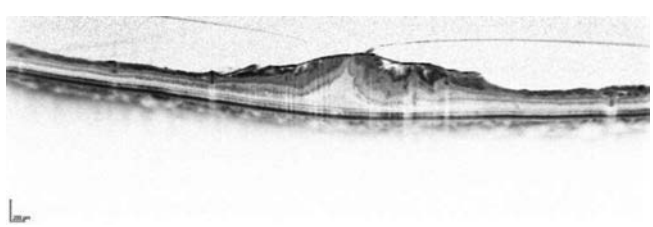

Epiretinal membrane without PVD
(Case 31E, page 68)

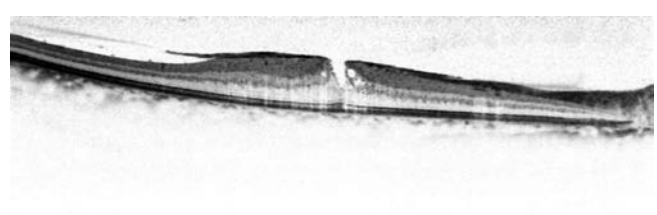

Macular pseudohole without PVD
(Case 34D, page 71)

Macular thickening

Thickening due to traction

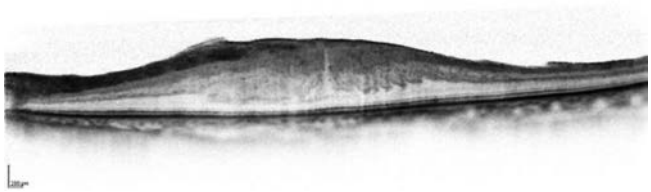

Epiretinal membrane
(Case 28D, page 65)

Vitreomacular traction syndrome
(Case 35E, page 74)

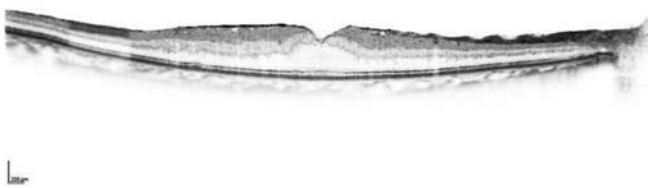

Macular pseudohole with PVD
(Case 33D, page 70)

Thickening with cystoid spaces

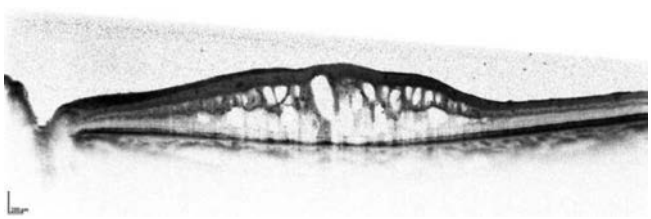

Diabetic macular edema
(Case 41 G, page 89)

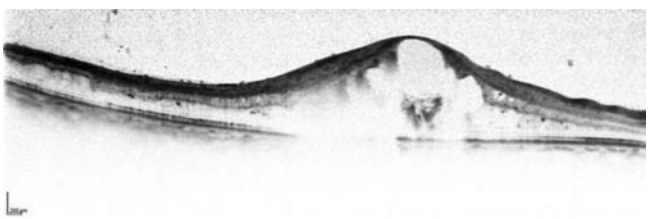

Branch retinal vein occlusion
(Case 57C, page 114)

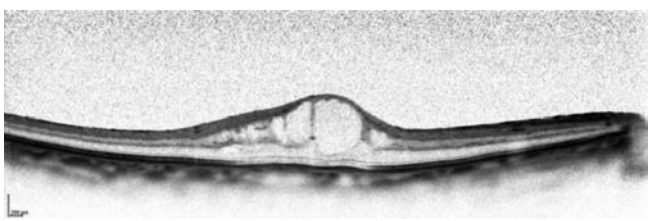

Sarcoidosis
(Case 154E, page 283)

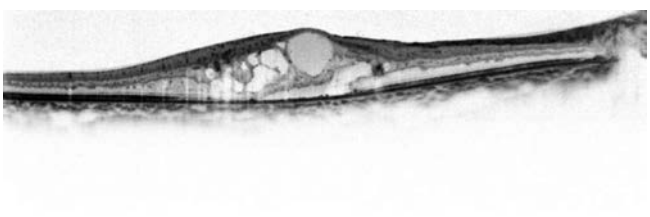

Macular telangiectasia Type 1
(Case 64E, page 124)

Thickening with retinoschisis

Myopic foveoschisis
(Case 170B, page 316)

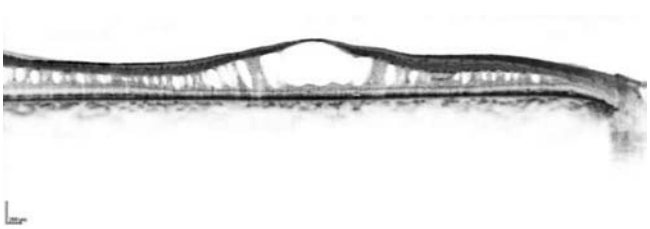

X-linked juvenile retinoschisis
(Case 131C, page 243)

Foveal detachment and macular retinal detachment

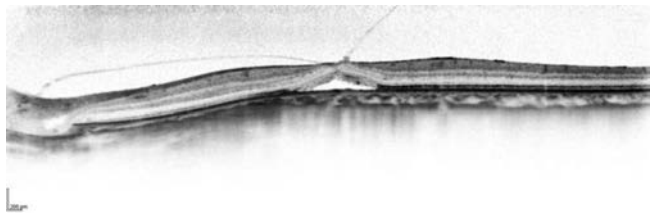

Stage 1 idiopathic macular hole
(Case 4C, page 32)

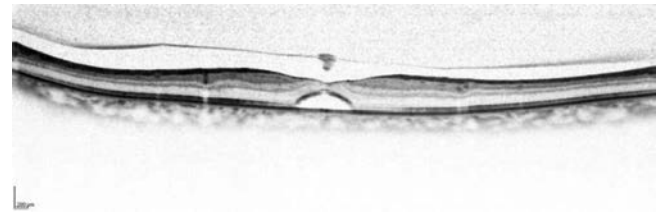

Idiopathic macular hole with spontaneous closure
(Case 18E, page 50)

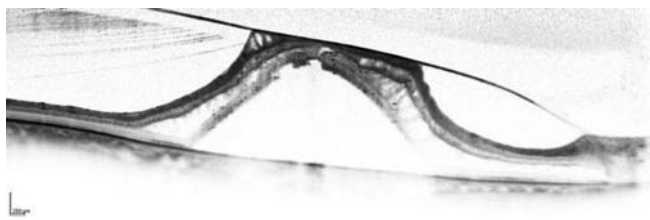

Vitreomacular traction syndrome
(Case 36B, page 75)

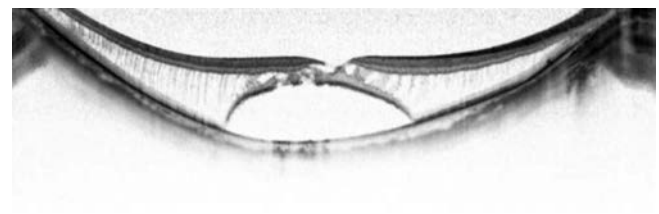

Myopic foveoschisis
(Case 170B, page 316)

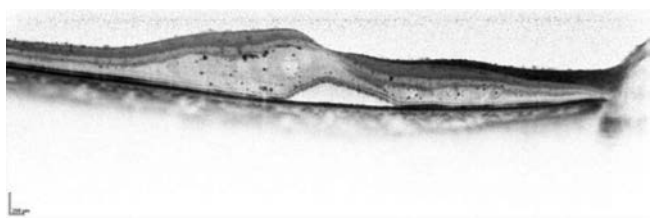

Diabetic macular edema
(Case 46E, page 95)

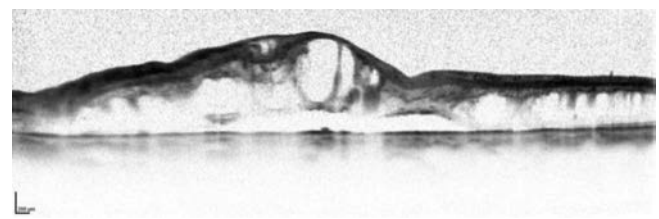

Central retinal vein occlusion
(Case 55E, page 112)

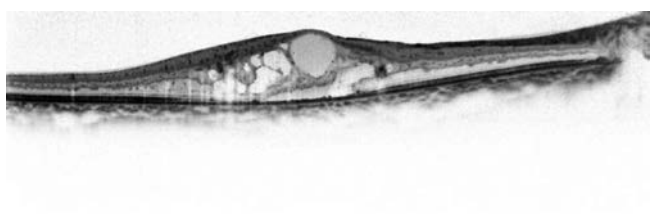

Macular telangiectasia Type 1
(Case 64E, page 124)

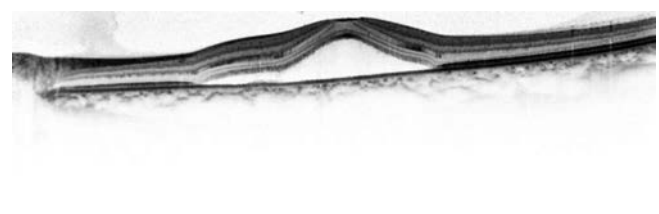

Central serous chorioretinopathy
(Case 72D, page 140)

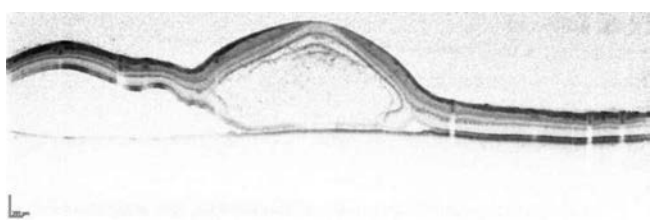

Vogt-Koyanagi-Harada syndrome
(Case 156E, page 287)

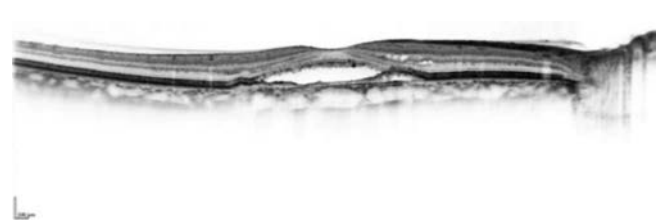

Type 1 CNV in exudative age-related macular degeneration
(Case 98G, page 184)

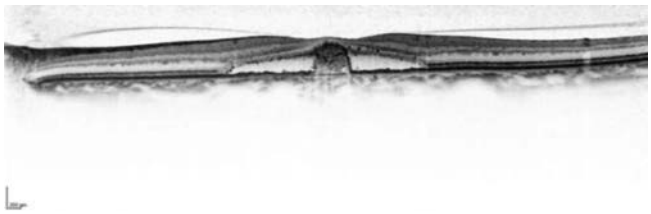

Polypoidal choroidal vasculopathy
(Case 105D, page 195)

Inferior staphyloma
(Case 182G, page 335)

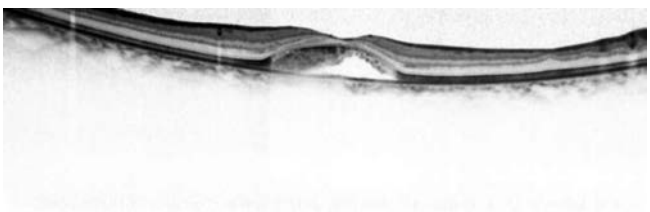

Adult-onset foveomacular vitelliform dystrophy
(Case 135E, page 252)

Outer retinal layer atrophy

Atrophic age-related macular degeneration
(Case 95D, page 178)

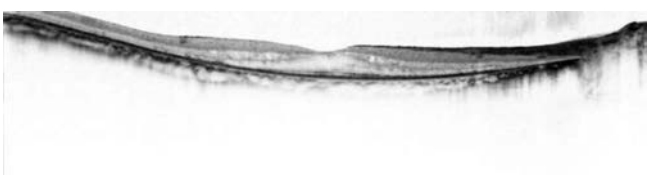

Retinitis pigmentosa
(Case 145E, page 267)

Stargardt disease
(Case 133F, page 247)

Oguchi disease
(Case 149C, page 275)

Bietti's crystalline dystrophy
(Case 143D, page 265)

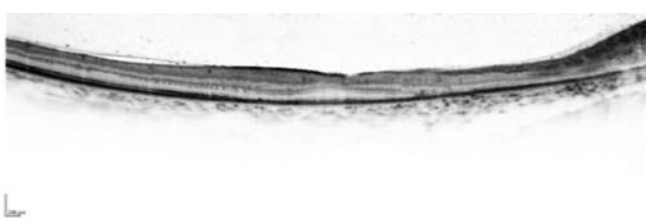

Cancer-associated retinopathy
(Case 142E, page 263)

Retinal pigment epithelium protrusions and undulations

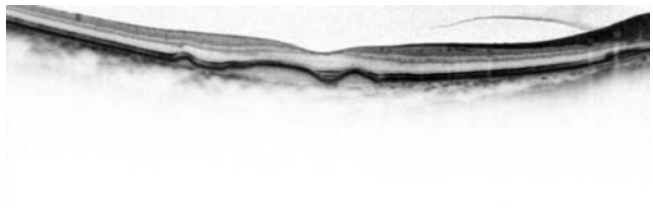

Drusen
(Case 80C, page 158)

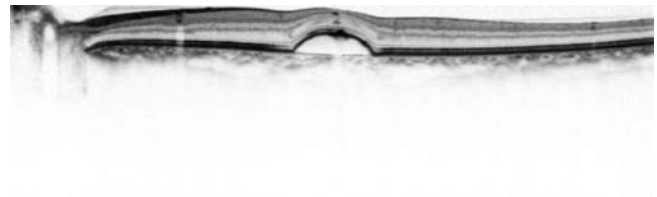

Serous pigment epithelial detachment
(Case 86D, page 164)

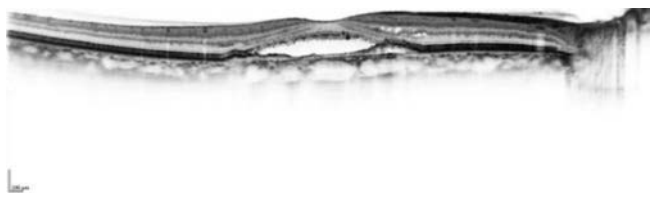

Type 1 CNV in exudative age-related macular degeneration
(Case 98G, page 184)

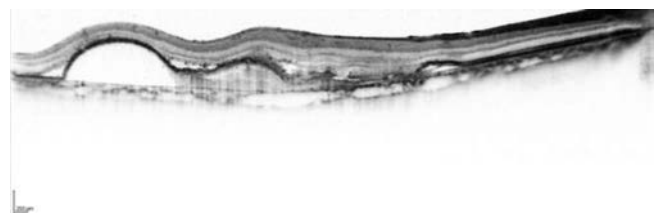

Polypoidal choroidal vasculopathy
(Case 113G, page 208)

Choroidal thickening and thinning

Retinal angiomatous proliferation stage 2B
(Case 120D, page 217)

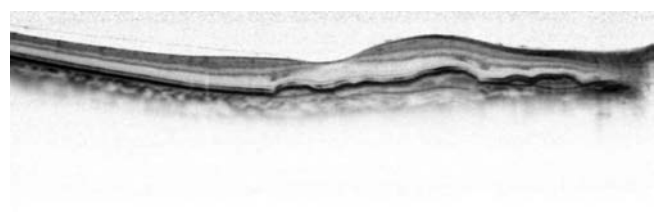

Pseudoxanthoma elasticum
(Case 137D, page 255)

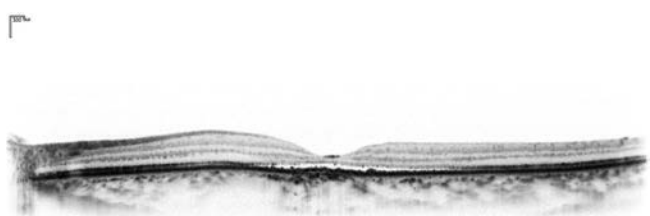

Central serous chorioretinopathy (EDI-OCT)
(Case 74D, page 142)

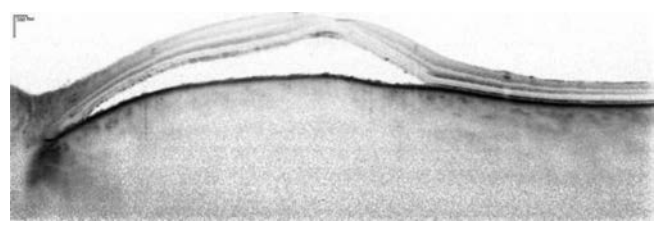

Vogt-Koyanagi-Harada syndrome (EDI-OCT)
(Case 157D, page 289)

Myopic foveoschisis
(Case 170B, page 316)

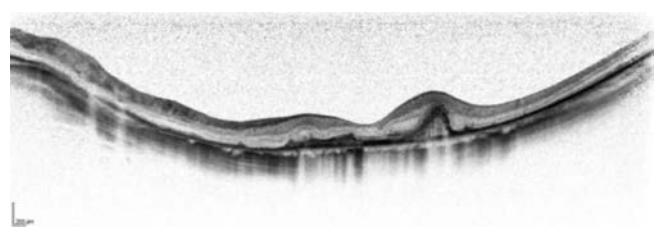

Myopic choroidal neovascularization
(Case 178D, page 327)

Service Part

Subject Index – 348

Case Index – 350

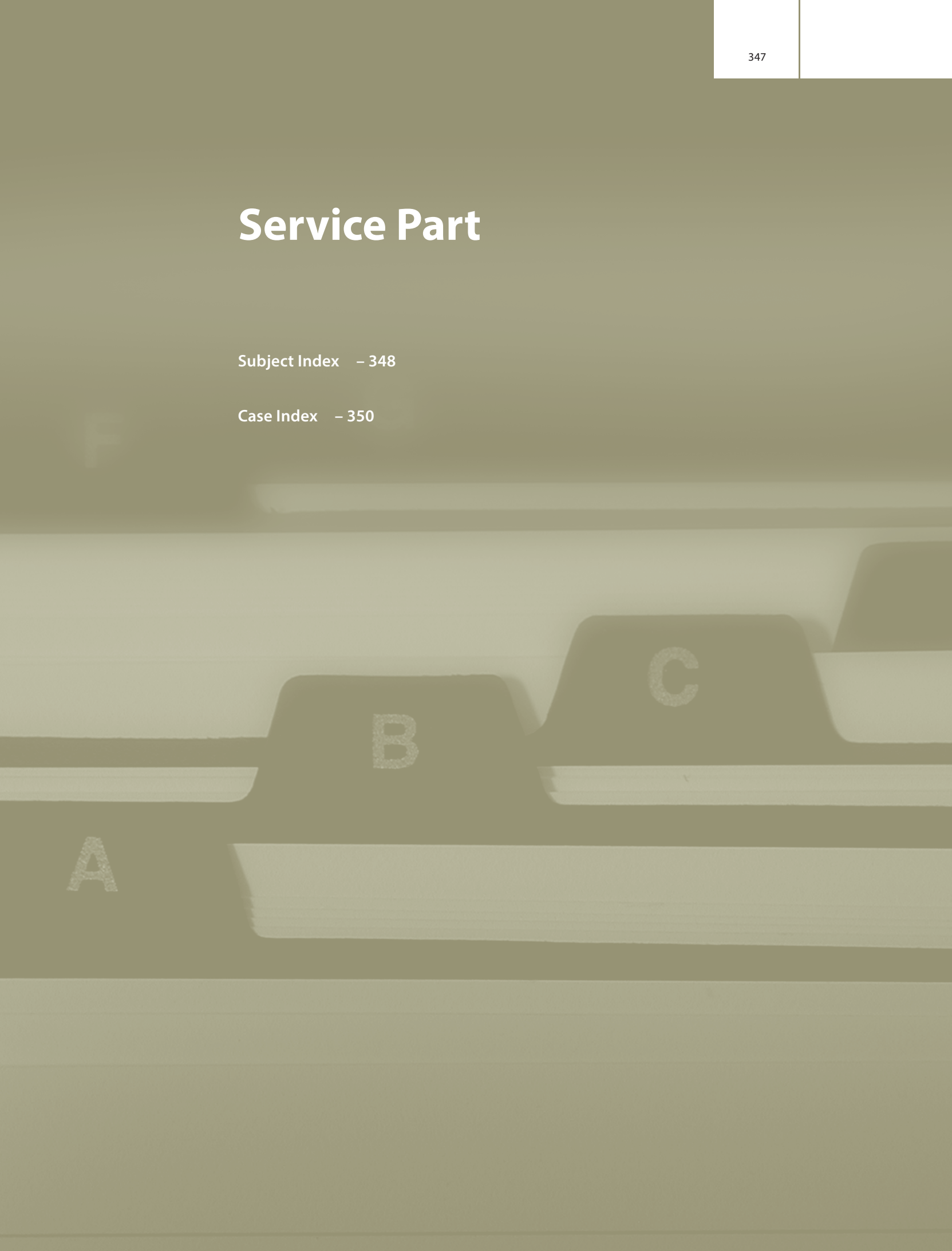

Subject Index

A

ABCA4 gene mutation 246
acute CSC 136
acute retinal necrosis 299, 301
acute zonal occult outer retinopathy (AZOOR) 235
adult-onset foveomacular vitelliform dystrophy (AOFVD) 249
age-related macular degeneration (AMD) 173
– and outer segment 7
angioid streaks (AS) 254
anti-VEGF treatment 326, 329
area of nonperfusion 110
arterial macroaneurysm 132
artifacts 13, 14, 15, 16, 17
– caused by the optical properties of tissue 14
– high-reflectivity 14
– involuntary eye imovement 13
– low-reflectivity 14
– shadows 14
atrophic age-related macular degeneration 173, 174
atrophic AMD 173
atrophy of the photoreceptor layer 96
autoimmune 295
AZOOR 237
– complex 235

B

Behçet disease 278, 279
Best disease 249
Bietti crystalline dystrophy 262
blind spot enlargement 237
boundary surface 4, 6
branch retinal vein occlusion (BRVO) 106
breakdown of the outer blood-retinal barrier 134
Bruch's membrane tears 241
B-scan interpretation 2
B-scans 10
– displaying false colours 10
– displaying reflection intensity 10
bullous retinal detachment 337

C

cancer-associated retinopathy (CAR) 259
capillary aneurysms 124
central retinal vein occlusion 104, 105, 109, 111
central scotomas 235
central serous chorioretinopathy (CSC) 56, 134, 137
cherry-red spot 115, 116
choroid 9, 10, 137
choroidal folds 293, 294
choroidal imaging 9
– choroidal thickness 10
– EDI-OCT 9
– swept source OCT (SS-OCT) 10
choroidal neovascularization (CNV) 179, 180, 181, 182, 183, 185, 186, 187, 188, 189, 190
choroidal permeability 134
choroidal thickening 137, 286, 289, 290
choroidal thinning 308, 313, 334
choroidal vessel hyperpermeability 137
chronic central serous chorioretinopathy 135, 144
chronic CSC 136
classic CNV 324, 325, 328
CME 122
Coat's disease 128
cone outer segment tip (COST) 6
cone sheath 7
contact cylinder 7
COST line 6
cotton-wool spots 78
cryopexy 128
Curtin classification 304
cuticular drusen 153, 159, 160
cyclosporine 296
cystic degeneration 122
cystoid macular edema 98, 104, 106, 109, 110, 121, 124, 278, 280, 282, 284, 336, 338
cystoid spaces 81, 82, 86, 95, 97, 105
– intracavity reflectivity 80
– typical locations 80

D

dark choroid 247
defocusing 16, 17
degenerative myopia 304, 305
depth resolution 2, 11, 12
– misinterpretations 11
diabetic macular edema 78, 79, 88
– injure
– photoreceptor layer 84
diabetic retinopathy 78
dome-shaped macula 331, 332
DONFL 36, 39
drusen 153, 159, 160, 161
drusenoid PED 153, 167

E

EDI-OCT 9
Ehlers-Danlos syndrome 254
ellipsoids 7
enhanced depth imaging (EDI) 10
enlargement of blind spot 233
epiretinal membrane 60, 61, 70
extensibility 305
exudative age-related macular degeneration 179
exudative chorioretinal spots 284
eye movement 13

F

false colours 10
fibrin 141
fibrin membrane 285
fibrovascular membrane 101, 102
flap 24
fluorescein angiography 134
fovea centralis thinning 146
foveal atrophy 99
foveal avascular zone (FAZ) 78
foveal cystoid spaces 132
foveal detachment 40, 42, 47, 48, 49, 50, 124, 132, 279, 284, 336
foveal detachment 344
foveal IS/OS reflectivity 111
foveal retinal thinning 315
foveal retinoschisis 312, 314, 316
foveal RPE atrophy 315
foveal thinning 281
fringe washout 14
fundus albipunctatus 271, 273
fundus flavimaculatus 246

G

Gass's Stage 24
gas tamponade 131
genetic predisposition 295
granulomatous iridocyclitis 285
granulomatous lesions 297, 298

H

hard drusen 153
hard exudate 84, 128, 132
hemi-retinal vein occlusion 104
hemorrhage 84
Henle fiber layer (HFL) 4, 25
herpes simplex virus 299
HFL 4, 5
hyperreflective foci 82, 91, 95

I

idiopathic choroidal neovascularization 223, 226, 228
idiopathic CNV 223, 328
idiopathic epiretinal membrane 60
idiopathic juxtafoveolar retinal telangiectasia 121
idiopathic macular holes 23
ILM detachment 307, 313
ILM peeling 315, 317
incomplete central retinal artery occlusion 118
indocyanine angiography 134
inferior staphyloma 331, 334
infiltrated leukocytes 281
inflammatory cells 297
ink-blot 135
ink-blot pattern 135, 140
inner nuclear layer cystoid edema 245
inner nuclear layer cystoid spaces 244
inner retinal atrophy 116
inner segment 7, 8
interpretation, B-scan 2
intracavity reflections 80, 81
intrachoroidal cavitation (ICC) 305, 308
intraretinal microvascular abnormalities (IRMAs) 78, 98
intraretinal separation 336
irregular retinal whitening 118
ischemic maculopathy 84
IS/OS abnormalities 235
IS/OS defect 232, 233, 234
IS/OS line 7
IS/OS line irregularities 125

L

lacquer crack 305, 311, 312, 330
lamellar cystic degeneration 125, 126, 127
lamellar macular hole 25, 46, 54
laser photocoagulation 137, 141
leakage mechanism 79

M

macular dystrophy 246
macular hole 23, 24, 25, 26, 27, 306
– Myopia 306
– postoperative OCT findings 26
– postoperative visual prognosis 26
– spontaneous closure 26
– stage classification 24
macular hole formation 319
macular hole retinal detachment 305, 320
macular microhole 25, 56, 57
macular pseudohole 55, 61
macular retinal detachment 316, 344

macular serous retinal detachment 340
macular thickening
– thickening due to traction 343
– thickening with cystoid spaces 343
– thickening with retinoschisis 343
Malattia leventinese 220, 222
Marfan syndrome 254
measurement principles 16
membrane-like material 292
MEWDS 235, 237
microaneurysms (MAs) 79, 88
middle-aged men 134
mild lacquer cracks 311
Müller cell cone 26, 27, 33, 35
multifocal choroiditis and panuveitis (MCP) 238
multilocular subretinal detachment 287
multiple B-scan averaging 3
multiple evanescent white dot syndrome (MEWDS) 232, 234
myopia 304
myopic CNV 307, 310, 325, 326, 327, 328
myopic foveoschisis 305, 318
myopic simple hemorrhage 322, 323

N

neovascularization, idiopathic choroidal 226, 228
noncaseating epithelioid granuloma 282
non-ischemia 113
nonperfusion area 83
nonproliferative diabetic retinopathy 78
normal choroidal imaging 9
normal retina 4
– cellular layer 4
– fiber layer 4
normal retinal layer structure 7

O

OCT findings 61, 136
Oguchi disease 274
operculum 24
outer photoreceptor shedding 296, 334
outer plexiform layer edema 81, 95, 132
outer retinal layer atrophy 345
outer retinal thinning 235
outer segment 7, 8
outer segment photoreceptor abnormalities 143, 144
outer segment shedding 294

P

Paget's disease 254
panretinal photocoagulation 99
papilledema 293
parafoveal cystoid spaces 94
paravascular retinal cysts 306
pathological myopia 304, 306
perifoveal PVD 23, 26
– foveal form abnormalities 25
– spontaneous separation 25
peripapillary atrophy 314
photodynamic therapy 137
photoreceptor cell inner 7
photoreceptor cells 83
photoreceptor defects 316
photoreceptor dehiscence 24
photoreceptor layer damage 84
PIC 241
pigment epithelial detachment 134, 135, 147, 155, 172, 201, 205
polypoidal choroidal vasculopathy (PCV) 155, 167, 191, 192, 196, 201, 202, 205, 207
posterior staphyloma 304, 320
posterior synechia 279
posterior vitreous cortex 100
posterior vitreous detachment (PVD) 23
proliferative diabetic retinopathy 101, 102
proliferative membrane 298
prolonged subretinal detachment 144
pseudoxanthoma elasticum (PXE) 254
punctate inner choroidopathy (PIC) 238
PVD 23

R

RAP
– schematic diagram 212
reactive RPE hyperplasia 146
recurrence 144
reflection intensity 10
reflection of virtual images 16
reflectivity 4, 5, 14, 15
reticular pseudodrusen 153, 154, 161, 162, 163
retinal angiomatous proliferation 212, 213, 219
retinal arterial macroaneurysm 129, 131
retinal artery occlusion 115
retinal atrophy 280
retinal capillary bed 78
retinal capillary lesions 78
retinal capillary network 78
retinal clouding 281
retinal detachment 300, 301, 336
retinal edema 79
– classification 79
retinal folds 298, 338, 339
retinal granulomatous lesions 282
retinal hemorrhages 110
retinal macroaneurysm 130
retinal microaneurysms 83
retinal nerve fiber layer 7, 8
retinal nerve fiber layer clouded edema 79
retinal nerve fiber layer thinning 317
retinal periphlebitis 283
retinal pigment epithelium protrusions and undulations 346
– Choroidal thickening and thinning 346
retinal pigment epithelium (RPE) 6, 134
retinal thickening 120, 122
retinal thinning 126, 127, 292, 299, 301
retinal traction 297
retinal vasculitis 278
retinal vein occlusion 104
retinal whitening 115, 119, 120
retinitis pigmentosa 265, 268
retinoschisin 242
retinoschisis 319, 330, 338, 340
rhegmatogenous retinal detachment (RRD) 299, 336
right-angled retinal venules 126
rod outer segment tip (ROST) 6
RPE 4, 6
atrophy 135
defects 238
depigmentation 237
hyperplasia 127
line 6
thickening 296
RS1 gene mutation 242

S

sarcoidosis 282
scar contraction 298
scotoma 234
SD-OCT findings 80
sensitivity attenuation 16, 17, 18
serous retinal detachment (SRD) 134, 181, 285
shadows 14
silicone oil tamponade 301
smoke-stack 134, 135
pattern 137, 139, 143
soft drusen 153, 157
soft exudate (cotton-wool spots) 78
solar retinopathy 56
speckle noise 2, 3, 11
– removal 11
– removing 3
spectral-domain OCT (SD-OCT) 2
SS-OCT 10
Stargardt disease 246, 248
steroid resistance 294
steroids 134
steroid therapy 288, 290, 291
subfoveal atrophic lesions 315
sub-ILM hemorrhage 130
subretinal deposits 145
subretinal detachment 104, 106, 109, 128, 135, 147
subretinal hemorrhage 130, 131
supraciliary effusion 289, 293, 294
swept source OCT 142
sympathetic ophthalmia 295, 296

T

temporal cystoid macular edema 123
thickened posterior vitreous cortex 318
third line 6
thrombus 115
tilted disc syndrome with inferior staphyloma 332
toxocariasis 297
tractional posterior vitreous detachment 312
traumatic macular hole 52
Type 2 CNV 238, 240, 325, 328

V

vacuoles 340
varicella-zoster virus 299
vascular microfolds 306, 313
vasculitis 299
venous beading 98
virtual images 16, 17
visual impairment 78
vitelliform macular dystrophy (VMD) 249
vitreomacular traction syndrome 67, 71, 72, 73, 100, 102
vitreoretinal interface lesions 342
vitreous hemorrhage 99, 129
vitreous inflammation 300
vitreous macular traction syndrome 318
vitreous surgery 296
VKH syndrome 288
Vogt-Koyanagi-Harada disease (VHD)
– Harada type 285
– Vogt-Koyanagi type 285
Vogt-Koyanagi-Harada disease (VKH) 285

X

X-linked juvenile retinoschisis 242

Y

yellowish-white dots 232
yellowish-white lesions 238
yellowish-white spots 239

Case Index

A

acute bullous retinal detachment
– A typical example 147
acute central serous chorioretinopathy
– a slowly leaking ink-blot pattern 140
– Intense leakage with ink-blot pattern 141
– Smoke-stack pattern 139
acute retinal necrosis
– typical example 300
acute zonal occult outer retinopathy
– Eye with a history of MEWDS 236
adult-onset foveomacular vitelliform dystrophy
– course 253
– peudohypopyon stage 252
– vitelliform stage 251
after surgery 42, 45
anti-VEGF treatment 186, 196, 219, 226, 326
atrophic age-related macular degeneration
– atrophic lesions of various sizes 177
– fellow eye of PCV 178
– typical example 176

B

Behçet disease
– acute attack 281
– cystoid edema and foveal detachment 279
– retinal atrophy 280
Bietti crystalline dystrophy
– outer retinal tubulation 264
– typical example 263
aranch retinal artery occlusion
– case of good visual acuity 119
– incomplete occlusion 120
aranch retinal vein occlusion
– Significant inner retinal layer ischemia 114

C

cancer-associated retinopathy
– damage to the outer retinal layers 260
– retinal vasculitis 261
central retinal artery occlusion 116
– cilioretinal artery not occluded 117
– incomplete occlusion 118
central retinal vein occlusion
– ischemic type 112
– progression from non-ischemic to ischemic 108, 110
chronic central serous chorioretinopathy
– case of recurrence 143
– changes in the photoreceptor outer segment 145
– choroidal thickening 142
– example of poor visual acuity 146
Coats' disease 128
cuticular drusen
– case with vitelliform detachment 159
– fellow eye 160
cystoid macular edema 87
– CME limited to layers anterior to the ELM 87
– exacerbation 89
– foveal detachment with recurrence 90
– ME extending to the outer retina 88
– microaneurysms 97
– photoreceptor damage from outer plexiform layer edema 95
– subfoveal accumulation 91
– subfoveal leakage from a foveal cystoid space 94
– subretinal leakage from a parafoveal cystoid space 92
cystoid spaces 87

D

diabetic macular edema
– Early-stage case 86
dome-shaped macula
– typical example 332
dot and blot hemorrhages 88
drusenoid PED
– case where CNV is suspected 166

E

enlargement of hemorrhagic pigment epithelial detachment 201
enlargement of the abnormal vascular network 202
epiretinal membrane 69
exudative age-related macular degeneration
– case with extensive Type 1 and 2 CNV exudative changes 185
– Type 1 and 2 CNV with cystic changes 188
– Type 1 and 2 CNV with extensive serous retinal detachment 187
– Type 1 CNV with a SRD 181
– Type 1 CNV with low activity 182
– Type 1 CNV with relatively strong exudative changes 183
– Type 2 CNV localized in the fovea centralis 189
– Type 2 CNV with strong exudative changes 190

F

foveal cystoid spaces 90, 94
foveal detachment 90
foveal photoreceptor layer degeneration 92
fundus albipunctatus
– typical example 272

H

hard exudate 88, 91, 92, 96
hemi-central retinal vein occlusion
– non-ischemic type 113
– idiopathic choroidal neovascularization
– envelopment by RPE cells 225
– fresh case 224
– scarring process 227

I

idiopathic epiretinal membrane
– typical example 63
– exposure of the fibrocellular membrane 64
– macular PVD has been complete 68
– macular PVD has not been complete 67
– membrane with significant whitening 65
– significant columnar structure formation 66
idiopathic macular hole
– case just before progression from stage 1 to stage 2 35
– postoperative course for macular hole closure 40
– postoperative course for macular hole closure under gas tamponade 38
– progression from lamellar to full-thickness macular holes 46
– progression from stage 1 30
– Stage 1 foveal cystoid space formation type 31
– Stage 1 foveal detachment type 32
– Stage 1 photoreceptor dehiscence type 33
– Stage 1 small foveal detachment type 34
– typical example of stage 2 36
– typical example of stage 3 41
– typical example of stage 4 43
ILM detachment
– case without foveoschisis 312
inferior staphyloma
– Serous retinal detachment 333
intrachoroidal cavitation
– connection with the vitreous cavity 309
– typical example 308
ischemic maculopathy
– cystoid macular degeneration 98
– thinned macula 99

L

lacquer cracks
– mild case 311
– typical example 310
lamellar macular hole 53, 54, 55
large pigment epithelial detachment
– case where CNV is present 171
– case where CNV is suspected 168

M

macular hole 29, 42, 51, 52
– Stage 1, macular microhole formation 48
– Stage 1, spontaneous separation of perifoveal PVD 47
– Stage 2, spontaneous closure 49
– Stage 3, Spontaneous closure 50
– Stage 4, spontaneous closure 51
– traumatic, a typical example 52
macular microhole
– case without PVD 59
– with complete PVD 58
– with macular PVD 57
macular pseudohole 53, 70, 71
macular telangiectasia
– Yannuzzi classification Type 1 123, 124
– Yannuzzi classification Type 2 Stage 2 125
– Yannuzzi classification Type 2 Stage 3 126
– Yannuzzi classification Type 2 Stage 4 127
Malattia leventinese
– typical example 221
multilayered petaloid 89

multiple evanescent white dot syndrome
– typical example 233
myopic choroidal neovascularization
– anti-VEGF treatment 328
– foveoschisis 330
– Large CNV 327
– Small CNV 325
– typical example 324
– young example 328
myopic foveoschisis
– before and after surgery for MHRD 321
– case with foveal detachment 314
– case with macular retinal detachment 316
– case without foveal detachment 313
– macular hole formation 319
– MHRD 320
– traction from the thickened posterior vitreous cortex 318
myopic subretinal hemorrhages
– typical example 322

N

nonperfusion area 88, 93

O

Oguchi disease
– cystoid space formation and golden sheen fundus reflex 276
– typical example 275
optic disc pit maculopathy 340
outer plexiform layer cystoid spaces 94

P

physiological PVD
– flattening of foveal depression 29
pigment epithelial detachment
– case with type 1 CNV 169, 170
– reactive proliferation of retinal pigment epithelial cells 165
polypoidal choroidal vasculopathy
– large branching vascular network 199
– large hemorrhagic pigment epithelial detachment 203, 204
– massive lesion 211
– case confused with central serous chorioretinopathy 195
– case where the branching vascular network has detached 210
– fibrin deposits 197, 198
– large foveal cystoid space 200
– optic disc type 206
– polypoidal lesions and pigment epithelial detachment 208
– small lesions 194
– tomographic notch sign 209
proliferative diabetic retinopathy 101
pseudoxanthoma elasticum
– outer retinal tubulation 258
– polypoidal lesions 257
– Type 1 CNV 255
– Type 2 CNV 256
punctate inner choroidopathy
– atrophic pigmented scars 239
– case complicated by CNV 240
– yellowish-white spots and CNV 241

R

reticular pseudodrusen 163
– case with atrophic age-related macular degeneration (atrophic AMD) 162
– fellow eye of RAP 161
retinal angiomatous proliferation
– Stage 1 214
– Stage 2A 215
– Stage 2B 216, 217
– Stage 3 218
retinal arterial macroaneurysm 132
retinal arterial macroaneurysm
– subretinal hemorrhages 130
retinitis pigmentosa
– cystoid macular edema 269
– typical example 267
– vitreomacular traction syndrome 270
rhegmatogenous retinal detachment
– case where retinal detachment has stopped at the fovea centralis 337
– foveal inner segment defects 339
– macular detachment 338

S

sarcoidosis
– cystoid macular edema 283
– foveal detachment 284
serous pigment epithelial detachment
– case without CNV 164
soft drusen 163
– confluent drusen 158
– example 157
soft exudate 91
stargardt disease
– typical example 247
sympathetic ophthalmia
– after vitreous surgery 296

T

toxocariasis
– proliferative membrane 298

V

venous beading 98
vitreomacular traction syndrome 73, 74, 75, 76, 100
Vogt-Koyanagi-Harada disease
– choroidal folds 293
– large foveal cystoid space 287
– prominent choroidal thickening 289
– reattachment process 291

X

X-linked juvenile retinoschisis
– retinoschisis confined to the macula 245
– retinoschisis over a wide area 243